PETROLOGY, GEOCHEMISTRY AND TECTONIC IMPLICATIONS OF MAGMATISM ALONG THE NORTHERN HUNTER RIDGE AND KADAVU ISLAND GROUP, FIJI

by

Alicia Verbeeten BSc. (Hons) LaTrobe University

Submitted in fulfilment of the requirements
for the degree of Doctor of Philosophy (Geology)
University of Tasmania, Hobart
December, 1996

STATEMENT

This thesis contains the result of research done in the Geology Department, University of Tasmania, between 1993 and 1996. This thesis contains no material which has been accepted for the award of any other degree or diploma in any tertiary institution and, to the best of the author's knowledge and belief, this thesis contains no material previously published or written by another person, except where due reference is made in the text of the thesis.

(i) I agree/d~~o not agree~~ that the thesis may be made available for loan
(ii) I agree/d~~o not agree~~ that the thesis may be made available for photocopying

A. Verbeeten

Alicia Verbeeten
University of Tasmania
December, 1996

ABSTRACT

The submarine Hunter Ridge separates the inactive South Fiji Basin from the actively spreading North Fiji Basin, and is a newly recognised intra-oceanic arc in the SW Pacific. Magmatic activity along the Hunter Ridge is linked to the northward subduction of the crust of the Oligocene (26.0-32.5Ma) South Fiji back-arc basin. Subduction began in response to establishment of an E-W orientated spreading ridge at ~7Ma across the North Fiji Basin, and the accompanying anticlockwise rotation of the Fiji Platform.

Rocks suites dredged along the northern part of the Hunter Ridge include basalts to dacites transitional between high-Ca boninites and typical arc tholeiites, and calc-alkaline basalts to rhyolites. Mineral compositions (e.g. Cr-spinel with Cr#>70), coupled with whole rock high CaO/Al_2O_3 (0.91-1.13) and low abundances of HFSE (0.37-0.54% TiO_2; 0.27-0.86ppm Nb; 0.02-0.05ppm Ta), Y (11-15ppm) and HREE of the basalts relative to N-MORB show that both the arc tholeiite and calc-alkaline basalts are derived from sources more refractory than the N-MORB source, probably peridotite residual after production of North Fiji Basin oceanic crust. The enrichment in LILE and LREE of the Hunter Ridge rocks reflects addition to this refractory source of a slab-derived fluid for the arc tholeiitic suite and a slab melt component for the calc-alkaline suite.

The Kadavu Island Group, in southwesternmost part of the Fiji archipelago, is the northeastern exposed end of the Hunter Ridge and can be divided into four geochemically distinct magmatic groups.

The Astrolabe Group shoshonites (~3.4Ma) have major and trace element and isotopic compositions very similar to other shoshonites in Fiji. The low HFSE abundances (~0.64%TiO_2, 0.11ppm Ta, 2.0ppm Nb), high CaO/Al_2O_3 values (0.88-1.1) and high Cr# of Cr-spinel ($Cr^{\#}$~85) of the mafic lavas (absarokites) of the shoshonite suite indicate a particularly refractory peridotite source for the Astrolabe lavas. The strong LILE and LREE enrichments of the Astrolabe shoshonites are extreme variants of the same enrichment shown by primitive arc tholeiites on the Hunter Ridge and in the Vanuatu arc, and are attributed to relatively low degrees of partial melting of a mantle source similarly affected by ingress of slab-derived hydrous fluids. The mantle metasomatism responsible for producing the source peridotite of the Astrolabe suite magmas may have

occurred during Oligocene to Miocene subduction associated with the Vitiaz arc system. Emplacement of the Fijian shoshonites, including the Astrolabe Group, is considered to be related to lithospheric extension in the early-mid Tertiary Fijian arc, in response to reorganisation of spreading systems in the North Fiji Basin and initiation of spreading in the adjacent Lau Basin.

Pleistocene to Recent (2.9-0.48Ma) volcanism on Kadavu is represented by the Western Kadavu and Central/Eastern/Ono Groups, and records the effects of initiation of subduction of the South Fiji Basin crust beneath Fijian arc lithosphere. The dominant rock types are medium to high-K adakitic andesites and dacites. Low abundances of Y (15.6-19.6ppm), high Sr contents (553-1667ppm), high Sr/Y (79.2-88.9), and strongly fractionated REE patterns (La/Yb_N=12-25), are consistent with an origin involving partial melting of subducted basaltic oceanic crust consisting mainly of garnet and clinopyroxene (eclogite). Furthermore, Sr, Nd and Pb isotopic analyses plot within the range of Pacific MORB, consistent with derivation of these magmas by partial melting of subducted MORB, with no pelagic sediment involvement.

Lavas of the Ngaloa Group form a volumetrically small part of the Kadavu Island Group and consist of unusual basalts and basaltic andesites with high Na_2O (2.7-5.5%), TiO_2 (1.4-1.7%), and Sr (2055-2957ppm) and low FeO* (5.8-6.8%) and relatively high Nb contents (8-16ppm) for supra-subduction basalts. They are temporally and spatially associated with the Western Kadavu adakitic andesites and dacites, but major and trace element considerations rule out any direct genetic link between them through differentiation. However, Ngaloa Group lavas also have specific geochemical features (Sr/Y=93-205, La/Yb_N=19-29 and MORB-like isotopic compositions) similar to the Western Kadavu and Central/Eastern/Ono Group adakites, indicating involvement in their petrogenesis of a component formed by partial melting of the subducted oceanic crust. Their high MgO (5.1-7.9%), and Ni (up to 200ppm) contents and primitive phenocryst compositions (e.g. Fo_{89-91}) however, preclude their derivation solely from the partial melting of the subducted crust. Trace element considerations suggest that the Ngaloa Group basalts were produced by partial melting of mantle wedge peridotite that had interacted with and been strongly modified by slab melts probably similar to the Western Kadavu adakitic lavas. Lavas compositionally similar to the Ngaloa Group volcanics in some other arcs also occurring in close association with adakitic andesites, have been termed Nb-enriched arc basalts (NEAB)

and are also thought to have formed by melting of a slab-melt metasomatised mantle wedge.

Partial melting of subducted oceanic crust in eclogite facies (~50-80km depth) is thus implicated in the petrogenesis of the Ngaloa Group and the Central/Eastern/Ono and Western Kadavu adakitic lavas. As the subducted slab is too cool to partially melt at the amphibolite-eclogite transition beneath normal forearc regions of oceanic arcs, a mechanism to elevate the isotherms beneath the northern end of the Hunter Ridge is required. The subducting South Fiji Basin oceanic crust is too old (26.0-32.5Ma) and cold to provide the necessary heat. An alternative heat source is ascending asthenospheric mantle beneath the northwestern end of the Lau backarc basin. This convecting MORB-source mantle is hypothesised to move via the mantle window at the end of the subducting plate to abut subducted South Fiji Basin oceanic crust. Conductive heat transfer from this hot asthenospheric mantle enabled partial melting of the subducted South Fiji Basin slab, and partial melting of the same asthenosphere mantle is considered to be responsible for generation of the unusual OIB-type basalts that occur directly above the slab window between Viti Levu and Vanua Levu, Fiji.

ACKNOWLEDGMENTS

Many people have provided advice, assistance, support and friendship over the last three and a half years, and although the following list attempts to cite and thank all these, I also extend a general acknowledgment to any others I may have overlooked.

- My supervisor, Dr Tony Crawford provided constant support and encouragement. He contributed immeasurably to the development of the ideas and the assessment of the data presented in this thesis.

- Dr. Leonid Danyushevsky, Dr. Vadim (Dima) Kamenetsky and Professor Rick Varne offered invaluable advice and assistance.

- Professor David Green for access to the laboratory facilities (clean lab) and the ICP-MS at the Research School of Earth Sciences (RSES) at the Australian National University, and Dr. Richard Price for access to laboratory facilities at LaTrobe University.

- Dr. Steve Eggins (RSES) for his time analysing my samples (ICP-MS) and for his enthusiasm and advice.

- Dr. Roland Mass (Latrobe University), supervised the radiogenic isotope work and spent long days running the Finnigan MAT 262 mass spectrometer with me. A further thanks to Roland for providing a detailed description of the analytical procedure outlined in Appendix 2.

- I am grateful to the Mineral Resources Department, Fiji and the District Chiefs of the Kadavu Islands for allowing me to do fieldwork and to the people of Kadavu (especially Pauliasi Gudru from Waisomo Village, Tavuki) whose friendly help and hospitality made working in their country extremely enjoyable.

- Crew and Captain of the R.V Alis are thanked for an enjoyable and productive cruise along the northern part of the Hunter Ridge.

- Numerous post doctoral fellows and fellow Ph.D students at the University of Tasmania (Geology/CODES department) provided friendship and support throughout my Ph.D years. In particular the people I have shared an office with over the last three and a half years: Ingvar Sigurdsson, Fernando Della Pasqua, Massimo Gasparon, Ruth Lanyon, Robina Sharpe, Rohan Wolfe (thanks Rohan for helping with many computer problems and for drafting the last diagram) and Cathryn Gifkins. Many thanks also to Karen Orth, Andrew McNeill, Ali Raos, Mark Doyle, Paul Kitto, Anthea Hill, Bill Wyman, Briony Sinclair, and many others. I would like to make a special thanks to Fernando and Robina who have been enormous support throughout my Ph.D.

- Invaluable technical assistance was provided by Peter Cornish, Marylin Feast, Jeanette Harris, June Pongratz, Christine Higgins, Simon Stevens, Phil Robinson (XRF), Wislaw Jablonski (electron microprobe), Nilar Hliang and Katie McGoldrick

- Dr. Peter Fleming (Bald Eagle) and Dr. Peter Jackson (Jacko) from LaTrobe University for their continuing support and friendship.

- A special thanks to my extremely supportive housemates Megan Humrich, Ross Edwards and Paul Scott.

Finally, I dedicate this thesis to my family. To my parents Harry and Denise for their on-going support throughout my long years as a student and their emotional support in the final months and to Danny, Sonja, Peter, Andrew, Simone and Darren just for being there.

TABLE OF CONTENTS

LIST OF FIGURES

Chapter 1: Introduction

Chapter 2: Tectonic setting and geochemical evolution of Fiji

Chapter 3: Hunter Ridge

Chapter 4: Astrolabe Group

Chapter 5: Ngaloa Group

Chapter 6: Western Kadavu and Central/Eastern/Ono Groups

Chapter 7: Synthesis

LIST OF TABLES

LIST OF PLATES

Chapter 3: Hunter Ridge

Chapter 4: Astrolabe Group

Chapter 5: Ngaloa Group

Chapter 6: Western Kadavu and Central/Eastern/Ono Group

Chapter 1

INTRODUCTION

1.1 SETTING OF THE HUNTER RIDGE AND THE KADAVU ISLAND GROUP

This study examines the petrology, geochemistry and tectonic implications of magmatism of the Kadavu Island Group in Fiji, and its southern submarine continuation along the Hunter Ridge.

Fiji, including the Kadavu Islands and the Hunter Ridge, lies in a tectonically complex area between the oppositely-dipping Tongan and Vanuatu subduction zones and their associated arc-backarc systems (Fig. 1.1a).

The Hunter Ridge forms the boundary between the actively spreading North Fiji Basin and the South Fiji Basin (26-33Ma; Weissel and Watts, 1975; Watts et al., 1977), and joins the southern end of the Vanuatu island arc and the northern end of the Tongan island arc. It has been considered to be a transform zone almost parallel to the motion vector of the Australian Plate. However, the data presented in this thesis show that the Hunter Ridge rocks are unambiguously subduction-related. The Hunter Ridge, therefore, is a newly recognised island arc in the SW Pacific region.

Kadavu is the emergent northern termination of the Hunter Ridge, and with the small islands of Ono and Ngaloa, and a number of islets lying within the Great Astrolabe Reef, it forms the Kadavu Islands (Kadavu Island Group) (Fig. 1.1b). The main island of Kadavu is elongated along an ENE-WSW axis, parallel to the Hunter Ridge.

Igneous rocks on Fiji record four major tectonic and magmatic events; the early arc stage (>10Ma), the mature arc stage (~10-5Ma), the early rifting stage (5.5-3.0Ma) and the late rifting stage (3Ma to the present) (see chapter 2 for relevant references and a review of the tectonic development and geochemical evolution of Fiji). Over most of Fiji during the late rifting stage, volcanism had compositional affinities with ocean island basalts. In contrast, at this time, volcanism on Kadavu was

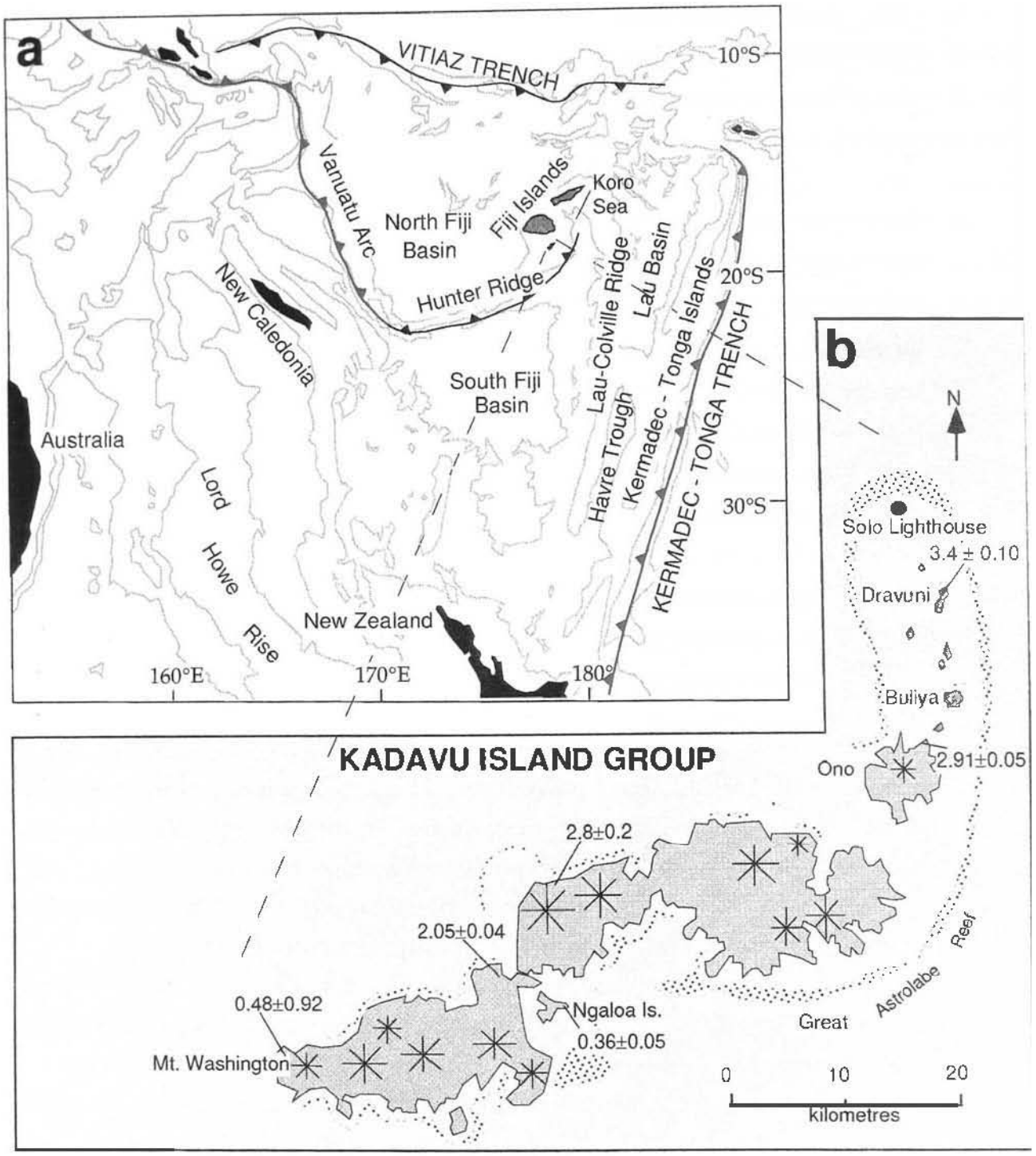

Figure 1.1a: Bathymetric map of the southwest Pacific after Inokuchi et al. (1992), showing present day locations of the Indo-Australia and Pacific Plate boundaries and the location of the Fiji Islands. Water depth is shown by the 2000m contour. Active spreading occurs in the North Fiji and Lau Basin-Havre Trough. Convergence is occurring along the Vanuatu and Kermadec -Tonga arcs. **b**: Sketch map of the Kadavu Island Group showing the main volcanic peaks (asterisks) (after Woodrow, 1980). Radiometric ages are from Whelan et al. (1985). The distributions of the four geochemical groups are shown by the different colours. The northern islands, in orange, represent the Astrolabe Group, the green area represents the CEO Group, the mauve area represents the WK Group, and the yellow area plus isolated small areas around the coast of the main island (not marked; see chapter 5) represent the Ngaloa Group volcanics.

dominated by subduction-related lavas, implying a complex tectono-magmatic setting for Fiji since 3Ma.

1.2 PREVIOUS WORK ON THE KADAVU ISLAND GROUP

Romanu et al. (1959) carried out the first major investigation of the Kadavu Island Group, involving coastal traverses, petrographic study of samples collected, and the interpretation of aerial photos. In 1971 the Geological Survey of Fiji collected stream sediment samples for geochemical study, and from 1972-1974 similar work was undertaken by Island Mines Limited. During 1974-1976, Woodrow (1980) carried out geological mapping of the Kadavu Island Group, and confirmed that Kadavu formed by the coalescence of many dominantly andesitic volcanoes, and that the smaller islands are remnants of other volcanoes.

In the limited geochemical studies of Fiji, the Kadavu Island Group is referred to in context with the rest of Fiji (Gill, 1984; Gill et al., 1984; Gill and Whelan, 1989b; Rodda, 1994). A general consensus from the more recent literature (Gill, 1984; Rodda, 1994) interprets the Kadavu Island Group to have formed by limited oblique subduction of South Fiji Basin crust. However, Gill and Whelan (1989b) claimed that lavas constituting Ngaloa island formed during the late rifting stage as one of the ocean island basalt-type volcanoes erupting in Fiji since 2.8Ma. This thesis presents evidence that Ngaloa Island is a product of subduction-related magmatism, albeit compositionally unusual.

Aside from limited data presented in the geological mapping report by Woodrow (1980), there has been no later specific geochemical studies of the Kadavu Islands. Whelan et al., (1985) presented $^{40}Ar/^{39}Ar$ ages on random samples taken from across the Kadavu Island Group and showed that the oldest rocks (~3.4Ma) occurred in the northeast (Astrolabe Islands) and the youngest in the southwest (Fig. 1.1b).

1.3 FIELDWORK

Approximately two and a half months were spent on the Kadavu Island Group (June - August, 1993) mapping and sampling. Fieldwork involved mainly coastal traverses, but where possible (due to the thick rainforest covering most of the island) inland traverses were completed. As a result, the majority of samples were collected from coastal outcrops. With the use of aerial photos in connection with Woodrow's (1980) geological map, samples were accurately located (Appendix 1).

Samples of between 300-400g were collected from all the major volcanoes outlined by Woodrow (1980). On the western part of Kadavu, and on Ono Island, fresh samples were difficult to attain. The central and eastern areas showed more fresh rock exposures that allowed more detailed sampling.

During late October-early November, 1993, I took part in a research cruise of the French vessel R.V. Alis, which dredged at depths of less than 1500m, along the central and northern part of the Hunter Ridge. Samples were collected from sixteen dredge locations. This part of the Hunter Ridge was surveyed by numerous transects using a EDO 12kHz single beam echosounder.

All samples collected from the Kadavu Island group and the Hunter Ridge were examined petrographically and selected rocks were analysed for major and trace elements and radiogenic isotopes (Sr, Nd and Pb).

1.4 AIMS AND PRESENTATION OF THIS THESIS

The main aim of this thesis is to report the geochemical data and interpret it to reveal the nature of arc volcanism for lavas recovered from the submarine Hunter Ridge and lavas collected from the Kadavu Island Group.

Geochemically, the lavas from the Kadavu Island Group fall into four distinct suites (Fig. 1.1b) referred to in this study as:

(i) Astrolabe Group
(ii) Ngaloa Group
(iii) Western Kadavu Group (WK)
(iv) Central/Eastern/Ono Group (CEO)

This introductory chapter is followed by one in which the broad tectonic setting and geochemical evolution of Fiji is reviewed within the framework of the southwest Pacific. In chapters 3, 4, 5, and 6 the different magmatic groups comprising the Hunter Ridge and the Kadavu Island Group are discussed under the following headings:

Geology
Petrography and Mineral chemistry
Major Element Geochemistry
Trace Element Geochemistry
Radiogenic Isotope Chemistry
Petrogenesis
Summary

Chapter 3 provides an extensive new set of analyses of magma suites dredged from along the northern part of the Hunter Ridge. Magma suites were found to include calc-alkaline basaltic andesites-rhyolites and arc tholeiitic basalts-andesites with transitional boninitic affinities. Results of this study, together with those from Sigurdsson, (1994) and Sigurdsson et al., (1993) show the diversity in geochemical composition of rocks along the Hunter Ridge.

Chapter 4 describes the oldest rocks found on the Kadavu Islands; the Astrolabe Group. The LIL enrichments and other compositional characteristics of the Astrolabe Group are similar to those of the 'shoshonite rock association' as defined by Morrison (1980) and these lavas also have very similar compositions to shoshonites produced during the early rifting stage of Fiji's evolution, such as those making up the Tavua Caldera on Viti Levu (Rogers and Setterfield, 1994)

Chapter 5 reports a study of the Ngaloa Group basalts and basaltic andesites, an unusual suite of lavas that are a volumetrically small part of the Kadavu Islands. They have high incompatible element abundances more typical of OIB type lavas, and for this reason have been claimed to be derived from a similar source to that which yielded the OIB volcanics of the same age elsewhere in Fiji (Gill and Whelan 1989b). However, as shown in this thesis, the Ngaloa Group show some typical characteristics of subduction related magmatism, and have radiogenic isotopes typical of N-MORB.

Chapter 6 describes the final two suites of lavas from the Kadavu Islands; the Western Kadavu and Central/Eastern/Ono Group andesites and dacites. These suites show similar geochemical affinities, and are therefore described together.

The main conclusions of this thesis are summarised, and the tectonic implications of magmatism along the northern part of the Hunter Ridge and the Kadavu Island Group are described in Chapter 7.

1.5 ACRONYMS AND ABBREVIATIONS

The following acronyms and abbreviations are used throughout the main text of this thesis.

An	Anorthite content of plagioclase = 100Ca/(Na+Ca+K)
BABB	Back Arc Basin Basalt
CEO	Central/Eastern/Ono group
$Cr^{\#}$	100Cr/(Cr+Al) for Cr-spinel

DMM	Depleted MORB mantle
E-MORB	Enriched Mid-Ocean Ridge Basalt
$Fe^{\#}$	$Fe^{3+}/(Fe^{3+}+Fe^{2+})$ for Cr-spinel
FeO*	$(0.8998 \times Fe_2O_3)+FeO$
FMQ	Fayalite Magnetite Quartz oxygen buffer
Fo	Forsterite content of olivine = $100Mg/(Mg+Fe^{2+})$
fO_2	Oxygen fugacity
HFSE	High Field Strength Elements (ionic potential >2.0)
HREE	Heavy Rare Earth Elements
IAT	Island Arc Tholeiite
ICP-MS	Inductively Coupled Plasma-Mass Spectrometry
$(La/Sm)_N$	La/Sm normalised to chondrite
LILE	Large Ion Lithophile Elements (ionic potential <2.0)
LOI	Loss On Ignition
LREE	Light Rare Earth Elements
$Mg^{\#}$	$100Mg/(Mg+Fe^{2+})$
MREE	Middle Rare Earth Elements
MORB	Mid-Ocean Ridge Basalt
NHRL	Northern Hemisphere Reference Line
N-MORB	Normal Mid-Ocean Ridge Basalt
OIB	Ocean Island Basalt
REE	Rare Earth Elements
WK	Western Kadavu group
XRF	X-Ray Fluorescence spectrometry

Chapter 2

TECTONIC SETTING AND GEOCHEMICAL EVOLUTION OF FIJI

2.1 INTRODUCTION

The SW Pacific is a prime locality for the study of convergent plate margin processes involving intra-oceanic arc-backarc basin systems, particularly that part between the Tonga-Kermadec arc and the Vanuatu (nee New Hebrides) arc which has been the subject of numerous geodynamic and tectonic studies and reconstructions over the last 20 years. Although both the Tongan and Vanuatu arcs are by no means tectonically or magmatically simple, the intervening area, represented by the Fijian Islands and adjacent seas, is even further complicated by its removal from the site of active subduction over the last 5 m.y., and the appearance of intraplate basalts.

The regional tectonic setting and evolution of the Fiji Islands has been summarised from several perspectives, resulting in some conflicting interpretations (Malahoff et al., 1982; Colley and Hindle, 1984; Gill et al., 1984; Rodda and Kroenke, 1984; Hathway, 1994). This chapter reviews the tectonic setting and geochemical evolution of Fiji through four tectonic stages: (i) the early arc stage, (ii) the mature arc stage, (iii) the early rifting stage, (iv) and the late rifting stage, paying particular attention to the latter two stages, since it was during this time that the Kadavu Island Group was forming.

2.2 REGIONAL SETTING OF FIJI

The Fiji Islands lie close to the active boundary between the Pacific and Indo-Australian plates, a region characterised by a complex array of island arcs, backarc basins, troughs and ridges. In this region, two subduction zones with opposite convergence face each other (Fig. 1.1a). At the Tonga-Kermadec trench, Pacific lithosphere is being subducted in a westerly direction, whereas younger Indo-Australian lithosphere is being subducted beneath the Pacific plate at the Solomon and New Hebrides trenches. Periodic arc rotation, fragmentation and dislocation have all

contributed to the complex morphology of this region, which reflects the on-going interaction between the Indo-Australian and Pacific plates.

The Fiji Platform is an area of relatively shallow water (depths <2000m) upon which the major Fiji Islands are situated (Fig. 1.1a). The largest island of Fiji, Viti Levu, and the second largest island Vanua Levu, are encircled by about 320 smaller islands. The Kadavu Island Group, the individual islands of the Moala Group and various other islands and seamounts, rise from water more than 2000m deep.

The Fiji Islands are situated at the northern end of the 2400km long, mainly submarine Lau-Colville Ridge (Cole et al., 1990), and are flanked by the actively forming North Fiji and Lau backarc basins to the west and east respectively. The presently inactive backarc basin, the South Fiji Basin (26-33Ma), is located to the south of the platform.

2.3 PLATE TECTONIC HISTORY OF FIJI

Throughout the last decade, most syntheses of SW Pacific tectonic development have joined Vanuatu, Fiji and Tonga into the once-continuous Vitiaz Arc system, that lay along the northeastern edge of the Indian Plate during the early Tertiary. Figure 2.1a-d shows reconstructions of the SW Pacific from >10 Ma to the present, after Kroenke (1984). During this time, the setting of the Vitiaz arc may have been similar to the modern Mariana arc, involving west-directed subduction of relatively old Pacific lithosphere. Late Eocene basement rocks of Fiji correlate with those in the Tongan forearc, and also appear as east-derived clasts in Late Oligocene sediments in Vanuatu (Gill, 1976; Coleman and Packham, 1976).

The position of the arc at the onset of arc volcanism is known only approximately, because during much of the Oligocene, the South Fiji Basin was forming (Weissel and Watts, 1975; Kroenke, 1984), introducing more spreading ridges and thus complicating the tectonics along the Indo-Australia and Pacific plate margin. The South Fiji Basin probably formed behind an arc system now represented by the Three Kings Rise - Loyalty Islands Ridge - D'Entrecasteaux Ridge, and Inokuchi et al. (1992) suggested that Viti Levu may have rotated clockwise ~45°, during opening of the South Fiji Basin.

About 10Ma, the Ontong-Java Plateau is thought to have collided with the northern end of the Vitiaz subduction system (Fig. 2.1b), shutting it down and forcing a reversal in subduction polarity to east-directed subduction of Indo-Australian lithosphere beneath the Pacific plate. Also around this time, backarc basin formation led to initial opening of the North Fiji Basin. In

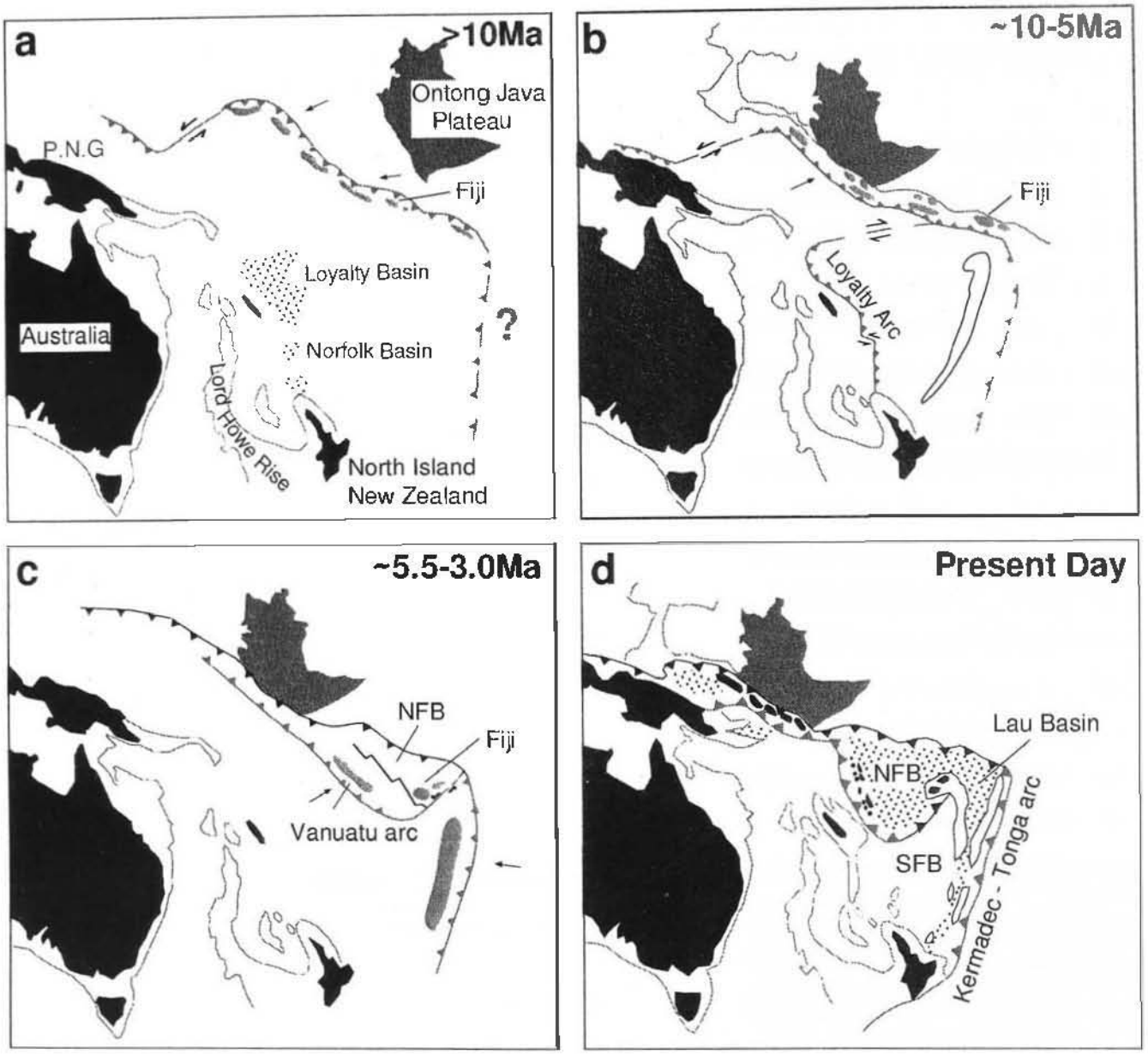

Figure 2.1 Reconstruction of Indo - Australia and Pacific Plates from >10Ma to the present day (after Kroenke, 1984). **a**: >10Ma Convergence probably started (~42Ma) along the Vitiaz Arc (southwestward subduction). **b**: ~10Ma the Ontong Java Plateau collided with the northern end of the Vitiaz subduction system, possibly shutting it down, forcing a reversal in subduction polarity and the eventual opening of the North Fiji Basin (NFB). **c**: ~5.5 the North Fiji Basin (NFB) continues to open, rotating the Vanuatu arc in a clockwise direction and the Fiji Platform in an anticlockwise direction. **d**: Present day locations of the Indo-Australian and Pacific Plate boundaries. The NFB and Lau Basin are still actively spreading. Convergence is occurring along the Vanuatu arc (northeastward subduction) and the Tonga-Kermadec arc (westward subduction). SFB= South Fiji Basin

response to North Fiji Basin opening, the Fiji segment of the Vitiaz arc, recently detached from the eastern part of the New Hebrides forearc, began to rotate in an anticlockwise direction. Falvey (1978) proposed about 35° rotation of Viti Levu beginning later than 6Ma, based on plate reconstruction and palaeomagnetic data from Viti Levu and Vanuatu. James and Falvey (1978) estimated the anticlockwise rotation to be approximately 21° since 4Ma. Rotation of the Fiji platform is considered to have been accommodated by subduction along the Hunter Fracture Zone, with resulting volcanism building the Kadavu Islands (Gill, 1984; Rodda, 1994).

In late Miocene to early Pliocene time (5Ma), seafloor spreading began in the Lau Basin just east of the North Fiji Basin. Formation of these backarc basins caused profound changes in the region, and removed the Fiji Platform from the proximity of subducted lithosphere. Basalts erupted in most of Fiji from 3Ma to the present show almost no arc-like chemical characteristics, and are alkali basalts or their hawaiitic differentiates, with OIB-type affinities.

2.4 GEOCHEMICAL EVOLUTION OF FIJI

2.4.1 INTRODUCTION

The geology of the Fiji Islands is dominated by arc-related volcanic and intrusive rocks and thick sequences of volcaniclastic sediments. The early history of Fiji, from mid?-Eocene through to the late Miocene, records the progressive development of an early- to mature-stage island arc, the igneous component of which indicates a gradual evolution from island arc tholeiites to calc-alkaline basalts and andesites (Gill et al., 1984). During the period ~5.5-3.0Ma (early rifting stage), a transition from calc-alkaline to shoshonitic volcanism occurred, dominantly in western Fiji, and has been considered to be related to the disruption of the Vitiaz arc, although North Fiji Basin opening almost certainly commenced earlier, around 12-10Ma (Auzende et al., 1996). Post-disruption volcanism (late rifting stage, 3-0Ma) has been dominated by alkali basalts, apparently derived from a deeper, intra-plate OIB-like magma source.

2.4.2 EARLY ARC STAGE (>10Ma)

On Viti Levu, Vitiaz arc magmatic activity is represented by the Yavuna and Wainimala Groups. The Late Eocene-Early Oligocene rocks of the Yavuna Group are the oldest known rocks in Fiji. They consist of basaltic to andesitic massive and pillowed lavas, pillow breccias and reworked volcaniclastic rudites (Inokuchi et al., 1992; Hathway 1994; Rodda, 1994).

This group includes the Yavuna tonalitic stock (34 Ma), and is intruded by a N-W striking dyke swarm composed of primitive island arc tholeiites transitional to high-Ca boninites (Wharton et al., 1995). The succeeding Wainimala Group, located in the southern part of Viti Levu and on a number of smaller islands to the west at the southern end of the Yasawa Chain, lies with angular unconformity on Yavuna Group rocks (Fig. 2.2a). Oldest Wainimala rocks (southernmost Yasawa Chain) are basaltic pillow lavas and volcaniclastics, with subordinate pelagic limestone, all intruded by dyke swarms. In southwestern Viti Levu, similar pillowed, massive and brecciated basalts with minor dacitic rocks are intercalated with pelagic limestones.

Hathway (1994) divided the Wainimala Group into two assemblages, an arc assemblage and a basinal assemblage, separated by faults. The arc assemblage has been interpreted as representing the axial part of an island arc developed in the late Early Oligocene in which the main volcanic centres may have existed over areas now occupied by stocks of the Colo Plutonic suite (middle and late Miocene). These intrusions range from 75-150km^2 in outcrop area, range from olivine-augite gabbro and quartz gabbro to tonalite and quartz tonalite in composition, and were emplaced synorogenically, mainly in anticlinal folds in the Wainimala Group across southern and central Viti Levu. The basinal assemblage lies unconformably on the Yavuna Group to the north of the arc assemblage, and consists of volcaniclastic rudites, basaltic lavas and rhyolite lava domes (Hathway, 1994). Most rocks of the Wainimala Group have been regionally metamorphosed to prehnite-pumpellyite to greenschist facies, and are overlain by Mid-Late Miocene undeformed sedimentary rocks.

Volcanism in Fiji, representing crust formed during or shortly after initiation of subduction in the Middle Eocene, shows geochemical signatures ranging from island arc tholeiite to transitional boninite types (Gill, 1987; Wharton et al., 1995). Early stage tholeiites correspond to the classic 'island arc tholeiitic series' of Jakes and Gill (1970) and Pearce (1982). Noting the low-K tholeiitic nature of the basement rocks of Viti Levu, Colley and Hindle (1984) and Colley (1984) suggested that these rocks may represent upthrust South Fiji Basin backarc basin crust emplaced as an ophiolite during the Mid-Miocene. However limited available data for drilled SFB basalts (Gill, 1987) indicate that these are typically N$^-$ to E$^-$MORB, characteristic of stable mature backarc basins, compositionally unlike the more arc tholeiitic to transitional high-Ca boninites of the Viti Levu basement.

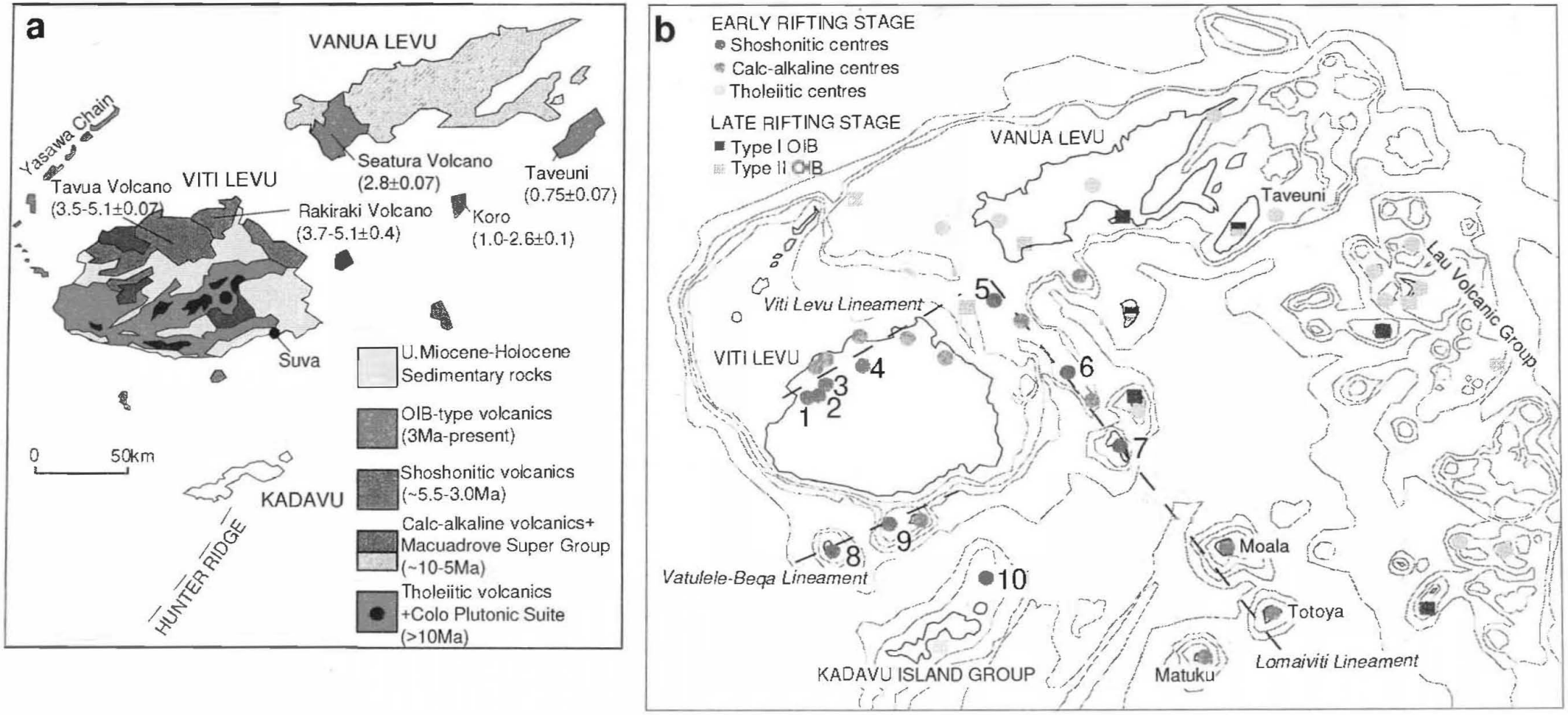

Figure 2.2 **a**: Simplified geological map of Fiji (after Kroenke, 1984). Radiometric dates from Malahoff et al. (1982) and Whelan et al. (1985). **b**: Sites of volcanism during the early rifting and late rifting stages after Gill and Whelan (1989a,b). The numbers denote individual shoshonitic centres: 1 = Sabeto, 2 = Nausori, 3 = Koroyanitu, 4 = Tavua, 5 = Vatu-i-cake, 6 = Wakaya, 7 = Gau, 8 = Vatulele, 9 = Yanuca, 10 = Astrolabe Islands (see chapter 4). The dashed lines represent the three zones along which the calc-alkaline and shoshonitic volcanics were produced during the early rifting stage.

2.4.3 MATURE ARC STAGE (~ 10 - 5Ma)

The late Miocene-Early Pliocene was a time of widespread volcanism across Fiji, and a broad change in the chemistry of lavas, from arc tholeiite volcanics to calc-alkaline volcanics occurred. The rocks of this stage are mostly medium-K, and have higher incompatible trace element concentrations and LREE enrichment than the preceding arc tholeiitic lavas.

The Namosi Formation of Viti Levu is representative of the Mature Arc Stage, and is a typical calc-alkaline suite characterised by andesite with subordinate amounts of basaltic andesite and dacite, with relatively high Al_2O_3 contents, no Fe-enrichment trend and moderate K_2O contents at a given SiO_2 (Gill, 1974). Gill and Gorton (1973) argued that it is one of several Fijian volcanic suites associated with underthrusting of the Pacific beneath the Indo-Australian plate along the northern and eastern edges of the Lau-Colville Ridge during the late Miocene.

Voluminous high-Si, low-K dacites and trondhjemite plutons were emplaced during the Miocene, on northeastern Vanua Levu when Fiji was probably still an active island arc (Gill and Gorton, 1973; Gill and Stork, 1979). These have been considered to be partial melts of amphibolitic lower Fijian crust (Gill and Stork, 1979).

The temporal compositional change from tholeiitic to calc-alkaline has been discussed by Gill (1970, 1981, 1984) and Gill et al. (1984). Gill (1981) initially attributed this change to progressively smaller percentages of melting of a periditote source, which became increasingly more refractory yet more metasomatised with time, due to fluid/mass transfer from altered, subducted ocean crust (including sedimentary cover). In a general sense, Gill's (1981, 1984) models suggest that island arc tholeiites are generated by higher degrees of partial melting of a MORB-source or a MORB-residue mantle source, produced early in the arc development history by rapid (?) subduction of old Pacific lithosphere. By implication, percent melting decreased as the onset of arc rifting approached, reaching a minimum in the rifting-related shoshonitic series. However, isotopic and other key compositional features suggest that the differences between the tholeiitic volcanics from the early arc stage and the calc-alkaline rocks from this mature arc stage cannot be reconciled with derivation from a common source. Later, Gill (1984) suggested that the increasing LILE (including LREE) of the calc-alkaline relative to the island arc tholeiite lavas may reflect input from an OIB-source component, possibly present as blobs or pods in a MORB-source mantle wedge beneath Fiji; smaller degrees of fusion produced the calc-alkaline magmas. This model remains unproven, and the reasons for changing mantle sources involved in the temporal change from

the arc tholeiite to calc-alkaline magma associations in Fiji are still unresolved.

2.4.4 EARLY RIFTING STAGE (~5.5 - 3.0Ma)

In the Early Pliocene, intermediate and basic high-K lavas of the shoshonite association were erupted, initially in NW Viti Levu. Shoshonite-dominated volcanism in Fiji (5.5-3.0Ma) coincides with well-developed spreading in the North Fiji Basin, and was also accompanied by the eruption of subordinate volumes of calc-alkaline and tholeiitic rocks (Gill and Whelan, 1989a). The following summary of the post-5.5 Ma shoshonitic, calc-alkaline and tholeiitic rocks of this stage is drawn from Gill and Whelan, (1989a).

Shoshonitic rocks erupted from 10 volcanic centres (Sabeto, Koroyanitu, Tavua, Wakaya, Vatu-i-cake, Gau, Vatulele, Yanuca, Nausori and the Astrolabe Islands north of Kadavu) in Fiji between 5.5 and 3.0Ma, and lie along three broad lineaments (Viti Levu Lineament, Lomaiviti Lineament and Vatulele-Beqa Lineament) (Fig. 2.2b). These lavas were divided by Gill and Whelan (1989a) into three different types based on the levels of K enrichment with respect to SiO_2, MgO and Na_2O (Fig. 2.3). These were termed low- (LKS), medium- (MKS) and high-K shoshonites (HKS). At the well-studied Tavua Caldera, the LKS, MKS and HKS groups are all represented amongst the absarokites and shoshonites (Rogers and Setterfield, 1994). HKS and MKS rocks are more silica-undersaturated, have higher K_2O/Na_2O (0.9-1.5) and have higher P_2O_5 contents (0.5-0.7) than do LKS rocks (0.25-0.5). The Sabeto volcanics generally have lower SiO_2 but are more sodic than the LKS or MKS shoshonites at Tavua. Most Sabeto shoshonites have higher concentrations of LREE, U, and Zr and higher $^{87}Sr/^{86}Sr$ (0.7037-43) and lower Ba/La than the Tavua shoshonites, especially the samples richest in P_2O_5 and LREE. Koroyanitu volcano lies north of the Sabeto volcanics and its lavas are compositionally close to the MKS shoshonites of Tavua volcano, i.e., they have lower concentrations of Na_2O, LREE and K_2O than Sabeto volcanics at comparable SiO_2 and MgO, and slightly lower $^{87}Sr/^{86}Sr$. The islands Vatu-i-cake, Wakaya and Gau lie at 35-55km intervals along the Lamoaiviti Lineament, and become larger and younger to the SSE. Absarokites at Vatu-i-cake and Wakaya are HKS type. Their concentrations of P_2O_5, LREE and Zr are 1.5-2 times higher than in the absarokites in Tavua. Vatulele contains the most K-rich shoshonites in Fiji. Their K_2O, Sr and Pb contents exceed those of the Sabeto volcanics, but the greatest difference is the much higher levels of REE and HFSE, and the resulting OIB-like element ratios (Zr/Y=10; Y/Nb = 1-2). Yanuca and Ugaga lie 40-55km ENE of Vatulele, and are younger, less potassic, and less rich in

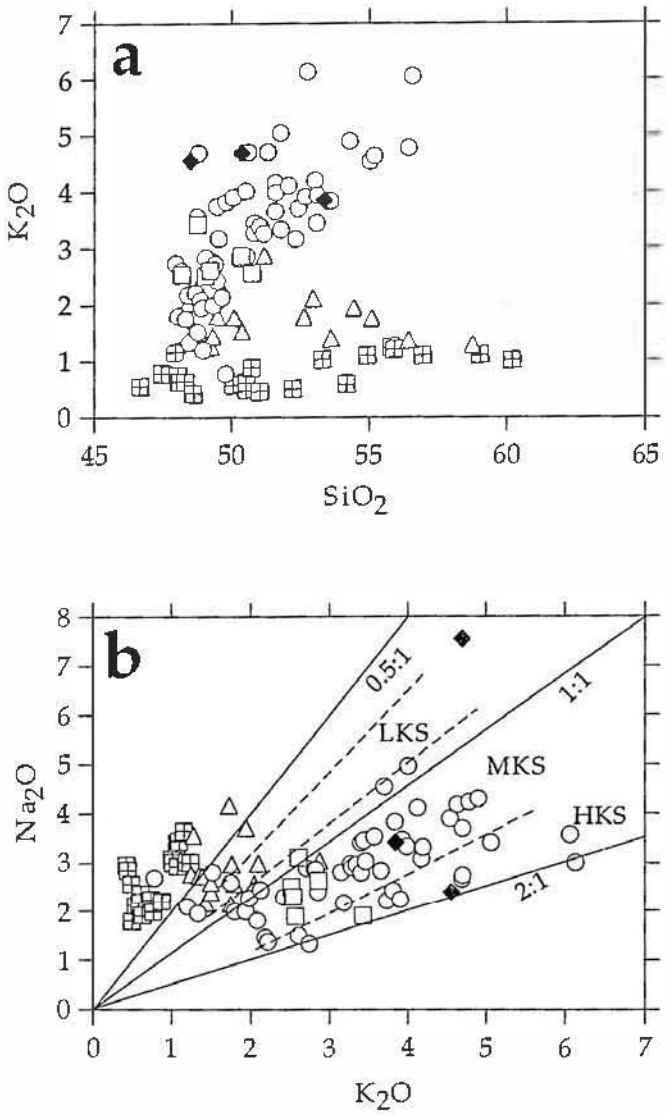

Figure 2.3 a: SiO_2 vs K_2O variation in shoshonitic lavas along the three lineaments (Lomaiviti, open squares; Vatulele-Beqa, closed diamonds; Viti Levu, open cirlces), and the calc-alkaline and tholeiitic series lavas during the early rifting stage after Gill and Whelan (1989a). Data sources: Dickinson et al. (1968), Gill (1970, 1976, 1984), Gill and Whelan (1989a), Rogers and Setterfield (1994). b: K_2O vs Na_2O variation of all the volcanics from the early rifting stage. Solid lines are Na_2O:K_2O ratios and dashed lines are the divisions into LKS, MKS and HKS after Gill and Whelan (1989a).

HFSE and REE than Vatuele. Rocks from Yanuca are MKS type, whereas the Ugaga rocks are LKS.

Gill and Whelan's (1989a) K_2O content-based division of Fijian shoshonite suite lavas in the three series (HKS, MKS, LKS) may well be an artefact of sampling. They report only 3 analyses from the Vatulele Beqa Lineament, and it is clear from Figure 2.3 that rocks from the Viti Levu Lineament (including new Tavua data from Rogers and Setterfield (1994)) plot dominantly in the MKS field, with some falling into the LKS field, and ten in the HKS field. It is not obvious therefore, that there is any value in maintaining the notion that the Fijian shoshonites can be separated into three different series based on K-enrichment.

Calc-alkaline magmas erupted from adjacent volcanoes at the same time as the shoshonitic lavas (Fig. 2.2b). Their maximum K_2O contents lie within or below the LKS field, and most samples have up to one third less K_2O, Rb, Sr, Pb, Th and U at comparable SiO_2 or MgO contents to LKS rocks. LREE contents in calc-alkaline basalts and andesites are at the low end of those in LKS rocks, whereas concentrations of Y, Ti, Zr, V, Sc and Ni are similar at comparable $Mg^{\#}$ numbers. Low concentrations and MORB-like ratios of HFSE and HREE characterise both suites (Gill and Whelan, 1989a).

Gill and Whelan (1989a) claimed that in all three lineaments noted above the westernmost volcanoes are HKS-type shoshonitic, whereas the easternmost volcanoes are calc-alkaline and generally have the youngest ages; however from Figure 2.2b, this progression is not obvious.

Tholeiites of similar age to the calc-alkaline and shoshonitic rocks occur on Vanua Levu and also constitute the Lau Volcanic Group on the Lau Islands (Figure 2.2b). These have typical arc-like signatures (e.g., Ba/La>30 ; Table 2.1) and arc tholeiitic K_2O and LILE levels. The Vanua Lava - Lau Islands tholeiites probably reflect ongoing subduction beneath the north Tongan arc and western Fiji.

In summary, the shoshonitic and calc-alkaline lavas of the early rifting stage all have low concentrations and MORB-like ratios of HFSE and HREE. In general, they mostly have Zr<60ppm at >6%MgO, Zr/Nb>25 and Zr/Y<3, and arc-like Ba/La>30 and Ti/V<20. These traits also characterise most older arc volcanic rocks in Fiji (Table 2.1). However, rocks of the early rifting stage are variably enriched in K, Rb, Cs, Ba, Sr (and especially $^{87}Sr/^{86}Sr$) and Pb, compared to magmas erupted along the volcanic front during the preceding stage of normal arc volcanism. Gill et al. (1984) suggested that the shoshonites do not necessarily represent magmatism following cessation of subduction beneath Fiji. Shoshonite-dominated volcanism is concentrated near the western rifted arc margin of Fiji, furthest from the Pacific convergent

plate boundary, and Gill et al. (1984) suggested that shoshonitic eruptions may mark a time interval during which limited lithospheric extension led to extraction of small melt fractions from highly metasomatised, yet HFSE-depleted lithospheric mantle residual from earlier arc depletion events (Gill et al., 1984).

	Zr	Zr/Nb	Zr/Y	La/Yb	Ba/La	Ti/V	K/Rb	Sr/Rb
Early arc stage	62 (9)	33 (7)	2.8 (8)	2.8 (7)	52 (8)	19 (9)	615 (9)	36 (9)
Mature arc stage	42 (1)	44 (1)	3.8 (1)	-	38 (1)	12 (1)	557 (1)	37 (1)
Early rifting: shoshonites	45 (19)	26 (10)	2.8 (19)	5.8 (12)	75 (18)	19 (17)	366 (19)	19 (19)
Early rifting: calc-alkaline	59 (5)	25 (5)	3.1 (5)	-	82 (4)	14 (5)	428 (5)	18 (5)
Early rifting: tholeiite	42 (9)	19 (3)	2.2 (2)	2.9 (1)	56 (3)	17 (9)	452 (8)	33 (8)
Late rifting stage	191 (16)	4 (14)	6.1 (16)	10.5 (4)	14 (11)	57 (14)	437 (16)	26 (16)
Samoa	292 (16)	6 (16)	7.8 (16)	23 (16)	67 (16)	-	365 (16)	21 (16)

	$^{87}Sr/^{86}Sr$	$^{143}Nd/^{144}Nd$	$^{206}Pb/^{204}Pb$	$^{207}Pb/^{204}Pb$	$^{208}Pb/^{204}Pb$
Early arc stage	0.70305-0.7050	0.5131	18.36-18.90	15.53-15.58	37.98-38.47
Mature arc stage	0.7035-0.7039	0.5130	18.88	15.57	38.55
Early rifting: shoshonites	0.7036-0.7043	0.51297-0.51303	18.79-18.89	15.54-15.57	38.49-38.64
Early rifting: calc-alkaline	0.7037	0.5130	18.85-18.98	15.55-15.58	38.49-38.60
Early rifting: tholeiite	0.7032-0.7041	-	-	-	-
Late rifting stage	0.7033-0.7039	0.5128-0.5129	18.55-18.83	15.57-15.58	38.38-38.52
Samoa	0.7044-0.7074	0.5126-0.5129	18.85-19.33	15.58-15.63	38.78-39.58

Table 2.1: Comparison of trace elements at >6%MgO presented as averages, and isotopic abundances for the early arc, mature arc, early rifting, and late rifting stages during Fiji's geochemical evolution. Numbers in parentheses indicate the number of analyses obtained from the literature to calculate the average. Data for Samoa is also presented as a comparison to the late rifting stage in Fiji. Data sources include: Dickinson et al. (1968), Gill (1970, 1974, 1976, 1984, 1987), Gill and McDougall (1973), Hindle and Colley (1981), White and Hofmann (1982), Newsom et al. (1986), Palacz and Saunders (1986), Wright and White (1987), Gill and Whelan (1989a,b), Cole et al. (1990), Rogers and Setterfield (1994), Wharton et al. (1995),

2.4.5 LATE RIFTING STAGE (3Ma to present)

The character of volcanism in Fiji changed at about 3Ma when the mode of formation of the adjacent Lau backarc basin shifted from rifting to active spreading, leaving Fiji as a remnant arc (Gill and Whelan, 1989b). The most voluminous volcanism of the Late Rifting stage involved eruption of predominantly subduction-related andesitic-dacitic centres that collectively constitute the Kadavu Island Group in southwest Fiji. However, Kadavu magmatism contrasts markedly with other volcanism of the same age elsewhere in Fiji, which was dominated by the eruption of OIB-types basalts and hawaiites. Twelve subaerial OIB volcanoes have been identified (Fig. 2.2b). Three formed large shield volcanoes (Seatura, Koro and Taveuni), and the rest are small cinder cones or plugs. They surround the hook in the northern Lau Ridge (Koro Sea), which contracted during the counter-clockwise rotation of Fiji and the accompanying formation of adjacent backarc basins (Gill and Whelan, 1989b).

Gill and Whelan (1989b) divided the Fijian OIB (FOIB) into two types on the basis of chemical composition. Type II rocks are the most abundant, are more differentiated, and have lower concentrations of LILE and HFSE at a given MgO compared to type I. All type I FOIB have higher Nb contents (50-60ppm) and higher ratios of K, P, Zr and Y than do the type II samples. Sr and Nd isotopic compositions are generally similar in both FOIB types. Although the Sr and Pb isotopic characteristics of the OIB lavas are within the range of subduction-related Fijian basalts (Table 2.1), the Nd isotopic values of both types of FOIB are lower than in all earlier, subduction-related Fijian rocks.

2.5 SUMMARY

From Mid-Eocene to ~5.5Ma, the Fijian Islands lay above actively subducting Pacific lithosphere, and resulting arc magmas varied from early arc tholeiites to later calc-alkaline lavas. Around 5.5Ma, poorly-understood lithospheric extension in the backarc region led to generation of shoshonitic lavas, whereas closer to the Pacific plate boundary, calc-alkaline to arc tholeiitic rocks continued to be erupted on the Lau Ridge and Vanua Levu. Since 3Ma, intraplate OIB-type basalts have erupted from a number of major shield volcanoes and smaller cinder cones in that part of Fiji east of Viti Levu.

Gill and Whelan (1989b) suggested that the Fijian OIB source is sub-Pacific plate mantle which moved southward once the plate boundary changed from convergent to a transform boundary. Fijian OIB may have been emplaced beneath the transform fault system between the Lau Basin

and Samoa. If this was the case, the Fijian OIB volcanics should have the same isotopic signature as the Samoan plume. However, the limited isotopic data available for the Fijian OIB, show the source for these rocks have less radiogenic $^{87}Sr/^{86}Sr$, $^{206}Pb/^{204}Pb$, $^{207}Pb/^{204}Pb$ and $^{208}Pb/^{204}Pb$ (Table 2.1).

An alternative explanation for the presence of the Fijian OIB is presented in chapter 7, in relation to the tectonic implications for the Kadavu Island Group and Hunter Ridge volcanics.

Chapter 3

THE HUNTER RIDGE

A Newly Recognised Intra-oceanic Arc in the SW Pacific

3.1 INTRODUCTION

An important unresolved problem in understanding petrogenesis in arc-backarc basin systems concerns the composition of primary magmas generated during the earliest stages of intra-oceanic arc evolution. One reason why this problem is difficult to address is that the key evidence usually occurs in the deep ocean, or else in mountain belts as ophiolites or greenstone belts; in the latter case, interpretations of the original tectonic setting and the pristine lava compositions are compromised.

In 1993, the 'Alize' cruise dredged numerous sites at depths of less than 1500m along the northern part of the Hunter Ridge, between the southernmost Vanuatu arc and Kadavu Island in Fiji, and recovered lavas with strong subduction-related affinities. Notable among these dredges are high-Mg lavas from two dredge stations that are characterised by high $Mg^{\#}$ olivines (up to Fo_{93}) and which are important, as they have appropriate characteristics to be primary or near-primary magmas. These lavas are also very fresh, so that their trace element and isotopic characteristics can be confidently used in evaluating potential source components.

This study aims to use petrology and geochemistry to better understand the evolution and tectonic significance of the Hunter Ridge, presently considered to be a major transform fault system linking the opposite-facing Tongan and Vanuatu arcs. It is demonstrated that the Hunter Ridge is, in fact, a primitive intra-oceanic arc system, probably aborted only a few million years after its inception.

3.1.1 TECTONIC SETTING AND PREVIOUS STUDIES

There has been little research work done on the rocks from the Hunter Ridge (also known as the Hunter Fracture Zone) and it remains one of the least known major bathymetric features in the SW Pacific. It is a well-defined curvilinear belt of ridge/trough topography extending

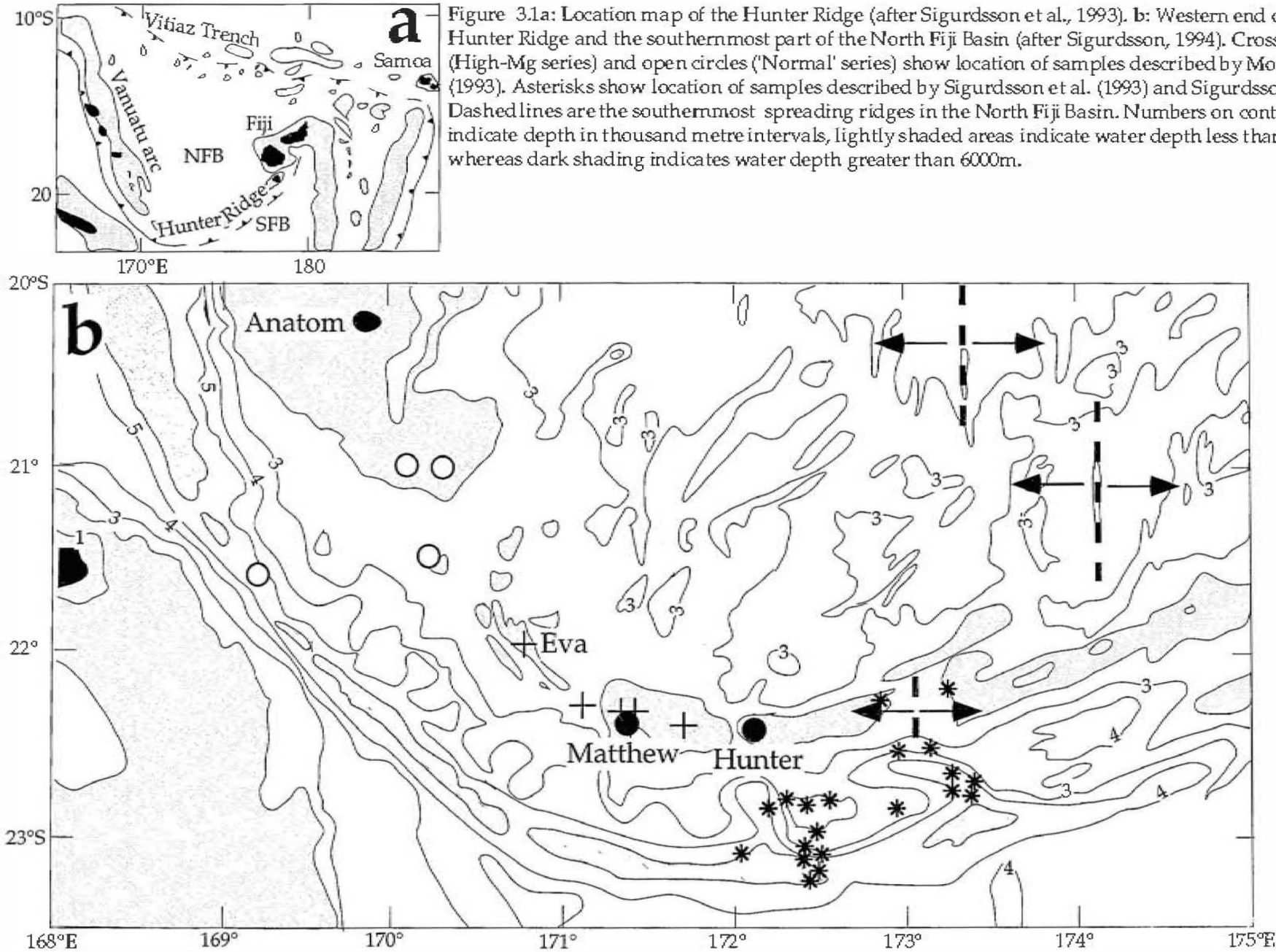

Figure 3.1a: Location map of the Hunter Ridge (after Sigurdsson et al., 1993). **b**: Western end of the Hunter Ridge and the southernmost part of the North Fiji Basin (after Sigurdsson, 1994). Crosses (High-Mg series) and open circles ('Normal' series) show location of samples described by Monzier et al. (1993). Asterisks show location of samples described by Sigurdsson et al. (1993) and Sigurdsson (1994). Dashed lines are the southernmost spreading ridges in the North Fiji Basin. Numbers on contour lines indicate depth in thousand metre intervals, lightly shaded areas indicate water depth less than 2000m, whereas dark shading indicates water depth greater than 6000m.

from Fiji to the southern Vanuatu arc (Fig. 3.1a). At its western end, it sweeps around into the southern termination of the New Hebrides Trench. The Koro Sea (between Fiji and the Lau Ridge) represents its eastern termination (Hamburger and Isacks, 1987). The crest of the Hunter Ridge generally lies around 2000m below sea-level, although individual peaks not uncommonly extend to <1000m below sea level. The volcanic islands of Matthew and Hunter represent the exposed southwestern tip of the Hunter Ridge (Fig. 3.1b), and the island of Kadavu the north-eastern exposed tip. Matthew and Hunter mark the transition zone between the Vanuatu arc and the Hunter Ridge, and also lie close to the southern limb of the active southern spreading ridge of the North Fiji Basin. Along that section of the southernmost Vanuatu arc from Hunter Island to Anatom, at least 6 submarine arc volcano seamounts occur, several extending to <500m below sea level (Monzier et al., 1993) (Fig. 3.1b). A marked bathymetric trough on the Hunter Ridge at 173°E has been interpreted by Maillet et al. (1989) to be a short N-S trending spreading centre, the southernmost limb of the main N-S spreading ridge in the North Fiji Basin, propagating into the Hunter Ridge.

Although the Hunter Ridge has been generally considered to mark the trace of a transform fault system linking the opposite-facing Tongan and Vanuatu arc systems (e.g., Kroenke, 1984), bathymetric and seismic reflection profiles across the Hunter Ridge show a subduction margin morphology that is preserved well into the Fiji platform (Brocher and Holmes, 1985). Malahoff et al. (1982) and Gill et al. (1984) proposed that the Hunter Ridge may have accommodated some oblique subduction of the South Fiji Basin lithosphere, an interpretation supported by oblique truncation of magnetic anomalies in the South Fiji Basin (Malahoff et al., 1982). The absence of an inclined seismic zone and shallow thrust type focal mechanisms suggest that currently the Hunter Ridge is not accommodating plate convergence (Hamburger and Isacks, 1987).

Figure 3.2 shows a tectonic model for the development of the North Fiji Basin proposed by Auzende et al. (1996). This model shows the initiation of a major E-W orientated spreading ridge at ~7Ma across the North Fiji Basin. Spreading on this new ridge system probably triggered subduction along the Hunter Ridge ~7Ma. Subduction continued until a major reorganisation of spreading geometry in the North Fiji Basin occurred around 3Ma (Fig. 3.2), broadly synchronous with the initial opening of the Lau Basin. This new N-S spreading ridge terminated subduction along the Hunter Ridge plate boundary around 3Ma, and subsequent motion along the Hunter Ridge has been essentially

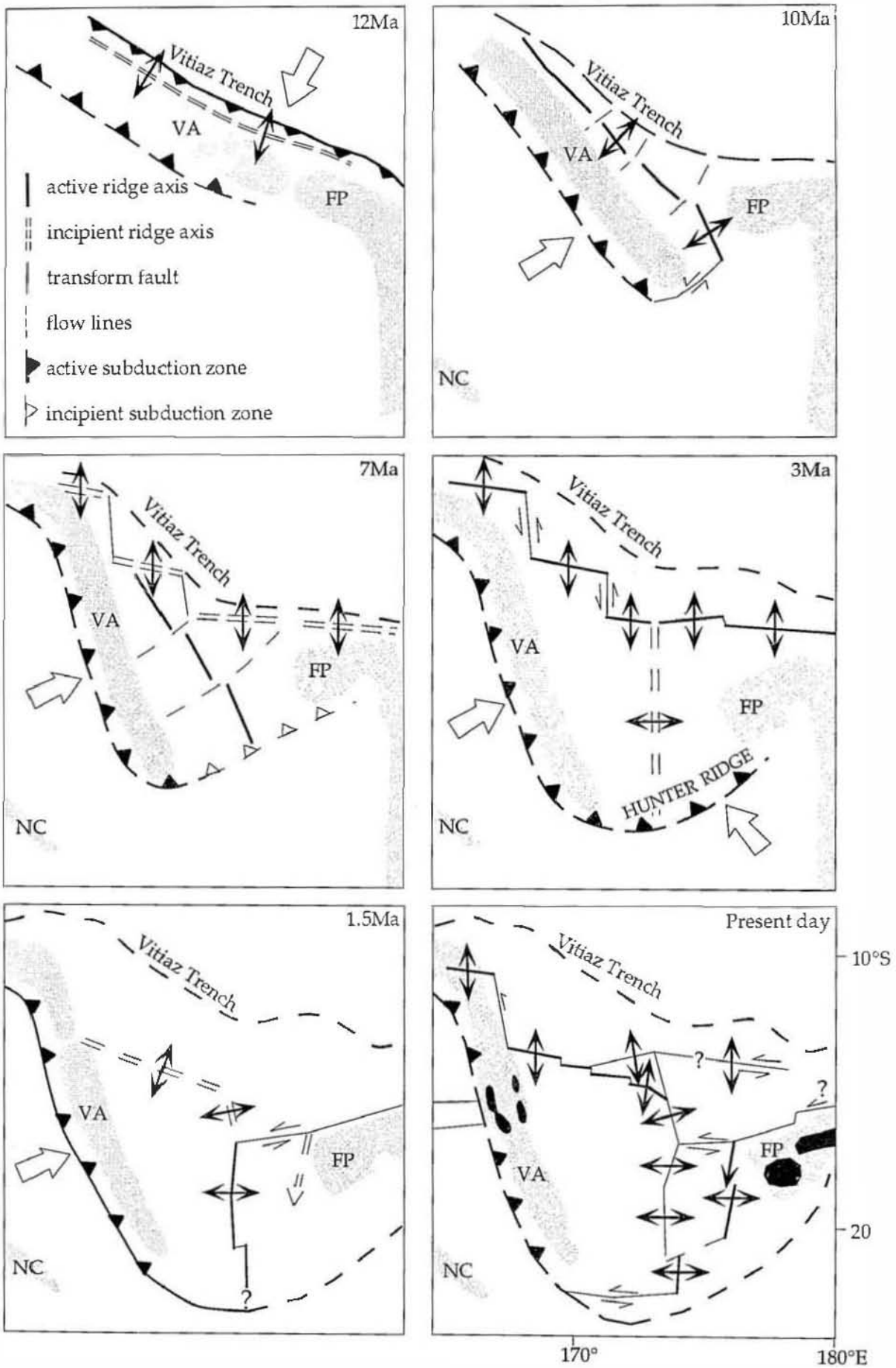

Figure 3.2: Geodynamic evolution of the North Fiji Basin (after Auzende et al., 1996). VA=Vanuatu arc; FP=Fiji Platform; NC=New Caledonia. See text for further explanation.

transcurrent/transform. The proposed demise of subduction and associated arc magmatism along the Hunter Ridge ~3Ma is strongly supported by nanno-foram oozes dredged from the tops and upper sides of several Hunter Ridge volcanic edifices during the 'Alize' cruise, which have been dated at 2.5 - 1.5Ma (P.G. Quilty, pers. comm. 1995).

Lavas from the southernmost, submarine volcanoes of the Vanuatu arc between Hunter and Anatom (Fig. 3.1b) have been studied by Monzier et al. (1993) and Crawford et al. (1993). Those seamounts north of 22°S are characterised by typical medium-K arc tholeiites and are similar to the lavas of the main Vanuatu arc volcanoes further north. South of 22°S, however, lavas constitute an unusual high-Mg suite for which the more mafic end-members have some affinities to adakites (Crawford et al., 1993), and their petrogenesis may have involved a slab melt component. The marked change in magma suites in the submarine arc volcanoes at 22°S in this region is believed to reflect the position of a tear in the subducted slab at this latitude, with a steeply dipping slab to the north, and a much shorter and more shallowly dipping slab to the south (Monzier et al., 1993). The combination of an unusually shallow slab and an unusually hot ambient geotherm due to proximity over the last several million years to the rising diapirs of the intersecting backarc spreading axis, may explain the unusual affinities of the southern seamount arc volcanics (Monzier et al., 1993; Crawford et al., 1993).

The first geochemical study of rocks from the Hunter Ridge was undertaken by Maillet et al. (1986), and focussed on the two active volcanoes, Matthew and Hunter, that occur in the transition zone between the westernmost Hunter Ridge and the southernmost Vanuatu island arc (Fig. 3.1b). These small subaerial cones are composed of medium-K calc-alkaline high-Mg andesites with unusually low TiO_2 contents (0.37-0.45% TiO_2 at 60-62% SiO_2), and strong geochemical similarities to the high-Mg suite lavas of the southernmost submarine volcanoes in the Vanuatu arc.

In 1990, the Soviet research vessel 'Academician A. Nesmeyanov' dredged along the southwestern section of the Hunter Ridge east of Matthew and Hunter islands (Fig. 3.1b), and recovered a diverse assemblage of rocks, including several suites of primitive arc tholeiites and high-Ca boninites (Sigurdsson et al., 1993; Sigurdsson, 1994). The discovery of boninites confirmed the prediction by Crawford et al. (1989) that the juxtaposition of hydrous, metasomatised supra-subduction zone mantle beneath the Hunter Ridge arc against hot MORB mantle supplying the south-propagating southernmost spreading centre in the

North Fiji Basin could produce boninitic magmas in this region. Andesitic and dacitic lavas dredged close to the spreading ridge that cuts through the Hunter Ridge show clear evidence of magma mixing, involving both primitive (IAT and BABB) and more fractionated melts (Sigurdsson et al., 1993; Sigurdsson, 1994). In the forearc region of the same area just south of the Hunter Ridge, Sigurdsson et al. (1993) also discovered primitive MORB-like backarc basin basalts, containing olivine to Fo_{91}, in close proximity to both island arc tholeiites and boninites. This confirmed the tectonic scenario proposed by Maillet et al. (1989) in which this depression in the Hunter Ridge was interpreted to be a pull-apart structure due to the southward propagation of the southernmost segment of the North Fiji Basin spreading centre through the Hunter Ridge.

In 1993, I was a crew member of the 'Alize' scientific cruise of the French research vessel R.V. Alis, which surveyed the seafloor over the northern and central Hunter Ridge using a EDO 12kHz single beam echo sounder, and dredged rocks from 16 selected stations (Table 3.1) further northeast than the Nesmeyanov study area reported by Sigurdsson et al. (1993) (Fig. 3.3). All 'Alize'-dredged samples have been examined petrographically and 21 representative samples selected from different dredges have been analysed for major and trace elements (Ni, Y, Rb, Nb, Zr, Sr, Cr, Ba, Sc and V) by XRF spectrometry. From these 21 samples, a representative least-altered 8 rocks were chosen for further trace element analysis using the ICP-MS, and radiogenic isotope (Sr, Nd and Pb) analysis (Table 3.2). Analytical techniques are described in Appendix 2.

3.2 PETROGRAPHY AND MINERAL CHEMISTRY

3.2.1 PETROGRAPHY

Major petrographic features of the 21 selected representative rocks from the Hunter Ridge are summarised below. Appendix 3 has more detailed petrographic descriptions of all the dredged samples.

DR3-2: This sample is a strongly porphyritic, weakly vesicular andesite with subhedral to euhedral plagioclase phenocrysts (5 modal%) which commonly occur in aggregates with subhedral to euhedral clinopyroxene and anhedral to euhedral orthopyroxene phenocrysts. It has a slightly altered glassy groundmass consisting of tiny plagioclase and clinopyroxene euhedral laths and rounded to equant FeTi oxide (Ti-magnetite) grains.

Dredge no.	Latitude	Longitude	Water Depth (m)	Rock Types
DR 1	19° 35.69	177° 46.50	850	1 large block (~50cm) and numerous small fragments of altered andesite with Mn coating, pumice fragments
DR 2	19° 55.07	177° 24.45	1140	pumice, shell limestone with micro-bivalves, breccia with pumice fragments
DR 3	20° 05.85	177° 02.73	1000	pumice, altered andesite
DR 4	20° 34.36	177° 22.12	750	very altered hornblende diorite, mylonitized, strong green colour
2DR 4	20° 32.33	177° 24.58	1000	hornblende diorite
DR 5	20° 42.26	177° 04.97	740	large block of altered breccia, altered volcanic fragments, tuff
DR 6	20° 27.13	176° 47.92	1100	volcaniclastics
2DR 6	20° 26.21	176° 49.98	1050	altered volcanic breccia, with vesicular lava fragments (boninite)
DR 7	20° 21.79	176° 52.46	840	coral fragments
DR 8	21° 22.88	176° 01.89	680	fragment of brown tuff
2DR 8	21° 22.49	176° 01.67	700	microporphyritic basalt and pillow rims with fresh glass
DR 9	21° 39.10	174° 50.09	1030	basalt
DR 10	21° 45.59	174° 35.13	1200	porphyritic basalt-andesite
DR 11	21° 54.84	174° 17.02	800	lost dredge
2DR 11	21° 54.68	174° 18.49	800	altered basalt and tuff
DR 12	21° 59.24	174° 04.47	300	coral
2DR 12	21° 59.41	174° 07.90	600	fragments of porphyritic basalt, pumice fragments, altered tuffs and breccias
DR 13	22° 02.25	173° 55.02	1200	tuff
DR 14	22° 08.36	173° 45.48	1100	pumice fragments, tuff
DR 15	22° 06.13	173° 45.05	650	empty dredge
2DR 15	22° 06.39	173° 44.24	800	porphyritic basalt, breccia with calcareous matrix, tuff
DR 16	21° 52.34	173° 22.00	1450	fresh vesicular basalt, tuffs, pumice fragments

Table 3.1. Location, water depth and description of rock types of the sixteen individual dredge stations from the northern part of the Hunter Ridge sampled during the 1993 'Alize' cruise of the R.V Alis.

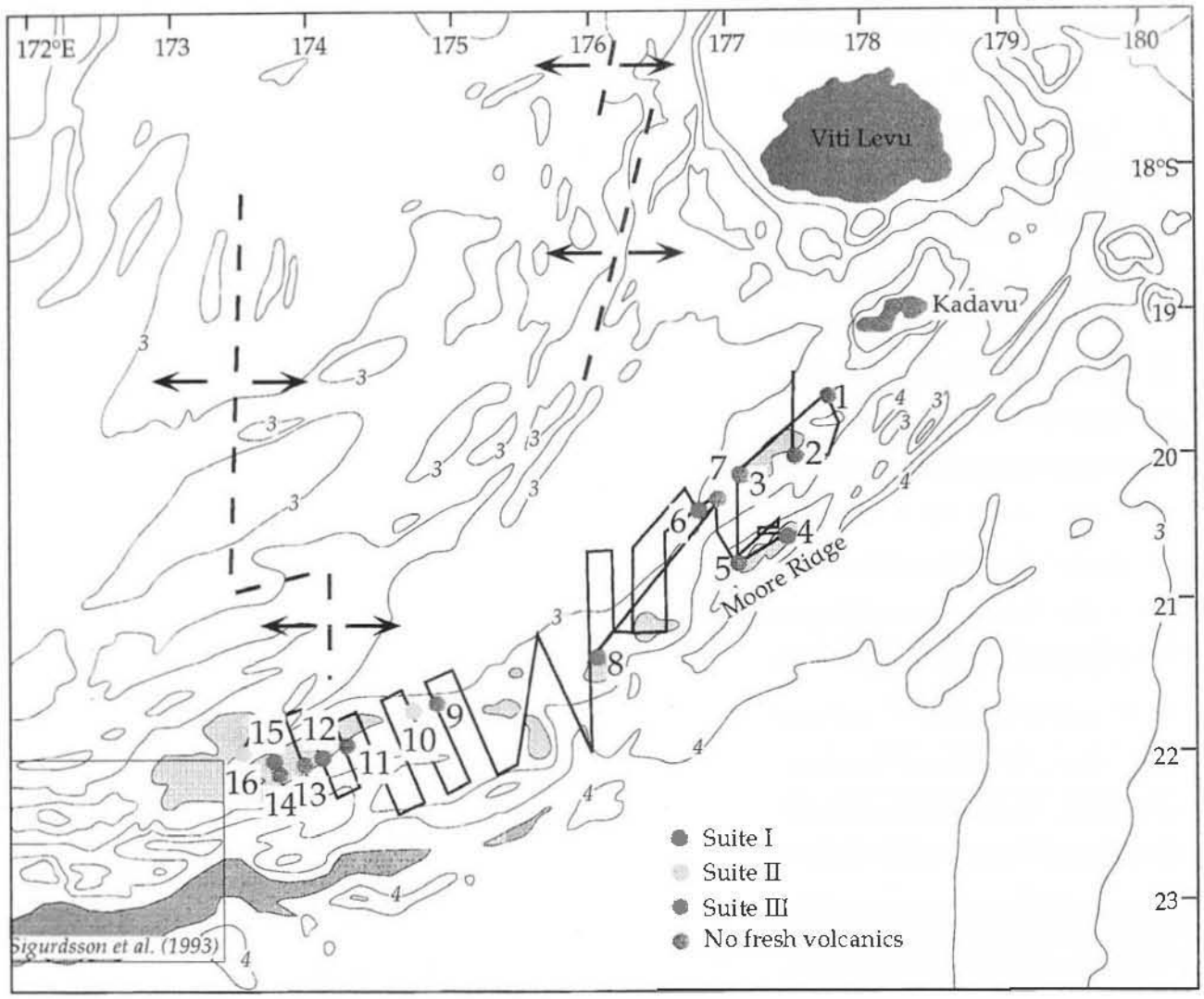

Figure 3.3. The northern part of the Hunter Ridge and ship tracks for the 'Alize' cruise. Dredge locations are shown by coloured filled cirlces. Italic numbers on contour lines indicate water depth in thousand metre intervals. Lightly shaded areas indicate water depth less than 2000m, whereas dark areas indicate water depth greater than 5000m.

The northern Hunter Ridge rocks are divided into three different suites based on their geochemistry, represented by the different coloured cirlces. Suite I (red cirlces) is low-K, high Ti/Zr and low P2O5; suite II (yellow circles) is medium-K, low Ti/Zr, low P2O5; suite III (green circles) are high K2O, low Ti/Zr, low P2O5.

	SUITE I									
									(altered)	
	2DR6-1	DR12-8	DR12-3	DR8-2	DR12-2	2DR4-9	DR15-2	DR15-4	2DR4-1	2DR4-5
SiO_2	52 57	50 27	53 77	55.18	60.73	60.77	58.32	63.16	65.72	63.91
TiO_2	0 37	0 34	0.36	0.45	0.35	0.55	0.52	0.45	0.47	0 47
Al_2O_3	11 09	14 39	14 27	15.63	13.95	15.56	14.82	15.12	16.90	17.29
FeO*	7 80	10 77	9 97	7.84	8.16	6.47	9.68	7.32	4.18	3.38
MnO	0.15	0 20	0.19	0.13	0.15	0.14	0.17	0.14	0.06	0.06
MgO	12.77	8.48	7.46	5.91	4.58	4.18	3.06	1 84	1.70	1.42
CaO	10 10	11 10	10 60	9.40	8.36	6.81	8.02	7.02	5.92	7.03
Na_2O	1 33	2 20	2.15	2.63	2.22	4.41	2.49	2.77	3.84	4.04
K_2O	0 26	0.45	0.69	0.68	0.48	0.23	0.51	0.66	0.21	0 24
P_2O_5	0.08	0 15	0 13	0.10	0.12	0.09	0.10	0.10	0.13	0.15
LOI	2.93	0.88	0 00	2.19	0.22	1.33	1.29	0.17	0.79	2.36
Total	100 31	100 42	100.69	101.01	100.23	101.26	100.06	99.57	100.37	100.71
Mg#	74.5	58.4	57 1	57.3	50.0	53 5	36.0	30.9	42.0	42 8
Ni	258	47	37	59	18	27	10	2	3	2
Y	11	14	12	14	12	30	15	16	22	13
Rb	4	5	9	11	6	1	7	8	1	2
Nb	0 27	0 45	<1	0 75	<1	3.04	<1	<1	2.1	3.3
Zr	21	25	29	43	28	49	34	36	76	82
Sr	66	210	211	252	204	264	233	215	255	173
Cr	925	317	272	113	86	51	14	1	4	46
Ba	19	89	131	93	105	64	91	102	57	51
Sc	41	54	45	33	39	41	41	30	8	27
V	244	341	310	275	247	251	385	171	75	207
Li	5.40	7.32		4.73		0.79				
Be	0.16	0.28		0.54		0.79				
Co	44.13	44.88		31.12		19.20				
Cu	51.80	46.20		66.74		5.91				
Zn	47.70	74.48		60.96		35.66				
Ga	9.35	11.38		14.38		14.07				
Mo	0 38	0.64		0.82		0.09				
Sn	0.48	0.35		0.53		1.22				
Sb	0.17	0.20		0.11		0.02				
Cs	0.20	0.01		0.25		0.02				
La	0.56	2 56		2.86		6.52				
Ce	1.63	5 32		6.90		17.40				
Pr	0 29	0 85		1.04		2.50				
Nd	1.77	4 20		5.16		11.26				
Sm	0.73	1 22		1.58		3.01				
Eu	0.29	0.38		0.52		0.82				
Gd	1 14	1.46		1.89		3.45				
Tb	0.22	0.26		0.33		0.62				
Dy	1.56	1.71		2.14		4.13				
Ho	0.37	0.40		0.49		0.95				
Er	1 13	1.22		1 48		2.95				
Yb	1 15	1.31		1.46		3.26				
Lu	0.18	0.21		0.23		0.52				
Hf	0.63	0 76		1.21		0.85				
Ta	0 02	0 03		0.05		0.23				
Tl	0 03	0 03		0.10		0.02				
Pb	0.67	2 19		2.72		0.72				
Th	0 04	0.22		0.35		0.30				
U	0 05	0.36		0.21		0.11				

	$^{87}Sr/^{86}Sr$	±2σ	$^{143}Nd/^{144}Nd$	±2σ	$^{206}Pb/^{204}Pb$	±2σ	$^{207}Pb/^{204}Pb$	±2σ	$^{208}Pb/^{204}Pb$	±2σ
2DR6-1	0 70344	21	0 51311	9	18.594	3	15.543	3	38 218	9
DR12-8	0 70366	17	0.51302	10	18 607	2	15 532	2	38.308	6
DR8-2	0.70339	19	0 51304	11	18.841	1	15.528	2	38 350	5
2DR4-9	0 70338	27	0 51305	9	18 684	4	15 504	3	38 195	8
DR15-1	0 70283	22	0.51310	10	18.665	4	15.485	3	38 117	7
DR10-2	0.70310	24	0 51307	9	18.679	4	15.512	3	38 219	8
DR16-6	0.70294	28	0 51309	10	18.646	2	15.494	2	38 141	6
DR9-2	0.70365	18	0.51300	10	18.630	2	15.517	2	38.271	6

	SUITE II						SUITE III			ALTERED	
	DR15-1	DR10-1	DR10-3	DR16-5	DR10-2	DR16-6	DR9-3	DR9-1	DR9-2	DR5-5	DR3-2
SiO_2	51.00	56.13	57.89	58.82	60.44	60.99	62.42	62.39	62.21	47.35	68 78
TiO_2	0.54	0.69	0.68	0.78	0.69	0.92	0.88	0.86	0.84	0.87	0 36
Al_2O_3	10.22	14.73	15.45	16.07	15.58	16.18	15.50	15.22	15.14	19.96	13 77
FeO*	9.11	7.59	7.03	6.55	6.00	6.32	5.70	5.42	5.31	8.16	3 95
MnO	0.17	0.14	0.12	0.14	0.12	0.11	0.11	0.11	0.11	0.15	0 08
MgO	11.54	5.42	4.50	4.24	3.22	2.53	1.93	1.73	1.67	5.38	1.11
CaO	11.57	8.13	7.33	7.16	5.95	5.57	4.16	3.81	3.68	6.95	4.09
Na_2O	1.86	3.58	3.64	4.13	4.16	4.70	5.00	4.96	4.84	4.95	3.39
K_2O	0.68	1.20	1.55	0.82	1.76	1.07	2.73	2.73	3.05	0.28	1.56
P_2O_5	0.23	0.27	0.25	0.21	0.27	0.25	0.34	0.33	0.33	0.15	0.10
LOI	1.83	1.08	0.82	0.50	0.63	-0.20	1.70	1.81	2.57	6.09	2.13
Total	99.77	99.79	100.04	100.14	99.48	99.13	101.11	99.97	100.33	101.19	99.76
Mg#	69.3	56.0	53.3	53.6	48.9	41.6	37.6	36.3	35.9	54.0	33.4
Ni	84	28	20	40	9	8	4	4	3	39	2
Y	15	18	18	19	22	25	28	28	29	20	16
Rb	7	16	22	11	25	14	39	41	42	3	19
Nb	0.86	2	2.8	3.1	3.32	3.49	6.9	6.8	6.96	2.4	1.8
Zr	68	126	153	114	182	154	247	258	260	103	79
Sr	817	620	606	524	585	451	414	383	379	254	232
Cr	649	78	49	63	30	7	4	2	2	2	2
Ba	82	136	159	143	189	188	346	355	362	76	137
Sc	47	28	24	21	18	20	14	12	12	9	15
V	251	263	229	216	182	192	158	140	137	74	77
Li	4.35				12.02	7.77			10.92		
Be	0.74				1.40	1.23			1.98		
Co	44.86				18.00	16.18			12.11		
Cu	89.30				71.42	31.71			72.84		
Zn	57.53				63.46	59.92			70.05		
Ga	10.90				17.59	17.98			17.91		
Mo	0.38				1.41	0.84			2.19		
Sn	1.75				1.22	1.25			1.73		
Sb	0.14				0.11	0.05			0.17		
Cs	0.08				0.33	0.09			0.54		
La	10.37				18.68	11.84			32.96		
Ce	27.84				45.65	29.36			71.14		
Pr	4.24				6.34	4.33			9.76		
Nd	19.66				28.00	19.43			39.81		
Sm	4.48				6.05	4.68			7.94		
Eu	1.28				1.48	1.36			1.79		
Gd	3.68				5.04	4.52			6.38		
Tb	0.50				0.70	0.70			0.91		
Dy	2.68				3.79	4.08			4.91		
Ho	0.52				0.74	0.85			0.97		
Er	1.40				2.05	2.43			2.73		
Yb	1.22				1.89	2.27			2.57		
Lu	0.18				0.29	0.35			0.40		
Hf	1.74				4.61	3.93			6.54		
Ta	0.05				0.21	0.22			0.41		
Tl					0.13	0.05			0.30		
Pb	3.17				5.01	2.99			8.09		
Th	0.91				2.40	1.50			5.08		
U	0.37				1.06	0.61			1.92		

Table 3.2. Major (wt%) and trace element (ppm) analyses, and isotopic data for the northern Hunter Ridge rocks. Major and elements and Ni, Y, Rb, Zr, Sr, Cr, Ba, Sc and V analysed by XRF. Other trace elements analysed by ICP-MS. Sr and Nd isotopte data has been normalised to $^{86}Sr/^{88}Sr=0.1194$ and $^{146}Nd/^{144}Nd=0.7219$. SRM gave a mean value of 0.710212±32, and the LaJolla standard gave a mean value of 0.511862±9 during this study. Pb isotopic data has been corrected for instrumental mass fractionation. For the Sr, Nd and Pb isotope data the $2\sigma_{mean}$ values associated with individual sample measurements indicate within-run precision only.

2DR4-1, 2DR4-5, 2DR4-9: All samples from the second dredge from station 4 are hornblende diorites, with slightly different textures, comprising varying amounts of quartz, plagioclase, hornblende and Ti-magnetite. 2DR4-1 and 2DR4-5 are equigranular and more quartz-rich, with common interstitial, anhedral hornblende. Both samples show weak chlorite-smectite alteration. 2DR4-9 is weakly porphyritic, with ragged hornblende (20%; 0.2-1.0mm) and plagioclase (3%; 0.4-1.2mm) phenocrysts set in an equigranular groundmass composed of quartz, plagioclase and Ti-magnetite.

DR5-5: This sample is a strongly porphyritic, rather altered andesite, dominated by subhedral to euhedral plagioclase phenocrysts (25%) with lesser amounts of anhedral clinopyroxene (10%), set in an altered glassy groundmass containing abundant plagioclase microlites.

2DR6-1: This rock is a matrix-supported volcanic breccia composed of strongly vesicular basaltic clasts, set in a carbonate matrix. Most of the mainly angular basaltic fragments (4 to 60mm) are slightly altered, as shown by carbonate-clay pseudomorphs after olivine, and/or yellow Fe-stained clayey material dispersed throughout the groundmass. However, a number of the larger clasts are not altered.

The basaltic clasts in this lava breccia are olivine-phyric, with a hyalopilitic groundmass composed mainly of quenched clinopyroxene with a 'cockscomb' appearance of curved, branching dendrites (Plate 3.1) and sheaf morphologies typical of pillow margins. The olivine phenocrysts (25%; 0.05-0.2mm) frequently display 'hopper' morphologies (Plate 3.1) indicative of rapid cooling, and suggesting that they probably nucleated during magma ascent immediately prior to or upon eruption (Cameron, 1985; MacLeod, 1988). Cr-spinel occurs as euhedral inclusions in olivine phenocrysts and as individual crystals scattered throughout the groundmass.

DR8-2: This lava is a porphyritic and weakly vesicular basaltic andesite with glassy rims typical of pillow lavas. Subhedral to euhedral plagioclase (20%; 0.1-0.8mm) and clinopyroxene (10%; 0.4-0.8mm) dominate the phenocryst assemblage with rare (<1%), large (up to 2mm) olivine phenocrysts and minor amounts of orthopyroxene (2%; 0.2-0.4mm) phenocrysts. The large olivines are mainly euhedral, but have occasional embayments, interpreted as resorption features. Orthopyroxene forms equant or slightly elongate subhedral to euhedral prisms. Clinopyroxene

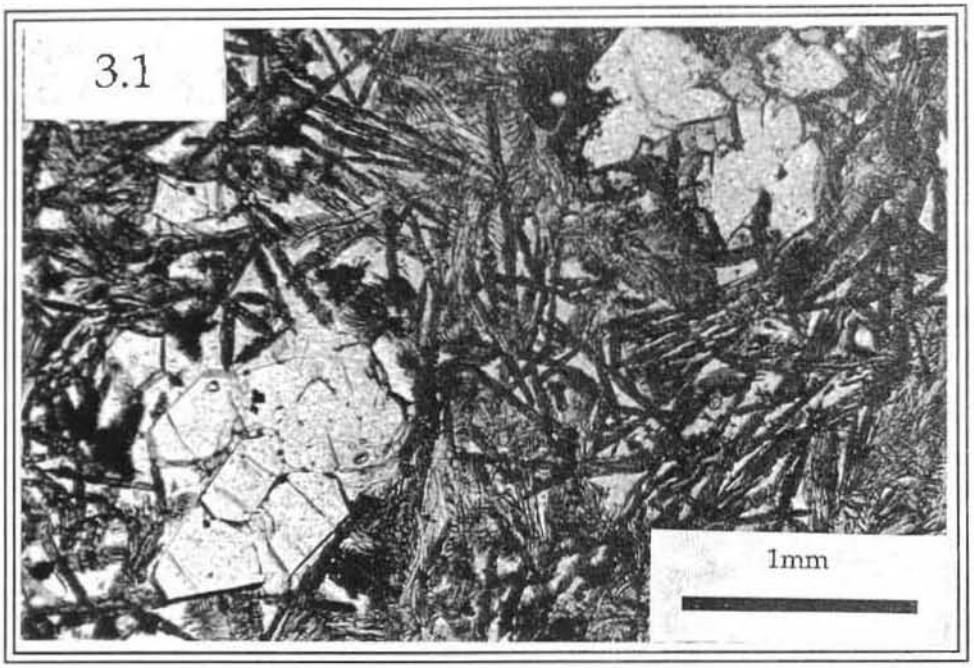
3.1
1mm

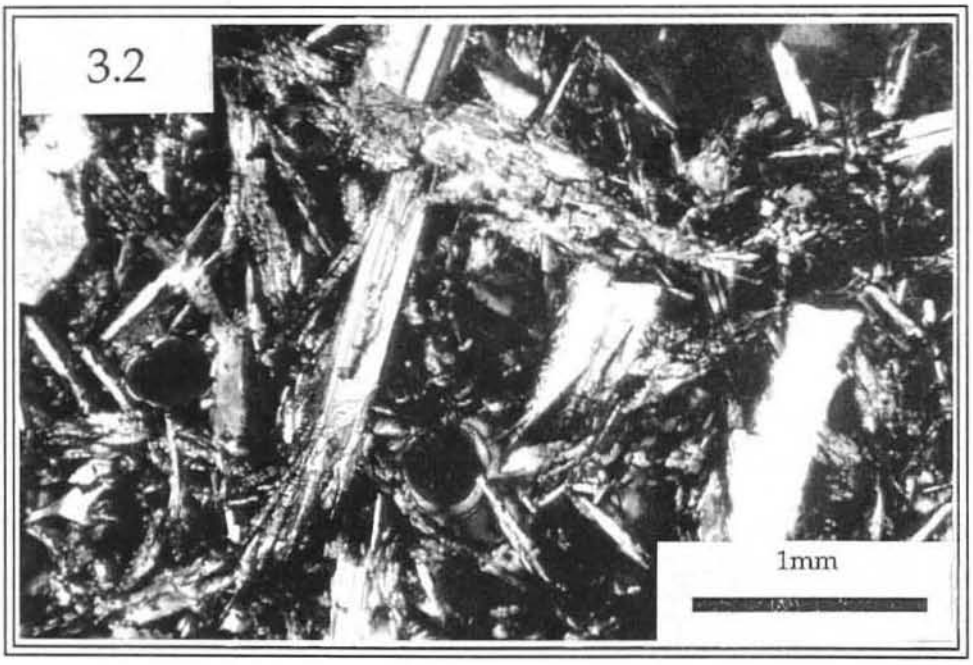
3.2
1mm

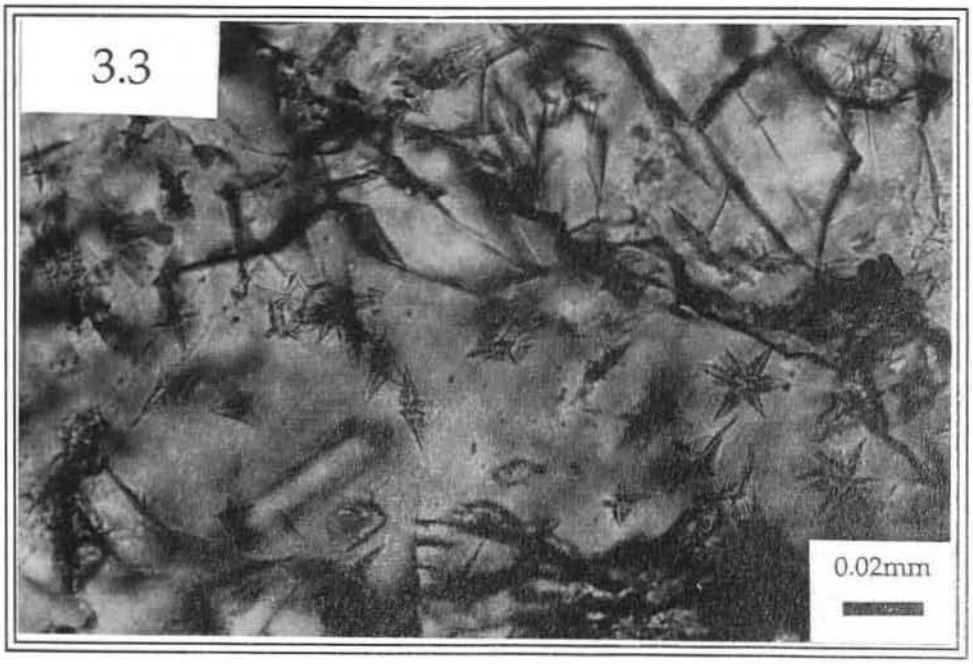
3.3
0.02mm

and plagioclase frequently form irregular blocky aggregates. Cr-spinel occurs as small inclusions in olivine phenocrysts, and also as occasional equant, euhedral microphenocrysts up to 0.15mm in the groundmass. The latter is vitrophyric to glassy, consisting of plagioclase laths and abundant acicular clinopyroxene microlites, with clinopyroxene sometimes nucleating on larger plagioclase and pyroxene grains (Plate 3.2).

DR9-1, DR9-2, DR9-3: Dredge 9 lavas are strongly porphyritic, vesicular dacites, with glassy groundmasses containing microlites of plagioclase. Textures vary slightly between samples. The phenocryst assemblage is dominated by subhedral to euhedral plagioclase (5-7%; 0.2-2mm) showing strong normal and oscillatory zoning. Lesser amounts of subhedral to euhedral clinopyroxene (3-5%; 0.2-0.8mm) and orthopyroxene (1-2%; 0.1-0.4mm) and Ti-magnetite phenocrysts commonly occur in clusters with plagioclase. Vesicles make up ~10% of the rock.

DR10-1, DR10-2, DR10-3: Dredge 10 lavas are strongly porphyritic, weakly vesicular andesites, varying slightly in texture and modal abundances of phenocryst phases. Subhedral to euhedral plagioclase (10-15%; 0.2-3mm) is the dominant phenocryst phase. Clinopyroxene occurs as subhedral to euhedral phenocrysts (5-10%; 0.2-1.5mm), and also rims many orthopyroxene phenocrysts. Anhedral to euhedral orthopyroxene varies between 3-7% and often occurs in clusters with plagioclase and clinopyroxene. The groundmass is glassy and charged with plagioclase and clinopyroxene microlites. Vesicles make up ~1% of the rock. Disequilibrium textures present to varying extents in the dredge 10 andesites include embayed rims on clinopyroxene and orthopyroxene, and partial to complete rim resorption of plagioclase phenocrysts.

DR12-2, DR12-3, DR12-8: Andesites from dredge 12 are plagioclase+clinopyroxene+orthopyroxene-phyric, with a glassy, spherulitic groundmass. Subhedral to euhedral plagioclase phenocrysts (7-10%; 0.2-1mm) often contain glassy inclusions in zones following the crystal margins. Clinopyroxene (7-10%; 0.2-1.2mm) and orthopyroxene (5%; 0.2-1.2mm) often occur in aggregates with plagioclase. The glassy groundmass contains plagioclase and clinopyroxene microlites showing flow alignment.

DR15-1, DR15-2, DR15-4: The three samples from dredge 15 have different textures. DR15-1, a clast from a coarse-grained, poorly-sorted volcanic breccia, is a strongly vesicular (40% vesicles), porphyritic basalt with rare large olivine phenocrysts (up to 1.5mm) and abundant olivine (15%; 0.2mm) and clinopyroxene (7%; 0.4-0.8mm) microphenocrysts. The groundmass is glassy and contains tiny rosettes and sheaves of quenched pyroxene (Plate 3.3). DR15-2 and DR15-4 are strongly porphyritic, less vesicular (10% vesicles) andesites. DR15-2 contains subhedral to euhedral altered plagioclase (7%; 0.2-0.8mm) and anhedral to subhedral clinopyroxene (3%; 0.1-0.4mm) phenocrysts set in a fine-grained to glassy groundmass. The latter consists of tiny plagioclase laths, frequently flow-aligned, and small (~0.02mm) equant clinopyroxene grains. DR15-4 has the same phenocryst assemblage in slightly different proportions (10% plagioclase; 5% clinopyroxene) set in a vitrophyric to glassy groundmass containing only plagioclase microlites.

DR16-5, DR16-6: Dredge 16 andesites are plagioclase+clinopyroxene+ orthopyroxene-phyric, with a fine-grained to glassy groundmass. Subhedral to euhedral plagioclase (15-20%; 0.4-2mm) dominates the phenocryst assemblage, and larger plagioclase phenocrysts contain variable amounts of glassy inclusions and show partial to total resorption of the rims. Subhedral to euhedral clinopyroxene (3-5%; 0.1-0.8mm) and orthopyroxene (2-3%; 0.2-0.8mm) occur as individual phenocrysts and as glomerocrysts with plagioclase and Ti-magnetite (3%; 0.4mm). The fine-grained to glassy groundmass consists of plagioclase microlites and small equant augite and Ti-magnetite grains.

3.2.2 PHENOCRYST MINERAL CHEMISTRY

Compositions of phenocryst phases in selected Hunter Ridge samples have been determined by routine analysis using the Cameca SX-50 electron microprobe at the University of Tasmania. Analytical techniques are described in Appendix 2. Microprobe analyses are listed in Tables A4.1-A4.4 in Appendix 4.

Olivine

Olivine phenocrysts in mafic rocks 2DR6-1, DR8-2 and DR15-1 range in composition from Fo_{88} to Fo_{93} (Fig. 3.4). The most magnesian olivine detected is $Fo_{92.9}$ from DR8-2. Figure 3.5 shows CaO contents of olivines from these three samples compared to olivine from island arc tholeiites (IAT) and high-Ca boninitic lavas from the Sigurdsson et al.

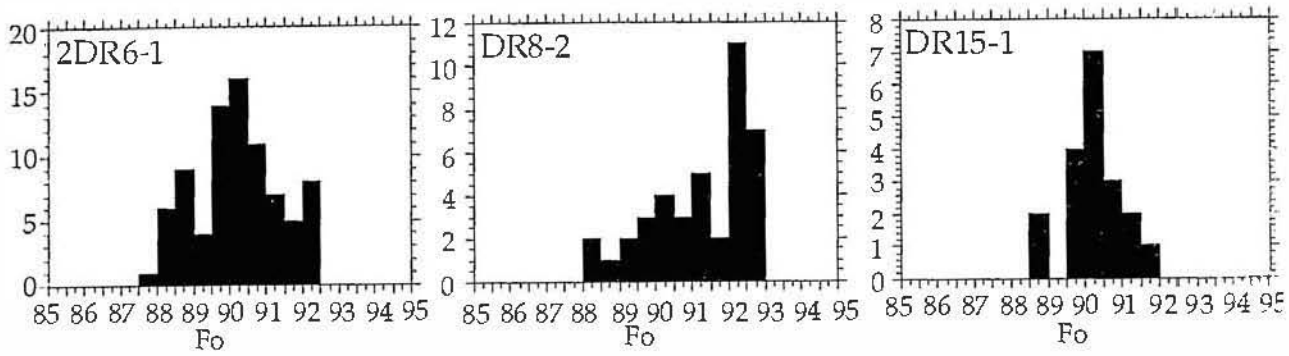

Figure 3.4. Histograms showing the range in Fo values in olivine phenocrysts from Hunter Ridge lavas

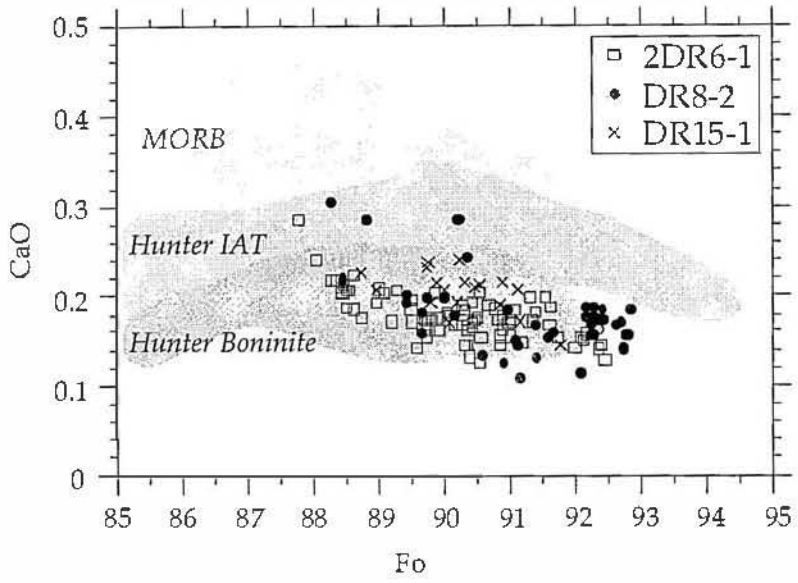

Figure 3.5. Variation of CaO vs Fo in olivine phenocrysts from Hunter Ridge lavas. Hunter IAT = Hunter Ridge island arc tholeiites; Hunter Boninite = Hunter Ridge high-Ca boninites. Data for MORB from Sobolev et al. (1989), Dmitriev et al. (1991), McNeill and Danyushevsky (1996); Hunter IAT and Hunter boninites from Sigurdsson et al. (1993).

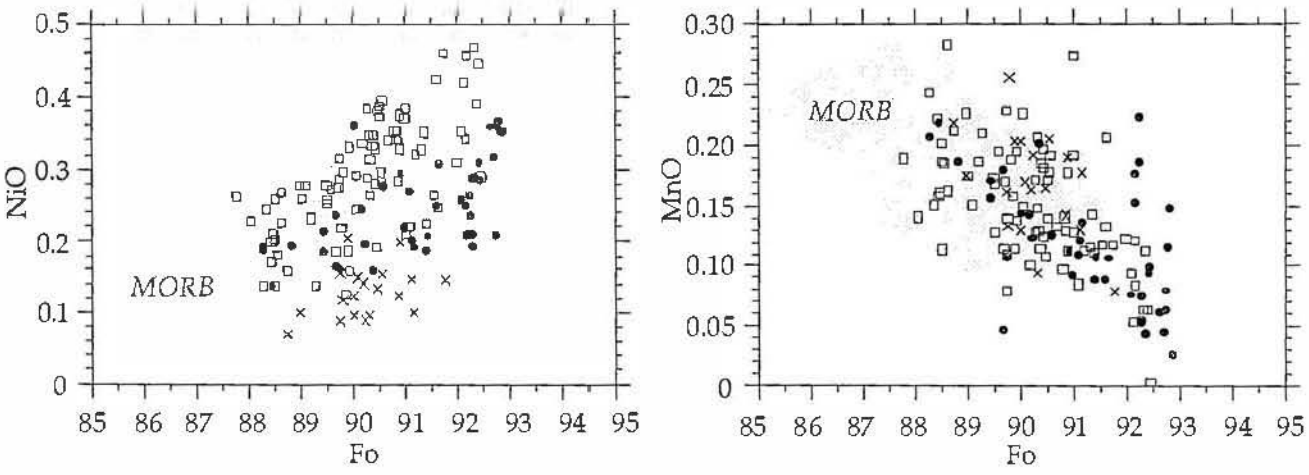

Figure 3.6. NiO and MnO variation in olivine phenocrysts from Hunter Ridge lavas. Symbols are the same as in Figure 3.5. Olivine NiO and MnO data are unavailable for the lavas studied by Sigurdsson et al. (1993).

(1993) study of the southwestern Hunter Ridge. Olivines from 2DR6-1, DR8-2 and DR15-1 have CaO contents mainly between 0.10% and 0.20%. The broad rise in olivine CaO contents with decreasing Fo value is characteristic of crystallisation in the absence of clinopyroxene. Jurcewicz and Watson (1988) studied CaO partitioning between olivines and coexisting melt and found that the CaO contents of magmatic olivines reflect CaO abundance in coexisting equilibrium melt. 2DR6-1 and DR8-2 olivine CaO contents overlap the fields defined by olivines in Hunter Ridge high-Ca boninites, suggesting crystallisation from similar transitional boninitic magmas. CaO contents of olivines in DR15-1 are slightly higher on average, and overlap into the lower range for Hunter Ridge arc tholeiites. MnO contents in olivine phenocrysts decrease with increasing Fo and overlap with MORB around Fo_{87} to Fo_{90} (Fig. 3.6).

At a given Fo value, NiO contents in olivine from 2DR6-1 overlap with values for MORB and are higher than those in DR8-2 and DR15-1 (Fig. 3.6), whereas the lowest NiO contents at Fo_{90} occur in DR15-1. In general, NiO in olivine from all three samples decreases with decreasing Fo, along trajectories parallel to, but below those of MORB olivines, consistent with olivine-dominated fractionation. Variations in olivine NiO contents at, for example, Fo_{90}, between the three studied samples might reflect the varying parental magma FeO contents. Major controls on melt FeO contents during mantle melting include (Falloon et al., 1988) pressure of melt segregation (higher pressure, higher FeO), extent of partial melting (lower degrees of partial melting, lower FeO content) and oxidation state (higher oxidation giving more Fe_2O_3 and therefore less FeO). Fractionation of high-Mg olivine has little effect on melt FeO contents. Therefore, assuming the constancy of the olivine-liquid K_D for Fe-Mg partitioning in mafic systems (Roeder and Emslie, 1970; Ford et al., 1983; Ulmer, 1989), to crystallise Fo_{90} olivine for example, a more Fe-rich magma will require higher MgO contents to achieve the required $Mg^{\#}$ than a relatively low-Fe magma. As NiO contents of mafic magmas closely follow MgO, a magma crystallising Fo_{90} that has 8% MgO will have higher NiO (and therefore higher olivine NiO) than a more Fe-poor magma that requires, for example, only 6% MgO to achieve the appropriate $Mg^{\#}$ value to crystallise Fo_{90}. On this basis, the highest-FeO sample DR15-1 should have the highest olivine NiO content of the three samples studied, since it required more MgO to crystallise Fo_{90} olivine. This is the opposite of the observed case (Fig. 3.6), suggesting that other factors, especially melt oxidation state, played a major role in controlling olivine NiO contents (see section 3.3; magma crystallisation conditions).

Cr-spinel

Cr-spinel occurs mainly as inclusions in olivine and rarely as discrete phenocrysts. Compositional relationships of olivine-spinel pairs for 2DR6-1, DR8-2 and DR15-1 are presented in Figure 3.7, together with olivine-spinel data from MORB, and from Hunter Ridge high-Ca boninites and IAT. Northern Hunter Ridge spinel $Cr^{\#}$ values are mainly >70 and <86 (Fig. 3.7a), overlap with $Cr^{\#}$ values of spinels in high-Ca boninites and arc tholeiites from further southwest on the Hunter Ridge, and indicate strongly depleted harzburgitic mantle sources (Arai, 1992). $Cr^{\#}$ values are relatively constant with decreasing Fo, consistent with olivine ± minor pyroxene fractionation without plagioclase. At $Mg^{\#}$ = 55-60, DR15-1 Cr-spinels have higher TiO_2 contents (0.36-0.46%) than those in the other two samples (Fig. 3.7b), and in each rock, Cr-spinel TiO_2 contents increase with advancing fractionation. Cr-spinels in DR8-2 and DR6-1 have Fe^{3+} contents <0.23, whereas DR15-1 has Fe^{3+} contents in Cr-spinel up to 0.3 (Fig. 3.7c).

Pyroxenes

Orthopyroxene phenocrysts occur in lavas from dredges 8, 9, 10, 12 and 16, and include bronzite and hypersthene (Fig. 3.8). Maximum $Mg^{\#}$ values for the orthopyroxene phenocrysts are around 80-85 and occur in sample DR8-2 (Fig. 3.9). Orthopyroxene phenocrysts from the other dredges have $Mg^{\#}$ <80. Cr_2O_3 contents are below 0.30% and are broadly inversely related to Al_2O_3 contents, which range from ~0.6-1.40% (Fig. 3.10).

Clinopyroxene phenocrysts occur in samples from dredges 8, 9, 10, 12, 15 and 16 and span a compositional range from endiopside through to augite (Fig. 3.8). Maximum $Mg^{\#}$ values are around 90 (Fig. 3.11) and contents of Al_2O_3, TiO_2 and Na_2O increase with decreasing pyroxene $Mg^{\#}$ (Fig. 3.12), reflecting increases in melt contents of these elements with advancing fractionation, and the absence of FeTi oxide crystallisation over this interval. Early-crystallised clinopyroxenes have low Al_2O_3 contents (<2% Al_2O_3), indicative of low pressure fractionation. The decrease in the Al_2O_3 contents of clinopyroxene in the DR10 and DR16 lavas at $Mg^{\#}$~78 may reflect the start of plagioclase crystallisation in these magmas.

Plagioclase

The cores of plagioclase phenocrysts in the Hunter Ridge lavas cover a wide range in compositions (Fig. 3.13). Those from dredge 8 and 12 lavas are highly calcic (An_{80-88}), as is characteristic of plagioclase

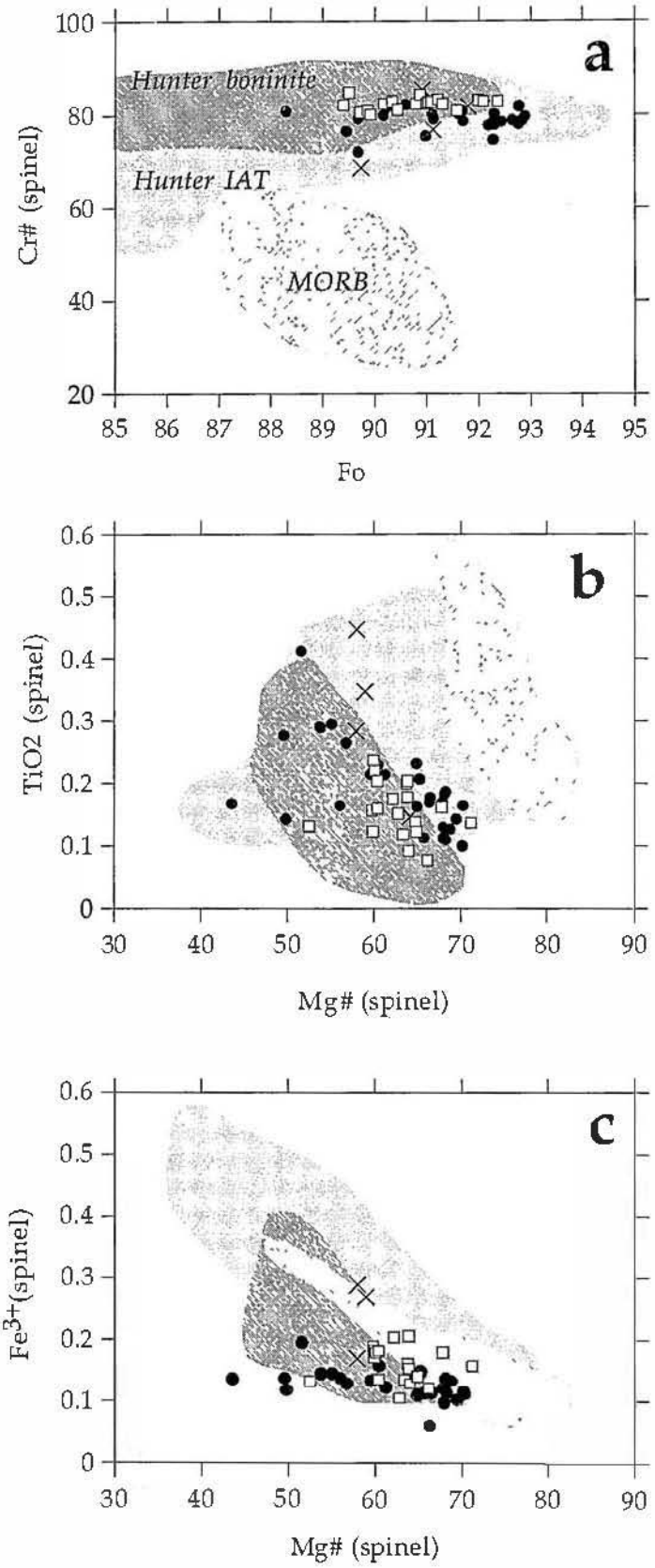

Figure 3.7a, b, c. Compositional variations in spinel inclusions in olivine phenocrysts from the Hunter Ridge lavas. Symbols and fields as for Figure 3.6.

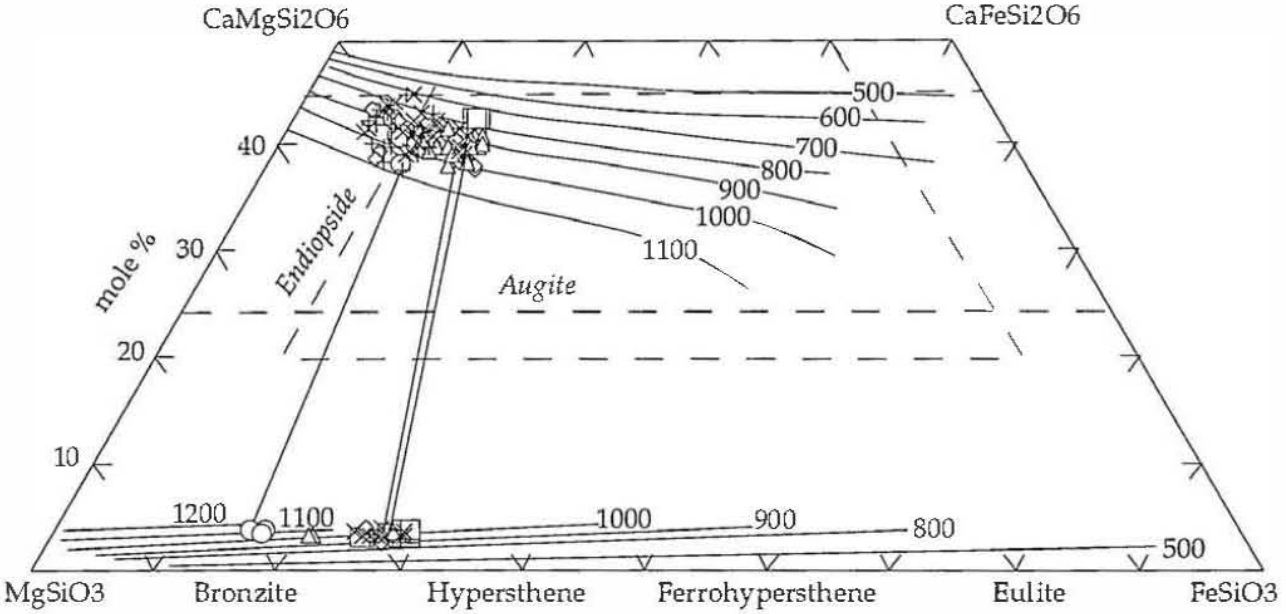

Figure 3.8. Quadrilateral components of clinopyroxene and orthopyroxene phenocryst cores from Hunter Ridge lavas. Circles = DR8; squares = DR9; diamonds = DR10; triangles = DR12; + = DR15; X = DR16. The graphical pyroxene thermometer (Lindsley and Anderson, 1983) show crystallization temperatures of coexisting pyroxene phenocrysts cores in Hunter Ridge lavas. Tielines join coexisting phenocryst assemblages

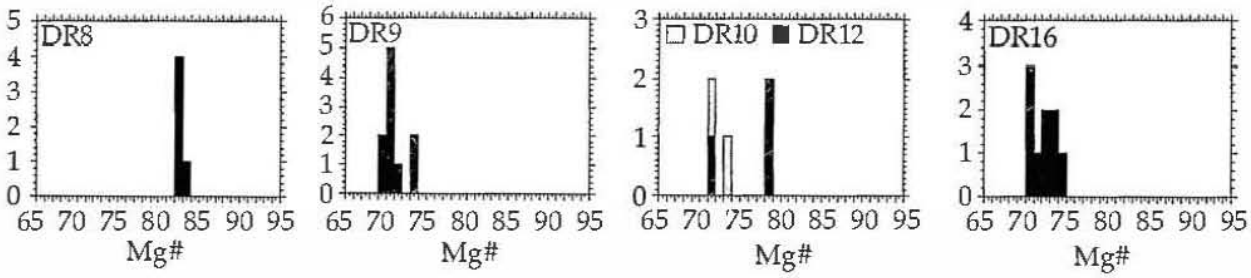

Figure 3.9. Histograms showing the range in Mg# values in orthopyroxene phenocrysts from Hunter Ridge lavas.

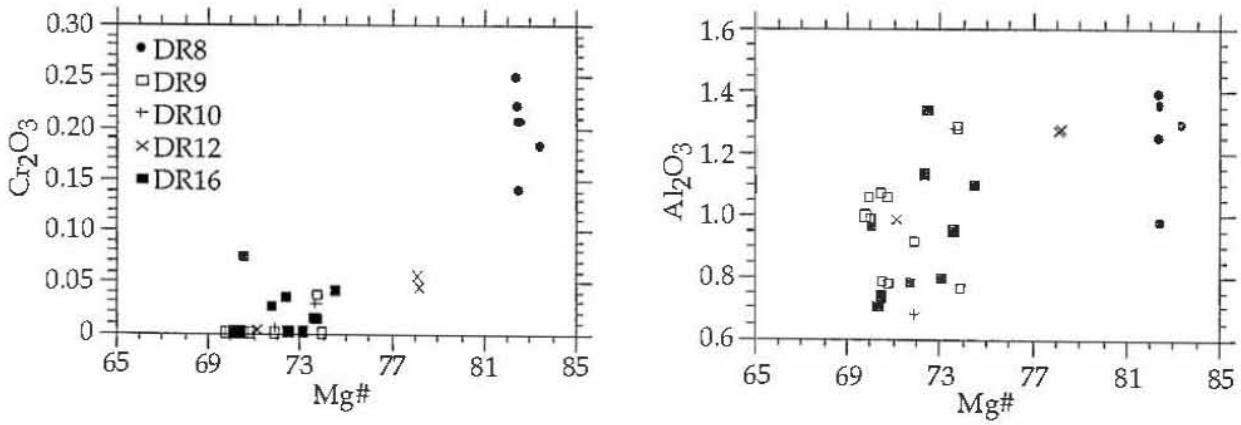

Figure 3.10. Cr2O3 and Al2O3 contents in orthopyroxene phenocrysts from Hunter Ridge lavas

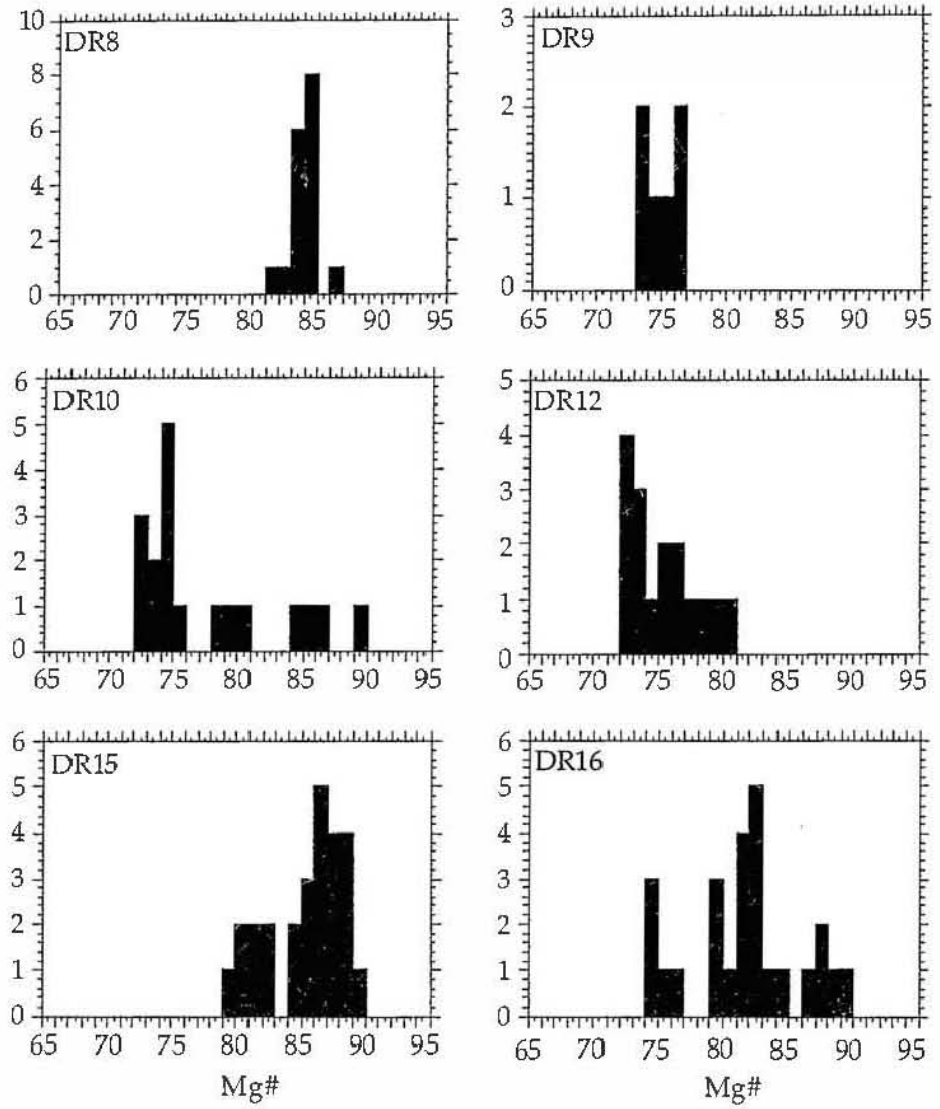

Figure 3.11. Histograms showing the range in Mg# in clinopyroxene phenocrysts from Hunter Ridge lavas.

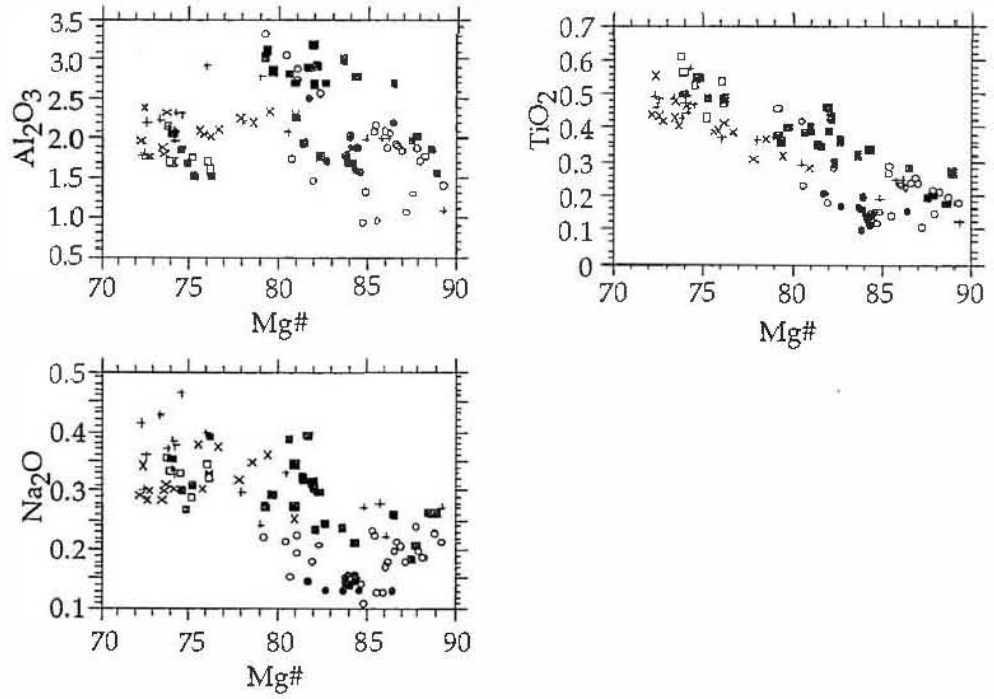

Figure 3.12. Al_2O_3, TiO_2, and Na_2O contents in clinopyroxene phenocrysts from Hunter Ridge lavas. Symbols same as in Figure 3.10.

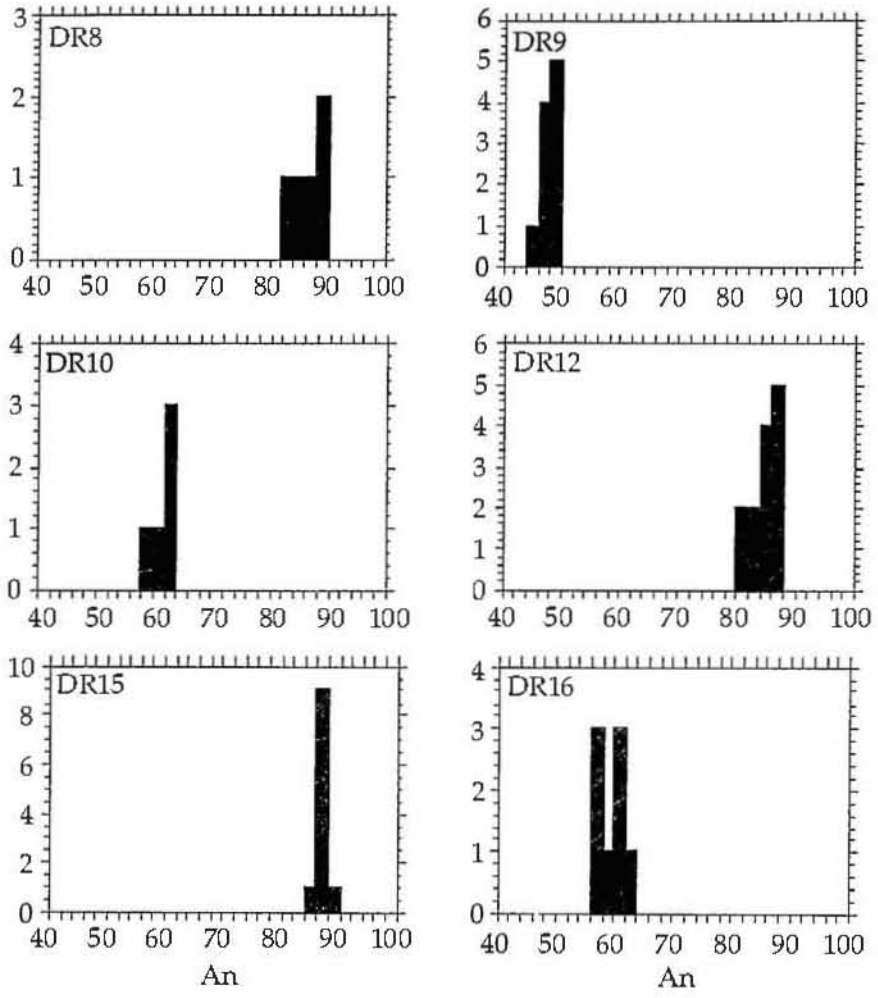

Figure 3.13. Histograms showing the range in anorthite content in plagioclase phenocrysts from Hunter Ridge lavas

phenocrysts in some oceanic forearc lavas compositionally transitional from arc tholeiites to high-Ca boninites, such as those from the northern Tongan forearc (Falloon and Crawford, 1991). Panjasawatwong et al. (1995) showed that the bulk $Ca^{\#}$ (100Ca/Ca+Na) of a magma exerts a pronounced control on the composition of crystallising plagioclase. They found that at 5kbar, An_{95} plagioclase crystallises from a bulk composition with $Ca^{\#} = 90$ under anhydrous conditions, and also with 2% H_2O added. DR8-2 has plagioclase phenocryst cores with compositions of An_{82-88}, and a bulk composition $Ca^{\#} = 89$, and would be expected to crystallise plagioclase around An_{90}. The slightly lower An content of plagioclase phenocrysts in this sample may be due to clinopyroxene crystallisation prior to plagioclase appearance. Water is well known to markedly suppress plagioclase appearance temperatures, leading to crystallisation of olivine and/or pyroxene as liquidus and near-liquidus phases at low pressures (Yoder and Tilley, 1962; Sekine et al., 1979).

The plagioclase phenocrysts in dredge 15 andesites have An contents (An_{84-89}) far higher than expected for plagioclase crystallising from magmas with CaO/Na_2O values around 2-3. Presumably, these crystallised from more primitive precursors to these andesitic lavas, and have remained 'floating' in the magma despite fractionation and removal of mafic phases, because of their relatively low density. Further studies of the melt inclusions in these plagioclase phenocrysts are required to determine the nature of the magma from which they crystallised.

Plagioclase phenocryst cores in andesites from dredges 10 and 16 and the dacites from dredge 9 lie between An_{45-62}, more typical of plagioclase in calc-alkaline andesites and dacites (Gill, 1981).

3.3 MAGMA CRYSTALLISATION CONDITIONS

3.3.1 TEMPERATURE

Estimates of the equilibration temperature of olivine-spinel pairs in DR6-1, DR8-2 and DR15-1 have been obtained using the Ballhaus et al. (1991) calibration for the olivine-spinel Fe^{2+}/Mg exchange geothermometer, which is based on the reaction

$$Fe_2SiO_4^{ol} + 2MgAl_2O_4^{sp} <-------> Mg_2SiO_4^{ol} + 2FeAl_2O_4^{sp} \qquad (3.1)$$

Resultant temperatures of the most high-$Mg^{\#}$ pairs are just above 1200°C for DR6-1, 1170°C for DR8-2, and 1070°C for D15-1 (Table A4.2), and are clearly dependent on the $Mg^{\#}$ of the individual spinels (Fig 3.14). These olivine-spinel equilibration temperatures are probably lower than

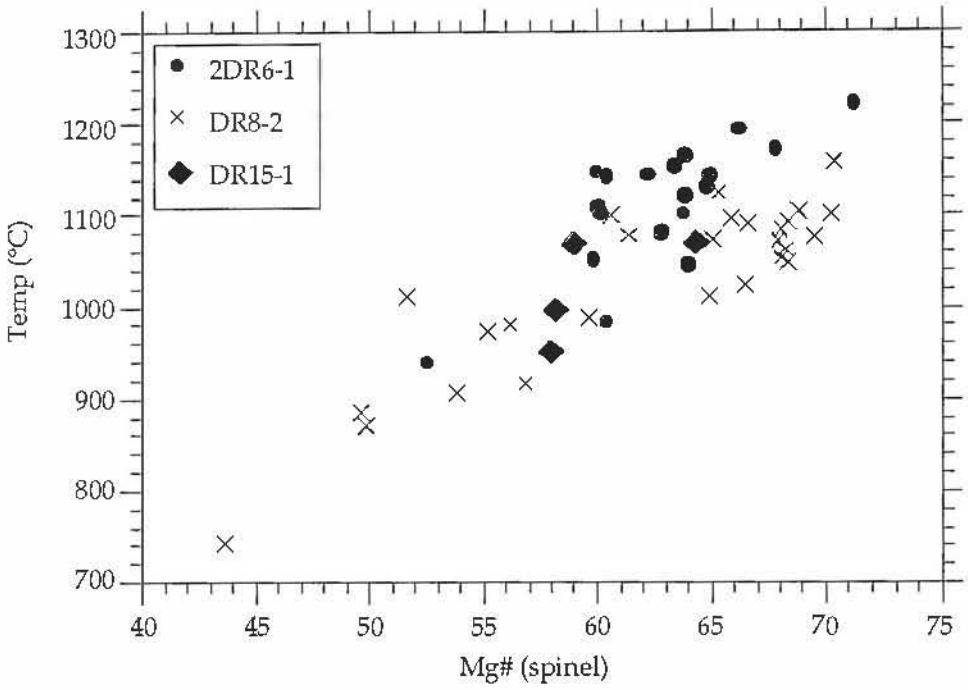

Figure 3.14. Temperature vs Mg# of Cr-spinel. Temperature, calculated using the Ballhaus et al. (1991) calibration for the olivine-spinel Fe2+/Mg exchange geothermometer.

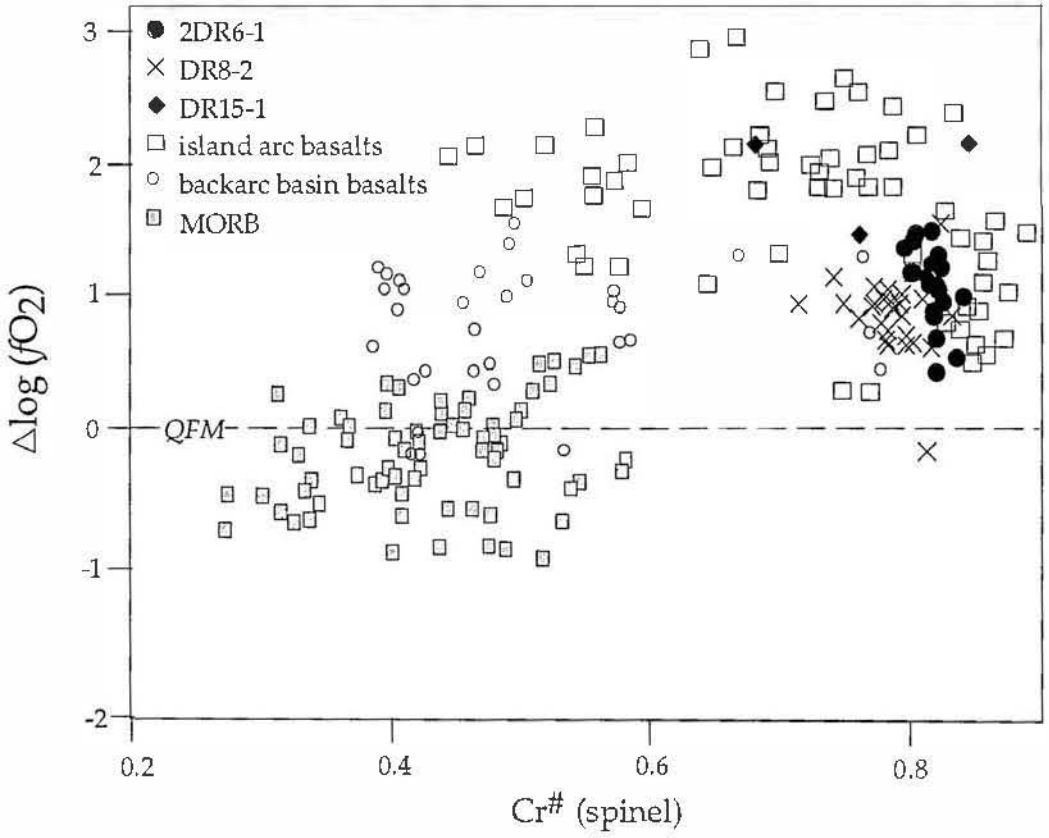

Figure 3.15. Oxidation states of 2DR6-1, DR8-2, and DR15-1 spinels plotted against Cr# in Cr-spinel compared to Cr-spinels in island arc basalts, backarc basin basalts and MORB (see Ballhaus, 1993 Fig.8 for refernces); oxidation expressed as log units above or below the quartz-fayalite-magnetite (QFM) buffer.

magmatic equilibration temperatures, since they were probably affected by subsolidus diffusion of Fe^{2+} - Mg; only relatively short times are required to alter the primary $Mg^{\#}$ of spinel cores by diffusive processes (Ozawa, 1983; Eggins, 1989). This is supported by application of the Ford et al. (1983) olivine/liquid Mg - Fe^{2+} thermometer to estimate the pre-eruption temperatures of basic lavas. Temperatures derived from DR6-1, DR8-2 and DR15-1 using this method are 1312°, 1159° and 1292°C respectively.

Calculated crystallisation temperatures of coexisting clino- and orthopyroxene phenocrysts in the more evolved northern and central Hunter Ridge dredged lavas are shown in Figure 3.8, and were derived using the Lindsley and Anderson (1983) graphical pyroxene thermometer and projection scheme. Temperatures range from ~970°C to 1000°C. Temperatures for the same coexisting pairs calculated using the solution models of Wells (1977) are slightly higher (1002-1090°C) than those indicated by Figure 3.8. These relatively low temperatures are reasonable, since the only coexisting 'equilibrium' pyroxene pairs discovered in the samples have $Mg^{\#}$ values of 65 - 75, and are thus quite evolved. The absence of amphibole, despite the crystallisation extending to temperatures below 1000°C, suggests that these magma did not achieve enough H_2O pressure to crystallise amphibole. The two pyroxene geothermometer of Lindsley and Anderson (1983) was also applied to DR8-2 pyroxene pairs, yielding temperature around 1100°C, consistent with the olivine-spinel pair thermometry.

3.3.2 OXYGEN FUGACITY

The Ballhaus et al. (1991) calibration of the olivine-orthopyroxene-spinel geobarometer can be applied to olivine-spinel assemblages of the Hunter Ridge lavas. Where orthopyroxene is absent, as in DR6-1 and DR15-1, silica activities may be estimated from thermodynamic models for silicate melts, according to values given by Ghiorso and Carmichael (1987). The leucite basanite and tholeiitic compositions they model can be used to bracket SiO_2 activity in the Hunter Ridge melt compositions to between -0.4 and -0.7 log units over the range 1000 to 1300°C (see Fig. 3 in Ghiorso and Carmichael, 1987). However Ballhaus et al (1991) state that for orthopyroxene-undersaturated rocks, the correction required for fO_2 calculations rarely exceeds -0.2 log units. On this basis, fO_2 estimates for DR6-1 and DR15-1 range between 0.5 to 1.6 log units and 1.2 to 2.2 log units, respectively, above the QFM oxygen buffer, within the range for other island arc basalts (Fig. 3.15; Ballhaus, 1993).

3.4 MAJOR ELEMENT GEOCHEMISTRY

3.4.1 MAJOR ELEMENTS

On the K_2O-SiO_2 classification diagram of Peccerillo and Taylor (1976), rocks from Hunter Ridge dredges 1 to 16 show a compositional range from basalts to rhyolites (52-70.7% SiO_2), with the majority falling in the low-K field (Fig. 3.16a). For the purposes of discussion, three different suites can be identified on this diagram, a low-K, a medium-K and a high-K suite, referred to herein as suites I, II and III respectively. There appears to be no regular pattern of occurrence or distribution of these three suites along the northern part of the Hunter Ridge (Fig. 3.3), and this subdivision does not imply that all rocks in any of Suite I, II or III are necessarily comagmatic. Suites I and II overlap around 0.5-0.7% K_20 between 52 and 60% SiO_2; however these suites at 6% MgO have significantly different TiO_2 and P_2O_5 contents (Fig. 3.17), and are clearly separated on a Ti/Zr vs P_2O_5 plot (Fig. 3.16b), with the medium-K suite II being clearly more TiO_2- and P_2O_5-rich than low-K suite I.

Four samples (DR3-2, 2DR4-1, 2DR4-5 and DR5-5) show petrographic evidence for seawater alteration (or possible low-grade hydrothermal alteration for the DR4 dioritic rocks), which may have significantly modified the original compositions of these rocks (Staudigel et al., 1981; Staudigel and Hart, 1983; Bienvenu et al., 1990). Altered diorites 2DR4-1 and 2DR4-5 might reasonably be assigned to the low-K suite, since fresh and originally petrographically almost identical diorite 2DR4-9 from the same dredge can be confidently assigned to the low-K suite. Because of alteration affects on K-group and other mobile elements (Na, Sr, Ca), these elements are excluded from further discussion.

Figure 3.17 shows major element vs MgO variations for rocks from the northern Hunter Ridge, compared with compositional fields for high-Ca boninites and island arc tholeiites dredged from further southwest along the Hunter Ridge (Sigurdsson et al., 1993). Also plotted for comparison are the high-Mg series rocks from Matthew and Hunter islands and adjacent submarine seamounts in the southern Vanuatu arc (Monzier et al., 1993), and island arc tholeiites from the Tongan arc (Ewart et al., 1973).

Suite I rocks have 13.2% to 1.4% MgO at SiO_2 contents from 51.1 to 64.1%. As might be expected from the distribution of the analysed samples along more than 400km of the Hunter Ridge, irregular variations in FeO* (where FeO* is total Fe expressed as FeO) and P_2O_5 contents suggest that individual samples constituting Suite I are not likely to be comagmatic.

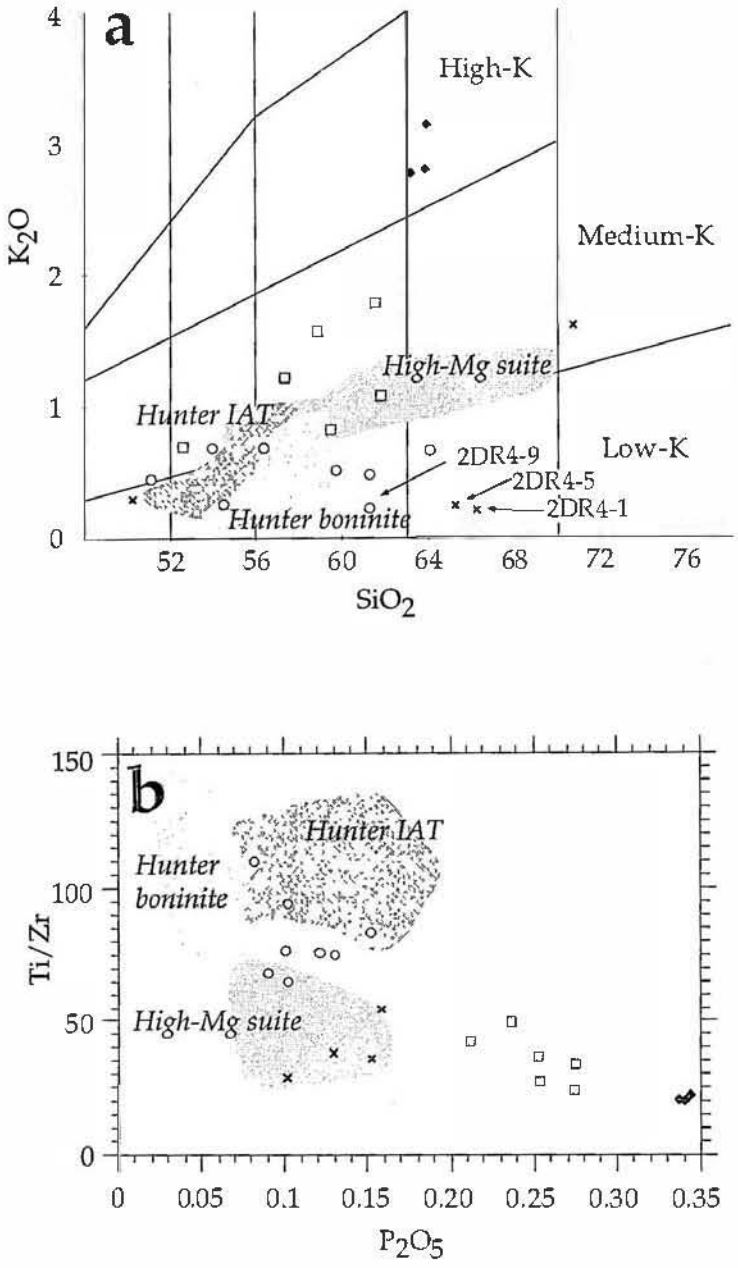

Figure 3.16 **a.** SiO_2 vs K_2O classification diagram of Peccerillo and Taylor (1976), showing the separation of three suites, the low-K (suite I; open circles), medium-K (suite II; open squares) and the high-K suite (suite III; filled diamonds). The crosses represent altered samples. 2DR4-1 and 2DR4-5 (marked) are assigned to suite I since 2DR4-9 from the same dredge is fresh and originally petrographically identical. Hunter IAT = Hunter Ridge island arc tholeiites and Hunter boninite = Hunter Ridge high-Ca boninites from Sigurdsson et al. (1993). High-Mg suite = high-Mg suite rocks from Matthew and Hunter islands and adjacent seamounts (Monzier et al., 1993). All major element data has been normalised to 100%. **b.** Ti/Zr vs P_2O_5 for Hunter Ridge rocks showing marked separation of the three suites defined above. Symbols and fields as for Figure 3.16a.

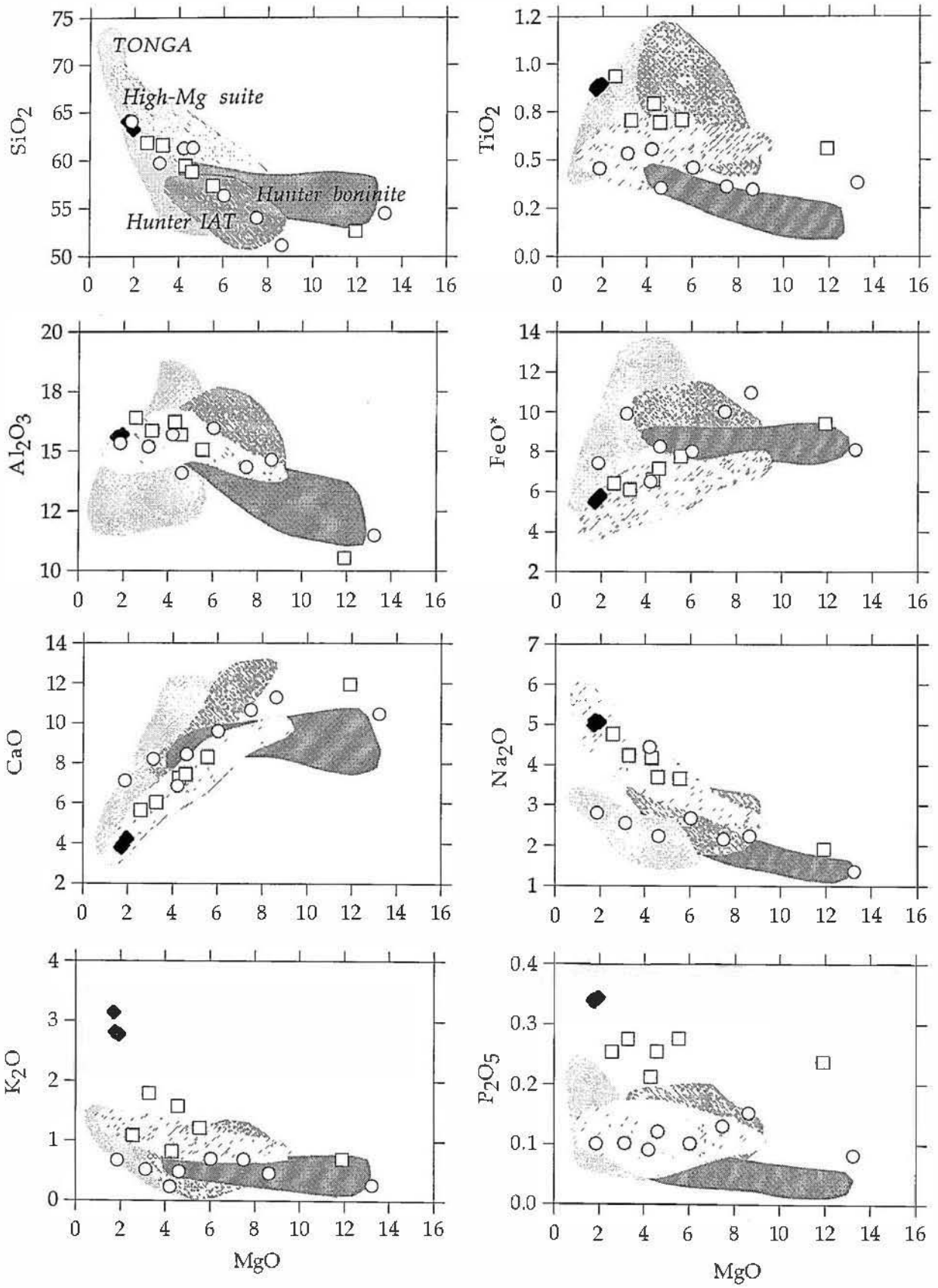

Figure 3.17. Major element covariation diagrams for the Hunter Ridge rocks compared to high-Ca boninites (Hunter boninite) and island arc tholeiites (Hunter IAT) dredged from further southwest along the Hunter Ridge (Sigurdsson et al., 1993), the high-Mg series rocks representing Matthew and Hunter islands (Fig. 3.1b) and surrounding seamounts (Monzier et al., 1993) and island arc tholeiites from the Tonga arc (Ewart et al., 1973). Symbols for the Hunter Ridge rocks as for Figure 3.16a,b. All major element data has been normalized to 100%.

Relative to the Tonga arc low-K tholeiites at ~5% MgO, the Hunter Ridge rocks are less FeO*-rich. As a consequence of their relatively high SiO_2 contents at any MgO level (and low FeO*/MgO), nearly all of the low-K suite I rocks plot in the calc-alkaline field of Miyashiro's (1974) discriminant diagram, as do the majority of lavas with boninitic affinity from further southwest along the Hunter Ridge, and from the Hunter-Matthew high-Mg seamount suite (Fig. 3.18). In contrast, the southwestern Hunter Ridge arc tholeiites and Tongan tholeiites plot clearly within the tholeiitic field on Figure 3.18, as a result of their higher FeO* contents. At any MgO value, the suite I rocks have TiO_2 contents always <0.6%, slightly above the Hunter Ridge high-Ca boninites, but below Hunter Ridge arc tholeiites for similar levels of MgO. The Na_2O contents range from 1.38 to 2.81%, comparable to Hunter Ridge high-Ca boninites, and increase with increasing fractionation. Excluding 2DR6-1 at 13.2% MgO, suite I rocks have CaO values generally higher (7.1-11.3%) than suite II and III lavas at equivalent MgO .

Suite II medium-K lavas have MgO contents from 2.6-11.9% at relatively high SiO_2 (52.6-70.8%), and also plot in the calc-alkaline field on Figure 3.18. Both FeO (9.4-6.1%) and CaO (11.9-5.6%) decrease and Na_2O increases (1.92-4.76%) with decreasing MgO, following trends similar to the high-Mg suite seamount lavas from the Hunter-Matthew area. P_2O_5 remains fairly constant at ~0.25%, and is significantly higher than in either the Hunter Ridge boninites and IAT, or the Hunter-Matthew high-Mg suite lavas.

Suite III samples are all high-K andesites from dredge 9, midway along the length of the Hunter Ridge (Fig. 3.3). In terms of FeO* and TiO_2 contents, they are little different at 2-3% MgO from Suite 2 lavas, but they have significantly higher P_2O_5 and K_2O contents. They have important compositional differences from the high-K andesites and dacites occurring on Kadavu island 300km further north (see Chs. 5 and 6), best shown by the much lower Sr contents and flat HREE patterns of the DR9 lavas.

Based on the major elements and mineral chemistry, suite I rocks are best considered to be transitional between typical high-Ca boninites and arc tholeiites and are here classified as transitional boninites. Suite II and III are more typical calc-alkaline series arc lavas.

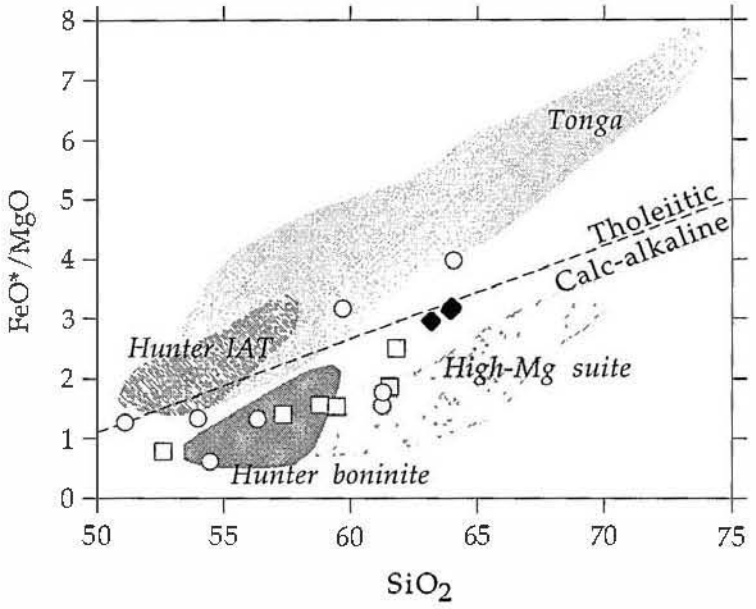

Figure 3.18. FeO*/MgO vs SiO2 discrimination diagram of Miyashiro (1974). Suite I (open circles) nearly all fall in the calc-alkaline field with Hunter Ridge high-Ca boninites (Sigurdsson et al., 1993) and the high-Mg suite (Monzier et al., 1993) because of high SiO2 contents at any MgO value. Symbols as for Figure 3.17.

3.4.2 PRIMARY MAGMAS

2DR6-1 in suite I has been identified as a possible primary magma with 12.8% MgO and $Mg^{\#}$ = 74.5 (calculated assuming ΣFe=FeO); although it contains abundant olivine, these are almost all hopper-type microphenocrysts that probably crystallised during eruption, rather than during magma chamber storage or transit. Thus 2DR6-1 can be considered to represent a liquid composition. Olivines in 2DR6-1 are dominated by compositions of $Fo_{\sim 90\pm 1}$ (Fig. 3.4). If sample 2DR6-1 represents a melt which crystallised as a closed system under equilibrium conditions, then the olivine observed in the sample should be in equilibrium with the host melt. For the whole rock $Mg^{\#}$ (74.5) and an olivine-liquid Fe-Mg K_D of 0.3, equilibrium olivine is $Fo_{90.5}$, consistent with the microphenocryst olivine composition. Ni (>200ppm) and Cr contents (>400ppm) are also consistent with the hypothesis that sample 2DR6-1 is close to a primary melt composition (e.g., Hart and Davis, 1978; Kinzler et al., 1990).

Sample DR15-1 from suite II has $Mg^{\#}$ = 69.3, appropriate for a candidate for a primary magma, but it contains common olivine and clinopyroxene phenocrysts, so does not represent a liquid composition. Olivines in DR15-1 range in composition from $Fo_{88.5}$ to $Fo_{91.8}$. If the wholerock composition were to represent a liquid composition, and Fe^{3+}/Fe^{2+} = 0.15, the equilibrium olivine is $Fo_{89.9}$, and for Fe^{3+}/Fe^{2+} = 0.25, equilibrium olivine is $Fo_{90.9}$. As most phenocrystal olivines in DR15-1 are more Mg-rich than Fo_{90} (Fig. 3.4), and at least 25% of the analysed olivines are even more Mg-rich than $Fo_{90.9}$, it is concluded that (i) the composition has not been significantly affected by olivine (and clinopyroxene) accumulation, and (ii) that either the magma was significantly more oxidised than required to give Fe^{3+}/Fe^{2+} = 0.25, or the wholerock composition is that of a liquid from which significant amount of olivine had already separated prior to eruption of this basalt. Addition of 1.5-2 wt% equilibrium olivine to the wholerock composition for Fe^{3+}/Fe^{2+} = 0.25 produces a liquid in equilibrium with the most forsteritic olivine measured in this rock, $Fo_{91.8}$. On this basis, and constrained by the assumptions of Fe^{3+}/Fe^{2+} ~0.25 and K_D = 0.3, it can be concluded that the wholerock composition of DR15-1 is also a near-primary magma composition. The higher Fe^{3+}/Fe^{2+} for DR15-1 relative to 2DR6-1 required to match observed olivine and wholerock compositions is supported by olivine-spinel barometry (Fig. 3.15).

3.5 TRACE ELEMENT GEOCHEMISTRY

Selected trace elements (Ni, Cr, Zr, Sr, Rb, Ba, Sc and V) vs MgO diagrams for the dredged Hunter Ridge lavas are given in Figure 3.19. The chemical groups proposed on major element grounds can also be resolved as distinct groups on many trace element diagrams, notably Zr, Rb, Ba and Sr. However, the range in V and Sc contents of the suites overlap and are variable.

Suite I lavas are characterised by relatively high Cr (113-925ppm) and Ni (47-258) at andesitic SiO_2 contents. Rb (4-11ppm), Sr (66-252ppm) and Ba (19-131ppm) do not show a strong variation with decreasing MgO relative to suite II lavas. Also Zr abundances are strikingly low, being still <50ppm at 2% MgO, and vary from around 20 to only ~50 ppm over the MgO range 13% to 2% (Fig. 3.19).

In contrast to the suite I lavas, trace elements in suite II lavas show more pronounced variations with MgO. Both Rb and Ba follow the trend for K_2O, increasing with decreasing MgO, whereas Sr shows a reverse trend; V and Sc broadly follow the trend defined for FeO*.

Suite III lavas tightly cluster on all trace element variation diagrams. Their potassic character is reflected in elevated abundances of Rb (39-42ppm) and Ba (346-362ppm), but not Sr (379-414ppm). For most elements but excluding Ba and Rb, suite III lavas lie on the broad fractionation trends defined by suite II lavas, but at lower MgO values.

Chondrite-normalised REE diagrams for all three suites are shown in Figures 3.20. REE abundances are low in suite I lavas and show a range from LREE-depleted patterns (2DR6-1) to patterns with weak LREE enrichment [$(La/Sm)_N$=0.49-1.35; $(La/Yb)_N$=0.35-1.40]. All patterns have flat HREE patterns but at levels well below those of N-MORB, and even the hornblende diorite 2DR4 -9 with 60% SiO_2 and 4.1% MgO still has HREE at the N-MORB level. The REE patterns for DR8-2 and DR12-8 lavas are subparallel and reflect similar mantle sources. Suites II and III lavas show more sloping HREE patterns and stronger LREE-enrichment than those in Suite I [$(La/Yb)_N$=3.74-7.10] (Fig. 3.10b). All have HREE levels below those of N-MORB. Very small negative Eu anomalies are also present in the more evolved lavas, reflecting plagioclase fractionation.

MORB-normalised trace element patterns (Fig. 3.21) are all characterised by the enrichment in LILE relative to the HFSE typical of arc-related lavas, and enrichment levels increase from the low-K suite I lavas through to the higher-K suite III lavas. Within suite I, most

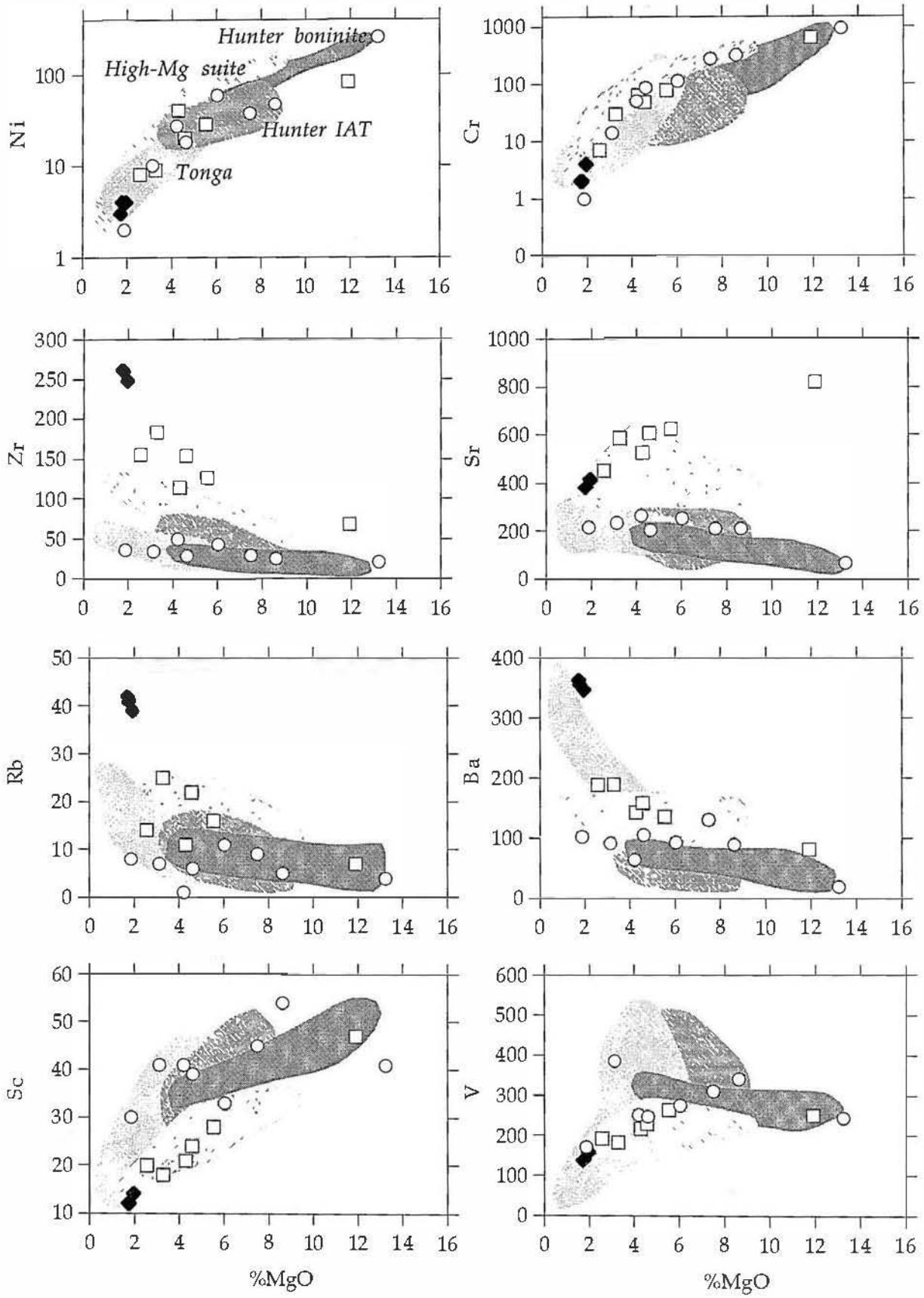

Figure 3.19. Trace element (ppm)-MgO covariation diagrams for the Hunter Ridge rocks. Symbols and fields are the same as in Figure 3.18.

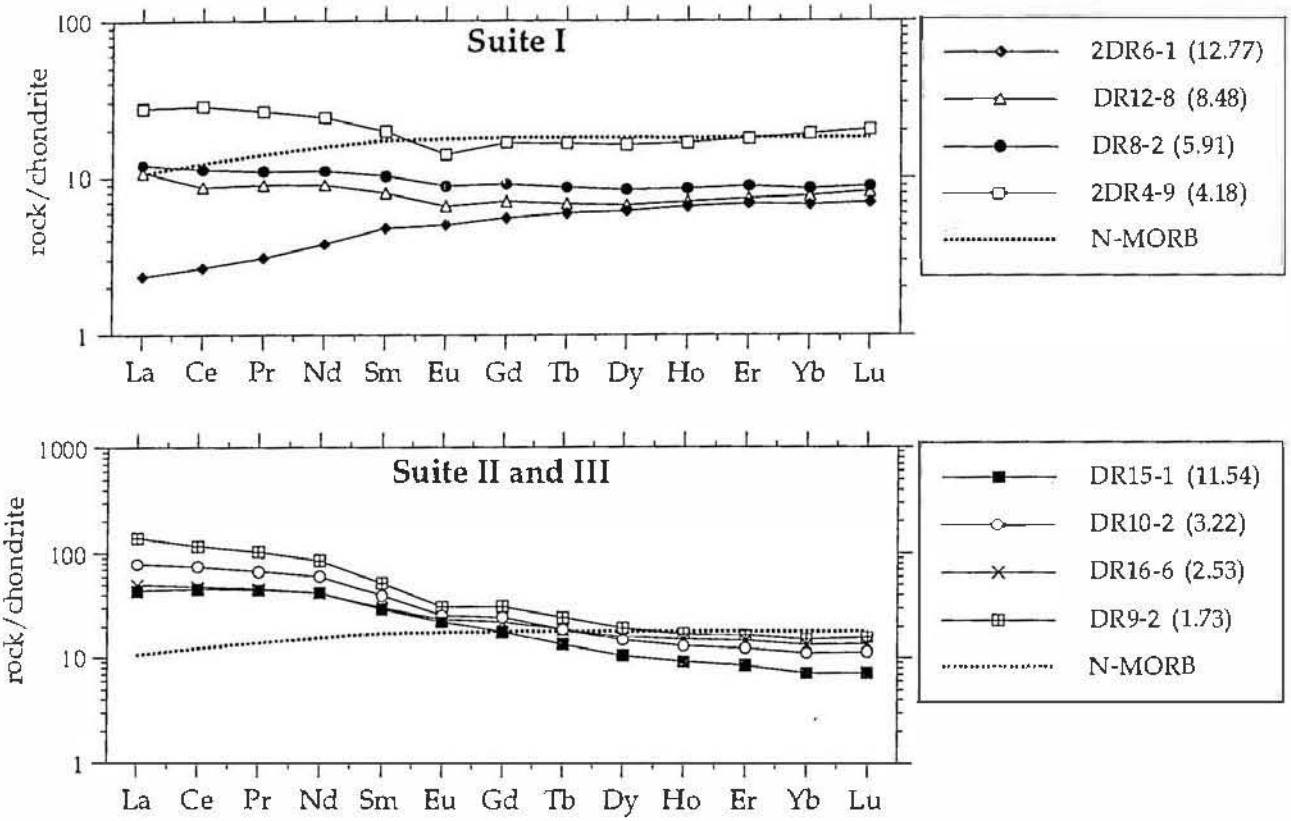

Figure 3.20. REE concentrations for the Hunter Ridge rocks normalised to chondrite. MgO content for each sample in brackets. Chondrite normalising values and N-MORB composition are those from Sun and McDonough (1989).

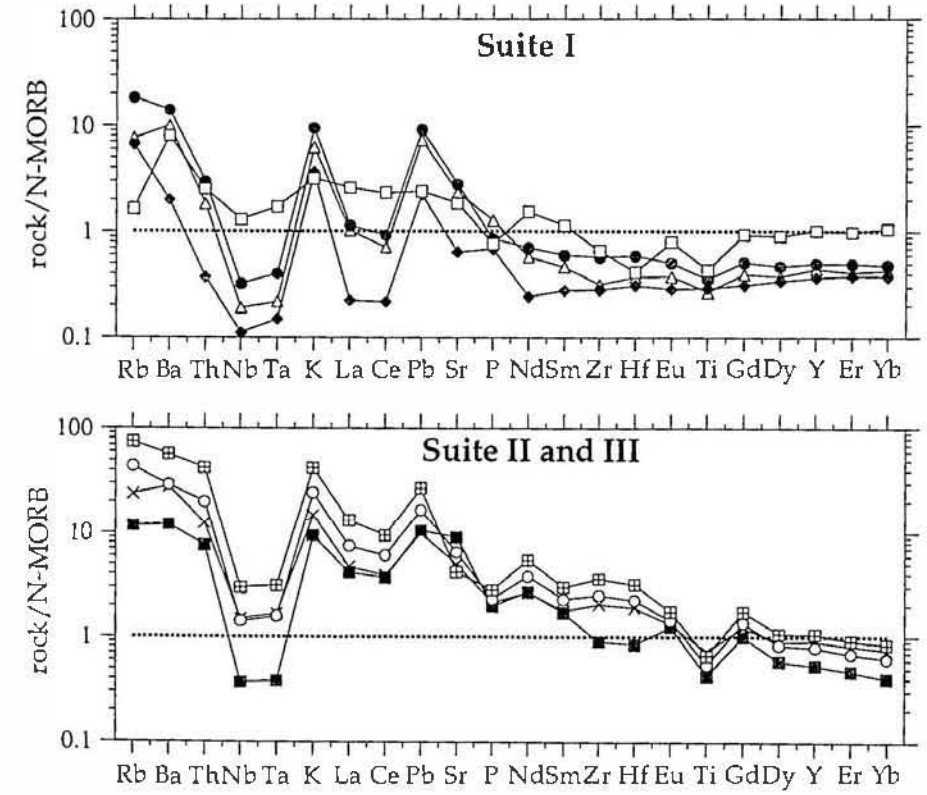

Figure 3.21. N-MORB normalised multi-element diagrams for the Hunter Ridge rocks. Symbols are the same as those in Figure 3.20. Normalising values used are those from Sun and McDonough (1989).

magnesian sample (2DR6-1) has a relatively flat pattern for the HFSE and the REE (Nd to Yb). In contrast to the suite I lavas, suite II and III show strong depletions in Nb and Ta relative to the neighboring REE, due to the more pronounced enrichment of the LILE and LREE in these rocks compared to the Suite I lavas.

3.6 RADIOGENIC ISOTOPE CHEMISTRY

Figure 3.22 shows the standard isotope covariation plots for the Hunter Ridge lavas. Also plotted are data from the North Fiji back arc basin basalts (Price et al., 1990; Price and Kroenke, 1991; Nohara et al., 1994) as representative of the back arc mantle and possibly, the mantle wedge before Hunter Ridge - related subduction. The limited available data (Pb isotopes only) from the South Fiji Basin (Gill, 1987) are plotted as representative of the subducting plate. Also plotted are fields for the intra-oceanic South Sandwich arc (Hawkesworth et al., 1977; Cohen and O'Nions, 1982; Barreiro, 1983; Pearce et al., 1995) and the Vanuatu arc (Briqueu et al. 1994; Crawford et al. 1995).

The Hunter Ridge lavas have a restricted range in Nd isotopic composition ($^{143}Nd/^{144}Nd$ = 0.51299-0.51310) and slightly more radiogenic $^{87}Sr/^{86}Sr$ (0.70282-0.70366) at equivalent $^{143}Nd/^{144}Nd$ compared to Pacific MORB; they plot at the radiogenic Sr side of the field defined by North Fiji Basin backarc basin basalts. Suite II lavas have significantly less radiogenic Sr isotope values, and lie in the mantle array and the fields for Pacific MORB and North Fiji Basin basalts, whereas the analysed suite III lava has a $^{87}Sr/^{86}Sr$ value of 0.70362, slightly outside the mantle array and similar to the most radiogenic Suite I sample analysed. The Sr-Nd isotopic differences between the Suite II and Suite III lavas preclude any broad comagmatic relationships between the lavas of these suites. The range in $^{87}Sr/^{86}Sr$ is considered to be a source feature and not to be due to 'post-magmatic' sea water alteration effects, as leached and unleached samples show only very small differences in $^{87}Sr/^{86}Sr$ (see Appendix 2).

The plot of $^{207}Pb/^{204}Pb$ and $^{208}Pb/^{204}Pb$ against $^{206}Pb/^{204}Pb$ shows that most Hunter Ridge lavas lie close to the NHRL, with no systematic variation between the suites. Unlike the South Sandwich and Vanuatu arc lavas, the Pb isotope data for the Hunter Ridge samples do not extend towards values for subducted sediment and lie close to or within the Pacific MORB field similar to values for the South Fiji Basin crust.

The major implication of these data is that any hydrous fluids involved in the petrogenesis of the Hunter Ridge lavas studied must

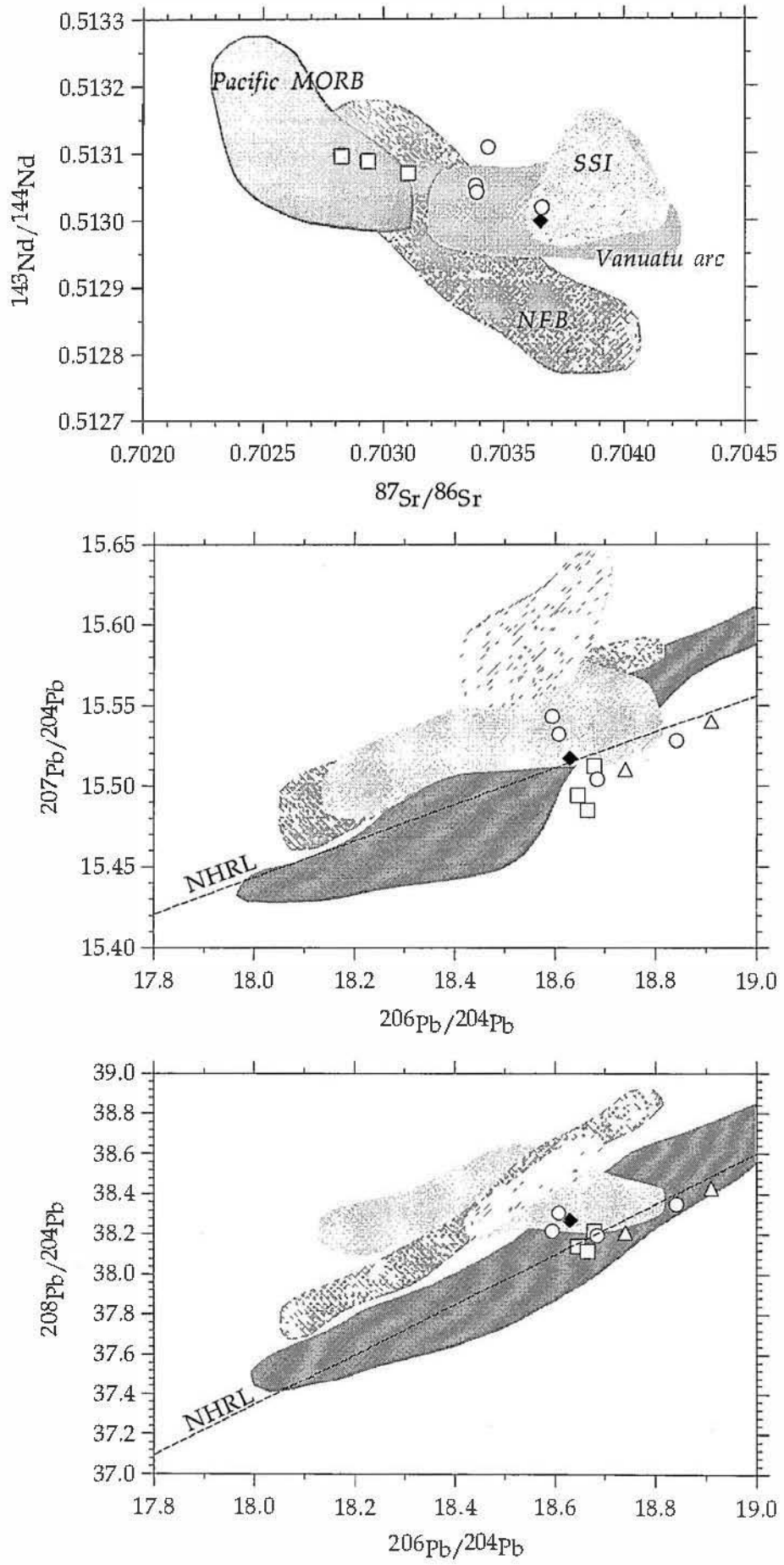

Figure 3.22. Sr vs Nd and Pb isotopic compositions for the Hunter Ridge rocks shown relative to fields for Pacific MORB (Ito et al., 1987), the North Fiji Basin (NFB; Price et al., 1990; Price and Kroenke, 1991; Nohara et al., 1994) BABB, South Sandwich arc (SSI; Hawkesworth et al., 1977; Cohen and O'Nions, 1982; Barreiro, 1983; Pearce et al., 1995) and the Vanuatu arc (Briqueu et al. 1994; Crawford et al. 1995). Hunter Ridge symbols as for Figure 3.17. The limited Pb isotope data for the South Fiji Basin (Gill, 1987) are represented by the open triangles.

have been derived from deeper levels of the subducting South Fiji Basin oceanic crust, rather than from the pelagic sedimentary carapace.

3.7 PETROGENESIS

3.7.1 INTRODUCTION

The differences between the individual suites from the northern part of the Hunter Ridge cannot be explained by crystal fractionation processes, as shown by major and trace element variation diagrams and isotopic data, and instead are a consequence of variations in the composition and/or degree of partial melting of their sources. The following section focuses on what inferences may be made about the nature of the mantle sources of these lavas.

Petrogenesis of island arc lavas requires the mixing of two or more components (e.g. Gill, 1981). Although the nature of these sources is still a controversial topic, the petrogenesis of the Hunter Ridge rocks is best explained by a model involving a depleted mantle source (more depleted than N-MORB sources) and an 'enriched' metasomatic phase. The discussion below outlines the evidence for these components.

3.7.2 DEPLETED COMPONENT

In Figure 3.23, the CIPW molecular normative compositions of 2DR6-1 and DR15-1 are shown in the projection from diopside onto the base of the basalt tetrahedron, with apices jadeite plus Ca-Tschermaks molecule (Jd+CaTs)-quartz (Qtz)-olivine (Ol) (Falloon and Green, 1987, 1988; Falloon et al., 1989). These compositions are compared with the fields of Cape Vogel low-Ca boninites (Jenner, 1981), high-Ca boninites from the Troodos Upper Pillow Lavas (Cameron, 1985, Duncan and Green, 1987), high-Ca boninites transitional to arc tholeiites from station 21 in the northern Tongan forearc (Falloon et al., 1987; Falloon, unpubl. data), and primitive MORB glasses (references in Falloon and Green, 1987). Also shown on this diagram are olivine+orthopyroxene± clinopyroxene+liquid cotectics defined by partial melting experiments on (a) a MORB pyrolite composition at 10, 15, 20 and 30kbar (Falloon and Green 1987, 1988) and (b) the more refractory Tinaquillo lherzolite at 5kbar (Jaques and Green 1980, Falloon et al., 1989). Sample 2DR6-1 from the Hunter Ridge plots below the olivine control line through MORB pyrolite, suggesting that the mantle source was more refractory than MORB source peridotite. Compositions slightly more depleted than the Tinaquillo lherzolite are more capable of producing 2DR6-1 by partial

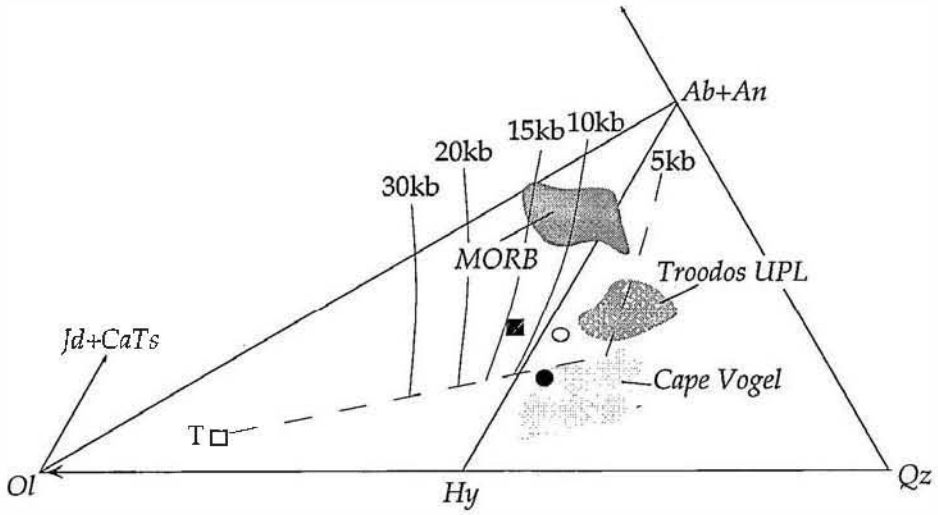

Figure 3.23. 2DR6-1 (closed cirlce) and DR15-1 (closed square) compositions plotted on a CIPW molecular normative projection from Di onto the base of the basalt tetrahedron jadeite plus Ca-tschermaks molecule (Jd + CaTs) - olivine (Ol) - quartz (Qtz). After Falloon et al. (1989). Hy = hypersthene; Ab = albite; An = anorthite. Open circle is the calculated parental magma composition to Troodos Group II and III Upper Pillow Lavas (Duncan and Green, 1987). Open square T is Tinaquillo lherzolite (Jaques and Green, 1980). See text for a more detailed explanation.

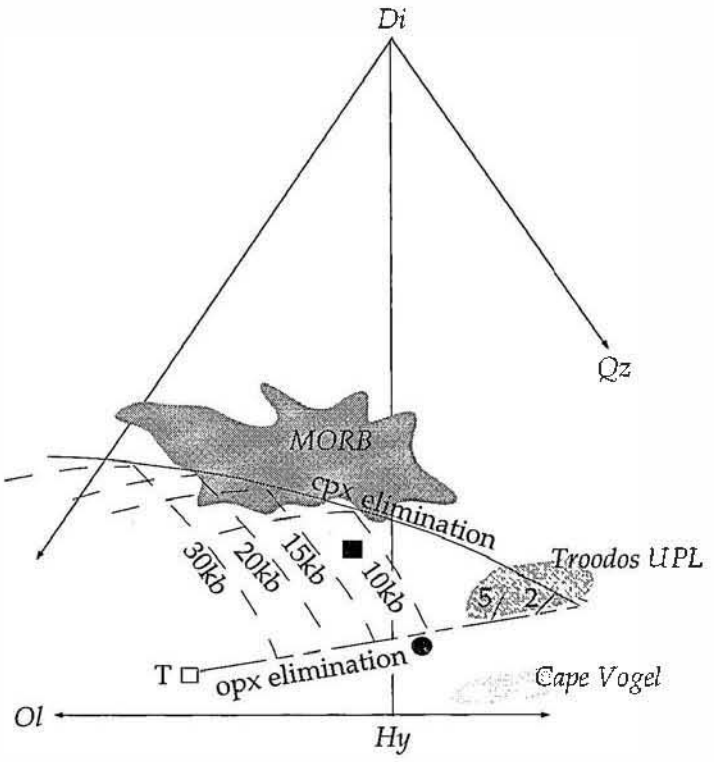

Figure 3.24. 2DR6-1 and DR15-1 compositions plotted on a CIPW normative projection from plagioclase onto the base of the basalt tetrahedron Di-Ol-Qz (after Falloon et al., 1989). Cotectic lines for a range of pressures are shown (Falloon et al., 1989) together with the representative compositional fields outlined in Figure 3.23 and the Tinaquillo lherzolite composition (open square T).

melting. The calculated parental composition for the more depleted (types II and III) Troodos Upper Pillow Lavas, studied experimentally by Duncan and Green (1987), is very similar to 2DR6-1. They determined that this composition segregated from depleted upper mantle peridotite at about 25km, 8kbar, 1360°C in the presence of 0.5-1% water, leaving a harzburgite residue. The hydrous nature of these magmas is confirmed by the presence in some samples of primary quenched amphibole (Cameron, 1985). The low-Ca boninites from Cape Vogel, Papua New Guinea (Jenner, 1981) plot at even lower Jd+CaTs than 2DR6-1, indicating that these unusual lavas require a significantly more refractory mantle source (Falloon et al., 1989). Potential primary magma DR15-1 may be derived from a source such as the Tinaquillo lherzolite at P<15kb, but only if the extent of partial melting was high enough to eliminate clinopyroxene. This is better shown in Figure 3.24.

The projection from plagioclase for the proposed primary liquid compositions is shown in Figure 3.24, together with the comparative suite compositional fields and the Tinaquillo lherzolite composition. This figure also shows the locus points marking clinopyroxene and orthopyroxene elimination for equilibrium melting at different pressures and the olivine-orthopyroxene-clinopyroxene and olivine-orthopyroxene equilibrium cotectics experimentally determined for the Tinaquillo lherzolite at different pressures (Falloon et al., 1989). 2DR6-1 lies just below the line of orthopyroxene elimination for the Tinaquillo lherzolite; therefore, as shown above, it may have been produced by melting of a source that is slightly more depleted than the Tinaquillo lherzolite composition. DR15-1 could have been generated from a source similar to the Tinaquillo lherzolite only if the degrees of melting had been sufficiently high to eliminate clinopyroxene. Alternatively, it may have been produced by lower degrees of partial melting of a source more depleted than the Tinaquillo lherzolite. Of particular importance however, is that the two primary magmas are not related by any partial melting trend, and probably were derived from sources characterised by different degrees of depletion.

The CaO/Al_2O_3 value provides a further constraint on the nature of the mantle sources of these proposed primary magmas. Peridotite melting experiments (Jaques and Green, 1980; Falloon and Green, 1988) show that for a given composition, increasing degrees of partial melting yield first melts with gradually increasing CaO/Al_2O_3, until the point of clinopyroxene elimination, after which this ratio decreases dramatically in subsequent partial melts. For 2DR6-1, the CaO/Al_2O_3 value is 0.91, and

for DR15-1 it is 1.13, both being higher than the CaO/Al_2O_3 of primitive MORB glasses (0.67-0.88) and notably higher than CaO/Al_2O_3 of clinoenstatite-bearing boninites from Cape Vogel (<0.66), the source for which was probably clinopyroxene-free (Crawford et al., 1989). This is consistent with the source for both DR15-1 and 2DR6-1 being more refractory than MORB sources, but still containing clinopyroxene.

The minor element and HFSE characteristics of suites I, II and III rocks also suggest a refractory mantle source, taking into account the effect of subsequent enriching events. Their low TiO_2, Y and HREE abundances compared to N-type MORB mantle (Figs. 3.20 & 3.21) and their relatively high Al_2O_3/TiO_2 (17-42) and CaO/TiO_2 (8-33) are also consistent with a mantle source more depleted than a MORB source mantle. Finally mineral chemical features also suggest a refractory mantle source for the Hunter Ridge parental magmas. The very magnesian olivine phenocrysts (up to Fo_{93}), and the particularly refractory Cr-spinels in these lavas ($Cr^{\#}$ averaging 80-85 (2DR6-1), 75-80 (DR8-2), and 70-85 (DR15-1), values significantly greater than those for MORB and BABB Cr-spinels, and at the high end of the range for island arc basalt chromites (Fig. 3.15; Dick and Bullen, 1984; Ballhaus, 1993), lend support to a strongly depleted mantle source for these lavas.

In summary, the CIPW molecular normative compositions, major and trace element chemistry, and near-liquidus mineral compositions of the primitive lavas from the Hunter Ridge, all suggest that the mantle sources of these lavas were more refractory than the sources to MORB, but not as refractory as low-Ca boninite sources. They may have been clinopyroxene-poor lherzolite and harzburgite (<5 % clinopyroxene by definition) residues following the extraction of BABB that formed the North Fiji Basin oceanic crust.

3.7.3 ENRICHED COMPONENT

The most striking feature of the trace element patterns in Figure 3.21 is the strong enrichment of LILE relative to the REE and HFSE that is apparent for all Hunter Ridge lava suites. The degree of LILE enrichment can be seen using the Th/Yb vs Ta/Yb diagram of Pearce (1982) (Fig. 3.25). The normalising factor used (Yb) is effective in largely eliminating variations due to partial melting and fractional crystallisation, while having minimal participation in the various enrichment processes. Any melt-related enrichment processes will affect Th and Ta equally because of their similar Kd's during mantle melting, and thus any mantle-derived magmas will lie in the 'mantle array' trend on Figure 3.25. The Hunter

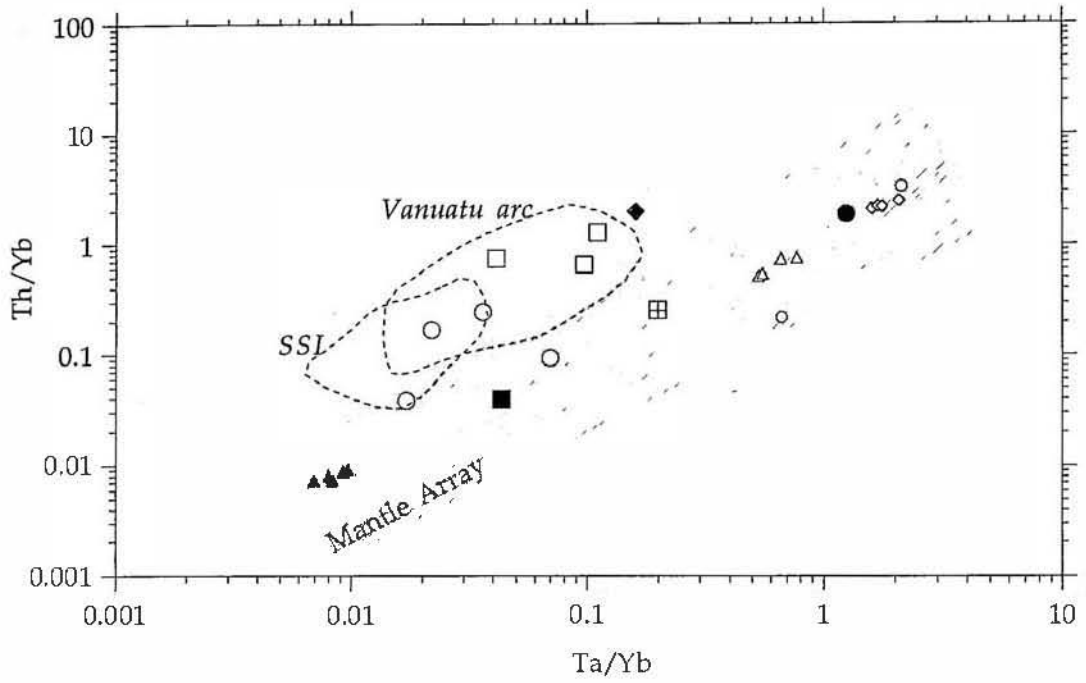

Figure 3.25. Th/Yb vs Ta/Yb for selected Hunter Ridge rocks. The shaded area represents the 'mantle array' extending from highly depleted MORB (closed triangles; McNeill and Danyushevsky, 1996), through N-MORB (closed square; Sun and McDonough, 1989) and E-MORB (square with cross; Sun and McDonough, 1989) to OIB (closed circle; Sun and McDonough, 1989). The SW Seamounts from the Juan de Fuca Ridge (open triangles; Cousens et al., 1995), Macquarie Island lavas (small open circles; Crawford et al. unpubl. data) and the Tuzo Wilson Volcanic Field (open diamonds; Allan et al., 1993) represent small degree melts of MORB source mantle. SSI = South Sandwich Islands and the Vanuatu arc are representative of intra-oceanic arcs. Data for the SSI from Pearce et al. (1995); Vanuatu arc from Crawford et al. unpubl. data. Symbols for the Hunter Ridge rocks as for Figure 3.17.

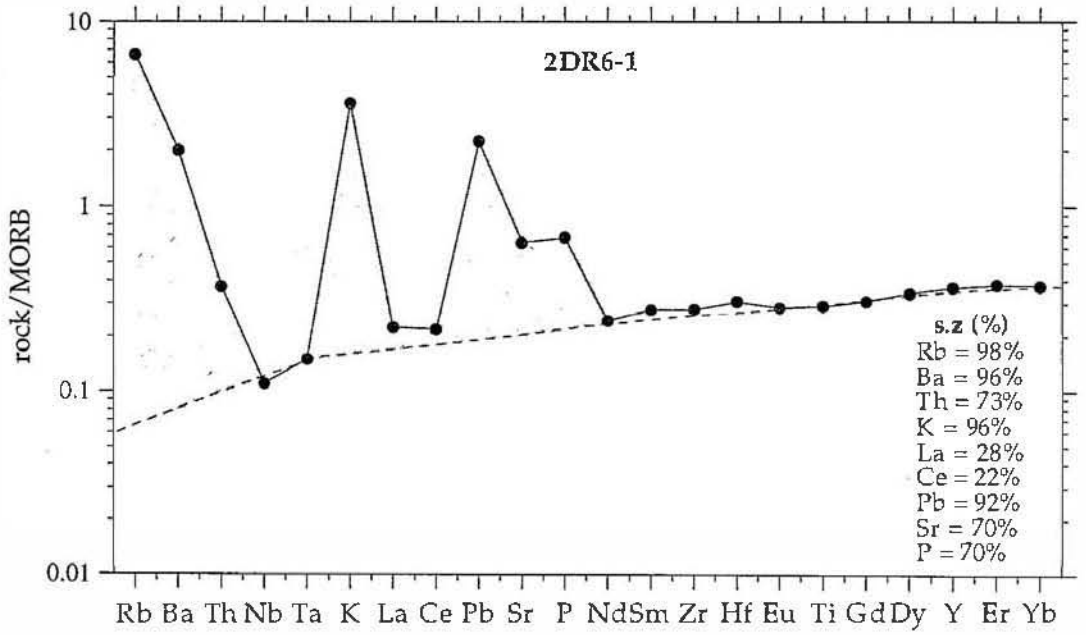

Figure 3.26. Geochemical pattern for sample 2DR6-1. Dashed line is drawn through the elements that are considered to be not accommodated in the subduction component (Ta, Nb, Zr, Hf, Ti, Y and Yb). The shaded area represents the subduction component. s.z (%) = percentage of the subduction component in 2DR6-1 for the elements listed. After Pearce (1983).

Ridge lavas, like those from the intra-oceanic South Sandwich and Vanuatu island arcs, are all displaced above this trend to higher Th/Yb, implying ingress of Th in the LILE-enriched hydrous fluids invoked in the petrogenesis of arc magmas. The enrichment in other incompatible elements is also evident from the N-MORB normalised patterns in Figure 3.21. Pearce (1983) proposed that an estimation of the slab-derived budget of LILE in primitive arc lavas may be made by drawing a line through the HFSE on a MORB-normalised diagram, and, assuming that Nb and Ta were not added from the slab, calculating directly the proportion of each LILE above its predicted abundance in the 'pre-metasomatised' mantle source. It is apparent, for example, for 2DR6-1 that the LILE owe a major proportion of their concentrations in the mantle wedge to an enriched component. Using Pearce's (1983) method, the calculated contribution of the subduction zone component to the elemental concentration of the source of 2DR6-1 is shown on Figure 3.26. It is likely, therefore, that more than three quarters of the observed K, Rb, Ba, and Pb and more than half of the Sr, P and Th have a slab origin. This enrichment in LILE has long been recognised as an important feature of subduction-related magmatism (e.g. Gill, 1981; Pearce, 1982; Pearce and Peate, 1995).

Two points of interest derive from the above treatment and the pertinent figures. First, the enrichment of P, also shown in a recent study by Pearce and Peate (1995) to be widespread in arc lavas, contrasts with its expected behaviour as a nominally HFSE-type element and its immobile nature during greenschist- to amphibolite facies metamorphic alteration of metabasic lavas. Although this is not investigated here, it suggests that high-temperature complexing of P may occur in slab-derived hydrous fluids, or alternatively, that a carbonatitic fluid may also take part in subduction zone metasomatism, as suggested by Wallace and Green (1988) and Falloon and Crawford (1991). Second, it was suggested above, and in Figure 3.26, that 92% of the Pb in sample 2DR6-1, for example, may derive ultimately from the subducted slab, and similar or slightly lower values may apply for the Suite II lavas. However, the clustering of the Hunter Ridge lavas (particularly Suite II) near the NHRL on the Pb isotope variation diagrams (Fig. 3.22) indicates that the added Pb had the isotopic characteristics of typical Pacific Ocean MORB, precluding any pelagic sediment involvement in the petrogenesis of these arc lavas.

The three Hunter Ridge lava suites have varying shaped chondrite normalised REE patterns (Fig. 3.20). Normalised heavy REE abundances in suite I samples are very similar and sub-parallel. Gross differences,

however exist between the samples with respect to their LREE abundances and patterns. It is not possible to account for the differences in the LREE abundances between the samples simply by varying the degree of melting of a single source given the similarity of their HREE abundances. Increasingly high degrees or repeated partial melting of a (MORB-depleted) peridotite source will result in progressively lower La/Sm, and a REE profile decreasing towards La. Thus, the kick in the REE pattern (La>Sm) displayed by most suite I samples except 2DR6-1, must imply that the LREE have been added to the source by some other mechanism. This is also shown on Figure 3.27, on which most Hunter Ridge lavas, like lavas from the South Sandwich and Vanuatu arcs (except 2DR6-1), plot above the mantle array, implying some addition of La relative to the similarly incompatible Ta. Suites II and III have stronger LREE enrichments compared to suite I. In general, addition of a LREE-enriched component, i.e. a hydrous metasomatic fluid, to the Hunter Ridge lavas provides a credible mechanism to account for their LILE and LREE abundances.

A notable trace element feature of suite II and III is their elevated Zr and Hf contents relative to Ti, Y, and the M-HREE (Sm to Yb). Figure 3.28 shows a plot of Zr/Yb vs Nb/Yb on which the suite I samples (and lavas from the South Sandwich and Vanuatu intra-oceanic arcs) lie on or very close to the mantle array. In contrast, suite II and III lavas plot significantly above the mantle array, and overlap with high-K andesitic lavas with adakitic affinities from Kadavu (see chapter 5 & 6), further north along the Hunter Ridge. A slab melt component, rather than simply hydrous slab-derived fluids, are implicated in the petrogenesis of the adakitic lavas from Kadavu. It is possible, therefore, that the Suite II and III lavas from the central Hunter Ridge may also have involved a slab melt component as a modifier of their refractory mantle sources prior to or during magma generation. However, the amount of slab melt involved in the Suite II and III lavas is probably less than invoked in the genesis of the Kadavu adakitic lavas, although this is difficult to quantify. Melting in this instance is more likely to have been in the amphibolite facies with no residual garnet, otherwise the intermediate and heavy REE would be strongly fractionated (Brophy and Marsh, 1986).

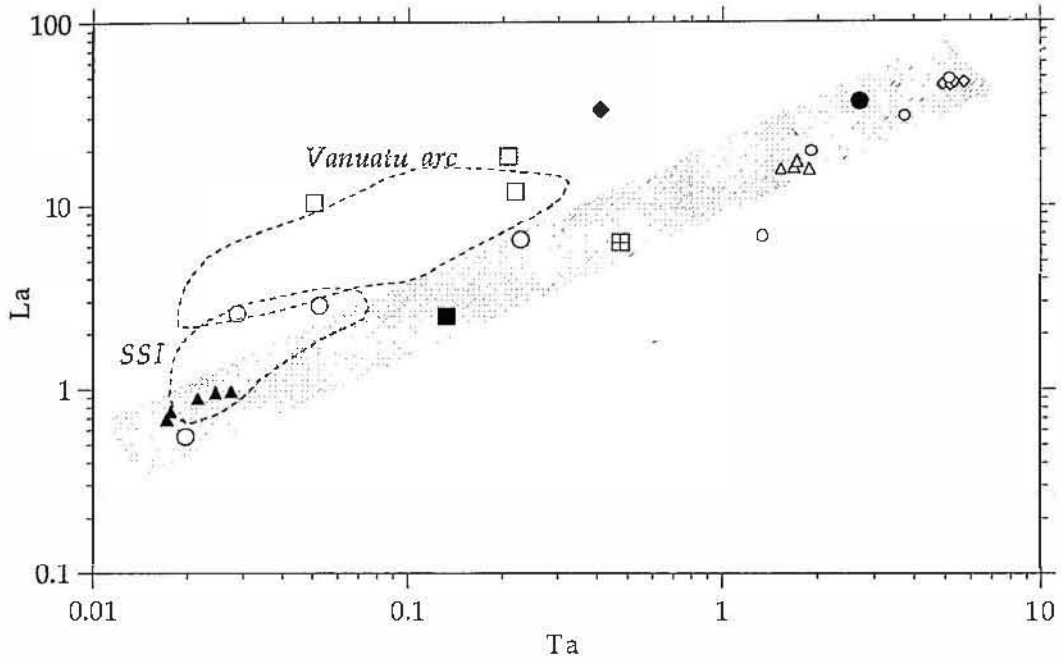

Figure 3.27. La vs Ta for selected Hunter Ridge rocks. Symbols and fields as for Figure 3.25.

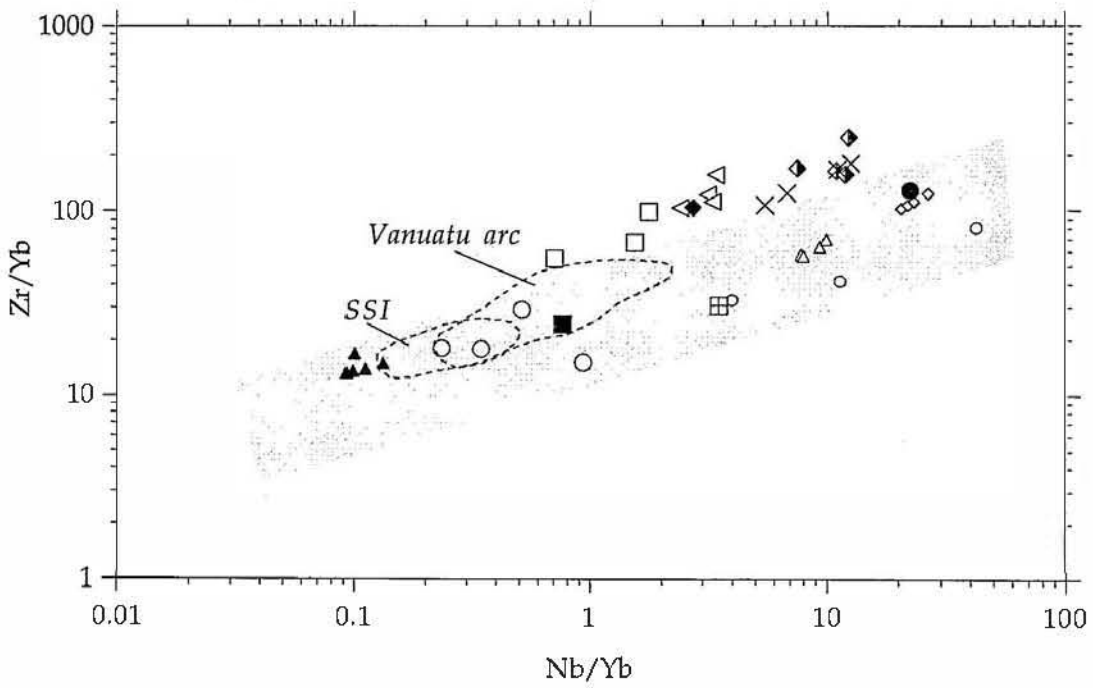

Figure 3.28. Nb/Yb vs Zr/Yb for selected Hunter Ridge rocks compared to the Ngaloa Group (half closed diamonds), Western Kadavu (crosses) and Central/ Eastern/Ono Group (large open triangles) lavas which are part of the Kadavu Island Group (see chapters 5 & 6). Symbols and fields as for Figure 3.25.

3.8 CONCLUSION

The Hunter Ridge, extending from the southern end of the Vanuatu arc in the southwest to the Kadavu Island group in the northeast, is a newly recognised intra-oceanic arc in the SW Pacific region, where the onset of north-directed subduction ~7Ma was triggered by initiation of an E-W oriented spreading ridge in the North Fiji Basin. After approximately 3Ma, subduction ceased due to establishment of a new N-S spreading system in the North Fiji Basin (Auzende et al., 1996).

The southern end of the Hunter Ridge including the islands of Matthew and Hunter and related seamounts based on available dredging information, appears to be constructed of rocks that vary from:
(1) high-Mg andesites where slab melt involvement seems likely (Crawford et al. 1993) at the southernmost end of the Hunter Ridge arc, to
(2) along the south central part of the Hunter Ridge primitive arc tholeiites, and high-Ca boninites compositionally transitional to the latter tholeiites were produced (Sigurdsson et al. 1993), in which the dominant metasomatic agent was hydrous fluids derived from the subducted slab. Subduction immediately beneath young hot backarc basin crust may be responsible for the boninite genesis (Crawford et al. 1989).
(3) this study shows that rocks recovered from the northern part of the Hunter Ridge comprise transitional boninitic basalts and andesites and calc-alkaline basaltic andesites to rhyolites. The presence of calc-alkaline lavas along the Hunter Ridge dispels the notion of calc-alkaline lavas being only a feature of mature arcs.

The mantle source prior to subduction along the northern part of the Hunter Ridge can be inferred from mineral chemistry, major and trace elements to be more refractory than the source to MORB, but less refractory than sources for low-Ca boninites. The trace element and isotopic data indicate two subduction components. One component contains only the most mobile elements (such as LILE), and has affected sources of suite I, II and III; this is conventionally interpreted as an aqueous fluid derived via dehydration of hydrated ocean crust, with little pelagic sediment involvement. The other contains both LILE and HFSE and affected only suite II and III. Lead isotope data indicate that pelagic sediments were not the source for this component and that it may have been the product of slab melting.

Chapter 4

ASTROLABE GROUP

The Shoshonitic Lavas

4.1 INTRODUCTION

Shoshonitic magmas have interested petrologists for many years, with most attention being directed at explaining both the difference between shoshonites and normal basaltic rocks, and between shoshonites and other types of K-rich volcanics, particularly as a function of their tectonic setting. The nature and importance of the source of K and related elements in K-rich magma genesis is the subject of continuing debate. Furthermore, the nature of the enriching process (encompassing both fluids and melts) and their timing is also not well understood.

The term shoshonite was first formalised by Iddings (1895), who recognised a range of rock types he called the absarokite-shoshonite-banakite series from the Absaroka volcanic field of Montana and Wyoming. Absarokites have abundant phenocrysts of olivine and augite, and lack phenocrystal feldspar, whereas shoshonites and banakites were defined as having progressively more feldspar and less mafic minerals. The term 'shoshonite association' was revived by Joplin (1968), who suggested that it be restricted to K-rich rocks showing some affinities with calc-alkaline rocks. Subsequent work on the geochemistry of island arc lavas (e.g. Gill, 1970; Jakes and White, 1972) distinguished the shoshonite association as the most potassic of typical island arc magmas. Jakes and White (1972) among others, stressed the gradational geochemical relationships between island arc tholeiites, calc-alkaline volcanics and shoshonites. Shoshonites were recognised as products of mature, well-developed island arcs, and Ewart and Bryan (1973) pointed out that they are mostly restricted to areas of thick crust.

More recently, Morrison (1980) defined the shoshonite association as consisting of near silica-saturated, K-rich suites with little Fe-enrichment and high contents of large ion lithophile elements (LILE). He emphasised that shoshonitic rocks show features common to both calc-alkaline (AFM trend; low ferromagnesian and HFSE abundances; high

Al_2O_3) and alkaline (total alkalis vs SiO_2; high LILE and LREE) magma types. He concluded that since shoshonitic rocks cannot be unambiguously classified as alkalic or calc-alkaline, they must be considered as a distinct rock association.

The shoshonitic rock association has been reported in a variety of settings in island arcs and continental arcs. High-K shoshonitic rocks are among the youngest eruptives in the Eolian arc (Barberi et al., 1973). In southern Peru and the Sunda Arc there is a zonation in erupted rock types away from the trench from tholeiitic to calc-alkaliine to shoshonitic (Whitford and Nicholls, 1976), and in Fiji the youngest rocks in the arc sequence are shoshonitic, succeeding tholeiitic and calc-alkaline lavas (Gill, 1970; Gill and Whelan, 1989a). Morrison (1980) suggested that in general, the arc shoshonitic suite is intimately associated with calc-alkaline volcanics, that the shoshonitic rocks occur above the deeper part of the Benioff zone, and that in supra-subduction zone areas without an obvious spatial zonation of magmatic suites, they are younger and associated with oblique convergence, possibly related to steepening of the Benioff Zone.

The LIL enrichments and other compositional characteristics of the Astrolabe group of Kadavu are very similar to those of the 'shoshonite rock association' as defined by Morrison (1980). Unlike many island arcs however, where shoshonites occur generally late in the eruptive sequence, the Astrolabe group are the oldest rocks (~3.4Ma, Whelan et al., 1985) within the Kadavu Island Group. In this chapter, rock nomenclature follows that outlined above in which absarokite denotes mafic basalt with little or no phenocrystal plagioclase, shoshonite denotes plagioclase-phyric, more evolved lava, and banakite denotes olivine-free, intermediate composition lava with biotite phenocrysts.

4.2 GEOLOGY

The Astrolabe Islands make up the northern extension of the Kadavu Island Group, and include, from south to north, the islets of Vurolevu, Yambu, Buliya, Yaukuvelailai, Yaukuvelevu, Qasimbale, Namara, Yanuyanu-I-Loma, Yanuyanu-I-Sau, Dravuni, Vanuakula and the Solo Lighthouse lying within the Great Astrolabe Reef (Figure 4.1).

Vurolevu and Yambu islets are composed of silicified volcanics, and have been considered to belong to the island of Ono (Woodrow, 1980). The islands from Buliya north to Namara are composed entirely of basalt flows and breccias, cut by a few dykes which generally strike

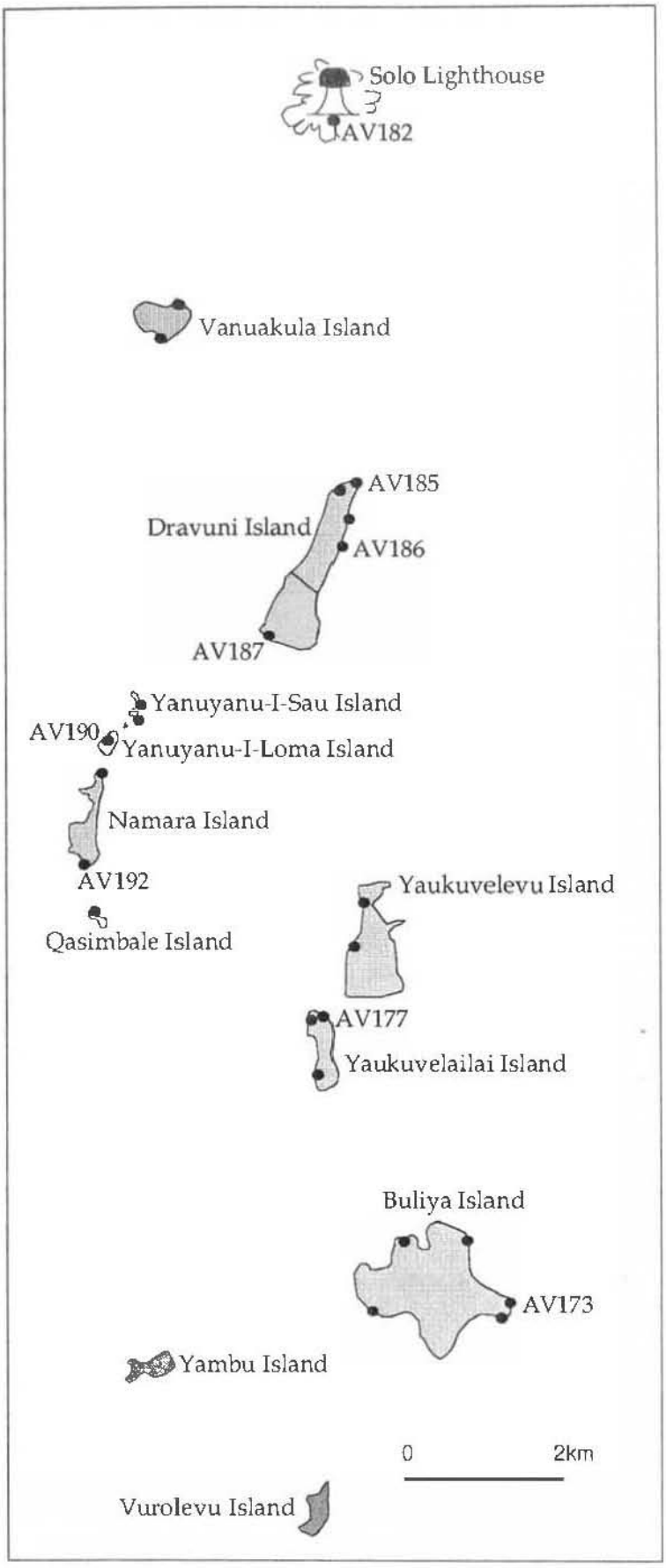

Figure 4.1: Simplified map of the Astrolabe Islands (after Woodrow, 1980). Black dots show location of samples. Numbered locations (eg AV173) were samples selected for detailed geochemical analysis. Dravuni island is composed of basaltic (green area) and andesitic (yellow area) flows and breccias. Vurolevu and Yambu islands consist of silicified volcanics.

northwest. Dravuni is also composed of basalt flows and breccias, but andesite lavas are also present. Columnar jointing is common in the lava flows on Dravuni. Solo (meaning 'rock' in the local dialect) is little more than a rock supporting a lighthouse.

Twenty four samples were collected from the Astrolabe Islands, from coherent lava outcrops (Figure 4.1). These were all examined petrographically, and eight representative samples were selected for XRF geochemical analysis. From these, four were selected for ICP-MS and radiogenic isotope analysis. Table 4.1 lists the geochemical analyses for the Astrolabe lavas.

4.3 PETROGRAPHY AND MINERAL CHEMISTRY

The absarokites of the Astrolabe Islands are dominated by clinopyroxene (10-15 modal%) and lesser olivine phenocrysts (5-10%), with abundant microphenocrysts of clinopyroxene and embayed Fe-Ti oxides (Plate 4.1). The shoshonites are characterised by an increase in modal plagioclase (Plate 4.2), so that the abundance of phenocrystal plagioclase (15%) can equal that of clinopyroxene, but these lavas have fewer olivine phenocrysts (~1%) than the absarokites. Plagioclase phenocrysts are euhedral, with some resorption textures. The most evolved lava, from Dravuni and the Solo lighthouse, are the banakites (Plate 4.3), in which the plagioclase phenocrysts (20%) exceed clinopyroxene (10%). Biotite (7%) and minor hornblende (~1%) phenocrysts are less abundant, and olivine is absent from these lavas. The groundmass in all lavas is generally dominated by plagioclase laths, anhedral K-feldspar, equant granular clinopyroxene, Ti-magnetite, and minor amounts of interstitial glass; the shoshonites contain occasional small crystals of groundmass olivine.

Clinopyroxene forms subhedral to euhedral phenocrysts up to 2mm long. In the absarokites it commonly occurs in glomerocrysts of 5 to 20 grains, sometimes with Ti-magnetite and plagioclase. Some phenocrysts show concentric and hour glass zoning. Absarokite clinopyroxene phenocrysts are diopsides (Fig. 4.2), whereas the shoshonites and banakite clinopyroxene phenocrysts range from diopside to salite, although the banakite clinopyroxene phenocrysts have a higher CaO content (>23%CaO) at comparable $Mg^{\#}$ than shoshonite clinopyroxene phenocrysts. The $Mg^{\#}$ values of clinopyroxene phenocrysts are high in the absarokites ($Mg^{\#}$=90-93), and shoshonite clinopyroxene phenocrysts extend to high $Mg^{\#}$ (up to 92), but have a larger range, from

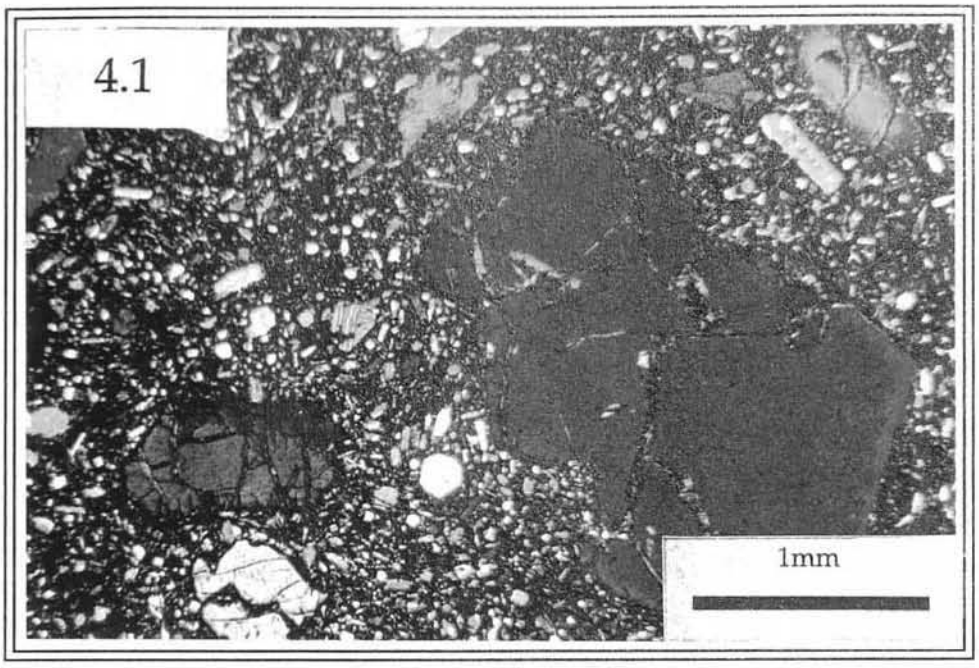
4.1
1mm

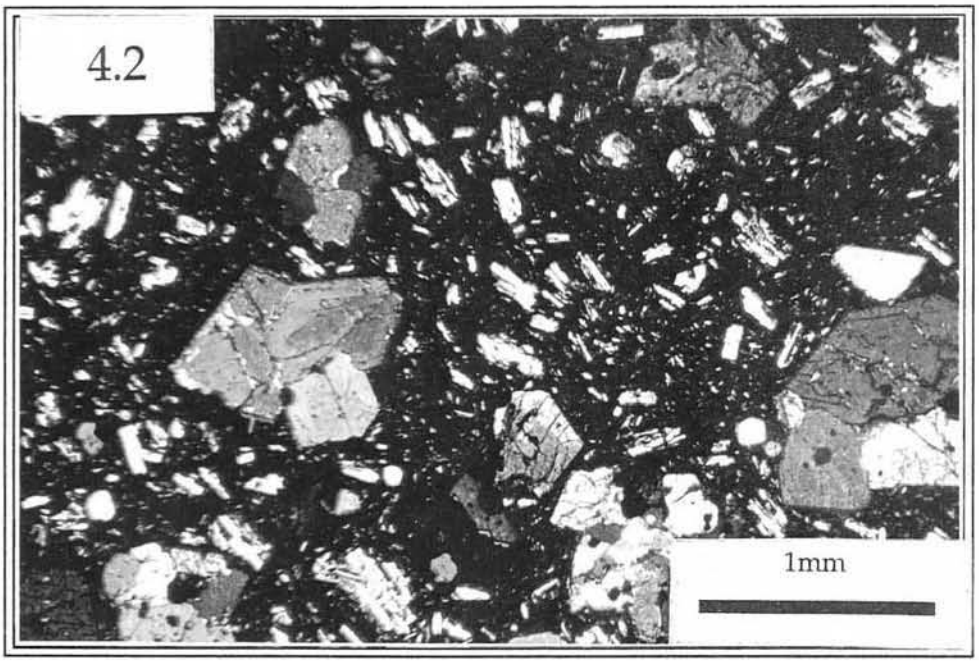
4.2
1mm

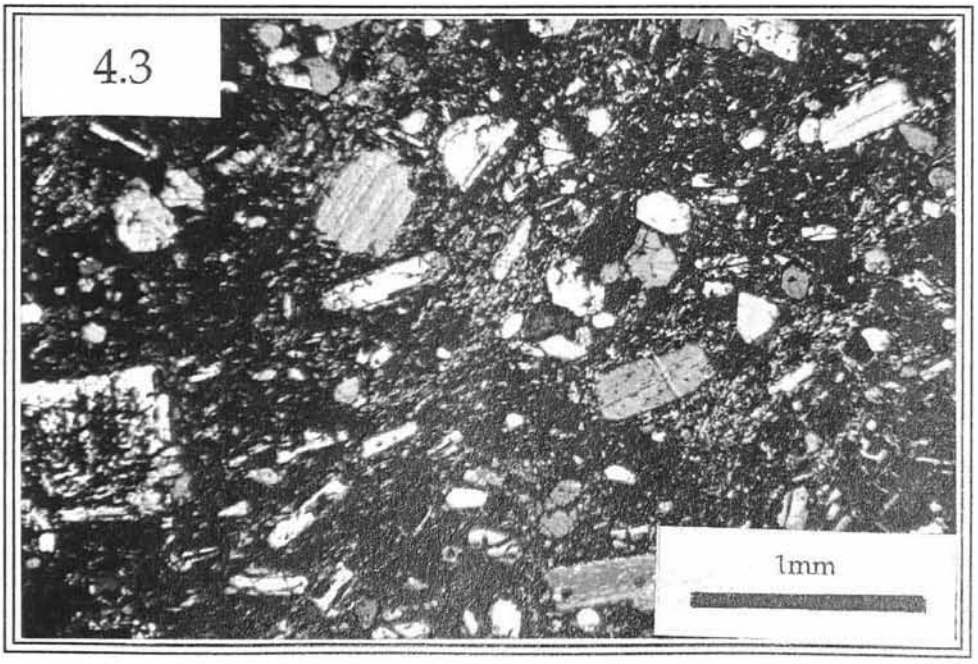
4.3
1mm

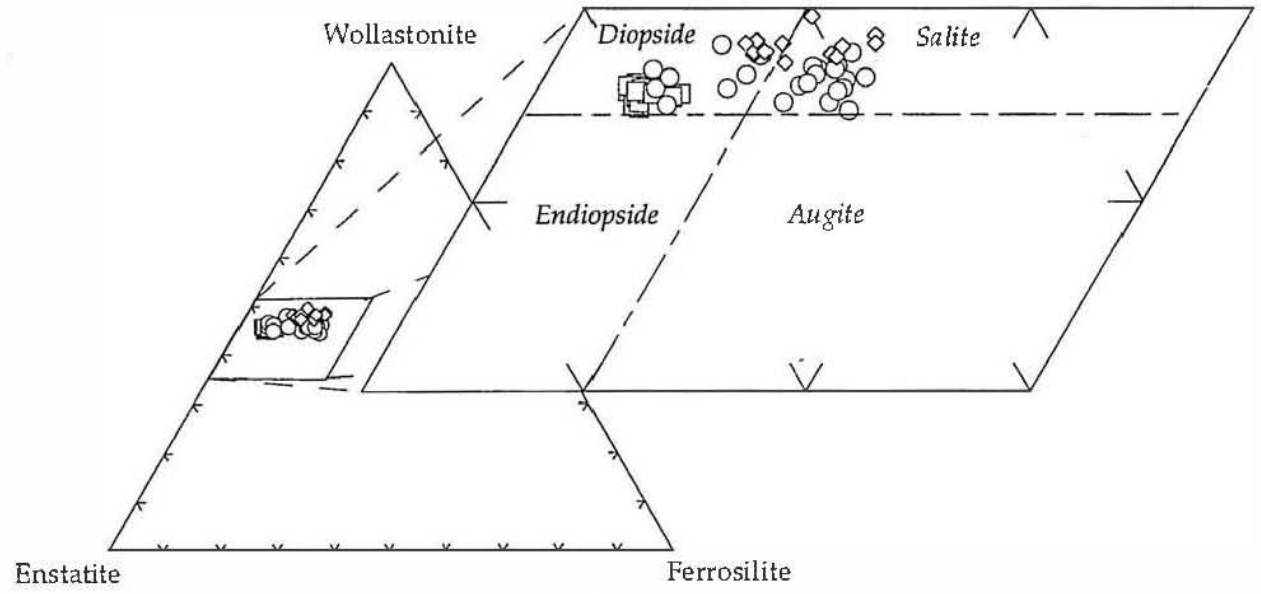

Figure 4.2. Clinopyroxene phenocryst core compositions from the Astrolabe Group. Squares = absarokite clinopyroxene phenocrysts, circles = shoshonite clinopyroxene phenocrysts, diamonds = banakite clinopyroxene phenocrysts.

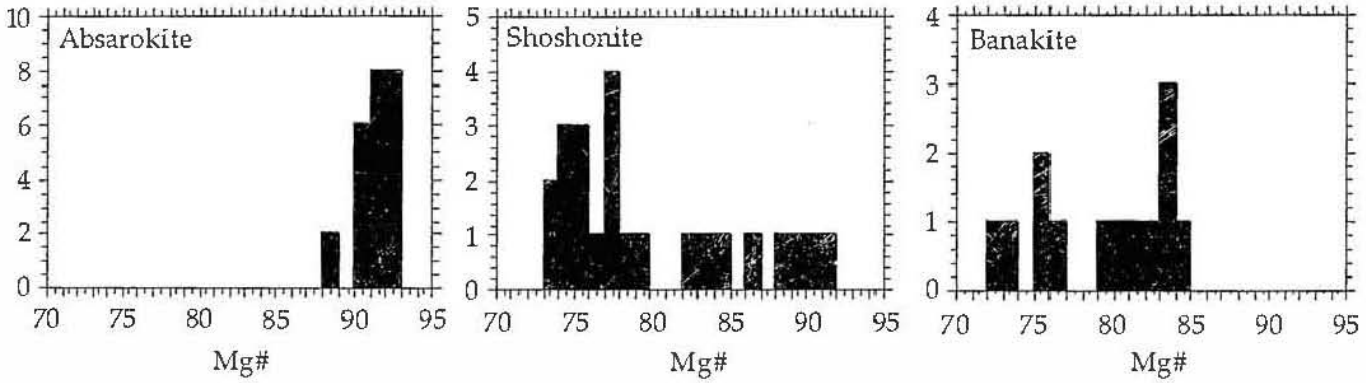

Figure 4.3. Histograms showing the range in Mg# in clinopyroxene phenocryst cores from the absarokites, shoshonites and banakites of the Astrolabe Group.

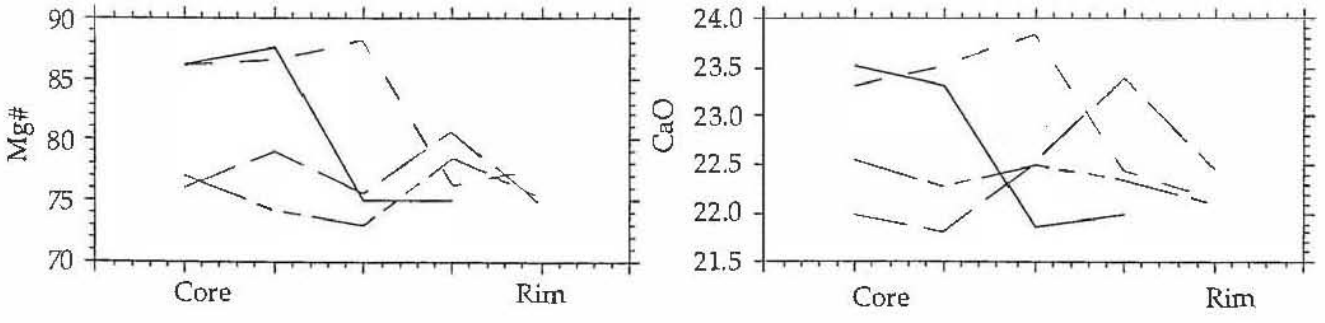

Figure 4.4. Variation of Mg# and CaO along a traverse line (core - rim) across clinopyroxene phenocrysts from the Astrolabe shoshonites

72 to 92 (Fig. 4.3). Banakite clinopyroxene phenocrysts range from $Mg^{\#}$=72 to 86. Optical zoning in the clinopyroxene phenocrysts (Fig. 4.4) generally is characterised by sharp, chemically discontinuous boundaries between adjacent zones. Crystals may zone outward either to more enriched Fe-rich or Mg-rich compositions from core to rim, but marked Fe enrichment only occurs close to crystal margins.

Minor elements in clinopyroxene phenocrysts show systematic variation with decreasing $Mg^{\#}$ from absarokites to shoshonites. Cr_2O_3 decreases with decreasing $Mg^{\#}$, whereas TiO_2 and Al_2O_3 increase (Fig. 4.5). Clinopyroxene phenocrysts from the banakites are characterised by lower TiO_2 and Al_2O_3 at similar $Mg^{\#}$ to shoshonite clinopyroxene phenocrysts. This may reflect relatively lower pressures of crystallisation, and/or co-crystallisation of the more evolved banakitic clinopyroxenes with Ti-magnetite and plagioclase; however, crystallographic studies have suggested that melt K/Na and Fe^{2+}/Fe^{3+} may also exert a significant effect on clinopyroxene compositions (Dal Negro et al., 1985).

Olivine occurs as euhedral phenocrysts and as subrounded partly resorbed and reacted 0.5-2mm grains in the absarokites, most being slightly oxidised and veined with iddingsite; olivine phenocrysts in the shoshonites are generally totally replaced by iddingsite. Olivines in the absarokites are unzoned and fall within a compositional range of Fo_{80-92}, although most lie between Fo_{89-91} (Fig. 4.6). MnO contents range from ~0.45-0.5% correlating negatively with Fo, whereas NiO (~0.05-0.22%) has a positive correlation with Fo (Fig. 4.7). The low Ni contents in olivines Fo_{90-92} are notable, and are typical of highly forsteritic olivines in arc ankaramites (Della Pasqua and Varne in press; A.J. Crawford, pers. comm. 1995). CaO in olivine shows little variation (0.27-0.36%) with Fo.

Cr-spinels occurring as inclusions in olivine phenocrysts have compositions of $Mg^{\#}$= 25-52, $Cr^{\#}$=81.0-86.6 and $Fe^{\#}$= 28.1-37.8. Most Cr-spinels show unusually high $Cr^{\#}$ values, even higher than for the refractory Cr-spinels in Hunter Ridge IAT (Fig 4.8), and they match Cr-spinels crystallised from magmas derived from refractory mantle sources, such as the Hunter Ridge boninites. Despite their higher $Cr^{\#}$ values, Astrolabe Cr-spinels have higher Fe^{3+} contents than Cr-spinels in Hunter Ridge IAT. Magma oxygen fugacity values for representative olivine - spinel pairs have been calculated using the equations of Ballhaus et al. (1991), Maurel and Maurel (1982) and Borisov and Shapkin (1990) which yield consistent fO_2 values ~QFM buffer.

Plagioclase is present as phenocrysts in the shoshonites and banakites as subhedral-euhedral laths generally ≤2mm, and is also present

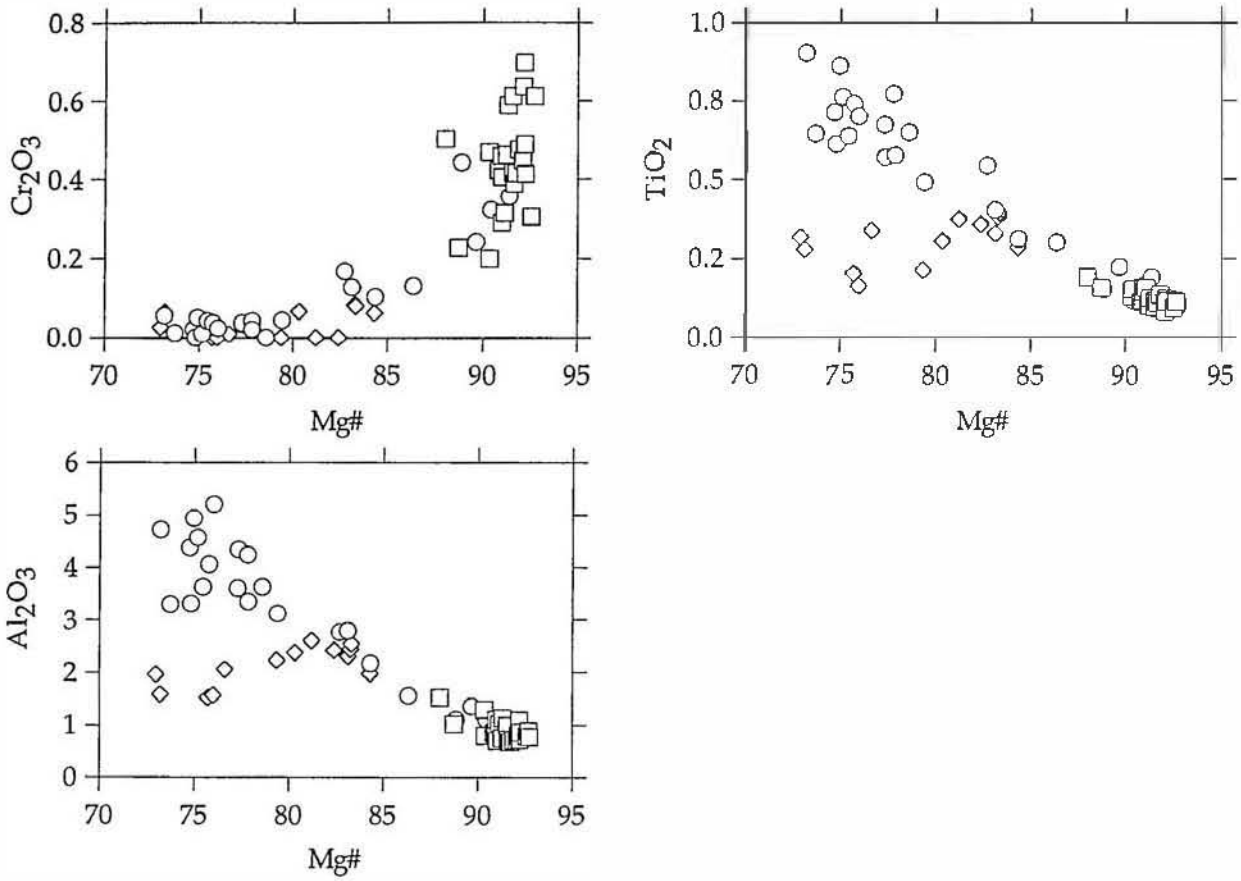

Figure 4.5. Variation of Cr_2O_3, TiO_2 and Al_2O_3 vs Mg# in clinopyroxene phenocryst cores from the Astrolabe absarokites (squares), shoshonites (circles) and banakites (diamonds).

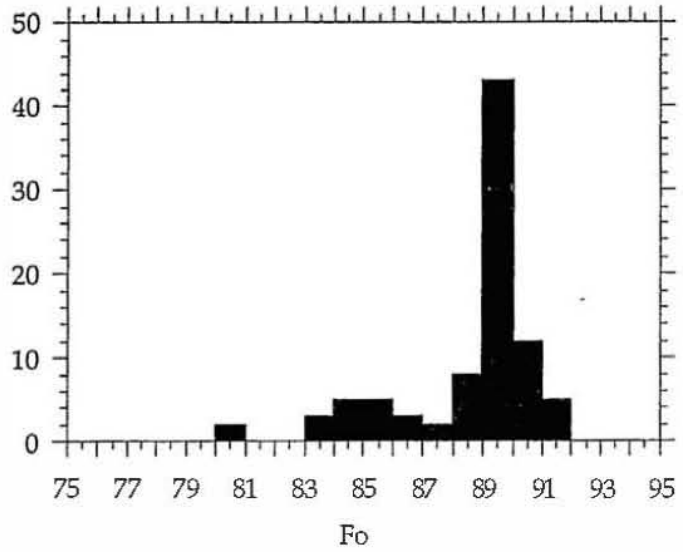

Figure 4.6. Histogram showing the range of Fo in olivine phenocryst cores in the absarokites from the Astrolabe Group.

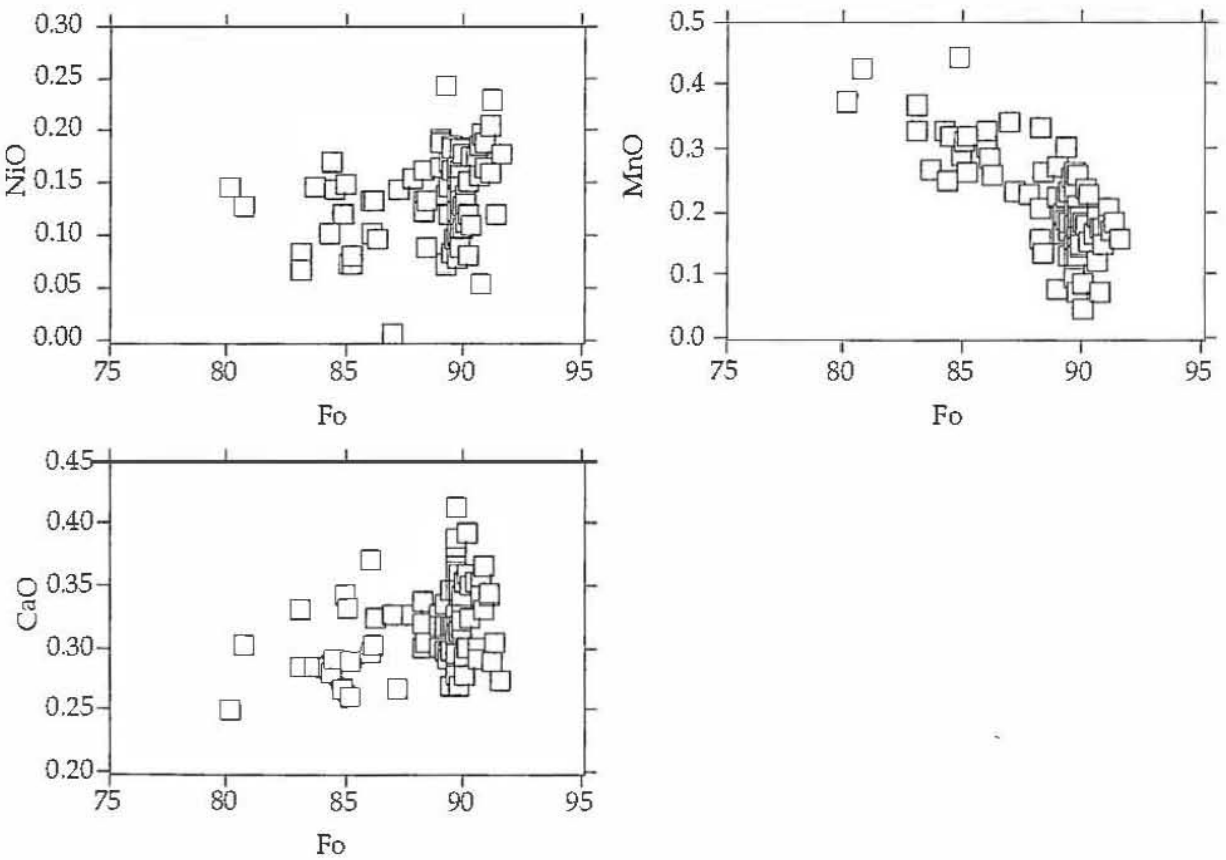

Figure 4.7. Variation of NiO, MnO and CaO vs Fo in olivine phencrysts in absarokites from the Astrolabe Group

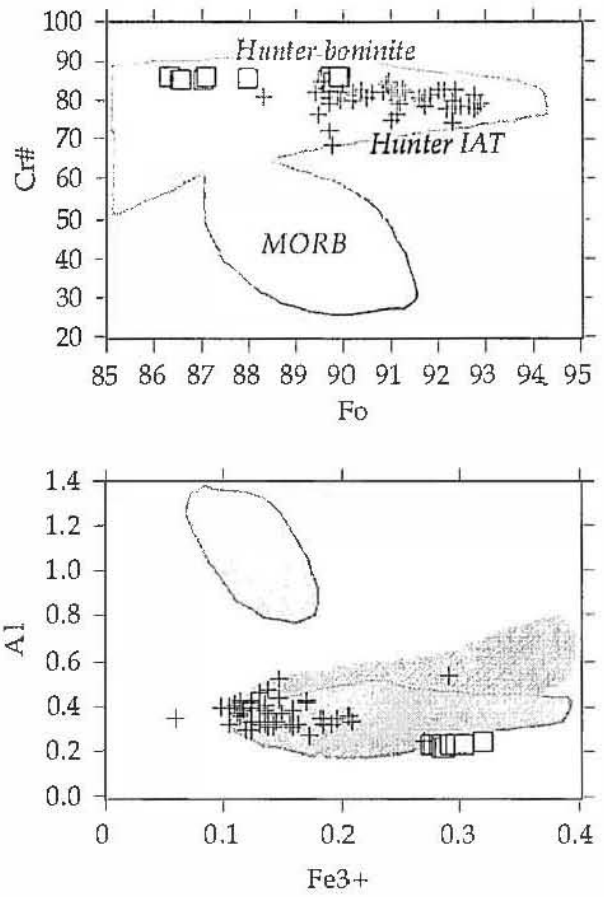

Figure 4.8. Composition of Cr-spinel inclusions in olivine phenocrysts from the absarokite lavas. Squares= absarokite spinel inclusions; crosses= spinel inclusions in olivine phenocrysts from the Hunter Ridge lavas (chapter 3). Hunter IAT and Hunter boninite fields represent data from Sigurdsson et al. (1993) and Sigurdsson (1994). Data for MORB from Sobolev et al. (1989), Dmitriev et al. (1991) and McNeill and Danyushevsky (1996).

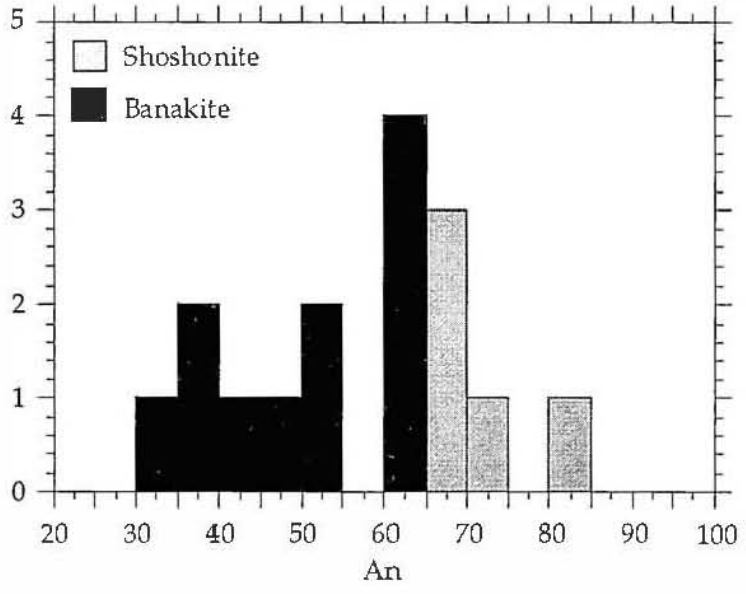

Figure 4.9. Histogram showing the range in Anorthite content in plagioclase phenocryst cores from the shoshonites and banakites from the Astrolabe Group

in the groundmass of all lavas. The compositional range of plagioclase phenocryst cores in the shoshonites is An_{65-85} and those in the banakites extend to lower An contents (An_{30-65}) (Fig. 4.9).

4.4 GEOCHEMISTRY OF THE ASTROLABE LAVAS

4.4.1 MAJOR AND TRACE ELEMENT GEOCHEMISTRY

Major and trace element compositions of the Astrolabe Group are shown on variation diagrams in Figure 4.10 and 4.11. For comparison, trends are also shown for the shoshonites from the Tavua Caldera in Fiji (Rogers and Setterfield, 1994). The Tavua shield volcano in north central Viti Levu is the largest, most mineralised, and therefore the best studied example of shoshonitic volcanism in Fiji, and is representative of the widespread shoshonites of Viti Levu (Fiji) which are of similar age (~3.4Ma) to the Astrolabe shoshonites (Whelan et al., 1985; Gill and Whelan, 1989a; Rogers and Setterfield, 1994).

For the absarokite -> shoshonite -> banakite fractionation series, the increase in SiO_2 is accompanied by enrichment in Al_2O_3, Na_2O and K_2O and depletion in MgO, FeO and CaO. Both TiO_2 and P_2O_5 show a well defined change in slope at approximately 51% SiO_2. The K_2O enrichment is accompanied by enrichment of other LILE, including Rb (33-101ppm), and Ba (334-777ppm). Sr also shows a significant increase (838-2092ppm).

The analysed Astrolabe lavas plot within or very close to the Tavua shoshonitic suite for all major and trace elements, and both suites show significant separation in compositional space between those lavas with <6-7% MgO, and those with >8 % MgO. Rogers and Setterfield (1994) suggested that the Tavua absarokites represent ~30% accumulation of a 2:1 mixture of clinopyroxene and olivine in a shoshonitic magma. It is unlikely that the Astrolabe absarokites represent liquid compositions, since they contain up to 30% phenocrysts. No attempt has been made to model the crystallisation sequence linking the Astrolabe absarokites, shoshonites and banakites, for the following reasons:

1: It was not possible to determine groundmass (liquid) compositions for any Astrolabe lava.
2: Significant compositional differences exist between individual Astrolabe samples at a given MgO; for example, at 4.5-6% MgO, samples AV190 and 192 from the westernmost Astrolabe Islands (Fig. 4.1) have 0.97-1.05% TiO_2, compared with ~0.6-0.8% inferred from Fig. 4.10 for samples from the Astrolabe islets further to the east.

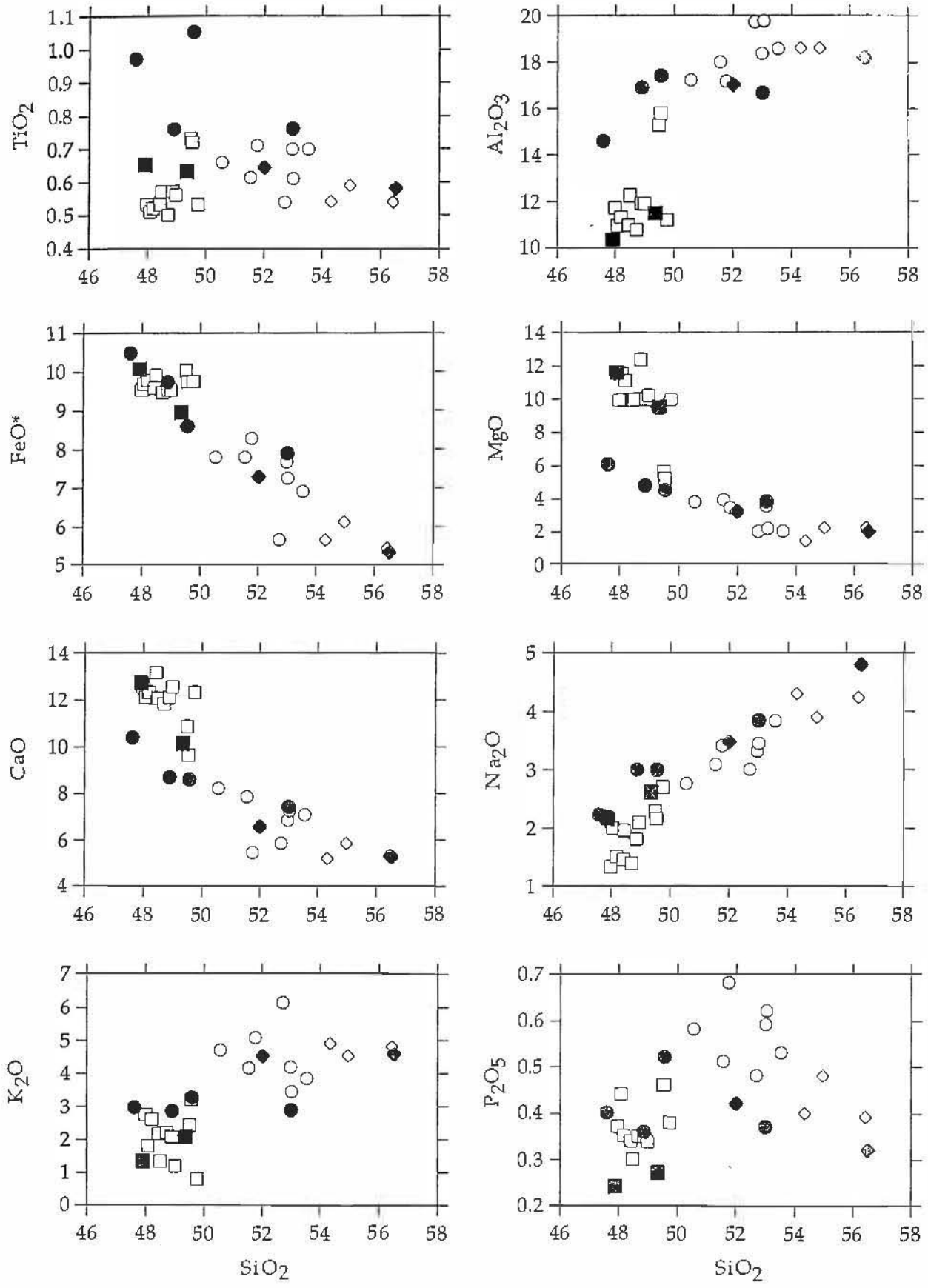

Figure 4.10. Major element covariation diagrams for the Astrolabe lavas (filled symbols) compared to the Tavua lavas (open symbols; Rogers and Setterfield, 1994). Squares = absarokites, circles = shoshonites and diamonds = banakites.

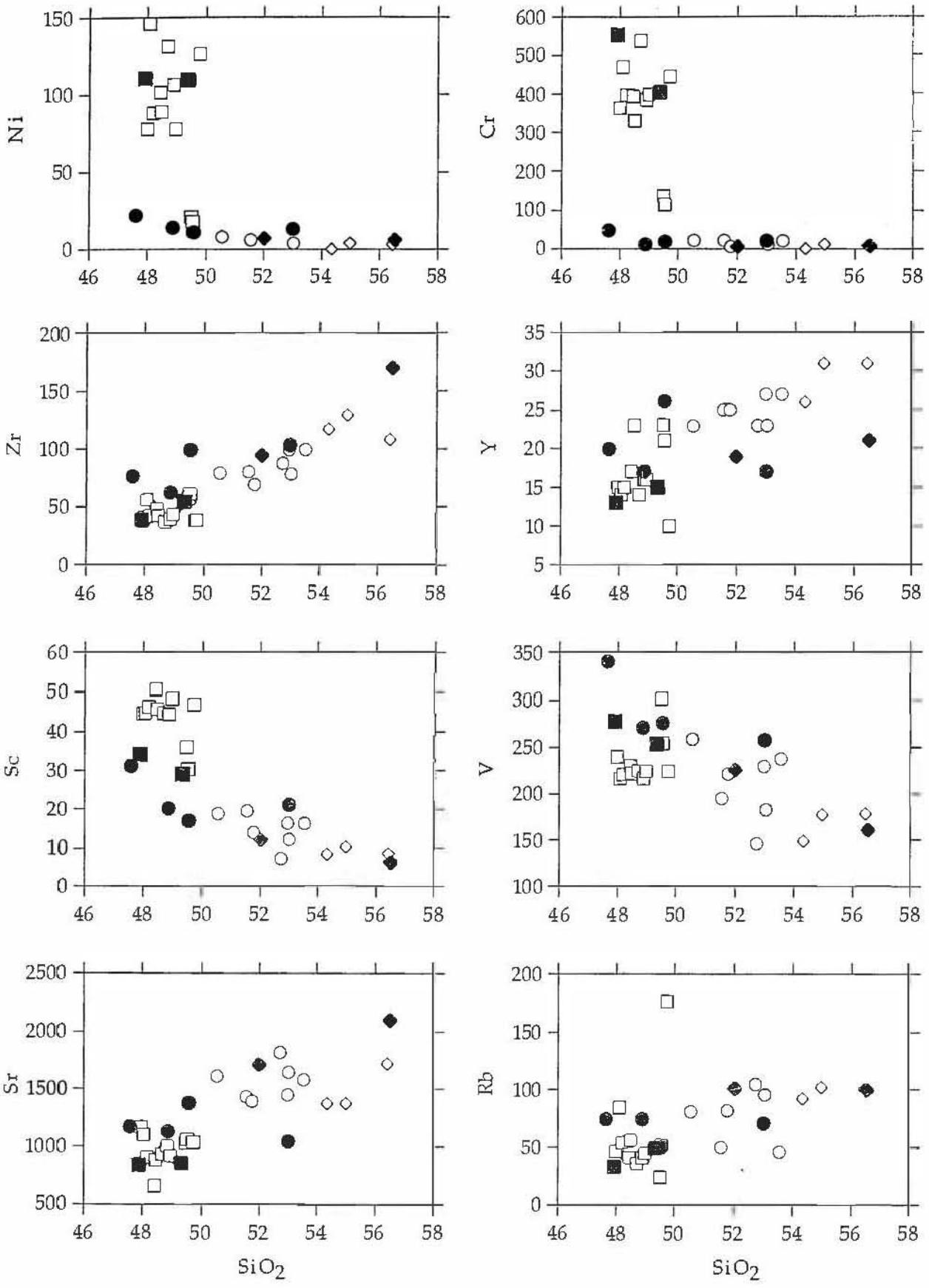

Figure 4.11. Trace element covariation diagrams for the Astrolabe lavas compared to the Tavua lavas. Symbols as in Figure 4.10.

3: Element ratios such as Zr/Nb and La/Yb, normally unfractionated during olivine+clinopyroxene+plagioclase-dominated fractionation, show significant variation for the Astrolabe (and Tavua) suites.

Therefore, individual analysed Astrolabe samples are unlikely to be directly comagmatic with other analysed Astrolabe shoshonitic lavas. The subdued but significant compositional differences probably reflect slight variations in parental magmas, and mixing in subvolcanic magma chambers, the latter for example, being reflected in the occasional high-Mg absarokitic clinopyroxenes occurring in Astrolabe shoshonites. However, the general coherence of compositional features, including isotopic signatures, plus the similarity with the Tavua absarokite-shoshonite-banakite suite, all argue that the Astrolabe lavas may be classed as a shoshonitic suite, linked by a similar mantle source, melting processes and broad fractionation scheme.

In the interval 47 to 49% SiO_2, clinopyroxene + olivine ± minor chromite are the only fractionating phases. Ni concentrations within the Astrolabe lavas range from 6-110ppm. The unusually low Ni concentrations (~100 ppm) for lavas with 9-12% MgO are reflected in the low-Ni highly forsteritic olivines. In contrast, Cr contents in the high MgO lavas are >400ppm (403-552ppm Cr). High Cr relative to Ni is consistent with accumulation of clinopyroxene, and is supported by the broadly decreasing Sc concentrations with increasing SiO_2. V shows a similar trend to FeO* and TiO_2.

At approximately 51% SiO_2, Ti-magnetite started to crystallise, causing the contents of TiO_2 and less strikingly, FeO and V, to decrease. The continuous increase in Al_2O_3 contents with increasing SiO_2 indicates that plagioclase is not an important fractionating phase within the Astrolabe Group lavas, although its modal abundance in the shoshonite and banakite lavas suggests that it crystallised, but was not removed from the evolving magmas. This may be due to the small difference in density of melt and plagioclase (0.05-0.1 g/cm^3; Drake and Weill, 1975), and is supported by the observations that Sr increases with increasing SiO_2, and the normalised REE diagrams lack Eu anomalies.

Although it is not obvious petrographically, apatite starts to fractionate at around 51% SiO_2, causing a reduction in the P_2O_5 content and also effecting the REE abundances. The partitioning of REE between apatite and silicate melts varies systematically with atomic number, the middle REE (Sm, Eu, Gd) being more easily accommodated than either the light or the heavy elements (Irving, 1978; Watson and Green, 1981). Consequently when apatite starts fractionating at ~51% SiO_2, the middle

REE tend to be extracted from the melt at a greater rate than the other elements, thereby increasing La/Sm and also leading to a distinct jump observed in the REE profiles between Sm and Nd in the more evolved lavas (AV182b and AV187).

Fractionation from shoshonite to banakite produced stronger enrichment of Ta, Nb and LREE than of the K-group elements of similar incompatibility, probably reflecting separation of hornblende and/or biotite. However, Nb/Ta values are little changed during the fractionation from absarokite (17.8) to banakite (16.6-18.0).

Chondrite-normalised REE diagrams for the more mafic Astrolabe lavas (Fig. 4.12a) are characterised by moderate LREE enrichment (La/Yb_N = 3-5). Heavy REE patterns are flat, precluding garnet involvement as a significant residual phase in the petrogenesis of this suite. The more evolved shoshonitic and banakitic lavas from the Astrolabe Group show steeper (more fractionated) REE patterns, with higher $(La/Yb)_N$ values (to 12.2), yet retain flat HREE patterns, and show no enrichment of HREE during fractionation from shoshonite to banakite..

N-MORB-normalised multi-element diagrams for the Astrolabe lavas (Fig. 4.12b) have geochemical features common to subduction-related magmas in general, although they attain a more extreme expression of these features than do K-poor arc basalts. The K-group elements, and Pb and Sr, show anomalous enrichment relative to adjacent REE, whereas Ta and Nb show characteristic subduction-related negative anomalies. Contents of Nb, Ta and the HREE and HFSE in the absarokites are less than those of N-MORB.

The REE and multi-element patterns for the Astrolabe lavas, particularly for the absarokites, are essentially identical to those of the Tavua lavas of similar MgO, implying very similar mantle sources and petrogenetic processes in the evolution of both suites.

4.4.2 RADIOGENIC ISOTOPE CHEMISTRY

Isotopic ratios of Sr, Nd and Pb in the Astrolabe suite lavas are shown in conventional isotope diagrams in Figure 4.13 relative to other Fijian lavas of the different magmatic stages described in chapter 2, the field for Pacific MORB, NFB and the Vanuatu arc. The $^{87}Sr/^{86}Sr$ and $^{143}Nd/^{144}Nd$ values show minimal variation, ranging from 0.70405 - 0.70412 and 0.51296 - 0.51298 respectively, and overlap those of other lavas of the early rifting stage which include the Tavua lavas, although the latter extend to lower $^{87}Sr/^{86}Sr$ (to 0.7035). The Astrolabe lavas and early

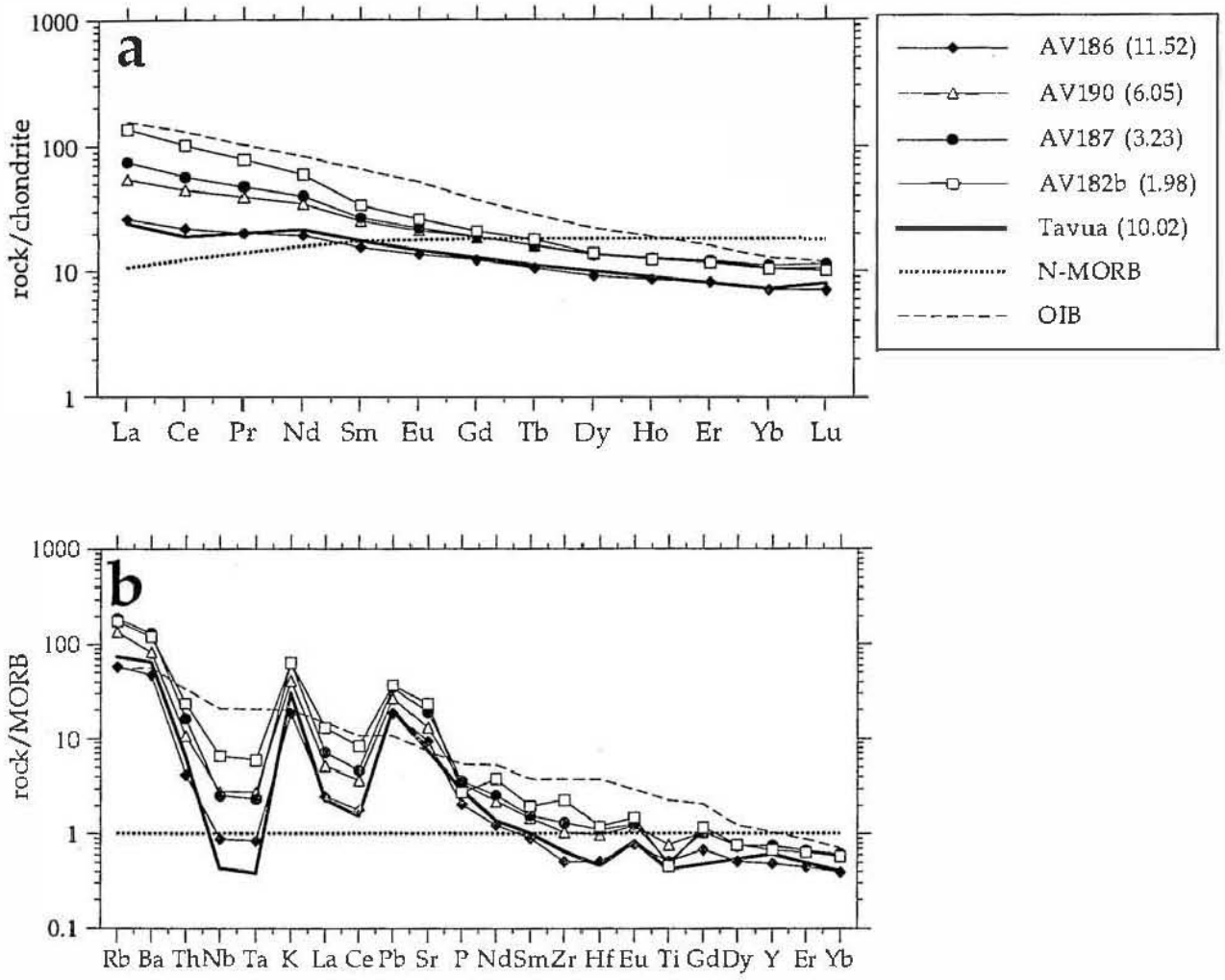

Figure 4.12 **a.** REE concentrations for the Astrolabe lavas normalised to chondrite. MgO content for each sample in brackets. OIB and N-MORB compositions and normalising values from Sun and McDonough (1989). Tavua absarokite composition from Rogers and Setterfield (1994). **b.** N-MORB normalised multi-element diagrams for the Astrolabe lavas.

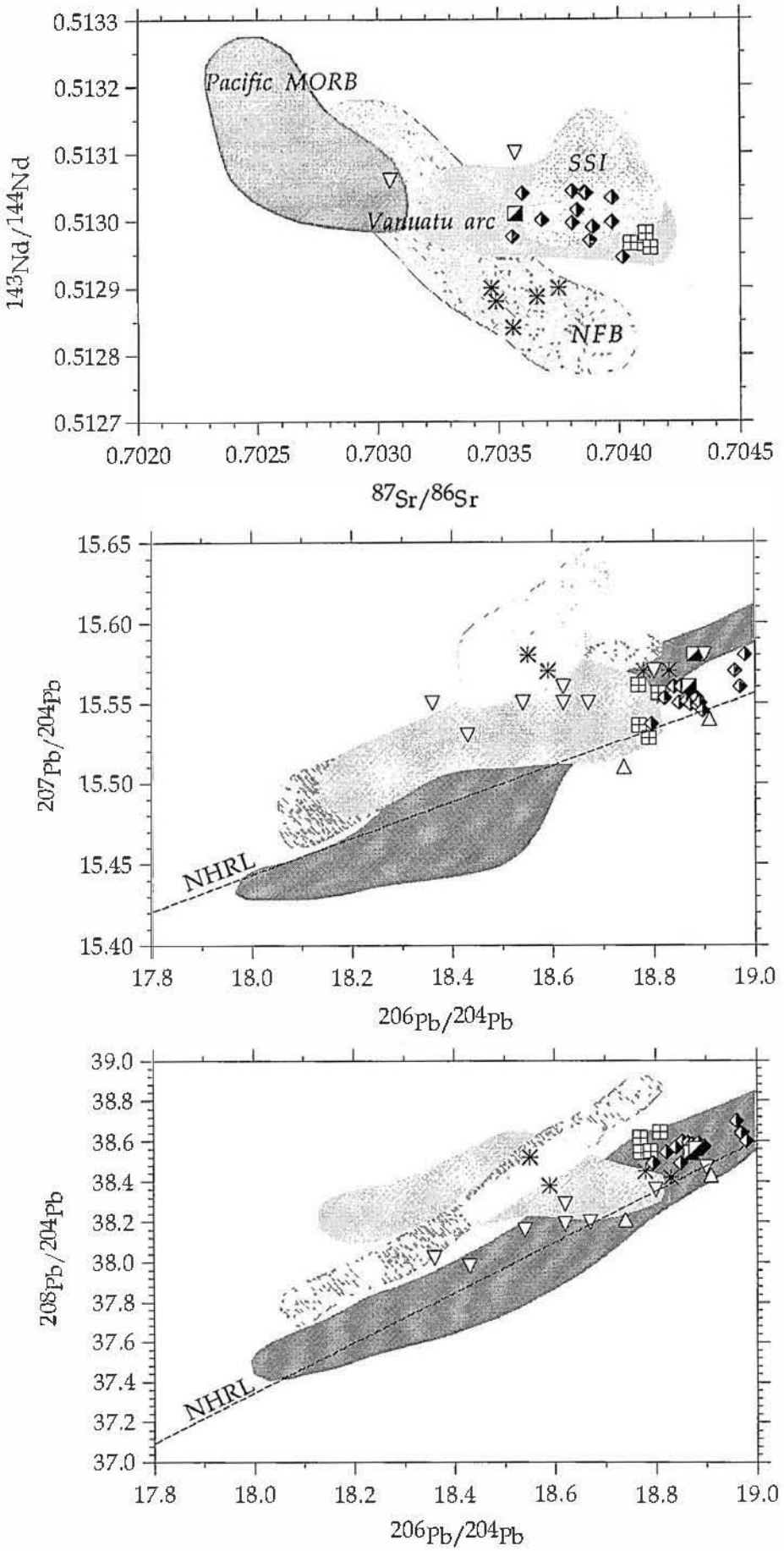

Figure 4.13. Sr vs Nd and Pb isotopic compositions for the Astrolabe lavas (squares with crosses) shown relative to fields for Pacific MORB, the North Fiji Basin (NFB) BABB, South Sandwich arc tholeiites (SSI) and the Vanuatu arc basalts. Also plotted for comparison are the isotopic data representing the different magmatic stages during the evolution of Fiji. Upside down open triangles = early arc stage; half filled squares = mature arc stage; half filled diamonds = early rifting stage including the Tavua lavas; asterisks = late rifting stage (Fijian OIB). The limited Pb isotope data for the South Fiji Basin are represented by the open upright triangles. Data sources for Pacific MORB, NFB, SSI and the Vanuatu arc are listed in Figure 3.22. Data sources for the different magmatic stages in Fiji are listed in Table 2.1.

rifting stage shoshonitic suites plot at notably higher $^{143}Nd/^{144}Nd$ than Fijian OIB of Gill's (1987) 'late rifting stage'.

Pb isotopic values of the Astrolabe lavas are also almost identical to those for Gill and Whelan's (1989a) early rifting stage lavas, show very little variation, and plot just above NHRL of Hart (1984) and at the more radiogenic end of the Pacific MORB field. For both $^{207}Pb/^{204}Pb$ and $^{208}Pb/^{204}Pb$ plotted against $^{206}Pb/^{204}Pb$, the Fijian shoshonites (early rifting stage) plot at more radiogenic values compared to typical lavas from all other magmatic stages in Fiji. The more ^{206}Pb-rich Fijian OIB have similar Pb isotopic compositions to the Fijian shoshonites, but other Fijian OIB extend down to $^{206}Pb/^{204}Pb = 18.55$. Rogers and Setterfield (1994) showed that if subducted pelagic sediment was involved in the petrogenesis of the Tavua shoshonites, its contribution was <4%, and petrogenetic scenarios totally excluding subducted sediment are equally valid.

4.5 DISCUSSION

4.5.1 INTRODUCTION

The Astrolabe and Tavua shoshonite suite lavas are high-K, high-LILE basaltic to basaltic andesite compositions with Nb-Ta depletion, high $^{143}Nd/^{144}Nd$, slightly elevated $^{87}Sr/^{86}Sr$ relative to N-MORB, and Pb isotopic compositions falling close to the more radiogenic end of the Pacific MORB spectrum, and only slightly above the NHRL. The strong geochemical similarities between the Astrolabe and Tavua shoshonitic suites suggest that these suites, despite being erupted at least 200 km apart, were derived from similar source regions. In this perspective therefore, the magmatic evolution of the Astrolabe lavas are likely to have been governed by petrogenetic processes similar to those for other shoshonitic lavas in Fiji.

The geochemical and petrological evidence presented above is used in the following section to evaluate more closely the petrogenesis of the Fijian shoshonites, and to attempt to put some constraints on the nature of the components involved, including the mantle wedge and the metasomatic fluid/melt responsible for the high-K composition.

4.5.2 NATURE OF THE MANTLE WEDGE

Three lines of evidence suggest that the source peridotite of the Astrolabe shoshonites was particularly refractory, and had been depleted in basaltic component during prior melting events.

(i) Cr-spinel compositions in these lavas, with $Cr^{\#}$~85, indicate a particularly refractory source for the Astrolabe lavas, even more depleted than the source of the Hunter Ridge arc tholeiites, and matching values for high-Ca boninites from the Hunter Ridge and North Tongan forearc,
(ii) the low HREE and Zr, Y levels (only 0.4-0.6 N-MORB levels; Fig. 4.12b) in Astrolabe lavas yet relatively flat HREE patterns (Fig. 4.12a) also demand a mantle source that was significantly more depleted than the source of N-MORB basalts, and
(iii) the unusually high CaO/Al_2O_3 values of the Fijian absarokites (0.88-1.1) also match those of high-Ca boninites (Crawford et al., 1989) and argue for a refractory source (Crawford et al., 1989). Although it could be argued that these high CaO/Al_2O_3 values reflect clinopyroxene accumulation, two lines of evidence rule against this possibility. First, taking as a typical depleted primary magma, an average primitive MORB with CaO/Al_2O_3 = 0.70, and adding to this the average 10 modal% of clinopyroxene phenocrysts present in the Astrolabe absarokites only increases CaO/Al_2O_3 to around 0.83, still significantly lower than the analysed Astrolabe absarokite values (0.88-1.2), or the range of values for Tavua absarokites (1.0-1.2). Second, Della Pasqua and Varne (in press) have recently shown that for three different arc ankaramite suites which have CaO/Al_2O_3 >0.9, melt inclusions that were trapped in primitive olivines (>Fo_{91}) from these clinopyroxene-rich lavas before the appearance of clinopyroxene as a crystallising phase, still have very high CaO/Al_2O_3, mainly >0.9, indicating that these high wholerock CaO/Al_2O_3 values are not due to clinopyroxene accumulation. It is concluded that the high CaO/Al_2O_3 values of the Astrolabe shoshonitic suite are features of the primary magmas of this suite, and indicate a refractory source.

As in Chapter 3, a mantle array is defined for various HFSE/Yb plots, extending from highly depleted MORB (D-MORB), through N-MORB and E-MORB to OIB and very low-degree melts of MORB source mantle. For a broadly MORB source mantle, extent of partial melting can also slide a magma composition along the mantle array, from high HFSE/Yb for very low degree melts (e.g. Tuzo Wilson alkaline volcanics, Allan et al. 1993), to low values for high degree partial melts. Also shown on such plots are several well-studied arc-related suites, for which the South Sandwich Islands arc tholeiites represent a strongly depleted source, southern Vanuatu arc a broadly N-MORB source, and Santorini lavas an E-MORB source.

In the Nb/Yb vs Zr/Yb plot (Fig 4.14), and also in the Ta/Yb vs Ta plot (Fig. 4.15) used by Rogers and Setterfield (1994), lavas from the

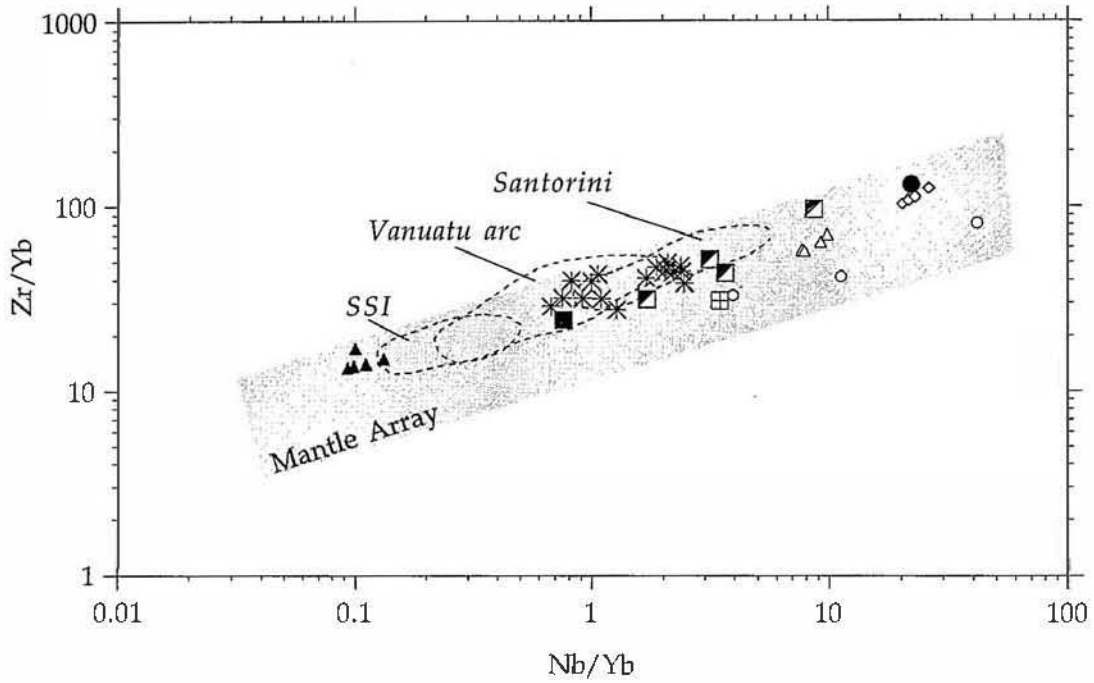

Figure 4.14. Nb/Yb vs Zr/Yb for selected Astrolabe lavas (half filled squares) and Tavua lavas (asterisk). The linear relationship defines the mantle array controlled by the mantle melting regime. Symbols and fields as for Figure 3.25.

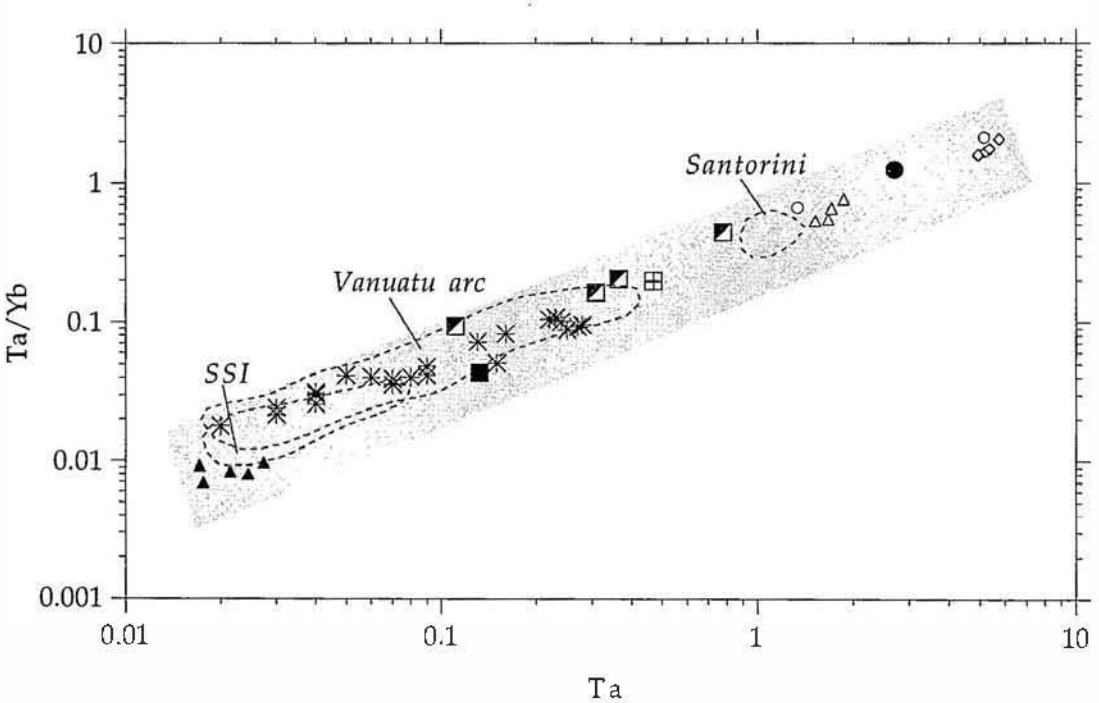

Figure 4.15. Ta/Yb vs Ta for the Astrolabe and Tavua lavas. Symbols as for Figure 4.14. Low degrees of partial melting 'slides' the Astrolabe lava compositions up the mantle array towards high Ta/Yb and Ta.

Astrolabe group (and Tavua) plot within the mantle array at Zr/Yb and Nb/Yb values suggestive of a mantle source compositionally between an N-MORB source and an E-MORB source, significantly more 'fertile' than the refractory source indicated above. Note that many Tavua shoshonites plot on the Ta/Yb vs Ta plot (Fig. 4.15) at more refractory levels than N-MORB, but these are believed to reflect the unreliable, and almost certainly too low Ta values determined by instrumental neutron activation analysis at levels < 0.07 ppm reported by Rogers and Setterfield (1994) (H.M. Waldron, Becquerel Labs., pers. comm., 1996).

In summary, key lines of evidence indicate that the Fijian shoshonitic parent magmas (absarokites) were produced from sources significantly more refractory than those which yield N-MORB, yet HFSE systematics suggest sources between those of N-MORB and E-MORB are more appropriate. These conflicting interpretations can be reconciled by interpreting the Astrolabe parental magmas as having been low degree partial melts of a highly depleted mantle that had already been depleted by previous MORB (or BABB or IAT) extraction, but had been subsequently metasomatised. For low degrees of partial melting, magmas shift along the HFSE mantle array towards OIB compositions, probably as a result of the small amount of amphibole required in MORB mantle sources to provide the small but significant amounts of H_2O in N- to E-MORB. Thus small degrees of fluid-fluxed partial melting of a very refractory mantle source will produce melts with HFSE systematics between N- and E-MORB.

The conclusion that the Astrolabe and Tavua parental magmas were produced by low degrees of partial melting contrasts with that of Rogers and Setterfield (1994), who argued, based mainly on the Tavua high $Ca_{6.0}$ and low $Na_{6.0}$ values (Plank and Langmuir, 1988), that the Tavua parental magmas represent high degree partial melts. However, these authors did not take into account the refractory nature and prior melting history of the Tavua source, which can equally as effectively account for the compositional features of Fijian shoshonite suite magmas as high degree partial melting. Furthermore, it is far easier to account for the high-K, high-P_2O_5 and high-LILE nature of the parent magma(s) of these shoshonites within the framework of a low degree partial melting model. However, even very low degree partial melts of an N-MORB or E-MORB source mantle cannot yield K_2O contents >~0.8% (based on MORB from the Tuzo Wilson Seamounts (Allan et al., 1993) and Macquarie Island (A.J. Crawford, pers. comm. 1996), so that the high K_2O contents of the Fijian shoshonitic suites requires metasomatic enrichment of the

mantle source in at least K-group elements prior to the melting event that produced the Astrolabe parent magmas.

4.5.3 INCOMPATIBLE ELEMENT ENRICHMENT AND THE NATURE OF THE SUBDUCTION COMPONENT

The incompatible element enrichment of the mantle source of the Fijian shoshonites may reasonably be attributed to metasomatic processes caused by fluids derived from the subducted slab before or during production of the Astrolabe parent magmas. Current petrogenetic models for such metasomatic enrichment invoke slab-derived hydrous fluids, which probably leave the slab and migrate into the shallow mantle wedge as serpentinitic and amphibolitic facies slab lithologies dehydrate (Tatsumi and Eggins, 1996). These form amphibole peridotite in the mantle wedge, which is dragged down with the slab by induced convection, until pressure-controlled amphibole dehydration reactions are initiated around 25-30 kbar. Fluids released are then involved in fluxing the mantle wedge and inducing peridotite melting reactions, producing magmas which segregate and may increase in volume as they rise through the hot mantle wedge (Tatsumi and Eggins, 1996).

The composition and characteristics of the slab-derived hydrous fluids are not well known at present. For example, the amount of fluid input into the wedge derived from subducted pelagic sediments is poorly constrained. However, in the case of the Astrolabe and Tavua shoshonitic suites, their isotopic similarities to Pacific MORB support insignificant material input from subducted sediments. It is likely, therefore, that the hydrous fluids responsible for the metasomatic enrichment of LILE in the Fijian shoshonites were derived in large part from altered oceanic crust. The detectable shift away from the mantle array towards higher $^{87}Sr/^{86}Sr$ in the Astrolabe shoshonites and other Fijian shoshonites is consistent with limited isotopic exchange of the subducted ocean crust with seawater. Such alteration leads to insignificant modification of Nd and Pb isotopic compositions (Cohen and O'Nions, 1982).

Shoshonitic lavas are enriched in K-group LILE and to a lesser extent LREE relative to other arc basalts and andesites. A key aspect of the petrogenesis of the Fijian shoshonitic lavas, therefore, is to evaluate whether this LILE-enrichment is simply an enhanced version of the same enrichment present in typical intra-oceanic arc lavas, or whether an entirely different metasomatic agent (and process?) may be implicated. In their study of the Tavua shoshonitic suite, Rogers and Setterfield (1994) argued that the parent magmas of this suite were produced by relatively

high degrees of partial melting of a metasomatised peridotitic mantle. They further claimed that the source enrichment in LILE and related elements was simply an extreme example of that operating beneath intra-oceanic arcs in general, requiring unusually massive input of hydrous fluids from the slab. However, they did not attempt to explain the anomalous enrichment of P in the Tavua shoshonites relative to typical arc basalts, especially since (increasingly) high degree melts will have (progressively) lower P_2O_5 contents. The Rogers and Setterfield (1994) model does not explain the nature of the metasomatic enrichment undergone by the source peridotite of the Tavua shoshonites.

Trace and minor element compositions of a Tavua and an Astrolabe absarokite with ~11-12% MgO are compared with a similarly magnesian island arc tholeiite from the Vanuatu arc, and a Tavua and an Astrolabe shoshonite with ~5-7% MgO are compared with a less magnesian (7% MgO) arc tholeiite from the South Sandwich arc in the MORB-normalised element variation diagrams in Figure 4.16. This diagram shows that the element enrichments in the Fijian shoshonite parental magmas are indeed simply extreme variants of the same enrichment shown by the two primitive arc tholeiites. Furthermore, the convergence of the element distribution patterns of the arc tholeiites and shoshonites towards less incompatible elements (Y to Yb) is exactly the style of element variation expected if the shoshonitic source(s) were partially melted to a significantly lower degree than was involved in arc tholeiite production.

The only significant difference between the arc tholeiite and shoshonite element variation patterns is the lower Ba/Rb for the shoshonites relative to the arc tholeiites. This reflects the greater incompatibility of Rb relative to Ba, leading to increased separation of these highly incompatible elements. It may be considered as simply an enhanced version of the same progressive increase shown by La relative to Ce in the shoshonites compared with the arc tholeiites. This same feature is shown on Figure 4.17, a Ba/Rb vs Rb plot for several arc tholeiite suites and the Fijian shoshonites, which shows that the South Sandwich and southern Vanuatu mafic volcanics all show a progressive decrease of Ba/Rb with increasing Rb (corresponding to progressively lower degrees of partial melting), reflecting the enhanced incompatibility of Rb relative to Ba.

An alternative explanation for the lower Ba/Rb in the Fijian shoshonites relative to arc tholeiites is that this feature may reflect a small amount of residual amphibole or phlogopite during the low degree

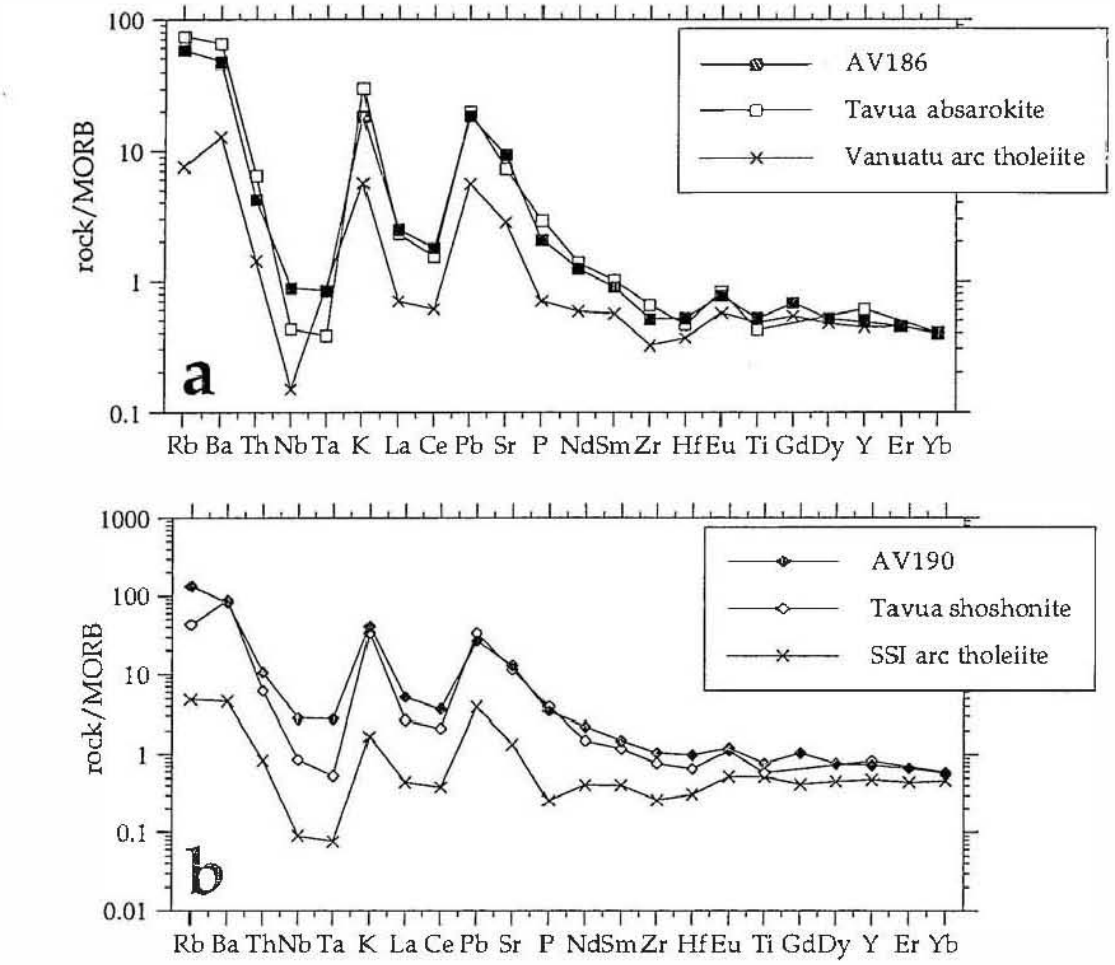

Figure 4.16 a. N-MORB normalised multi-element diagram of an Astrolabe and Tavua absarokite compared to a typical arc tholeiite from the Vanuatu arc. b. N-MORB normalised multi-element diagram of an Astrolabe and Tavua shoshonite compared to an arc tholeiite from the South Sandwich Islands (SSI; Pearce et al., 1995).

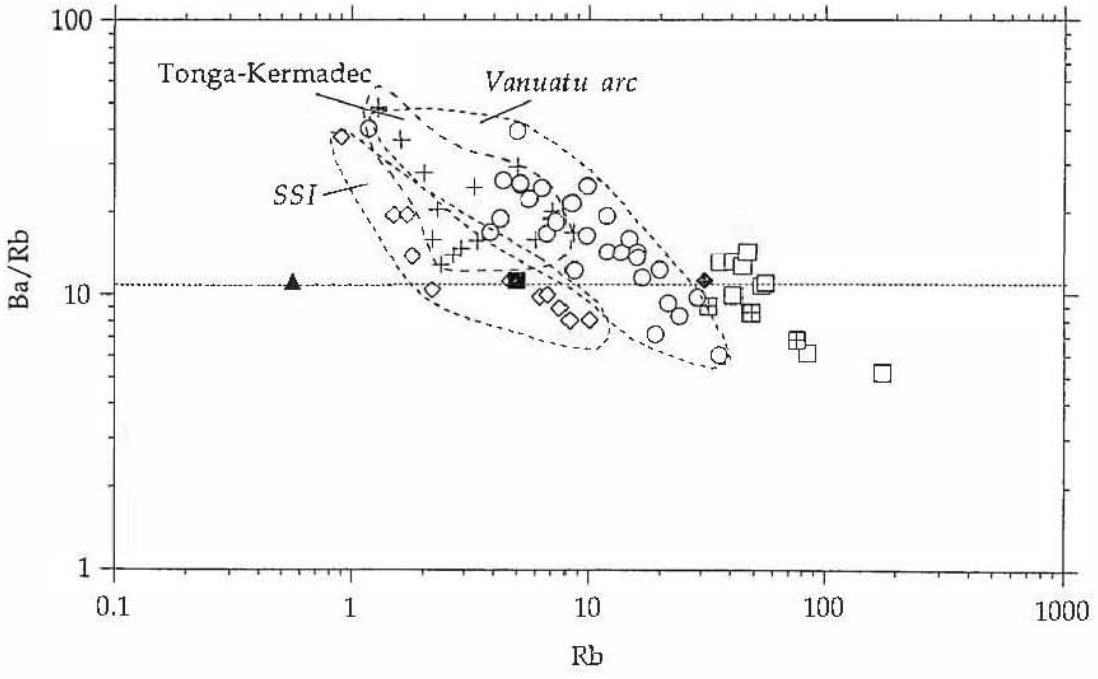

Figure 4.17. Ba/Rb vs Rb of Astrolabe and Tavua lavas at >6% MgO compared to arc tholeiites from the Vanuatu arc, SSI and Tonga-Kermadec arc at >6% MgO. Filled triangle= DMM, filled square= N-MORB, filled diamond= E-MORB. The increase of Rb with a decreasing Ba/Rb shown by arc volcanics reflects the greater incompatibility of Rb relative to Ba.

melting invoked here to have produced the Fijian shoshonite parent magmas. Phlogopite in Alpine-type lherzolites and harzburgites such as in the Finero complex in northern Italy (Exley et al., 1982) have Ba/Rb values typically around 3-6, whereas pargasites have significantly higher values relative to micas, due to their low Rb contents (Brenan et al., 1995). Thus residual phlogopite may be a better candidate. The parallelism of the element variation patterns for the shoshonites and primitive arc tholeiites suggests that if residual phlogopite was involved in Fijian shoshonite petrogenesis, it must have been in such low abundance in the harzburgite residuum that it did not significantly affect other element fractionations in the lava produced.

4.6 RELATIONSHIP TO TECTONICS

The tectonic setting of the shoshonitic association in Fiji has important implications for the genesis of the Astrolabe shoshonites. The age of the lavas from the Astrolabe Islands (3.4Ma) is very similar to other shoshonites in Fiji, so whatever mantle source has produced the shoshonites throughout Fiji extends as far south as the Astrolabe Islands.

Low mantle velocity values (~7.6km/s; Hamburger et al., 1990) indicate that a cold, rigid mantle lid which makes up the bulk of the lithosphere, is substantially thinned beneath Fiji (Hamburger et al., 1990). Thermal thinning of the Fiji lithosphere has been linked to processes of backarc magmatism in the neighboring Lau and North Fiji Basins (Hamburger and Isacks, 1987; Hamburger et al., 1990), and suggests that the Fiji Platform is characterised by an extensional tectonic regime. The shoshonitic series lavas in Fiji are not directly related to current subduction; however, a subduction-related origin for the Fijian shoshonites is not in contradiction with the extensional tectonic setting of Fiji at shoshonitic type volcanism. The processes responsible for mantle metasomatism may have occurred in different times and, accordingly, in a different tectonic setting, to that associated with the formation and emplacement of the Fijian shoshonites. The extensional tectonic regime responsible for the opening of the NFB and Lau Basin facilitated melting and emplacement of the Fijian shoshonitic magmas. Early subduction processes associated with the Vitiaz arc system brought upper crustal material into the mantle beneath Fiji. A fluid rich in K-group elements and Sr isotopes and depleted in HFSE was responsible for contamination of a depleted mantle. Subduction related fluids rising through the upper mantle reacted with mantle peridotite producing enriched mantle

domains which may have escaped melting while subduction was still active. After the cessation of subduction, an uprise of the isotherms caused the enriched mantle domains to melt which produced the shoshonitic magmas in Fiji.

Chapter 5

NGALOA GROUP VOLCANICS

An example of interaction between siliceous melts from the subducted slab and mantle wedge peridotite?

5.1 INTRODUCTION

Fiji is now a remnant oceanic arc which developed on the north eastern edge of the Indo-Australian Plate since the Late Eocene. It was a mature arc during the Miocene, characterised by low-K tholeiitic to medium-K calc-alkaline andesites. During arc fragmentation 8-5Ma, and lasting until 3Ma on Kadavu, magmatic activity was dominated by eruption of shoshonites generally on the northern part of Viti Levu and the Astrolabe Islands. Throughout this stage, all Fijian volcanism retained arc-like geochemical characteristics, although magmatism became gradually more basaltic (Gill and Whelan, 1989a). From ~3Ma to the present, Fijian magmatism has been characterised by mafic volcanism with oceanic intraplate geochemical signatures, except for the Kadavu islands, where lavas retain arc-type signatures. This stage coincides with development of the present geometry of spreading centres in the North Fiji and Lau Basins at ~3Ma (Malahoff et al., 1982; Auzende et al., 1996).

One distinctive magmatic series on Kadavu is the Ngaloa Group, composed essentially of basaltic lavas with abnormally high Na_2O and low FeO contents, and major element compositions similar in some respects to intraplate ocean island basalts. These Ngaloa Group basalts are very likely the 'alkali olivine basalts with 5% normative nepheline present in southwest Kadavu' reported by Gill (1984). However, although the Ngaloa lavas have been classified as oceanic intraplate basalts (Gill and Whelan, 1989b), their relatively low TiO_2 (<1.7%) and FeO (<7%) contents, and their location so close to a Late Neogene subduction zone (Hunter Ridge-Hunter Fracture Zone) within a large province of subduction-related magmatism (Kadavu Island), casts doubt on their postulated "hot spot" origin.

This study of the Ngaloa Group volcanics aims to (1) provide comprehensive new mineralogical and geochemical data to better constrain their classification and petrogenesis, (2) to determine the nature

of the source(s) which may have produced the Ngaloa Group magmas, (3) to compare and contrast the Ngaloa Group source mantle and petrogenetic processes with those for the other magma suites (adakitic and shoshonitic) on Kadavu, described in chapters 4 and 6, and (4) to better constrain the tectonic setting of the Kadavu Islands in the framework of the Fiji archipelago (see chapter 7).

5.2 SETTING OF THE NGALOA GROUP VOLCANICS

Eight samples collected during the 1993 field season fall into a distinct geochemical group here called the Ngaloa Group, characterised by elevated TiO_2 contents compared to other Kadavu suites. The Ngaloa volcanics form Ngaloa Island and smaller areas at several places around the coast of central and eastern Kadavu (Fig. 5.1).

Ngaloa Island is one of the smaller islands making up the Kadavu Island Group, and is situated to the south of the main island (Fig. 5.1). It consists of lavas dated at 0.36 ± 0.05Ma (Whelan et al., 1985), which are the youngest rocks on the Kadavu Islands. Woodrow (1980) divided Ngaloa Island into three different areas - a volcanic cone, an area of lava, and an area of sandstone (Fig. 5.1). The symmetrical volcanic cone makes up the southeastern part of the island and consists mainly of interbedded flows and breccia. The area of sandstone makes up the southwestern part of the island and consists of well-bedded coarse volcaniclastic sandstones and associated fine breccias. The area of lava dominates most of the island and possibly consists of a series of flows erupted from the base of the volcanic cone. No breccias are associated with this unit. Two samples were collected from Ngaloa Island (AV98 and 99), from outcrops of coherent lava. No fresh samples could be found from the volcanic cone or area of sandstone.

Five samples were collected from the southern and eastern part of the main island of Kadavu from outcrops of coherent lava. Only one sample (AV208) with compositional characteristics of the Ngaloa Group was collected from the northern part of Kadavu (Fig. 5.1). Available evidence from the Kadavu Island occurrences of Ngaloa Group lavas is inconclusive as to whether they occur above, or within andesites that dominate this island. However, the compositional coherence of this suite, and the young K-Ar age and good state of preservation of the cone on Ngaloa all suggest that the Ngaloa Group basalts may be the youngest manifestation of magmatism on Kadavu.

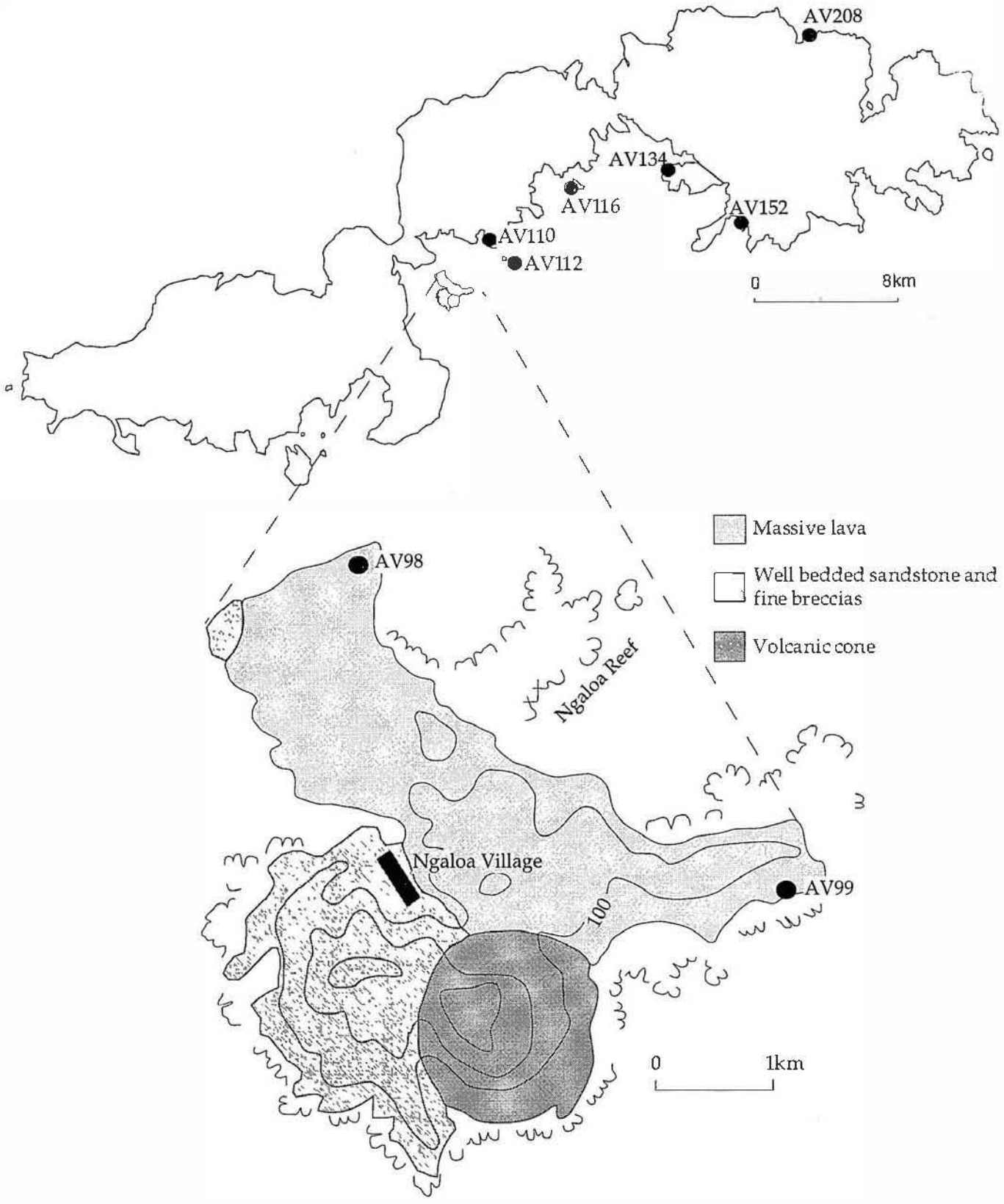

Figure 5.1: Sample locations of the Ngaloa group volcanics and simplified geological map (after Woodrow, 1980) of Ngaloa Island.

The eight samples noted above were analysed by X-ray fluorescence spectrometry for major elements and a suite of ten trace elements (Ni, Y, Rb, Nb, Zr, Sr, Cr, Ba, Sc, V). From these eight samples, four representative samples (at different MgO contents) were chosen for ICP-MS trace element analysis and radiogenic isotope analysis (Sr, Nd and Pb) (Table 5.1).

5.3 PETROGRAPHY AND MINERAL CHEMISTRY

This section describes the petrography and mineral chemistry of the Ngaloa Group volcanics, with comparisons being made to a well-studied (in this laboratory) intra-oceanic arc basaltic lava suite from Ambae, Vanuatu (Eggins, 1989). Detailed petrographic descriptions are given in Appendix 3 and microprobe analyses of phenocryst phases are listed in Appendix 4.

In hand-specimen, Ngaloa Group lavas are very fine-grained and show usually <15 modal% of subhedral phenocrysts of clinopyroxene (up to 2mm long) and olivine (<1mm). In thin section, phenocrysts of clinopyroxene and olivine occur in varying amounts; however most samples are dominated by clinopyroxene (7-10%). Plagioclase is a minor phenocryst phase (up to 3%), and phlogopite occurs sometimes as discrete phenocrysts (1-2%), but is more commonly found in aggregates with clinopyroxene and olivine. The groundmass varies from fine- to medium-grained and consists of plagioclase and clinopyroxene laths and euhedral magnetite and ilmenite needles

5.3.1 OLIVINE

Olivine forms anhedral to subhedral crystals 0.05-0.8mm long, some partly surrounded by phlogopite and equant grains of magnetite, suggestive of reaction with host melt. Cr-spinel occurs as rare, tiny, brown euhedral inclusions in olivine phenocrysts. This paucity of chromite inclusions is a striking feature of the Ngaloa volcanics compared with other arc, MORB or OIB suites with similarly Fo-rich olivines. Another most unusual feature of the Ngaloa olivines is that they host common, variably-shaped former melt inclusions now charged with tiny crystals of magnetite (Plate 5.1). Inclusions vary in abundance and shape from sample to sample. In AV208, olivine contains one or two former melt inclusions, whereas in other samples (e.g., AV99), olivines are riddled with inclusions (Plate 5.2). The long axes of these inclusions are sometimes aligned subparallel or parallel to the C-axis of their host

	AV112	AV110	AV116	AV134	AV99	AV98	AV152	AV208
SiO_2	54.06	53.93	52.48	52.74	51.00	50.40	51.47	50.18
TiO_2	1.44	1.44	1.60	1.56	1.58	1.66	1.40	1.65
Al_2O_3	16.72	16.52	16.08	14.63	15.74	16.09	15.04	14.86
FeO*	6.24	5.85	6.19	6.43	6.45	6.71	6.14	6.78
MnO	0.10	0.09	0.08	0.11	0.11	0.11	0.10	0.11
MgO	5.13	5.22	5.29	6.30	7.06	7.49	7.61	7.94
CaO	8.78	8.88	9.47	10.33	10.27	9.82	9.11	10.37
Na_2O	4.52	4.47	4.40	4.04	4.03	3.92	4.03	3.65
K_2O	1.68	1.66	1.79	1.71	1.58	1.65	1.68	1.71
P_2O_5	0.67	0.65	0.84	0.80	0.75	0.80	0.71	0.77
LOI	1.52	0.57	0.96	0.63	0.65	1.01	0.83	1.46
Total	101.56	99.93	99.86	99.99	99.96	100.40	98.79	100.23
Mg#	67.99	69.75	68.83	71.69	73.88	74.26	76.21	75.16
Ni	33	111	140	121	168	156	192	199
Y	13	18	20	17	20	22	15	18
Rb	13	12	14	13	18	20	16	21
Nb	11.5	9.6	9.9	7.4	15.7	16.7	8.7	16.2
Zr	234	225	225	221	237	246	255	213
Sr	2751	2709	2862	2680	2144	2055	2957	2129
Cr	85	109	209	236	213	213	245	288
Ba	414	415	501	474	442	456	456	491
Sc	13	13	17	19	20	20	17	23
V	194	198	235	230	219	216	218	261
Li	7.02		6.79		5.25			5.72
Be	1.90		1.92		1.86			2.06
Co	24.97		35.16		30.72			33.60
Cu	107.29		83.89		114.93			121.66
Zn	77.80		92.44		67.96			80.26
Ga	23.62		23.36		18.98			18.87
Mo	0.40		0.41		0.39			0.52
Sn	1.50		1.42		1.56			1.39
Sb	0.02		0.02		0.03			0.03
Cs	0.05		0.04		0.08			0.10
La	37.98		46.36		38.38			37.72
Ce	85.72		109.82		89.18			89.03
Pr	11.15		14.58		12.20			12.07
Nd	43.88		58.73		49.83			48.95
Sm	6.98		9.49		8.51			8.25
Eu	1.96		2.68		2.40			2.34
Gd	4.58		6.09		5.94			5.64
Tb	0.58		0.72		0.76			0.72
Dy	2.63		3.34		3.71			3.52
Ho	0.46		0.58		0.69			0.64
Er	1.15		1.48		1.77			1.64
Yb	0.94		1.33		1.44			1.36
Lu	0.14		0.22		0.22			0.20
Hf	5.08		4.96		5.08			4.69
Ta	0.61		0.52		0.85			0.85
Tl	0.03		0.04					0.02
Pb	5.20		9.33		5.30			9.72
Th	4.53		4.62		3.62			4.18
U	1.29		1.22		0.96			1.16

	$^{87}Sr/^{86}Sr$	±2σ	$^{143}Nd/^{144}Nd$	±2σ	$^{206}Pb/^{204}Pb$	±2σ	$^{207}Pb/^{204}Pb$	±2σ	$^{208}Pb/^{204}Pb$	±2σ
AV99	0.70292	25	0.51302	10	18.783	2	15.534	2	38.336	4
AV112	0.70288	17	0.51305	8	18.754	5	15.518	4	38.256	10
AV116	0.70296	25	0.51304	7	18.810	1	15.518	1	38.303	2
AV208	0.70300	21	0.51302	8	18.800	3	15.516	2	38 313	6

Table 5.1: Major (wt%) and trace element (ppm) analyses, and isotopic data for the Ngaloa Group volcanics. Mg# has been calculated using Fe^{2+} derived via wholerock Fe^{2+}/Fe^{3+} melt (=1.8) which was calculated from data on Cr-spinel-silicate melt equilibria (Maurel and Maurel, 1982) through the equation $\log_{10}(Fe^{2+}/Fe^{3+})_{sp} = 0.764*\log_{10}(Fe^{2+}/Fe^{3+})_{melt} - 0.343$. Major elements and Ni, Y, Rb, Zr, Sr, Cr, Ba, Sc and V analysed by XRF. Other trace elements analysed using ICP-MS. LOI=Loss On Ignition. Sr and Nd isotope data has been normalised to $^{86}Sr/^{88}Sr=0.1194$ and $^{146}Nd/^{144}Nd=0.7219$ respectively. Pb isotope data has been corrected for instrumental mass fractionation. For the Sr, Nd, and Pb isotope data, the $2\sigma_{mean}$ values associated with individual sample measurements indicate within-run precision only.

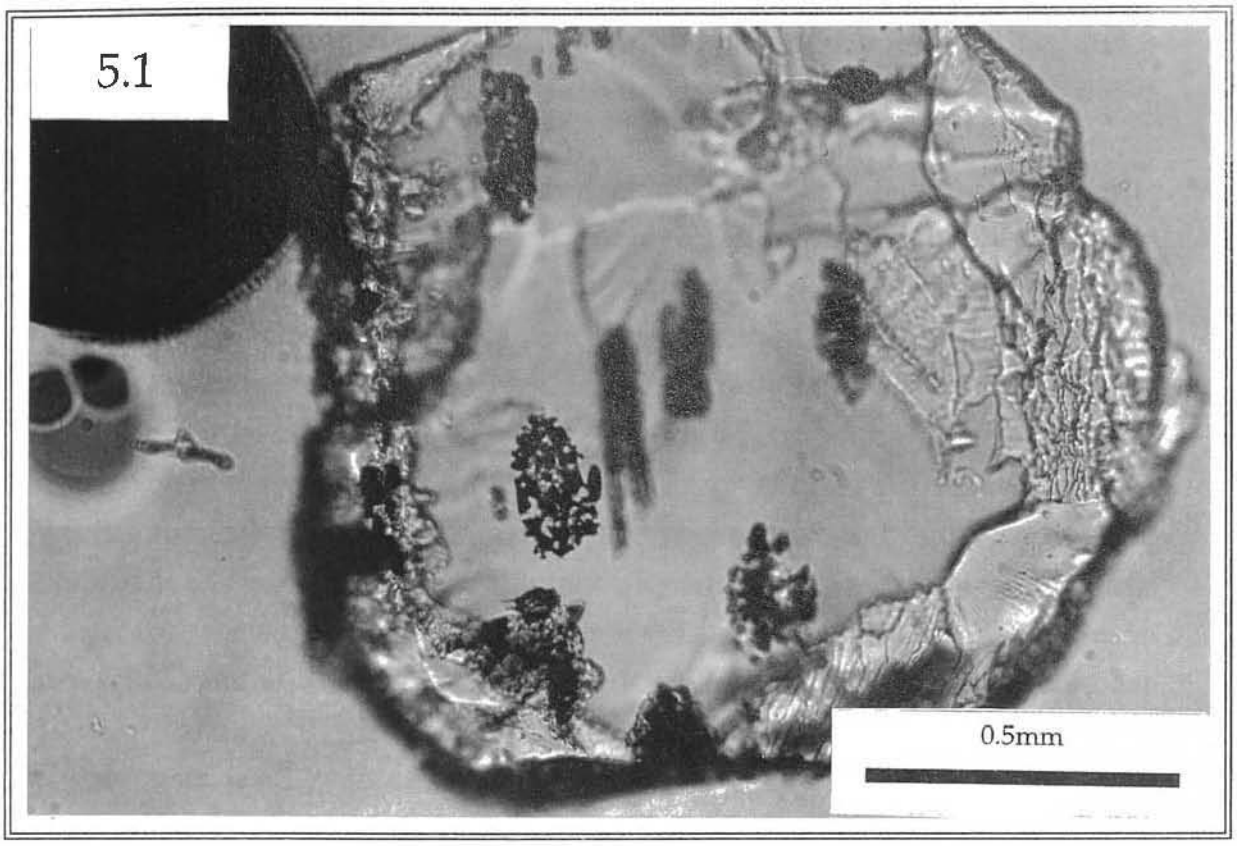
5.1
0.5mm

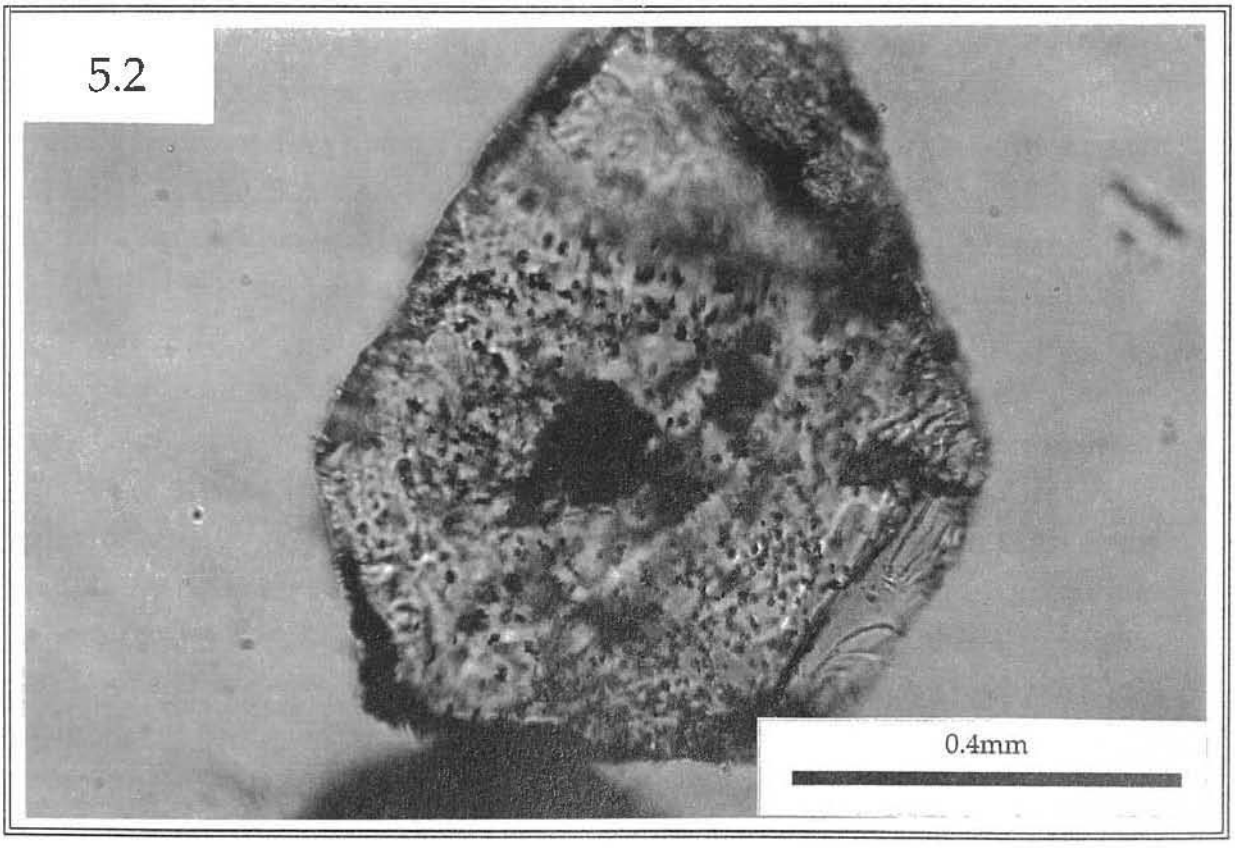
5.2
0.4mm

olivine crystals. Inclusions also form irregular, or crystallographically orientated inclusion trails; the latter may have been trails of secondary melt inclusions along cleavage traces. To the best of my knowledge, this is the first reported occurrence of such inclusions in olivines in primitive island arc magmas.

Rare olivine-hosted primary melt inclusions lacking magnetite have spherical or subspherical morphologies, and were probably trapped during growth along non-planar interfaces. These inclusions have been analysed by electron microprobe, and are discussed later in this chapter .

Olivine phenocrysts in Ngaloa lavas are notable for their restricted range in Fo compositions ($Fo_{85.5-91.2}$) (Fig. 5.2) compared to other arc basalt suites such as those from Ambae (Eggins, 1989: A.J. Crawford and V.S. Kamenetsky, unpubl. data) and the Hunter Ridge (Sigurdsson et al., 1993; A.J. Crawford and V.S. Kamenetsky, unpubl. data). They also have maximum Fo contents extending to levels significantly higher than in any OIB lavas with around 8% MgO, for which maximum Fo values are usually $<Fo_{89}$ (Eggins, 1989). The maximum Fo content of olivine phenocrysts is 91.2, in sample AV99, which generally contains the most magnesian olivines of all samples in the Ngaloa volcanics (Fig. 5.2b). Sample AV98 has lower Fo concentrations in olivine phenocrysts ($Fo_{86.3-88.6}$; Fig. 5.2a), whereas AV110 shows a wider range in olivine compositions ($Fo_{85.5-91}$; Fig. 5.2c) relative to the other Ngaloa lavas studied. Olivine phenocrysts in sample AV208 show a limited range in Fo values between $Fo_{88.5}$ and Fo_{91}, and a symmetric distribution with a peak at $Fo_{89.5-90}$ (Fig. 5.2e).

On the basis of Cr-spinel-silicate melt equilibria, Maurel and Maurel (1982) suggested that the Fe^{2+}/Fe^{3+} value of a magma could be calculated from spinel compositions crystallising from that magma. On this basis, the calculated Fe^{2+}/Fe^{3+} value for this suite averages close to 1.8. Using this value, and established Fe/Mg partitioning relationships between olivine and basaltic melts (Roeder and Emslie, 1970), olivine phenocrysts in AV99 (K_d=0.27-0.34) are broadly in equilibrium with their whole rock composition, as are a significant fraction of the olivine phenocrysts in AV110 and AV208 (Fig. 5.2f-j). However, those in AV98 and AV112 are not in equilibrium with their wholerock compositions, due to either accumulation of clinopyroxene phenocrysts, or trapping/retention of earlier formed olivines in more evolved magmas.

Measured olivine phenocryst CaO contents vary between 0.10 and 0.20% and show no systematic variation with decreasing Fo (Fig. 5.3). This contrasts with regular trends shown by olivines in Ambae high-K arc

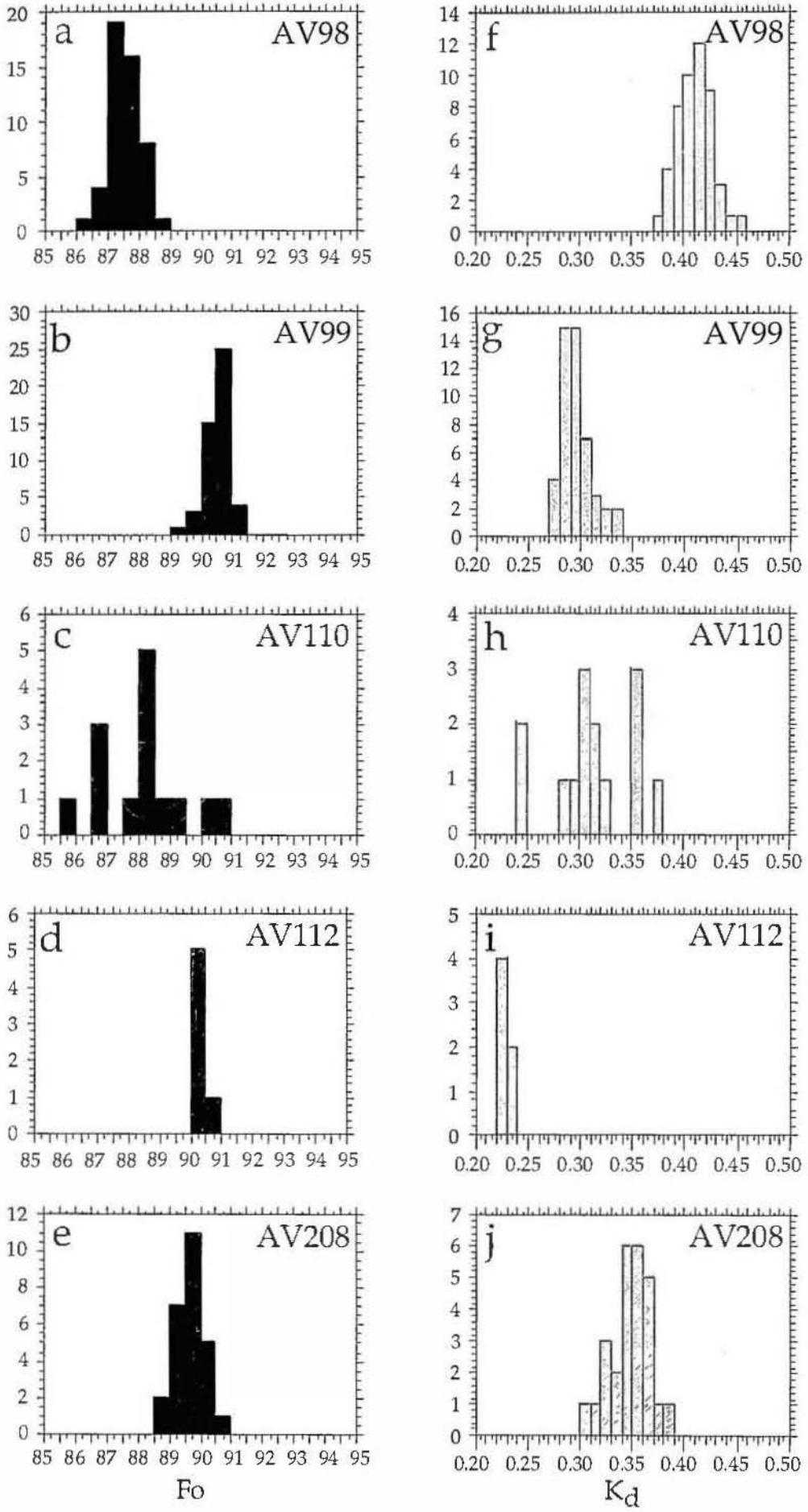

Figure 5.2 a-e: Histograms showing the range in Fo values in olivine phenocrysts in the Ngaloa Group volcanics. f-j: Histograms showing the range in the distribution coefficient (K_d) relating the partitioning of iron and magnesium between olivine and liquid for wholerock Fe^{2+}/Fe^{3+}=1.8 calculated from the Cr-spinel-silica melt equilibria (Maurel and Maurel, 1982).

basalts and Hunter Ridge low-K arc tholeiites (A.J. Crawford, V.S. Kamenetsky and S.M Eggins, unpubl. data; Sigurdsson, 1994), for which olivine CaO contents increase until clinopyroxene joins the crystallisation sequence at $Fo_{\sim 89}$, leading to lower CaO contents in later-crystallising olivines. These CaO levels at Fo_{87-91} are significantly lower than for Hunter Ridge arc tholeiites and Ambae olivines, which are always higher than 0.2%, and usually between 0.2 and 0.4% (A.J. Crawford and V.S. Kamenetsky, unpubl. database, 1996). Such low CaO contents in olivine phenocrysts have been attributed to a xenocrystic (cumulate) origin (Simkin and Smith, 1970); however the euhedral crystals, the presence of melt inclusions and rare Cr-spinel inclusions, all favor a phenocrystic origin for the Ngaloa olivines.

The controls on olivine CaO contents are poorly understood, but certainly include melt CaO content (Jurewicz and Watson, 1988) and probably SiO_2 activity, as indicated by Figure 5.4. This figure shows that for three basaltic suites with almost identical CaO-MgO relationships but with distinctly different SiO_2 contents at any MgO (low SiO_2 transitional alkaline Ambae basalts; 'normal' SiO_2 Hunter Ridge arc tholeiites; high SiO_2 Hunter Ridge boninites), olivines show quite different CaO contents for a given Fo level. As the SiO_2 levels of the Ngaloa basalts are within the range shown by the Hunter Ridge arc tholeiites, the significantly lower olivine CaO contents in Ngaloa basalts compared to those in the Hunter Ridge tholeiites may reflect lower CaO in the Ngaloa parental melts than in the Hunter Ridge tholeiites. However, the effect of melt oxidation state on olivine CaO contents is unknown.

Figure 5.5 shows the variation of NiO and MnO contents in olivine phenocrysts from the Ngaloa Group volcanics. Olivine populations in AV110 and AV99 show systematic decreases in MnO over a broadly similar range (0.55%/0.40% to ~0.15%) as Fo decreases, and the other three samples show greater scatter around similar trends. The MnO-Fo slope defined by AV110 and AV99 are steep, and almost perpendicular to the regular and expected MnO increase with decreasing Fo shown by Ambae olivines. Furthermore, the MnO content of the Ambae (and other arc-related or MORB) olivines at Fo>85 is rarely >0.3%, so the 0.4-0.5% MnO contents of Ngaloa olivines with Fo>90 are most unusual. Similarly, NiO -Fo relationships of the Ngaloa olivines are unusual and contrast with those of any other suite for which data are available. All but sample AV208 show NiO levels between 0.15% and 0.56%, with no apparent systematic relationship between Fo and NiO. Sample AV208 shows olivine NiO contents mainly greater than 0.40%, extending up to ~0.58%

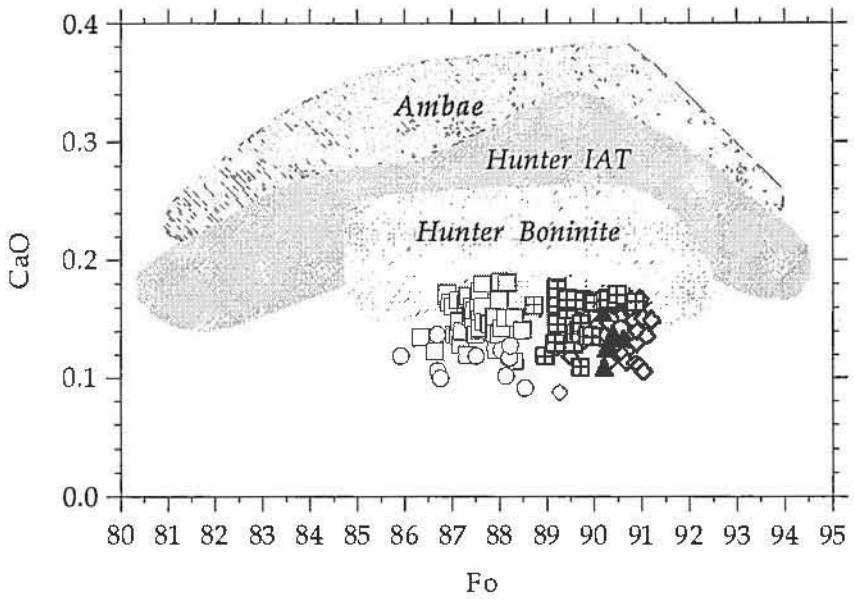

Figure 5.3. CaO content in olivine phenocrysts from the Ngaloa Group volcanics compared to CaO content in olivine phenocrysts from the Hunter Ridge island arc tholeiites (Hunter IAT), Hunter Ridge boninites (Hunter Boninite) and Ambae high-K arc basalts. Squares with crosses=AV208; filled triangles=AV112; open circles=AV110; open diamonds=AV99; open squares=AV98. Sources for Hunter boninite, IAT and Ambae data from A.J Crawford, V.S Kamenetsky, S.M Eggins, unpubl. data, Eggins, (1989) and Sigurdsson (1994).

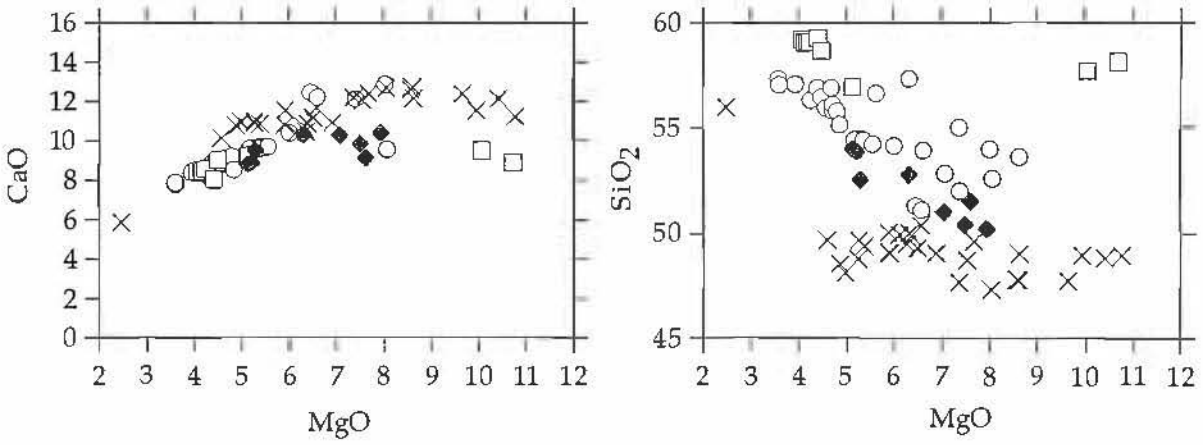

Figure 5.4. MgO vs CaO and SiO_2 of several different mafic lava suites from the Vanuatu-Hunter Ridge arc system, showing the similar CaO contents but significantly different SiO_2 levels at 6-8% MgO. Filled diamonds=Ngaloa Group volcanics; crosses=Ambae lavas; open squares=Hunter Ridge boninites; open circles=Hunter Ridge island arc tholeiites. Sources for Hunter Ridge IAT and boninite data from Sigurdsson (1994); Ambae data from A.J Crawford, S.M Eggins, unpubl. data and Eggins (1989).

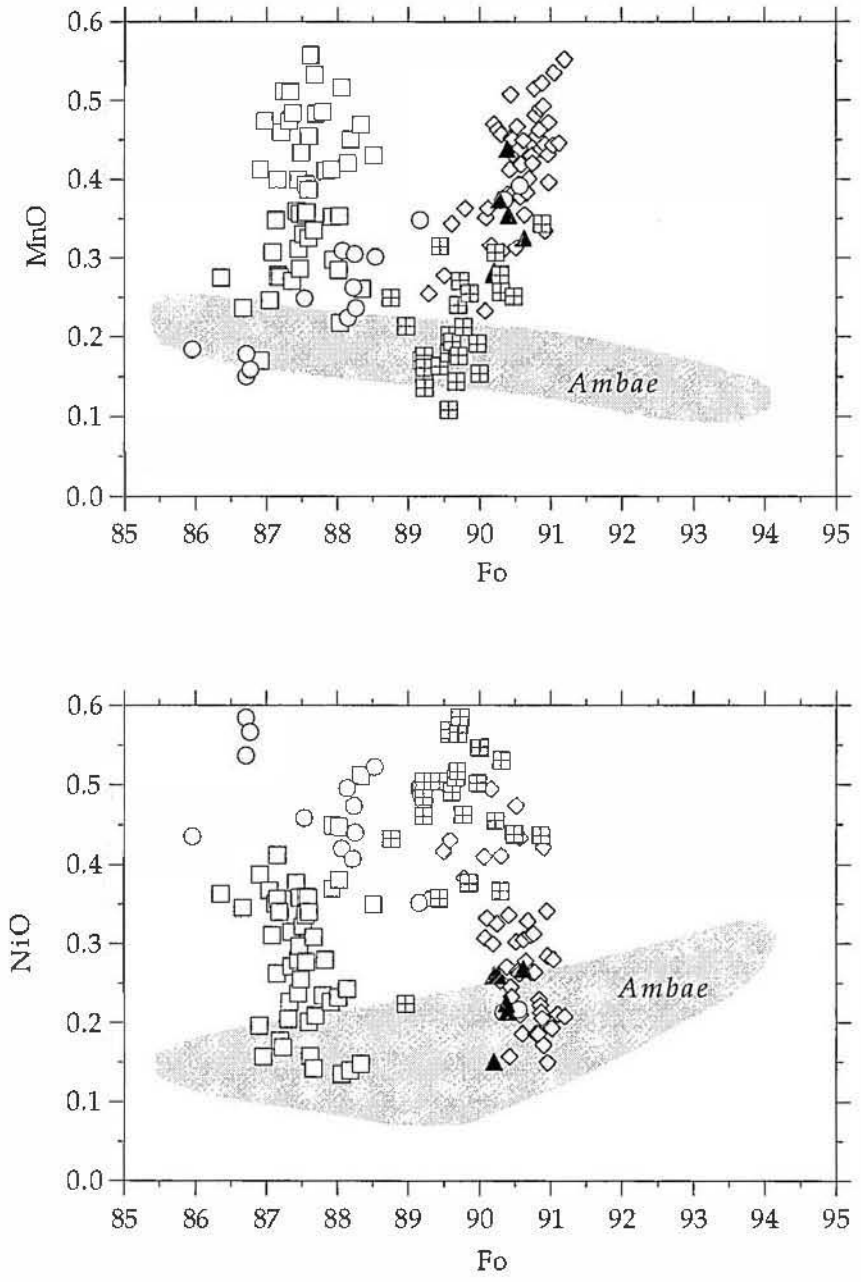

Figure 5.5. MnO and NiO variation in olivine phenocrysts from the Ngaloa Group volcanics compared to MnO and NiO content in olivine phenocrysts from the Ambae lavas (Eggins, 1989). Symbols as for Figure 5.3.

at Fo_{89}, far in excess of the 0.25-0.30% NiO recorded in Ambae olivines with Fo_{94}. The range of NiO contents in olivines from any Ngaloa sample is far greater than that recorded from Ambae, and the expected gradual decrease of NiO with decreasing Fo is absent. The high NiO contents of the Ngaloa olivines are therefore particularly unusual for arc lavas.

Rim to rim analyses (Fig. 5.6) of single olivine phenocrysts in sample AV99 were determined, since this sample shows a large range in olivine NiO and MnO contents. Although zoning profiles are variable, on average a slight increase in the Fo content towards the rims of grains is paralleled by a decrease in NiO and increase in MnO contents. CaO does not vary systematically across the grains, although in grain 4 an excursion to notably lower Fo midway across the crystal shows a corresponding drop in olivine CaO content.

The unusual Fo-NiO, Fo-MnO and Fo-CaO relationships of the Ngaloa olivines compared to Ambae (and other arc, OIB and MORB suites) olivines suggest that regular olivine-melt partitioning during the evolution of the Ngaloa magmas was affected by some other factor(s?) that was not operative, for example, during the magmatic evolution of Ambae picrite-basalt suite. This is further assessed following presentation of data for the Ngaloa clinopyroxenes, plagioclase and spinels.

5.3.2 CLINOPYROXENE

Three textural groups of clinopyroxene phenocrysts can be identified (Plates 5.3 & 5.4) in the Ngaloa lavas.

(i) subhedral to euhedral crystals up to 2mm long with optically strong compositional zoning,

(ii) a smaller (0.1-1mm) more abundant, anhedral to euhedral phenocryst population, characterised by dark bottle green cores and pale green rims. Cores are subhedral or rounded and embayed, indicating some resorption prior to mantle (pale green rim) overgrowth.

(iii) large phenocrysts with sieved cores. Textures show that reactions causing sieved core textures apparently took place subsequent to crystallisation of the rim.

Considerable compositional variability in all clinopyroxene phenocryst variants is shown by random spot analyses of phenocryst cores, which span a compositional range from endiopside via diopside and salite to augite (Fig. 5.7). Only sample AV112 shows a limited range in $Mg^{\#}$ in clinopyroxene phenocrysts (Fig. 5.8), whereas most other samples show a significant range, from 91 to 65. Figure 5.9 shows Al_2O_3 and TiO_2 vs $Mg^{\#}$ variations in clinopyroxene phenocrysts. The most Mg-rich

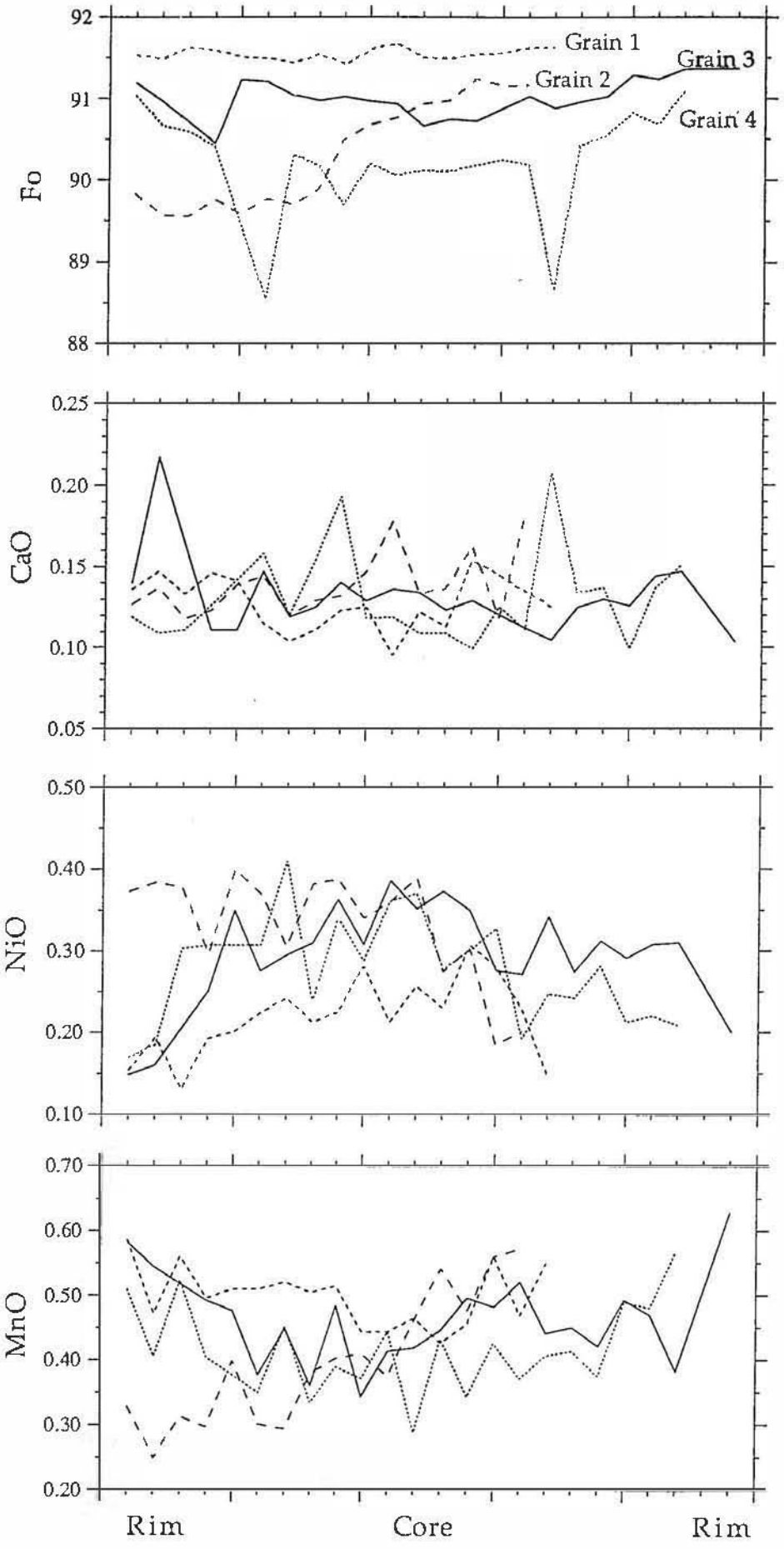

Figure 5.6. Rim-core-rim analyses of olivine phenocrysts from sample AV99

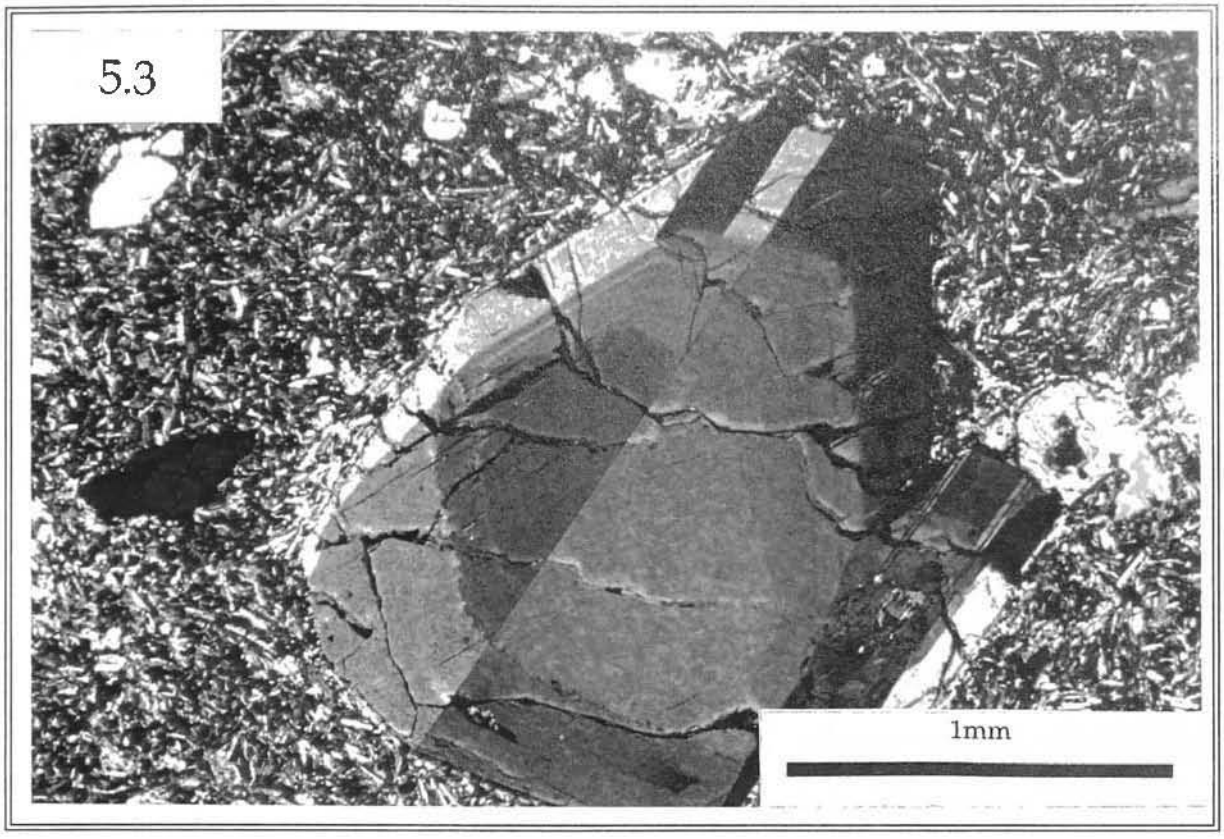
5.3
1mm

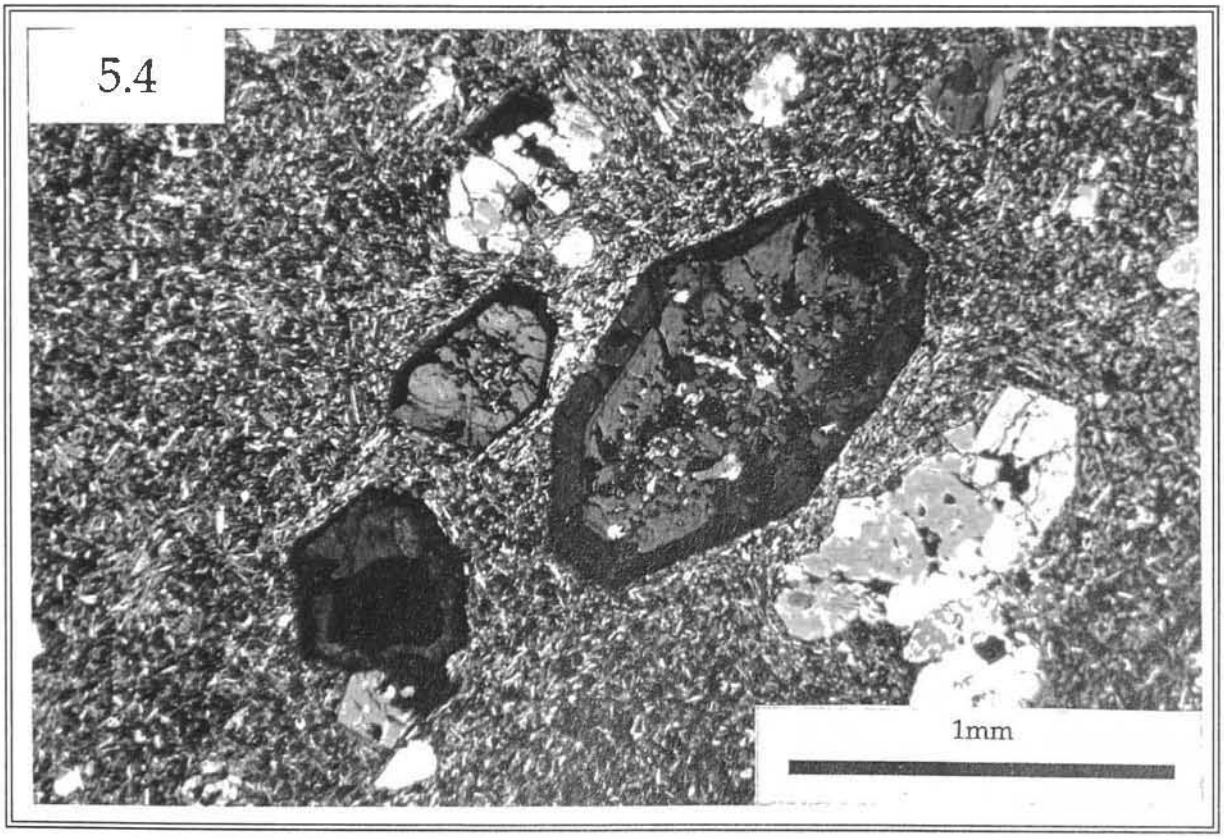
5.4
1mm

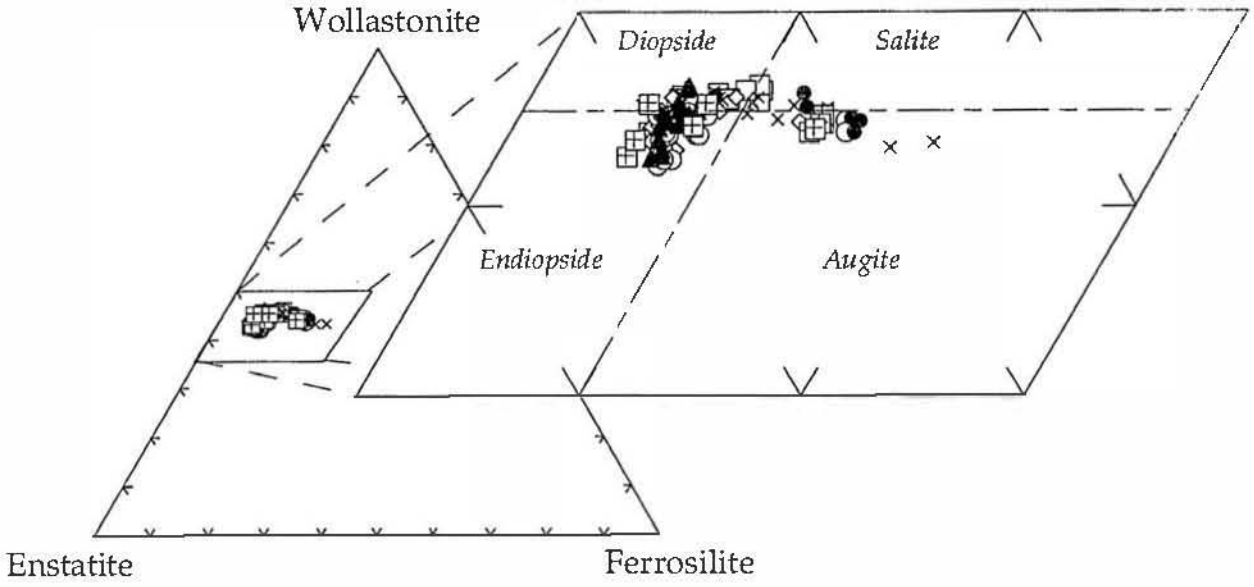

Figure 5.7. Clinopyroxene phenocryst compositions from the Ngaloa Group volcanics. Open squares=AV98; open diamonds=AV99; open circles=AV110; filled triangles=AV112; filled circles=AV116; crosses=AV152; crosses in squares=AV208.

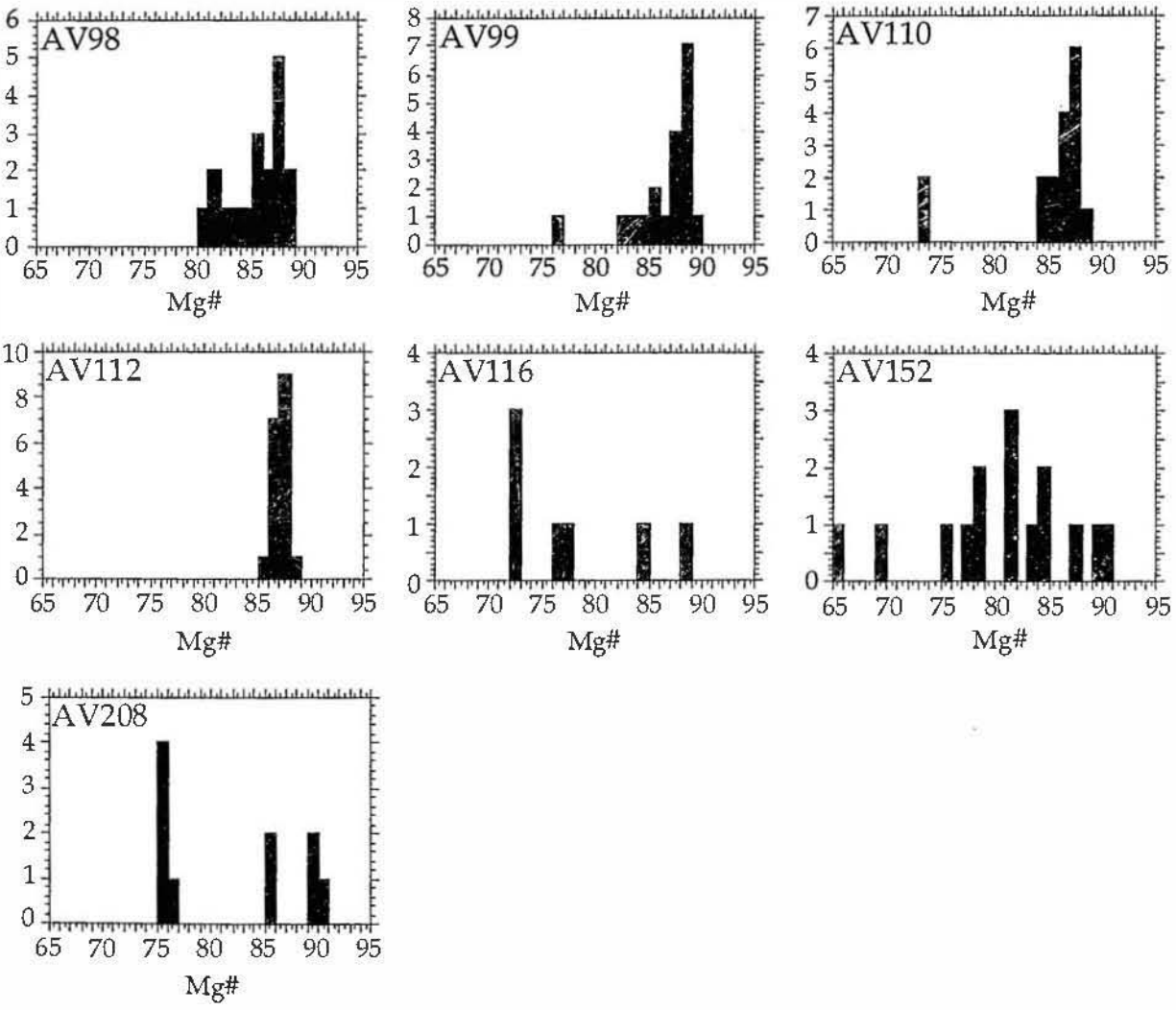

Figure 5.8. Histograms showing the range in Mg# of clinopyroxene phenocrysts from the Ngaloa Group volcanics.

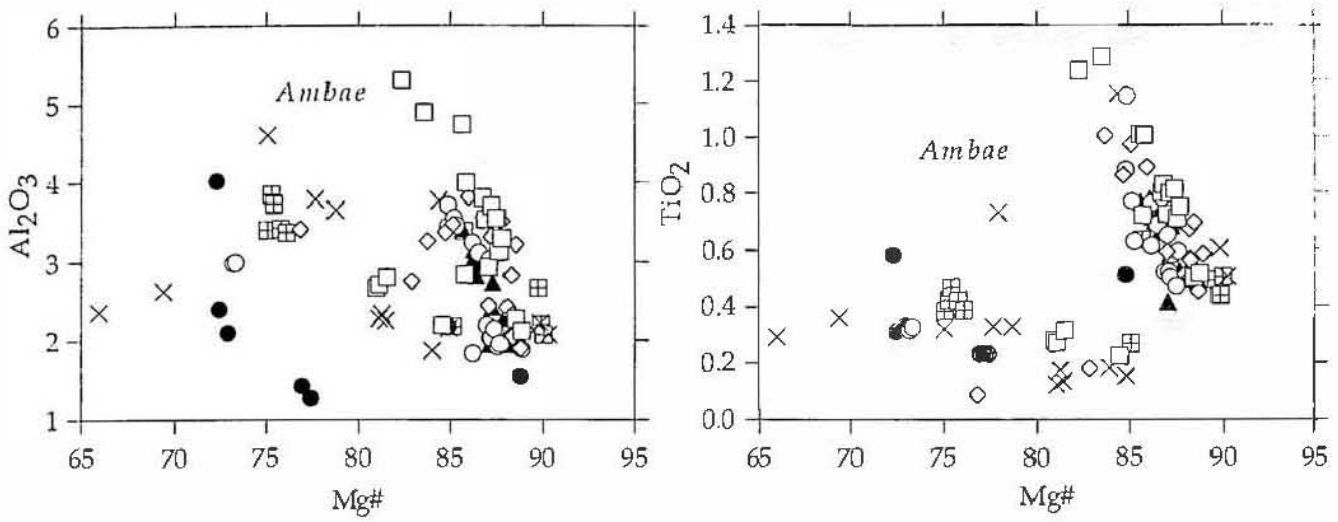

Figure 5.9. Al_2O_3 and TiO_2 variation in clinopyroxene phenocrysts from the Ngaloa Group volcanics. Symbols as for Figure 5.7.

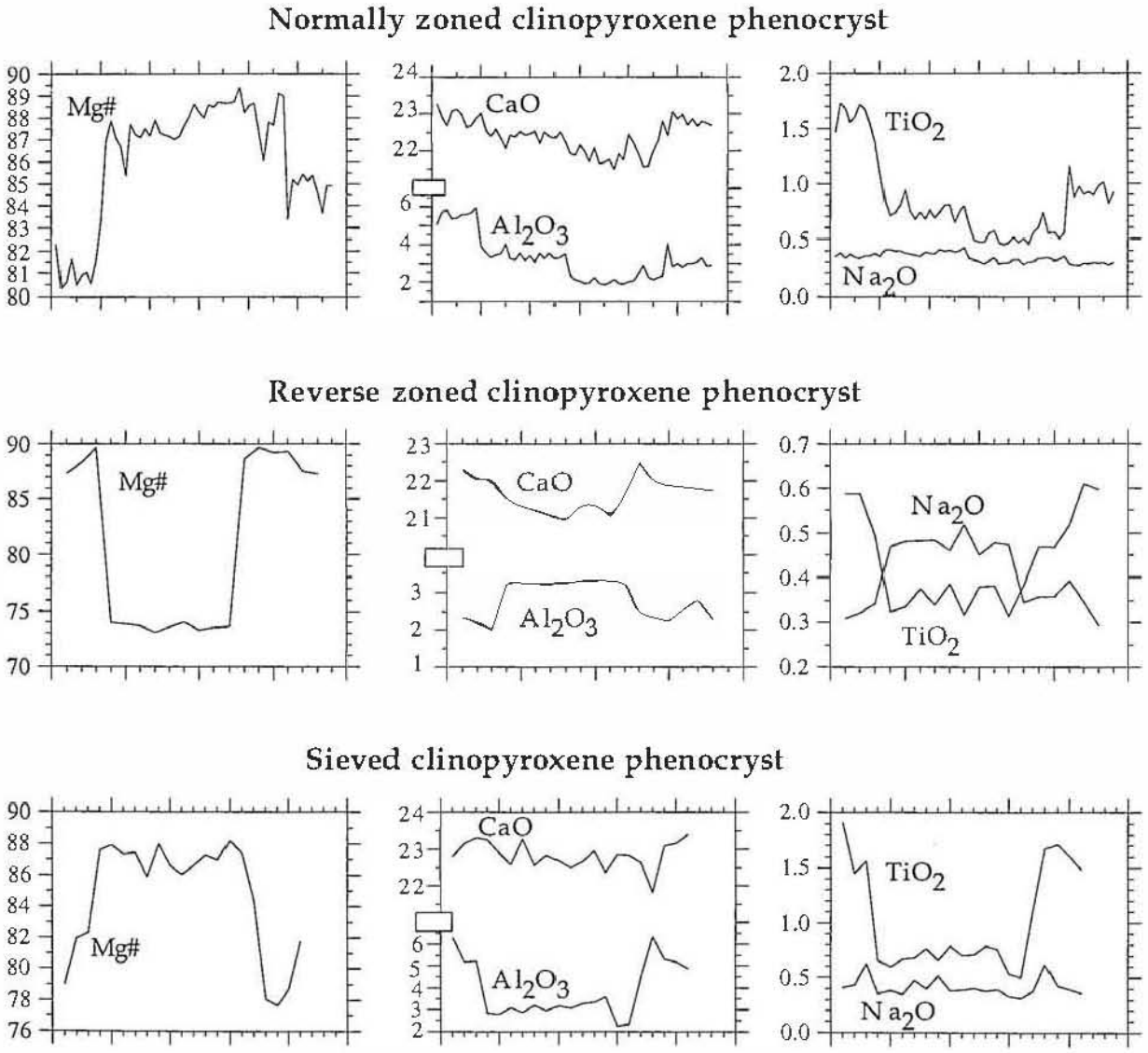

Figure 5.10. Rim-core-rim analyses of the three different types of clinopyroxene phenocrysts from the Ngaloa Group volcanics.

clinopyroxene phenocrysts are particularly Al_2O_3-poor (1.5-2%), suggesting a low pressure (<5kbar) origin (Thy and Lofgren, 1993). With decreasing $Mg^{\#}$, Al_2O_3 increases, as there is no plagioclase crystallisation taking up melt Al; at 4-5% Al_2O_3 and $Mg^{\#}$ 80-85, the sudden sharp drop in Al_2O_3 in clinopyroxene may reflect initiation of plagioclase crystallisation. The Ngaloa clinopyroxene phenocrysts also show a large range in Na_2O contents (0.28-0.62% Na_2O) and are notably higher in Na_2O than Ambae clinopyroxenes (~0.25%). As the low Al_2O_3 contents of these clinopyroxene phenocrysts indicate a low pressure origin, the higher Na_2O at comparable Al_2O_3 and $Mg^{\#}$ relative to Ambae clinopyroxene phenocrysts presumably reflects the higher melt Na for the Ngaloa magmas rather than a high pressure-related jadeite component. The TiO_2 contents in clinopyroxene phenocrysts of the Ngaloa volcanics show a distinct trend broken into two parts with decreasing $Mg^{\#}$; a steep increase in TiO_2 (0.5-1.5%) from $Mg^{\#}$ = 90 to 82 is well-defined, and for $Mg^{\#}$ = 85 to ~70, a more shallow increase at lower TiO_2 values of 0.1 to ~0.5% occurs. Although compositions intermediate between these two broad trends have been analysed (Fig. 5.10), the trends may reflect the onset of Ti-magnetite crystallisation at $Mg^{\#}$ = ~80-85. Ambae clinopyroxene phenocrysts show a trend falling between the two Ngaloa trends.

Detailed microprobe rim-core-rim zoning profiles (Fig. 5.10) for optically zoned clinopyroxene phenocrysts reveal strong compositional zoning. The zoned phenocrysts lacking green cores show weakly normally-zoned cores with $Mg^{\#}$ = 87-90, then a sharp drop to rims of lower $Mg^{\#}$, around 80-84, and higher Al_2O_3 and TiO_2, probably produced during quenching upon eruption. Zoning profiles for the sieved phenocrysts show very similar profiles and compositions to the other zoned phenocrysts lacking green cores, and lack high-$Mg^{\#}$ rims or other compositional features that might suggest late stage trapping of these phenocrysts in a hotter, more primitive magma with subsequent partial disequilibrium and patchy breakdown. The origin of the sieved textures remains unknown.

The common small phenocrysts with green cores show striking reverse zoning profiles, with a sudden jump from homogeneous cores with $Mg^{\#}$ = 70-75, to considerably more magnesian, broad rims with $Mg^{\#}$ = 86-90. The cores show significantly higher Na_2O and slightly higher Al_2O_3 contents, and significantly lower TiO_2 and slightly lower CaO contents than the rims (Fig. 5.10). The usually subhedral to euhedral crystal shapes and the absence of intergrowth with other phases such as olivine, suggest that these unusual clinopyroxene phenocrysts probably

clinopyroxene phenocrysts are particularly Al_2O_3-poor (1.5-2%), suggesting a low pressure (<5kbar) origin (Thy and Lofgren, 1993). With decreasing $Mg^{\#}$, Al_2O_3 increases, as there is no plagioclase crystallisation taking up melt Al; at 4-5% Al_2O_3 and $Mg^{\#}$ 80-85, the sudden sharp drop in Al_2O_3 in clinopyroxene may reflect initiation of plagioclase crystallisation. The Ngaloa clinopyroxene phenocrysts also show a large range in Na_2O contents (0.28-0.62% Na_2O) and are notably higher in Na_2O than Ambae clinopyroxenes (~0.25%). As the low Al_2O_3 contents of these clinopyroxene phenocrysts indicate a low pressure origin, the higher Na_2O at comparable Al_2O_3 and $Mg^{\#}$ relative to Ambae clinopyroxene phenocrysts presumably reflects the higher melt Na for the Ngaloa magmas rather than a high pressure-related jadeite component. The TiO_2 contents in clinopyroxene phenocrysts of the Ngaloa volcanics show a distinct trend broken into two parts with decreasing $Mg^{\#}$; a steep increase in TiO_2 (0.5-1.5%) from $Mg^{\#}$ = 90 to 82 is well-defined, and for $Mg^{\#}$ = 85 to ~70, a more shallow increase at lower TiO_2 values of 0.1 to ~0.5% occurs. Although compositions intermediate between these two broad trends have been analysed (Fig. 5.10), the trends may reflect the onset of Ti-magnetite crystallisation at $Mg^{\#}$ = ~80-85. Ambae clinopyroxene phenocrysts show a trend falling between the two Ngaloa trends.

Detailed microprobe rim-core-rim zoning profiles (Fig. 5.10) for optically zoned clinopyroxene phenocrysts reveal strong compositional zoning. The zoned phenocrysts lacking green cores show weakly normally-zoned cores with $Mg^{\#}$ = 87-90, then a sharp drop to rims of lower $Mg^{\#}$, around 80-84, and higher Al_2O_3 and TiO_2, probably produced during quenching upon eruption. Zoning profiles for the sieved phenocrysts show very similar profiles and compositions to the other zoned phenocrysts lacking green cores, and lack high-$Mg^{\#}$ rims or other compositional features that might suggest late stage trapping of these phenocrysts in a hotter, more primitive magma with subsequent partial disequilibrium and patchy breakdown. The origin of the sieved textures remains unknown.

The common small phenocrysts with green cores show striking reverse zoning profiles, with a sudden jump from homogeneous cores with $Mg^{\#}$ = 70-75, to considerably more magnesian, broad rims with $Mg^{\#}$ = 86-90. The cores show significantly higher Na_2O and slightly higher Al_2O_3 contents, and significantly lower TiO_2 and slightly lower CaO contents than the rims (Fig. 5.10). The usually subhedral to euhedral crystal shapes and the absence of intergrowth with other phases such as olivine, suggest that these unusual clinopyroxene phenocrysts probably

did not originate as disintegrated wall rock xenoliths as suggested by Barton and Bergen (1981) for green-cored augite phenocrysts in K-rich rocks from the Leucite Hills. Models proposed for green (Fe-rich) cores in clinopyroxene phenocrysts in alkali basalt provinces suggests that the reverse zoning might be caused by increasing fO_2 (Frisch and Schmincke, 1969), or magma mixing in which an evolved magma, parental to the green clinopyroxenes, is mixed with a more primitive magma at crustal levels (Thompson, 1977). The strong compositional similarity of the Fe-rich cores in the type (ii) reverse-zoned clinopyroxene phenocrysts of the Ngaloa Group volcanics with clinopyroxene phenocrysts in the high-K andesites from western and central Kadavu (see Ch. 6) favor the concept of formation in an evolved melt, with subsequent incorporation into a more mafic magma by magma mixing.

5.3.3 SPINEL

Compared to most lava suites with olivines between Fo_{86-91}, Cr-spinel is a remarkably rare phase as inclusions in the Ngaloa olivines, and it is not present in other phases or the groundmass, in which Ti-magnetite (and also ilmenite in the groundmass) is present. The rare Cr-spinel inclusions in olivine (Fo_{89-91}) fall within the compositional limits of $Cr^{\#}$ = 71.6-75.6, $Mg^{\#}$ = 41.4-48.5 and $Fe^{\#}$= 55.2-61.4. The Ngaloa Cr-spinels have higher $Cr^{\#}$ compared to MORB spinels, but are comparable with chromites in Ambae lavas (Fig. 5.11) and those in Hunter Ridge arc tholeiites. Ngaloa Cr-spinels are lower in Al and significantly higher in Fe^{3+} relative to MORB chromites, and are also higher in Fe^{3+} relative to Ambae chromites, and chromites in Hunter Ridge arc tholeiites and boninites (Fig. 5.11).

Calculations to determine magma oxygen fugacity of the Ngaloa magmas have been performed using appropriate equations from Ballhaus et al. (1991), Maurel and Maurel (1982) and Borisov and Shapkin (1990) based on olivine-spinel geothermometers. Calculated fO_2 values for equilibration of the few available Ngaloa olivine-spinel pairs are ~ 3 ± 0.2 log units above the FMQ oxygen buffer (~2.3 log units above the NNO oxygen buffer), well above MORB (FMQ-1 to FMQ) and OIB values (0.8 units above FMQ; Ballhaus, 1993), at the high end of the fO_2 range for Ambae lavas (Eggins, 1989, 1993), and significantly higher than values similarly calculated for Hunter Ridge arc tholeiites. The Ngaloa parental magmas were clearly strongly oxidised compared to MORB and OIB, and even more oxidised than other arc lavas in the Vanuatu-Hunter Ridge arc system.

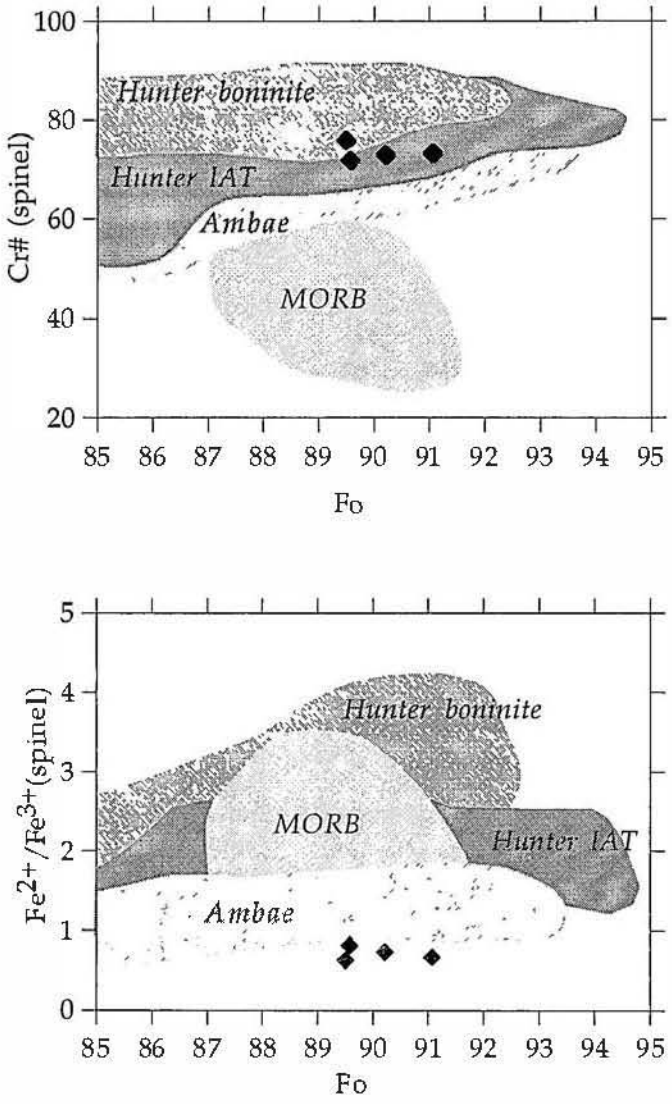

Figure 5.11. Cr# and Fe^{2+}/Fe^{3+} variation of rare Cr-spinel inclusions in olivine phenocrysts from the Ngaloa Group volcanics (closed diamonds). Sources for Hunter Ridge boninite (Hunter boninite), Hunter Ridge island arc tholeiites (Hunter IAT) and MORB data are listed in the caption for Figure 3.5. Sources for data for Ambae from A.J Crawford, S.M Eggins unpubl. data.

5.3.4 PLAGIOCLASE

Plagioclase is a rare phenocryst phase in the Ngaloa volcanics. It forms subhedral to euhedral grains (0.06-0.8mm long) and is commonly found in clusters with clinopyroxene. Plagioclase phenocrysts span a range of compositions from An_{30-70} (Table A4.12, Appendix 4), significantly lower than those in most other primitive arc lavas such as Ambae (An_{66-95}; Eggins, 1989). Ambae and Ngaloa parental magmas both crystallised at low pressures, and if they contained comparable H_2O contents, the more albitic compositions of the Ngaloa phenocrysts imply higher melt Na/Ca for the Ngaloa magmas (Panjasawatwong et al., 1995), an implication strongly supported by whole rock geochemistry. The plagioclase phenocrysts in Ngaloa magmas probably grew together with the green evolved cores of clinopyroxene phenocrysts with $Mg^{\#}$ ~ 72-80, since very similar plagioclase and clinopyroxene compositions coexist in andesites from central and eastern Kadavu (see Chapter 6) that lack any evidence of magma mixing that has clearly affected magmas that yielded the Ngaloa lavas.

5.3.5 PHLOGOPITE

Phlogopite is present as individual anhedral phenocrysts (~0.08-0.8mm), in crystal aggregates with clinopyroxene and olivine and rimming olivine phenocrysts. Microprobe analyses of individual phlogopite phenocrysts are given in Table A4.13 in Appendix 4.

Phenocryst phlogopites all have broadly similar compositions with 3.8-5.7% TiO_2, 8.0-9.8% K_2O, and 0.73-0.98% Na_20. All micas have Mg/Fe>2 and are properly classified as phlogopite (Deer et al., 1989).

Compared to phenocryst compositions of phlogopite from the Colima basanite-minette suite (Luhr and Carmichael, 1981), the Ngaloa Group phlogopite phenocrysts have higher TiO_2 and Na_2O and lower K_2O, consistent with the lower whole rock K_2O content of the Ngaloa Group basalts.

5.3.6 MELT INCLUSIONS IN OLIVINE PHENOCRYSTS

The rare, olivine-hosted melt inclusions lacking disseminated magnetite 'dust' in the olivine phenocrysts, now consist of glass, tiny indeterminate crystalline phases and gas bubbles. These were originally a small portion of melt trapped by growing crystals that later solidified during cooling. 'Shrinkage bubbles' occur in some of the melt inclusions, due to the smaller volume of the solidified melt inclusion to the volume of the originally trapped melt.

Melt inclusions can be classified as primary or secondary. Primary inclusions formed during the growth of the crystal and indirectly reflect the composition of the melt from which the host mineral crystallised. Secondary inclusions form by healing of fractures in the host crystal, and offer no useful petrogenetic information.

Primary melt inclusions from sample AV99 were heated up to temperatures of homogenisation (at which point the shrinkage bubble disappears into the melt; Sobolev et al. 1980, 1991), and then rapidly quenched. It could be argued that the composition of the homogenised inclusion should be the same as the original composition of the trapped melt. However, major problems can arise during the heating process. For example, it may be that the melt already contained phases at the time of trapping, or phases inside the inclusions may not homogenise (dissolve back into the melt) due to their refractoriness or due to the changes in the pressure and pH_2O conditions. Other chemical reactions between the melt inclusion and the host olivine crystal (e.g. Fe-Mg diffusion) might have occurred (see Sobolev and Danyushevsky, 1994), thus modifying the chemical composition of the melt inclusion. For these reasons, the melt inclusion results presented here should be regarded as preliminary and are used as a broad support to the geochemical and mineral chemical data, recalling that addition or subtraction of olivine from the melt inclusion will not affect ratios of elements incompatible in olivine.

Melt inclusions in Ngaloa olivines show a wide range in K_2O/Na_2O=0.29-0.59 values (Table 5.2; Fig. 5.12) which show no regular relationship to SiO_2 contents, and they have SiO_2 (49.1-51.4%) contents overlapping with the whole rock compositions between 50 and 52% SiO_2. All melt inclusions have $CaO/Al_2O_3 < 0.8$, extending to values just greater than the host rocks (0.71 max.), and implying little if any addition of clinopyroxene trapped in melt inclusions prior to homogenisation. They show, however, a remarkably wide range in TiO_2 (1.6-4.0%) and P_2O_5 (0.77-1.76%) contents at similar MgO levels (Fig. 5.12) that cannot be explained by any crystallisation process, and testify to the existence of different, compositionally quite variable primary melts involved in the petrogenesis of the Ngaloa lavas. Independent support for this claim comes from the evaluation of trace element (Ca, Ni, Mn) systematics in olivine phenocrysts, which show opposite (or no) trends relative to those shown by (and expected on theoretical grounds) olivine phenocrysts in other arc lava suites. This will be evaluated further from the assessment of isotope and trace element data.

	MI1	MI2	MI3	MI4	MI5	MI6	MI7
SiO2	48.48	49.95	49.29	46.78	49.14	49.65	51.38
TiO2	1.81	2.49	2.01	4.00	3.36	1.86	2.15
Al2O3	14.41	14.29	14.44	15.39	13.83	13.45	14.60
FeO*	6.60	5.45	5.71	6.59	5.64	7.40	5.56
MnO	0.16	0.07	0.06	0.06	0.12	0.16	0.17
MgO	9.24	8.43	8.99	8.60	8.70	9.93	8.95
CaO	9.54	10.50	9.34	10.58	10.73	8.52	8.35
Na2O	2.51	4.39	3.29	4.42	4.42	3.38	4.54
K2O	1.49	1.76	1.63	1.31	1.59	1.52	1.88
P2O5	0.81	0.78	0.84	1.14	1.76	1.24	0.91
Cr2O3	0.06	0.02	0.00	0.34	0.09	0.05	0.02
S	0.33	0.20	0.49	0.16	0.26	0.04	0.10
Cl	0.30	0.15	0.22	0.14	0.20	0.32	0.73
Total	95.75	98.48	96.30	99.51	99.85	97.52	99.35

Table 5.2. Composition of melt inclusions trapped in olivine phenocrysts from the Ngaloa Group volcanics.

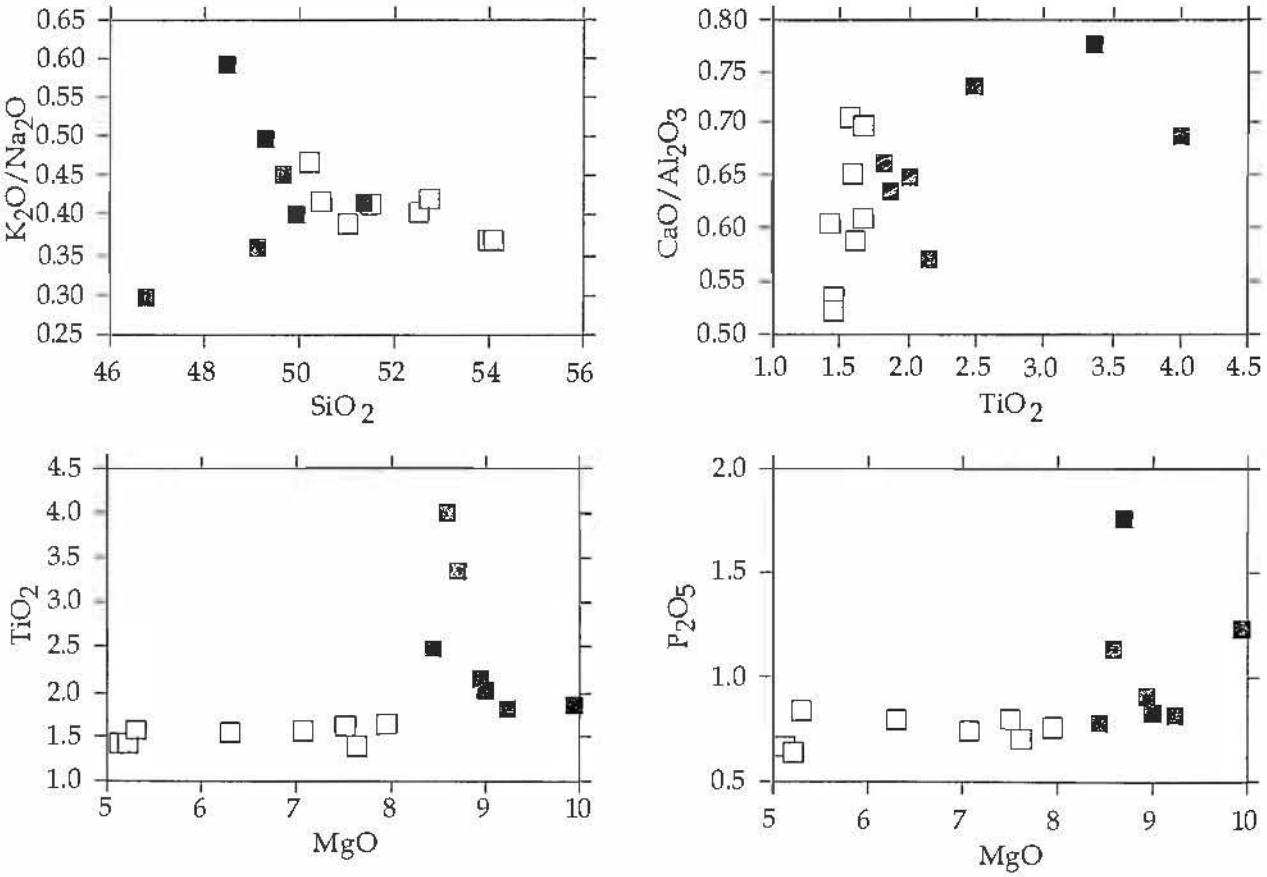

Figure 5.12. Composition of melt inclusions (filled squares) trapped in olivine phenocrysts from sample AV99 compared to the whole rock composition (open squares) of the Ngaloa Group volcanics.

5.4 GEOCHEMISTRY OF THE NGALOA GROUP

5.4.1 MAJOR ELEMENT GEOCHEMISTRY

The Ngaloa Group lavas are high-K basalts (Fig. 5.13) with the highest SiO_2 value (54.1%) slightly exceeding the nominal division of 53% between basalts and basaltic andesites. $Mg^{\#}$ (calculated based on total Fe as Fe^{2+}) varies from 67.9-75.2.

The most striking feature of the Ngaloa Group is the extremely low total Fe contents (~6.8% at 8% MgO), significantly lower than Ambae, or MORB or OIB suites at 8% MgO (Fig. 5.13). Despite the abundant clinopyroxene phenocrysts, CaO contents (8.8-10.4%) are low, and show no regular trend; however the more evolved lavas have slightly lower CaO contents than most of the primitive basalts. Ngaloa Al_2O_3 (14.6-16.7%) contents are normal for plagioclase-free arc lavas. High TiO_2 contents (1.4-1.66%) in the Ngaloa lavas are unusual compared to typical arc magmas (<1%TiO_2) and decrease with increasing MgO. High K_2O (1.6%) and Na_2O (3.65%) contents of the Ngaloa volcanics at 8%MgO are also unusual for typical primitive arc lavas, which commonly have 1.5 - 2.0% Na_2O and up to 2% K_2O (Tatsumi and Eggins, 1996). The P_2O_5 contents in the Ngaloa volcanics are high, significantly higher than Ambae and increase slightly to a maximum of 0.84% at 5.3% MgO, then decrease rapidly, presumably reflecting apatite fractionation in the most evolved basalts.

5.4.2 TRACE ELEMENT GEOCHEMISTRY

The Ngaloa Group basalts have extremely high Sr contents, mainly between 2000 and 3000ppm (Fig. 5.14), nearly four times the levels in Fijian OIB (~660ppm; Gill and Whelan, 1989b), twice the levels in Ambae high-K basalts, and an order of magnitude greater than those in the Hunter Ridge arc tholeiites. In keeping with their high-K affinities, Ngaloa lavas have high contents of Ba (415-501ppm) and Rb (12-21ppm), comparable to the Ambae lavas. The transition elements Sc and V follow FeO and decrease with decreasing MgO, consistent with fractional crystallisation of clinopyroxene, but Sc abundances are only half those of Ambae and most other arc basalts at 8% MgO. The Zr levels are high (213-255ppm), well above Ambae at 8% MgO and fall in the range for Fijian OIB (~280ppm; Gill and Whelan, 1989b); most orogenic lavas with 5-8% MgO have Zr contents around 50-150ppm (Gill, 1981).

Chondrite-normalised REE patterns for the Ngaloa Group basalts (Fig. 5.15A) are LREE-enriched with significant HREE depletion, and

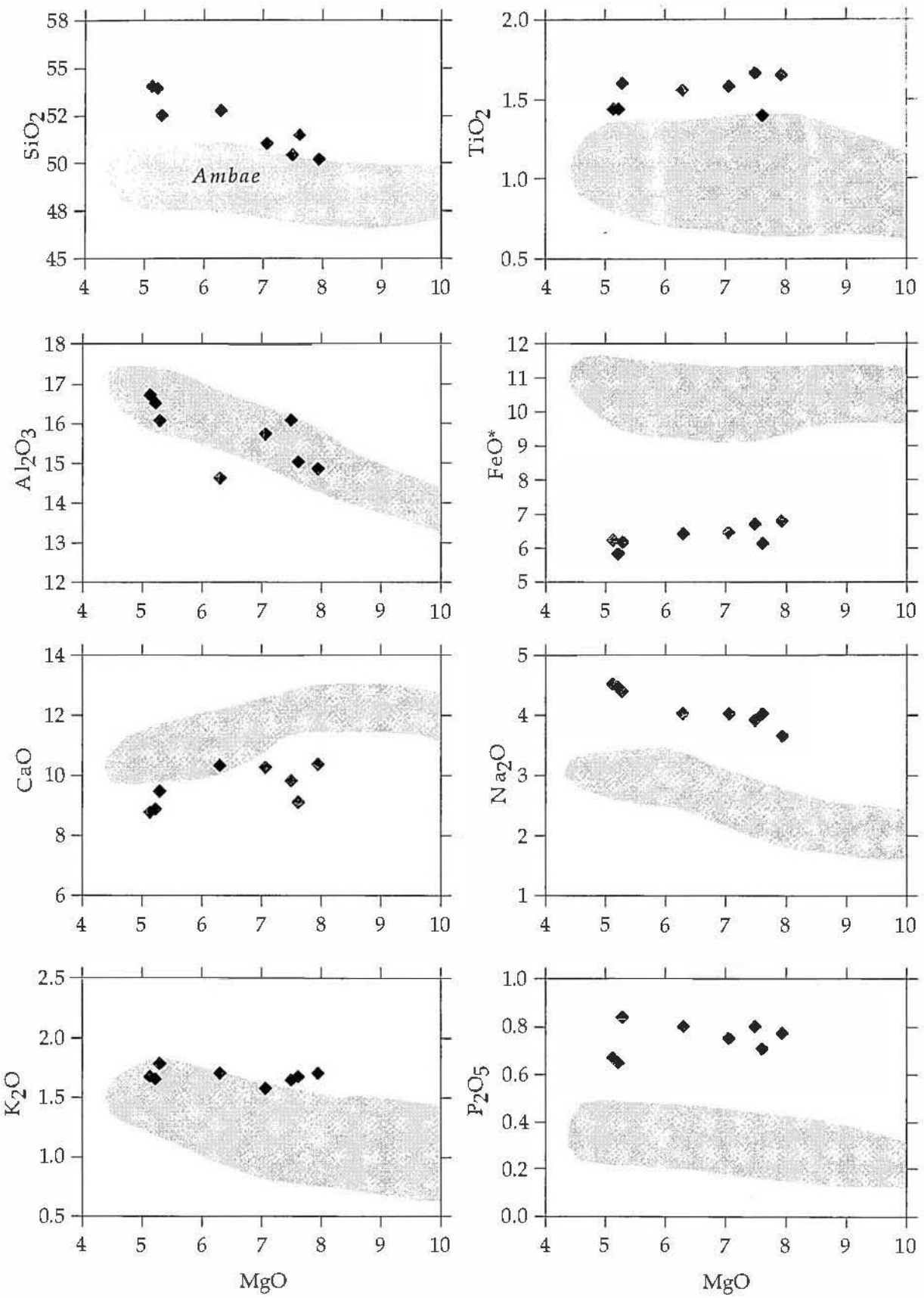

Figure 5.13. Major element covariation diagrams for the Ngaloa Group volcanics compared to field for lavas from Ambae volcano, Vanuatu (Eggins, 1989).

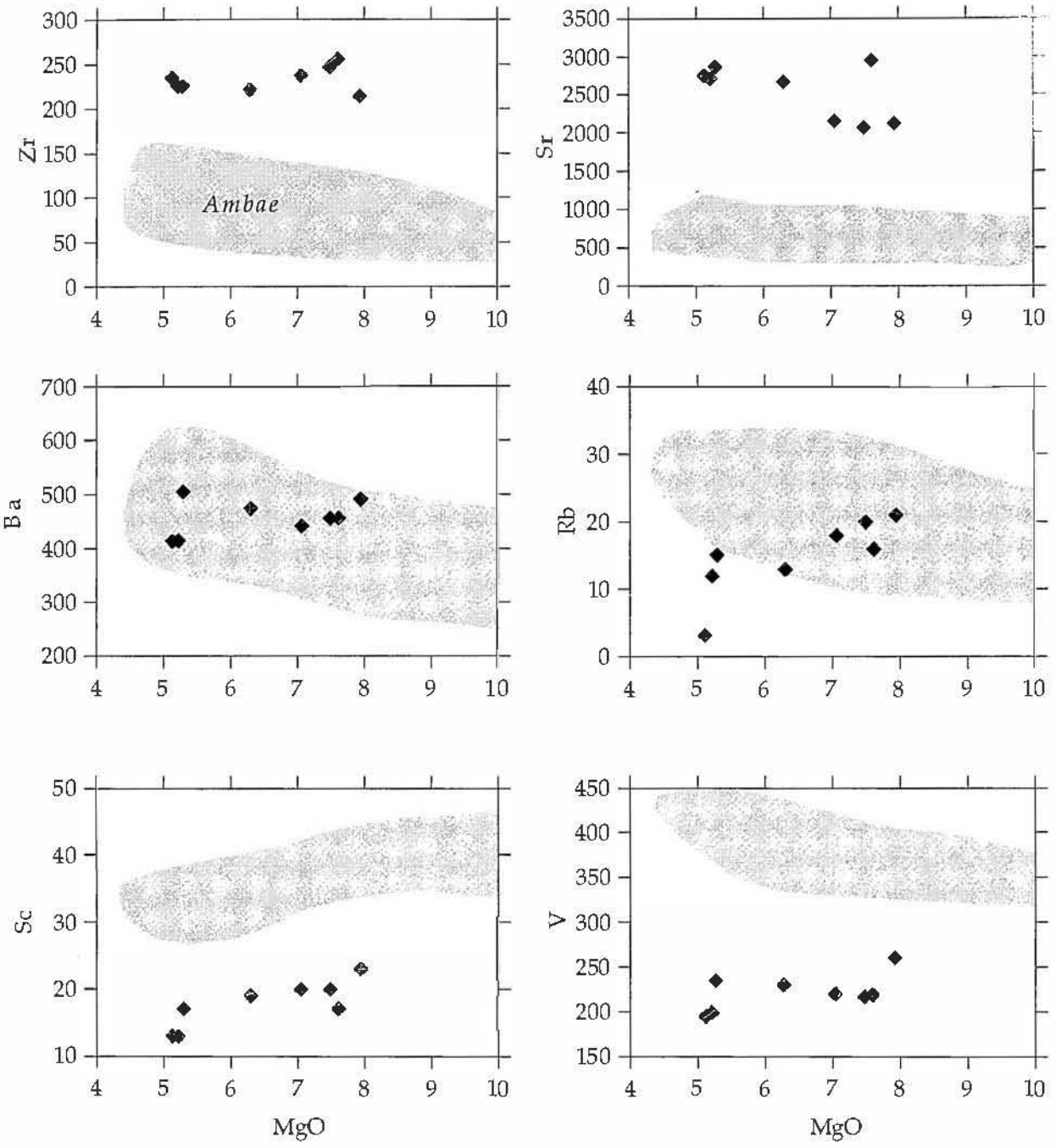

Figure 5.14. Trace element variation of the Ngaloa Group volcanics compared to field for lavas from Ambae volcano, Vanuatu (Eggins, 1989).

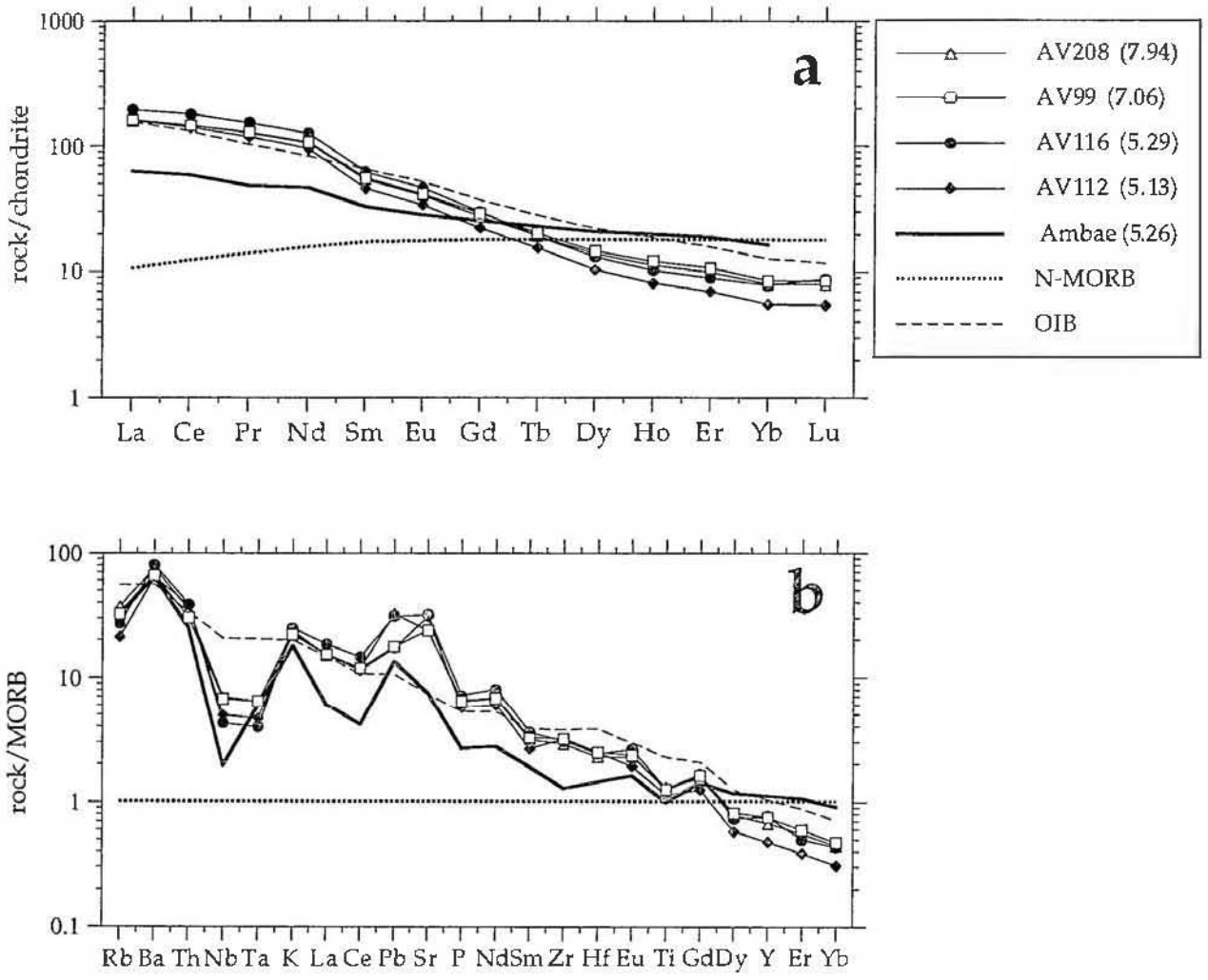

Figure 5.15a REE concentrations for the Ngaloa Group volcanics normalised to chondrite. MgO content for each sample in brackets. Ambae composition from Eggins, (1993). OIB and N-MORB compositions and normalising values from Sun and McDonough (1989).
b. N-MORB normalised multi element diagrams for the Ngaloa Group volcanics.

resemble those of OIB, but slopes of the Ngaloa basalts are even steeper than average and Fijian OIB. The significant depletion of HREE suggests that garnet was involved at some stage in the petrogenesis of these basalts.

N-MORB-normalised multi-element patterns (Fig. 5.15B) for the Ngaloa basalts show the broad features of typical arc volcanics (Perfit et al., 1980; Pearce, 1983; Hickey et al., 1986), including enrichment in LILE (Rb, Ba, K) relative to neighboring REE, significant negative Nb-Ta anomalies relative to K or La, and large positive anomalies for Sr and Pb relative to adjacent elements Ce and P. For the LREE, MREE and HFSE, the Ngaloa patterns are essentially parallel to, but at significantly higher levels than Ambae basalts, as represented by an evolved basalt with 5.26% MgO; however, K-group element patterns are very similar in shape and abundance to the Ambae lavas, and Y-HREE are clearly depleted.

5.4.3 RADIOGENIC ISOTOPE CHEMISTRY

Sr, Nd and Pb isotope ratios are plotted in standard isotopic covariation diagrams in Figure 5.16. The Ngaloa lavas fall within the more radiogenic end (av. 0.7029) of the Pacific MORB field for $^{87}Sr/^{86}Sr$, at very uniform $^{143}Nd/^{144}Nd$ (av. 0.51303), indicating derivation from a depleted mantle, and ruling out involvement of old, recycled continental crustal components (pelagic sediments, clays) in their petrogenesis.

Pb isotopic compositions of Ngaloa lavas are also very uniform ($^{206}Pb/^{204}Pb$=18.75-18.81; $^{207}Pb/^{204}Pb$=15.52-15.53; $^{208}Pb/^{204}Pb$=38.26-38.34), and plot very close to the NHRL of Hart (1984) and either just within ($^{208}Pb/^{204}Pb$) or very slightly below ($^{207}Pb/^{204}Pb$) the field defined for Pacific MORB. Importantly, the Ngaloa volcanics have very similar Pb isotope compositions to basalts from the North Loyalty Basin section of the South Fiji Basin.

5.5 SUMMARY

The petrography, mineral chemistry, major and trace element composition and the Sr-Nd-Pb isotopic compositions demonstrate the complex nature of the Ngaloa Group volcanics.

First, petrographic and mineral chemical data suggest that disequilibrium assemblages are common, and imply a complex mixing origin for the host magmas. The presence of phlogopite and magnetite surrounding some olivine phenocrysts indicates olivine reaction with the melt. Clinopyroxene phenocrysts show either well developed reverse

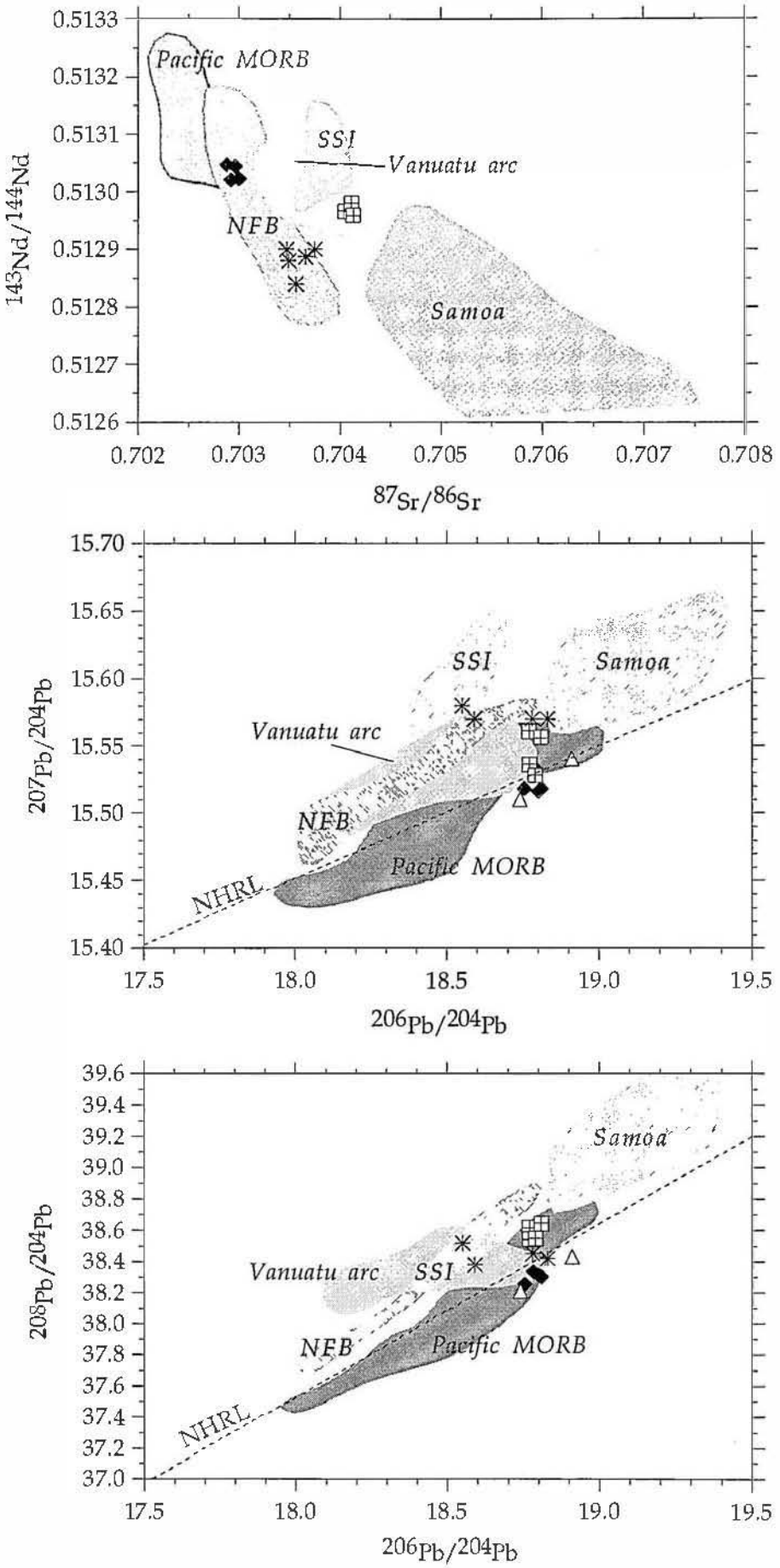

Figure 5.16. Sr vs Nd and Pb vs Pb isotopic compositions for the Ngaloa Group volcanics (filled diamonds) and Astrolabe lavas (squares with crosses) shown relative to fields for Pacific MORB, the North Fiji Basin (NFB) BABB, South Sandwich arc (SSI) and the Vanuatu arc. Asterisks = late rifting stage (Fijian OIB). The limited Pb isotope data for the South Fiji Basin are represented by the open upright triangles. Data sources for Pacific MORB, NFB, SSI and the Vanuatu arc are listed in Figure 3.22. Data for Samoa from White and Hofmann (1982), Palacz and Saunders (1986) and Wright and White (1987).

or normal zoning. The reverse zoned phenocrysts have cores of green augite that crystallised from evolved basaltic to andesitic lavas, and were subsequently incorporated into the more mafic, hotter, host basalts. Occasional plagioclase and phlogopite phenocrysts also probably crystallised in more evolved magmas than the host basalts. Both olivine and clinopyroxene phenocrysts extend to very high-Mg compositions ($Mg^{\#}$ =91-91.5), and trace element (Ca, Ni and Mn) abundances in the olivines show very anomalous abundances and trends that remain poorly understood. Furthermore, the olivine phenocrysts contain common melt inclusions, the majority of which have suffered strong oxidation, leading to crystallisation of abundant magnetite 'dust' throughout the melt inclusions. Cr-spinels in the Ngaloa basalts are extremely uncommon despite the mafic nature of these lavas, and have $Cr^{\#}$ values (~75) typical of arc lavas; they are strongly oxidised, and olivine-spinel geobarometry yields consistent values of fO_2 around FMQ + 3, values at the very highest end of the arc lava fO_2 spectrum, and significantly greater than MORB (FMQ -1 to FMQ).

The few unoxidised melt inclusions within olivine phenocrysts display an exceptional compositional range, extending to very P_2O_5- and TiO_2-rich compositions typical of very low degree mantle melts. The whole rock compositions are unusual in their very low total Fe and CaO and their high Na_2O contents, and TiO_2 levels (~1.6%) notably higher than other arc volcanics on Kadavu and the Hunter Ridge-Vanuatu arc systems.

Despite the high Sr, Nd, and Pb contents (2129-2862ppm Sr; 43.87-58.73ppm Nd; 5.2-9.71ppm Pb), the isotopic compositions of these elements are similar to those of MORB, and are well removed from Fijian OIB compositions. The Ngaloa volcanics thus are very unusual, both globally among arc volcanics, and even within the Vanuatu -Hunter Ridge arc systems. An understanding of their petrogenesis should contribute significantly to a better understanding of the tectonic development of Kadavu and Fiji.

5.6 ORIGIN OF THE NGALOA GROUP VOLCANICS

5.6.1 MIXING BETWEEN OIB AND ADAKITE MAGMAS?

At first glance, concentrations of SiO_2, TiO_2 and MgO in the Ngaloa basalts suggest that it is reasonable to hypothesise that they may be due to mixing between an adakitic magma such as the Western Kadavu dacites, and a high-TiO_2 lower SiO_2 magma such as a typical Fijian OIB. This

hypothesis is reasonable considering the proximity of Kadavu to young OIB centres in Fiji (<50 km). Furthermore, mixing was certainly involved in the petrogenesis of the Ngaloa basalts, as well shown by the green adakitic augite cores to clinopyroxene phenocrysts in these basalts. However, numerous considerations rule against this OIB-adakite mixing model. First, mineralogical evidence suggests that the magma that mixed with an adakitic magma at shallow crustal levels to produce the Ngaloa basalts was highly oxidised, and with chromite and olivine compositions far more refractory than recorded from Fijian (or other) OIB. Second, major- and trace element mixing models attempting to link Fijian OIB, Ngaloa basalts, and Kadavu adakites (Fig. 5.17) are singularly unsuccessful, and along with isotopic data (see Fig. 6.10) effectively preclude such a mixing model being relevant for the petrogenesis of the Ngaloa lavas. Another model is required.

5.6.2 NATURE OF THE MANTLE WEDGE

Figure 5.18 shows the Ngaloa Group volcanics plotted on a Nb/Yb vs Zr/Yb plot (Fig. 5.18a). As shown in previous chapters, a 'mantle array' is defined extending from D-MORB through N-MORB and E-MORB to OIB. Unlike the Astrolabe lavas and other arc lavas both in the Vanuatu-Fiji region and elsewhere (e.g. South Sandwich arc), the Ngaloa volcanics plot above the mantle array at very high Nb/Yb values appropriate for OIB. Does this mean that the Ngaloa volcanics were derived from melting of an enriched OIB-type mantle source? The presence of an extensive regional OIB mantle domain in the Fiji-Lau-Tonga area has been well established by the isotopic compositions of recent volcanics (<3Ma) from the northern part of the NFB (South Pandora Ridge-Rotuma; Price et al., 1990), Lau Ridge (Cole et al., 1990), northern Lau backarc basin (Volpe et al., 1988), and the alkali basalts in Fiji (Gill, 1984). However, the MORB-like isotopic ratios and some MORB-like key incompatible trace element ratios such as K/Rb of the Ngaloa volcanics (680-1180, cf. OIB 450-550) cannot be explained by involvement of an OIB-source.

It was argued in Chapter 4 with respect to the Astrolabe shoshonites that while the mantle array in plots such as Figure 5.18 reflects source compositions (as originally proposed by Pearce and coworkers), very low degrees of partial melting of a depleted source can also drive resultant melt compositions towards the 'fertile' OIB end of the mantle array. On all diagrams of this nature tested, using either HFSE or other incompatible elements (a selection are shown in Fig. 5.18), the

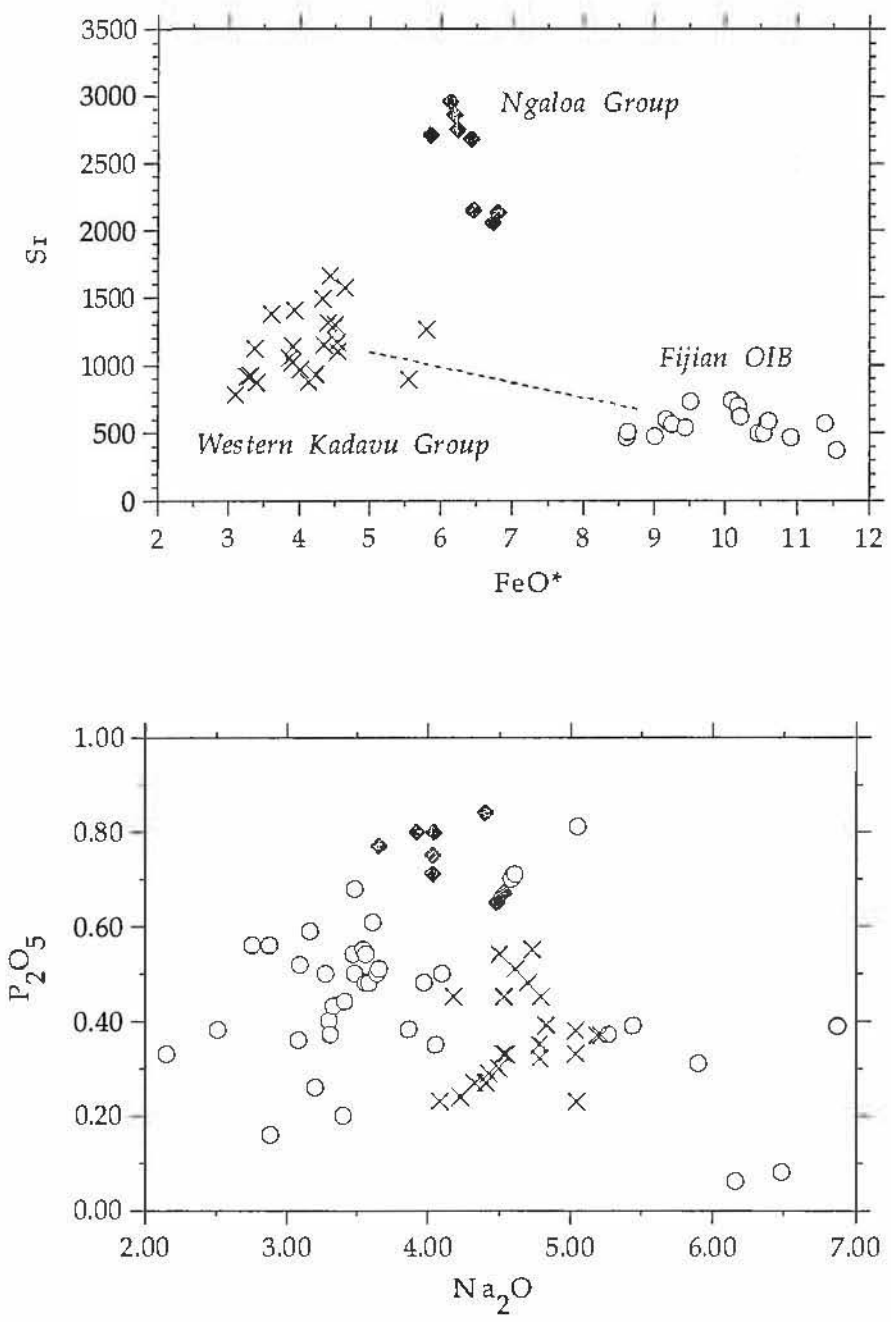

Figure 5.17. FeO* vs Sr and Na2O vs P2O5 plots showing that the Ngaloa Group volcanics cannot be produced by mixing between Western Kadavu adakites and Fijian OIB. Fijian OIB data from Cole et al. (1990), Gill and Whelan (1989b), Hindle and Colley (1981), Gill (1976).

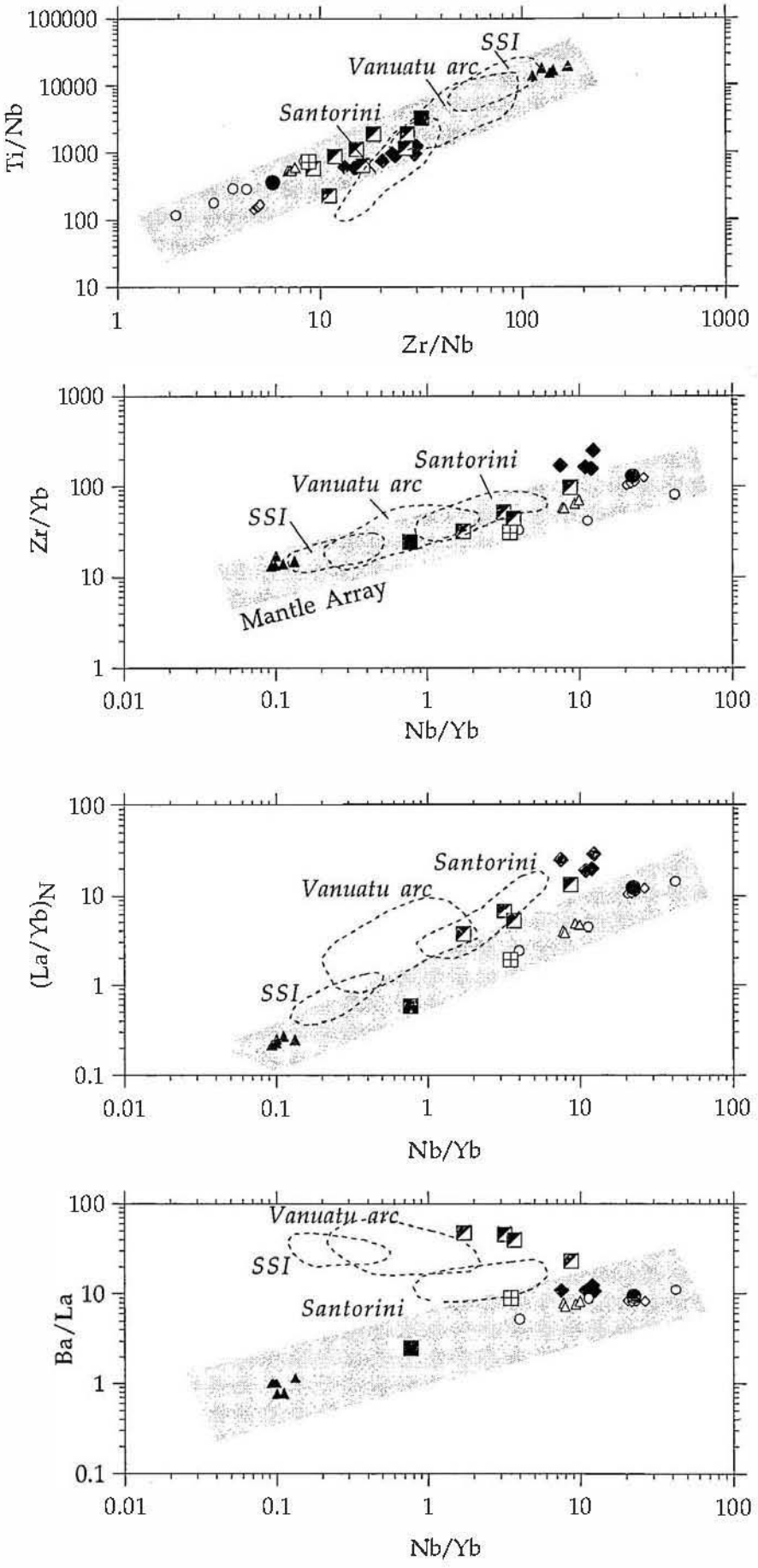

Figure 5.18. Yb-normalised incompatible element ratio plots showing the Ngaloa Group volcanics (filled diamonds) plotting at the OIB end of the mantle array. Symbols as for Figure 3.25. Data sources listed in Figure 3.25.

Ngaloa basalts plot at the OIB end of the mantle array, in some cases (La/Yb_N) extending above the mantle array, but along the same trend.

The relatively highly forsteritic olivines (to $Fo_{91.5}$) and the high-$Cr^{\#}$ Cr-spinels in the Ngaloa olivine phenocrysts are more depleted than those in MORB, indicating a rather refractory, arc-type peridotite source, although less depleted than the source for Hunter arc tholeiites and boninites. The paradox, therefore, between the mineralogical evidence for a depleted source and the mantle array plots arguing for an enriched source may be reconciled, as for the Astrolabe shoshonites, by invoking low degrees of partial melting of a metasomatised but relatively refractory peridotite source. This does not, however, provide a ready explanation for the significant major and trace element differences between the Astrolabe shoshonites and the Ngaloa basalts, best emphasised by the low Fe, low Sc, strongly HREE-depleted, high Na_2O, high Zr, high Sr Ngaloa basalts relative to the shoshonites. An alternative mechanism capable of producing key features of the unusual Ngaloa magma compositions is addition of hydrous, silicic slab melts to the mantle wedge. The possible involvement of a slab melt component in the petrogenetic evolution of the Ngaloa Group is discussed in the following section.

5.6.3 THE SLAB MELT SIGNATURE

In recent years, increasing attention has been paid to suites of andesitic to dacitic lavas that show unusually high Na_2O/K_2O, high Sr, and low Y, and strongly HREE-depleted REE patterns; these suites have been referred to as adakites (Defant and Drummond, 1990). Adakitic andesites and dacites have been identified in several subduction-related settings, e.g., the western Aleutians (Kay 1978; Yogodzinski et al., 1995), Panama and Costa Rica (Defant et al. 1991, 1992), northern Kamchatka (Hochstaedter et al. 1994; Kepezhinskas, 1989; Kepezhinskas et al. 1996), Cerro Pampa, Chile (Kay et al., 1993), Cook Island in the Andean Austral Volcanic Zone (Stern and Kilian, 1996), and in the Zamboanga Peninsula in the Philippines (Sajona et al., 1996). The distinctive compositional features of adakites have led most authors to invoke melting of subducting oceanic lithosphere in the evolution of these magmas (Peacock et al., 1994; Sen and Dunn, 1994). Subducted oceanic crust might normally be expected to include altered MORB and pelagic sediment, as well as fresh MORB, but available isotopic data for the Ngaloa Group (Fig. 5.16) indicate that if subducted oceanic crust was involved in the genesis of the Ngaloa volcanics, only MORB lacking $^{87}Sr/^{86}Sr$ evidence for seawater alteration could have been involved.

Defant and Drummond (1990) suggested that a plot of Sr/Y vs Y is sensitive in discriminating between slab-derived and peridotite mantle wedge-derived magmas. Partial melting of an amphibole eclogite source would generate melts that plot towards high Sr/Y but low Y, as the melt would contain high contents of Sr, due to the incompatible nature of this element in a clinopyroxene-garnet assemblage, and the absence of plagioclase. On the Sr/Y vs Y diagram (Fig. 5.19), the Ngaloa volcanics plot at high Sr/Y comparable to 'typical' adakites. Furthermore as noted above, their high Na_2O/CaO values, very high Sr contents, HREE depletion, and abnormally low Sc abundances also argue for involvement of a slab melt in the genesis of the Ngaloa basalts.

Further evidence for slab melt involvement in the genesis of the Ngaloa basalts comes from ratios of some incompatible elements. Partial melting of MORB eclogite will not result in extensive inter-element fractionation of Rb, Th, Ba, K and LREE because the distribution coefficients for these elements are very low in an essentially clinopyroxene and garnet assemblage (Green et al. 1989). Consequently any melt from the unaltered slab MORB will have broadly MORB-like ratios of these elements. Ba/La values (~10) of the Ngaloa volcanics are in the E-MORB range, and are significantly lower than typical arc lava values (Fig. 5.18d), for which dehydration of subducted oceanic crust and contamination of the sub-arc mantle by LILE-rich hydrous fluids is considered an important petrogenetic process (c.f., Vanuatu arc and South Sandwich Islands). Similarly, Ngaloa K/Rb values vary between 680 and 1180, and are significantly higher than typical values for the Vanuatu (mainly 400-700) or South Sandwich arc (200-400).

5.7 DISCUSSION

Many unusual compositional features noted above, and the MORB-like isotopic compositions of the Ngaloa volcanics, are consistent with derivation of these magmas by partial melting of subducted MORB. However, their primitive phenocryst compositions, coupled with their high whole rock $Mg^{\#}$ and Ni (to 200ppm) and Cr (>200ppm at MgO>6%) contents may result from the interaction of slab melts with mantle peridotite. This scenario has been suggested for adakitic lavas from several locations (Rogers et al., 1985; Kay et al. 1993; Stern and Kilian, 1996) including the type adakite from Adak Island (Kay 1978). This is because relatively small percentage melts (<15-20%; Rapp, 1995) of a

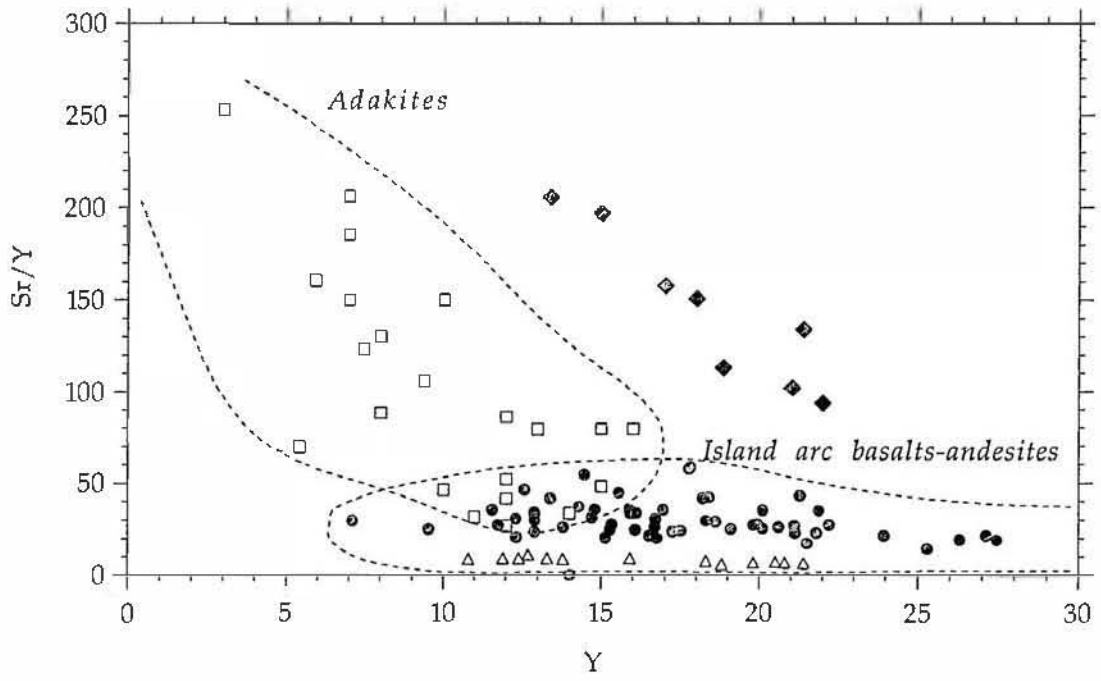

Figure 5.19. Ngaloa Group volcanics (filled diamonds) plotted on the Sr/Y vs Y discrimination diagram of Defant and Drummond (1990). Island arc field defined by South Sandwich Islands (open triangles; Pearce et al. 1995) and the Vanuatu arc (filled circles; Crawford et al. unpubl.data). Sources for adakites are Kay (1978), Drummond and Defant (1990), Defant et al. (1992), Kay et al. (1993) Sajona et al. (1993), Yogodzinski et al. (1995) and Kepezhinskas et al. (1996).

basaltic source (e.g., eclogite) are silicic (>60% SiO_2), with low concentrations of compatible elements (Cr, Ni and MgO). Although the details of the process involved during interaction of slab melts with mantle peridotite are poorly understood, and quantification is impossible, since the mantle wedge is undoubtedly hotter than either the slab or any slab melts, it is most unlikely that such interaction would *not* occur (Kelemen et al. 1993).

In this section I consider two hypotheses that explain the major, trace element and isotopic evidence for slab melting observed in the Ngaloa volcanics. First, they may represent adakites that have assimilated or interacted with mantle peridotite during ascent to the surface. Second, the Ngaloa volcanics may represent differentiated daughters of basaltic parents that were generated from a mantle that had been infiltrated and metasomatised by slab melts.

Hypothesis 1: Slab melt interaction with mantle peridotite.

Slab melts might interact with the mantle wedge en route to the surface by bulk assimilation of peridotite. Kelemen (1990, 1995) suggested that heating of hydrous slab-derived melts ascending through the mantle wedge, due either to the inverted temperature gradient in the wedge (Davis and Stevenson, 1992) or to heating resulting from isenthalpic ascent (Baker et al. 1994), provides substantial thermal energy for peridotite dissolution. In such reactions outlined by Kelemen et al. (1993), the mass assimilated is greater than the mass crystallised and the solid products are still peridotitic. However, Sen and Dunn (1995) conducted experiments reacting felsic partial melts of amphibolite with lherzolite, and found that olivine, clinopyroxene and spinel are consumed, and amphibole and more-Fe-rich orthopyroxene are produced. Clearly, it is not possible to quantitatively constrain such reactions even to a first degree without further detailed experimental studies. Bulk addition of peridotite, or peridotite-derived olivine and clinopyroxene, into silicic melts would primarily affect SiO_2, MgO and compatible element abundances of the migrating, evolving melts. Intuitively, reaction-induced addition of an olivine-clinopyroxene assemblage to a dacitic adakite slab melt during its ascent through the mantle wedge would produce a significant increase in CaO/Na_2O of resultant melts. As the vast majority of adakites reported have CaO/Na_2O values between 1 and 1.6, the Ngaloa values of 1.9 to 2.9 are in general accord that such assimilation of mantle material may have occurred during their production.

Despite these positive indicators of mantle assimilation by adakitic primary melts in the petrogenesis of the Ngaloa basalts, mass balance equations for the major elements SiO_2, FeO, MgO and CaO for models of assimilation of (any mixture of) peridotitic olivine, spinel, clinopyroxene and orthopyroxene into any typical adakitic magma with ~60-64% SiO_2 are particularly unsuccessful in matching even these major element features of the most mafic Ngaloa basalt (AV208). This is best shown by TiO_2, which is far higher in the Ngaloa basalts (1:4-1.65%) than in either any reported adakite or any mixture of mantle peridotite mineral assimilants. It is concluded, therefore, that the Ngaloa basalts were not produced by assimilation of peridotitic minerals in the mantle wedge by an adakitic slab melt during its ascent to eruption.

Hypothesis 2: Melting Products of an Slab melt-Metasomatised Mantle.

This hypothesis suggests that some adakitic melts generated beneath Kadavu by slab melting passed up in to the mantle wedge peridotite above the slab, and were trapped there through interaction with peridotite; in doing so, they imparted some of their distinctive geochemical traits upon the mantle wedge. Subsequent partial melting of this melt-metasomatised peridotite produced primary magmas that differentiated to form the Ngaloa Group basalts.

Hybridisation between slab-derived melts and adjacent peridotite is likely to be a complex process. The two systems are initially grossly out of chemical equilibrium, and would physically involve the reaction of mantle olivine and pyroxenes with silica-rich hydrous melts to produce new minerals (amphibole, pyroxenes, olivine, and/or garnet; Sekine and Wyllie 1983; Carroll and Wyllie 1989; Kelemen 1990, 1995; Sen and Dunn, 1995). Whether these reaction products are dispersed as pods or veins, or are pervasively distributed through the peridotite is unknown, although mantle xenoliths in adakites from northern Kamchatka contain the assemblage olivine, orthopyroxene, clinopyroxene, garnet and pargasite (Kepezhinskas et al., 1995).

Assuming then that the slab-melt metasomatised mantle wedge is an abnormally clinopyroxene-rich pargasite peridotite, perhaps bearing minor garnet, do the major element compositions of the Ngaloa basalts provide any information about the partial melting process? Evaluation of this problem is further compromised by the recognition that the Ngaloa basalts contain some significant added component, evident in the green-cored clinopyroxene phenocrysts, likely to have been an adakitic dacite/andesite magma such as on western Kadavu (see Ch. 6). Removing

as a first approximation, ~10wt% of a typical western Kadavu dacite (AV90) from most mafic Ngaloa Group basalt AV208 yields a magma with the following general composition: SiO_2 48.5%, TiO_2 1.8%, Al_2O_3 14.8%, total Fe ~7.2%, CaO ~11.1%, Na_2O 3.6%, K_2O 1.6%, P_2O_5 0.82%. The high P_2O_5 and K_2O are reminiscent of OIB-type melts, but the very low total Fe and low TiO_2 contents are atypical of OIB, which is precluded anyway by radiogenic isotope data. Although large extrapolations and assumptions are required (e.g., clearly the Ngaloa magmas were generated by hydrous partial melting), anhydrous peridotite melting experiments (Falloon et al., 1988; Hirose an Kushiro, 1993) show that the characteristic low Fe, high Na, high K and high K features of this reconstructed Ngaloa parent magma are best matched by low degree partial melts of MORB source-type peridotite compositions, at relatively low pressure (10-15 kbar).

5.8 CONCLUSIONS

As shown in Chapter 6, adakitic magmas derived in large part from partial melting of subducted oceanic crust constitute most of the exposed area of Kadavu, and have been generated in this region over the last million years. The Ngaloa basalts (0.36Ma) are the youngest lavas in Kadavu and are shown here to contain a component formed by melting of the subducted oceanic crust. However, their high MgO contents, Fo-rich olivines, and refractory chromites indicate that significant contamination by mantle material occurred during partial melting or ascent to eruption of the Ngaloa basalt magmas.

A preferred model for the petrogenesis of the Ngaloa basalts involves quite low degrees of partial melting of depleted peridotite in the mantle wedge that had been previously metasomatised by siliceous adakitic magmas formed by partial melting of unaltered subducted oceanic crust. Interaction (mixing?) of these magmas with ponded adakitic melts in subvolcanic conduits or magma chambers led to limited contamination of the basaltic magmas, clearly shown by the green Fe-rich cores of clinopyroxenes in all Ngaloa basalts.

Although this model is poorly constrained numerically, both the model and the range of magmas represented on Kadavu and Ngaloa, bear strong similarities to lavas exposed on the Zamboanga Peninsula in the Philippines (Sajona et al., 1996), where adakites and complex 'high-Nb basalts', very similar to the Ngaloa basalts, occur above subducting hot,

young Sulu Sea crust. The tectonic aspects of this adakite-basalt association are discussed in Chapter 7, following presentation in Chapter 6 of the petrology and geochemistry of the dominant adakitic lavas on Kadavu.

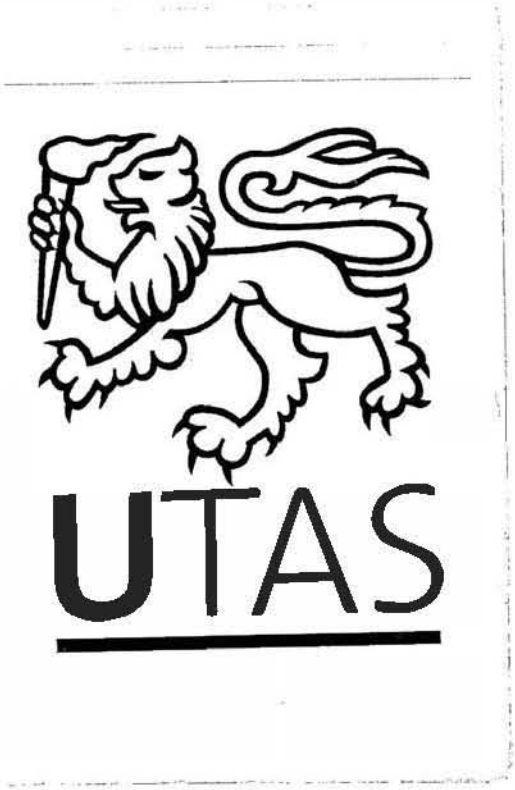

Chapter 6

WESTERN KADAVU AND CENTRAL/EASTERN/ONO GROUPS

Melts from subducted oceanic crust

6.1 INTRODUCTION

It is generally accepted that the source of arc volcanic rocks is predominantly metasomatised peridotite in the mantle wedge above the subducted slab (Kay, 1980; Perfit et al., 1980; Crawford et al., 1987; Morris et al., 1990). Interest in the geochemistry of arc volcanic rocks has increasingly focussed on the nature of slab-derived metasomatising agent (melt or a fluid?) and on processes that occur in the mantle wedge. However, recent studies of volcanic arc systems under which young, hot oceanic crust is being subducted has brought attention to an unusual rock assemblage considered to have been produced by melting of subducted young oceanic crust. Defant and Drummond (1990) termed these rocks adakites after Adak Island, Alaska, where they were first described by Kay (1978). These authors defined adakites as volcanic and intrusive rocks occurring mainly in Cenozoic arcs related to the subduction of oceanic crust ≤ 25m.y. old. Adakites are mineralogically similar to typical calc-alkaline andesites and dacites, with ubiquitous plagioclase phenocrysts, and amphibole phenocrysts are common in all but the more MgO-rich samples. Clinopyroxene, orthopyroxene, biotite and FeTi-oxide phenocrysts may also occur. They have $SiO_2 \geq 56\%$, $Al_2O_3 \geq 15\%$ (rarely lower), MgO usually <3% (rarely above 6%), low Y (<18ppm), Sc (<20ppm) and HREE (Yb <1.9 ppm), high Sr (rarely <400ppm), low HFSE (e.g., Nb and Ta anomalies on normalised diagrams), and $^{87}Sr/^{86}Sr$ <0.7040. Their low Y, Sc and HREE contents and high La/Yb and Sr/Y values are attributed to residual garnet and omphacite in the partially melted eclogitic slab, and their high Sr contents are due to the incompatibility of Sr in this residual eclogite assemblage.

In this chapter, I describe a new adakite suite from the Kadavu Island Group. Andesites and dacites make up the main island of Kadavu, and also Ono, an islet north of Kadavu. Geochemically, these rocks can be separated into two groups, the Western Kadavu (WK) and Central/Eastern/Ono (CEO) Groups. I present a petrological and geochemical study of these rocks

and a petrogenetic model, stressing the importance of slab melting for the origin of the WK and CEO groups.

6.2 GEOLOGY

6.2.1 INTRODUCTION

The main island, Kadavu, is ~93km long and varies in width from several hundred metres to 13km (Fig. 6.1). It has a young mountainous topography with several peaks rising more than 600m. Mount Washington, the highest peak, is 822m high (Plate 6.1). Numerous creeks flow into narrow, steep-sided valleys. Level ground is rare, being restricted to small areas along the coast. The coasts are deeply indented and are generally fringed with coral reefs, the most famous being the 48km loop of the Great Astrolabe Reef on Kadavu's northern extension (Fig. 1.1).

The island is almost completely covered by thick rainforest, but gives way in many places to reeds, especially on the northern part of western Kadavu, where there has been the most cultivation. The deeply embayed, southern shoreline consists of deeply weathered rock or large rounded boulders of lava. Mangrove swamps are common at the heads of the bays. There are few tracks across the island and along the coast, so nearly all travel is by boat.

The morphology of some of the Kadavu volcanoes suggests that they may have been modified by faulting, and the shape of Kadavu itself suggests the possibility of a north-south fault between western and central-eastern Kadavu; however there is no obvious evidence for this on land (Woodrow, 1980). Very little mineralisation has been found. Native copper occurs as tiny specks in basalt from the Astrolabe Islands (Woodrow, 1980), and an extensive area of silicification occurs on the northeastern tip of the island.

Together, the WK and CEO geochemical groups cover the main island Kadavu, and Ono, the small island directly northeast of Kadavu. Ages range from 2.9-0.48Ma (Whelan et al. 1985). There is a temporal geochemical trend towards less potassic magmatism with time, and from high-K through to medium-K rocks progressing west on the main island of Kadavu.

6.2.2 LITHOLOGY

Figure 6.1 shows the outline of the main volcanoes and volcanic features determined from photo interpretation and topography (Woodrow, 1980). Generally, steep-sided (presumably due to the high viscosity lavas, as pyroclastics appear to be subordinate), overlapping circular volcanic cones

Figure 6.1: Sample locations (dots) and the distribution of Western Kadavu and Central/Eastern/Ono groups.
The outline of the major volcanoes and volcanic features after Woodrow, 1980.

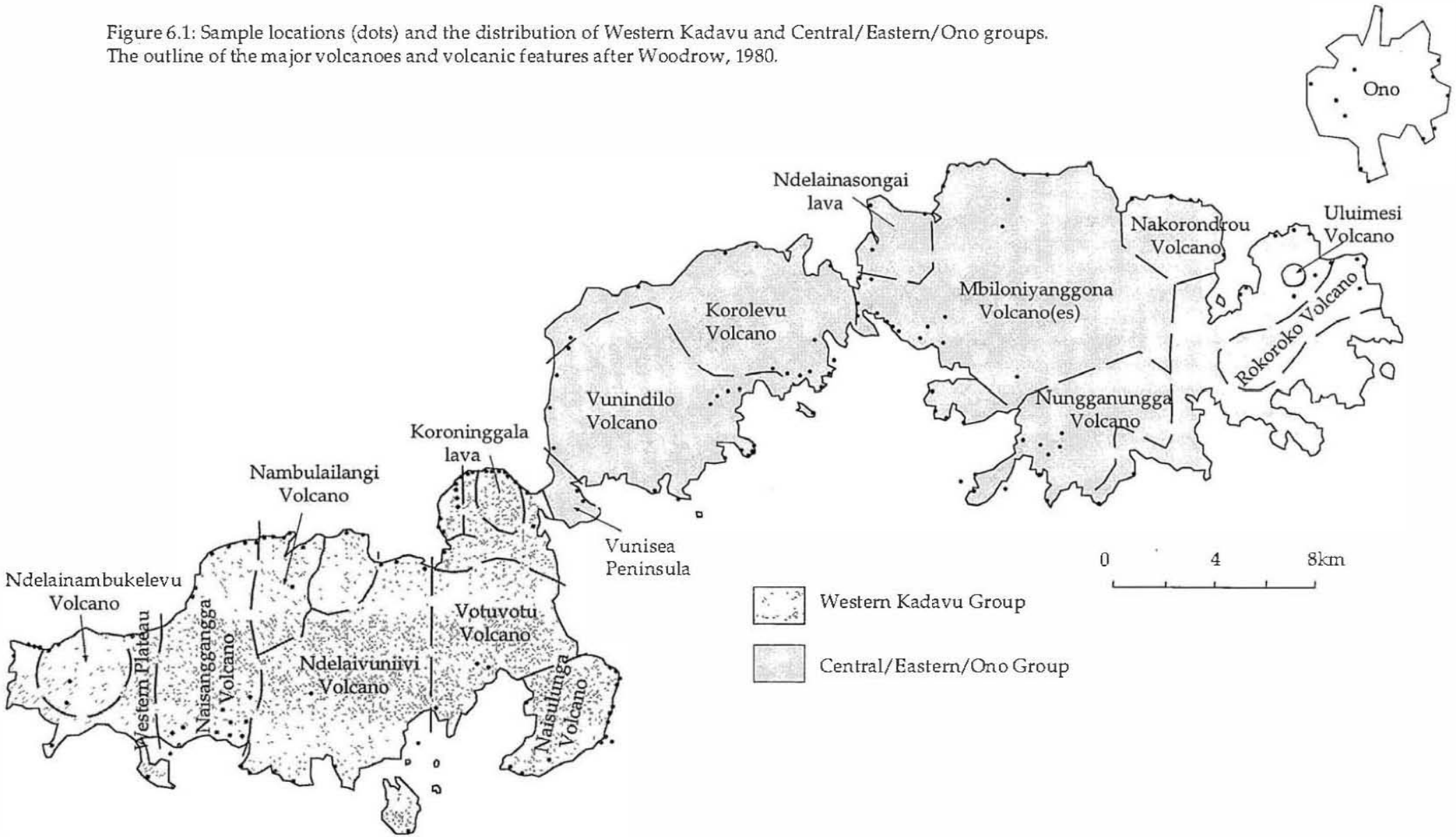

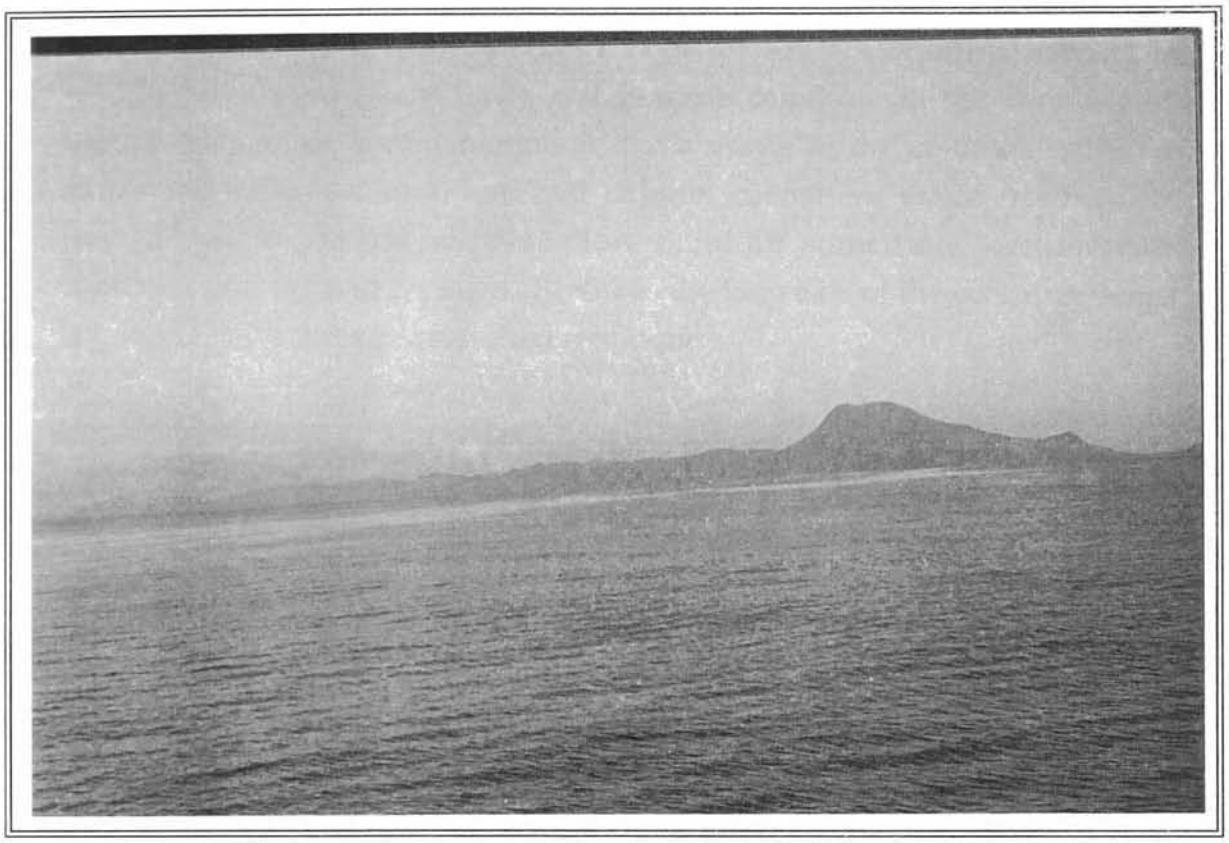

Plate 6.1. Northern side of Kadavu Island. Mt Washington, the highest peak on the island is 822m high, and composed of interbedded flows and coarse breccias of adaktic composition.

make up western Kadavu. Eastern Kadavu consists of more irregular-shaped, ill-defined hills indicating older eruptive centres and more erosion.

Lava Flows

Most lava flows are at least 10m thick and probably thicker, since tops and bases of flows are rarely exposed. A notable feature of the lava flows of Kadavu is the common occurrence of flow banding. Columnar jointing is well developed in many flows and is more common on the central and eastern part of Kadavu. Changes in the attitude of the columns within a single exposure are common, and column diameters range from a few centimetres to several metres. Flow banding sometimes occurs with columnar jointing and is perpendicular to the long axis of the columns. Some lava types show strong spheroidal weathering.

Interbedded flows and breccias

These rocks form the bulk of Kadavu. Flows are generally <2m thick and in some areas predominate over breccias. Some breccias are clearly insitu hyaloclastite, formed by the non-explosive fracturing and disintegration of quenched lavas (Yamagishi and Dimroth, 1985; McPhie et al., 1993). These hyaloclastites are monolithic and have gradational boundaries against coherent and fractured lava (Plate 6.2). Fragments range in size from 5cm to 60cm and fit more or less neatly together (jigsaw fit texture; Plate 6.3); they are sometimes bounded by curviplanar surfaces and generally get larger and more tabular towards the more massive lava. The angular fragments have very sharp contacts with the matrix, which increases in modal abundance towards the more fractured lava areas. In some exposures, flow banding in the lava can be traced continuously from fragment to fragment (Plate 6.4). Where lava flows have possibly flowed into or channelled through wet sediment, peperites have formed and adjacent sediment is baked (Plate 6.5).

6.2.3 SAMPLE LOCATIONS

One hundred and fifty five samples were collected from all the major volcanoes outlined by Woodrow (1980) (Fig. 6.1), mainly from in-situ outcrops of coherent lava along the coast and in the creeks. Occasionally, fragments from monomict breccias were collected. All samples have been examined petrographically and 60 selected rocks were analysed for major and trace elements (Ni, Y, Rb, Nb, Zr, Sr, Cr, Ba, Sc, V) by X-Ray Fluorescence (XRF) spectrometry. From these analyses, 8 carefully selected samples were analysed using ICP-MS for further trace elements, and for Sr,

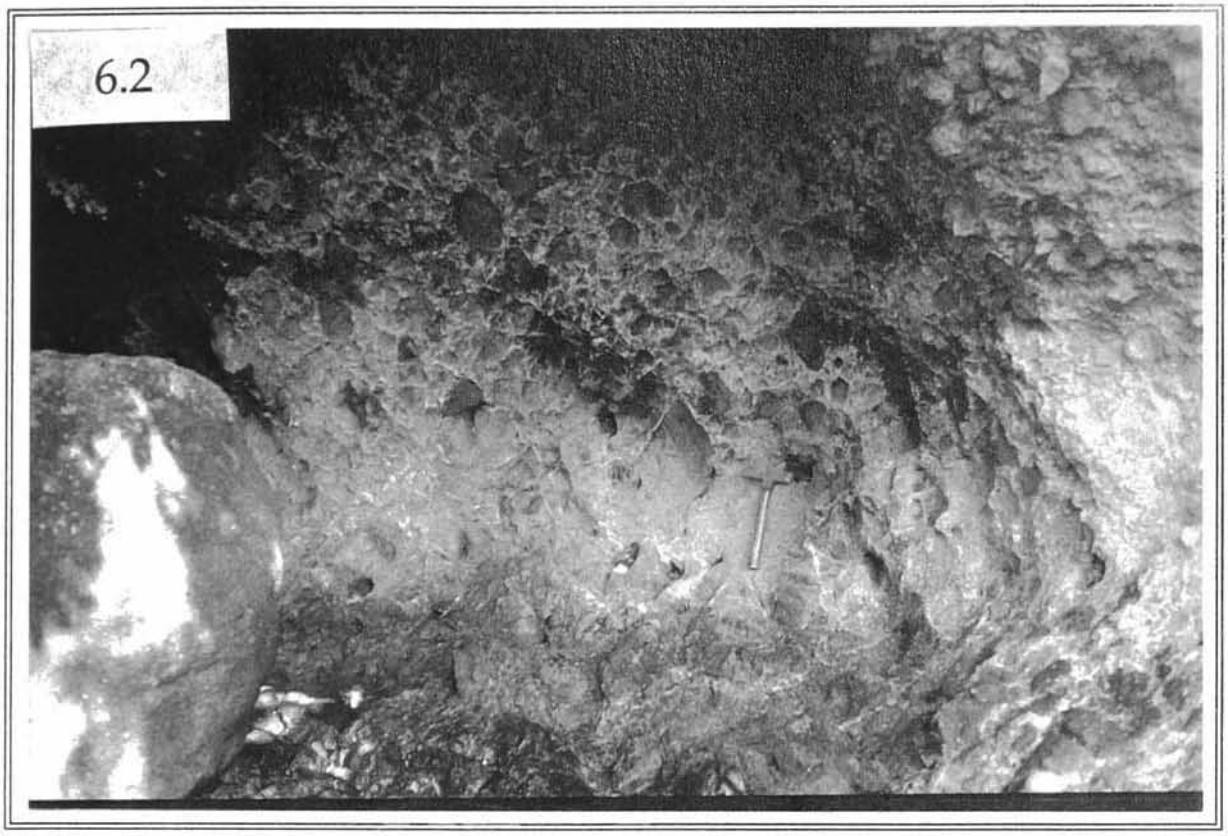
6.2


6.3


6.4


6.5

Nd and Pb isotopes. Analytical procedures are discussed in Appendix 2. Geochemical analyses are listed in Table 6.1.

6.3 PETROGRAPHY AND MINERAL CHEMISTRY

A general petrographic description of rocks from the WK and CEO groups is given below. To avoid repetition, more detailed petrographic descriptions are presented in Appendix 3. Electron microprobe data for representative silicate and oxide phenocrysts and/or microphenocryst phases, are presented in Appendix 4.

The andesites and dacites of the WK group are usually highly porphyritic, with up to 40% phenocrysts of plagioclase, clinopyroxene, orthopyroxene, Ti-magnetite, hornblende and biotite. The relative abundances of the individual phenocryst phases differ markedly among these lavas, with plagioclase and clinopyroxene being the only ubiquitous phenocryst phases. Textures are extremely variable, and groundmasses are usually microcrystalline to glassy, and made up of plagioclase laths, with intergranular clinopyroxene (augite), variable amounts of Ti-magnetite and rare patches of glass.

The lavas of the WK group generally fall into three categories, based on the dominant phenocryst phases:

(i) plag + hornblende + biotite + cpx

(ii) plag + cpx + hornblende ± opx

(iii) plag + cpx.

Rocks from the first category can be easily distinguished in handspecimen from the other types by their large (to 15mm) tabular phenocrysts of plagioclase and euhedral biotite crystals. These rocks weather more easily than other lava types and are restricted to western Kadavu.

In contrast, lavas from the CEO group generally have finer-grained phenocrysts. Excluding Ono Island, biotite is scarce and orthopyroxene is slightly more abundant than in the WK lavas. These lavas generally fall into two main categories based on the dominant phenocrysts phases:

(i) plag + cpx + opx + hornblende

(ii) plag + cpx + opx.

Plagioclase is the most abundant (>10 modal%) phenocryst phase in all samples from the WK and CEO groups. It is commonly present in two size ranges as phenocrysts, occurring as stumpy prisms (1.5-10mm) and relatively small (0.05-1mm) laths. As is characteristic of 'orogenic' andesites, plagioclase phenocrysts in both groups display well-developed complex

Western Kadavu Group

	AV37	AV84	AV54	AV70	AV78	AV76	AV77	AV48	AV72	AV62	AV73
SiO_2	60 70	56.88	58 28	59.46	58.96	61.19	60.73	61.84	61.38	61.08	61.91
TiO_2	0.87	0 81	1.00	0.90	0.51	0 68	0.91	0.87	0 76	0.62	0.67
Al_2O_3	15.92	16.67	16.27	16.21	17 50	16.51	16.01	15.45	16.24	16.71	16.67
FeO*	4 40	5.81	4 64	4.31	5 56	4.55	4.54	3.60	4.35	4.12	3.86
MnO	0.08	0.09	0 08	0 07	0.09	0.08	0.08	0.07	0.08	0.07	0.06
MgO	4 05	3 83	3.80	3 80	3.70	3.47	3.42	3.29	3.29	3.17	3.17
CaO	6.32	6.77	7.13	5 73	6.48	5.83	5.97	5.42	5.47	5.98	4.90
Na_2O	4.61	4.18	4.73	4.53	4.08	4.49	4.70	4.50	4.52	4.32	4.78
K_2O	2 29	1.85	1.69	1.76	1.58	1.92	2.04	1.98	2.00	2.12	1.83
P_2O_5	0.51	0.45	0.55	0.45	0.23	0.30	0.48	0.54	0.33	0.27	0.32
LOI	0.45	1.86	0.96	2.91	1.28	0.71	0.83	1.34	0.81	1.20	0.76
Total	100.69	99 85	99.65	100.62	100.58	100.24	100.21	99.30	99.72	100.10	99.36
Mg#	62.1	54.0	59.3	61.1	54.3	57.6	57.3	62.0	57.4	57.8	59.4
Ni	56	13	114	48	19	22	45	55	27	25	46
Y	16	10	13	13	13	13	16	14	17	15	14
Rb	34	7	23	25	20	30	31	31	32	36	29
Nb	15.5	8.3	12.1	11.9	3.2	9.1	13.8	11.3	10.8	10.0	9.6
Zr	204	176	174	191	102	132	182	172	151	162	150
Sr	1317	1263	1580	1488	888	1102	1171	1377	1151	870	1048
Cr	97	59	109	54	15	24	56	51	27	29	34
Ba	491	471	371	484	343	423	424	417	453	459	412
Sc	14	19	14	11	20	14	13	9	14	14	12
V	129	198	158	130	178	139	144	108	136	122	116
Li			8.20					13.30			
Be			1.64					2.01			
Co			24					14			
Cu			44					41			
Zn			57					51			
Ga			19					18			
Mo			0.32					1.30			
Sn			1.07					1.01			
Sb			0.04					0.11			
Cs			0.10					0.47			
La			33.33					34.48			
Ce			71.83					74.27			
Pr			9.11					9.15			
Nd			34.89					35.42			
Sm			5.83					5 87			
Eu			1.54					1.58			
Gd			3 98					4.08			
Tb			0.51					0.52			
Dy			2 44					2.52			
Ho			0.44					0.46			
Er			1.13					1.20			
Yb			0.96					1.03			
Lu			0.14					0.15			
Hf			3.07					2.36			
Ta			0.71					0.75			
Tl			0.04								
Pb			3.60					5.62			
Th			3.94					5.44			
U			1.05					1.91			

Table 6.1. Major (wt%) and trace element (ppm) analyses, and isotopic data for the Western Kadavu and Central/Eastern/Ono Groups. Major elements and Ni, Y, Rb, Zr, Sr, Cr, Ba, Sc and V analysed by XRF. Other trace elements analysed by ICP-MS. Sr and Nd isotope data have been normalised to $^{86}Sr/^{88}Sr=0.1194$ and $^{146}Nd/^{144}Nd=0.7219$ respectively. Pb isotopic data has been corrected for instrumental mass fractionation. For the Sr, Nd and Pb isotope data the $2\sigma_{mean}$ values associated with individual sample measurements indicate within-run precision only.

	AV85	AV91	AV94	AV14	AV50	AV40	AV5	AV66	AV57	AV59	AV90	AV31
SiO_2	61.78	61.55	61.86	64.69	64.89	63.54	63.09	61.92	60.05	60.18	65.64	63.81
TiO_2	0.73	0.58	0.63	0.55	0.59	0.51	0.57	0.67	0.86	0.63	0.45	0.69
Al_2O_3	16.28	17.15	16.86	16.28	15.99	17.52	16.34	17.54	17.35	17.89	15.88	17.40
FeO*	3.90	4.51	4.01	3.27	3.31	3.36	3.39	3.91	4.42	3.92	3.10	4.23
MnO	0.05	0.08	0.07	0.07	0.07	0.05	0.07	0.07	0.07	0.05	0.06	0.08
MgO	3.06	2.86	2.70	2.69	2.60	2.53	2.46	2.44	2.23	2.20	1.98	1.09
CaO	4.88	5.46	5.08	4.42	4.17	4.79	4.38	5.33	6.14	5.22	3.87	4.26
Na_2O	4.78	4.54	4.42	5.03	4.83	5.04	4.40	5.18	4.79	5.21	4.22	5.03
K_2O	2.36	1.80	2.19	2.18	1.98	1.45	2.55	1.70	1.75	1.77	2.72	2.11
P_2O_5	0.35	0.33	0.29	0.38	0.39	0.23	0.27	0.37	0.45	0.37	0.24	0.33
LOI	2.31	1.54	1.65	1.42	1.71	1.49	2.06	1.16	1.28	0.91	2.49	1.86
Total	100.91	100.89	100.20	101.33	100.88	100.89	99.96	100.71	99.89	98.78	101.01	101.36
Mg#	58.3	53.1	54.5	59.5	58.3	57.3	56.4	52.7	47.3	50.0	53.2	31.5
Ni	29	15	18	24	38	50	19	17	32	28	10	18
Y	36	29	14	13	13	10	12	14	20	14	16	15
Rb	44	25	34	34	32	17	53	23	23	26	50	34
Nb	13.4	7.6	10.4	9.4	9.9	5.3	10.7	9.7	8.7	8.0	9.9	10.7
Zr	164	134	175	147	180	129	171	161	178	171	185	152
Sr	1015	1304	961	909	914	1120	867	1136	1667	1411	779	927
Cr	39	12	18	21	34	33	20	8	46	29	16	24
Ba	483	536	490	414	409	402	567	413	466	480	588	482
Sc	13	13	11	8	11	10	11	9	11	10	9	15
V	123	139	108	78	94	97	90	111	133	105	70	115
Li									9.70		6.40	
Be									2.29		1.90	
Co									14		9	
Cu									63		34	
Zn									70		38	
Ga									21		16	
Mo									0.99		2.14	
Sn									1.00		0.95	
Sb									0.06		0.19	
Cs									0.41		0.85	
La									30.56		28.14	
Ce									64.03		56.64	
Pr									8.74		6.82	
Nd									35.74		25.48	
Sm									6.20		4.46	
Eu									1.75		1.10	
Gd									4.58		3.40	
Tb									0.59		0.49	
Dy									2.99		2.60	
Ho									0.59		0.52	
Er									1.65		1.49	
Yb									1.60		1.48	
Lu									0.26		0.23	
Hf									3.74		2.97	
Ta									0.50		0.58	
Tl									0.13		0.31	
Pb									5.28		7.56	
Th									3.80		5.36	
U									1.20		1.82	

Table 6.1. Continued

Central/Eastern/Ono Group

	AV117	AV214B	AV219	AV141	AV232	AV103	AV127	AV118	AV154	AV153	AV223	AV199
SiO_2	56.84	55.76	57.44	55.47	59.31	60.86	57.15	57.13	57.75	57.31	59.68	56 80
TiO_2	0.55	0.60	0.57	0.79	0.51	0.58	0.65	0.56	0.55	0.60	0.52	0 67
Al_2O_3	15.20	15.84	15.41	16.07	15.76	15.94	16.18	17.08	15.60	15.77	16.24	16.16
FeO*	5.86	6.63	5.79	6.55	5.43	4.75	6.41	6.10	6.38	5.81	5.16	7 41
MnO	0.11	0.13	0.10	0.12	0.10	0.10	0.14	0.11	0.11	0.11	0.09	0 18
MgO	6.61	4.79	4.52	4.37	4.27	4.24	4.21	4.19	4.04	3.77	3.73	3 71
CaO	7.79	7.64	6.81	7.58	6.25	5.89	7.06	7.20	6.78	6.74	6.17	7.31
Na_2O	3.48	3.41	3.59	3.82	3.75	3.91	3.66	3.64	3.01	3.41	3.88	3.03
K_2O	2.16	2.15	2.55	2.09	2.28	2.91	2.46	1.95	2.18	2.78	2.25	2.45
P_2O_5	0.35	0.37	0.34	0.50	0.31	0.39	0.45	0.30	0.21	0.46	0.26	0.26
LOI	1.42	1.20	2.36	1.10	2.29	0.51	1.53	1.24	2.03	2.26	0.83	1.31
Total	101.01	99.26	100.12	99.19	100.86	100.61	100.61	100.18	99.34	99.67	99.39	100.12
Mg#	66.8	56.3	58.2	54.3	58.4	61.4	53.9	55.0	53.0	53.6	56.3	47.2
Ni	81	19	90	6	21	75	16	15	14	8	30	8
Y	16	16	14	23	18	16	34	14	18	23	20	19
Rb	37	32	44	36	40	52	40	31	45	50	35	54
Nb	3.7	3.4	4.1	5.4	3.3	4 5	4.7	2.8	2.9	3.3	2.5	3.9
Zr	143	123	146	180	144	198	160	116	105	187	124	121
Sr	1097	1292	1258	1394	941	1088	1284	1040	553	1414	1195	655
Cr	224	61	199	35	37	100	35	29	52	23	40	10
Ba	511	462	871	547	476	605	626	476	360	733	584	466
Sc	23	24	20	25	20	15	21	22	26	18	17	26
V	192	248	198	244	174	154	217	213	207	229	184	262
Li	5.42			9.45	7.54							
Be	2.07			2.20	1.90							
Co	25			24	20							
Cu	83			115	74							
Zn	49			65	50							
Ga	16			18	17							
Mo	1.19			0.44	0.75							
Sn	0.86			0.58	0.78							
Sb	0.12			0.06	0.09							
Cs	0.75			0.51	0.62							
La	26.06			43.05	23.74							
Ce	55.90			92.40	52.13							
Pr	7.36			11.77	7.04							
Nd	29.99			47.67	29.07							
Sm	5.79			8.83	5.75							
Eu	1.60			2.37	1.58							
Gd	4.33			6.40	4.64							
Tb	0.56			0.81	0.61							
Dy	2.75			3.98	3.07							
Ho	0.51			0.72	0.58							
Er	1.35			1.90	1.57							
Yb	1.17			1.65	1.38							
Lu	0.18			0.25	0.22							
Hf	3.30			4.06	3.34							
Ta	0.19			0.29	0.19							
Tl				0.17	0.21							
Pb	8.63			9.25	6 70							
Th	3.78			5.50	3.37							
U	1.47			1.91	1.38							

	AV150	AV123	AV205	AV201	AV231	AV211	AV107	AV133	AV137	AV213	AV140	AV207
SiO_2	57.56	61.15	58.27	57.69	59.79	58.63	61.87	61.08	58.88	56.84	58.88	59.84
TiO_2	0.61	0.49	0.68	0.63	0.51	0.42	0.52	0.46	0.56	0.51	0.46	0.52
Al_2O_3	16.13	15.82	16.88	15.89	16.65	17.22	16.39	15.27	17.15	17.30	17.62	16.15
FeO*	6.28	5.09	7.32	6.62	5.19	5.63	4.50	5.18	5.86	6.33	5 73	5.39
MnO	0.11	0.11	0.14	0.13	0.09	0.11	0.08	0.10	0.12	0.11	0.12	0.10
MgO	3.69	3.65	3.63	3.61	3 44	3.31	3.25	3.24	3.22	3.21	3.08	3.02
CaO	6.65	6.09	7.19	6.74	5 65	6.41	5.33	5.79	6.30	6.60	6.51	5.66
Na_2O	3.88	3.94	3.32	3.21	4.10	3.64	4.21	3.58	4.10	3.61	3.60	3.85
K_2O	2.34	2.56	2 54	2.87	2.31	1.98	2.79	2.65	2.11	1.65	2.11	2.56
P_2O_5	0.54	0.28	0.27	0.24	0.31	0.20	0.31	0.22	0.33	0.22	0.23	0.32
LOI	1.45	0.90	2.44	1.32	0.93	1.59	0.67	1.31	1.50	3.06	2.58	1.51
Total	99.94	100 66	103 51	99.70	99.55	99.77	100.40	99.44	100.77	100.15	101.55	99.51
Mg#	51.2	56.1	46.9	49 3	54.2	51.2	56.3	52.7	49.5	47.5	48 9	50.0
Ni	9	17	5	7	23	6	25	7	5	11	3	5
Y	24	17	18	18	15	13	18	14	16	11	15	16
Rb	50	43	48	56	40	32	46	47	41	26	31	48
Nb	4.7	4.0	3.6	3.9	3.5	1.9	4.5	2.7	3.8	1.4	1.7	4.2
Zr	212	147	119	135	150	101	174	124	128	91	104	153
Sr	1272	990	673	563	950	955	939	870	997	1031	914	915
Cr	25	59	8	22	25	9	42	25	4	16	4	9
Ba	740	629	467	492	473	432	532	584	492	417	428	567
Sc	19	16	24	22	17	18	14	18	18	23	18	16
V	238	162	224	208	170	173	143	168	205	226	180	176

	AV196	AV227	AV158	AV164	AV126	AV142	AV169	AV100	AV129	AV101	AV113	AV216	AV225
SiO_2	60.31	61.12	56.21	61.25	61.25	60.68	56.44	63.02	61.41	61.02	65.84	63.60	61.03
TiO_2	0.53	0.50	0.69	0.55	0.59	0.43	0.60	0.47	0.50	0.57	0.40	0.45	0.40
Al_2O_3	16.41	16.55	18.06	16.03	16.72	16.74	18.18	16.26	16.57	17.36	15.52	15.81	17.93
FeO*	5.27	4.40	6.41	4.94	5.00	4.42	6.22	4.07	5.13	5.25	3.27	4.40	4.63
MnO	0.13	0.07	0.18	0.07	0.10	0.07	0.21	0.07	0.09	0.06	0.04	0.07	0.07
MgO	2.97	2.87	2.70	2.60	2.51	2.39	2.38	2.36	2.29	2.21	1.96	1.85	1.60
CaO	5.59	5.51	6.35	5.17	5.00	4.90	6.50	4.43	5.59	5.32	3.30	4.38	3.91
Na_2O	3.97	4.07	4.30	4.42	3.86	4.28	4.22	4.35	4.22	4.26	4.17	4.08	4.34
K_2O	2.05	2.80	3.07	3.09	2.68	1.95	2.13	2.95	2.55	2.70	3.21	2.91	2.15
P_2O_5	0.27	0.29	0.37	0.30	0.27	0.27	0.35	0.30	0.25	0.37	0.23	0.22	0.21
LOI	1.32	0.66	0.77	1.13	1.76	2.10	1.07	1.08	1.52	1.41	1.65	0.66	2.22
Total	99.40	99.33	99.82	100.09	100.30	98.71	98.99	99.82	100.71	101.12	99.95	98.92	99.01
Mg#	50.1	53.8	42.9	48.4	47.2	49.1	40.5	50.8	44.3	42.9	51.7	42.8	38.1
Ni	15	33	3	17	18	17	3	18	29	18	31	4	8
Y	14	14	1	15	55	40	18	15	16	19	31	18	6
Rb	37	43	54	48	40	34	43	49	45	47	56	51	8
Nb	3.9	3.4	4.2	3.5	2.7	2.0	3.0	4.0	2.8	4.1	3.7	2.6	2.0
Zr	115	159	105	156	152	131	85	166	122	176	161	148	103
Sr	865	1144	1178	1435	1084	1017	1106	896	1060	955	829	810	1427
Cr	32	43	1	39	16	18	1	16	34	28	41	6	9
Ba	536	650	545	841	631	497	508	583	620	539	576	595	1128
Sc	16	15	14	16	16	13	12	16	20	18	11	16	14
V	167	155	200	162	167	136	167	128	178	158	95	142	142
Li		8.07											
Be		2.19											
Co		17											
Cu		63											
Zn		48											
Ga		18											
Mo		0.80											
Sn		0.84											
Sb		0.09											
Cs		0.56											
La		22.93											
Ce		47.21											
Pr		6.30											
Nd		25.59											
Sm		4.93											
Eu		1.35											
Gd		3.73											
Tb		0.48											
Dy		2.36											
Ho		0.44											
Er		1.17											
Yb		1.01											
Lu		0.16											
Hf		3.78											
Ta		0.21											
Tl		0.19											
Pb		7.09											
Th		3.57											
U		1.47											

	$^{87}Sr/^{86}Sr$	±2σ	$^{143}Nd/^{144}Nd$	±2σ	$^{206}Pb/^{204}Pb$	±2σ	$^{207}Pb/^{204}Pb$	±2σ	$^{208}Pb/^{204}Pb$	±2σ
AV54	0.70296	22	0.51304	8	18.778	2	15.520	2	38.291	6
AV48	0.70301	17	0.51304	10	18.829	2	15.529	4	38.350	11
AV57	0.70298	21	0.51304	7	18.796	1	15.543	1	38.362	4
AV90	0.70326	23	0.51302	8	18.792	1	15.525	1	38.322	2
AV117	0.70332	18	0.51301	9	18.844	1	15.518	1	38.334	1
AV141	0.70321	20	0.51304	9	18.761	1	15.541	1	38.331	4
AV232	0.70335	21	0.51301	10	18.837	1	15.526	1	38.344	3
AV227	0.70325	18	0.51302	9	18.812	1	15.535	1	38.353	3

Table 6.1. Continued.

oscillatory zoning, which is usually more pronounced on crystal margins. Rounded to irregular brown glassy inclusions are often present in the plagioclase and may be concentrated in crystal cores, or in one or more distinct zones paralleling crystal margins. The appearance of these melt inclusions are evidence for a primary origin (Halsor, 1989), and suggests that they were trapped in plagioclase phenocrysts during rapid growth. 'Dusty' or resorbed plagioclase also occurs in the CEO group (Plate 6.6).

Plagioclase phenocryst core compositions span a wide range (WK: An_{30-70}; CEO: An_{25-75}), reflected in the histograms in Figure 6.2, and single crystal zoning of An contents (Table A4.15 and A4.19; Appendix 4) is always less than the range shown by phenocryst cores in any sample. The WK and CEO plagioclase phenocrysts are more sodic than the average plagioclase phenocryst composition in calc-alkaline series andesites recorded by Ewart (1982) (An_{50-70}). The WK plagioclase phenocrysts have lower K_2O at any An level compared to those in CEO lavas (Fig. 6.3), consistent with differences in wholerock K_2O contents between these groups. Glass inclusions in the plagioclase phenocrysts are rhyolitic (SiO_2 69-76%; Table A4.16 and A4.20, Appendix 4).

The most common pyroxene phenocrysts in the WK and CEO groups are subhedral to euhedral clinopyroxenes (3-15 modal%), which range in size from 0.02 to 1mm and are commonly found in glomeroporphyritic clusters with plagioclase and Ti-magnetite. Orthopyroxene (~3 modal%) occurs as subhedral to euhedral pink-pale green pleochroic crystals generally ≤1mm long, that are commonly associated with Ti-magnetite crystals.

Compositions of pyroxene phenocryst cores in the WK and CEO andesites and dacites are shown in Figure 6.4. The WK group clinopyroxenes are dominated by augite, but range from endiopside-diopside-salite to augite. The CEO group clinopyroxenes also show this range; however they are dominated by salite and augite. Orthopyroxene (hypersthene) ranges in composition from En_{70-75} ($Mg^{\#}$=71-76).

Clinopyroxene phenocryst cores show a greater range in $Mg^{\#}$ values (75-92) than most typical calc-alkaline andesites (e.g., Volcan Colima, Mexico Mg#=74-82; Luhr and Carmichael, 1980). The minor elements TiO_2 and Na_2O also show considerable variation in clinopyroxene phenocrysts (Fig. 6.5) and tend to increase with decreasing $Mg^{\#}$; TiO_2 contents of clinopyroxene at Mg>80 are slightly higher in the WK lavas. The range in TiO_2 and Na_2O in the WK and CEO group clinopyroxene phenocrysts compares well with the core compositions of the strongly reverse zoned clinopyroxene phenocrysts from the Ngaloa Group volcanics, although the latter are mainly slightly lower $Mg^{\#}$ (70-74). The presence of rare high-$Mg^{\#}$

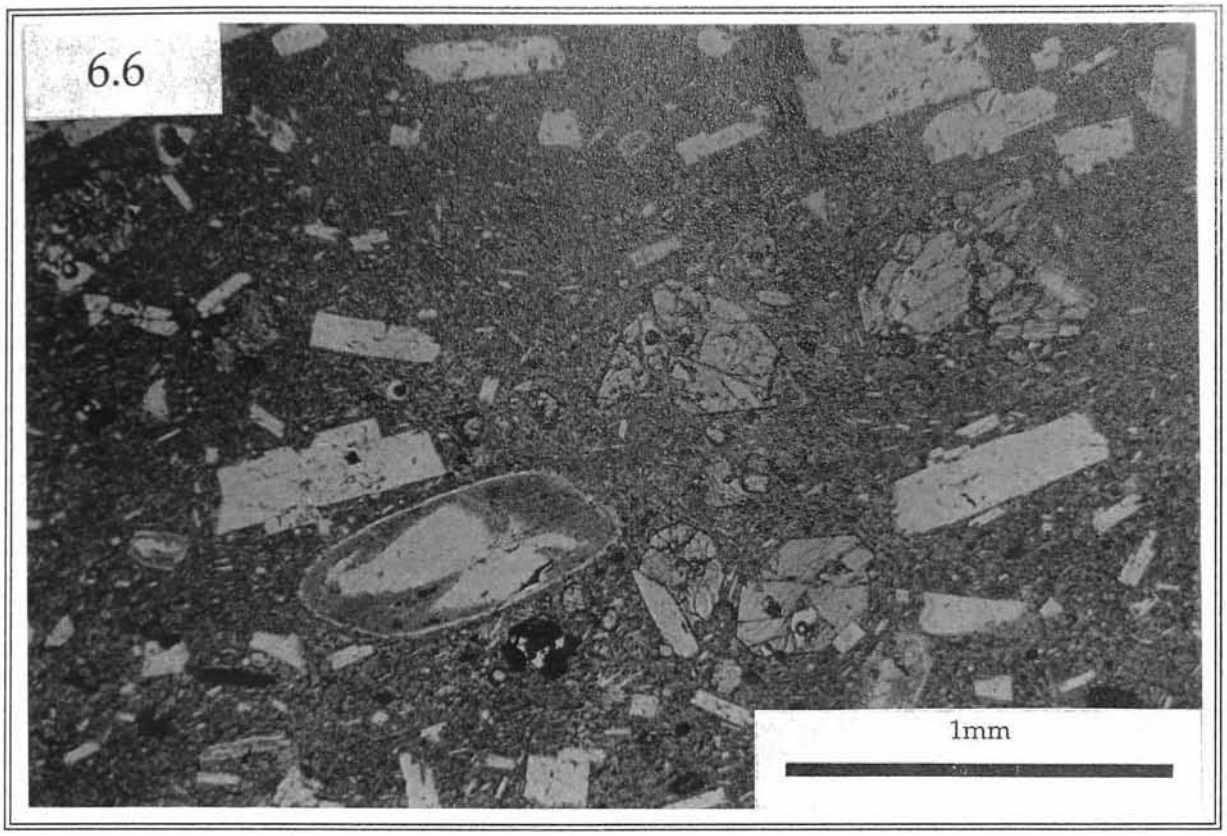
6.6
1mm

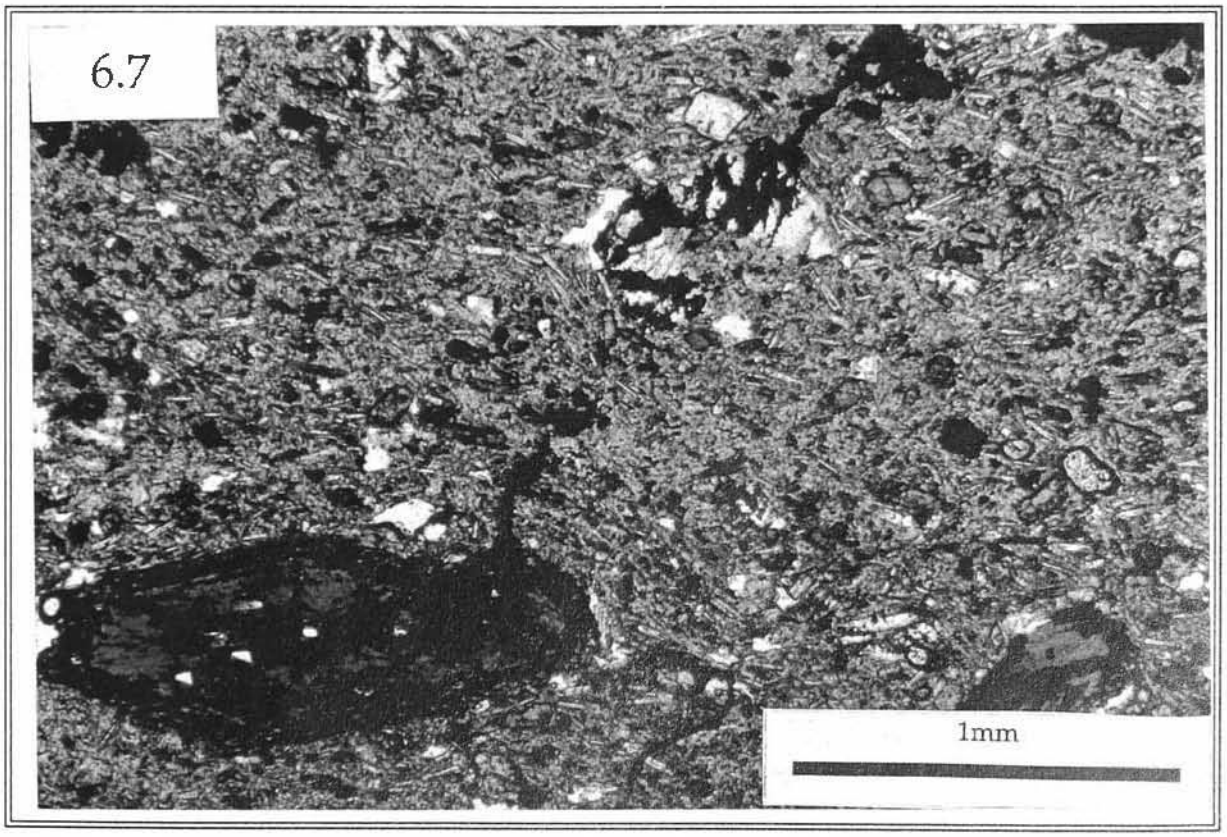
6.7
1mm

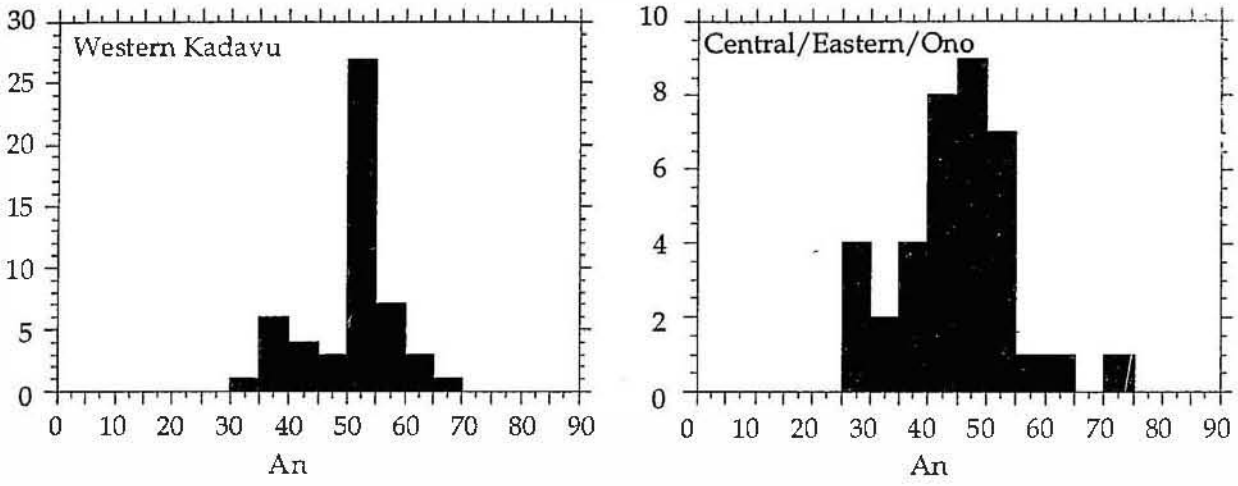

Figure 6.2. Anorthite content of plagioclase phenocryst cores from the Western Kadavu and Central/Eastern/Ono Groups.

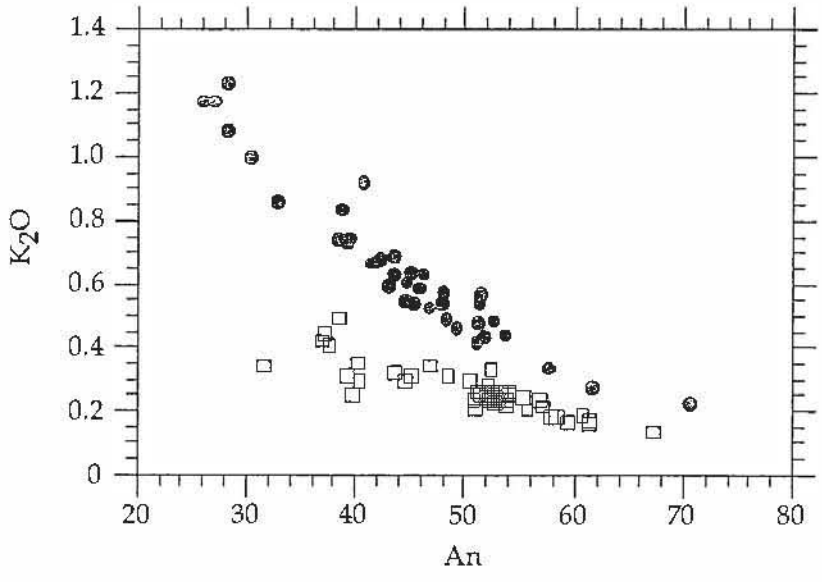

Figure 6.3. K_2O vs Anorthite content in plagioclase phenocryst cores from the Western Kadavu (open squares) and Central/Eastern/Ono (filled circles) Groups.

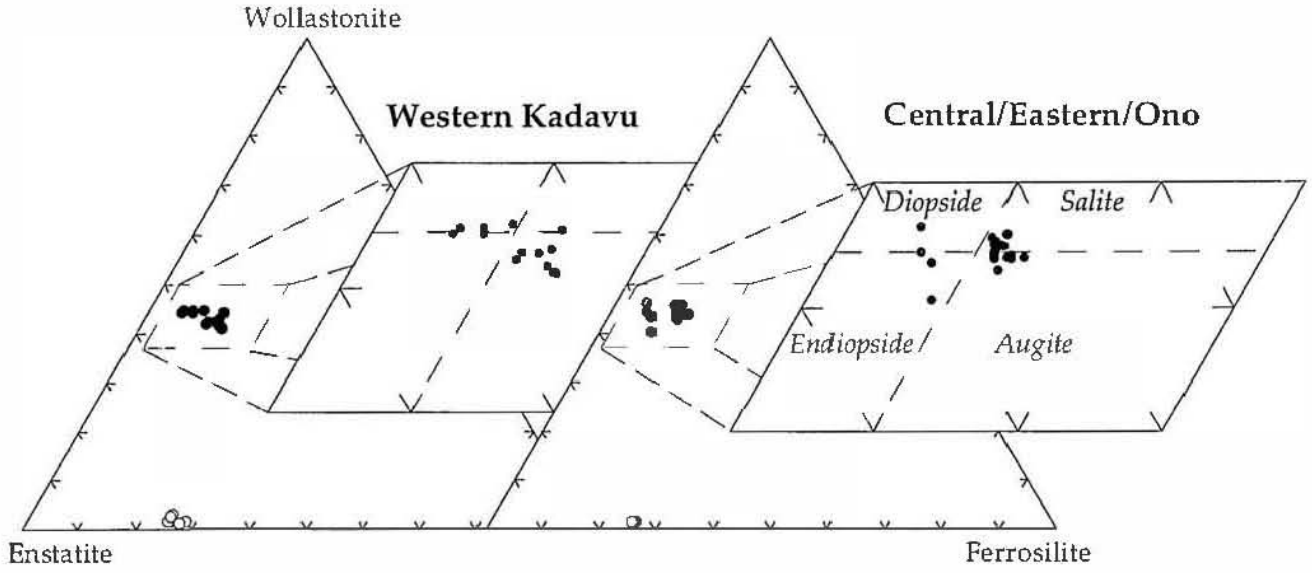

Figure 6.4: Composition of clinopyroxene (filled circles) and orthopyroxene (open circles) phenocrysts from the Western Kadavu and Central/Eastern/Ono Groups.

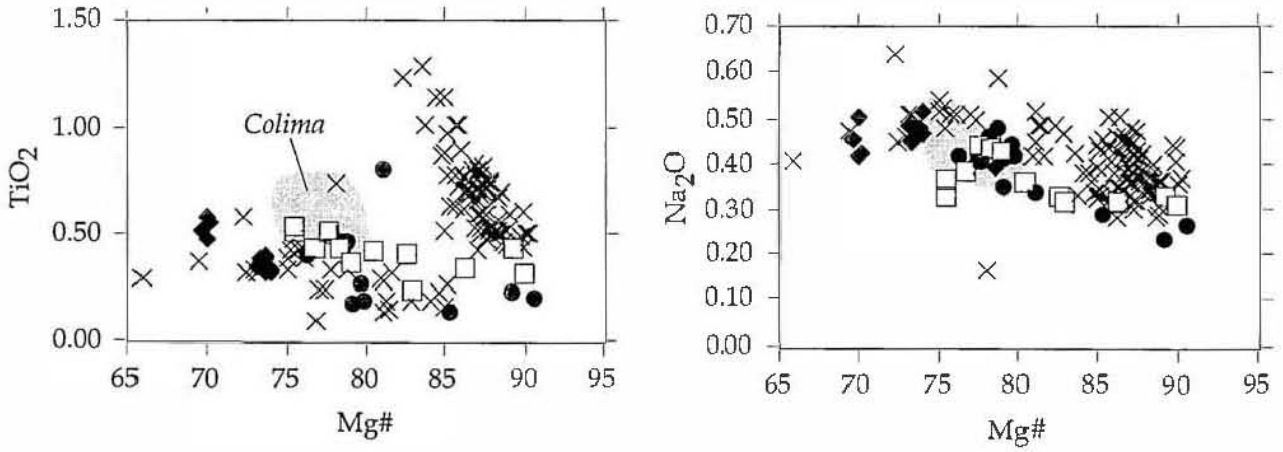

Figure 6.5. TiO_2 and Na_2O contents in clinopyroxene phenocryst cores from the Western Kadavu (open squares) and Central/Eastern/Ono (filled cirlces) Groups compared to the Ngaloa Group clinopyroxene phenocrysts (crosses), the green-cored Ngaloa phenocrysts, (filled diamonds) and clinopyroxene phenocryst cores from Colima calc-alkaline andesites (Luhr and Carmichael, 1980).

(89-91) clinopyroxene phenocrysts in both suites of andesites, and the similarity of these primitive phenocrysts in terms of TiO_2 and Na_2O abundances to the most primitive clinopyroxene phenocrysts in the Ngaloa suite basalts, suggests limited mixing of the andesites and dacites with more mafic magmas such as the Ngaloa basalts. However, direct derivation of these andesites from Ngaloa-type basalts can be confidently ruled out by trace element considerations (see next section).

Hornblende phenocrysts average ~4modal%, are <2mm long and are commonly euhedral or bladed. Polycrystalline aggregates are rare, and hornblende is generally absent from groundmass assemblages. Some degree of disequilibrium exists between the hornblendes and the host magmas, as phenocrysts show different degrees of resorption. Reaction rims consisting mainly of very fine-grained Fe-Ti oxide (opacite) are common (Plate 6.7). This disequilibrium may reflect decompression breakdown during ascent (perhaps due to loss of H_2O), or the influx of new higher temperature or low-H_2O magma into the storage region (Rutherford and Hill, 1993).

Electron microprobe analyses of hornblendes from the WK and CEO group lavas have been recalculated to the method recommended by Leake (1978) on an anhydrous basis of 23 oxygen atoms. According to Leake's (1978) classification, WK group hornblendes are magnesio-hornblendes (Fig. 6.6), whereas those in the CEO lavas range from tschermakite to tschermakitic hornblende. Hornblende $Mg^{\#}$ values for typical calc-alkaline andesites such as Colima and Stromboli are in the range 65-70 (Luhr and Carmichael, 1980). As hornblende $Mg^{\#}$ values are directly related to that of the liquid from which they crystallised (Allen et al., 1975), it is inferred that the Kadavu hornblendes grew from unusually high-$Mg^{\#}$ andesitic magmas, probably due to their low total Fe contents (5% FeO at 60% SiO_2) relative to typical calc-alkaline andesites.

Biotite appears as euhedral grains (up to 1.5mm) with the pleochroism ranging from light yellow to the characteristic dark mottled brown. Although conspicuous in handspecimen, it is sparse in thin section. Ti-magnetite is common in all samples as isolated microphenocrysts (usually 0.5-3 modal%), in crystal clusters with pyroxene and plagioclase, within hornblende reaction rims, and as groundmass grains. Apatite occurs as occasional typically subhedral microphenocrysts in the WK and CEO andesites, never longer than 0.2mm.

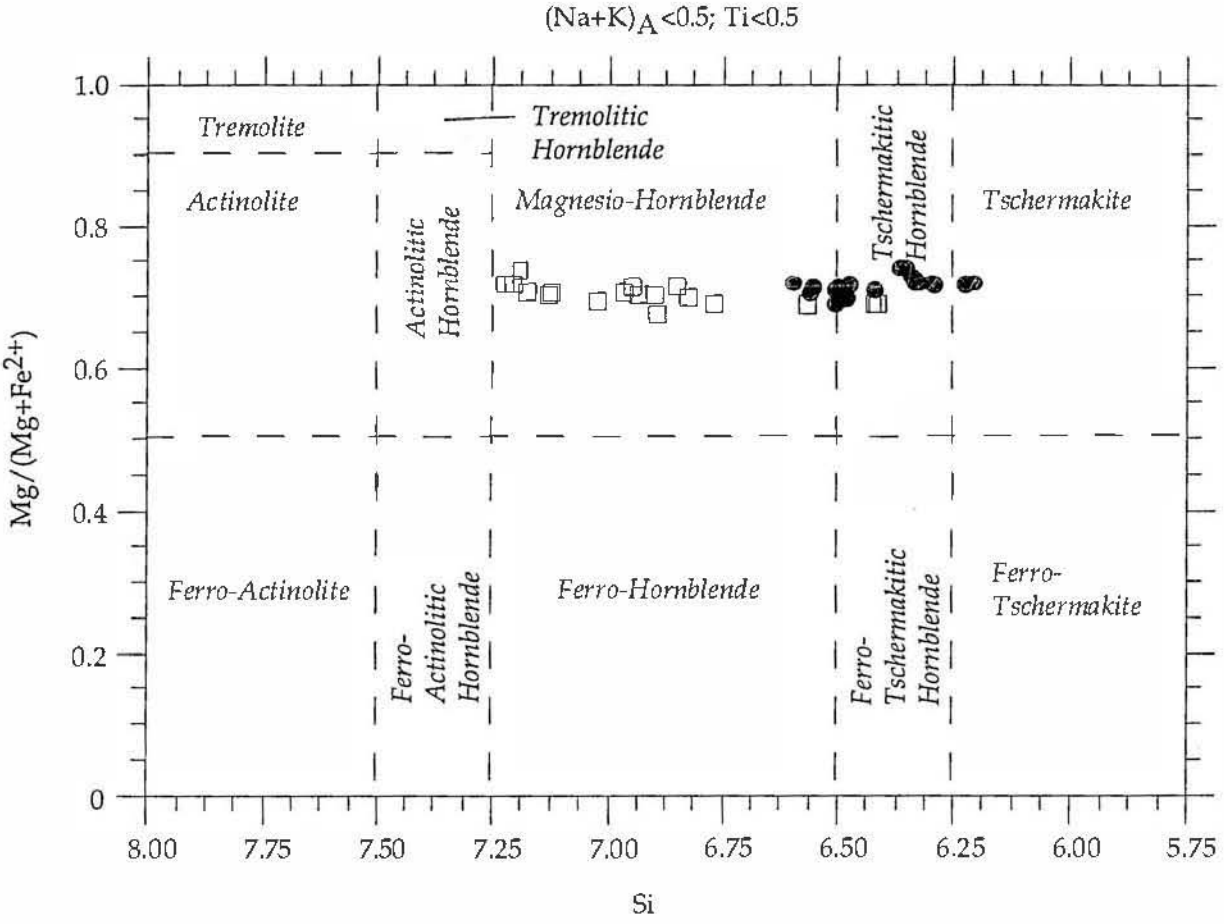

Figure 6.6: Composition of hornblende phenocryst cores from the Western Kadavu (open squares) and Central/Eastern/Ono Groups (filled circles).

6.4 GEOCHEMISTRY OF THE WESTERN KADAVU AND CENTRAL/EASTERN/ONO GROUPS

6.4.1 MAJOR ELEMENT GEOCHEMISTRY

The K_2O-SiO_2 variations for the WK and CEO group lavas indicates medium- to high-K affinities (Fig. 6.7). Despite their intra-oceanic setting, they have clearly higher abundances of K_2O (WK: 1.45-2.72%; CEO: 1.65-2.95%) and particularly P_2O_5 (WK: 0.23-0.55%; CEO: 0.20-0.54%) than typical medium-K calc-alkaline andesites (Fig. 6.7). Both the WK and CEO groups show a significant scatter in Al_2O_3 contents, indicating no strong control by phenocrystal plagioclase. Significant compositional differences between the WK and CEO suites are evident from Figure 6.7. At 4% MgO, the latter suite has lower TiO_2 and Na_2O and higher FeO and K_2O than the WK andesites. For SiO_2, Al_2O_3 and CaO, there are no significant differences between these suites. These contrasting fractionation trends for some of the major elements between the WK and CEO groups suggest differences in parental magma composition, and the extent of fractionation and mixing/contamination before eruption. However, the range of K_2O (1.7-2.9%) and P_2O_5 (0.22-0.55%) contents in CEO lavas having ~57% SiO_2 clearly indicates that even lavas in this group are unlikely to be comagmatic, but probably derived from a range of parental magmas. No attempt has therefore been made to model fractionation trends linking the most 'mafic' and most evolved members of each suite

6.4.2 TRACE ELEMENT GEOCHEMISTRY

Variation diagrams of selected trace elements are shown in Figure 6.8. The WK and CEO andesites and dacites differ from typical calc-alkaline orogenic arc andesites (Ewart, 1982) by having very high Sr contents, mainly between 800 and 1600 ppm, nearly twice the levels in Colima andesites. In keeping with the transitional high-K affinities of the WK and CEO groups, they have high contents of Rb, but Ba levels for the WK suite are similar to those for Colima. In contrast, the CEO group lavas have slightly higher Ba contents on average, though a few samples have >800ppm Ba. Abundances of Zr are quite variable within each group, although the WK lavas generally have greater Zr contents, particularly between 57 and 60% SiO_2. The WK and CEO lavas have similar contents of V and Sc to Colima andesites, and these elements emphasise the distinction between the CEO and WK groups already noted on the basis of the FeO-MgO, with both elements paralleling FeO and decreasing with advancing fractionation.

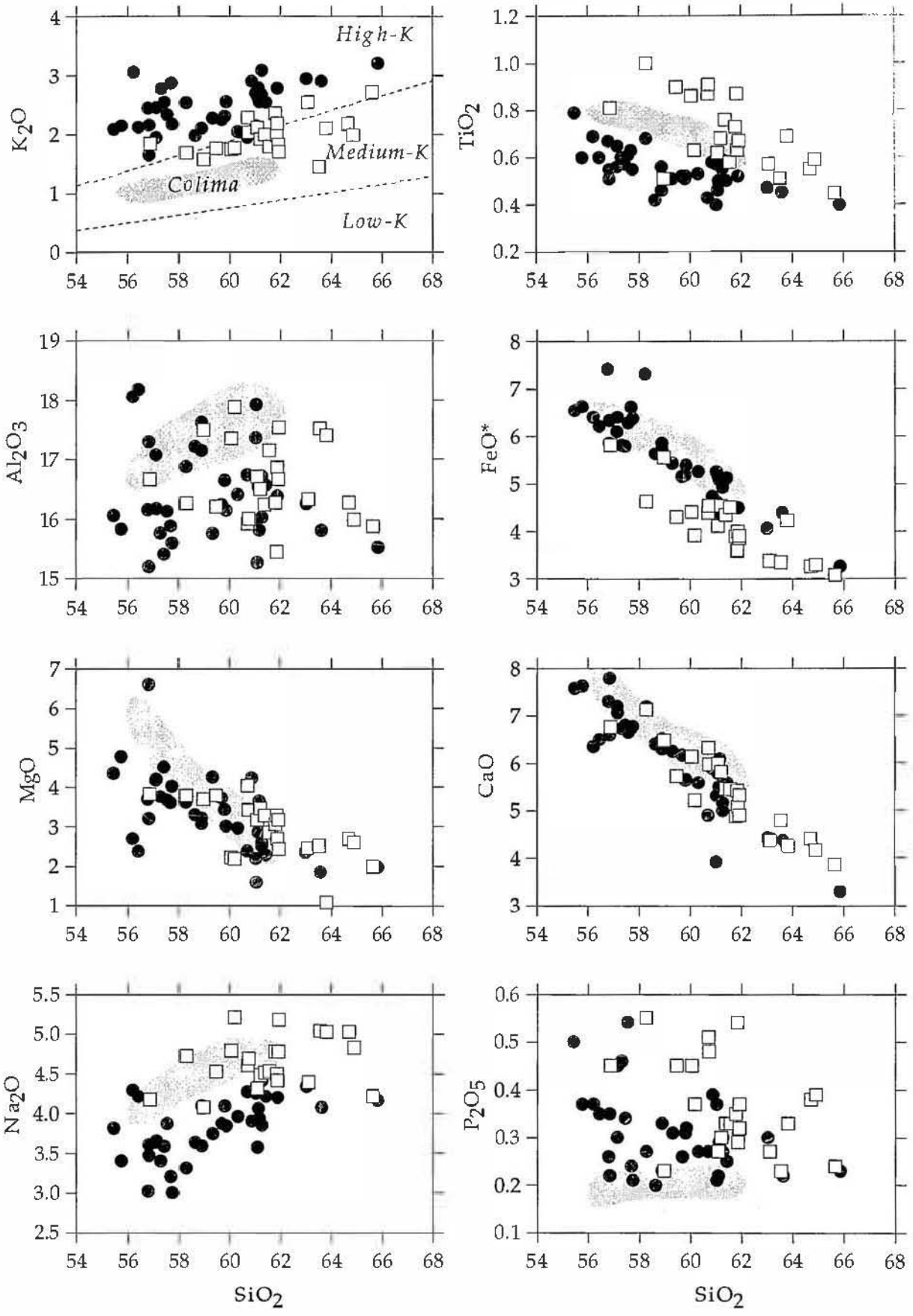

Figure 6.7. Major element covariation diagrams for the Western Kadavu (open squares) and the Central/Eastern/Ono (filled circles) Groups compared to the Colima medium-K calc-alkaline andesites (Luhr and Carmichael, 1980).

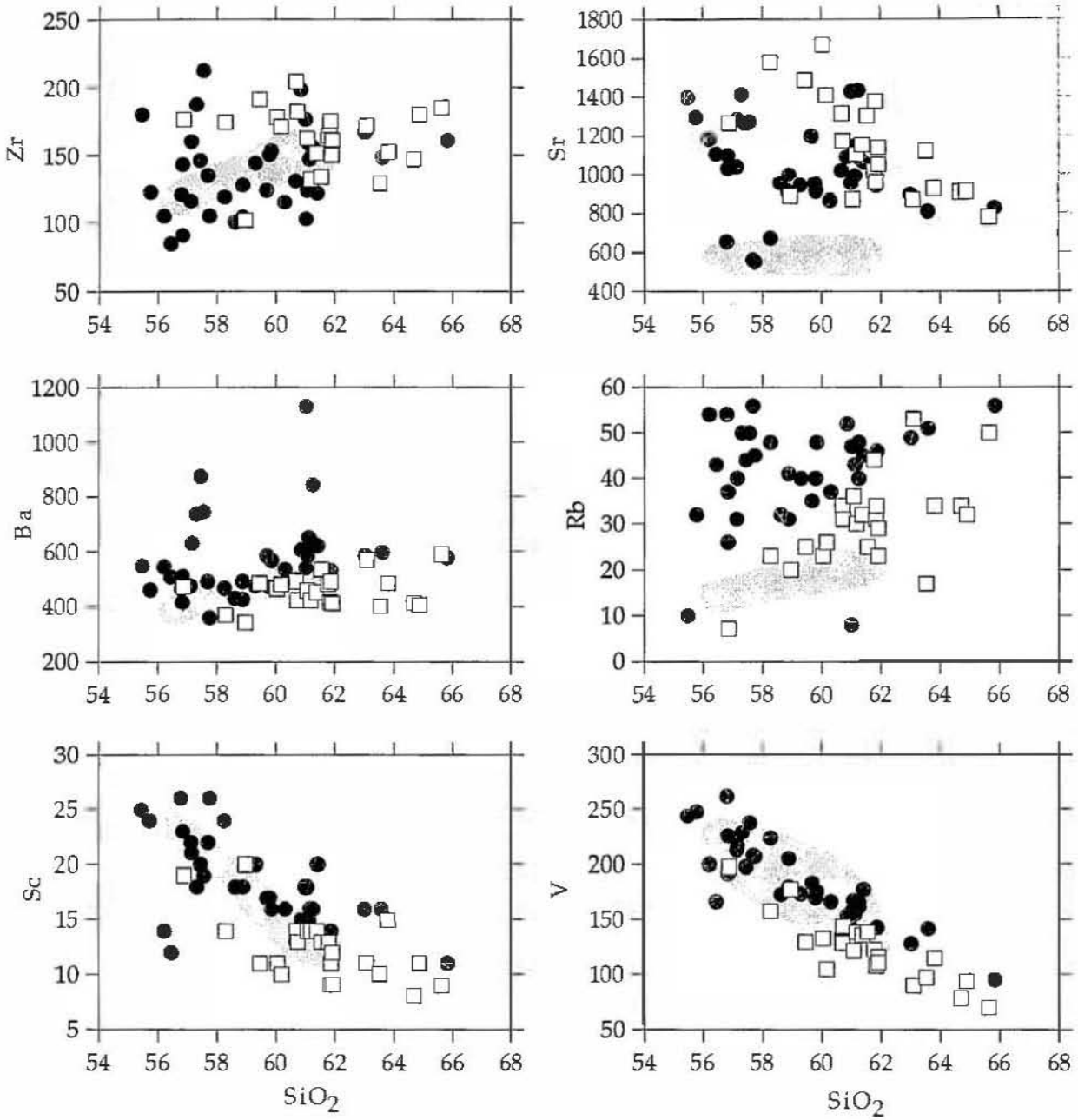

Figure 6.8. Trace element (ppm) covariation diagrams for the Western Kadavu and Central/Eastern/Ono Groups compared to Colima andesites. Symbols as for Figure 6.7.

Four samples from each group were analysed for REE, and chondrite-normalised patterns are plotted in Figure 6.9a. The REE patterns of the WK and CEO andesites show strong LREE-enrichment relative to the chondritic abundances, with La enriched by a factor of 100-200 times. The HREE are depleted in both groups, and are present at levels below those of the average OIB (Sun and McDonough, 1989) despite their andesitic compositions, consistent with garnet in the source.

On MORB-normalised element variation diagrams, both the WK and the CEO groups show the significant Nb-Ta negative anomalies and LILE enrichments that characterise island arc magmas (e.g., Gill, 1981; Perfit et al., 1980) (Fig. 6.9b). Also prominent are Pb and Sr enrichments, Ti depletion (due to fractionating Ti-magnetite in part), and negative P anomalies relative to adjacent Nd, perhaps reflecting separation of apatite.

6.4.3 RADIOGENIC ISOTOPE GEOCHEMISTRY

The Sr, Nd and Pb isotopic compositions of representative WK and CEO lavas are illustrated on conventional Sr-Nd-Pb covariation diagrams (Fig. 6.10); also shown are compositions of several Kadavu lavas reported by Gill (1984). $^{87}Sr/^{86}Sr$ values vary significantly, from 0.70296-0.70335, with the CEO group samples extending to more radiogenic values; both groups have $^{87}Sr/^{86}Sr$ values significantly below values even for highly depleted South Sandwich arc tholeiitic basalts. Their Sr isotopic compositions are less radiogenic than for the Astrolabe lavas, but slightly more radiogenic than the Ngaloa Group basalts. In contrast to the Sr-isotopic compositions, $^{143}Nd/^{144}Nd$ ratios are uniform in the rocks from both the groups (0.51301-0.51304), and match those of the Ngaloa basalts, although they are slightly higher values compared with the Astrolabe lavas. Both groups fall within or very close to the high $^{87}Sr/^{86}Sr$ - low $^{143}Nd/^{144}Nd$ end of the Pacific MORB field.

Pb isotopic compositions for the WK and CEO groups plot close to or on the NHRL and at the more radiogenic end for Pacific MORB, and overlap with those of the Ngaloa basalts; they have lower $^{207}Pb/^{204}Pb$ values than the Astrolabe lavas. As for the Ngaloa basalts, involvement of old continental crust or pelagic sediments in the petrogenesis of these lavas can be confidently ruled out.

6.4.4 SUMMARY

Petrographically, the WK and CEO group lavas have a phenocryst assemblage typical of medium- to high-K calc-alkaline andesites and dacites. The WK group, with the lower K_2O contents, is characterised by the

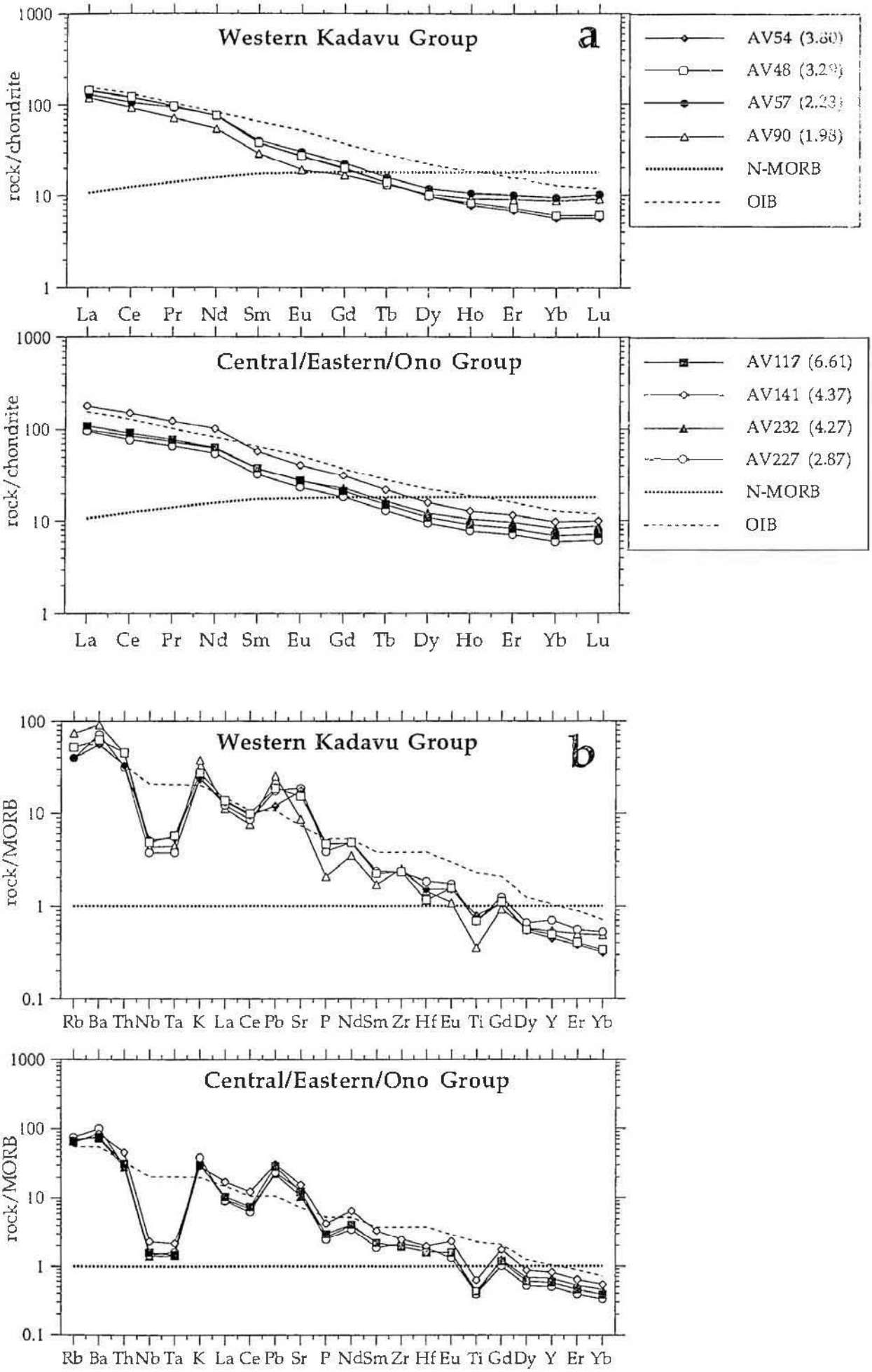

Figure 6.9 a. REE concentrations for the Western Kadavu and Central/Eastern/Ono lavas normalised to chondrite. MgO content of each sample in brackets. b. N-MORB normalised multi-element diagrams for the WK and C/E/O lavas. OIB and N-MORB compositions and normalising values from Sun and McDonough (1989).

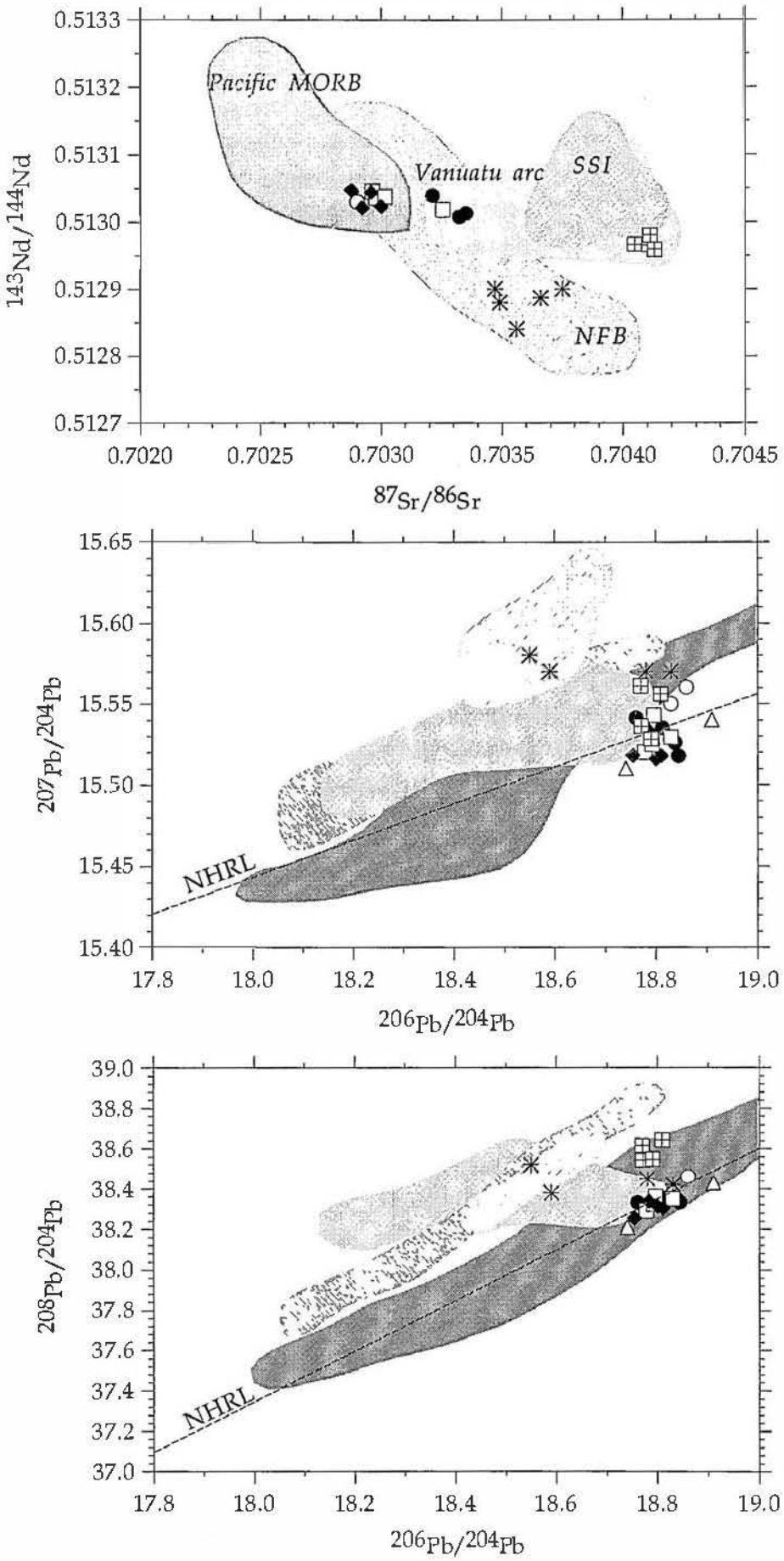

Figure 6.10. Sr vs Nd and Pb vs Pb isotopic compositions for the Western Kadavu (open squares) and the Central/Eastern/Ono (filled circles) Groups compared to the Ngaloa Group volcanics (filled diamonds) and Astrolabe lavas (squares with crosses). Also shown are the fields for Pacific MORB, the North Fiji Basin (NFB) BABB, South Sandwich arc tholeiites (SSI) and Vanuatu arc basalts. Asterisks = late rifting stage (Fijian OIB). The limited Pb isotope data for the South Fiji Basin are represented by the open upright triangles. Open cirlces are the limited isotope data for the Kadavu Island Group reported by Gill (1984). Data sources for Pacific MORB, NFB, SSI and the Vanuatu arc are listed in Figure 3.22.

phenocryst assemblage plagioclase + clinopyroxene (augite) + Ti-magnetite + hornblende + biotite, with minor amounts of orthopyroxene. In the CEO group, plagioclase + augite + Ti-magnetite is the common phenocryst assemblage; however orthopyroxene is slightly more abundant and biotite less abundant than in WK lavas. Oscillatory zoning and resorption and embayment along plagioclase phenocryst margins, and the wide range of pyroxene $Mg^{\#}$ values (extending to $Mg^{\#}$=91) suggests disequilibrium existed in both the WK and CEO group magma chambers during phenocryst crystallisation, probably due largely to magma mixing.

The medium- to high-K nature and lack of Fe- and Ti-enrichment of the Kadavu andesites with fractionation are typical calc-alkaline characteristics. Furthermore, as with all arc-related calc-alkaline magmas, the WK and CEO lavas are enriched in the LILE relative to MORB, but show strong depletion of Nb and Ta. However, radiogenic isotope ratios fall at the less depleted end of the Pacific MORB range, and low HREE abundances and HREE depletion suggest some garnet involvement in their petrogenesis.

6.5 GEOCHEMICAL CONSTRAINTS ON THE ORIGIN OF THE WESTERN KADAVU AND CENTRAL/EASTERN/ONO ANDESITES AND DACITES.

6.5.1 CRYSTAL FRACTIONATION FROM A MORE BASIC PARENT.

It has become apparent from both experimental and geochemical studies that most calc-alkaline andesites and dacites are derived from basaltic magmas through differentiation processes such as crystal fractionation (Crawford et al., 1987). Furthermore, the primary basaltic magmas are considered to originate by partial melting of mantle peridotite metasomatised by a slab-derived LIL-enriched hydrous fluid (Tatsumi, 1989).

Crystal fractionation as a possible mechanism involved in the generation of the WK and CEO andesites and dacites raises the question of possible parent magmas. Mafic precursors are scarce from the Kadavu Island Group. Simple closed system crystallisation of a basalt from the Astrolabe Group or the Ngaloa Group to yield the WK and CEO group lavas is unlikely for the following reasons:

(i) Sr and Nd isotopic compositions are significantly different between the Astrolabe lavas and the WK and CEO Groups. Furthermore, Ba/La values are higher and K/Rb slightly lower in the Astrolabe basalts relative to the WK and CEO Groups. Amphibole fractionation will change these ratios and has been suggested as a mechanism for generating calc-alkaline lavas in

island arcs (Gill, 1981). However, amphibole (+plagioclase) - dominated fractionation from an Astrolabe basalt with high Ba/La will result in an andesite with higher Ba/La and lower K/Rb, and is incapable of producing the WK and CEO andesites and dacites.

(ii) Although Ngaloa radiogenic isotope values are permissible for these basalts to be parental to the WK or CEO andesites, trace element considerations appear to be less supportive of this hypothesis. For example, even though Zr and Y normally increase in the sequence basalt-andesite-dacite, the WK and CEO andesites lavas have lower Zr values compared to the Ngaloa Group basalts (Fig. 6.11). Also, Figure 6.12 shows that chondrite-normalised REE patterns of the most evolved lavas from the WK and CEO groups plot below those of the least evolved basalts from the Ngaloa Group, inconsistent with a hypothesis linking the WK or CEO andesites to the Ngaloa basalts by crystal fractionation.

6.5.2 SOURCE VARIATIONS AND PARTIAL MELTING

Several key geochemical features of the WK and CEO group lavas are consistent with those expected in adakite-type magmas derived from partial melting of basalt in the subducted lithosphere. In particular, on the adakite discrimination diagram (Fig. 6.13a) of Defant and Drummond (1990), lavas with >58% SiO2 of both the WK and CEO groups fall within the field defined for adakites, due to their abnormally low Y and high Sr abundances relative to typical arc andesites. A series of other diagrams constructed for this study using a larger data base of Tertiary adakites (Fig. 6.13b-f) confirms this assignment and also serves to reinforce the notion that adakitic magmas are fundamentally different in composition from andesites and dacites derived by simple fractionation from mantle-derived basalts.

Partial melting experiments by Rapp (1995) showed that typically high SiO_2 (64-68%) tonalitic/adakitic magmas require at least 20-30% batch melting of a hornblende eclogite or garnet amphibolite basaltic source rock, leaving a dry eclogitic residuum. Low Y and HREE abundances in adakitic magmas reflect retention of these elements in residual garnet in the partially melted subducted slab eclogite. The lack of Eu anomalies and very high Sr abundances implies that plagioclase was not likely to have been a residual phase. These diagnostic geochemical features are well shown by the WK and CEO andesites and dacites, and an origin via partial melting of subducted slab eclogite (18-30kbar) or garnet amphibolite (~10-18kbar) is strongly implied.

Rapp and Watson (1995) performed dehydration melting experiments at 8 - 32 kbar on four natural basaltic/amphibolitic compositions, all within

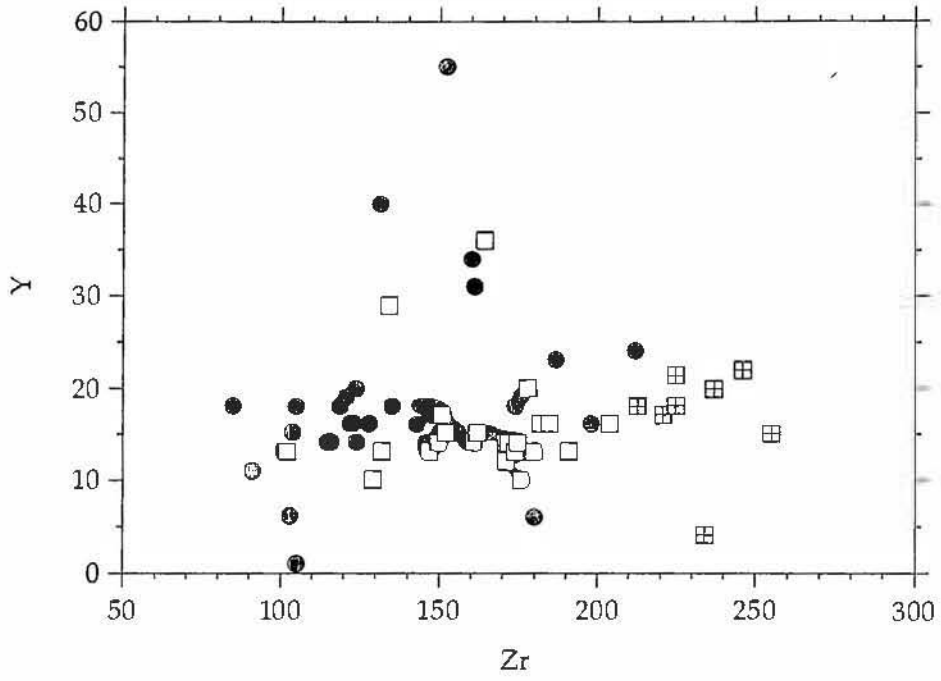

Figure 6.11. Zr vs Y variation showing the low Zr contents of the Western Kadavu (open squares) and Central/Eastern/Ono (filled cirlces) andesites and dacites compared to the Ngaloa Group basalts (squares with crosses).

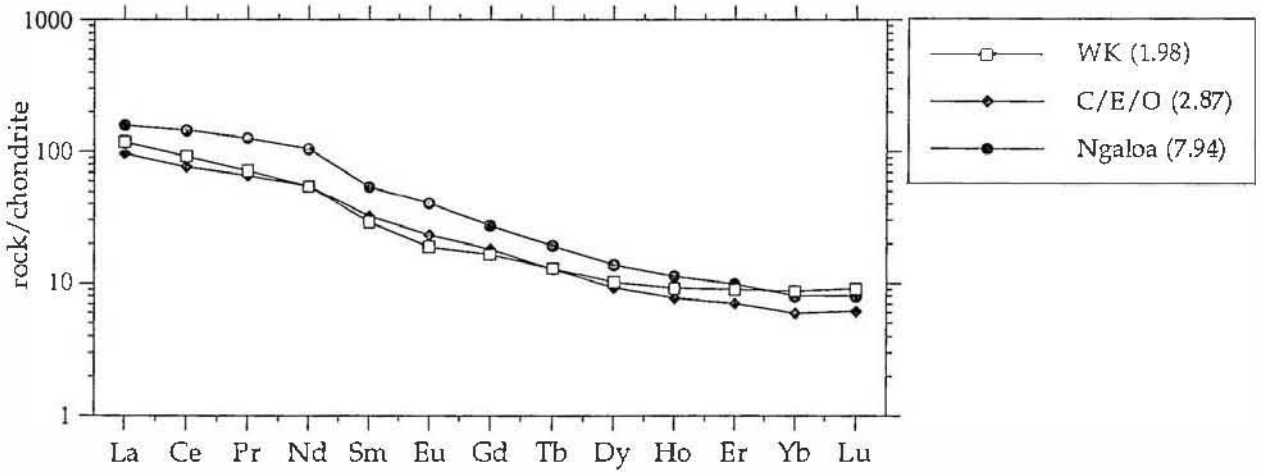

Figure 6.12. REE abundance patterns normalised to chondrite of the most evolved lavas from the Western Kadavu and Central/Eastern/Ono Groups compared to the least evolved basalt from the Ngaloa Group.

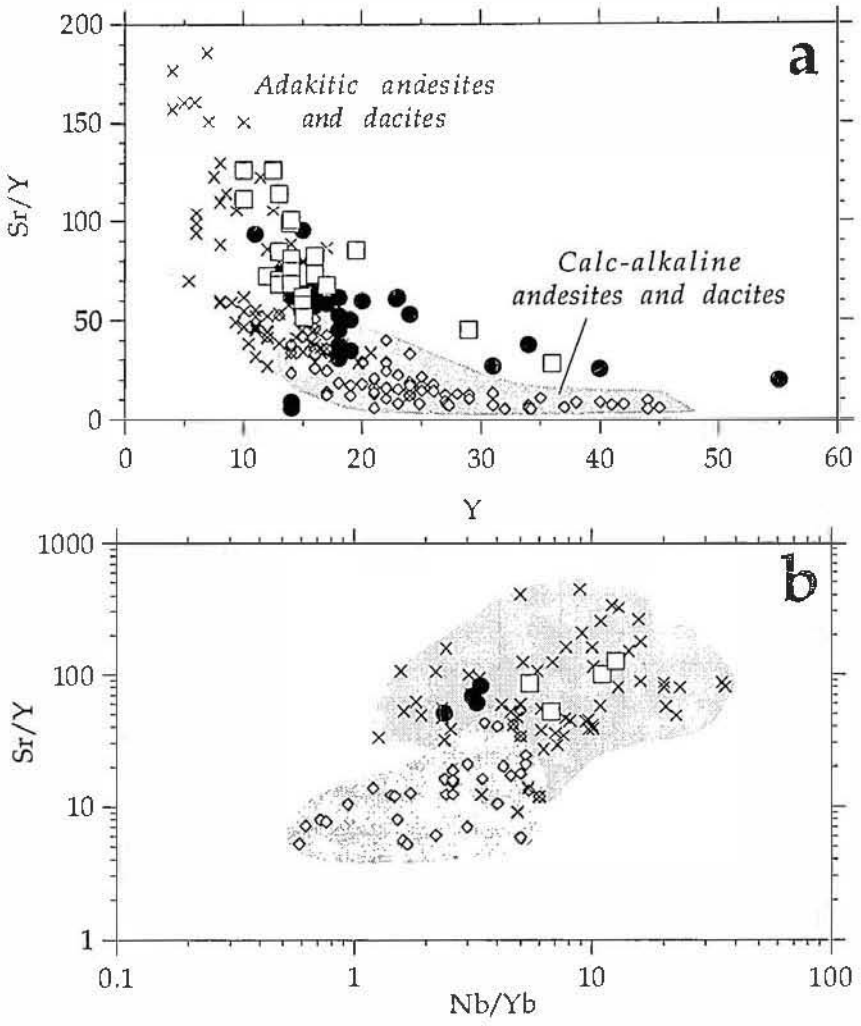

Figure 6.13. a. Western Kadavu (open squares) and Central/Eastern/Ono (filled circles) andesites and dacites plotted on the Sr/Y vs Y discrimination diagram of Defant and Drummond (1990). Partial melting of an eclogite source generates melts that plot towards high Sr/Y and low Y (adakites). Melts generated via partial melting of the mantle wedge and subsequent differentiation ('normal' calc-alkaline andesites and dacites) trend towards high Y and low Sr/Y values. b-f. Western Kadavu and Central/Eastern/Ono andesites and dacites plotted on various incompatible element diagrams showing the difference in composition to calc-alkaline andesites and dacites derived by fractionation from mantle-derived basalts. Adakitic magmas are characterised by high La/Yb, low HREE (e.g. Yb). Sources for adakites: Kay (1978), Drummond and Defant (1990), Defant et al. (1991a, 1991b, 1992), Kay et al. (1993), Sajona et al. (1993), Hochstaedter et al. (1994), Morris (1995), Yogodzinski et al. (1995), Kepezhinskas et al. (1996), Sajona et al. (1996), Stern and Kilian (1996). Sources for calc-alkaline andesites and dacites: Luhr and Carmichael (1980), Huijsmans et al (1988), Defant et al. (1991a, 1991b), Pearce et al. (1995)

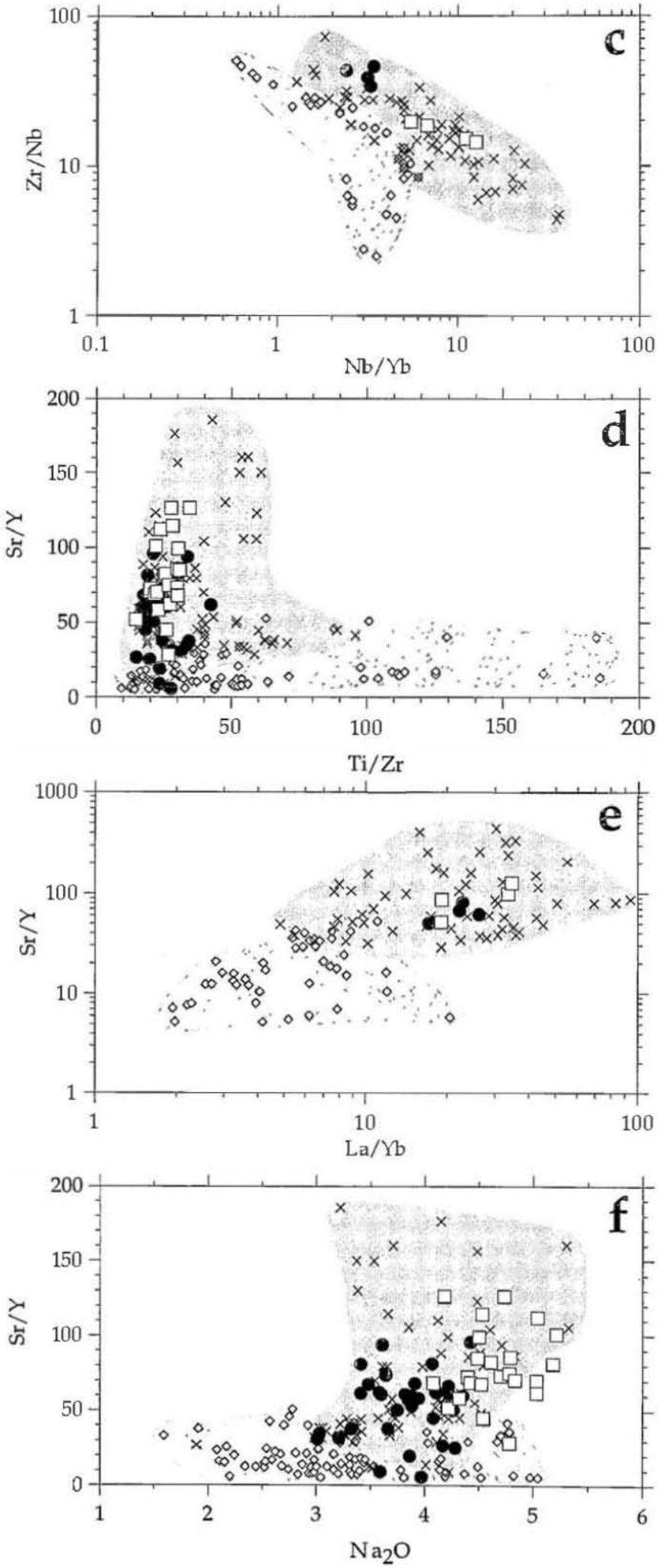

Figure 6.13 continued.

the range of ocean floor basalt compositions, although one is relatively enriched in alkalis (51.2% SiO_2, 4.3% Na_2O, K_2O 0.82%). Melt compositions for runs in which plagioclase was not a residual phase (16-32 kbar) are shown in Figure 6.14, and several important points may be derived from these plots. First, melt compositions are strongly controlled by starting compositions for TiO_2 and K_2O irrespective of pressure and temperature, and a strong starting composition control is also evident for Na_2O and CaO. Second, melt FeO and MgO contents show little relation to starting composition, despite the latter showing a range from FeO/MgO from 1.3 to 2.0.

Assuming that WK and CEO lavas are melts of subducted slab mafic rocks, several compositional constraints relating to the source of these suites can be determined from Figure 6.14:

i): given the strong correlation between starting composition TiO_2 and melt TiO_2 compositions in the Rapp and Watson (1995) experiments, it is reasonable to assume that the mafic composition melted to produce the WK andesites and dacites probably had around 0.7% TiO_2, somewhat higher than that which yielded the CEO lavas. The sources of the WK and CEO suites must have had Al_2O_3 contents probably close to or below 14%.

ii): on the same basis, the WK suite source probably had Na_2O contents below 2.5% and at least 11% CaO, whereas the source of the CEO suite had even lower Na_2O and probably similar CaO contents, and they fall within the field for experimental melts for Al_2O_3 and Na_2O. The K_2O contents of the WK and CEO lavas plot at the high-K_2O end whereas the Na_2O and FeO* plot at the low end of the experimental melts range.

iii): K_2O contents of both the WK and CEO suites are notably greater than melts from low-K basalt starting compositions with K_2O<~0.2%, and thus their source composition probably was more K-rich than the highest-K starting composition used by Rapp and Watson (0.82%); sources of the Kadavu lavas probably had ~0.8-1% K_2O. Clearly, the CEO source was more K_2O-rich than that of the WK lavas.

iv): the major difference between the experimental eclogite melt compositions produced in the Rapp and Watson experiments, and the Kadavu adakites is their respective MgO abundance trends. The Kadavu lavas are strongly and uniformly displaced towards higher MgO levels, and perhaps slightly lower FeO contents. These differences cannot be ascribed to

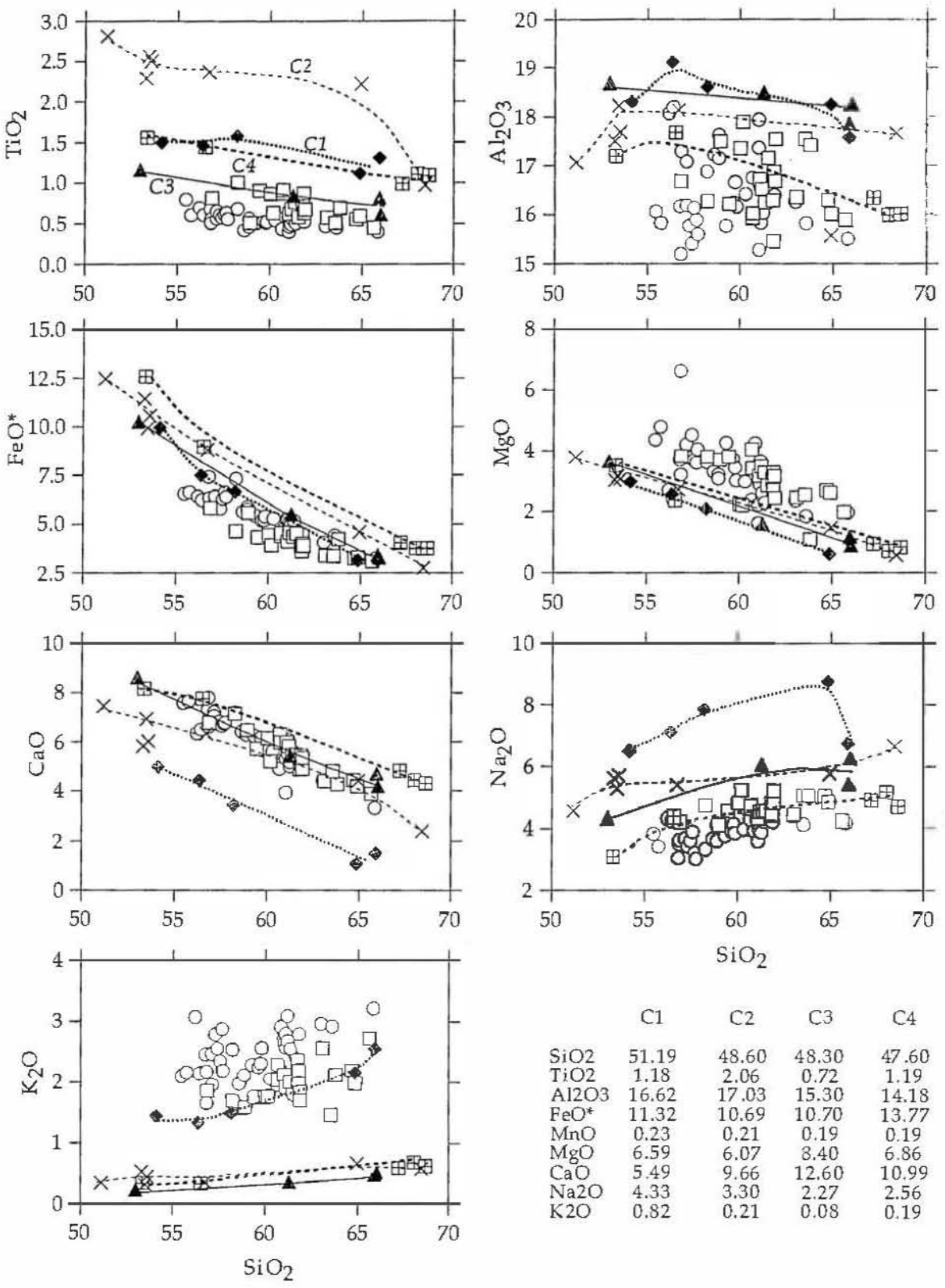

	C1	C2	C3	C4
SiO2	51.19	48.60	48.30	47.60
TiO2	1.18	2.06	0.72	1.19
Al2O3	16.62	17.03	15.30	14.18
FeO*	11.32	10.69	10.70	13.77
MnO	0.23	0.21	0.19	0.19
MgO	6.59	6.07	8.40	6.86
CaO	5.49	9.66	12.60	10.99
Na2O	4.33	3.30	2.27	2.56
K2O	0.82	0.21	0.08	0.19

Figure 6.14. Western Kadavu and Central/Eastern/Ono Group andesites and dacites compared to liquids produced in dehydration melting experiments (8-32kbar) on four natural basaltic/amphibolite compositions (Rapp and Watson, 1995) for which plagioclase is not a residual phase. Composition 1 (C1; filled diamonds) is an alkali rich basalt, composition 2 (C2; crosses) is a high-Al basalt, composition 3 (C3; filled triangles) is a low-K olivine tholeiite and composition 4 (C4; squares with crosses) is a low-K Archean greenstone. See text for further explanation. WK lavas are open squares, CEO lavas open circles.

the influence of starting composition, as the experimental melts define smooth overlapping trends, whatever the FeO and MgO contents of the starting compositions, at least within the compositional range of the starting materials used by Rapp and Watson (1995).

A more complicated scenario than simple batch partial melting of an appropriate metabasaltic composition is required to explain the petrogenesis of these lavas. It is possible that an eclogite derived from a more mafic, gabbroic source in subducted oceanic crust may have yielded the Kadavu suites. This would be consistent with the higher $Mg^{\#}$, higher CaO, lower Na_2O and lower Al_2O_3 and lower TiO_2 contents of the Kadavu lavas. However, it does not account for the strikingly high K_2O contents of the latter relative to melts of basaltic compositions with K_2O contents typical of those in the oceanic crust (usually <0.2%).

An alternative possibility is that the primary eclogite melts ultimately parental to the Kadavu adakites gained MgO and K_2O during passage from the melting slab source to the surface. Kay (1978) first suggested that the high MgO contents of some adakites were produced by interaction of hydrous slab melts with peridotitic minerals in the mantle wedge. The net result of such interaction with olivine and pyroxenes will be to enrich the melts in MgO and, to a lesser extent, CaO (Sen and Dunn, 1993). However, the enrichment of K_2O implies interaction with pargasite or phlogopite (or both) present in the mantle wedge, probably as metasomatic veins (Kepezhinskas et al., 1996), but also possibly dispersed pervasively throughout regions of metasomatised peridotite. This means that the characteristic major element trends produced by slab melting are not substantially disrupted by the hybridisation process, but some modification to melt trace element patterns might be expected, especially for those elements concentrated in the pargasite or phlogopite.

Trace element data for subduction zone-metasomatised peridotites are sparse and incomplete. Peridotite xenoliths in andesitic lavas from Bataan Island in the Luzon arc show well-developed metasomatic phlogopite, and have Ba/Rb values around 0.3 (Chen, 1993; A.J Crawford pers. comm.), significantly lower than values for N- to E-MORB (~10). Their Sr/Rb (12) values are considerably lower than values for N-MORB (160) or E-MORB (30), reflecting the low Sr/Rb values of phlogopite (Hartmann and Wedepohl, 1993). As Sr/Rb values for the WK and CEO adakites are mainly well within the N- to E-MORB range, it is assumed that assimilation/digestion of phlogopite did not play a significant role in the evolution of these magmas. This implies that the abnormally high K_2O

contents of these adakites relative to otherwise compositionally similar experimental melts, may be largely due to pargasite assimilation. Pargasites in the Finero peridotite in northern Italy have Sr/Rb values mainly between 20 and 40 (Hartmann and Wedepohl, 1993), supporting this contention, although it is acknowledged that more rigorous evaluation of this hypothesis requires better trace element data for pargasites in subduction-related peridotite xenoliths.

6.6 CONCLUSION

The WK and CEO andesitic and dacitic lavas were derived via partial melting of subducted basaltic ocean crust, probably with an eclogitic mineralogy. Compositionally and mineralogically, these Kadavu lava suites are appropriately classified as adakites. However, the higher MgO contents at any SiO_2 level relative to experimental partial melts of eclogites suggest that the primary slab-derived adakitic magmas reacted to some limited extent with mantle wedge peridotite. Abnormally high K_2O contents of the adakites relative to experimental melts of low-K basaltic derived eclogite suggest that ascending and reacting melts may have assimilated pargasite, distributed in veins or interstitially throughout mantle wedge peridotite. The paucity of mafic lavas throughout Kadavu, and the failure to relate (using key trace element ratios) the WK and CEO andesites to the Ngaloa basalts, suggests that the adakites were not derived from more mafic liquids through differentiation processes.

The tectonic implications of the widespread occurrence of slab-derived magmas in the Kadavu Island Group is discussed in the following chapter.

Chapter 7

SYNTHESIS

Tectonic implications of the composition of the Hunter Ridge and Kadavu Island Group magmas

7.1 INTRODUCTION

This petrological and geochemical study of lavas from the Kadavu Island Group and northern Hunter Ridge provides important constraints on the regional tectonic evolution and mantle wedge processes occurring in this area over the last 5 million years. In addition the 600km-long section of supra-subduction zone magmatism enables an investigation of the geochemical effects of the variation in mantle sources along the Hunter 'arc' and into the older Fijian lithosphere.

The Kadavu Island Group and the Hunter Ridge were produced by subduction of South Fiji Basin (SFB) crust, which accompanied spreading in the North Fiji Basin (Auzende et al., 1996) and the anticlockwise rotation of the Fiji Platform between 7 and 3-2 Ma. The geometry of the subducted slab and mantle wedge below the Kadavu Island Group and the Hunter Ridge cannot be determined because of the lack of seismicity along the Hunter Fracture Zone (Hamburger and Isacks, 1987). The oblique truncation of linear magnetic anomalies in the SFB (Malahoff et al., 1982) suggests that SFB crust may have subducted obliquely beneath the Kadavu Island Group.

The Kadavu Island Group represents the youngest apparently subduction-related volcanism in Fiji (3.4-0.36Ma) and is associated in time with intraplate lavas (Fijian OIB) that were erupted mainly around the hook in the Koro Sea (Fig. 2.2). A working model for the tectonic evolution of the Fiji region has been developed by several authors, notably Gill (1984) and Gill and Whelan (1989a, b) and is summarised in chapter 2. This model holds that before ~10Ma, the Fijian arc was part of a continuous volcanic arc (the Vitiaz arc) extending along the Vanuatu arc through Fiji to the then-contiguous Lau-Tonga Ridge as a product of subduction of the Pacific Plate along the Vitiaz Trench. Following reversal of subduction polarity at ~10 Ma, claimed to be due to collision of the immense Ontong Java Plateau with the northern Vitiaz arc (Kroenke,

1984), clockwise rotation of the Vanuatu arc and anticlockwise rotation of the Fiji Platform occurred as the North Fiji Basin opened in a complex and unstable configuration. Oceanward migration of the Tonga arc led to creation of the Lau Basin commencing around 5Ma, and in the isolation of the Lau Ridge and the Fiji Platform (Gill, 1976).

The origin and evolution of the Kadavu Island Group and Hunter Ridge lavas has been described in the previous chapters, and key geochemical features will be reviewed here, before these magma suites are fitted within the tectonic scenario briefly outlined above.

7.2 TECTONO-MAGMATIC EVOLUTION OF THE HUNTER RIDGE

Previous studies of the southwestern section of the Hunter Ridge (Sigurdsson et al., 1993; Eggins and Crawford, 1993) have recorded arc tholeiitic basalts and high-Ca boninites, the latter best represented on that section of the Hunter Ridge adjacent to the N-S orientated southernmost spreading centre in the North Fiji Basin. At the southwestern termination of the Hunter Ridge, where it swings around to become the southernmost Vanuatu arc, Monzier et al. (1993) described an unusual suite of high-Mg andesites that were subsequently argued to have been produced by interaction of slab-derived melts with refractory peridotite (Crawford et al., 1993). Although detailed mineralogical studies of these lavas are still underway (A.J. Crawford and L.V. Danyushevsky, work in progress), they bear strong compositional similarities to the more evolved Ngaloa Group basaltic andesites, and are discussed later in this chapter.

Three geochemical suites based on K_2O contents have been identified for rocks dredged along the northern section of the submarine Hunter Ridge. Based on major element compositions and mineral chemistry, suite I (0.21-0.69%K_2O) rocks are classified as basalts to andesites and diorites transitional between high-Ca boninites and arc tholeiites. They are essentially similar to those erupted further southwest along the Hunter Ridge, and record normal to slightly 'hotter than normal' arc magma generation in a young intra-oceanic arc. Suites II (0.68-1.76% K_2O) and III (2.73-3.05% K_2O) are classified as calc-alkaline basalts to rhyolites, and are interpreted to have transitional adakite affinities, their petrogenesis involving some role (albeit relatively minor compared to the Kadavu adakites) for partial melts of the subducted slab, possibly amphibolitic rather than eclogitic. The occurrence of rocks along the northern Hunter Ridge with affinities to adakites suggests that slab

melting was not only restricted to beneath the Kadavu Island Group area, but extended at least 250km further southwest along the Hunter Ridge. This, in turn, implies that slab temperatures along all the northern Hunter Ridge were higher than those normally present in slabs at depths of 50-100km beneath intra-oceanic arcs. This important point is discussed in detail in a later section.

7.3 TECTONO-MAGMATIC EVOLUTION OF THE KADAVU ISLAND GROUP

7.3.1 INTRODUCTION

Four distinct geochemical suites within the Kadavu Island Group have been identified in this study (Fig. 7.1). The Astrolabe Group shoshonitic basalts and andesites in the northeast, the CEO Group high-K adakitic andesites and dacites, the WK Group medium-K adakitic andesites and dacites, and the high-K basalts and basaltic andesites of the Ngaloa Group volcanics.

7.3.2 THE ASTROLABE GROUP

Gill et al., (1984) and Rodda (1994), noted a geochemical trend of decreasing K_2O content with decreasing age of the rocks along the Kadavu Island Group, from 3.4Ma shoshonites (Astrolabe Group) in the northeast through high-K CEO Group andesites and dacites aged from ~2.9m.y. to 0.48m.y. medium-K andesitic and dacitic WK Group lavas in the west.

As shown in chapter 4, the shoshonites of the Astrolabe Group (3.4Ma), despite being over 50km from the nearest shoshonitic volcanoes in Fiji (Vatulele and Yanuca; Fig. 2.3b) and up to about 200km from the Tavua Caldera (Fig 2.3b), have striking major and trace element and isotopic compositional similarities to other shoshonites on Viti Levu, particularly the best studied suite, from the Tavua Caldera.

The remarkable similarity of these Tavua shoshonites and absarokites to those of the Astrolabe Group suggests that similar processes were involved in the generation of both suites. The high $Cr^{\#}$ values (81.0-86.6) of Cr-spinel inclusions in olivine phenocrysts from the Astrolabe absarokites match those in high-Ca boninites ($Cr^{\#}$=70-85), the sources of which are considered to be more refractory than those of MORB or typical arc basalts, due to one or more prior melt extraction events (Crawford et al., 1989). High CaO/Al_2O_3 values (0.88-1.1 for Astrolabes; high Ca boninites = 0.7-1.0) and the low HREE, Zr and Y abundances, well below N-MORB levels (Fig. 7.1), further supports the argument for a refractory

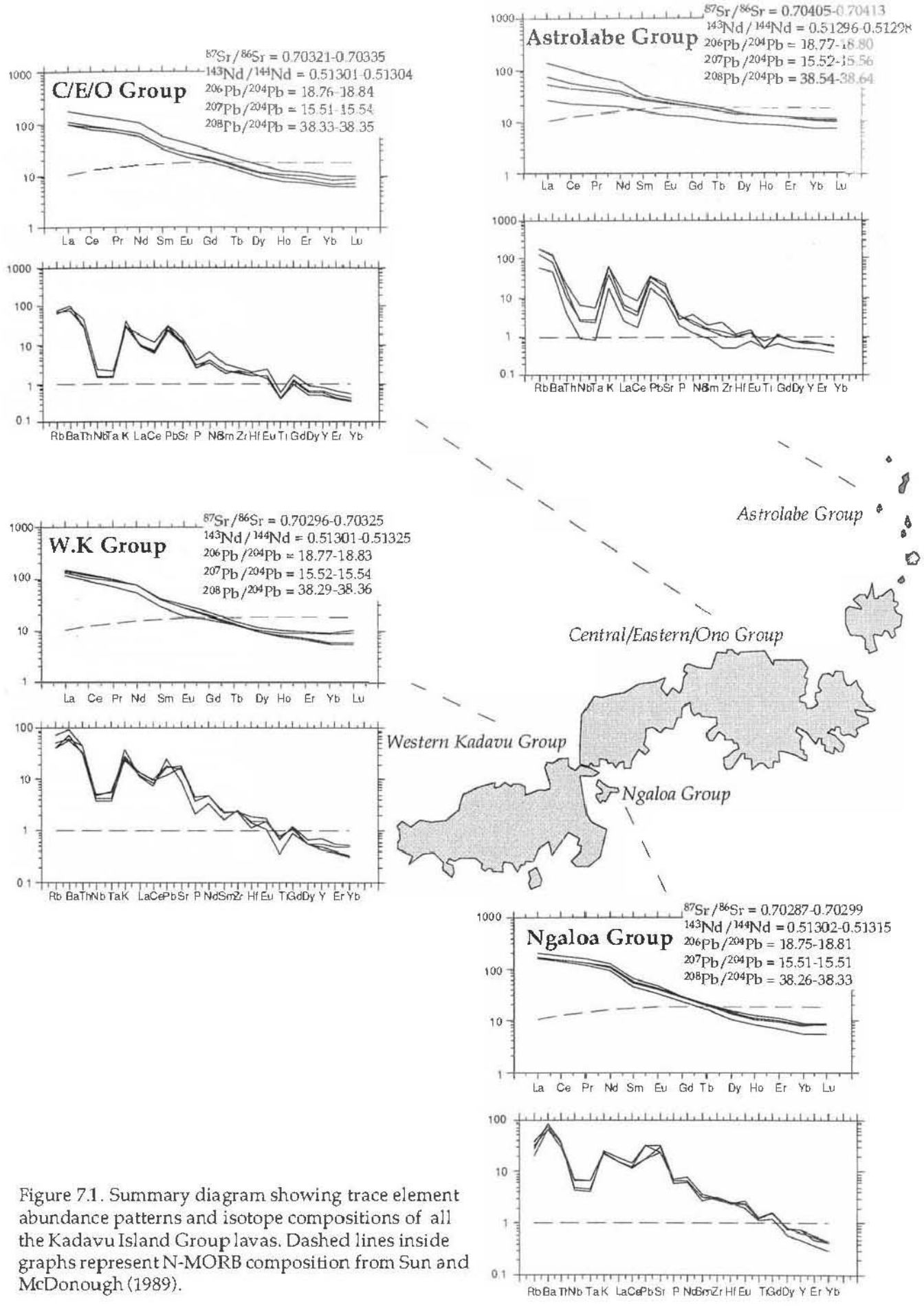

Figure 7.1. Summary diagram showing trace element abundance patterns and isotope compositions of all the Kadavu Island Group lavas. Dashed lines inside graphs represent N-MORB composition from Sun and McDonough (1989).

source. Trace element considerations suggest that the nature of the fluid responsible for the LILE enrichment in the Astrolabe and Tavua shoshonite suite lavas was a hydrous fluid, very similar compositionally to that invoked in fluxing the mantle wedge sources of typical, much lower-K suites, such as arc tholeiites, and no 'unusual' metasomatic fluid need be invoked to generate the Astrolabe shoshonites. The strong K-group element enrichment in the Fijian shoshonites, and also their elevated (relative to Zr and N-MORB, for example) Nb-Ta abundances, can be accounted for by an origin involving very low degrees of partial melting, not high degrees as claimed by Rogers and Setterfield (1994). The shift in $^{87}Sr/^{86}Sr$ (0.70405-0.70413) at equivalent $^{143}Nd/^{144}Nd$ levels to Pacific MORB (see Fig. 4.13) is consistent with this metasomatic fluid phase being derived from subducted altered oceanic crust, and Pb isotope concentrations of the Astrolabe and Tavua lavas preclude any involvement of a component derived from subducted pelagic sediment.

The ages of the Fijian shoshonites range between 5.5 and 3.0Ma (Gill and Whelan, 1989a) and they are clearly not associated directly with contemporaneous subduction along the Vitiaz trench, as subduction along the Vitiaz arc system had ceased by this time. Although the model of Auzende et al. (1996) for opening of the North Fiji Basin provides an appropriate tectonic setting for initiation of subduction along the Hunter Ridge following the reorganisation of spreading centres in the North Fiji Basin ~ 7Ma, the 3Ma Astrolabe shoshonites occur only ~40km from the trench, whereas the compositionally almost identical Tavua shoshonites occur some 220 km from the trench. This precludes these two suites being produced immediately above the same actively subducting slab, which would have been at least 2 - 3 times deeper beneath the Tavua caldera.

It is concluded, therefore, that the Astrolabe Group lavas were unlikely to be associated with contemporaneous subduction of the SFB crust beneath the Kadavu Island Group. Rather, the Fijian shoshonites may have been generated when lithospheric stretching associated with the rotation of Fiji and reorganisation of spreading in the North Fiji Basin led to limited passive ascent and decompression melting of peridotite that was metasomatised above the older Vitiaz subduction zone.

7.3.3 WESTERN KADAVU, CENTRAL/EASTERN/ONO AND NGALOA GROUP VOLCANICS

Ngaloa Group

Some compositional features of the volumetrically minor Ngaloa Group basalts, particularly their high Na_2O, P_2O_5, K_2O, strikingly low FeO* contents, and their strong enrichment of incompatible elements, are typical features of low degree partial melts of peridotite (Langmuir et al., 1992). However, important geochemical criteria, including their distinctive MORB-like isotopic signatures, their low HREE (Fig. 7.1) and Y (4-22ppm) contents, and their high Sr/Y (93-205) values similar to those of the WK and CEO andesites and dacites, suggest at first glance derivation via partial melting of subducted oceanic basalts metamorphosed to eclogite facies. The mafic nature of the Ngaloa Group volcanics and their primitive phenocryst compositions, including common olivine phenocryst with compositions of Fo_{89-91}, however, precludes their derivation solely from the partial melting of the subducted basaltic crust, and requires significant involvement of mantle wedge peridotite. It is hypothesised that siliceous adakitic melts (andesites or dacites) broadly similar to those constituting the WK and CEO suites were produced by melting of eclogite in the subducted slab, but reacted with, and stalled in the overlying mantle wedge peridotite. Subsequent partial melting of this slab melt-metasomatised peridotite produced the parental magmas of the Ngaloa Group.

Western Kadavu and Central/Eastern/Ono Groups

The WK and CEO andesites and dacites meet the diagnostic geochemical and mineralogical criteria established for adakites, as defined by Defant and Drummond (1990). Their steep REE patterns (Fig. 7.1), low Sc, Y and HREE abundances, very high Sr contents, and high Sr/Y and La/Yb values are consistent with an origin involving partial melting of eclogite in the subducted slab, a hypothesis supported by their Pacific MORB-like Sr, Nd and Pb isotopic compositions.

The higher MgO content of these Fijian adakitic rocks compared to experimental slab melts suggests that these lavas have had some limited interaction with the mantle wedge peridotite probably involving significant 'scavenging' of metasomatic pargasite. This is not unexpected, since the primary slab melt must ascend through at least 70km of mantle wedge peridotite before eruption.

7.3.4 PETROGENETIC RELATIONSHIPS BETWEEN THE NGALOA GROUP VOLCANICS & ADAKITES OF THE WK AND CEO GROUPS

A cogenetic relationship between basalts of the Ngaloa Group and andesites and dacites of the WK and CEO Groups through fractionation is precluded on firm geochemical grounds (for example, concentrations of REE in the basalts are greater than those in the WK and CEO andesites). However, the similarity of key trace element features and radiogenic isotopes between the WK and CEO group adakites and the Ngaloa group basalts and their close spatial and temporal relationship suggests that there may be a petrogenetic relationship between them.

Several authors have documented the occurrence of basalts spatially and temporally associated with adakites. Some of these occurrences include the northern Kamchatka arc (Hochstaeder et al., 1994; Kepezhinskas et al., 1995, 1996), western Panama and southeastern Costa Rica (Defant et al., 1992), and Mindanao in the Philippines (Sajona et al., 1993, 1996). Basalts associated with the adakitic andesites and dacites have been classified as either Nb-enriched arc basalts or high-Nb basalts, due to their relatively high concentrations of Nb (>15ppm) (Reagan and Gill, 1989; Defant et al., 1991) and other HFSE (1-2%TiO_2) compared to typical island arc basalts (Nb<10ppm; TiO_2< 1%).

Two main hypotheses have been proposed to explain the origin of the higher concentrations of HFSE in Nb-enriched arc basalts (NEAB). These include:

(i) 'OIB hypothesis' (Verma and Nelson, 1989; Leeman et al., 1990), which proposes a heterogenous sub-arc mantle such as the plum pudding model of Morris and Hart (1983), in which MORB and OIB sources are intermixed on a relatively small scale, for the source of arc lavas, and,

(ii) the 'reaction hypothesis', in which reaction between adakitic melts (slab melts) and mantle peridotite produces phases such as phlogopite and amphibole (Johnston and Wyllie, 1988; Carroll and Wyllie, 1989), which break down during partial melting of the mantle, releasing HFSE into the melt (O'Reilly et al. 1991).

The OIB hypothesis has been rejected for a number of reasons. First, although the NEAB are high in Nb (15-25 ppm), they are significantly lower in Nb than OIB (usually >40ppm; av. 48ppm; Sun and McDonough, 1989). Second, despite having higher Nb concentrations than IAB, NEAB still have typical subduction-related trace element signatures on multi element diagrams, such as the depletion in HFSE relative to LILE and LREE. Gill and Whelan (1989b) argued for an OIB-type mantle in the source of the Ngaloa volcanics. However, this

argument can be confidently excluded for the Ngaloa volcanics, since they have MORB-like isotopic compositions.

The second hypothesis suggests that slab melt hybridisation should add HFSE to the mantle, because small percentage melting of the slab should mobilise the most incompatible elements, including Nb (Kesson and Ringwood, 1989). Defant et al. (1991, 1992) and Kepezhinskas et al. (1995) suggested on the basis of geochemical modelling and studies of mantle xenoliths, that the NEAB are derived from the mantle during or after interaction of mantle peridotite with slab melts. The latter study on Cr-diopside and Al-augite series xenoliths in NEAB from the northern Kamchatka arc provided strong evidence for mantle hybridisation processes produced by mantle peridotite-slab melt interaction, including the presence of veins of trondhjemitic magma through lherzolite. A similar origin for the Ngaloa basalts is proposed herein.

7.3.5 WHY DID THE SOUTH FIJI BASIN SUBDUCTED SLAB MELT ?

The subduction of South Fiji Basin crust beneath the Kadavu Island Group is demonstrated by the occurrence of a well developed subduction margin morphology preserved well into the Fiji Platform (Brocher and Holmes, 1985), and the presence of arc tholeiites, high-Ca boninites, and calc-alkaline and adakitic rocks further south along the Hunter Ridge demand that subduction has occurred beneath this area. From Auzende et al.'s (1996) study of the NFB spreading centres, the age of initiation of subduction along the Kadavu - Hunter Ridge trench is thought to be around 7Ma.

Melting of subducted oceanic crust requires a thermal regime several hundreds of degrees hotter than more typical subduction zones at depths of 50-100km (Peacock, 1990; Peacock et al., 1994). Peacock et al. (1994) proposed that the generation and maintenance of the high temperatures required for slab melting must involve either high shear stresses (>100MPa), or the subduction of relatively young (≤25Ma), hot oceanic crust. In most areas where adakites are documented (Table 7.1), the subduction of young hot oceanic crust is well demonstrated, and provides appropriately high temperatures to melt the subducted slab. Based on thermal modelling by Peacock et al. (1994), during the early stages of subduction, the top of the oceanic crust may be up to 300°C warmer than in mature subduction zones, and provides ambient conditions appropriate for slab melting, even more so if the slab being subducted is young and hot.

In the case of subduction beneath the Kadavu Island Group, the former convergence rate is unknown, so the possible role of high shear stresses cannot be evaluated. Furthermore, the subducting SFB crust (~20-30Ma at the time of subduction; Weissel and Watts, 1975; Malahoff et al., 1982; Davey, 1982) is older than required by the thermal modelling of Peacock (1990) to induce slab melting. Given the strong geochemical evidence for the involvement of slab melts in the generation of the WK, CEO and Ngaloa volcanics, an alternative mechanism is required to account for the melting of what should have been a barely warm or cool subducting slab of South Fiji Basin crust. Also, unlike in other arcs in which calc-alkaline volcanism occurs 100-150km from the trench, the anomalously 'near trench' (~30-50km) volcanism of the Kadavu Island Group is in agreement with the hypothesis that slab melting is induced at relatively shallow depths, probably 70-85km (23-26kbar), corresponding to the amphibolite-eclogite window of the subducted slab (e.g. Drummond and Defant, 1990).

Volcanic area	Reason for slab melting	Source
Aleutian Komandorsky area	highly oblique convergence that produced a slow subduction path into the sub-arc mantle	Kay, (1978); Yogodzinski et al., (1994, 1995)
Panama-southeast Costa Rica	subduction of hot oceanic crust (12-24Ma)	Defant et al., (1991, 1992)
Southwest Japan	Young (21Ma) lithosphere slab subducting at a shallow angle (10°)	Morris (1995)
Mount St Helens	Subduction of hot oceanic crust (3Ma)	Halliday et al. (1983); Leeman et al. (1990)
northern Kamchatka	subduction of young (<25Ma) hot basin crust	Hochstaedter et al. (1994); Kepezhinskas et al. (1996)
Andean Austral Volcanic Zone	slow subduction (2cm/yr) and young age (<24Ma) of subducted oceanic lithosphere	Stern and Kilian, (1996)
Zamboanga Peninsula, Philippines	subduction of young and hot oceanic crust and initiation of subduction	Sajona et al (1993, 1996).

Table 7.1. Locations of adakites and the reasons for slab melting in these areas.

The occurrence of adakites on the Kadavu Island Group may be explained in part by the initiation of subduction around 7Ma, leading several million years later to penetration of the slab into an unusually hot mantle wedge due to the proximity of rising diapirs supplying the NFB backarc basin spreading centres. Heat flow studies in the North Fiji

Basin indicate high heat flow values existing over the whole basin (Sclater and Menard, 1967; MacDonald et al., 1973).

A remarkably similar suite of adakites and high-Nb arc basalts to the WK and Ngaloa suites has been reported recently by Sajona et al. (1996) from the Zamboanga Peninsula in western Mindanao. These authors suggested that this adakitic association was produced during Late Miocene initiation of subduction of young Sulu Sea backarc basin crust, and in fact the spreading centre in this basin is currently being subducted beneath the Zamboanga Peninsula.

7.3.6 THE SIGNIFICANCE OF FIJIAN ALKALI BASALTS

The occurrence of alkali basalts in Fiji is remarkable, considering that subduction had been operative beneath this region for about 25-30Ma until around 2-3Ma. The scattered occurrences around the hook of the Koro Sea, and their chemical diversity (Gill and Whelan, 1989b) suggests that the Fijian OIB magmas may have resulted from thermal convective disturbances in the mantle caused by the deformation of the SFB crust at the northeastern 'corner' of the Kadavu Trench, rather than the occurrence of a deep mantle plume at this location.

A temporal relationship between the cessation of subduction and the eruption of alkalic basalts has also been documented in several other areas, including the Antarctic Peninsula (Hole, 1988, 1990; Hole et al., 1991), Baja California (Storey et al., 1989) and British Columbia (Thorkelson and Taylor, 1989; Thorkelson, 1990). For the Baja California area, Dickinson and Snyder (1979) introduced the concept of a 'slab window', where the active continental margin is not underlain by subducted oceanic lithosphere due to subduction of a spreading ridge, leaving a 'window' into the asthenosphere. A similar occurrence along the Antartica Peninsula produced a slab window to the asthenosphere as a result of the subduction of a spreading ridge and its subsequent detachment from the trailing oceanic plate (Hole, 1988, 1990). Broadly OIB-type basaltic magmas are generated at both locations when asthenospheric mantle convects up into the slab hole or window.

In the Kadavu Island Group area, the subducted spreading centre-slab window hypothesis may not be appropriate, as there is clearly no young spreading centre on the downgoing plate. However, Fijian OIB occur directly above the northeastern termination of the (until 1-2 Ma) northwest-dipping subducted slab, leaving a northwest-orientated window into the asthenosphere. Convection of asthenospheric mantle into this slab window might produce both the Fijian OIB, and also

contribute to the production of adakitic magmas in this region, via the emplacement of hot deep-derived mantle against the subducted slab and overlying metasomatised mantle wedge peridotite (Fig. 7.2). It is worth noting that the few analysed Fijian OIB (Gill and Whelan 1989b) have isotopic compositions distinctively different from the nearest OIB-providing plume, in this case, the Samoan plume (Fig. 5.16).

7.4 SUMMARY

Geodynamic constraints on the geochemical evolution of the Kadavu Island Group and northern Hunter Ridge are:

Stage 1 (~5.5-3Ma): Thermal thinning of the Fijian lithosphere associated with the backarc basin development in the Lau and North Fiji Basins may have triggered small degrees of partial melting of lithosphere beneath Fiji that had been enriched by 'normal' slab-derived hydrous fluids during previous subduction along the Vitiaz arc. Melting of this lithospheric source produced the shoshonitic lavas that occur mainly in the northwestern part of Viti Levu, but also extend to the Astrolabe Islands in the northern Kadavu Island Group.

Stage 2 (<3Ma): in response to initiation of an E-W-trending spreading ridge in the North Fiji Basin probably ~7-5Ma, and to subsequent rotation of the Fiji Platform, 28-32 m.y. old South Fiji Basin crust began to subduct beneath young, hot MORB-depleted mantle wedge of the North Fiji Basin. Along the main part of the Hunter Ridge, high-Ca boninites, primitive arc tholeiites, and magmas transitional between these suites were generated. Further north along the Hunter Ridge, calc-alkaline lavas with some adakitic affinities were erupted, implying initiation of slab melting beneath this part of the ridge. In the Fiji area, however, subduction was initially beneath older, cooler arc lithosphere, and magma generation was suppressed. Eventual migration and decompression melting of asthenospheric mantle from around the northern end of the subducting slab produced the Fijian OIB, and possibly provided extra heat to induce slab melting beneath this northern section of the ridge, producing the WK and CEO adakites. Some adakitic melts were trapped in, and reacted with the mantle wedge, and subsequent partial melting of this source produced the Ngaloa Group high-Nb basalts.

A final consideration centres on the reason for the absence of lavas with adakitic affinities in the south-central part of the Hunter Ridge. It is likely that subduction beneath the young (<5m.y. old) hot backarc basin lithosphere of the North Fiji Basin led to anomalously shallow and

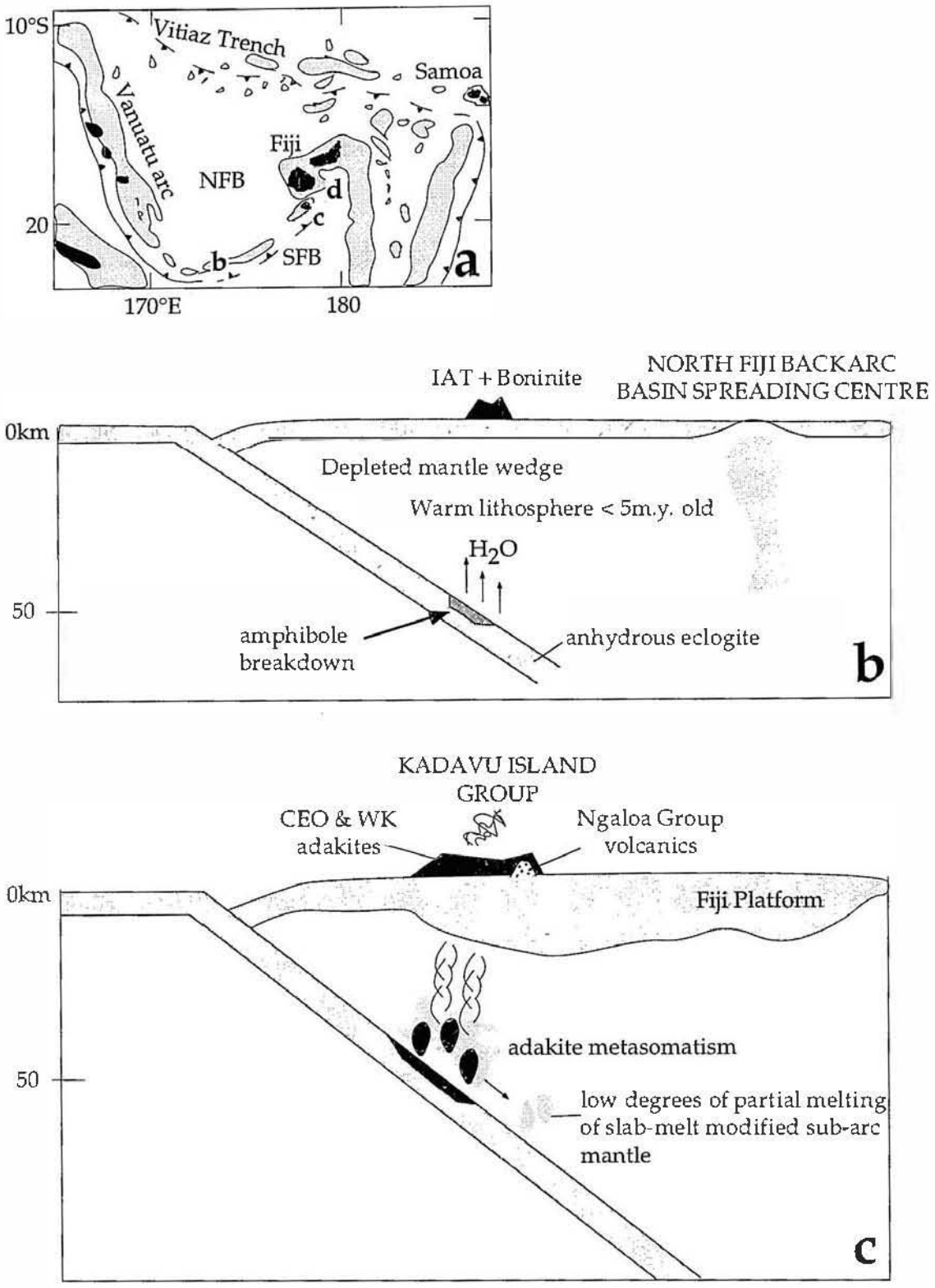

Figure 7.2 Schematic cross-sections below the Hunter Ridge and the Kadavu Island Group.
a: Location of the b, c and d sections along the Hunter Ridge to Kadavu Island Group.
b: Release of hydrous fluids from the subducted slab into the overlying depleted mantle wedge. The juxtaposition of hydrous, metasomatised subduction zone mantle beneath the Hunter Ridge against hot MORB mantle supplying North Fiji Basin oceanic crust produces magmas with affinities to both adakites and boninites.
c. Subduction of South Fiji Basin lithosphere below the Kadavu Island Group. Melting of the subducting slab produces dacitic (adakitic) magmas that infiltrate the mantle wedge. Ascent of these adakitic liquids, with limited assimilation of mantle wedge peridotite produces the Western Kadavu and Central/Eastern/Ono adakitic andesites and dacites. Some slab melt is consumed through slab melt-metasomatic reactions and hybridises the mantle wedge. The metasomatised mantle may be dragged to deeper levels, where it could melt producing the Ngaloa Group volcanics.

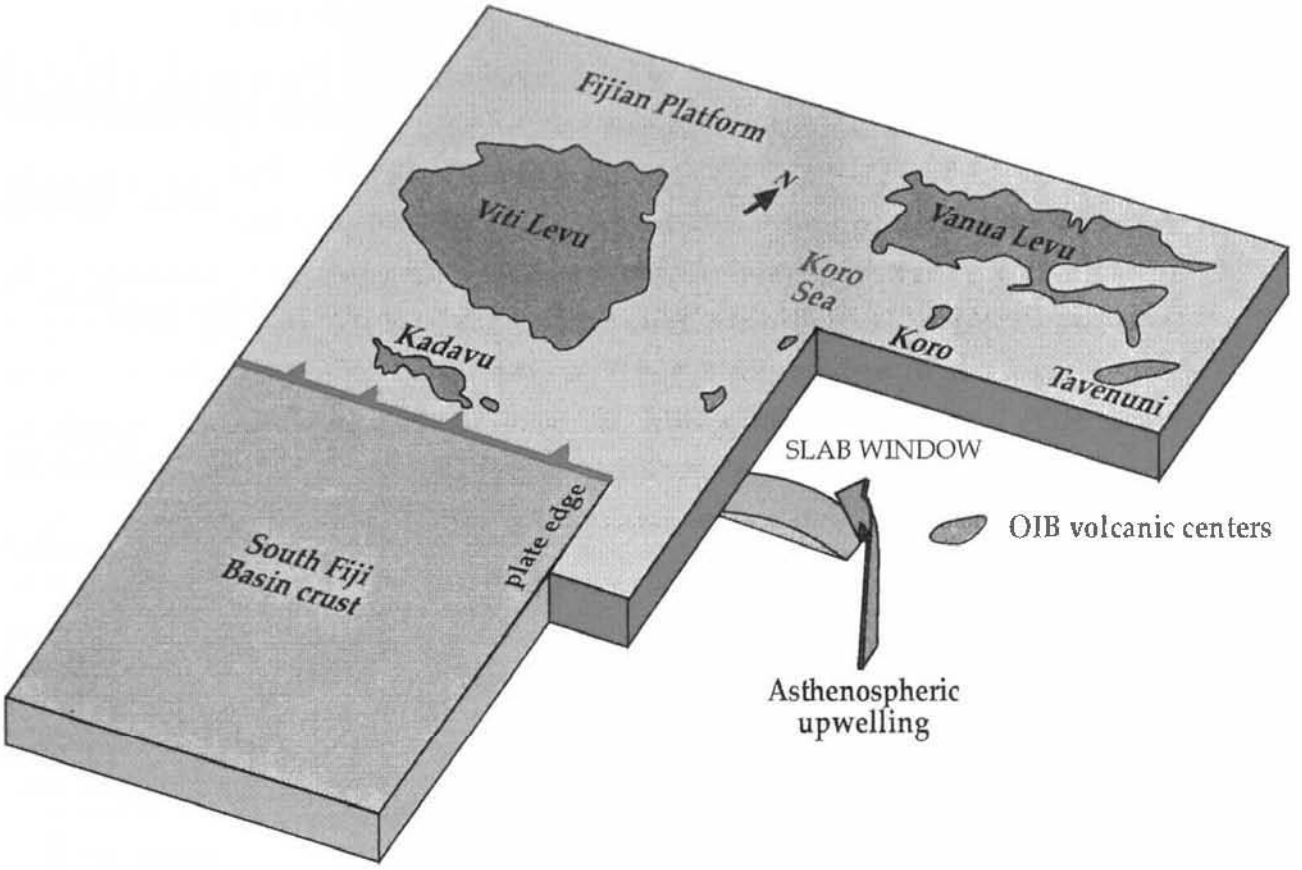

Figure 7.2 continued..
d. Schematic diagram of the 'slab window' at the northeastern edge of the subducted (SFB) slab, and the geographic location of some of the OIB volcanic centres in Fiji in relation to the subducted slab beneath the Kadavu Island Group. Emplacement of hot asthenospheric mantle against the subducted slab may also contribute heat for melting of the subducted slab producing the Western Kadavu and Central/Eastern/Ono Group andesites and dacites and the Ngaloa Group basalts.

thorough dehydration of the subducting slab, rendering it effectively anhydrous and infertile at deeper levels. In contrast, subduction beneath the slightly thicker and cooler lithosphere beneath the southern Vanuatu arc, and the extending thicker arc lithosphere of the Fiji Platform, stalled dehydration, and thermal effects from adjacent hot lithosphere of the North Fiji Basin (SW Hunter Ridge), or associated with ascent of asthenospheric mantle around the northern termination of the slab (NE Hunter Ridge), led to slab melting.

In conclusion, the range and diversity of magmas along the Hunter Ridge, including high-Ca boninites, arc tholeiites, primitive calc-alkaline lavas and lavas with adakitic slab-melt affinities, all reflect abnormal thermal and tectonic conditions in the mantle wedge of the over-riding plate, coupled with variations in lithospheric thickness. The brief existence of the Hunter Ridge arc reflects regional plate kinematics and the transient nature of spreading systems in the over-riding plate.

REFERENCES

Allan, J.F., Chase, R.L., Cousens, B., Michael, P.J., Gorton, M.P. & Scott, S.D. (1993). The Tuzo Volcanic Field, NE Pacific: Alkaline Volcanism at a complex, diffuse, transform-trench-ridge triple junction. *Journal of Geophysical Research*, 98(B12): 22367-22387.

Allen, J.C., Boettcher, A.L. & Marland, G. (1975). Amphiboles in andesite and basalt: I. Stability as a function of P-T-fO_2. *American Mineralogist*, 60: 1069-1085.

Arai, S. (1992). Chemistry of chromian spinel in volcanic rocks as a potential guide to magma chemistry. *Mineralogical magazine*, 56: 173-184.

Auzende, J.M., Pelletier, B. & Eissen J.P. (1996). The North Fiji Basin: geology, structure and geodynamic evolution. In: Taylor, B (ed). *Backarc basins: tectonics and magmatism*, Plenum Press, New York. pp 139-175

Baker, M.B., Grove, T.L. & Price, R. (1994). Primitive basalts and andesites from the Mt Shasta region, N California: products of varying melt fraction and water content. *Contributions to Mineralogy and Petrology*, 118: 111-129.

Ballhaus, C. (1993). Redox states of lithospheric and asthenospheric upper mantle. *Contributions to Mineralogy and Petrology*, 114: 331-348.

Ballhaus, C., Berry, R.F. & Green, D.H. (1991). High pressure experimental calibration of the olivine-orthopyroxene-spinel oxygen geobarometer: implications for the oxidation state of the upper mantle. *Contributions to Mineralogy and Petrology*, 107: 27-40.

Barberi, F., Gasparini, P., Innocenti, F. & Villari, L. (1973). Volcanism in the Southern Tyrrhenian Sea and its geodynamic implications. *Journal of Geophysical Research*, 78: 5221-5232.

Barreiro, B. (1983). Lead isotopic compositions of South Sandwich Island volcanic rocks and their bearing on magma genesis in intra-oceanic island arcs. *Geochimica et Cosmochimica Acta*, 47: 817-822.

Barton, M. & Bergen, M.J. (1981). Green clinopyroxenes and associated phases in a potassium-rich lava from the Leucite Hills, Wyoming. *Contributions to Mineralogy and Petrology*, 77: 101-114.

Bienvenu, P., Bougault, H., Joron, J.L., Treuil, M. & Dmitriev, L. (1990). MORB alteration: rare earth element/non rare earth hygromagmaphile element fractionation. *Chemical Geology*, 82: 1-14.

Borisov, A.A., & Shapkin, A.I. (1990). A new empirical equation rating Fe^{3+}/Fe^{2+} in magmas to their composition, oxygen fugacity, and temperature. *Geochemistry International*, 27: 111-116.

Brenan, J.M., Shaw, H.F., Ryerson, F.J. & Phinney, D.L. (1995). Experimental determination of trace-element partitioning between pargasite and a synthetic hydrous andesitic melt. *Earth and Planetary Science Letters*, 135: 1-11.

Briqueu, L., Laporte, C., Crawford, A.J., Hasenaka, T., Baker, P.E. & Coltorti, M. (1994). Temporal magmatic evolution of the Aoba Basin, central New Hebrides island arc: Pb, Sr, and Nd isotopic evidence for the coexistence of two mantle components beneath the arc. In:

Green, H.G., Collot, J-Y., Stokking, L.B et al., *Proceedings of the Ocean Drilling Program, Scientific Results*, 134: 393-401, Ocean Drilling Program, College Station, TX.

Brocher, T.M. & Holmes, R. (1985). The marine geology of sedimentary basins south of Viti Levu, Fiji. In: Brocher, T.M. (ed), *Investigations of the northern Melanesian Borderland, Circum Pacific Council for Energy and Mineral Resources Earth Science Series*, Circum-Pacific Council for Energy and Mineral Resources, Houston , Texas. pp: 123-138.

Brophy, J.G. & Marsh, B.D. (1986). On the origin of high-alumina basalt and the mechanics of melt extraction. *Journal of Petrology*, 27: 763-789.

Cameron, W.E. (1985). Petrology and origin of primitive lavas from the Troodos ophiolite, Cyprus. *Contributions to Mineralogy and Petrology*, 89: 239-255.

Carroll, M.R. & Wyllie, P.J. (1989). Experimental phase relations in the system tonalite-peridotite-H_2O at 15 kb; Implications for assimilation and differentiation processes near the crust-mantle boundary. *Journal of Petrology*, 30: 1351-1382.

Chen, C-H. (1993). Hydrous minerals in metasomatisedultra mafic xenoliths from Batan Island, Philippines. *Journal of Geological Society of China*, 36: 401-418.

Cohen, R.S. & O'Nions, R.K. (1982). Identification of recycled continental material in the mantle from Sr, Nd and Pb isotope investigations. *Earth and Planetary Science Letters*, 61: 73-84.

Cole, J.W., Graham, I.J. & Gibson, I.L. (1990). Magmatic evolution of late Cenozoic volcanic rocks of the Lau Ridge, Fiji. *Contributions to Mineralogy and Petrology*, 104: 504-554.

Coleman, P.J. & Packham, G.H. (1976). The Melanesian Borderland and Indian-Pacific plate boundary. *Earth Science Reviews*, 12: 197-263.

Colley, H. & Hindle, W.H. (1984). Volcano-tectonic evolution of Fiji and adjoining marginal basins. In: Kokelaar, B.P. & Howells, M.F. (eds), *Marginal Basin Geology*. Geological Society of London, pp 151-162.

Colley, H. (1984). An ophiolite suite in Fiji. In: Gass, I.G., Lippard, S.J. & Shelton, A.W., (eds). *Ophiolites and oceanic lithosphere*. Special publication Geological Society of London, 13: 133-140. Blackwell Scientific Publications, Oxford.

Cousens, B.L., Allan, J.F., Leybourne, M.I., Chase, R.L & Wagoner, N.Y. (1995). Mixing of magmas from enriched and depleted mantle sources in the northeast Pacific: West Valley Segment, Juan de Fuca Ridge. *Contributions to Mineralogy and Petrology*, 120: 337-357.

Crawford, A.J., Beccaluva, L. & Serri, G. (1981). Tectonic-magmatic evolution of the West Philippine-Mariana region and the origin of boninites. *Earth and Planetary Science Letters*, 54: 346-356.

Crawford, A.J., Danyushevsky, L., Sigurdsson, I., Monzier, M. & Eggins, S.M. (1993). Tectonic controls on magmatism in the southern New Hebrides (Vanuatu) Island arc. In: *Ancient volcanism and modern analogues*, IAVCEI, Canberra, abstracts pp 24.

Crawford, A.J., Falloon, T.J. & Eggins, S. (1987). The origin of island arc high-alumina basalts. *Contributions to Mineralogy and Petrology*, 97: 417-430.

Crawford, A.J., Falloon, T.J. & Green, D.H. (1989). Classification, petrogenesis and tectonic setting of boninites. In: Crawford, A.J (ed). *Boninites and related rocks*. London. Unwin Hyman. pp 1-49.

Crawford, A.J., Briqueu, L., Laporte, C. & Hasenaka, T. (1995). Coexistence of Indian and Pacific Oceanic upper mantle reserviors beneath the central New Hebrides Island Arc. In: Taylor, B. & Natland, J (eds). *Active margins and marginal basins of the Western Pacific.* Geophysical monograph 88, American Geophysical Union, 199-217.

Dal Negro, A., Carboin, S., Salviulo, G., Piccirillo, E.M. & Cundari, A. (1985). Crystal chemistry and site configuration of the clinopyroxene from leucite-bearing rocks and related genetic significance; the Sabatini lavas, Roman region, Italy. *Journal of Petrology,* 26: 1027-1040.

Davey, F.J. (1982). The structure of the South Fiji Basin. *Tectonophysics,* 87: 185-241.

Davis, J.H. & Stevenson, D.J. (1992). Physical model of source region of subduction zone volcanics. *Journal of Geophysical Research,* 97: 2037-2070.

Deer, W.A., Howie, R.A. & Zussman, J. (1989). *An introduction to the rock-forming minerals.* Longmas Scientific and Technical, United States.

Defant, M.J. & Drummond, M.S. (1990). Derivation of some modern arc magmas by melting of young subducted lithosphere. *Nature,* 347: 662-665.

Defant, M.J., Jackson, T.E., Drummond, M.S., de Boer, J.Z., Bellon, H., Feigenson, M.D., Maury, R.C. & Stewart, R.H. (1992). The geochemistry of young volcanism throughout western Panama and southeastern Costa Rica: An overview. *Geological Society of London Journal,* 149: 569-579.

Defant, M.J., Clark, L.F., Stewart, R.H., Drummond, M.S., deBoer, J.Z., Maury, R.C., Bellon, H., Jackson, T.E. & Restrepo, J.F. (1991a). Andesite and dacite genesis via contrasting processes: the geology and geochemistry of El Valle Volcano, Panama. *Contributions to Mineralogy and Petrology,* 106: 309-324.

Defant, M.J., Richerson, P.M., De Boer, J.Z., Stewart, R.H., Maury, R.C., Bellon, H., Drummond, M.S., Feigenson, M.D. & Jackson, T.E. (1991b). Dacite genesis via both slab melting and differentiation: Petrogenesis of La Yeguada Volcanic Complex, Panama. *Journal of Petrology,* 32: 1101-1142.

Della-Pasqua, F.N. & Varne, R. (1996). Primitive ankaramitic magmas in volcanic arcs: a melt inclusion approach. *(in press).*

Dick, H.J.B. & Bullen, T. (1984). Chromian spinal as petrogenetic indicator in abyssal and alpine-type peridotites and spatially associated lavas. *Contributions to Mineralogy and Petrology,* 86: 54-76.

Dickinson, W.R. & Snyder, W.S. (1979). Geometry of subducted slabs related to the San Andreas transform. *Journal of Geology,* 87: 609-627.

Dickinson, W.R., Rickard, M.J., Coulson, F.I., Smith, J.G. & Lawrence, R.L. (1968). Late Caenozoic shoshonitic lavas in north-western Viti Levu, Fiji. *Nature,* 219: 148.

Dmitriev, L.V., Magakian, R., Danyushevsky, L.V. & Kamenetsky, V.S. (1991). New data on primitive tholeiites from the Atlantic Ocean (12th cruise of the R/V 'Academic Boris Petrov'. *Volcanology and Seismology (Vulkanologai Seismologia),* 6: 78-94 (in Russian).

Drake, M.J. & Weill, D.F. (1975). Partition of Sr, Ba, Ca, V, Eu^{2+}, Eu^{3+} and other REE between plagioclase feldspar and magmatic liquid; an experimental study. *Geochimica et Cosmochimica Acta,* 39: 689-712.

Drummond, M.S. & Defant, M.J. (1990). A model for trondhjemite-tonalite-dacite genesis and crustal growth via slab melting: Archean to modern comparisons: *Journal of Geophysical Research,* 95: 21503-21521.

Duncan, R.A. & Green, D.H. (1987). The genesis of refractory melts in the formation of oceanic crust. *Contributions to Mineralogy and Petrology*, 96: 326-342.

Eggins, S.M. & Crawford, A.J. (1993). Primitive arc volcanism on the Hunter Ridge, SW Pacific. Extended abstracts. In: Smellie, J.L. (ed) *Volcanism associated with extension at subducting plate margins*. Cambridge, U.K.

Eggins, S.M. (1989). The origin of primitive ocean island and island arc basalts. Unpublished Ph.D thesis , University of Tasmania.

Eggins, S.M. (1993). Origin and differentiation of picritic arc magmas, Ambae (Aoba), Vanuatu. *Contributions to Mineralogy and Petrology*, 114: 79-100.

Eggins, S.M., Woodhead, J.D., Kinsley, L.P.J., Sylvester, P., McCulloch, M.T., Hergt, J.M. & Handler, M.R. (1996). A simple method for the precise determination of 40 or more trace elements in geological samples by ICPMS using enriched isotope internal standardisation. *Chemical Geology* (in press).

Ewart, A. & Bryan, W.B. (1973). The petrology and geochemistry of the Tongan Islands (1973). In: The Western Pacific; island arcs, marginal seas, geochemistry. *University of Western Australia. Press, Nedlands.* pp 503-522.

Ewart, A. (1982). The mineralogy and petrology of Tertiary-Recent orogenic volcanic rocks: with special reference to the andesite-basaltic compositional range. In: Thorpe, R.S., *Andesites*. John Wiley and Sons, New York.

Ewart, A., Bryan, W.B. & Gill, J.B. (1973). Mineralogy and geochemistry of the younger volcanic islands of Tonga, S.W. Pacific. *Journal of Petrology*, 14: 429-465.

Exley, R.A., Sills, J.D. & Smith, J.Y. (1982). Geochemistry of Micas from the Finero Spinel-Iherzolite, Italian Alps. *Contribution to Mineralogy and Petrology*, 81: 59-63.

Falloon, T.J. & Crawford, A.J. (1991). The petrogenesis of high-calcium boninite lavas dredged from the northern Tonga ridge. *Earth and Planetary Science Letters*, 102: 375-394.

Falloon, T.J. & Green, D.H. (1987). Anhydrous partial melting of MORB pyrolite and other peridotite compositions at 10 kbar: implications for the origins of primitive MORB glasses. *Mineralogy and Petrology*, 37: 181-219.

Falloon, T.J. & Green, D.H. (1988). Anhydrous partial melting of peridotite from 8 to 35 kbars and the petrogenesis of MORB. *Journal of Petrology, Special Lithosphere Issue*, pp 379-444.

Falloon, T.J., Green, D.H. & Crawford, A.J. (1987). Dredged igneous rocks from the northern termination of the Tofua magmatic arc, Tonga and adjacent Lau Basin. *Australian Journal of Earth Sciences*, 34: 487-506.

Falloon, T.J., Green, D.H., Hatton, C. J. & Harris, K.L. (1988). Anhydrous partial melting of a fertile and depleted peridotite from 2 to 30 kb and application to basalt petrogenesis. *Journal of Petrology*, 29: 1257-1282.

Falloon, T.J., Green, D.H. & Mc Culloch, M.T. (1989). Petrogenesis of high-Mg and associated lavas from the north Tonga Trench. In: Crawford, A.J (ed). *Boninites and related rocks*, London, Unwin Hyman.

Falvey, D.A. (1978). Analysis of palaeomagnetic data from the New Hebrides. *Bulletin of Australian Society of Exploration Geophysics*, 9: 117-123.

Ford, C.E., Russell, D.G., Craven, J.A. & Fisk, M.R. (1983). Olivine-liquid equilibria: temperature, pressure and composition dependence of the crystal/liquid cation partition coefficients for Mg, Fe^{2+}, Ca and Mn. *Journal of Petrology*, 24: 256-265.

Frisch, T. & Schmincke, H.U. (1969). Petrology of clinopyroxene-amphibole inclusions from the Roque Nublo Volcanics, Gran Canaria, Canary Islands (petrology of Roque Nublo Volcanics I). *Bulletin of Volcanologique*, 33: 1073-1088.

Ghiorso, M.S. & Carmichael, I.S.E. (1987). Modelling magmatic systems: petrologic application. *Reviews in Mineralogy*, 17: 467-499.

Gill, J.B. & Gorton, M. (1973). A proposed geological and geochemical history of Eastern Melanesia. In: Coleman, P. (ed). *The Western Pacific Island arcs, Marginal seas, geochemistry*, pp 543-566. University of Western Australia, Press Nedlands.

Gill, J.B. & McDougall, I. (1973). Biostratigraphic and geological significance of Miocene-Pliocene volcanism in Fiji. *Nature*, 241: 176-180.

Gill, J.B. & Stork, A.L. (1979). Miocene low-k dacites and trondhjemites of Fiji. In: Barker, F. (ed), *Trondhjemites, dacites and related rocks*, Elsevier, Amsterdam.

Gill, J.B. & Whelan, P. (1989a). Early rifting of an oceanic island arc (Fiji) produced shoshonitic to tholeiitic basalts. *Journal of Geophysical Research*, 94: 4561-4578.

Gill, J.B. & Whelan, P. (1989b). Post subduction ocean island alkali basalts in Fiji. *Journal of Geophysical Research*. 94: 4579-4588.

Gill, J.B. (1970). Geochemistry of Viti Levu, Fiji, and its evolution as an island arc. *Contributions to Mineralogy and Petrology*. 27: 179-203.

Gill, J.B. (1974). Role of underthrust oceanic crust in the genesis of a Fijian calc-alkaline suite. *Contributions to Mineralogy and Petrology*, 43: 29-45.

Gill, J.B. (1976). Composition and age of Lau Basin and Ridge volcanic rocks: implications for evolution of an interarc basin and remnant arc. *Geological Society of America Bulletin*, 87: 1384-1395.

Gill, J.B. (1981). Orogenic andesites and plate tectonics. *Springer-Verlag*, Berlin - Heidelberg. pp 390.

Gill, J.B. (1984). Sr - Pb - Nd isotopic evidence that both MORB and OIB sources contribute to oceanic island arc magmas in Fiji. *Earth and Planetary Science Letters*, 68: 443-458.

Gill, J.B. (1987). Early geochemical evolution of an oceanic island arc and backarc: Fiji and the South Fiji Basin. *Journal of Geology*, 95: 589-615.

Gill, J.B., Stork, A.L. & Whelan, P.M. (1984). Volcanism accompanying backarc basin development in the southwest Pacific. *Tectonophysics*, 102: 207-224.

Green, T.H., Sie, S.H., Ryan, C.G. & Cousens, D.R. (1989). Proton microprobe-determined partitioning of Nb, Ta, Zr, Sr and Y between garnet, clinopyroxene and basaltic magma at high pressure and temperature. *Chemical Geology*, 74: 201-216.

Halliday, A.N., Fallick, A.E., Dicken, A.P., Mackenzie, A.B., Stephens, W.E. & Hildreth, W. (1983). The isotopic and chemical evolution of Mount St Helens. *Earth and Planetary Science Letters*, 63: 241-256.

Halsor, S.P. (1989). Large glass inclusions in plagioclase phenocrysts and their bearing on the origin of mixed andesitic lavas at Toliman Volcano, Guatemala. *Bulletin of Volcanology*, 51: 271-280.

Hamburger, M.W. & Isacks, B.L. (1987). Deep earthquakes in the southwest Pacific: a tectonic interpretation. *Journal of Geophysical Research*, 92: 13841-13854.

Hamburger, M.W., Everingham, I.B., Isacks, B.L. & Barazangi, M. (1990). Seismicity and crustal structure of the Fiji Platform, Southwest Pacific. *Journal of Geophysical Research*, 95: 2553-2573.

Hart, S.R. & Davis, K.E. (1978). Nickel partitioning between olivine and silicate melt. *Earth and Planetary Science Letters*, 44: 159-161.

Hart, S.R. (1984). A large-scale isotope anomaly in the Southern Hemisphere mantle. *Nature*, 309: 753-757.

Hartmann, G. & Wedepohl, K.H. (1993). The composition of peridotite tectonites from the Ivrea complex, Northern Italy: Residues from melt extraction. *Geochimica et Cosmochimica Acta*, 57: 1761-1782.

Hathway, B. (1994). Sedimentation and volcanism in an Oligocene-Miocene intra-oceanic arc and fore-arc, southwestern Viti Levu, Fiji. *Journal of the Geological Society of London*. 151: 499-514.

Hawkesworth, C.J., O'Nions, R.K., Pankhurst, R.J., Hamilton, P.J. & Evensen, N.M. (1977). A geochemical study of island arc and backarc tholeiites from the Scotia Sea. *Earth and Planetary Science Letters*, 36: 253-262.

Hickey, R.L., Frey, F.A. & Gerlach, D.C. (1986). Multiple sources for basaltic rocks from the southern volcanic zone of the Andes (34-41 degrees south): trace element and isotopic evidence for contributions from subducted oceanic mantle and continental crust. *Journal of Geophysical Research*, 91: 5943-5962.

Hindle, W.H. & Colley, H. (1981). An oceanic volcano in an island arc setting-Seatura volcano, Fiji. *Geological Magazine*, 118: 1-14.

Hirose, K. & Kushiro, I. (1993). Partial melting of dry peridotites at high pressures; determination of compositions of melts segregated from peridotite using aggregates of diamond. *Earth and Planetary Science Letters*, 114: 477-489.

Hochstaedter, A.G., Kepezhinskas, P.K., Defant, M.J., Drummond, M.S. & Bellon, H. (1994). On the tectonic significance of Arc volcanism in northern Kamchatka. *Journal of Geology*, 102: 639-654.

Hole, M.J. (1988). Post-subduction alkaline volcanism along the Antarctic Peninsula: *Geological Society of London Journal*, 145: 985-988.

Hole, M.J. (1990). Geochemical evolution of Pliocene-Recent post-subduction alkalic basalts from Seal Nunataks, Antarctic Peninsula. *Journal of Volcanology and Geothermal Research*, 40: 149-167.

Hole, M.J., Rogers, G., Saunders, A.D. & Storey, M. (1991). Relation between alkalic volcanism and slab-window formation. *Geology*, 19: 657-660.

Huijsmans, J.P.P., Barton, M. & Sallers, V.J.M. (1988). Geochemistry and evolution of the calc-alkaline volcanic complex of Santorini, Aegean Sea, Greece. *Journal of Volcanology and Geothermal Research*, 34: 283-306.

Iddings, J.P. (1895). Absarokite-shoshonite-banakite series. *Journal of geology*, 3: 935-959.

Inokuchi, H., Yaskawa, K. & Rodd, P. (1992). Clockwise and anticlockwise rotation of Viti Levu, Fiji - in relation to the tectonic development of the North and the South Fiji Basin. *Geophysical Journal International*, 110: 225-237.

Irving, A.J. (1978). A review of experimental studies of crystal/liquid trace element partitioning. *Geochimica et Cosmochimica Acta* 42: 743-770.

Ito, E., White, W.M. & Gopel, C. (1987). The O, Sr, Nd and Pb isotope geochemistry of MORB. *Chemical Geology*, 62: 157-176.

Jakes, P. & Gill, J.B. (1970). Rare earth elements and the island arc tholeiitic series. *Earth and Planetary Science Letters*. 9: 17-28.

Jakes, P. & White, A.J.R. (1971). Composition of island arcs and continental growth. *Earth and Planetary Science Letters*. 12: 224-230.

Jakes, P. & White, A.J.R. (1972). Major and trace element abundance in volcanic rocks of orogenic areas. *Geological Society America Bulletin*, 83: 29-39.

James, A. & Falvey, D.A. (1978). Analysis of palaeomagnetic data from Viti Levu, Fiji. *Bulletin Australian Society of Exploration Geophysics*, 9: 115-117.

Jaques, A.L. & Green, D.H. (1980). Anhydrous melting of peridotite at 0-15 kbar pressure and the genesis of tholeiitic basalts. *Contributions to Mineralogy and Petrology*, 73: 287-310.

Jarosewich, E.J., Nelen, J.A. & Norberg, J.A., (1980). Reference samples for electron microprobe analysis. *Geostandards Newsletter*, 4: 43-47.

Jenner, G.A. (1981). Geochemistry of high-Mg andesites from Cape Vogel, Papua New Guinea. *Chemical Geology*, 33: 307-332.

Johnston, A.D. & Wyllie, P.J. (1988). Interaction of granite and basic magmas: experimental observations on contamination processes at 10 kbar with H_2O. *Contributions to Mineralogy and Petrology*, 98: 352-362.

Joplin, G.A. (1968). The shoshonite association: A review. *Journal of Geological Society of Australia*, 15: 275-294.

Jurcewicz, A.J.G. & Watson, E.B. (1988). Cations in olivine, Part 1: calcium partitioning and calcium-magnesium distribution between olivines and co-existing melts, with petrologic applications. *Contributions to Mineralogy and Petrology*, 99: 176-185.

Kay, R.W. (1978). Aleutian magnesian andesites: Melts from subducted Pacific Oceanic crust: *Journal of volcanology and Geothermal Research*, 4: 117-132.

Kay, R.W. (1980). Volcanic arc magmas; Implications of a melting-mixing model for element recycling in the crust-upper mantle system. *Journal of Geology*, 88: 497-522.

Kay, S.M., Ramos, V.A. & Marquez, M. (1993). Evidence in Cerro Pampa volcanic rocks for slab melting prior to ridge-trench collision in southern South America. *Journal of Geology*, 101: 703-714.

Kelemen, P,B. (1995). Genesis of high $Mg^{\#}$ andesites and the continental crust. *Contributions to Mineralogy and Petrology*, 120: 1-19.

Kelemen, P.B. (1990). Reaction between ultramafic rock and fractioning basaltic magma I. Phase relations, the origin of calc-alkaline magma series, and the formation of discordant dunite. *Journal of Petrology*, 31: 51-98.

Kelemen, P.B., Shimizu, N. & Dunn, T. (1993). Relative depletion of niobium in some arc magmas and the continental crust: Partitioning of K, Nb, La and Ce during melt/rock reaction in the upper mantle. *Earth and Planetary Science Letters*, 120: 111-134.

Kepezhinskas, P.K. (1989). Origin of the hornblende andesites of northern Kamchatka. *International Geology Reviews*, 31: 246-252.

Kepezhinskas, P.K., Defant, M.J. & Drummond, M.S. (1996). Progressive enrichment of island arc mantle by melt-peridotite interaction inferred from Kamchatka xenoliths. *Geochimica et Cosmochimica Acta*, 60: 1217-1229.

Kepezhinskas, P.K., Defant, M.J. & Drummond, M.S. (1995). Na metasomatism in the island-arc mantle by slab melt-peridotite interaction: Evidence from mantle xenoliths in the north Kamchatka arc. *Journal of Petrology*, 36: 1505-1527.

Kesson, S.E. & Ringwood, A.E. (1989). Slab-mantle interactions I. sheared and refertilized garnet peridotite xenoliths-samples of Wadati-Benioff zones? *Chemical Geology*, 78: 83-96.

Kinzler, B.J., Grove, T.L. & Recca, S.I. (1990). An experimental study on the effect of temperature and melt composition on the partitioning of nickel between olivine and silicate melt. *Geochimica et Cosmochimica Acta*, 54: 1255-1265.

Kroenke, L.W. (1984). *Cenozoic tectonic development of the southeast Pacific.* UN, ESCAP, CCOP/SOPAC Technical Bulletin no.6.

Langmuir, C.H., Klein, E.M. & Plank, T. (1992). Petrological systematics of mid-ocean ridge basalts: constraints on melt generation beneath ocean ridges. In: Phipps, M.J., Blackman, D.K., Sinton, J.M (eds). *Mantle flow and melt generation at mid-ocean ridges.* AGU, Washington, D.C.

Lavrentev, Y.G., Pospelova, L.N. & Sobolev, A.V. (1974). Rock-forming mineral compositions determination by X-ray microanalysis. *Zavodskaya Laboratoria*, 40: 657-666 (in Russian).

Leake, B. (1978). Nomenclature of amphiboles. *American Mineralogist*, 63: 1023-1052.

Leeman, W.P., Smith, D.R., Hildreth, W., Palacz, Z. & Rogers, N. (1990). Compositional diversity of Late Cenozoic basalts in a transect across the Southern Washington Cascades: Implications for subduction zone magmatism. *Journal of Geophysical Research*, 95: 19561-19582.

Lindsley, D.H. & Anderson, D.J. (1983). A two pyroxene thermometer. *Journal of Geophysical Research*, 88: A887-A906.

Luhr, J.F. & Carmichael, I.S.E. (1980). The Colima Volcanic Complex, Mexico. I. Post-caldera andesites from Volcan Colima. *Contributions to Mineralogy and Petrology*, 71: 343-372.

Luhr, J.F. & Carmichael, I.S.E. (1981). The Colima Volcanic Complex, Mexico: Part II. Late Quaternary cinder cones. *Contributions to Mineralogy and Petrology*, 76: 127-147.

MacDonald, K.C., Luyendyk, B.P. & Von Herzen, R.P. (1973). Heat flow and plate boundaries in Melanesia. *Journal of Geophysical Research*, 78: 2537-2546.

MacLeod, C.J. (1988). The tectonic evolution of the Eastern Limassol Forest Complex, Cyprus. Unpublished Ph.D thesis. The Open University.

Maillet, P., Monzier, M. & Lefevre, C. (1986). Petrology of Matthew and Hunter volcanoes, south New Hebrides island arc (southwest Pacific). *Journal of Volcanology and Geothermal Research*, 30: 1-27.

Maillet, P., Monzier, M., Eissen, J.P. & Lovat, R. (1989). Geodynamics of an arc-ridge junction: the case of the New Hebrides arc/North Fiji Basin. *Tectonophysics*, 165: 251-268.

Malahoff, A., Hammond, S.R., Naughton, J.J., Keeling, D.L. & Richmond, R.N. (1982). Geophysical evidence for post-Miocene rotation of the island of Viti Levu, Fiji, and its relationship to the tectonic development of the North Fiji Basin. *Earth and Planetary Science Letters*, 57: 398-414.

Maurel, C. & Maurel, P. (1982). Etude experimentale de l'equilibre Fe^{2+}-Fe^{3+} dans les spinelles chromiferes et les liquides slicates basiques coexistants, a 1 atm. *C.R. Academy Science Paris*, 285: 209-215.

McNeill, A.W. & Danyushevsky, L.V. (1996). Compositions and crystallization temperatures of primary melts for hole 896A: Evidence from melt inclusions studies. *Proceedings ODP, Scientific results*, 148: 21-35.

McPhie, J., Doyle, M. & Allen, R. (1993). *Volcanic textures. A guide to the interpretation of textures in volcanic rocks.* Centre for Ore Deposit and Exploration studies, University of Tasmania. pp 198.

Meijer, A. & Reagan, M. (1983). Origin of K_2O - SiO_2 trends in volcanoes of the Mariana Arc. *Journal of Geology*, 11: 67-71.

Miyashiro, A. (1974). Volcanic rock series in island arcs and active continental margins. *American Journal of Science*, 274: 321-355.

Monzier, M., Danyushevsky, L.V., Crawford, A.J., Bellon, H. & Cotton, J. (1993). High-Mg andesites from the southern termination of the New Hebrides island arc (SW Pacific). *Journal of Volcanology and Geothermal Research*, 57: 193-217.

Morris, J.D. & Hart, S.R. (1983). Isotopic and incompatible element constraints on the genesis of island arc volcanics from Cold Bay and Amak Island, Aleutians, and implications for mantle structure. *Geochimica et Cosmochimica Acta*, 47: 2015-2030.

Morris, J.D., Leeman, W.P. & Tera, F. (1990). The subducted component in island arc lavas: constraints from Be isotopes and B-Be systematics. *Nature*, 344: 31-36.

Morris, P.A. (1995). Slab melting as an explanation of Quaternary volcanism and aseismicity in southwest Japan. *Geology*, 23: 395-398.

Morrison, G.W. (1980). Characteristics and tectonic setting of the shoshonitic rock association. *Lithos*, 13: 97-108.

Newson, H.G., White, W.M., Jochum, K.P. & Hofman, A.W. (1986). Siderophile and chalcophile element abundances in oceanic basalts, Pb isotope evolution and growth of the Earth's core. *Earth and Planetary Science Letters*, 80: 299-313.

Nohara, M., Hirose, K., Eissen, J.P., Urabe, T., & Joshima, M. (1994). The North Fiji Basin basalts and their magma sources: Part II. Sr-Nd isotopic and trace element constraints. *Marine Geology*, 116: 1-17.

Norrish, K. & Chappell B.W. (1977). X-ray fluorescence spectrography. In: Zussman, J. (ed), *Physical methods in determinative mineralogy.* Academic Press: 161-214.

Norrish, K. & Hutton, J.T. (1969). An accurate X-ray spectrographic method for the analysis of a wide range of geological samples. *Geochimica et Cosmochimica Acta*, 33: 431-455.

O'Reilly, S.Z., Griffin, W.L & Ryan, C.G. (1991). Residence of trace elements in metasomatized spinel lherzolite xenoliths: a proton-microprobe study. *Contributions to Mineralogy and Petrology*, 109: 98-113.

Ozawa, K. (1983). Evaluation of olivine-spinel geothermometry as an indicator of thermal history of peridotites. *Contribution to Mineralogy and Petrology*, 82: 52-65.

Palacz, Z.A. & Saunders, A.D. (1986). Coupled trace element and isotope enrichment in the Cook-Austral-Samoa Islands, Southwest Pacific. *Earth and Planetary Science Letters*, 79: 270-280.

Panjasawatwong, Y., Danyushevsky, L.V., Crawford, A.J. & Harris, K.L. (1995). An experimental study of the effects of melt composition on plagioclase: melt equilibria at 5 and 10 kbar: implications for the origin of magmatic high-An plagioclase. *Contributions to Mineralogy and Petrology*, 118: 420-432.

Peacock, S.M. (1987). Creation and preservation of subduction-related inverted metamorphic gradients. *Journal of Geophysical Research*, 92: 12763-12781.

Peacock, S.M. (1990). Numerical simulation of metamorphic pressure-temperature-time paths and fluid production in subducting slabs. *Tectonics*, 248: 329-337.

Peacock, S.M., Rushmer, T. & Thompson, A.B. (1994). Partial melting of subducting oceanic crust. *Earth and Planetary Science Letters*, 121: 227-244.

Pearce, J.A. & Peate, D.W. (1995). Tectonic implications of the composition of volcanic arc magmas. *Annual Reviews of Earth and Planetary Sciences*, 24: 251-285.

Pearce, J.A. (1982). Trace element characteristics of lavas from destructive plate boundaries. In: Thorpe, R.S. (ed) *Andesites: Orogenic Andesites and Related Rocks.* Chichester: John Wiley, pp 525-548.

Pearce, J.A. (1983). Role of the sub-continental lithosphere in magma genesis at active continental margins. In: Hawkesworth, C.J. & Norry, M.J. (eds) *Continental basalts and mantle xenoliths.* Nantwich: Shiva, pp 230-249.

Pearce, J.A., Baker, P.E., Harvey. P.K. & Luff, I.W. (1995). Geochemical evidence for subduction fluxes, mantle melting and fractional crystallization beneath the South Sandwich Island Arc. *Journal of Petrology*, 36: 1073-1109.

Peccerillo, A. & Taylor, S.R. (1976). Geochemistry of Eocene calc-alkaline volcanic rocks from the Kastamonu area, northern Turkey. *Contributions to Mineralogy and Petrology*, 58: 63-81.

Perfit, M.R., Gust, D.A., Bence, A.E., Arculus, R.J., Taylor, S.R. (1980). Chemical characteristics of island arc basalts: implications for mantle sources. *Chemical Geology*, 30: 227-256.

Plank, T. & Langmuir, C.H. (1988). An evaluation of the global variations in the major element chemistry of arc basalts. *Earth and Planetary Science Letters*, 90: 349-370.

Price, R.C. & Kroenke, L.W. (1991). Tectonics and magma genesis in the northern North Fiji Basin. *Marine Geology*, 98: 241-258.

Price, R.C., Johnson, L.E. & Crawford, A.J. (1990). Basalts of the North Fiji Basin: the generation of backarc basin magmas by mixing of depleted and enriched mantle sources. *Contributions to Mineralogy and Petrology,* 105: 106-121.

Rapp, R.P. & Watson, B. (1995). Dehydration melting of metabasalt at 8-32 kbar: Implications for continental growth and crust-mantle recycling. *Journal of Petrology,* 36: 891-931.

Rapp, R.P. (1995). Amphibole-out phase boundary in partially melted metabasalt, its control over liquid fraction and composition, and source permeability. *Journal of Geophysical Research,* 100: 15601-15610.

Reagan, M.K. & Gill, J.B. (1989). Co-existing calc-alkaline and high niobium basalts from Turrialba volcano, Costa Rica: Implications for residual titanates in arc magma sources. *Journal of Geophysical Research,* 94: 4619-4633.

Rodda, P. & Kroenke, L.W. (1984). Fiji: A fragmented Arc. In: Kroenke, L.W. (ed) *Cenozoic tectonic development of the southwest Pacific.* UN, ESCAP, CCOP/SOPAC Technical Bulletin no.6 . pp 87-111.

Rodda, P. (1994). Geology of Fiji. In: Stevenson, A.J., Herzer, R.H. & Ballance, P.F. (eds). *Geology and submarine resources of the Tonga Lau - Fiji Region.* SOPAC Technical Bulletin, 8: 131-151.

Roeder, P.L. & Emslie, R.F. (1970). Olivine-liquid equilibrium. *Contributions to Mineralogy and Petrology,* 29: 275-289.

Rogers, G., Saunders, A.D., Terrell, D.J., Verma, S.P. & Marriner, G.F. (1985). Geochemistry of Holocene volcanic rocks associated with ridge subduction in Baja, California, Mexico. *Nature,* 315: 389-392.

Rogers, N.W. & Setterfield, T.N. (1994). Potassium and incompatible element enriched in shoshonitic lavas from the Tavua volcano, Fiji. *Chemical Geology,* 118: 43-62.

Romanu, J.M., Ibbotson, P. & Harvey, S. R. M. (1959). Geological reconnaissance of Kadavu. *Geological Survey of Fiji report no. 48.* (unpublished).

Rutherford, M.J. & Hill, P.M. (1993). Magma ascent rates from amphibole breakdown; an experimental study applied to the 1980-1986 Mount St. Helens eruptions. *Journal of Geophysical Research,* 98: 19667-19685.

Sajona, F.G., Maury, R.C., Bellon, H., Cotten, J. & Defant, M. (1996). High field strength element enriched of Pliocene-Pleistocene island arc basalts, Zamboanga Peninsula, Western Mindanao (Philippines). *Journal of Petrology,* 37: 693-726.

Sajona, F.G., Maury, R.C., Bellon, H., Cotton, J., Defant, M.J. & Pubellier, M. (1993). Initiation of subduction and the generation of slab melts in western and eastern Mindanao, Philippines. *Geology,* 21: 1007-1010.

Sclater, J.G. & Menard, H.W. (1967). Topography and heat flow of the Fiji Plateau. *Nature,* 216: 991-993.

Sekine, T. & Wyllie, P.J. (1982). Phase relationships in the system $KAlSiO_4$-Mg_2SiO_4-SiO_4-H_2O as a model for hybridization between hydrous siliceous melts and peridotite. *Contributions to Mineralogy and Petrology,* 79: 368-374.

Sekine, T. & Wyllie, R.S. (1983). Experimental simulation of mantle hybridization in subduction zones. *Journal of Geology,* 91: 511-528.

Sekine, T., Katsura, T. & Aramaki, S. (1979). Water-saturated phase relations of some andesites with application to the estimation of the initial temperature and water pressure at the time of eruption. *Geochimica et Cosmochimica Acta* : 1367-1376.

Sen, C. & Dunn, T. (1993). Experimental productions of modally metasomatised mantle. *Geological Association Canada/Mineral Association Canada program*-abstract 18: A-95.

Sen, C. & Dunn, T. (1994). Dehydration melting of a basaltic composition amphibolite at 1.5 and 2.0 GPa: implications for the origin of adakites. *Contributions to Mineralogy and Petrology*, 117: 394-409.

Sen, C. & Dunn, T. (1995). Experimental model metasomatism of a spinel lherzolite and the production of amphibole-bearing peridotite. *Contributions to Mineralogy and Petrology*, 119: 422-432.

Sigurdsson, I.A. (1994). Primitive magmas in convergent margins and at oceanic spreading ridges: evidence from early formed phenocryst phases and their melt inclusions. Unpublished Ph.D thesis, University of Tasmania.

Sigurdsson, I.A., Kamenetsky, V.S., Crawford, A.J., Eggins, S.M. & Zlobin, S.K. (1993). Primitive Island Arc and Oceanic Lavas from the Hunter Ridge-Hunter Fracture Zone. Evidence from glass, olivine and spinel compositions. *Mineralogy and Petrology*, 47: 149-169.

Simkin, T. & Smith, J.Y. (1970). Minor element distribution in olivines. *Journal of Geology*, 78: 304-325.

Sobolev, A.V. & Danyushevsky, L.V. (1994). Petrology and geochemistry of boninites from the north termination of the Tonga Trench; constrainsts on the generation conditions of primary high-Ca boninite magmas. *Journal of Petrology*, 35: 1183-1211.

Sobolev, A.V., Danyushevsky, L.V., Dimitriev, L.V. & Sushchevskaya, N.M. (1989). High-alumina magnesian tholeiite as the primary basalt magma at midocean ridge. *Geochemistry International*, 26: 128-133.

Sobolev, A.V., Dmitriev, L.V., Barsukov, V.L., Nevsorov, V.N. & Slutsky, A.B (1980). The formation conditions of the high-magnesian olivines from monomineralic fraction of Luna 24 regolith. *Proceedings of Lunar Planetary Science conference 11th Pergamon Press*, 105-116.

Sobolev, A.V., Dmitriev, L.V., Tsameryan, O.P., Kononkova, N.N., Robinson, P.T. (1991). A possible primary melt composition for the ultramafic lavas of the Margi area, Troodos Ophiolite, Cyprus. In: Gibson, I.L., Malpas, J., Robinson, P.T & Xenophontos, C (eds), *Cyprus crustal study project*: initial report, holes CY-1 and 1a. Geological Survey of Canada paper 90-20, 203-216.

Staudigel, H. & Hart, S.R. (1983). Alteration of basaltic glass, mechanisms and significance for the oceanic crust-seawater budget. *Geochimica et Cosmochimica Acta*, 47: 337-350.

Staudigel, H., Hart, S.R. Richardson, S.H. (1981). Alteration of the oceanic crust, processes and timing. *Earth and Planetary Science Letters*, 52: 311-327.

Stern, C.R. & Kilian, R. (1996). Role of the subducted slab, mantle wedge and continental crust in the generation of adakites from the Andean Austral Volcanic Zone. *Contributions to Mineralogy and Petrology*, 123: 263-281.

Storey, M., Rogers, G., Saunders, A.D. & Terrell, D.J. (1989). San Quintin volcanic field, Baja California, Mexico: 'Within-plate' magmatism following ridge subduction. *Terra Nova*, 1: 195-202.

Sun, S.S. & McDonough, W.F. (1989). Chemical and isotopic systematics of oceanic basalts: implications for mantle composition and processes. In: Saunders, A.D. and Norry, M.J. (eds), *Magmatism in the ocean basins*, Geological Society Special Publication no. 42: 313-345.

Taras, B.D. & Hart, S.R. (1987). Geochemical evolution of the New England seamount chain; isotopic and trace element constraints. *Chemical Geology*, 64: 35-54.

Tatsumi, Y. (1989). Migration of fluid phases and genesis of basalt magmas in subduction zones. *Journal of Geophysical Research*, 94: 4697-4707.

Tatsumi, Y. & Eggins S.M. (1996). *Subduction zone magmatism.* Blackwell Science, Australia, pp 211.

Thompson, R.N. (1977). Primary basalts and magma genesis III Alban Hills, Roman comagmatic province, Central Italy. *Contributions to Mineralogy and Petrology*, 60: 91-108.

Thorkelson, D.J. & Taylor, R.P. (1989). Cordilleran slab windows. *Geology*, 17: 833-836.

Thorkelson, D.J. (1990). Tectonic and magmatic aspects of slab windows: Geological Association of Canada with Abstracts. 15: A131.

Thy, P. & Lofgren, G.E. (1993). Experimental constraints on the low-pressure evolution of transitional and mildly alkalic basalts; multisaturated liquids and co-existing augites. *Contributions to Mineralogy and Petrology*, 112: 196-202.

Ulmer, P. (1989). The dependence of the Fe^{2+}-Mg cation partitioning between olivine and basaltic liquid on pressure, temperature and composition. An experimental study to 30 kbars. *Contributions to Mineralogy and Petrology*, 101: 261-273.

Verma, S.P. & Nelson, S.A. (1989). Isotopic and trace element constraints on the origin and evolution of alkaline and calc-alkaline magmas in the northwestern Mexican volcanic belt. *Journal of Geophysical Research*, 94: 4531-4544.

Volpe, A.M., McDougall, J.D. & Hawkins, J.W. (1988). Lau Basin basalts (LLB): trace element and Sr-Nd isotope evidence for heterogeneity in backarc basin mantle. *Earth and Planetary Science Letters*, 90: 174-186.

Wallace, M.E. & Green, D.H. (1988). An experimental determination of primary carbonatite magma composition, *Nature*, 355: 343-346.

Watson, E.B. & Green, T.H. (1981). Apatite/liquid partition coefficients for the rare earth elements and strontium, *Earth and Planetary Science Letters*, 56: 405-421.

Watts, A.B, Weissel, J.K. & Davey, F.J. (1977). Tectonic evolution of the South Fiji marginal basin. In: Talwani M. & Pitman, W.C. (eds), *Island Arcs Deep Sea Trenches and Backarc Basins.* American Geophysical Union, Maurice Ewing Ser., 1: 419-427.

Weissel, J.K. & Watts, A.B. (1975). Tectonic complexities in the South Fiji marginal basin. *Earth and Planetary Science Letters*, 28: 121-126.

Wells, P.R.A. (1977). Pyroxene thermometry in simple and complex systems. *Contributions to Mineralogy and Petrology*, 62: 129-139.

Wharton, M.R., Hathway, B. & Colley, H. (1995). Volcanism associated with extension in an Oligocene-Miocene Arc, southwestern Viti Levu, Fiji. In: Smellie, J.L. (ed), *Volcanism associated with extension at consuming plate margins.* Geological Society Special Publication, no. 81: 95-114.

Whelan, P.M., Gill, J.B., Kollman, E., Duncan, R.A. & Drake, R.E. (1985). Radiometric dating of magmatic stages in Fiji. In: Scholl, D.W & Vallier, T.L. (eds), *Geology and offshore resources of Pacific island arcs - Tonga region. Circum-Pacific Council for Energy and Mineral Resources Earth Science Series,* V.2. Houston, Texas.

White, W.M. & Hofmann, A.W. (1982). Sr and Nd isotope geochemistry of oceanic basalts and mantle evolution. *Nature,* 296: 821-825.

Whitford, D.J. & Nicholls, I.A. (1976). Potassium variation in lavas across the Sunda Arc in Java and Bali. In: Johnson, R.W. (ed). *Volcanism in Australasia,* Elsevier, Amsterdam. pp 63-76.

Woodrow, P.J. (1980). Geology of Kadavu. *Mineral Resources Department, Fiji. Bulletin no. 7.*

Wright, E. & White, W.M. (1987). The origin of Samoa: new evidence from Sr, Nd and Pb isotopes. *Earth and Planetary Science Letters,* 81: 151-162.

Yamagishi, H. & Dimroth, E. (1985). A comparison of Miocene and Archean rhyolite hyaloclastites: Evidence for a hot and fluid rhyolite lava. *Journal of Volcanology and Geothermal Research,* 23: 337-355.

Yoder, H.S. & Tilley, C.E. (1962). Origin of basalt magmas: an experimental study of natural and synthetic rock systems. *Journal of Petrology,* 3: 342-532.

Yogodzinski, G.M., Kay, R.W., Volynets, O.N., Koloskov, A.V. & Kay, S.M. (1995). Magnesian andesite in the western Aleutian Komandorsky region: Implications for slab melting and processes in the mantle wedge. *Geological Society of America Bulletin,* 107: 505-519.

Yogodzinski, G.M., Volynets, O.N., Koloskov, A.V., Seliverstov, N.I. & Matvenkov, V.V. (1994). Magnesian andesites and the subduction component in a strongly calc-alkaline series at Piip volcano, Far Western Aleutians. *Journal of Petrology,* 35: 163-204.

APPENDIX 1

Catalogue of rocks from the Kadavu Island Group and the northern part of the Hunter Ridge

Samples collected by A.C Verbeeten, May - August, 1993 (Kadavu Island Group) and October-November, 1993 (northern part of Hunter Ridge)

Explanation of Table A.1.1

UT# - University of Tasmania, Department of Geology collection number

Field# - Number of sample given when collected in the field

Suite - Geochemical suite or group that the sample has been assigned to.
WK = Western Kadavu Group
CEO = Central/Eastern/Ono Group
NG = Ngaloa Group
AG = Astrolabe Group
HR1 = Hunter Ridge suite I
HR2 = Hunter Ridge suite II
HR3 = Hunter Ridge suite III
HR4 = Hunter Ridge altered samples
HR5 = Hunter Ridge sedimentary/pumice

Description - Type of outcrop from where the sample has been taken from.

Sheet - Sample locality.
Kadavu 1 = Geology of Western and Central Kadavu (Woodrow, 1980), 1:50 000 series mapsheet (Mineral Resources Department-Fiji)
Kadavu 2 = Geology of Eastern Kadavu and Astrolabe Islands (Woodrow, 1980), 1:50 000 series mapsheet (Mineral Resources Department - Fiji)

	Nabukelevu = Nabukelevu 1:250 000 Bathymetric map series MRD 819. (Mineral Resources Department - Fiji) S.Vanuatu = Bathymetry map of the southern part of the New Hebrides arc and North Fiji Basin (Monzier et al., 1992). ORSTOM 1: 500 000 mapseries.
Grid Reference	- sample locality, grid reference
T	- x if thin section available
X	- x if XRF major and trace element analyses available
I	- x if ICPMS trace element analyses available
R	- x if radiogenic isotope (Sr, Nd and Pb) analyses available

Table A1.1: Catalogue of Kadavu Island Group and Hunter Ridge rocks.

UT#	Field#	Suite	Description	Sheet	Grid Reference	T	X	I	R
134022	AV5	WK	lava flow	Kadavu 1	19°02.7', 178°08.8'	x	x		
134023	AV14	WK	lava flow	Kadavu 1	19°06.7', 177°58.1'	x	x		
134024	AV31	WK	clast in breccia	Kadavu 1	19°04.9', 178°07.0'	x	x		
134025	AV37	WK	lava flow	Kadavu 1	19°04.2', 178°03.9'	x	x		
134026	AV40	WK	float in creek	Kadavu 1	19°05.3', 178°01.7'	x	x		
134027	AV48	WK	lava flow	Kadavu 1	19°08.9', 177°58.4'	x	x	x	x
134028	AV50	WK	float in creek	Kadavu 1	19°07.8', 177°59.0'	x	x		
134029	AV54	WK	lava flow	Kadavu 1	19°08.9', 178°01.2'	x	x	x	x
134030	AV57	WK	lava flow	Kadavu 1	19°08.7', 178°02.5'	x	x	x	x
134031	AV59	WK	lava flow	Kadavu 1	19°08.3', 178°02.4'	x	x		
134032	AV62	WK	lava flow	Kadavu 1	19°08.0', 178°03.2'	x	x		
134033	AV66	WK	float on beach	Kadavu 1	19°09.7', 178°03.8'	x	x		
134034	AV70	WK	lava flow	Kadavu 1	19°10.8', 178°06.7'	x	x		
134035	AV72	WK	lava flow	Kadavu 1	19°07.8', 178°04.8'	x	x		
134036	AV73	WK	lava flow	Kadavu 1	19°06.2', 178°04.2'	x	x		
134037	AV76	WK	float in creek	Kadavu 1	19°07.1', 178°08.4'	x	x		
134038	AV77	WK	lava flow	Kadavu 1	19°08.0', 178°07.3'	x	x		
134039	AV78	WK	lava flow	Kadavu 1	19°08.3', 178°11.2'	x	x		
134040	AV84	WK	lava flow	Kadavu 1	19°09.3', 178°10.3'	x	x		
134041	AV85	WK	lava flow	Kadavu 1	19°07.9', 178°09.3'	x	x		
134042	AV90	WK	lava flow	Kadavu 1	19°07.0', 178°11.4'	x	x	x	x
134043	AV91	WK	lava flow	Kadavu 1	19°07.0', 178°11.3'	x	x		
134044	AV94	WK	lava flow	Kadavu 1	19°04.0', 178°09.4'	x	x		
134045	AV100	CEO	lava flow	Kadavu 1	19°03.4', 178°10.6'	x	x		
134046	AV101	CEO	lava flow	Kadavu 1	19°03.2', 178°10.5'	x	x		
134047	AV103	CEO	lava flow	Kadavu 1	19°02.2', 178°10.8'	x	x		
134048	AV107	CEO	lava flow	Kadavu 1	19°02.5', 178°14.3'	x	x		
134049	AV113	CEO	float on beach	Kadavu 1	19°03.2', 178°12.2'	x	x		
134050	AV117	CEO	lava flow	Kadavu 1	19°01.5', 178°15.6'	x	x	x	x
134051	AV118	CEO	lava flow	Kadavu 1	19°00.8', 178°16.1'	x	x		
134052	AV123	CEO	lava flow	Kadavu 1	19°00.8', 178°14.1'	x	x		
134053	AV126	CEO	lava flow	Kadavu 1	19°00.8', 178°15.5'	x	x		
134054	AV127	CEO	lava flow	Kadavu 1	19°00.8', 178°15.7'	x	x		
134055	AV129	CEO	lava flow	Kadavu 1	18°59.4', 178°17.1'	x	x		
134056	AV133	CEO	lava flow	Kadavu 1	18°59.7', 178°17.5'	x	x		
134057	AV137	CEO	float on beach	Kadavu 2	19°01.8', 178°19.3'	x	x		
134058	AV140	CEO	lava flow	Kadavu 2	18°59.7', 178°18.3	x	x		
134059	AV141	CEO	lava flow	Kadavu 2	19°00.0', 178°18.8'	x	x	x	x
134060	AV142	CEO	lava flow	Kadavu 2	19°02.7', 178°19.3'	x	x		
134061	AV150	CEO	float in creek	Kadavu 2	19°02.2', 178°21.6'	x	x		
134062	AV153	CEO	clast in breccia	Kadavu 2	19°03.4', 178°21.2'	x	x		
134063	AV154	CEO	lava flow	Kadavu 2	19°03.5', 178°22.3'	x	x		
134064	AV158	CEO	lava flow	Kadavu 2	18°56.2', 178°28.9'	x	x		
134065	AV164	CEO	float on beach	Kadavu 2	18°52.1', 178°29.7'	x	x		
134066	AV169	CEO	lava flow	Kadavu 2	18°53.7', 178°30.6'	x	x		
134067	AV196	CEO	lava flow	Kadavu 2	18°58.2', 178°28.4'	x	x		
134068	AV199	CEO	lava flow	Kadavu 2	18°58.7', 178°26.7'	x	x		
134069	AV201	CEO	clast in breccia	Kadavu 2	18°57.4', 178°26.8'	x	x		
134070	AV205	CEO	lava flow	Kadavu 2	18°58.1', 178°25.3'	x	x		
134071	AV207	CEO	clast in breccia	Kadavu 2	18°56.8', 178°23.9'	x	x		
134072	AV211	CEO	lava flow	Kadavu 2	18°56.4', 178°20.8'	x	x		
134073	AV213	CEO	lava flow	Kadavu 2	18°57.6', 178°20.2'	x	x		
134074	AV214B	CEO	float in creek	Kadavu 2	18°57.1', 178°20.2'	x	x		
134075	AV216	CEO	lava flow	Kadavu 2	18°56.4', 178°19.0'	x	x		
134076	AV219	CEO	lava flow	Kadavu 1	18°58.1', 178°17.0'	x	x		

UT#	Field#	Suite	Description	Sheet	Grid Reference	T	X	I	R
134077	AV223	CEO	lava flow	Kadavu 1	18° 59.9', 178°15.8'	x	x		
134078	AV225	CEO	float on beach	Kadavu 1	18°58.4', 178°16.2'	x	x		
134079	AV227	CEO	lava flow	Kadavu 1	18°58.2', 178°13.3'	x	x	x	x
134080	AV231	CEO	float on beach	Kadavu 1	19°01.0', 178°09.9'	x	x		
134081	AV232	CEO	lava flow	Kadavu 1	19°00.2', 178°10.1'	x	x	x	x
134082	AV98	NG	lava flow	Kadavu 1	19°04.0', 178°11.0'	x	x		
134083	AV99	NG	lava flow	Kadavu 1	19°04.8', 178°12.1'	x	x	x	x
134084	AV110	NG	lava flow	Kadavu 1	19°03.4', 178°13.0'	x	x		
134085	AV112	NG	lava flow	Kadavu 1	19°03.5', 178°13.1'	x	x	x	x
134086	AV116	NG	lava flow	Kadavu 1	19°01.5', 178°15.2'	x	x	x	x
134087	AV134	NG	lava flow	Kadavu 2	19°00.9', 178°18.5'	x	x		
134088	AV152	NG	lava flow	Kadavu 2	19°02.9', 178°21.0'	x	x		
134089	AV208	NG	lava flow	Kadavu 2	18°56.8', 178°23.2'	x	x	x	x
134090	AV173	AG	lava flow	Kadavu 2	18°50.4', 178°32.6'	x	x		
134091	AV177	AG	lava flow	Kadavu 2	18°48.5', 178°31.4'	x	x		
134092	AV182b	AG	lava flow	Kadavu 2	18°38.0', 178°31.9'	x	x	x	x
134093	AV185	AG	lava flow	Kadavu 2	18°45.3', 178°31.8'	x	x		
134094	AV186	AG	lava flow	Kadavu 2	18°45.7', 178°31.6'	x	x	x	x
134095	AV187	AG	lava flow	Kadavu 2	18°46.2', 178°31.2'	x	x	x	x
134096	AV190	AG	lava flow	Kadavu 2	18°46.8', 178°30.1'	x	x	x	x
134097	AV192	AG	lava flow	Kadavu 2	18°47.6', 178°29.9'	x	x		
134098	DR1-1	HR5		Nabukelevu	19°35.6', 177° 46.5'	x			
134099	DR1-2	HR4		Nabukelevu	19°35.6', 177° 46.5'	x			
134100	DR1-3	HR5		Nabukelevu	19°35.6', 177° 46.5'	x			
134101	DR2-1	HR5		Nabukelevu	19°55.0', 177°24.4'	x			
134102	DR2-2	HR5		Nabukelevu	19°55.0', 177°24.4'	x			
134103	DR2-3	HR5		Nabukelevu	19°55.0', 177°24.4'	x			
134104	DR3-1	HR5		Nabukelevu	20°05.8', 177°02.7'	x			
134105	DR3-2	HR4		Nabukelevu	20°05.8', 177°02.7'	x	x		
134106	1DR4-1	HR4		Nabukelevu	20°34.3', 177°22.1'	x			
134107	1DR4-2	HR4		Nabukelevu	20°34.3', 177°22.1'	x			
134108	1DR4-3	HR4		Nabukelevu	20°34.3', 177°22.1'	x			
134109	1DR4-4	HR4		Nabukelevu	20°34.3', 177°22.1'	x			
134110	1DR4-5	HR4		Nabukelevu	20°34.3', 177°22.1'	x			
134111	1DR4-6	HR4		Nabukelevu	20°34.3', 177°22.1'	x			
134112	2DR4-1	HR1		Nabukelevu	20°32.3', 177°24.5'	x	x		
134113	2DR4-2	HR1		Nabukelevu	20°32.3', 177°24.5'	x			
134114	2DR4-3	HR1		Nabukelevu	20°32.3', 177°24.5'	x			
134115	2DR4-4	HR1		Nabukelevu	20°32.3', 177°24.5'	x			
134116	2DR4-5	HR1		Nabukelevu	20°32.3', 177°24.5'	x	x		
134117	2DR4-6	HR1		Nabukelevu	20°32.3', 177°24.5'	x			
134118	2DR4-7	HR1		Nabukelevu	20°32.3', 177°24.5'	x			
134119	2DR4-8	HR1		Nabukelevu	20°32.3', 177°24.5'	x			
134120	2DR4-9	HR1		Nabukelevu	20°32.3', 177°24.5'	x	x	x	x
134121	DR5-1	HR4		Nabukelevu	20°42.2', 177°04.9	x			
134122	DR5-2	HR4		Nabukelevu	20°42.2', 177°04.9	x			
134123	DR5-3	HR4		Nabukelevu	20°42.2', 177°04.9	x			
134124	DR5-4	HR4		Nabukelevu	20°42.2', 177°04.9	x			
134125	DR5-5	HR4		Nabukelevu	20°42.2', 177°04.9	x	x		
134126	1DR6-1	HR5		Nabukelevu	20°27.1', 176°47.9'	x			
134127	1DR6-2	HR5		Nabukelevu	20°27.1', 176°47.9'	x			
134128	2DR6-1	HR1		Nabukelevu	20°26.2', 176°49.9'	x	x	x	x
134129	DR7-1	HR5		Nabukelevu	20°21.7', 176°52.4'	x			
134130	DR7-2	HR4		Nabukelevu	20°21.7', 176°52.4'	x			
134131	DR8-1	HR5		S.Vanuatu	21°22.8', 176°01.6'	x			
134132	DR8-2	HR1		S.Vanuatu	21°22.8', 176°01.6'	x	x	x	x

UT#	Field#	Suite	Description	Sheet	Grid Reference	T	X	I	R
134133	DR9-1	HR3		S.Vanuatu	21°39.1', 174°50.0'	x	x		
134134	DR9-2	HR3		S.Vanuatu	21°39.1', 174°50.0'	x	x	x	x
134135	DR9-3	HR3		S.Vanuatu	21°39.1', 174°50.0'	x	x		
134136	DR9-4	HR3		S.Vanuatu	21°39.1', 174°50.0'	x			
134137	DR10-1	HR2		S.Vanuatu	21°45.5', 174°35.1'	x	x		
134138	DR10-2	HR2		S.Vanuatu	21°45.5', 174°35.1'	x	x	x	x
134139	DR10-3	HR2		S.Vanuatu	21°45.5', 174°35.1'	x	x		
134140	DR10-4	HR4		S.Vanuatu	21°45.5', 174°35.1'	x			
134141	DR10-5	HR5		S.Vanuatu	21°45.5', 174°35.1'	x			
134142	DR11-1	HR4		S.Vanuatu	21°54.6', 174°18.4'	x			
134143	DR11-2	HR4		S.Vanuatu	21°54.6', 174°18.4'	x			
134144	DR12-1	HR4		S.Vanuatu	21°59.4', 174°07.9'	x			
134145	DR12-2	HR1		S.Vanuatu	21°59.4', 174°07.9'	x	x		
134146	DR12-3	HR1		S.Vanuatu	21°59.4', 174°07.9'	x	x		
134147	DR12-4	HR5		S.Vanuatu	21°59.4', 174°07.9'	x			
134148	DR12-5	HR4		S.Vanuatu	21°59.4', 174°07.9'	x			
134149	DR12-6	HR4		S.Vanuatu	21°59.4', 174°07.9'	x			
134150	DR12-7	HR5		S.Vanuatu	21°59.4', 174°07.9'	x			
134151	DR12-8	HR1		S.Vanuatu	21°59.4', 174°07.9'	x	x	x	x
134152	DR12-9	HR4		S.Vanuatu	21°59.4', 174°07.9'	x			
134153	DR13-1	HR4		S.Vanuatu	22°02.2', 173°55.0'	x			
134154	DR14-1	HR5		S.Vanuatu	22°08.3', 173°45.4'	x			
134155	DR14-2	HR4		S.Vanuatu	22°08.3', 173°45.4'	x			
134156	DR15-1	HR2		S.Vanuatu	22°06.3', 173°44.2'	x	x	x	x
134157	DR15-2	HR1		S.Vanuatu	22°06.3', 173°44.2'	x	x		
134158	DR15-3	HR4		S.Vanuatu	22°06.3', 173°44.2'	x			
134159	DR15-4	HR1		S.Vanuatu	22°06.3', 173°44.2'	x	x		
134160	DR15-5	HR4		S.Vanuatu	22°06.3', 173°44.2'	x			
134161	DR16-1	HR4		S.Vanuatu	21°52.3', 173°22.0'	x			
134162	DR16-2	HR5		S.Vanuatu	21°52.3', 173°22.0'	x			
134163	DR16-3	HR4		S.Vanuatu	21°52.3', 173°22.0'	x			
134164	DR16-4	HR4		S.Vanuatu	21°52.3', 173°22.0'	x			
134165	DR16-5	HR2		S.Vanuatu	21°52.3', 173°22.0'	x	x		
134166	DR16-6	HR2		S.Vanuatu	21°52.3', 173°22.0'	x	x	x	x

APPENDIX 2

ANALYTICAL TECHNIQUES

A2.1 WHOLE ROCK MAJOR AND TRACE ELEMENT ANALYSES

X-ray fluorescence (XRF) spectrometry major and trace element analyses were performed at the University of Tasmania Geology/CODES department, using an automated Philips PW 1410 spectrometer. Instrumental conditions are listed in Table A2.1. Trace elements concentrations were determined using mass absorption coefficients calculated from major element XRF analyses. Spectrometer calibration were maintained using international and secondary standards used at the University of Tasmania and specpure silica blanks. Data precision was monitored by repeated analyses of several internal standards including TasBas and TasGran (Table A2.2)

Sample preparation included soaking Hunter Ridge breccias in concentrated HCL to dissolve carbonate matrix material, followed by washing constituent clasts with distilled water prior to crushing. Other samples were prepared by removing any weathered surfaces with the hydraulic splitter. Approximately 700-1000g of fresh rock samples were crushed in a steel jaw-crusher. 1cm fragments were hand-picked and washed in distilled water. Approximately 50-70g of rock chips were crushed to powder in a ceramic mill. This powder fraction was used for all the whole rock and isotope analyses.

Major elements were analysed on fused glass discs following the method described by Norrish and Hutton (1969). Loss on ignition (LOI) was measured as the weight percent loss of 1g of powdered sample heated to 1000°C for 12 hours, followed by 5 hours at 400°C. Negative LOI values (DR16-6) indicate that the gain in weight during the ignition because of the oxidation of FeO to Fe_2O_3 was larger than the loss in volatiles. Trace elements (Ni, Y, Rb, Nb, Zr, Sr, Cr, Ba, Sc, V) were analysed on 6g pressed powder pellets coated with boric acid using the method described by Norrish and Chappell (1977).

Table A2.1. Instrumental conditions for routine XRF major and trace element analysis at the University of Tasmania, Geology Department. The X-ray tube was operated at 60kv 40mA for all elements except Ba and Sc where 50kv, 50mA was used. Detection limits are 3 sigma (99%) confidence levels.

Major elements			
Oxide	Emission Line	X-ray Tube	Time (sec)
SiO2	K alpha	Rh	100
TiO2	K alpha	Rh	20
Al2O3	K alpha	Rh	100
Fe2O3	K alpha	Rh	20
MnO	K alpha	Rh	40
MgO	K alpha	Rh	100
CaO	K alpha	Rh	20
Na2O	K alpha	Rh	100+100
K2O	K alpha	Rh	20
P2O5	K alpha	Rh	40

Trace Elements				
Element	EmissionLine	X-ray Tube	Detection Limit	Precision
Sc	K alpha	Au	1	10±1, 30±1
V	K alpha	Au	3	30±2, 100±1
Cr	K alpha	Au	2	10±2, 400±4
Ni	K alpha	Mo	1	3±0.5, 20±0.5, 200±2
Rb	K alpha	Mo	2	10±1, 70±1, 170±2
Sr	K alpha	Au	2	10±1, 200±2, 500±5
Y	K alpha	Mo	1.5	10±2, 20±1, 100±2
Zr	K alpha	Au	1	100±2, 250±4, 500±10
Nb	K alpha	Au	1	10±0.5, 20±1
Ba	L alpha	Au	3	500±5, 1200±5

TableA2.2. XRF major and trace element data for two internal standards (TasBas and TasGran), measured at the University of Tasmania, Geology Department.

TasBas				TasGran		
		±1σ	σ%		±1σ	σ%
Major Elements (wt%)						
SiO2	44.54	0.24	0.5	72.62	0.15	0.2
TiO2	2.32	0.04	1.8	0.29	0.02	7.0
Al2O3	14.15	0.10	0.7	13.56	0.05	0.1
Fe2O3	12.73	0.09	0.8	2.30	0.03	2.3
MnO	0.17	0.01	5.5	0.04	0.002	0.0
MgO	8.29	0.12	1.4	0.59	0.03	4.8
CaO	7.85	0.06	0.8	1.85	0.02	0.3
Na2O	5.39	0.09	1.5	2.75	0.05	0.9
K2O	1.95	0.04	2.0	4.60	0.05	1.3
P2O5	0.94	0.97	2.4	0.12	0.01	5.5
Trace Elements (ppm)						
Nb	54.0	1.1	2.0	18.2		
Zr	256.9	4.0	1.7	158.0		
Sr	1001.8	10.3	1.0	151.4		
Cr	184.1	4.1	2.1	10.0		
Ba	203.6	3.0	1.3	465.2		
Sc	12.8	0.5	3.8	6.8		
V	152.8	2.3	1.4	26.0		
Ni	147.3	2.6	1.8	3.9		
Y	21.2	0.8	2.6	36.4		
Rb	16.4	0.7	4.2	250.9		

Trace element, including REE contents of selected samples were analysed by inductively coupled plasma-mass spectrometry (ICP-MS) on the VG PlasmaQuad II STE at the Research School of Earth Sciences, the Australian National University. Samples were dissolved by conventional digestion methods, using concentrated HF/HNO_3 mixtures detailed in Eggins et al (1996). Various laboratory and international standards were interspersed with sample analyses to monitor accuracy and precision. Table A2.3 shows the comparison for elements analysed by both XRF and ICP-MS.

A2.2 WHOLE ROCK RADIOGENIC ISOTOPE ANALYSES

Sr, Nd and Pb isotopes were analysed at LaTrobe University, Melbourne, using a Finnigan MAT262 mass spectrometer.

A2.2.1 PREPARATION

Following established practice (Taras and Hart 1987), all powdered samples were leached in hot 6N HCl for up to 12 hours to remove labile (seawater-) alteration. The residues were dissolved in HF, HNO_3 and HCl.

Sr and REE were initially separated from other elements using precalibrated cation exchange columns equilibrated with 2N HCl. Sr was collected with 2N HCl and the REE with 5.25N HCl. Nd was collected with 0.2N HCl using secondary stage cation exchange columns (Kel-F teflon powder coated with di(2-ethylhexyl)orthophosphoric acid) equilibrated with 0.2N HCl. Samples were dried down prior to filament loading.

Sr samples were loaded onto single Ta filaments and Nd samples were loaded onto the Ta filament of a Re-Ta pair.

Aliquots containing at least 100ng Pb were processed using conventional HBr-HCl column chemistry (AG-1 X8 anion resin, 200-400 mesh), on either 0.38 ml (7 mm ID, 10 mm height, 1 pass) or 0.1 ml (4 mm ID, 8 mm height, 2 passes) columns. The Pb fractions were loaded onto single Re filaments using silica gel/H_3PO_4.

A2.2.2 Sr AND Nd ANALYTICAL METHODS

Samples were run in static multi-collector mode. Individual analytical results represent the mean and $2\sigma_{mean}$ errors of 10 blocks. To correct for mass fractionation effects, measured $^{87}Sr/^{86}Sr$ was normalised to $^{86}Sr/^{88}Sr = 0.1194$ and $^{146}Nd/^{144}Nd = 0.7219$ respectively.

Table A2.3. Comparison of XRF and ICP-MS analysis of the Kadavu Island Group and Hunter Ridge rocks

Sample no.	AV48		AV54		AV57		AV90		AV117		AV141	
	ICPMS	XRF	ICPMS	XRF	ICPMS	XRF	ICPMS	XRF	ICPMS	XRF	ICPMS	XRF
Li	13.3		8.2		9.7		6.4		5.4		9.4	
Be	2.01		1.64		2.29		1.90		2.07		2.20	
Sc	9.4	9	13.2	14	11.3	11	7.9	9	23.4	23	23.6	25
Ti	5257	5216	5586	5995	4975	5156	3120	2698	3207	3297	4650	4736
V	125	108	155	158	156	133	92	70	195	192	241	244
Cr	58	51	117	109	49	46	19	16	190	224	39	35
Co	14		24		14		9		25		24	
Ni	56	55	117	114	35	32	12	10	86	81	14	6
Cu	41		44		63		34		83		115	
Zn	51		57		70		38		49		65	
Ga	18.0		18.7		20.5		16.3		16.2		18.3	
Rb	29.2	31	22.3	23	22.3	23	41.5	50	37.5	37	35.6	40
Sr	1338.1	1377	1513	1580	1618	1667	732	779	1081	1097	1396	1394
Y	13.9	14	12.5	13	19.5	20	15.1	16	16.3	16	22.9	16
Zr	97.7	172	130.6	174	172.0	178	114.9	185	143.9	143	183.9	180
Nb	11.34	10.1	12.09	11.2	8.73	8.6	9.99	9.1	3.69	3.4	5.40	5.5
Mo	1.300		0.324		0.993		2.137		1.191		0.437	
Cd	0.035		0.042		0.057		0.041		0.050		0.033	
Cd	0.031		0.032		0.037		0.030		0.034		0.025	
Sn	1.006		1.067		0.999		0.946		0.860		0.576	
Sb	0.112		0.089		0.057		0.185		0.123		0.057	
Cs	0.467		0.101		0.408		0.847		0.747		0.511	
Ba	399	417	351	371	452	466	572	588	483	511	540	547
La	34.48		33.33		30.56		28.14		26.06		43.05	
Ce	74.27		71.83		64.03		56.64		55.90		92.40	
Pr	9.15		9.11		8.74		6.82		7.36		11.77	
Nd	35.42		34.89		35.74		25.48		29.99		47.67	
Sm	5.87		5.83		6.20		4.46		5.79		8.83	
Eu	1.584		1.542		1.753		1.099		1.603		2.368	
Gd	4.08		3.98		4.58		3.40		4.33		6.40	
Tb	0.516		0.508		0.589		0.485		0.561		0.813	
Dy	2.52		2.44		2.99		2.60		2.75		3.98	
Ho	0.463		0.437		0.594		0.521		0.509		0.718	
Er	1.195		1.130		1.647		1.486		1.354		1.896	
Yb	1.028		0.962		1.599		1.479		1.172		1.646	
Lu	0.154		0.144		0.258		0.231		0.182		0.250	
Hf	2.36		3.07		3.74		2.97		3.30		4.06	
Ta	0.753		0.712		0.495		0.583		0.194		0.286	
Tl			0.044		0.128		0.308				0.174	
Pb	5.62		3.60		5.28		7.56		8.63		9.25	
Th	5.44		3.94		3.80		5.36		3.78		5.50	
U	1.912		1.050		1.198		1.815		1.472		1.914	

Sample no.	AV227		AV232		AV99		AV112		AV116		AV208	
	ICPMS	XRF	ICPMS	XRF	ICPMS	XRF	ICPMS	XRF	ICPMS	XRF	ICPMS	XRF
Li	8.1		7.5		5.3		7.0		6.8		5.7	
Be	2.19		1.90		1.86		1.90		1.92		2.06	
Sc	15.0	15	19.2	20	16.7	20	13.4	13	17.3	16.0	21.4	23
Ti	3117	2998	3285	3057	10040	9472	9215	8633	9628	9592	10508	9892
V	161	155	173	174	224	219	217	194	235	229	269	261
Cr	47	43	41	37	227	213	99	85	209	200	302	288
Co	17		20		31		25		35		34	
Ni	39	33	24	21	176	168	114	33	140	132	197	199
Cu	63		74		115		107		84		122	
Zn	48		50		68		78		92		80	
Ga	18.2		16.6		19.0		23.6		23.4		18.9	
Rb	42.5	43	39.8	40	18.0	18	11.83	13	15.15	14.0	20.9	21
Sr	1100	1144	923	941	2069	2144	2784	2751	2862	2830	2118	2129
Y	14.1	14	18.7	18	21.0	18	13.4	14	21	20	18.8	18
Zr	158.0	159	143.7	144	236.5	238	233.7	230	225	225	213.7	212
Nb	3.42	3.6	3.31	3.2	15.69	14.5	11.50	9.8	9.90	9.8	16.16	14.8
Mo	0.802		0.752		0.393		0.397		0.406		0.515	
Cd	0.047		0.049		0.075		0.070		0.064		0.070	
Cd	0.023		0.028		0.049		0.038		0.037		0.045	
Sn	0.844		0.779		1.561		1.497		1.415		1.387	
Sb	0.095		0.093		0.030		0.015		0.019		0.032	
Cs	0.556		0.622		0.083		0.046		0.041		0.101	
Ba	637	650	469	476	418	442	406	414	506	501	471	491
La	22.93		23.74		38.38		37.98		46.35		37.72	
Ce	47.21		52.13		89.17		85.72		109.82		89.03	
Pr	6.30		7.04		12.20		11.15		14.58		12.07	
Nd	25.59		29.07		49.83		43.87		58.73		48.95	
Sm	4.93		5.75		8.51		6.98		9.49		8.25	
Eu	1.346		1.584		2.402		1.963		2.679		2.338	
Gd	3.73		4.64		5.94		4.58		6.09		5.64	
Tb	0.480		0.607		0.757		0.579		0.716		0.722	
Dy	2.36		3.07		3.71		2.63		3.34		3.52	
Ho	0.438		0.584		0.686		0.457		0.582		0.640	
Er	1.166		1.570		1.771		1.150		1.476		1.636	
Yb	1.007		1.384		1.439		0.937		1.327		1.358	
Lu	0.155		0.220		0.216		0.138		0.222		0.203	
Hf	3.78		3.34		5.08		5.08		4.96		4.69	
Ta	0.213		0.188		0.845		0.615		0.523		0.847	
Tl	0.186		0.213				0.032		0.041		0.018	
Pb	7.09		6.70		5.30		5.20		9.33		9.71	
Th	3.57		3.37		3.62		4.53		4.62		4.18	
U	1.471		1.379		0.963		1.289		1.221		1.164	

Table A2.3. Comparison of XRF and ICP-MS analysis of the Kadavu Island Group and Hunter Ridge rocks

Sample no.	AV182b		AV186		AV187		AV190		2DR4-9		2DR6-1	
	ICPMS	XRF	ICPMS	XRF	ICPMS	XRF	ICPMS	XRF	ICPMS	XRF	ICPMS	XRF
Li	8.9		11.5		15.1		11.7		0.8		5.4	
Be	2.95		0.87		1.93		1.47		0.79		0.16	
Sc	8.8	6	42.1	34	14.8	12	35.0	31	23.8	41	41.1	41
Ti	3456	3477	3839	3897	3906	3837	6092		3848	3297	2525	2218
V	203	161	261	277	233	225	370	340	257	251	231	244
Cr	9	6	511	552	6	5	51	47	46	51	613	925
Co	13		50		21		38		19		44	
Ni	7	6	110	110	8	7	25	22	30	27	259	258
Cu	89		93		123		151		6		52	
Zn	53		69		70		86		36		48	
Ga	19.4		12.0		17.0		16.5		14.1		9.3	
Rb	98.3	99	32.3	33	105.1	101	75.5	74	0.92	1	3.70	4
Sr	1843	2092	834	838	1717	1706	1171	1170	167	264	58	66
Y	18.9	21	13.6	13	21.2	19	20.5	20	28.5	30	10.3	11
Zr	150.0	169	37.6	38	96.4	95	77.1	76	15.0	49	20.7	21
Nb	15.21	13.9	2.05	2.0	5.94	5.1	6.52	5.5	3.04	1.4	0.27	<1
Mo	0.189		0.303		0 120		0.400		0.093		0.375	
Cd	0.039		0.027		0.040		0.038		0.013		0.027	
Cd	0.033		0.038		0.034		0.046		0.030		0.043	
Sn	1.048		0.596		0.819		0.984		1.219		0.476	
Sb	0.031		0.018		0.029		0.028		0.017		0.174	
Cs	0.699		0.382		0.552		0.695		0.020		0.199	
Ba	756	777	293	334	825	866	519	560	49.2	64	14.9	19
La	32.42		6.17		17.68		12.88		6.52		0.558	
Ce	62.20		13.41		34.73		27.43		17.40		1.628	
Pr	7.42		1.91		4.51		3.71		2.50		0.293	
Nd	27.67		8.99		18.64		16.18		11.26		1.766	
Sm	5.15		2.36		4.07		3.86		3.01		0.730	
Eu	1.512		0.783		1.277		1.228		0.817		0.292	
Gd	4.29		2.49		3.87		3.80		3.45		1.142	
Tb	0.666		0.391		0.588		0.593		0.622		0.223	
Dy	3.49		2.32		3.38		3.44		4.13		1.561	
Ho	0.694		0.481		0.701		0.712		0.947		0.372	
Er	1.902		1.334		1.987		1.971		2.947		1.133	
Yb	1.748		1.193		1.870		1.772		3.255		1.148	
Lu	0.254		0.178		0.287		0.265		0.517		0.178	
Hf	2.45		1.05		2.26		2.00		0.853		0.633	
Ta	0.781		0.111		0.308		0.365		0.227		0.020	
Tl	0.416		0.054		0 177		0 036		0.017		0.034	
Pb	11.02		5.54		10.46		7.98		0.722		0.672	
Th	2.81		0.50		1.94		1.28		0.303		0.044	
U	1.122		0.198		0.857		0.385		0.110		0.050	

Sample no.	DR8-2		DR9-2		DR10-2		DR12-8		DR15-1		DR16-6	
	ICPMS	XRF	ICPMS	XRF	ICPMS	XRF	ICPMS	XRF	ICPMS	XRF	ICPMS	XRF
Li	4.7		10.9		12.0		7.3		4.4		7.8	
Be	0.54		1.98		1.40		0.28		0.74		1.23	
Sc	34.1	33	11.4	12	19.5	18	57.7	54	43.9	47	18.0	20
Ti	3172	2698	5171	5036	4046	4137	2035	2038	3885	3237	5264	5515
V	261	275	170	137	223	182	263	341	226	251	233	192
Cr	100	113	3	2	36	30	362	317	619	649	9	7
Co	31		12		18		45		45		16	
Ni	59	59	4	3	13	9	54	47	85	84	9	8
Cu	67		73		71		46		89		32	
Zn	61		70		63		74		58		60	
Ga	14.4		17.9		17 6		11.4		10.9		18.0	
Rb	10.31	11	41.7	42	24.5	25	4.26	5	6.55	7	13.3	14
Sr	247	252	369	379	571	585	197.9	210	814	817	436	451
Y	14.0	14	29.8	29	22.2	22	12.5	14	15.0	15	25.3	25
Zr	42.5	43	268.3	260	185.8	182	23.3	25	66.9	68	152.7	154
Nb	0.75	<1	6.96	6.0	3.32	2.6	0.45	1.2	0.86	<1	3.49	3.5
Mo	0.817		2.188		1.407		0.638		0.378		0.837	
Cd	0.033		0.092		0.066		0.033		0.039		0.056	
Cd	0.043		0.064		0.050		0.048		0 063		0.043	
Sn	0.527		1.729		1.223		0.345		1 747		1.252	
Sb	0.109		0.169		0.113		0.195		0.142		0.052	
Cs	0.250		0 544		0.326		0.011		0.078		0.087	
Ba	86.4	93	358	362	185	189	65.5	89	78.1	82	179	188
La	2.86		32.96		18 68		2.56		10 37		11.84	
Ce	6.90		71.13		45.65		5.31		27.84		29.36	
Pr	1.042		9.76		6.34		0.853		4.24		4.33	
Nd	5.16		39.81		27.99		4.20		19.66		19.43	
Sm	1.575		7.94		6.05		1.224		4 48		4.68	
Eu	0.515		1.790		1.482		0.383		1.281		1.357	
Gd	1.885		6.38		5.04		1.462		3.68		4.52	
Tb	0.326		0.908		0.701		0.257		0.505		0.698	
Dy	2.143		4.91		3.79		1 706		2.67		4.08	
Ho	0.486		0.967		0.738		0 400		0.519		0 850	
Er	1.475		2.731		2.047		1.224		1.396		2.427	
Yb	1.461		2.571		1.887		1.309		1.219		2.268	
Lu	0.226		0.400		0 288		0.209		0.183		0.347	
Hf	1.210		6.53		4 61		0.762		1 74		3.93	
Ta	0.053		0.412		0 209		0.029		0 050		0.220	
Tl	0.097		0.300		0.129		0.028				0.051	
Pb	2.72		8 09		5 01		2.19		3.17		2.99	
Th	0.354		5.08		2.40		0.219		0.907		1.50	
U	0.212		1.916		1 060		0.364		0 372		0.611	

During the course of the analyses, SRM987 gave a mean value of 0.710212±32 (1sd) and the La Jolla standard gave a mean value of 0.511862±9 (1sd).

For full preparation blanks, included at regular intervals, Sr≤500pg and Nd≤200pg.

One dredge sample (2DR6-1) was prepared using two different leaching regimes and the results show no significant differences in $^{87}Sr/^{86}Sr$ (Table A2.4).

Table A2.4. Sr isotope results for 2DR6-1 for the unleached fraction and leached residue. The leaching involved 12hrs in hot 6N HCl.

	Unleached	**Leached**
87Sr/86Sr	0.703426±28	0.703436±21

A2.2.3 Pb ANALYTICAL METHODS

Samples were run in static mode at filament temperatures of 1250 to 1350°C, at ^{208}Pb ion currents of 0.5 to $4x10^{-11}$ A. Typically, 3 blocks of 10x8 sec scans were collected, with in-run 2 sd errors of ≤0.05 %. However, the real error is larger and is dominated by mass fractionation, estimated to be 0.109 % per mass unit, based on many runs of the SRM 981 Pb standard; appropriate correction factors were applied to the data. External precisions (2 standard deviations) for 78 runs of SRM 981 were $^{206}Pb/^{204}Pb$ = ±0.097%, $^{207}Pb/^{204}Pb$ = ±0.130 %, and $^{208}Pb/^{204}Pb$ = ±0.175%.

Reproducibility was checked by running a sample several times throughout the course of the study. AV48 was prepared separately six times and the variation in Pb isotopic ratios is:

$^{206}Pb/^{204}Pb$	18.837 to 18.854, or ±0.045% range
$^{207}Pb/^{204}Pb$	15.534 to 15.555, or ±0.068% range
$^{208}Pb/^{204}Pb$	38.379 to 38.431, or ±0.068% range

The effect of leaching on the Pb isotopic systematics was explored for samples AV99 and 2DR6-1. Separate aliquots of AV99 were leached for 1 hour, 3 hours and 6 hours, followed by determination of Pb concentration and isotopic composition in the residues as well as in an unleached aliquot (Table A2.5).

Table A2.5. Leaching experiments for sample AV99.

	Pb (ppm)	206Pb/204Pb	207Pb/204Pb	208Pb/204Pb
AV99 ul	4.09	18.803	15.540	38.367
AV99 1hr	3.65	18.805	15.526	38.326
AV99 3hr	3.47	18.810	15.536	38.360
AV99 6hr	3.37	18.882	15.617	38.623

The Pb concentration drops by about 11% initially after 1 hour of leaching, followed by smaller increments after further leaching. Some Pb may have been leached from the powder; this may have been Pb held in sulfides and other HCl-soluble phases, or Pb held on microcracks and grain surfaces of silicate minerals. The isotope ratios do not change significantly except for the 6 hr residue which has more radiogenic ratios. A change to more radiogenic ratios after leaching (12 hrs) has also been observed for sample DR6-1 (Fig.A2.1).

The more radiogenic ratios are artefacts of poor Pb ion beams in the mass spectrometer. The AV99 6hr leach produced a small signal (300mV ^{208}Pb) that died after 1 block. The $^{206}Pb/^{204}Pb$, $^{207}Pb/^{204}Pb$ and $^{208}Pb/^{204}Pb$ ratios show differences of 0.38%, 0.52% and 0.68%, respectively, from the other residues. These differences may be explained by an unusually high degree of mass fractionation and a component of 204-error affecting the small 204 ion beam. The observation that all other Kadavu Island group samples (leached for 12 hours) plot in a coherent, less radiogenic cluster, further supports the spurious nature of the AV99 6hr residue result (Fig. A2.1).

Data for the unleached portion of DR6-1 were also obtained from a poor ion beam. In this case, the relative differences between the two samples are non-systematic (0.86%, 0.05%, 0.43%). This is not consistent with simple mass fractionation/204 error but probably reflects the influence of wide and random scatter during the (short) analysis.

The tight clustering of the Kadavu and dredge sample Pb results (Fig. A2.1) suggests that any alteration Pb remaining after the leaching did not influence data quality.

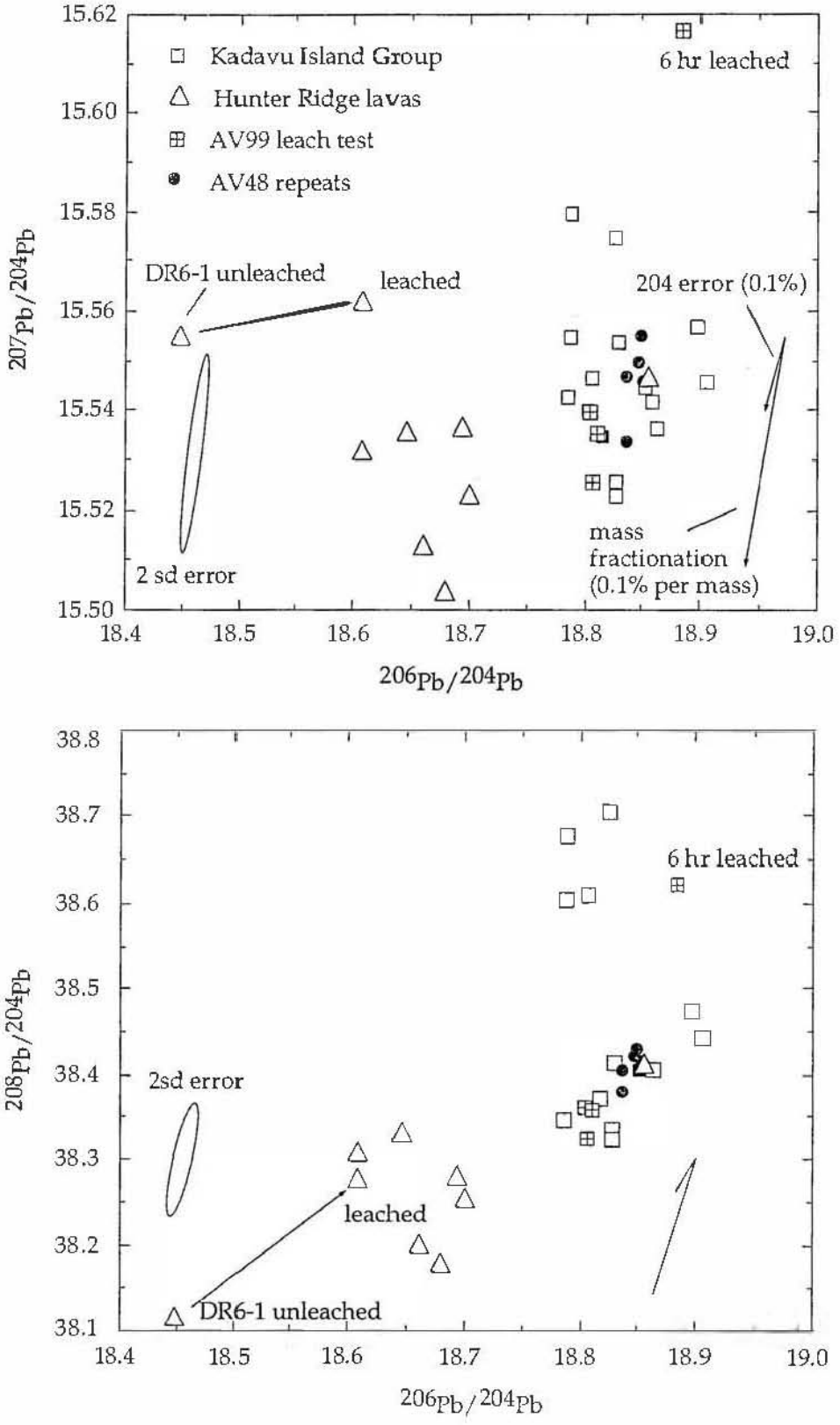

Figure A2.1. Pb isotope diagrms illustrating the effects of different leaching experiments on the Kadavu Island Group and Hunter Ridge rocks.

A2.3 MINERAL CHEMISTRY ANALYSES

Minerals were analysed either in thin section or in probe mounts with mineral separates. For mineral separates, samples were hand crushed, sieved and phenocrysts were hand picked from suitable size fractions, glued in epoxy and polished.

The analyses were performed using a fully automated, three spectrometer Cameca SX50 electron microprobe (University of Tasmania) calibrated with natural mineral standards. Standards were analysed at least twice during each probe session (5-7hrs). The standards used were the San Carlos olivine (USNM 111312/444), basaltic glass (USNM 111249/52), plagioclase LPL (USNM 115900), augite KA (USNM 122142) (Jarosewich et al., 1980) and spinel UV-126 (Lavrentev et al., 1974). Analytical conditions were 15kv accelerating voltage, 20nA beam current and a 1-2μm beam size.

Trace elements in olivine phenocrysts from the Ngaloa Group volcanics were analysed under two different labels, using two different sets of conditions and the results are displayed in Figure A2.2. Table A2.6 presents the analytical conditions and counting times for both analytical labels. However, as the trace element program has a matrix correction based on the San Carlos olivine standard, Fo contents cannot be determined at the point of analysis. Comparison of results using both analytical conditions (Fig. A2.2) show that CaO, MnO and NiO contents in olivine phenocrysts vary in a non-systematic fashion by only ±0.05wt% between the different analytical approaches. Therefore, as the normal analytical conditions also provided Fo contents during the same analysis, CaO, MnO and NiO concentrations reported in the thesis were determined using normal analytical conditions.

Table A2.6: Analytical conditions and counting times for the analytical labels used during microprobe analyses of the olivine phenocrysts from the Ngaloa Group volcanics. A matrix correction based on San Carlos olivine was applied using the trace element label Kspcoltr.

Oxide	Spectrometer	Miscellaneous label (normal conditions)	Kspcoltr (trace element label)
SiO2	TAP	20/10	
FeO	LIF	20/10	
MnO	LIF	20/10	120/60
MgO	TAP	20/10	
CaO	PET	20/10	120/60
Cr2O3	PET	20/10	120/60
NiO	LIF	20/10	120/60
Accelerating voltage		15kV	20kV
Beam current		20nA	200nA
Beam size		5μm	10μm

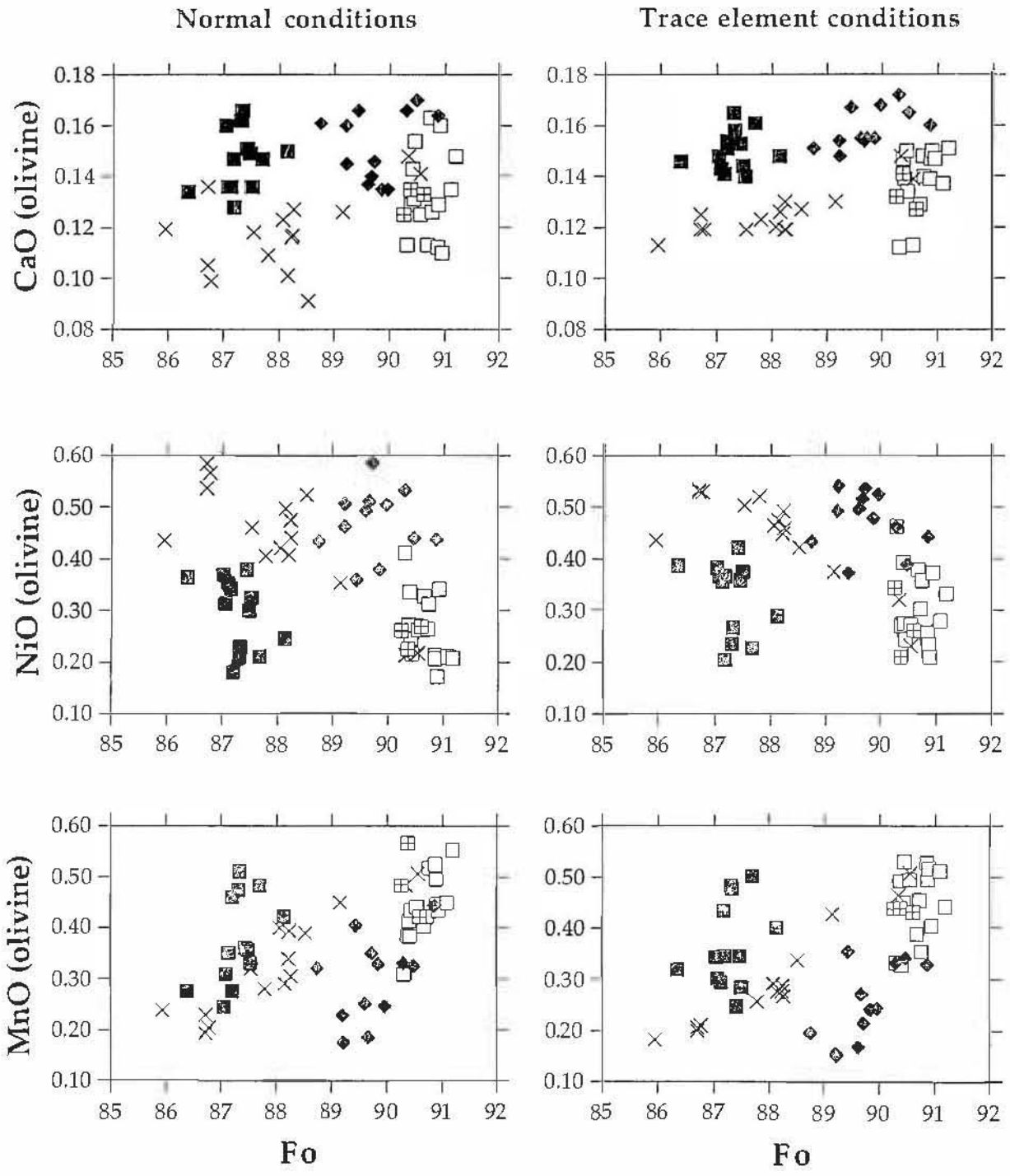

Figure A2.2. Comparison of CaO, NiO and MnO variation in olivine phenocrysts from the Ngaloa Group volcanics. a-c shows the elements analysed using the 'normal' conditions of 15kv and 20nA by the electron microprobe. d-f shows the same points analysed using the trace element program at extended counting times, high voltage (20kv) and high current (200nA). Closed squares=AV98; open squares=AV99; crosses=AV110; squares with crosses= AV112; closed diamonds=AV208.

APPENDIX 3

PETROGRAPHIC DESCRIPTIONS of the KADAVU ISLAND GROUP and NORTHERN HUNTER RIDGE ROCKS

Table A3.1. Petrographic descriptions of the Hunter Ridge rocks

Dredge no.	Sample no.	Rock type	Texture	Phenocrysts & microphenocrysts	Clast type	Groundmass
1	DR1-1	pumice	porphyritic	*plagioclase*: <1%, 0.2mm *pyroxene*: 2%, 0.2-0.6mm		
1	DR1-2	andesite	strongly porphyritic	*plagioclase*: 10%, 1-2mm, euhedral-subhedral, strong oscillatory, normal and reverse zoning, minor glass inclusions, in aggregates with cpx *hornblende*: 5%, 0.8-3mm, anhedral-euhedral, partially resorbed, embayed edges, inclusions of plagiolcase *cpx*: 2%, 2mm-1cm, subhedral-euhedral oxide: 2%, 0.5-1mm		glassy and extremely altered
1	DR1-3	limestone			100% planktonic foraminifera with a trace of Mn staining. *Orbulina universa, Globorotalia truncatulinoides truncatulinoides, G.tosaensis tenuitheca, G. tumida tumida, G. acostaensis acostaensis, G. a. humerosa, Globigerinoides conglobatus, G. quadrilobatus* subspp., *G. q. fistulosus, Hastigerina pelagica, Sphaeroidinella dehiscens, dehiscens, Pulleniatina obliqueloculata obliqueloculata*	
2	DR2-1	limetsone			occasional plagioclase and cpx grains, *Orbulina universa, Globorotalia menardii* subspp, *Globigerinoides conglobatus, G. quadrilobatus* subspp, *Sphaeroidinella dehiscens*	

Dredge no.	Sample no.	Rock type	Texture	Phenocrysts & microphenocrysts	Clast type	Groundmass
2	DR2-2	limestone			occasional cpx grains, dominantly planktinic foraminifera, *Orbulina universa, Globorotalia truncatulinoides truncatulinoides, G. tosaensis tosaensis, G. tumida tumida, G. menardii* subspp, *Hastigerina pelagica, Pulleniatina obliqueloculata obliqueloculata, Sphaeroidinella dehiscens dehiscens, Globigerinoides conglobatus*	
2	DR2-3	pumice				
3	DR3-1	pumice				
3	DR3-2	andesite	strongly porphyritic, weakly vesicular	*plagioclase*: 5%, 0.4-1mm, subhedral-euhedral, in aggregates with cpx and opx, glass inlcuions *cpx*: 3%, 0.2-0.6mm, subhedral-euhedral *opx*: 2%, 0.1-0.4mm, anhedral-euhedral *oxides*: 2% 0.1-0.2mm		glassy with fine laths of plagioclase, cpx, and rounded to equant oxides, extremely altered
4	1DR4-1 to 1DR4-6	cataclastic metagabbro	brittle textures typical of cataclastites			augen shaped porphyroblasts, strong planar fabric, areas of less deformation
4	2DR4-1	hornblende diorite	equigranular	*quartz*: 50%, 0.2-1mm, undulose extinction *plagioclase*: 25%, 0.5-1.5mm, subhedral-euhedral, strongly zoned *hornblende*: 20%, 0.4-0.8mm, anhedral *oxides*: 5%, 0.2mm		
4	2DR4-2	hornblende diorite	weakly porphyritic	*quartz*: 20%, 1mm *plagioclase*: 35%, 1-2mm, subhedral-euhedral, slightly altered *hornblende*: 10%, 0.5-2mm anhedral-subhedral, in aggregates		quartz, plagiolcase and oxides varying between 0.1-0.4mm, slight alteration on grain boundaries
4	2DR4-3	hornblende diorite	fine grained, equigranular, slightly altered			

Dredge no.	Sample no.	Rock type	Texture	Phenocrysts & microphenocrysts	Clast type	Groundmass
4	2DR4-4	hornblende diorite	equigranular, moderately altered, h.s: slickensides	*quartz*: 40%, 0.2-0.6mm *plagioclase*: 40%, 0.2-0.8mm, subhedral-euhedral *hornblende*: 20%, 0.4-0.8mm, anhedral, surrounds grain boundaries of plagioclase and quartz.		
4	2DR4-5	hornblende diorite	equigranular, moderately to strongly altered	*quartz*: 35%, 0.2-0.6mm *plagioclase*: 45%, 0.4-0.8mm, subhedral-euhedral *hornblende*: 25%, 0.2-0.8mm, anhedral calcite between grains		
4	2DR4-6	deformed hornblende diorite	equigranular, textures evidence for brittle deformation	*quartz*: 35%, 0.2-0.8mm *plagioclase*: 40%, 0.4-0.8mm *hornblende*: 25%		
4	2DR4-7	hornblende diorite	weakly porphyritic, moderately altered	*quartz*: 25%, 0.8-1mm *plagioclase*: 30%, 1-2mm, subhedral-euhedral *hornblende*: 10%, 0.5-2mm anhedral-subhedral, in aggregates		quartz, plagioclase, oxides varying between 0.2-0.6mm
4	2DR4-8	hornblende diorite	equigranular,moderately to strongly altered	*quartz*: 35%, 0.2-0.8mm *plagioclase*: 45%, 0.2-0.6mm, subhedral-euhedral *hornblende*: 25%, 0.2-0.6mm, anhedral		
4	2DR4-9	hornblende diorite	weakly porphyritic	*hornblende*: 20%, 0.2-1mm, anhedral-subhedral *plagioclase*: 3%, 0.4-1.2mm, subhedral-euhedral		*quartz*: 40%, 0.1-0.2mm *plagioclase*: 35%, 0.1-0.2mm, subhedral-euhedral *oxides*: 2%, 0.05-0.2mm
5	DR5-1	pumice				
5	DR5-2	volcaniclastic	fine grained, extremely altered		*cpx*: 3%, 0.2-0.4, subhedral-euhedral *olivine*: <1%, 0.2mm *quartz*: 2%, 0.2-0.6mm *plagioclase*: <1% *altered volcanic rock fragments*: 3%	carbonate, extremely altered in places

Dredge no.	Sample no.	Rock type	Texture	Phenocrysts & microphenocrysts	Clast type	Groundmass
5	DR5-3	volcaniclastic	medium grained		*andesite rock fragments*: 3%, 0.4-1mm, range from strongly to weakly porphyritic. *basaltic rock fragments*: 2%, 0.4-1mm, strongly vesicular, vesicles filled with quatrz or carbonate *plagioclase*: 3%, 0.4-2mm, anhedral-subhedral, glass inlcusions *cpx*: 2%, 0.2-0.6mm, anhedral-subhedral *olivine*: <1%, 0.1-0.3mm, anhedral-subhedral	carbonate
5	DR5-4	volcaniclastic	medium grained		fragments of DR5-3 embedded in matrix of foram ooze. *Orbulina universa, Pulleniatina sp., Sphaeroidinella* sp., *Globorotalia toaensis tosaensis,* *G. menardii* subspp, *G. tumida, G. acostaensis, Globigerinoides conglobatus, G. quadrilobatus* subspp.	foram ooze
5	DR5-5	andesite	strongly porphyritic, extremely altered	plagioclase: 25%, 0.5-2mm, subhedral-euhedral, commonly in clusters with cpx cpx: 10%, 0.2-0.8mm, anhedral, completely altered		glassy with fine plagioclase laths, extremely altered
6	1DR6-1	pumice				
6	1DR6-2	limestone			essentially planktonic foraminifera *Orbulina universa, Globorotalia tosaensis tosaensis, G. t. tenuitheca,* *G. tumida tumida, G. menardii* subspp., *G. acostaensis humerosa, G. multicamerata, Hastigerina pelagica, Pulleniatina obliqueloculata obliqueloculata, Globigerinoides conglobatus, G. quadrilobatus* subspp., *G quadrilobatus fistulosus, Sphaeroidinella deluscens dehiscens*	
6	2DR6-1	volcanic breccia	coarse grained, poorly sorted	basaltic fragment- *olivine*: 25%, 0.05-0.2mm, 'hopper' morphologies	basaltic rock fragments: 5%, 4mm-6cm, glassy rims, range from extremely altered to fresh.	groundmass of basalt fragments- acicular quenched cpx, and oxides

Dredge no.	Sample no.	Rock type	Texture	Phenocrysts & microphenocrysts	Clast type	Groundmass
7	DR7-1	limestone	Mn coated			
7	DR7-2	volcaniclastic	extremely altered			
8	DR8-1	limestone			planktonic foraminifera with very fine volcanic fragments and Mn staining. *Orbulina universa, Globorotalia truncatulinoides truncatulinoides, G. tosaensis tosaensis, G. t. tenuitheca, G. acostaensis acostaensis, G. tumida tumida, G. menardii* subspp., *G. scitula, Pulleniatina obliqueloculata obliqueloculata, Globigerinoides conglobatus, G. quadrilobatus* subspp.	carbonate
8	DR8-2	andesite	porphyritic, weakly vesicular	*plagioclase*: 20%, 0.1-0.8mm, subhedral-euhedral *cpx*: 10%, 0.4-0.8mm, subhedral-euhedral *opx*: 2%, 0.2-0.4mm, anhedral-subhedral, cores surrounded by cpx *olivine*: 1%, 0.5-2mm, anhedral-subhedral *vesicles*: <1%		fine grained to glassy with plagioclase and cpx laths; cpx laths nucleating on plagioclase phenocrysts
9	DR9-1	dacite	strongly porphyritic, moderately vesicular	*plagioclase*: 7%, 0.4-1.5mm, subhedral-euhedral, strongly zoned *cpx*: 5%, 0.2-0.6mm subhedral-euhedral, commonly in aggregates with plagioclase and opx *opx*: 2%, 0.1-0.3mm, subhedral-euhedral *vesicles*: 10%		glassy, microlites of plagioclase, slightly altered

Dredge no.	Sample no.	Rock type	Texture	Phenocrysts & microphenocrysts	Clast type	Groundmass
9	DR9-2	dacite	strongly porphyritic, moderately vesicular	*plagioclase*: 5%, 0.4-2mm, subhedral-euhedral, strongly zoned *cpx*: 3%, 0.2-0.8mm, subhedral-euhedral *opx*: 1%, 0.2-0.4mm, subhedral-euhedral *oxides*: 1%, 0.2mm phenocrysts mostle occur in aggregates, rarely as singular crystals *vesicles*: 10%		glassy, microlites of plagioclase vesicles are stretched with their long axis aligned subparallel to parallel
9	DR9-3	dacite	strongly porphyritic, moderately vesicular	*plagioclase*: 7%, 0.2-1.4mm, subhedral-euhedral *cpx*: 3%, 0.2-0.8mm, subhedral-euhedral *opx*: 2%, 0.1-0.4mm, subhedral-euhedral *oxides*: 1%, 0.2mm *vesicles*: 15%		glassy, microlites of plagioclase
9	DR9-4	volcanic breccia	coarse grained, poorly sorted		volcanic rock fragments of strongly porphyritic, vesicular, plagioclase phyric dacite similar to DR9-3; singular grains of plagioclase and cpx	carbonate
10	DR10-1	andesite	strongly porphyritic, weakly vesicular	*plagioclase*: 10%, 0.2-2.5mm, subhedral-euhedral, strong zoning, in aggregates, partially resorbed *cpx*: 7%, 0.4-1.5mm, subhedral-euhedral, sometimes rimming opx *opx*: 5%, 0.6-2mm, anhedral-euhedral *oxides*: 2%, 0.2-0.4mm anhedral, partially resorbed *vesicles*: 1%		extremely glassy, microlites of plagioclase and cpx

Dredge no.	Sample no.	Rock type	Texture	Phenocrysts & microphenocrysts	Clast type	Groundmass
10	DR10-2	andesite	strongly porphyritic, weakly vesicular	*plagioclase*: 15%, 0.2-2mm, subhedral-euhedral, partially resorbed *cpx*: 5%, 0.2-0.8mm, subhedral-euhedral, sometimes rimming opx *opx*: 3%, 0.4-1mm, subhedral-euhedral *oxides*: 2%, 0.1-0.4mm *vesicles*: 1%		glassy, microlites of plagioclase
10	DR10-3	andesite	strongly porphyritic	*plagioclase*: 10%, 0.2-3mm, subhedral-euhedral, larger phenocrysts riddled with glass inlcusions, partially to totally resorbed *cpx*: 10%, 0.2-1.5mm, subhedral-euhedral, minor glass inclusions and partially resorbed *opx*: 7%, 0.2-1.5mm, subhedral-euhedral *oxides*: 5%, 0.2mm phenocrysts commonly occurring in aggregates		glassy, fine laths of plagioclase and rare cpx
10	DR10-4	volcaniclastic	fine grained, poorly sorted		volcanic rock fragments similar to DR10-3 and singular crystals of cpx and olivine foraminifera not abundant *Globigerinoides conglobatus*, *G. quadrilobatus* subsp., *Globorotalia tosaensis tosaensis*, *G. menardii* subspp., *Pulleniatina* sp.	carbonate
10	DR10-5	andesite	strongly porphyritic, moderately altered	*plagioclase*: 10%, 0.4-3.2mm, subhedral-euhedral *cpx*: 10%, 0.2-1.5mm, subhedral-euhedral *opx*: 5%, 0.4-1mm, subhedral-euhedral *oxides*: 3%, 0.2mm		fine grained to glassy, laths of plagioclase

Dredge no.	Sample no.	Rock type	Texture	Phenocrysts & microphenocrysts	Clast type	Groundmass
11	DR11-1	volcaniclastic	fine grained, poorly sorted		abundant volcanic fragments (15%) of plagioclase, cpx, quartz, minor olivine and opx; altered volcanic rock fragments similar to DR10-1; *Globigerinoides conglobatus, Globorotalia tosaensis*	carbonate
11	DR11-2	volcaniclastic	coarse grained, poorly sorted		abundant volcanic fragments (20%) dominated by volcanic rock (up to 1.5mm) and lesser plagioclase, cpx, quartz, and olivine crystals.	carbonate
12	DR12-1	andesite	strongly porphyritic			
12	DR12-2	andesite	strongly porphyritic	*plagioclase*: 7%, 0.2-0.8mm, subhedral-euhedral, strong zoning, minor glass inclusions *cpx*: 10%, 0.2-1.2mm, subhedral-euhedral, commonly in aggregates with plagioclase and opx *opx*: 5%, 0.2-1.2mm, subhedral-euhedral		extremely glassy, spherilitic groundmass starting to crystallise
12	DR12-3	andesite	strongly porphyritic	*plagioclase*: 10%, 0.4-1mm, subhedral-euhedral, strong zoning, glass inclusions *cpx*: 7%, 0.4-1.2mm, subhedral-euhedral, rimming opx *opx*: 5%, 0.2-1.2mm, subhedral-euhedral		fine grained to glassy, fine plagioclase and cpx laths aligned subparallel to parallel
12	DR12-4	pumice				
12	DR12-5	volcaniclastic	fine grained, poorly sorted		volcanic fragments consist of plagioclase, cpx and pumice *Orbulina universa, Globorotalia truncatulinoides truncatulinoides, G. tosaensis tosaensis, G. acostaensis humerosa, G. tumida tumida, G. scitula, Globigerinoides quadrilobatus* subspp.	carbonate
12	DR12-6	volcaniclastic	fine grained, poorly sorted		volcanic fragments (7%) consist of plagioclase, cpx, quartz and andesitic rock fragments	carbonate
12	DR12-7	limestone	very altered			

Dredge no.	Sample no.	Rock type	Texture	Phenocrysts & microphenocrysts	Clast type	Groundmass
12	DR12-8	andesite	strongly porphyritic	*plagioclase*: 10%, 0.2-0.8mm, subhedral-euhedral, strong zoning, minor glass inclusions *cpx*: 10%, 0.2-1mm, subhedral-euhedral, commonly in aggregates with plagioclase and opx *opx*: 5%, 0.2-1.2mm, subhedral-euhedral		glassy
12	DR12-9	volcaniclastic	fine grained, poorly sorted		volcanic fragments (7%) consist of plagioclase, cpx, quartz and andesitic rock fragments	carbonate
13	DR13-1	volcaniclastic	fine grained		minor (5%) volcanic fragments - cpx, plagioclase, rock fragments similar to DR12-8	carbonate
14	DR14-1	pumice				
14	DR14-2	volcaniclastic	fine grained		minor (2%) volcanic fragments of plagioclase and cpx	carbonate
15	DR15-1	volcanic breccia	coarse grained, poorly sorted	Volcanic clasts - prophyritic *olivine*: 15%, 0.2-1.5mm, anhedral-euhedral *cpx*: 7%, 0.4-0.8mm, subhedral-euhedral *vesicles*: 40% cpx occurs as tiny rosettes in the groundmass	Volcanic fragments consist of extremely altered and fresh strongly vesicular basalt, no glassy rims, fragments range between 3mm to 2cm	carbonate
15	DR15-2	dacite	strongly porphyritic	*plagioclase*: 7%, 0.2-0.8mm, subhedral-euhedral, commonly in aggregates *cpx*: 3%, 0.1-0.4mm, anhedral-subhedral *vesicles*: 10%		fine grained to glassy, fine laths of plagioclase aligned subparallel to parallel and small (~0.02mm) rounded cpx
15	DR15-3	volcaniclastic	fine grained, moderatley sorted		minor (2%) volcanic fragments dominated by plagioclase	
15	DR15-4	dacite	strongly porphyritic	*plagioclase*: 10%, 0.2-0.8mm, subhedral-euhedral, commonly in aggregates *cpx*: 5%, 0.1-0.4mm, anhedral-subhedral *vesicles*: 10%		fine grained to glassy, fine laths of plagioclase

Dredge no.	Sample no.	Rock type	Texture	Phenocrysts & microphenocrysts	Clast type	Groundmass
15	DR15-5	dacite	strongly porphyritic	*plagioclase*: 7%, 0.4-1mm, subhedral-euhedral, commonly in aggregates *cpx*: 2%, 0.1-0.6mm, anhedral-subhedral *oxides*: 1% *vesicles*: 7%		fine grained to glassy, plagioclase laths and abundant oxides
16	DR16-1	volcaniclastic	medium grained, poorly sorted		volcanic fragments (5%) consist of plagioclase, cpx and altered andesitic rock fragments up to 1.5cm	carbonate
16	DR16-2	pumice				
16	DR16-3	volcaniclastic	fine grained, poorly sorted		volcanic fragments (7%) consist of cpx, plagioclase and altered andesitic rock fragments, *Orbulina universa, Globorotalia truncatulinoides truncatulinoides, G. tosaensis tosaensis, G. acostaensis humerosa, G. tumida tumida, G. menardii* subspp., *G. inflata, G. scitula, Globigerinoides quadrilobatus* subspp., *G. conglobatus, Pulleniatina obliqueloculata obliqueloculata, P. o. finalis, Sphaeroidinella dehiscens dehiscens, Candeina nitida nitida*	carbonate
16	DR16-4	volcaniclastic	medium grained, poorly sorted	volcanic clasts: strongly porphyritic *plagioclase*: 10%, 0.2-2mm, subhedral-euhedral, strongly zoned, minor glass inclusions *cpx*: 5%, 0.2-0.6mm, anhedral-euhedral *opx*: 2%, 0.4-0.8mm, subhedral-euhedral *groundmass:* fine grained to glassy, fine plagioclase laths aligned sub-parallel to parallel	volcanic fragments consist of altered plagioclase phyric dacite ranging in size between 0.5 to 3cm.	carbonate

Dredge no.	Sample no.	Rock type	Texture	Phenocrysts & microphenocrysts	Clast type	Groundmass
16	DR16-5	andesite	porphyritic	*plagioclase*: 15%, 0.4-2mm, subhedral-euhedral, strongly zoned, minor glass inclusions *cpx*: 3%, 0.1-0.6mm, anhedral-euhedral *opx*: 2%, 0.4-0.8mm, subhedral-euhedral		fine grained to glassy, fine plagioclase laths
16	DR16-6	andesite	strongly porphyritic	*plagioclase*: 20%, 0.4-1.5mm, subhedral-euhedral, strongly zoned, abundant glass inlcusions, partially resorbed *cpx*: 5%, 0.4-0.8mm, subhedral-euhedral *opx*: 3%, 0.2-0.8mm, subhedral-euhedral *oxides*: 3%, 0.4mm phenocrysts commonly occurring in aggregates		finegrained to glassy, fine laths of plagioclase aligned parallel to subparallel and oxides

Table A3.2. Petrographic descriptions of the Astrolabe Group absarokites, shoshonites and banakites

Sample no.	Rock type	Texture	Phenocrysts	Groundmass
AV173	shoshonite	porphyritic	*plagioclase*: 15%, 0.1-3mm, subhedral - euhedral, oscillatory zoning, *clinopyroxene*: 10%, 0.5-1.5mm, subhedral - euhedral, contains inclusions of plagioclase and spinel. *olivine*: 2%, 0.1-0.8mm, subhedral - anhedral, totally resorbed.	fine grained consisting of fine plagioclase laths, clinopyroxene, K-feldspar, spinel and minor olivine.
AV177	absarokite	porphyritic	*clinopyroxene*: 10%, 0.04-1.0mm, subhedral-euhedral, commonly in crystal clusters *olivine*: 5%, 0.8-1.5mm, subhedral-anhedral, partially veined with iddingsite	fine grained to glassy consisting of clinopyroxene, fine plagioclase laths, anhedral K-feldspar and spinel.
AV182b	banakite	porphyritic	*plagioclase*: 20%, 0.2-1.5mm, subhedral-euhedral *clinopyroxene*: 10%, 0.5-1mm, subhedral-euhedral *hornblende*: 3%, 0.2-0.6mm, anhedral-subhedral *biotite*: 3%, 0.05-0.4mm, anhedral-euhedral *spinel*: 7%, 0.2mm	fine grained consisting of plagioclase laths, clinopyroxene and spinel
AV185	absarokite	porphyritic	*clinopyroxene*: 15%, 0.02-1.0mm, subhedral-euhedral, commonly in crystal clusters *olivine*: 5%, 1-1.5mm, subhedral-anhedral, partially veined with iddingsite	fine grained to glassy consisting of clinopyroxene, fine plagioclase laths, anhedral K-feldspar and spinel.
AV186	absarokite	porphyritic	*clinopyroxene*: 15%, 0.05-2.0mm, subhedral-euhedral, commonly in clusters with other clinopyroxene. *olivine*: 5%, 0.5-2mm, subhedral-euhedral, partially veined with iddingsite, contains inclusions of Cr-spinel.	fine grained to glassy consisting of abundant clinopyroxene, fine plagioclase laths, anhedral K-feldspar and spinel.

Sample no.	Rock type	Texture	Phenocrysts	Groundmass
AV187	banakite	porphyritic	*plagioclase*: 20%, 0.5-2mm, subhedral-euhedral, partially resorbed. *clinopyroxene*: 10%, 0.5-1.5mm, subhedral-euhedral, commonly in aggregates. *biotite*: 3%, 0.6-1.0mm, anhedral-subhedral. *hornblende*: <1%, 0.4-0.8mm, anhedral-subhedral. *spinel*: 7%, 0.2mm	fine grained to glassy consisting of plagioclase laths and clinopyroxene.
AV190	shoshonite	porphyritic	*plagioclase*: 10%, 0.2-0.5mm, subhedral-euhedral. *clinopyroxene*: 15% 0.5-2mm, subhedral-euhedral, commonly in crystal aggregates with spinel. *olivine*: 2%, 0.5-0.8mm, anhedral, totally resorbed. *spinel*: 3%, 0.4mm, some deeply embayed.	fine grained to glassy consisting of plagioclase laths, K-feldspar, clinopyroxene and minor olivine.
AV192	shoshonite	porphyritic	*plagioclase*: 10%, 0.05-1.5mm, subhedral-euhedral. *clinopyroxene*: 5%, 0.2-0.6mm, anhedral-subhedral. *olivine*: 1%, anhedral, totally resorbed *spinel*: 5%, 0.05-0.4mm, some deeply embayed	fine grained consisting of plagioclase, clinopyroxene and spinel.

Table A3.3. Petrographic description of the Ngaloa Group basalts and basaltic andesites.

Sample no.	Rock type	Texture	Phenocrysts and microphenocrysts	Groundmass
AV 98	basalt	porphyritic	*clinopyroxene*: 10%, 0.1-1.2mm, subhedral-euhedral, strongly zoned, partial to total resorption, often in clusters with minor olivine and phlogopite. *olivine*: 3%, 0.1-0.4mm, anhedral-subhedral, often riddled with irregular shaped inclusions. *phlogopite*: 2%, 0.2-0.8mm, anhedral.	fine grained consisting of abundant plagioclase, clinopyroxene, equant shaped mgmetite and scattered ilmenite needles.
AV99	basalt	porphyritic	*clinopyroxene*: 7%, 0.4-2mm, subhedral-euhedral, partially resorbed, zoned, often in clusters with olivine and phlogopite *olivine*: 2%, 0.2-0.6mm, anhedral-subhedral, often riddled with inclusions (magnetite) *phlogopite*: 2%, 0.05-0.1mm, occurs as singular grains, in aggregtes with cpx and olivine and commonly surrounding olivine grains and as inclusions in cpx.	fine grained consisting of abundant plagiolase laths, clinopyroxene, equant shaped magmetite and ilmenite needles.
AV110	basaltic andesite	porphyritic	*clinopyroxene*: 7%, 0.2-0.8mm, subhedral-euhedral, partially resorbed, zoned *olivine*: 1%, 0.2-0.4mm, anhedral-subhedral, contain inclusions of magnetite *phlogopite*: 1%, 0.05-0.1mm, anhedral	finegrained consisting of plagioclase laths, clinopyroxene, magnetite and ilmenite needles

Sample no.	Rock type	Texture	Phenocrysts and microphenocrysts	Groundmass
AV112	basaltic andesite	porphyritic	*clinopyroxene*: 8%, 0.4-1mm, subhedral-euhedral, partially resorbed, zoned *olivine*: 2%, 0.4-0.6mm, anhedral-subhedral, inlcusions of magnetite *phlogopite*: 1%, 0.05-0.2mm, anhedral	fine grained consisting of plagioclase laths, clnopyroxene, magnetite and ilmenite needles
AV116	basaltic andesite	porphyritic	*clinopyroxene*: 8%, 0.4-1mm, strongly zoned, partially resorbed, inlcusions of phlogopite *olivine*: 2%, 0.4-0.8mm, anhedral-subhedral, minor inclusions *phlogopite*: <1%, 0.02-0.06mm anhedral	fine grained dominated by plagioclase laths sometimes aligned subparallel to parallel, less abundant cpx, phlogopite and ilmenite needles.
AV152	basalt	porphyritic	*clinopyroxene*: 10%, 0.05-1mm, subhedral-euhedral, some strongly zoned, partially to totally resorbed *olivine*: <1%, 0.05-1mm, anhedral-subhedral, minor inclusions *plagioclase*: 3%, 0.2-0.6mm, subhedral-euhedral, commonly in clusters with cpx	fine grained dominted by plagioclase laths, cpx euhedral magnetite, minor ilmenite and phlogopite
AV208	basalt	porphyritic	*clinopyroxene*: 10%, 0.2-0.8mm, subhedral-euhedral, rarely strongly zoned *olivine*: 7%, 0.2-0.6mm, subhedral-euhedral, riddled with inclusions *plagioclase*: 3%, 0.06-0.8mm, subhedral-euhedral, commonly in clusters with cpx *phlogopite*: 1%, 0.02-0.6mm, anhedral	fine grained domininated by plagioclase laths, cpx, euhedral magnetite, and lesser amounts of ilmenite needles and phlogopite

Table A3.4. Petrographic descriptions of the Western Kadavu and Central/Eastern/Ono adakitic andesites and dacites

Sample no.	Rock type	Texture	Phenocrysts & microphenocrysts	Groundmass
AV5	andesite	porphyritic	*plagioclase*: 15%, 0.08-2mm, subhedral-euhedral *clinopyroxene*: 5%, 0.08-1.5mm, subhedral-euhedral *hornblende*: 2%, 0.2mm, anhedral-subhedral, omphacitic rims *spinel*: 3%, 0.2mm, embayed edges	fine grained containing plagioclase laths, clinopyroxene and spinel.
AV14	dacite	porphyritic	*plagioclase*: 25%, 0.05-4mm, oscillatory zoned, subhedral-euhedral *clinopyroxene*: 2%, microphenocryst only, 0.05-0.1mm, anhedral-subhedral *spinel*: 5%, 0.1-0.3mm, phenocrysts have embayed edges *hornblende*: 3%, 0.1mm, microphenocrysts only, totally resorbed, anhedral *biotite*: 5%, 0.05-2mm, anhedral-subhedral, orange yellow-mottled black, inclusions of plagioclase, reaction rims	fine grained to glassy containing plagioclase laths, spinels and pyroxene.
AV31	dacite	porphyritic	*plagioclase*: 10%, 0.1-2mm, euhedral, oscillatory zoned, single crystals and clusters; microphenocrysts aligned subparallel to parallel and warp around phenocrysts phases *clinopyroxene*: 1%, 0.8mm *spinel*: 3%, 0.04-0.25mm, embayed edges *hornblende*: 5% 0.1-0.6mm anhedral-subhedral, partially to totally resorbed *biotite*: 2%, 0.8-1mm partially to totally resorbed	glassy, microlites of plagioclase.

Sample no.	Rock type	Texture	Phenocrysts & microphenocrysts	Groundmass
AV37	andesite	porphyritic	*plagioclase*: 10%, 0.2-3mm, subhedral-euhedral, oscillatory zoned *clinopyroxene*: 3%, 0.2-0.8mm; phenocrysts totally resorbed; microphenocrysts occur in clusters and single grains *orthopyroxene*: rare phenocrysts *spinel*: 3%, 0.4mm, embayed edges *hornblende*:10%, 0.1-0.8mm, partially to totally resorbed; microphenocrysts not as resorbed as phenocrysts *biotite*: 2%, 1mm, partially to totally resorbed, inclusions of *plagioclase*	fine grained to glassy
AV40	dacite	porphyritic	*plagioclase*: 20%, 0.5-2mm, subhedral-euhedral, strong oscillatory zoning *clinopyroxene*: 7%, 0.2-0.8mm, subhedral-euhedral, uncommon zoning; occurring in clusters; fine plagioclase inclusions *spinel*: 3%, 0.2mm	glassy with microlites of plagioclase, spinel and possibly pyroxene
AV48	andesite	porphyritic	*plagioclase*: 10%, 0.05-3mm, oscillatory zoned *clinopyroxene*: 1%, 0.02-0.05mm, subhedral-euhedral *spinel*: 1%, 0.2mm *hornblende*: 3%, 0.05-1mm, anhedral-subhedral, partially resorbed *biotite*: 4%, 0.05-2mm	fine grained to glassy consisting of plagioclase, hornblende, spinel and glass
AV50	dacite	porphyritic	*plagioclase:* 15%, 0.1-2mm, subhedral-euhedral, oscillatory zoned *clinopyroxene:* 3%, 0.1-0.5mm, commonly in clusters *spinel:* 2% 0.2-0.5mm *hornblende:* 10%, 0.5-1mm, partially to totally resorbed *biotite:* 3%, 0.5-1mm, inclusion of plagioclase; sometimes in clusters with hornblende *quartz:* one single grain	glassy

Sample no.	Rock type	Texture	Phenocrysts & microphenocrysts	Groundmass
AV54	andesite	porphyritic	*plagioclase:* 7%, 0.05-1.5mm, oscillatory zoned *clinopyroxene:* 5%, 0.01-0.5mm, subhedral-euhedral *spinel:* 3%, 0.05-0.1mm *hornblende:* 5%, 0.05-0.2mm, partially to totally resorbed *biotite:* 2%, 0.4-2mm, partially to totally resorbed	fine grained to glassy
AV57	andesite	porphyritic	*plagioclase:* 20%, 0.03-1mm, subhedral-euhedral, oscillatory zoning *clinopyroxene:* 7%, 0.1-0.5mm, subhedral-euhedral *spinel:* 3%, 0.1mm	glassy
AV59	andesite	porphyritic	*plagioclase:* 20%, 0.2-2mm, oscillatory zoned *clinopyroxene:* 17%, 0.1-0.6mm, subhedral, single grains and in clusters sometimes with orthopyroxene and spinel; inclusions of plagioclase *orthopyroxene:* 3%, 0.1-0.4mm, anhedral-subhedral, partially resorbed *spinel:* 2%, 0.1mm, scattered evenly throughout *biotite:* one single grain (0.8mm) partially resorbed	fine grained to glassy
AV62	andesite	porphyritic	*plagioclase:* 20%, 0.1-1.5mm, subhedral, oscillatory zoned; different stages of resorption; microphenocrysts not resorbed *clinopyroxene:* 15%, 0.1-0.8mm; phenocrysts are partially to totally resorbed *orthopyroxene:* 3%, 0.05-0.1mm, only microphenocrysts *spinel:* 3%, 0.05-2mm, embayed edges *hornblende:* 2%, 0.2-0.6mm, totally resorbed *biotite:* <1%, partially to totally resorbed	glassy

Sample no.	Rock type	Texture	Phenocrysts & microphenocrysts	Groundmass
AV66	andesite	porphyritic	*plagioclase:* 10%, 0.2-1.5mm, partially resorbed *clinopyroxene:* <1% as microphenocryst *spinel:* 3%, 0.05-0.1mm *hornblende:* 10%, 0.1-1mm, totally resorbed or reaction rims; microphenocrysts are totally resorbed *biotite:* <1% partially to totally resorbed *apatite:* <1%, 0.8mm long	fine grained to glassy with plagioclase laths, pyroxene and spinel
AV70	andesite	porphyritic	*plagioclase:* 7%, 0.2-2mm, subhedral-euhedral, uncommon resorption rims *clinopyroxene:* 2%, 0.5mm *spinel:* 3%, 0.4mm, deeply embayed edges *hornblende:* 10%, 0.2-1mm, partially to totally resorbed *biotite:* <1% different stages of resorption; inclusions of *plagioclase*	fine grained to glassy
AV72	andesite	porphyritic	*plagioclase:* 8%, 0.5-1.5mm, subhedral-euhedral, oscillatory zoning *clinopyroxene:* 3%, 0.6mm, anhedral-subhedral, some partially resorbed *spinel:* 3%, 0.1mm, embayed edges *hornblende:* 10%, 0.1-1mm, subhedral, partially to totally resorbed; microphenocrysts totally resorbed *biotite:* <1%, partially resorbed, plagioclase inclusions *apatite:* <1%	glassy containing fine plagioclase microlites
AV73	andesite	porphyritic	*plagioclase:* 10%, 0.4-1mm, subhedral-euhedral *clinopyroxene:* 5%, 0.2-0.6mm, anhedral-subhedral *hornblende:* 10%, 0.2-1mm subhedral, opacitic rims *biotite:* 1%, partially resorbed *spinel:* 2%, 0.1mm, embayed edges	glassy containing fine plagioclase microlites

Sample no.	Rock type	Texture	Phenocrysts & microphenocrysts	Groundmass
AV76	andesite	porphyritic	*plagioclase:* 7%, 0.2-3mm, some partially resorbed; minor glass inclusions; oscillatory zoned *clinopyroxene:* 3%, 0.5mm, subhedral-euhedral *spinel:* 3%, 0.1mm *hornblende:* 5%, 0.4-1.5mm, partially to totally resorbed *biotite:* <1%, partially resorbed, *plagioclase* inclusions *apatite:* <1%, 0.1mm	fine grained to glassy
AV77	andesite	porphyritic	*plagioclase:* 7%, 0.1-2mm, oscillatory zoned; sieve like textures *clinopyroxene:* 3%, 0.1-0.5mm, more common as a microphenocryst *spinel:* 3%, 0.2mm *hornblende:* 10%, 0.1-1mm, majority are totally resorbed *biotite:* <1%, 0.5-1mm, different stages of resorption *apatite:* <1%, 0.2mm	fine grained to glassy
AV78	andesite	porphyritic	*plagioclase*: 10%, 0.2-1mm, subhedral-euhedral *clinopyroxene*: 5%, 0.1-0.8mm, subhedral-euhedral, pockets of glass trapped between aggregates of clinopyroxene *orthopyroxene*: 2%, 0.2-0.6mm, subhedral-euhedral, sometimes rimmed by clinopyroxene *spinel*: 3%, 0.1mm, embayed edges.	glassy
AV84	andesite	porphyritic	*plagioclase*: 10%, 0.4-0.8mm, subhedral-euhedral *clinopyroxene*: 7%, 0.1-1mm, subhedral-euhedral *hornblende*: 3%, 0.1-0.8mm, subhedral-anhedral, some completely resorbed, sometimes see hornblende intergrown with clinopyroxene *spinel*: 3%, 0.08-0.4mm	fine grained to glassy

Sample no.	Rock type	Texture	Phenocrysts & microphenocrysts	Groundmass
AV85	andesite	porphyritic	*plagioclase*: 10%, 0.2-2mm, subhedral-euhedral, oscillatory zoned; some partially resorbed; sieve like textures *clinopyroxene*: 3%, 0.2-0.6mm, partially resorbed *spinel*: 3% 0.4mm, deeply embayed edges *hornblende*: 5%, 0.1-1.5mm majority totally resorbed *biotite*: <1% partially resorbed	fine grained to glassy
AV90	dacite	porphyritic	*plagioclase*: 15%, 0.5-3mm, subhedral-euhedral, oscillatory zoned *clinopyroxene*: 5%, 0.1-0.6mm, subhedral-euhedral *spinel*: 3%, 0.05mm *hornblende*: 7%, 0.2-1.5mm, subhedral-euhedral	glassy
AV91	andesite	porphyritic	*plagioclase*: 20%, 0.1-0.5mm, oscillatory zoning *clinopyroxene*: 15%, 0.2-0.6mm, common in glomeroporphyritic clusters with plagioclase and spinel *spinel*: 5%, 0.2mm embayed edges	very glassy with plagioclase microlites and spinel
AV94	dacite	porphyritic	*plagioclase*: 10%, 0.2-2mm, subhedral-euhedral *clinopyroxene*: 5%, 0.1-0.6mm, subhedral-euhedral *hornblende*: 7%, 0.1-0.6mm, subhedral-anhedral, minor opacitic rims *spinel*: 2%, 0.3mm *biotite*: <1%	fine grained to glassy
AV100	andesite	porphyritic	*plagioclase*: 15%, 0.1-2mm, oscillatory zoning; glass inclusions *spinel*: 5%, 0.05-0.2mm *hornblende*: 7%, 0.2-1mm, anhedral-subhedral, reaction rims *biotite*: 3%, 0.8mm, partially resorbed	very glassy, fine microlites of plagioclase aligned subparallel to parallel

Sample no.	Rock type	Texture	Phenocrysts & microphenocrysts	Groundmass
AV101	andesite	porphyritic	*plagioclase*: 7%, 0.1-1mm, subhedral oscillatory zoned, reaction rims *clinopyroxene*: 5%, 0.1-0.6mm, subhedral-euhedral, commonly in clusters with spinel and sometimes plagioclase *spinel*: 2%, 0.2mm *hornblende*: 3%, 0.3mm, subhedral-euhedral, reaction rims *biotite*: <1%, partially resorbed	fine grained with abundant plagioclase laths and pyroxene.
AV103	andesite	porphyritic	*plagioclase*: 7%, 0.1-4mm, oscillatory zoning not common, clinopyroxene inclusions *clinopyroxene*: 3%, 0.1-0.8mm, as single grains and cluster with spinel and plagioclase *orthopyroxene*: 2%, 0.15-0.4mm, subhedral-euhedral *spinel*: 3%, 0.2mm, some have embayed edges *hornblende*: 3%, 0.6mm, anhedral-subhedral, very thin reaction rims *biotite*: <1%, replaced by plagioclase and pyroxene	very glassy
AV107	andesite	porphyritic	*plagioclase*: 10%, 0.4-4mm, subhedral-euhedral, oscillatory zoning *clinopyroxene*: 3%, 0.8mm, subhedral-euhedral; inclusions of *plagioclase*, some concentric zoning *orthopyroxene*: 2%, 0.2mm subhedral-euhedral *spinel*: 3%, 0.2mm, some embayed edges *hornblende*: 2%, 0.2-0.6mm, anhedral-subhedral *biotite*: <1% *apatite*: <1%	glassy

Sample no.	Rock type	Texture	Phenocrysts & microphenocrysts	Groundmass
AV113	dacite	porphyritic	*plagioclase*: 10%, 0.6-4mm, anhedral-subhedral, minor oscillatory zoning, sieve like textures; glass inclusions; some resorption *clinopyroxene*: 2%, 0.1mm, as microphenocrysts only *spinel*: 2%, 0.3mm, some deeply embayed *hornblende*: 8%, 0.4-3mm, subhedral-euhedral; partially to totally resorbed; clusters with spinel *apatite*: <1%	extremely glassy
AV117	andesite	porphyritic	*plagioclase*: 20%, 0.5-3mm, subhedral-euhedral, oscillatory zoning *clinopyroxene*: 15%, 0.4-1mm, subhedral-euhedral	
AV118	andesite	porphyritic	*plagioclase*: 10%, 0.2-1mm, oscillatory zoned, glass inclusions; clusters with glass trapped between grains *clinopyroxene*: 17%, 0.2-1mm, subhedral-euhedral; glomeroporphyritic clusters with spinel *spinel*: 3%, 0.4mm, some deeply embayed	fine grained, fine plagioclase laths, scattered spinel and patches of clear brown glass
AV123	andesite	porphyritic	*plagioclase*: 10%, 0.1-2mm, subhedral-euhedral, oscillatory zoning, glass inclusions *clinopyroxene*: 7%, 0.3-1.5mm, subhedral-euhedral, some zoning *spinel*: 3%, 0.2mm, some with embayed edges *apatite*: <1%, 0.6mm	glassy with scattered spinels

Sample no.	Rock type	Texture	Phenocrysts & microphenocrysts	Groundmass
AV126	andesite	porphyritic	*plagioclase*: 10%, 0.2-1.5mm, subhedral-euhedral, minor oscillatory zoning *clinopyroxene*: 5%, 0.5-1.5mm, subhedral-euhedral, minor zoning, plagioclase inclusions *hornblende*: 5%, 0.5-1mm, anhedral-subhedral, partially to totally resorbed	fine grained consisting of plagioclase laths, clinopyroxene, and spinel
AV127	andesite	porphyritic	*plagioclase*: 15%, 0.1-1mm, partially resorbed; reaction rims *clinopyroxene*: 10%, 0.4-1.5mm, subhedral, plagioclase inclusions, some in clusters with oxides *orthopyroxene*: 10%, 0.2-1mm *spinel*: 5%, 0.05-0.2mm, larger grains are deeply embayed *apatite*: <1%, 0.4mm long	fine grained to glassy
AV129	andesite	porphyritic	*plagioclase*: 10%, 0.2-1mm, oscillatory zoning, clinopyroxene and plagioclase inclusions; partially to totally resorbed *clinopyroxene*: 3%, 0.2-0.8mm, subhedral-euhedral, inclusions of plagioclase *orthopyroxene*: 2%, 0.6mm euhedral *hornblende*: 5%, 0.2-1mm, subhedral-euhedral, reaction rims *biotite*: <1%, 0.8mm, partially resorbed	fine grained to glassy
AV133	andesite	porphyritic	*plagioclase*: 10%, 0.1-3mm, oscillatory zoning; some partially resorbed; glass inclusions *clinopyroxene*: 7%, 0.05-0.4mm, subhedral-euhedral *spinel*: 3%, 0.2mm; some with embayed edges *hornblende*: 5%, 0.2-1.5mm, subhedral-euhedral, partially to totally resorbed *biotite*: <1%, 0.6mm, partially resorbed, inclusions of plagioclase	fine grained
AV137	andesite	porphyritic	*plagioclase*: 10%, 0.1-2mm, subhedral-euhedral *clinopyroxene*: 5%, 0.1-1mm, anhedral-euhedral, sometimes in crystal clusters *hornblende*: 3%, 0.5mm subhedral-euhedral	fine grained to glassy

Sample no.	Rock type	Texture	Phenocrysts & microphenocrysts	Groundmass
AV140	andesite	porphyritic	*plagioclase*: 15%, 0.2-1.5mm, anhedral-subhedral; oscillatory zoning; some riddled with inclusions *clinopyroxene*: 5%, 0.2-0.8mm, anhedral-subhedral; sometimes in clusters with spinel and glass trapped between grains *orthopyroxene*: 3%, 0.2mm, subhedral *spinel*: 3%, 0.2mm, embayed edges	fine grained consisting of plagioclase laths and scattered spinel
AV141	andesite	porphyritic	*plagioclase*: 4%, 0.6-1mm, anhedral-subhedral, partially to totally resorbed *clinopyroxene*: 5%, 0.05-0.5mm, subhedral-euhedral *hornblende*: 5%, 0.2-2mm, anhedral-euhedral *orthopyroxene*: 3%, 0.3-1.5mm, anhedral-subhedral *spinel*: 1%, 0.2mm	glassy containing fine plagioclase laths and spinel
AV142	andesite	porphyritic	*plagioclase*: 10%, 0.15-1mm, subhedral-euhedral, oscillatory zoning not common; glass inclusions, sometimes in clusters with other grains *clinopyroxene*: 5%, 2mm, subhedral-euhedral, commonly in glomeroporphyritic clusters with glass trapped in between grains *hornblende*: 5%, 0.2-1.5mm, subhedral-euhedral, reaction rims; none completely resorbed	fine grained with patches of glass
AV150	andesite	porphyritic	*plagioclase*: 10%, 0.4-1mm, oscillatory zoned, subhedral-euhedral, clinopyroxene inclusions *clinopyroxene*: 7%, 0.2-1mm, subhedral-euhedral *orthopyroxene*: 3%, 0.3-1.5mm, anhedral-subhedral *spinel*: 5%, 0.2mm, deep embayed edges *hornblende*: 3%, 0.05-4mm, anhedral-subhedral; totally resorbed as a microphenocryst; partially resorbed phenocrysts *biotite*: <1%, partially resorbed *apatite*: <1%, 0.2mm	fine grained to glassy consisting of plagioclase laths, pyroxene, and spinel; plagioclase laths aligned subparallel-parallel and flow around phenocrysts

Sample no.	Rock type	Texture	Phenocrysts & microphenocrysts	Groundmass
AV153	andesite	porphyritic	*plagioclase*: 7%, 0.3-1.5mm, anhedral-subhedral; sometimes in clusters with glass trapped between grains; dusty texture with glass inclusions; oscillatory zoned; inclusions of clinopyroxene *clinopyroxene*: 10%, 0.05-1.5mm, anhedral-subhedral; sometimes in clusters with plagioclase, spinel and orthopyroxene with glass trapped between grains *orthopyroxene*: 3%, 1mm, subhedral *spinel*: 3%, 0.05-0.2mm, some edges embayed *hornblende*: 2%, 2.5mm, subhedral-euhedral, inclusions of biotite and plagioclase, phenocrysts have reaction rims; microphenocrysts are totally resorbed	fine grained with patches of glass consisting of plagioclase laths, clinopyroxene and spinel.
AV154	andesite	porphyritic	*plagioclase*: 10%, 0.2-1.5mm, subhedral; glass inclusions *clinopyroxene*: 7%, 0.1-0.6mm, subhedral-euhedral; glomeroporphyritic clusters with spinel *orthopyroxene*: 3%, 0.2-0.6mm, subhedral *spinel*: 2%, 0.1mm, some with embayed edges	fine grained to glassy; fine plagioclase laths, pyroxene and spinel
AV158	andesite	porphyritic	*plagioclase*: 10%, 0.2-2mm, subhedral-euhedral *clinopyroxene*: 7%, 0.1-0.8mm, subhedral-euhedral, crystal clusters with spinel *orthopyroxene*: 2%, 0.1-0.4mm, subhedral-euhedral *spinel*: 2%, 0.1mm *apatite*: <1%, 0.4mm	glassy
AV164	andesite	porphyritic	*plagioclase*: 10%, 0.2-1mm, subhedral, partially resorbed *clinopyroxene*: 7%, 0.4-1.4mm, subhedral-euhedral *hornblende*: 3%, 0.2-1.6mm, subhedral, partially resorbed with opacitic rims. *spinel*: 3%, 0.4mm *apatite*: 1%, 0.8mm *biotite*: <1%, 0.4mm, anhedral, totally resorbed	glassy containing fine plagioclase laths and pyroxene

Sample no.	Rock type	Texture	Phenocrysts & microphenocrysts	Groundmass
AV169	andesite	porphyritic	*plagioclase*: 15%, 0.2-1.5mm, subhedral; clinopyroxene inclusions; weak oscillatory zoning; partially resorbed *clinopyroxene*: 8%, 0.2-1mm, anhedral-subhedral *spinel*: 3%, 0.3mm, edges embayed	fine grained
AV196	andesite	porphyritic	*plagioclase*: 10%, 0.2-1.5mm, subhedral, oscillatory zoning, some have reaction rims *clinopyroxene*: 5%, 0.1-0.3mm, occurs as a microphenocryst only *orthopyroxene*: 2%, 1mm, subhedral-euhedral *spinel*: 2%, 0.25mm, some edges embayed *hornblende*: 3%, 0.2-1.5mm, anhedral-subhedral, totally resorbed *apatite*: <1%, 0.1mm	fine grained to glassy
AV199	andesite	porphyritic	*plagioclase*: 7%, 0.2-1.2mm, subhedral-euhedral, partially resorbed *clinopyroxene*: 7%, 0.1-0.8mm, subhedral-euhedral, crystal clusters with spinel *orthopyroxene*: 2%, 1mm , subhedral-euhedral *spinel*: 2%, 0.25mm, some edges embayed *hornblende*: <1%, totally resorbed	very glassy
AV201	andesite	porphyritic	*plagioclase*: 10%, 0.1-4mm, subhedral, inclusions of *clinopyroxene* and glass; some partially resorbed, in clusters, some have embayed edges *clinopyroxene*: 5%, 0.2-1mm, commonly in glomeroporphyritic clusters with orthopyroxene, *plagioclase*, *spinel* and glass trapped between grains *orthopyroxene*: 3%, 0.2-0.8mm, anhedral-subhedral, clinopyroxene rims *spinel*: 3%, 0.05-0.2mm *biotite*: <1%, 0.4mm partially resorbed	extremely glassy

Sample no.	Rock type	Texture	Phenocrysts & microphenocrysts	Groundmass
AV205	andesite	porphyritic	*plagioclase*: 10%, 0.1-2.5mm, subhedral-euhedral, some have reaction rims, minor oscillatory zoning *clinopyroxene*: 7%, 0.1-1mm, anhedral-subhedral, some in clusters with orthopyroxene, plagioclase and spinel *orthopyroxene*: 5%, 0.05-0.8mm, subhedral-euhedral *spinel*: 3%, 0.02-0.1mm, minor embayed edges	glassy
AV207	andesite	porphyritic	*plagioclase*: 7%, 0.1-1mm, subhedral-euhedral *clinopyroxene*: 5%, 0.04-0.6mm, anhedral-subhedral *orthopyroxene*: 3%, 0.05-0.8mm, subhedral *spinel*: 3%, 0.02-0.3mm, some embayed edges *hornblende*: 2%, 0.05-0.6mm, subhedral-euhedral, reaction rims	fine grained to glassy
AV211	andesite	porphyritic	*plagioclase*: 10%, 0.15-1mm, subhedral-euhedral, sometimes in clusters with other grains *clinopyroxene*: 5%, 2mm, subhedral-euhedral, commonly in glomeroporphyritic clusters *hornblende*: 2%, 0.2-1.5mm, subhedral-euhedral, opacitic reaction rims *spinel*: 2%, 0.2mm some with embayed edges	very glassy
AV213	andesite	porphyritic	*plagioclase*: 20%, 0.02-1.5mm, subhedral; inclusions of clinopyroxene and glass *clinopyroxene*: 5%, 0.2-0.6mm, anhedral-subhedral *orthopyroxene*: 7%, 0.2-0.8mm, anhedral, partially resorbed, in clusters with clinopyroxene *spinel*: 3%, 0.1-0.4mm, embayed edges	fine grained
AV214b	basaltic andesite	porphyritic	*plagioclase*: 1%, 0.2-0.6mm, subhedral-euhedral *clinopyroxene*: 5%, 0.15-2.5mm, subhedral-euhedral, commonly in glomeroporphyritic clusters with glass trapped between grains *olivine*: 2%, 0.4-0.8mm partially resorbed *spinel*: 2%, 0.2mm some with embayed edges	fine grained to glassy

Sample no.	Rock type	Texture	Phenocrysts & microphenocrysts	Groundmass
AV216	andesite	porphyritic	*plagioclase*: 10%, 0.1-2mm, minor oscillatory zoning, inclusions of glass *clinopyroxene*: 1%, 0.2mm, anhedral-subhedral, reaction rims *spinel*: 3%, 0.2-0.4mm some with embayed edges *hornblende*: 10%, 0.2-2mm, reaction rims, subhedral-euhedral, inclusions of plagioclase and clinopyroxene	fine grained to glassy
AV219	andesite	porphyritic	*plagioclase*: 7%, 0.2-1.5mm, partially resorbed *clinopyroxene*: 10%, 0.1-0.6mm, anhedral-subhedral; commonly in clusters with spinel and sometimes plagioclase; partially resorbed *orthopyroxene*: 2%, 0.2-0.6mm anhedral-subhedral *spinel*: 2%, 0.05-0.2mm embayed edges *hornblende*: 3%, 0.2-0.4mm totally resorbed and some with reaction rims *apatite*: <1%, 0.2mm, subhedral-euhedral	fine grained to glassy
AV223	andesite	porphyritic	*plagioclase*: 10%, 0.1-2mm, subhedral-euhedral, partially resorbed *clinopyroxene*: 5%, 0.2-0.6mm, anhedral-subhedral, sometimes in clusters with spinel and plagioclase *orthopyroxene*: 3%, 0.4-1mm, subhedral-euhedral *spinel*: 3%, 0.02-0.15mm, some with embayed edges	very glassy
AV225	andesite	porphyritic	*plagioclase*: 10%, 0.2-1.5mm, subhedral-euhedral, minor oscillatory zoning, partially resorbed *orthopyroxene*: 3%, 0.1-0.4mm, anhedral-subhedral *spinel*: 3%, 0.05-0.2mm *hornblende*: 2%, 0.4-1mm, partially resorbed	fine grained to glassy
AV227			*plagioclase*: 10%, 0.5-2.5mm, subhedral-euhedral *clinopyroxene*: 5%, 0.6-1.4mm, subhedral-euhedral *spinel*: 3%, 0.25mm *biotite*: <1%, 0.4mm, anhedral, partially to totally resorbed	fine grained containing plagioclase laths, clinopyroxene and interstitial glass

Sample no.	Rock type	Texture	Phenocrysts & microphenocrysts	Groundmass
AV231	andesite	porphyritic	*plagioclase*: 7%, 0.2-2mm, minor oscillatory zoning, some partially resorbed *clinopyroxene*: 5%, 0.2-4mm, subhedral-euhedral, some in clusters with *spinel* and *plagioclase* and glass trapped between grains *orthopyroxene*: 3%, 0.4-0.8mm, inclusions of *plagioclase* *spinel*: 2%, 0.05-0.2mm, some with embayed edges *hornblende*: <1%, anhedral-subhedral, reaction rims	fine grained to glassy consisting of fine plagioclase laths, clinopyroxene, and spinel
AV232	andesite	porphyritic	plagioclase: 7%, 0.5-3mm, subhedral-euhedral clinopyroxene: 7%, 0.1-2mm, subhedral-euhedral orthopyroxene: 2%, 0.05-1.5mm, subhedral-euhedral spinel: 2%, 0.2mm hornblende: 1%, 0.8mm, anhedral-subhedral biotite: <1%, 0.6mm	fine grained containing plagioclase laths, clinopyroxene and interstitial glass

APPENDIX 4

ELECTRON MICROPROBE ANALYSES OF MINERAL PHASES in the KADAVU ISLAND GROUP and NORTHERN HUNTER RIDGE ROCKS

Note. Traverse analyses across grains are recorded by analysis number, followed either by a 'C' or an 'R'. For example, for sample AV57 clinopyroxene phenocryst traverse, the analysis no. is 1C - 1R, indicating an analysis of the core (C) and the rim (R) with an analysis in between.

Table A4.1. Hunter Ridge olivine

Sample no.	2DR6-1												
Analysis no.	1	2	3	4	5	6	7	8	9	10	11	12	13
SiO2	40 98	41 63	40.73	40 61	40.76	41.46	40 57	41 27	41 08	41.51	41.33	40.89	40 69
Cr2O3	0 06	0.10	0 03	0.03	0 04	0 06	0.34	0.05	0.10	0.04	0.04	0.10	0.11
FeO	9.25	7 61	9 88	7 35	9 91	8.28	10.10	7.39	7.56	8.78	8.38	8.57	7 96
NiO	0.33	0.46	0.27	0 47	0 22	0 26	0 23	0.44	0 34	0.33	0.35	0.22	0.46
MnO	0 11	0.08	0.20	0 06	0 14	0.12	0.19	0.06	0.12	0.11	0.14	0.09	0.12
MgO	48.70	50.20	47.71	49.58	48 74	50.33	46.78	50.38	49.86	49.11	49 75	49.14	49.49
CaO	0.16	0.16	0 14	0.17	0 16	0.20	0.17	0.14	0.16	0.18	0.17	0.18	0.15
Total	99.60	100.24	98.95	98.32	99.97	100.71	98.38	99 75	99.22	100.06	100.16	99.19	98.98
Fo	90.37	92.16	89.59	92.32	89 76	91.55	89.19	92.39	92.16	90 89	91.36	91 09	91.72
Sample no.													
Analysis no.	14	15	16	17	18	19	20	21	22	23	24	25	26
SiO2	40.83	40.84	40.58	41.24	40.56	40.79	40.57	4036	41.47	41.24	40.94	41.11	4096
Cr2O3	0.09	0.05	0.15	0.12	0.03	0.05	0.11	0.10	0 05	0.17	0.24	0.16	0.63
FeO	8.09	9.03	9.28	7.34	8 28	7.52	7.71	8.32	8.20	8.86	9.75	9.28	8 70
NiO	0.25	0.30	0.35	0.29	0.22	0.42	0.31	0.33	0.42	0.35	0.16	0 19	0.37
MnO	0.21	0.18	0.15	0.00	0.11	0.05	0.12	0.12	0.13	0.10	0.14	0.13	0.19
MgO	49.75	48 54	48.65	50.50	49 30	49.44	49.67	49.01	50.23	49.03	48.79	49.28	49.30
CaO	0.19	0.13	0.15	0.13	0.18	0.15	0.14	0.20	0.17	0.19	0.18	0.19	0.17
Total	99.41	99.06	99.30	9962	98.69	98.42	98.63	98.43	100 67	9993	100.20	100.34	100.32
Fo	91.64	90.55	90.33	92.46	91.39	92.13	91.99	91.30	91.61	90.80	89.91	90.44	90.99
Sample no.													
Analysis no.	27	28	29	30	31	32	33	34	35	36	37	38	39
SiO2	41.30	40.53	40.82	41.13	40 67	40.25	40.20	4050	40.39	40.25	40.25	39.98	39 52
Cr2O3	0.10	0.33	0.13	0 09	0 21	0.07	0.12	0.23	0 05	0.03	0.11	0.05	0.05
FeO	7.41	8.66	8.62	9.34	7 61	8.37	9.29	10.12	9.60	9 15	8.86	10.98	10.99
NiO	0.39	0.28	0.21	0.31	0.35	0.32	0.34	0.25	0.19	0 39	0.34	0.14	0.21
MnO	0.11	0.13	0.13	0.13	0.09	0.11	0.10	0.13	0.11	0.17	0.14	0.20	0.16
MgO	50.27	48.33	49.06	48.96	49.68	48.76	47.85	48.42	47.87	48.88	49.26	47 51	47 36
CaO	0.14	0.14	0.16	0.15	0.15	0.15	0.17	0.17	0 18	0.18	0.17	0 21	0 21
Total	99.72	98.40	99.13	100.10	98 76	98.03	98.06	99.82	98.39	99.03	99.13	99.07	98.50
Fo	92.36	90 87	91 02	90.33	92 08	91 21	90.18	89.50	89 88	90.50	90.83	88 52	88.48
Sample no.													
Analysis no.	40	41	42	43	44	45	46	47	48	49	50	51	52
SiO2	40.07	39 89	39.84	39.86	39.73	39 71	39 88	40.05	39.96	40.03	39.92	40.03	39 72
Cr2O3	0.10	0.05	0.04	0.03	0.03	0.06	0.03	0.11	0.06	0.11	0.10	0.06	0 06
FeO	9.69	9.88	11.00	1062	10.08	10.93	11.16	11 01	11 18	1062	10.06	11.09	10.73
NiO	0.33	0.27	0.20	0.28	0.28	0.18	0.24	0.20	0.14	0.26	0.26	0.17	0.16
MnO	0.20	0 08	0.11	0.23	0 17	0.19	0.15	0.16	0.24	0.17	0.17	0 22	0.21
MgO	48.51	48.50	47.57	48.01	48.14	47.38	47 48	47.32	47.26	48 17	48.12	47 53	47 40
CaO	0.16	0 17	0.19	0.19	0 19	0.21	0 22	0.20	0 22	0.21	0 20	0 21	0.18
Total	99.06	98.84	9895	99.22	9861	98.65	99 15	99.04	99.04	99 57	98.81	99 31	98 46
Fo	89.92	89 74	88.51	88.95	89.49	88.53	88 35	88.45	88.28	88.99	89 50	88 42	88.72
Sample no.													
Analysis no.	53	54	55	56	57	58	59	60	61	62	63	64	65
SiO2	40 14	40 44	39 93	40.28	40 32	40.16	40 04	40 27	40.43	40 49	39.72	40.42	39 72
Cr2O3	0.04	0 10	0 07	0.10	0.04	0 08	0.07	0 07	0 02	0 08	0.07	0 06	0 07
FeO	9.92	9 39	1088	9.18	9.25	9 34	8 79	9.22	9 59	9 28	11 35	8.	11 44
NiO	0.18	0.29	0.22	0.38	0 35	0 38	0.35	0 28	0 29	0.26	0.23	0 38	0.26
MnO	0.11	0 17	0.16	0.11	0.18	0.13	0.13	0.20	0.15	0 21	0.14	0 27	0 19
MgO	48.39	48 92	47.61	48.98	48 79	48.61	49 01	48.93	48 66	48.63	46.85	49 36	46 18
CaO	0.16	0.19	0 22	0.17	0 13	0.17	0.16	0.16	0 18	0.18	0.24	0.17	0.28
Total	98.95	99.49	99.09	99.21	99.06	98.87	9854	99.13	99.30	99 13	98.60	99 34	98 14
Fo	89 68	90.28	88.63	90.48	90.38	90.27	90.86	90.43	90.05	90 32	88.03	91 02	87 79

Sample no.													
Analysis no.	66	67	68	69	70	71	72	73	74	75	76	77	78
SiO2	39.80	40.05	40.06	40.40	40.18	40.31	39.88	40.07	40.27	39.83	40.24	40.00	40.27
Cr2O3	0.04	0.05	0.04	0.10	0.04	0.12	0.09	0.03	0.09	0.04	0.07	0.08	0.11
FeO	10.36	9.25	11.06	9.94	9.51	9.11	9.80	9.11	9.93	10.92	9.14	9.95	8.97
NiO	0.28	0.33	0.26	0.31	0.24	0.28	0.30	0.37	0.29	0.27	0.40	0.27	0.34
MnO	0.15	0.18	0.19	0.11	0.23	0.18	0.19	0.14	0.23	0.28	0.19	0.17	0.13
MgO	47.51	49.10	47.80	48.68	48.34	48.88	48.44	48.68	48.78	47.64	49.26	48.69	48.95
CaO	0.21	0.17	0.19	0.18	0.18	0.20	0.17	0.18	0.16	0.19	0.15	0.17	0.19
Total	98.35	99.12	99.58	99.72	98.72	99.07	98.87	98.57	99.74	99.16	99.44	99.34	98.96
Fo	89.09	90.44	88.51	89.72	90.06	90.53	89.81	90.50	89.75	88.60	90.57	89.71	90.68
Sample no.				DR8-2									
Analysis no.	79	80	81	1	2	3	4	5	6	7	8	9	10
SiO2	40.10	40.33	40.02	40.95	40.61	40.89	40.38	40.74	40.23	41.33	41.07	41.29	40.83
Cr2O3	0.04	0.03	0.03	0.06	0.08	0.10	0.02	0.12	0.06	0.07	0.08	0.14	0.05
FeO	9.76	8.79	10.32	9.33	7.32	7.62	9.78	8.48	10.88	7.35	8.64	6.98	9.69
NiO	0.13	0.37	0.14	0.16	0.29	0.21	0.16	0.19	0.14	0.29	0.20	0.37	0.36
MnO	0.16	0.18	0.21	0.20	0.04	0.15	0.11	0.14	0.22	0.10	0.12	0.12	0.14
MgO	48.47	49.18	48.21	49.09	49.84	50.31	48.14	49.26	46.85	50.47	49.83	50.42	49.05
CaO	0.21	0.16	0.21	0.24	0.16	0.18	0.20	0.11	0.22	0.17	0.14	0.16	0.20
Total	98.86	99.04	99.13	100.03	98.35	99.45	98.79	99.04	98.59	99.77	100.09	99.46	100.31
Fo	89.85	90.89	89.28	90.37	92.39	92.17	89.77	91.19	88.47	92.45	91.13	92.79	90.02
Sample no.													
Analysis no.	11	12	13	14	15	16	17	18	19	20	21	22	23
SiO2	40.45	41.42	40.70	40.72	41.01	41.18	41.11	40.89	40.70	41.31	40.80	41.54	41.43
Cr2O3	0.05	0.29	0.13	0.14	0.07	0.12	0.13	0.15	0.12	0.17	0.16	0.12	0.15
FeO	10.70	7.54	9.49	8.70	9.98	7.10	8.73	7.64	8.31	8.73	7.11	7.00	7.47
NiO	0.19	0.23	0.24	0.22	0.21	0.31	0.27	0.26	0.21	0.29	0.36	0.35	0.29
MnO	0.19	0.19	0.14	0.09	0.17	0.04	0.11	0.08	0.11	0.11	0.06	0.03	0.05
MgO	47.69	50.52	48.80	49.24	47.39	50.63	50.20	49.99	49.75	49.10	50.26	51.22	50.32
CaO	0.29	0.16	0.18	0.18	0.20	0.17	0.15	0.11	0.13	0.13	0.17	0.18	0.15
Total	99.55	100.35	99.68	99.29	99.03	99.55	100.70	99.12	99.32	99.83	98.91	100.43	99.86
Fo	88.82	92.27	90.16	90.98	89.43	92.70	91.10	92.10	91.43	90.93	92.65	92.88	92.31
Sample no.													
Analysis no.	24	25	26	27	28	29	30	31	32	33	34	35	36
SiO2	40.70	40.99	41.01	40.89	40.53	41.21	40.35	41.08	41.22	40.74	40.71	40.75	40.37
Cr2O3	0.22	0.25	0.23	0.11	0.13	0.17	0.12	0.12	0.15	0.21	0.09	0.06	0.19
FeO	8.30	9.14	7.45	6.95	9.90	7.53	11.12	7.06	7.57	7.47	8.10	8.02	9.32
NiO	0.19	0.28	0.19	0.35	0.16	0.21	0.19	0.21	0.25	0.26	0.25	0.30	0.20
MnO	0.09	0.13	0.05	0.15	0.05	0.07	0.21	0.08	0.18	0.22	0.09	0.11	0.12
MgO	49.57	49.39	50.06	50.47	48.25	50.59	47.05	50.70	50.11	49.96	49.68	49.55	48.34
CaO	0.17	0.13	0.19	0.15	0.18	0.18	0.30	0.14	0.19	0.17	0.15	0.16	0.28
Total	99.23	100.31	99.18	99.06	99.19	99.95	99.33	99.39	99.65	99.03	99.06	98.94	98.82
Fo	91.41	90.59	92.30	92.83	89.68	92.30	88.29	92.76	92.18	92.26	91.62	91.68	90.23
Sample no.					DR15-1								
Analysis no.	37	38	39	40	1	2	3	4	5	7	8	9	10
SiO2	40.08	40.98	41.28	40.70	39.75	39.44	40.00	40.50	39.70	40.02	39.57	40.52	39.92
Cr2O3	0.24	0.09	0.13	0.38	0.13	0.09	0.06	0.07	0.11	0.05	0.05	0.04	0.04
FeO	10.06	9.95	7.33	7.00	10.02	9.92	8.57	7.88	9.19	9.29	10.67	8.80	9.62
NiO	0.18	0.23	0.31	0.36	0.16	0.09	0.15	0.15	0.15	0.13	0.10	0.12	0.15
MnO	0.16	0.18	0.09	0.06	0.13	0.16	0.13	0.08	0.21	0.17	0.17	0.14	0.17
MgO	47.85	48.49	50.17	50.35	49.26	48.61	49.32	49.40	49.33	49.49	48.26	49.03	49.04
CaO	0.19	0.16	0.18	0.14	0.24	0.23	0.21	0.15	0.21	0.21	0.21	0.19	0.17
Total	98.76	100.07	99.48	98.99	99.68	98.53	98.42	98.43	98.89	99.35	99.02	98.85	99.10
Fo	89.45	89.68	92.43	92.77	89.76	89.73	91.12	91.78	90.53	90.47	88.97	90.85	90.08

Sample no.										
Analysis no.	11	12	13	14	15	16	18	19	20	22
SiO2	40.05	40.66	40.31	39.83	39.83	39.95	40.11	38.91	39.55	39.26
Cr2O3	0.04	0.04	0.10	0.06	0.00	0.13	0.03	0.05	0.17	0.09
FeO	9.54	8.52	8.77	9.56	9.41	9.87	9.71	11.09	9.76	9.62
NiO	0.09	0.10	0.20	0.14	0.09	0.12	0.12	0.07	0.20	0.09
MnO	0.19	0.18	0.19	0.16	0.09	0.26	0.20	0.22	0.20	0.13
MgO	49.48	49.29	49.13	49.28	49.33	48.78	49.13	49.09	48.81	48.67
CaO	0.24	0.17	0.21	0.19	0.22	0.19	0.21	0.23	0.22	0.21
Total	99.62	98.96	98.91	99.22	98.98	99.31	99.51	99.65	98.91	98.08
Fo	90.23	91.15	90.90	90.19	90.33	89.80	90.02	88.75	89.91	90.01

Table A4.2. Hunter Ridge spinel

Sample no.	2DR6-1												
Analysis no.	1	2	3	4	5	6	7	8	9	10	11	12	13
SiO2	0.04	0 05	0.06	0 03	0.00	0.04	0.00	0.07	0 03	0.00	0.03	0.07	0 08
TiO2	0.16	0 12	0.24	0.26	0.16	0.18	0.20	0.20	0 22	0.12	0.15	0.14	0.08
Al2O3	9 08	8.30	8.90	8.27	8.26	9.10	8.22	8.59	8 78	8.40	8.27	8.23	7 59
Cr2O3	57.57	59 25	55.38	57 61	57 52	54.88	56.18	55 21	55.62	58.62	59.12	59.08	60 48
FeO	18.57	18.17	21 00	18.92	21 61	21.06	20.71	20 45	20.77	17.79	17.03	16.37	16.58
MnO	0.29	0 22	0.18	0 15	0.21	0.15	0 26	0 17	0.22	0.18	0.23	0.11	0.20
NiO	0 17	0.25	0 05	0.13	0.14	0.16	0.03	0.12	0 05	0.17	0.02	0.17	0.11
MgO	14.01	12.85	12.12	12.93	12.22	12.60	12.10	12.90	12 10	13.16	12.58	14.64	13.37
Total	99.90	99.20	97 92	98.24	100 12	98.15	97.70	97 72	97 79	98.43	97.43	98.80	98.50
Mg#	67.8	63.4	60	63.8	59.8	62.2	60.4	63 9	60.1	64.9	62.8	71 2	66.2
Cr#	80.9	82.7	80.6	82.3	82.3	80.1	82.1	81.1	80 9	82.4	82.7	82 8	84.2
Fe#	36.1	27.3	31.5	31	32 2	35.2	31.7	36.5	31.2	28.9	22	35 6	26 7
Fo (host olivine)	91.58	90.33	89.71	91.30	90.80	89.91	89 39	90 44	89.86	90.99	91.09	92.36	90.87
fO2	1.50	0.80	1.27	1.33	1.57	1.45	1.18	1.54	1.27	0.98	0 54	1.38	0.66
Temp(°C)	1173	1152	1108	1100	1052	1144	1143	1163	1100	1143	1081	1221	1195

							DR8-1						
	14	15	16	17	18	19	1	2	3	4	5	6	7
SiO2	0.04	0.03	0.08	0.05	0 03	0.06	0.08	0.08	0.07	0.04	0.06	0.06	0.08
TiO2	0.16	0 18	0.09	0.14	0 13	0.12	0. 21	0.18	0.17	0. 27	0. 21	0.17	0.14
Al2O3	7.99	8.15	8.21	7.89	8.24	7 03	10.12	12.52	9.61	11.96	9.72	7.97	7.67
Cr2O3	58.32	57.91	59.29	58.51	57.76	58.46	57.38	55.09	57. 20	54.75	58.00	57 65	59 41
FeO	19.07	18.59	17.63	17.67	21.59	20.48	19.80	17.03	20.98	20.71	18.46	24.70	22.10
MnO	0.09	0.12	0.21	0 25	0.15	0.15	0 29	0 25	0 16	0.17	0.16	0. 28	0 24
NiO	0.08	0.09	0.23	0 07	0.12	0 08	0 07	0.19	0 10	0.05	0.17	0.10	0.02
MgO	12.12	12.91	12.89	12.98	10.45	12.01	12.30	14.30	11.45	11.79	13.59	8 61	9.95
Total	97.86	97.98	98 63	97.57	98.48	98.39	100.25	99.64	99.74	99.75	100.35	99.54	99.60
Mg#	60.4	63.9	64	64.8	52.5	59.9	59.6	68.2	56 1	56.8	65.3	43 6	49 8
Cr#	83	82.6	82.8	83.2	82.4	84.8	79.1	74.6	79 9	75.4	80	82 9	83.8
Fe#	25.6	30	26.6	28.9	22	30.2	24.9	30.3	23.9	23	30.1	19 6	19.1
Fo (host olivine)	91.99	91.02	92.08	91 21	90.18	89 50	91.13	92.27	90 16	90.98	91.10	92.10	90 93
fO2	1.29	1.17	1.14	1 05	0 95	1.09	1 07	1.25	0.95	1 05	1.12	1.63	0 96
Temp(°C)	983	11 20	1046	1132	939	1147	989	1063	982	917	1125	742	871

	8	9	10	11	12	13	14	15	16	17	18	19	20
SiO2	0.08	0.07	0.06	0.03	0.04	0.02	0 07	0 07	0.07	0.05	0.07	0.06	0 07
TiO2	0.11	0 10	0.19	0.21	0.17	0 14	0. 29	0.13	0.18	0 41	0.11	0 13	0.23
Al2O3	10 54	10 08	10.46	8.60	9 88	10.48	13 60	10 94	10 56	8.76	10.96	11.03	10 72
Cr2O3	58.64	59.24	57 95	59.35	59 66	58 27	52.35	57 29	58 19	54.93	57 76	57.48	57 86
FeO	15 40	15 35	16.72	18.61	15 27	15 01	22 61	16.60	16 65	24.52	16.02	16 51	17 08
MnO	0.21	0 23	0.12	0 22	0 20	0.12	0. 24	0 21	0.21	0 22	0.14	0.31	0 14
NiO	0.10	0 13	0.12	0.06	0 19	0 20	0.11	0 14	0 06	0.10	0.03	0 04	0 07
MgO	14.08	14 60	14.29	12 54	14.67	14 35	11 24	14 36	13.86	10 46	14. 26	14 17	1354
Total	99.17	99.80	99.92	99 62	100 07	98 60	100.50	99.73	99 78	99 45	99.35	99 74	9971
Mg#	68	70 2	68.3	61.3	70 3	69 5	53 8	68 8	66 5	51 6	68.3	68	64.9
Cr#	78 8	79.7	78 8	82 2	80.2	78 8	72	77 8	78 7	80.8	77 9	77 7	78.3
Fe#	23 5	27.9	29 2	24 1	27 6	25 3	23 9	30.1	25 4	28 8	26 4	27 9	23 7
Fo (host olivine)	92.65	92.88	92.31	90.59	92.30	92 83	89 68	92 30	91.70	88.29	92.76	92 18	92 26
fO2	0.75	1.04	1 14	0.73	0.82	0 85	1 04	1.17	0 77	1. 27	1.04	1.02	0 91
Temp(°C)	1055	1102	1094	1078	1159	1077	906	1105	1092	1013	1050	1084	1011

								DR15-1			
	21	22	23	24	25	26	27	1	2	3	4
SiO2	0 05	0 01	0 08	0 00	0 06	0 07	0 09	0 05	0.02	0 05	0 05
TiO2	0 16	0 11	0 28	0 30	0 23	0 17	0 17	0 45	0 28	0 15	0.35
Al2O3	9 69	9 39	8 59	11 31	9 87	10.62	9 15	14 00	10.90	8.69	6 36
Cr2O3	58 56	58.95	57 06	55 04	56 04	58 08	61 40	45.89	53 87	58.38	55.23
FeO	16.93	16 60	22 87	21 95	20 23	16 54	14 50	26 53	21 49	18 18	24.34
MnO	0 03	0	0 29	0 17	0 14	0.10	0 15	0 29	0.27	0 25	0 17
NiO	0.11	0.12	0.09	0 12	0.11	0.12	0 20	0.09	0.20	0 18	0.01
MgO	13 40	13 46	9.91	11 41	12 40	14.23	13 61	12.18	11.82	13 04	11.87
Total	98 93	98 88	99 16	100 29	99 07	99.92	99.28	99 49	98 83	98 91	98.37
Mg#	65	65.8	49 6	55.1	60 5	67 9	66 4	58.0	58.0	64.2	59.0
Cr#	80 2	80.8	81.6	76.5	79.2	78.5	81 8	68 7	76.8	81.8	85.3
Fe#	24.1	25	21.5	24.4	28 6	27.6	15 2	40.8	29.0	28 8	39.5
Fo (host olivine)	91.62	91 68	90.23	89.45	89 68	92.43	92.77	89.73	91.12	91.78	90.90
fO2	0 75	0.77	1.08	0.94	1.00	1 07		2.19	1.54	1.24	2 21
Temp(°C)	1073	1096	887	973	1099	1073	1023	996	951	1068	1072

23

Table A4.3. Hunter Ridge pyroxene

OPX

Sample no.	DR8-2					DR9-1							
Analysis no.	1	2	3	4	5	1	2	3	4	5	6	7	8
SiO2	55 40	55 65	55 52	55 16	55.78	52.98	53.34	52.66	53.83	53.27	53.26	52 86	53.22
TiO2	0 09	0 08	0 08	0 12	0.06	0 27	0 30	0 29	0 17	0.36	0.31	0 33	0.34
Al2O3	1 25	1.29	1 35	1 39	0 97	1 07	0.91	1.28	0.76	0.78	0.78	1.06	0.99
FeO	11.31	1077	11.25	11 29	11 25	18 22	17.48	16 45	16.41	18.10	18.36	18.05	18.75
MnO	0.35	0.24	0 29	0.28	0.34	0.68	0.75	0 70	0.56	0.69	0.65	0.63	0 83
MgO	29.76	30.47	29 69	29.66	29.83	24.36	25 04	25.91	26.07	24.67	24.65	24.51	24.35
CaO	2.09	2 01	2.10	2 06	1.96	1.70	1.72	1.71	1.56	1.65	1.58	1.94	1.56
Na2O	0.03	0.01	0.02	0 01	0.02	0.04	0.02	0.01	0.02	0.03	0.03	0.04	0.02
Cr2O3	0.22	0.18	0.21	0.25	0.14	0.00	0 00	0.04	0.00	0.00	0.00	0.00	0.00
Total	100 50	100.71	100.51	100.22	100.35	99.31	99.55	99.04	99.39	99.54	99.62	99 41	100.06
Mg#	82.43	83.45	82.47	82.40	82.54	70 44	71.86	73.74	73.91	70 85	70.53	70.77	69.83
Enstatite	79.14	80.27	79.15	79.14	79.45	68.03	69.41	71.25	71.64	68.51	68.31	68.04	67.67
Ferrosilite	16 87	15.92	16.83	16.91	16.80	28.56	27.18	25.37	25.29	28.20	28.54	28 10	29.23
Wollastonite	4.00	3.81	4.02	3.95	3.75	3.42	3.42	3.38	3.08	3.30	3.15	3.86	3.11

Sample no.			DR10-4		DR12-5			DR16-3				DR16-6	
Analysis no.	9	10	1	2	1	2	3	1	2	3	4	1	2
SiO2	53.04	52.77	52.49	52.80	52.38	53.51	53 01	52 54	52.72	52 30	54.33	53 07	53.06
TiO2	0.36	0.31	0.22	0.26	0.28	0.16	0.16	0.29	0.25	0.22	0.32	0.21	0.27
Al2O3	0.98	1.06	1 28	0.68	0 98	1 27	1.28	0.77	1.09	1.13	0.94	0.73	0 70
FeO	18.48	18.29	16.23	17.33	17.86	13.98	13.93	17.71	15.78	17.17	16.07	18.27	18.26
MnO	0.78	0.77	0.53	1.11	0.66	0.43	0.44	0.79	0.57	0.64	0.67	0 58	0.53
MgO	24.30	23.88	25.50	24.88	24.71	28.00	28 12	25.30	25 94	25.23	25.24	24.51	24.34
CaO	1.80	2.01	1.90	1 29	1.80	1.73	1.69	1.62	1.71	1.93	1.65	1.63	1.66
Na2O	0.03	0.05	0.05	0 02	0.06	0.04	0.04	0.03	0.06	0.04	0.04	0 03	0 02
Cr2O3	0.00	0.00	0.03	0 01	0.00	0.06	0.05	0 03	0.04	0 04	0.01	0 07	0.00
Total	99.78	99.13	98 23	98.38	98.74	99 17	98.72	9908	98 15	98.70	99.27	99.09	98 83
Mg#	70 09	69.95	73 69	71 90	71 15	78 12	78.25	71 81	74.56	72.37	73.69	70.52	70.38
Enstatite	67 58	67.11	70.89	70.02	68.60	75.50	75.69	69.52	72.01	69 60	71.22	68 23	68.04
Ferrosilite	28 83	28.84	25.31	27 37	27.81	21.15	21 04	27 29	24 57	26 57	25.43	28 52	28 63
Wollastonite	3.59	4.05	3.80	2.61	3 59	3.35	3.27	3.20	3 42	3.83	3.34	3.25	3.34

CPX

Sample no.				DR8-2									
Analysis no.	3	4	5	1	2	3	4	5	6	7	8	9	10
SiO2	53 00	52 78	53.16	52.98	52.97	53.29	53 00	53.15	52 88	53.14	53.03	52 82	52.62
TiO2	0.26	0 29	0.21	0.16	0.13	0.15	0.10	0.16	0.15	0.16	0.13	0 20	0 14
Al2O3	1.33	0.95	0 79	1 66	1 67	1 57	1 73	1.71	1 79	1 75	1.87	2 04	1 88
FeO	16.93	18 33	16.56	6 06	6.00	5 81	6 04	6.89	6 16	6.27	5 85	6.03	5.80
MnO	0.52	0 63	0 47	0 25	0 23	0.19	0 11	0.26	0 25	0 24	0 17	0.16	0 22
MgO	25 10	24.18	25 29	17 75	18 10	18 00	17.69	18 59	1802	18 17	17 94	17 72	17.59
CaO	1.69	1 73	1 63	20 60	20 66	20.71	20 36	19.31	20 05	20 13	20.50	20 69	2065
Na2O	0.03	0.03	0.02	0.15	0.14	0 13	0.14	0.13	0 15	0.13	0 15	0 14	0 15
Cr2O3	0 00	0 00	0.00	0.21	0.30	0.28	0 16	0.23	0 31	0 23	0 37	0 37	0.38
Total	98 85	98 91	98.13	99 81	100.19	100.12	99 33	100 43	99.76	100 22	100 01	100.17	99 43
Mg#	72.55	70.16	73.14	83 93	84 32	84 67	83 92	82.78	83 90	83 79	84.55	83.97	84.38
Enstatite	70.09	67 73	70.75	49 37	49.84	49.80	49.53	5116	50 21	50 26	49.91	49.26	49.29
Ferrosilite	26.52	28.80	25.98	9 45	9.27	9.02	9 49	1064	9 63	9 72	9.12	9.40	9.12
Wollastonite	3.39	3 47	3 27	41 18	40 89	41 18	40.98	38.20	40 16	40 02	40 97	41 34	4158

Sample no.								DR9-2					
Analysis no.	11	12	13	14	15	16	17	1	2	3	4	5	6
SiO2	53 20	53.08	53 27	53 07	52.86	53 01	52.36	53.26	53 47	51.25	50.73	51.22	51.15
TiO2	0 16	0 12	0 13	0.11	0 15	0.13	0 20	0.54	0.48	0.56	0.61	0.43	0.53
Al2O3	2 00	1 65	1 66	1.59	2.17	1.88	2.48	1.72	1.62	1.69	2.16	1.76	1.85
FeO	6.05	6 00	5 88	5 93	4 93	6.03	7.00	8.72	8 73	9.44	9.38	8.88	9.14
MnO	0 20	0.19	0 25	0 18	0 17	0.20	0 23	0.51	0 41	0.36	0.36	0.27	0.32
MgO	17.81	17.97	17.75	17.98	17.82	17.88	17.54	15.56	15.64	15.04	14.82	15.09	14.99
CaO	20 39	20 67	20.98	20 72	21 45	20.52	19.97	19.54	19.25	20.51	20.71	20 79	20.73
Na2O	0.16	0 14	0.15	0.16	0.13	0.14	0.15	0.34	0.32	0.33	0.35	0.29	0 33
Cr2O3	0 39	0.30	0.32	0.30	0.67	0.36	0.31	0.00	0.00	0 00	0.00	0.03	0.01
Total	100.36	100.13	100 40	100.05	100.35	100.15	100.23	100.19	99.93	99.20	99.12	98 76	99.05
Mg#	84.00	84.23	84.33	84.38	86.57	84.09	81.71	76.08	76.15	73.96	73.80	75.19	74.51
Enstatite	49 68	49.66	49.14	49.67	49.49	49.66	48 97	45.11	45.50	42 89	42.39	43.10	42.81
Ferrosilite	9.47	9.30	9.13	9.19	7.68	9.40	10 96	14.18	14.25	15.10	15.05	14.22	14.64
Wollastonite	40 86	41.05	41.74	41.14	42.83	40.95	40.07	40.70	40.25	42.02	42.57	42.68	42.55

Sample no.	DR10-4												
Analysis no.	1	2	3	4	5	6	7	8	9	10	11	12	13
SiO2	50.28	50.26	50.72	51.79	51.54	51.87	50.54	50.38	50.13	50.28	52.64	50.55	51.33
TiO2	0.49	0.37	0.44	0.29	0.19	0.24	0.50	0.50	0.58	0.37	0.12	0.47	0.48
Al2O3	2.24	2.93	2.08	2.08	1.99	2 01	2.10	1.77	2.32	2.79	1.09	2.30	2.20
FeO	10.18	8 86	9.52	7.45	5.56	5.43	9.71	10.42	9.74	7.61	3.91	9.72	10.54
MnO	0.39	0.26	0.59	0.34	0 18	0.24	0 33	0.21	0.29	0.27	0.13	0.41	0.38
MgO	15.75	15.74	15.35	17.23	17.53	18.39	15 62	15.24	15.77	16.10	18.28	15.99	15 65
CaO	18.48	19.66	19.43	19.54	21.14	19.35	19.29	19.28	19.21	20.47	21.69	18.60	18.00
Na2O	0.43	0.40	0.33	0.33	0.27	0.28	0.38	0.41	0.37	0.24	0.27	0.46	0.36
Cr2O3	0 06	0.26	0.00	0.25	0.24	0.56	0.00	0.00	0.00	0.19	0.52	0.11	0.00
Total	98.30	98.73	98.46	99.30	98.64	98.36	98.45	98.21	98.41	98.31	98.66	98.62	98.96
Mg#	73.39	75 99	74.19	80 47	84.90	85.79	74.14	72.28	74.27	79.05	89.30	74.57	72.58
Enstatite	45.34	45.17	4429	48.60	48.91	52.03	44.71	43.62	45.00	45.89	50.70	45.93	45.37
Ferrosilite	16.44	14.27	15.41	11.79	8.70	8.62	15.59	16.73	15.59	12.17	6.08	15 67	17 14
Wollastonite	38.22	40.56	40.30	39 60	42.39	39 36	39 69	3965	39.41	41.94	43 23	38.41	37 50

Sample no.						DR12-5							
Analysis no.	14	15	16	17	18	1	2	3	4	5	6	7	8
SiO2	51.78	51 73	52.74	51.99	51 99	51 26	50.98	50.98	50.81	51 40	50.38	50.26	5102
TiO2	0 43	0.47	0 25	0 47	0.36	0.39	0.31	0.37	0.43	0 38	0.40	0.55	0.47
Al2O3	2.14	1.99	2 02	1.82	2.23	2.05	2 26	2 20	1.88	2.09	2.33	2.38	1 69
FeO	9.92	9 61	5 37	10 43	8 18	9.40	8 06	8.12	9 81	9.40	10.14	10.13	9 66
MnO	0.25	0 33	0.22	0.41	0 22	0.28	0.25	0 20	0 23	0.31	0.33	0 34	0 34
MgO	15.68	15.43	18 71	15.37	16.29	16 51	15 91	16 69	15 24	16 25	15 93	14.92	15 55
CaO	18 27	19.16	19.23	18.15	19.51	18.55	20 29	19.63	19 87	19 16	18 64	19.51	19.89
Na2O	0.37	0 34	0 22	0.30	0 30	0 30	0.32	0 35	0.28	0 38	0 31	0 34	0 30
Cr2O3	0.06	0.05	0 49	0.00	0 07	0.09	0.05	0 10	0.00	0.15	0.04	0.04	0 02
Total	98 89	99.12	99.24	98.93	99.15	98.84	98.43	98.63	98 55	99.51	98.51	98 47	98.94
Mg#	73.80	74 10	86 14	72.43	78.02	75 81	77.87	78.56	73.46	75.50	73.70	72 43	74 15
Enstatite	45.61	44.60	52.65	44.85	46.68	47.03	45.44	47 21	43.50	46.05	45.50	43 10	44 09
Ferrosilite	16.19	15 59	8.47	17 07	13 15	15 01	12.91	12.89	15.72	14 94	16.24	16 41	15.37
Wollastonite	38 21	39 81	38.89	38 08	40.17	37 97	41 65	39 90	40 78	39 01	38 26	40.49	40 53

Sample no.									DR15-1				
Analysis no.	9	10	11	12	13	14	15	16	1	2	3	4	5
SiO2	50 96	50 72	51 40	51 98	51 92	52 19	51 62	51.90	51 88	50 37	52.64	51.76	50.78
TiO2	0 39	0 42	0 32	0 28	0.44	0 41	0 44	0.48	0.26	0 42	0.12	0 23	0.38
Al2O3	2 11	1.76	2 33	2.28	1 78	2.03	1.95	1 81	2.06	3 05	0.92	1.87	2.72
FeO	8 72	10 08	7 87	7 07	10 05	8 94	10 30	9 81	5 44	7 00	5.96	5.03	7 06
MnO	0 29	0.29	0 33	0 33	0.38	0.22	0 45	0.41	0.12	0 23	0.16	0.16	0 16
MgO	16.10	15.12	17 03	16.83	14.93	15.98	15 00	15.32	17.92	16 22	18.58	17.60	17 04
CaO	19 30	19 96	19.45	19 61	19 04	18 62	19 26	19.20	21 06	21 16	20 26	21.35	20.55
Na2O	0.37	0 30	0 36	0.25	0.28	0.33	0.29	0.30	0 23	0 21	0.14	0.17	0.22
Cr2O3	0 21	0.00	0.22	0 28	0.02	0.10	0.01	0 01	0.63	0.24	0 19	0.63	0.20
Total	98.45	98 65	99 29	98.91	98 84	98 80	99.33	99.23	100 02	99 30	99.31	99.14	99.43
Mg#	76.69	72.79	79 42	80.94	72 59	76 12	72 19	73.58	85 45	80.51	84.74	86 18	81 15
Enstatite	46 17	43.05	48.08	48.25	43.59	46 49	43.33	44.25	49 63	45 88	50.92	49.20	47.63
Ferrosilite	14.03	16.09	12.46	11.36	16.46	14 59	16.69	15.89	8.45	11.11	9.17	7.89	11.07
Wollastonite	39.79	40 85	39.46	40.39	39.95	38.93	39.99	39.86	41 92	43 01	39.91	42.91	41.30

Sample no.													
Analysis no.	6	7	8	9	11	12	13	14	15	16	17	18	19
SiO2	52.74	51.78	53.12	52.18	51.62	51.58	51.93	52.42	52.62	49 77	52.11	52.72	53.55
TiO2	0.14	0.23	0.11	0.24	0.28	0.14	0.19	0.17	0.19	0 46	0.22	0.22	0.15
Al2O3	0 96	1 92	1.05	1.90	2.15	1.70	1.82	1.55	1.29	3.30	1.87	2 07	1.30
FeO	5 58	4.76	4.97	4.72	5.10	4 41	4.02	4.13	4.46	7.84	4.38	4 86	5 95
MnO	0 23	0 09	0.24	0.04	0.13	0.11	0 27	0 13	0 25	0 20	0.13	0.12	0.25
MgO	18.65	17.38	19 08	17 47	16.92	18.15	17 76	18.54	17.82	16 78	17.89	17.20	18 78
CaO	20.08	21.53	20.29	21.71	22.22	20 81	21.49	20.98	21 91	19 45	21.54	20.97	19 17
Na2O	0 13	0 20	0.18	0.21	0.22	0.20	0.26	0.23	0 18	0.22	0.24	0.18	0.11
Cr2O3	0.26	0.49	0.28	0 87	0 38	1.00	1 02	1 15	0.35	0 09	0 96	0 72	0 14
Total	99 08	98 36	99.30	99 34	99.01	98 09	98.76	99 29	99 06	98.11	99 33	99.0	99.39
Mg#	85 62	86.69	87.25	86.83	85.54	88 02	88.73	88 89	87.69	79.25	87 92	86 33	84.91
Enstatite	51 50	48.92	52.35	48 91	47.33	51.02	50.08	51.59	49 41	47.73	49.93	49.15	52.32
Ferrosilite	8.65	7.51	7 65	7 42	8.00	6.95	6 36	6.45	6 93	12.50	6 86	7 78	9.30
Wollastonite	39 85	43 57	40.00	43.67	44.67	42 03	43 56	41.96	43 66	39 77	43 21	43.07	38.38

Sample no.								DR16-3					
Analysis no.	20	21	22	23	24	25	26	1	2	3	4	5	6
SiO2	53.16	53 45	53.15	52 73	53.22	52.03	52.13	51.06	52.33	50 72	51 37	50.46	52 03
TiO2	0 24	0 17	0 23	0.21	0.17	0 28	0.39	0 40	0 27	0 36	0 48	0 36	0 35
Al2O3	1 84	1.46	2.10	1 77	1 40	2.56	2 87	2 25	1 55	2.69	1 52	3 10	1.93
FeO	4.65	7 15	5 12	4.23	3 87	6.49	7 04	7 09	4.07	6 26	8 68	7 43	7 10
MnO	0.18	0 32	0 07	0 19	0 07	0 25	0.15	0 27	0 07	0 23	0 49	0 31	0 18
MgO	17 48	18.32	17.65	17 85	18 11	17 04	16.92	16.99	18.48	16 75	15 63	16 08	17.50
CaO	20 98	18 88	20.68	20 90	20.76	20.20	20 17	19 48	20 41	20 80	20 28	20 50	19 43
Na2O	0.21	0 18	0.13	0 19	0 21	0 21	0 19	0 34	0 26	0 24	0.39	0 27	0 32
Cr2O3	0.73	0 02	0 41	1.07	1 02	0 08	0 10	0 26	0.63	0 23	0 02	0 27	0.17
Total	99 45	99.96	99 55	99.12	98 84	99.14	99 95	98 13	98 06	98 29	98 84	98 77	99.00
Mg#	87 02	82.04	86.01	88 27	89 30	82.41	81 08	81.03	89 01	82.67	76.25	79 42	81.45
Enstatite	49 71	51 03	49 88	50 65	51 45	48.42	47 85	48 59	52 16	47.58	44 56	45 96	49.36
Ferrosilite	7 41	11 17	8 12	6 73	6 17	10 34	11.16	11 38	6 44	9 97	13 88	11 91	11 24
Wollastonite	42 88	37 80	42 00	42 62	42 38	41 24	40.98	40 03	41 40	42.45	41 56	42 13	39.40

Sample no.													
Analysis no.	7	8	9	10	11	12	13	14	15	16	17	18	19
SiO2	50.62	51.31	52.37	50 94	50 51	53.08	52.36	51.54	51.32	53.37	52.23	52.98	51.67
TiO2	0.40	0.27	0.19	0.46	0.38	0.17	0.39	0.50	0.38	0.29	0.40	0.20	0.55
Al2O3	2.84	2.69	1.97	3.16	2 80	1.86	2.68	2 04	3.02	1.75	2.69	2.01	1.85
FeO	7.33	4.78	4.45	6.49	7.16	4 15	6.50	9.67	7.55	6.74	6.85	4.28	9.20
MnO	0.15	0.07	0.18	0.04	0.21	0.13	0.16	0.27	0.14	0.19	0.22	0.07	0.38
MgO	16.21	17.30	17.61	16.59	16.81	18.22	16.73	15.51	16.23	17.71	16.41	17.51	15.19
CaO	20.73	21.94	21.71	20.41	20.22	20.40	19.97	18.97	19.71	19.31	19.99	21.20	19.67
Na2O	0.29	0 26	0.18	0.31	0.39	0.26	0.31	0.35	0.27	0.30	0.27	0.21	0.30
Cr2O3	0.08	0 30	0.31	0.15	0.14	0.83	0.18	0 00	0.19	0 21	0.08	0.49	0 01
Total	98.66	98.93	98.98	98.55	98.62	99.10	99.27	98.86	98.82	99.86	99.14	98.94	98.81
Mg#	79.76	86.58	87.58	82.00	80.71	88.67	82.11	74.08	79.30	82.40	81.03	87.94	74 64
Enstatite	46.03	48.39	49.31	47.53	47.54	51.74	48.17	44.86	46.87	50.07	47.40	49 82	44.05
Ferrosilite	11.68	7.50	6.99	10.43	11.36	6.61	10.50	15.70	12.23	10.69	11.10	6.83	14.96
Wollastonite	42.29	44.11	43.70	42.04	41.10	41.65	41.34	39.44	40.90	39.24	41.50	43.35	40.99

Sample no.			DR16-6			
Analysis no.	20	21	1	2	3	4
SiO2	52.16	51 94	50.45	50.39	50.62	50.50
TiO2	0.32	0.34	0.49	0.54	0.33	0.43
Al2O3	2 99	2 89	1.53	1.69	2.76	2.90
FeO	5.98	6.87	9.67	9.82	5.51	6.47
MnO	0.30	0.22	0.41	0.42	0 20	0.19
MgO	17.27	17.24	16.54	16 45	16 71	16.72
CaO	20.15	19 08	20 16	19.92	22.36	21.49
Na2O	0.24	0.39	0.31	0.27	0.21	0.23
Cr2O3	0.19	0 34	0.00	0.04	0.23	0.10
Total	99.59	99.30	99.56	99.53	98.92	99.03
Mg#	83.74	81.74	75.31	74.92	84.40	82.16
Enstatite	49.19	49.53	45.38	45.35	46.60	46.71
Ferrosilite	9.55	11.07	14.88	15.18	8.61	10.14
Wollastonite	41.26	39.40	39.75	39.47	44.79	43 16

Table A4.4. Hunter Ridge plagioclase

Sample no.	DR8-2					DR9-1		DR9-2					
Analysis no.	1	2	3	4	5	1	2	1	2	3	4	5	6
SiO2	45 92	46 13	46 50	47.23	47 88	56 23	55 43	55 83	55 49	55 68	55 01	56 42	55.28
Al2O3	33 30	33 69	33.16	32 72	32.28	26 68	27 03	26 53	27 18	26 50	27 53	26.93	27.27
FeO	0 54	0 56	0 57	0 57	0 54	0 55	0 63	0 70	0 65	0 65	0 60	0 60	0.59
MgO	0 15	0 12	0 14	0 17	0.17	0 06	0 06	0 08	0 05	0 06	0 06	0 06	0.06
CaO	18 05	18 39	17 90	17 31	16 99	9 74	9 99	9 27	9 52	9 12	9.75	9 21	9.64
Na2O	1.34	1 28	1.35	1 72	1 95	5.41	5.37	5 56	5 42	5 64	5.32	5 73	5.44
K2O	0 02	0 04	0 01	0 01	0 03	0 32	0.33	0 45	0 33	0 38	0.32	0.34	0.31
Total	99 31	100 21	99 62	99 74	99 82	98 98	9884	98 40	98 64	98.03	98.58	99.30	99 09
Albite	11 81	11 17	12.00	15.26	17 14	49.16	48 36	50 66	49 74	51 63	48.72	51 91	49.58
Anorthite	88 10	88 63	87.96	84 66	82 69	48.93	49 70	46 66	48.30	46 11	49 36	46 07	48.57
Orthoclase	0 09	0.20	0 04	0.08	0.16	1 92	1.94	2 68	1 97	2.26	1 92	2 03	1 86

Sample no.			DR10-4					DR12-2					
Analysis no.	7	8	1	2	3	4	5	1	2	3	4	5	6
SiO2	56 44	56.20	51.02	51.01	52.59	51.56	52.67	47.17	46 74	49 81	47.60	47.95	47.34
Al2O3	26.43	26 72	30.05	30.13	29.93	30.15	30.48	32.39	32 63	29 94	32.18	31 92	32.27
FeO	0.59	0.61	0.92	0.83	0.69	0.76	0.85	0.88	0.82	1.50	0.89	0.83	1.02
MgO	0.08	0.07	0.10	0.05	0.09	0 07	0.08	0.06	0.06	0.18	0.07	0 06	0.08
CaO	8.89	9.17	12.94	12.85	12.65	11 96	12 38	17.00	17.35	15.60	16.98	16.70	17.30
Na2O	5.73	5 70	4.27	4.17	3.90	4.61	4.24	1.84	1.74	1.92	1.96	2.02	1.73
K2O	0.41	0.36	0.08	0.10	0.09	0.09	0.09	0 02	0.02	0.18	0.06	0 03	0.02
Total	98.57	98 83	99 37	99.14	99.93	99.20	100.79	99.35	99.36	99.15	99.73	99 51	99.75
Albite	52.49	51 80	37.19	36.76	35 61	40.88	38 02	16.36	15.33	18 05	17.24	17.91	15 29
Anorthite	45.02	46.04	62.33	62.69	63.86	58.58	61.43	83.53	84.54	80.82	82.42	81.94	84.62
Orthoclase	2.48	2.16	0.48	0 56	0.53	0.54	0 56	0.11	0.13	1.14	0.35	0.15	0 09

Sample no.		DR12-8						DR15-4					
Analysis no.	7	1	2	3	4	5	6	1	2	3	4	5	6
SiO2	46.36	46 35	46.75	45 87	46.35	46.75	45.87	45 51	46 05	45.67	47.15	44.93	45 61
Al2O3	32.87	33.08	32 82	33.32	33.08	32.82	33 32	32 77	33 14	33 17	32.28	33.27	33 10
FeO	0 82	1.06	1 04	1.07	1.06	1.04	1.07	0 93	0 90	0 85	0.93	0 96	1 05
MgO	0.05	0 07	0.10	0 08	0.07	0.10	0.08	0.05	0.07	0.05	0.08	0.06	0 07
CaO	17.51	17 07	16 98	17 15	17 07	16.98	17 15	17 76	17.33	17.79	17 21	18 46	17 75
Na2O	1.53	1.48	1 69	1.41	1.48	1.69	1.41	1 43	1 45	1.41	1.77	1.15	1.37
K2O	0 01	0.05	0.01	0 02	0 06	0.01	0 02	0 00	0.03	0 04	0.01	0 01	0 01
Total	99.15	99 16	99 38	98.93	99.16	99 38	98 93	98 44	98 95	98.98	99.43	98.83	98.95
Albite	13.60	13 53	15 21	12.94	13.53	15 21	12.94	12.72	13.10	12.55	15 71	10 08	12 22
Anorthite	86.32	86.19	84.71	86 94	86.19	84 71	86 94	87 28	86 75	87.22	84.22	89.85	87 71
Orthoclase	0.08	0 28	0.08	0.12	0 28	0.08	0 12	0.00	0.15	0.23	0.08	0 06	0 07

Sample no.						DR16-6							
Analysis no.	7	8	9	10	11	1	2	3	4	5	6	7	8
SiO2	46 04	45 49	46 03	45 92	46.12	53 38	52.68	53 27	53 96	52 49	52.66	52.62	53 56
Al2O3	32 89	32 97	32 96	32.76	32.92	2777	2858	2788	27.77	2848	28.58	28 49	2835
FeO	0 91	0.79	1.09	0.95	0.92	0.62	0 70	0 66	0 62	0 67	0 72	0.59	0.54
MgO	0 07	0.05	0 07	0 05	0.06	0.06	0 08	0 07	0 08	0.08	0.05	0.07	0.06
CaO	17 55	17 68	17.35	17 38	17 59	11.52	12 55	11 75	11.30	12 18	11.87	12 12	11 26
Na2O	1 48	1.36	1.42	1 53	1.41	4.55	4 10	4 52	4 63	4.22	4.26	4.22	4 71
K2O	0.03	0 03	0 04	0 01	0.04	0.11	0 09	0.09	0 11	0.10	0.07	0.09	0 09
Total	98.98	98.37	98 96	98 59	99 07	98 01	98 77	98 24	98.48	98 22	98 20	98 19	98.57
Albite	13 21	12.22	12.86	13 76	12 64	41 39	36.99	40 83	42 29	38 28	39 20	38 45	42 86
Anorthite	86.59	87 60	86.89	86 18	87 10	57 94	62 51	58 62	57 02	61.14	60.39	61 04	56 58
Orthoclase	0 19	0 18	0 25	0 06	0 26	0 67	0 51	0 56	0 69	0 59	0 41	0 52	0 56

Table A4.5. Astrolabe Group olivine

Sample no.	AV185												
Analysis no.	1	2	3	4	5	6	7	8	9	10	11	12	13
SiO2	39 99	4030	4038	40 27	40 61	39 87	39.72	40 20	40 65	4089	40.57	40.42	40.26
Cr2O3	0.05	0.01	0 07	0.01	0.07	0 04	0.03	0.06	0 09	0.06	0.06	0.01	0.05
FeO	10 29	9.01	8 57	9 57	8 52	9 70	12 29	9.50	8.98	8.70	8.28	10.25	11 22
NiO	0 14	0.20	0.23	0.08	0.12	0 12	0 15	0.18	0.06	0 21	0.18	0.09	0.09
MnO	0 17	0.18	0.17	0.18	0.19	0.19	0.23	0.23	0.08	0.18	0.16	0.23	0.27
MgO	47.59	49.06	49.68	48.98	49 57	48.45	46.48	49 00	49.05	49.65	49.87	48.06	47.51
CaO	0.34	0.35	0.29	0.36	0.31	0 28	0 27	0.35	0.34	0.35	0.27	0.32	0.31
Total	9856	99 12	99.39	99.45	9938	98.64	99 17	99.52	99 25	100 03	99.40	99.38	99.70
Fo	89 18	90 66	91.18	90 12	91.21	89.90	87 08	90.19	90.68	91.05	91.48	89 32	88.30
Sample no.									AV186				
Analysis no.	14	15	16	17	18	19	20	21	1	2	3	4	5
SiO2	40.68	40.54	40.27	40.53	39.05	40.57	40.49	40.72	40.10	40.14	39.61	39.92	39.68
Cr2O3	0.03	0 04	0 01	0.09	0.03	0.01	0.07	0.06	0.01	0 00	0 04	0.06	0.03
FeO	9.11	9.59	9.25	8.79	13.83	8.96	9.13	8.70	9.89	9 70	10.00	9.87	10.28
NiO	0.19	0.15	0.18	0.17	0.08	0.19	0.16	0.16	0 13	0.13	0.17	0.19	0.16
MnO	0.12	0.18	0.17	0.15	0.27	0.18	0.20	0.21	0.18	0.05	0.10	0.19	0.17
MgO	48.73	48.63	48.84	48.86	44.64	49.23	49.04	49.60	48.58	48.92	48.66	48.63	48.23
CaO	0.30	0.30	0.35	0.37	0.26	0.33	0.29	0.34	0.32	0.36	0.28	0.27	0.27
Total	99.17	99.44	99.06	98.94	98.16	99.47	99.38	99.80	99.20	99.30	98.86	99.12	98.82
Fo	90.51	90.04	90.40	90.83	85.19	90.74	90.54	91.04	89.75	8999	89.66	89.78	89.32
Sample no.													
Analysis no.	6	7	8	9	10	11	12	13	14	15	16	17	18
SiO2	39.99	40.21	40.02	39.75	39.42	39.62	39.92	40.03	40.05	40.46	39.61	39.83	39.55
Cr2O3	0.00	0.03	0.02	0.03	0.01	0.02	0.06	0.02	0.06	0.04	0.08	0.06	0.04
FeO	10.02	9.52	10.11	10.21	10.04	10.65	10.54	10.18	10 34	9.97	9.99	11 89	14.43
NiO	0.09	0.11	0.14	0.19	0.10	0.19	0.24	0.10	0.15	0 11	0.16	0.16	0.15
MnO	0.08	0.15	0.14	0.13	0.20	0.28	0.20	0.26	0.31	0.19	0.21	0.23	0.29
MgO	48.87	48 79	4859	48.21	48.32	48.14	48.38	48.41	48.40	49.36	48 68	47.56	45.36
CaO	0.34	0.33	0.37	0 30	0.33	0.32	0 30	0.32	0.29	0 34	0.32	0.33	0.34
Total	99.40	99.14	99.38	98.81	98.42	99.22	99.64	99.30	99.59	100 46	99.05	100.05	100.16
Fo	89 68	90 13	89.55	89.38	89.56	88.96	89.11	89.44	89.30	89.83	89 67	87.69	84.86
Sample no.													
Analysis no.	20	21	22	23	24	25	26	27	28	29	30	31	32
SiO2	40.59	40 61	39.74	39.75	40.20	39.23	40.07	40.03	40.52	40.59	40.36	40.15	39.69
Cr2O3	0.01	0.04	0.15	0.11	0.23	0.17	0.07	0.06	0.07	0.04	0.04	0 14	0.22
FeO	10.23	10 03	9.80	11.29	10.29	14.85	10 09	9.85	10.20	9.89	10.11	9.67	9.97
NiO	0.10	0 13	0.13	0.17	0.19	0.17	0.13	0.18	0.17	0.13	0.10	0 12	0.13
MnO	0.18	0 13	0.15	0.33	0 19	0.25	0.27	0.15	0.18	0 16	0.17	0 24	0.10
MgO	49.27	4940	48.62	47.50	48.75	44 75	48.78	48.70	49.36	49.08	49.25	49.11	48.35
CaO	0.41	0 35	0.32	0.32	0.35	0.28	0.36	0 32	0 30	0 34	0 32	0.40	0.39
Total	100.79	100.68	98.91	99.48	100.19	99 71	99.75	99.29	100.79	100.25	100.34	99 83	98 84
Fo	89 56	89.78	8984	88 23	89.41	84.30	89 60	89 81	89 61	89.84	89 68	90.05	89.63
Sample no.													
Analysis no.	33	34	35	36	37	38	39	40	41	42	43	44	45
SiO2	40 05	40 39	40 22	40 11	39.72	39.97	39.93	40.53	4056	3925	39 39	4059	40.30
Cr2O3	0.02	0.08	0.04	0.06	0.13	0.12	0.10	0.11	0.03	0 04	0.04	0 03	0 00
FeO	10.12	9.98	9.79	11.47	13.50	12.62	13.34	10.80	11.60	14.26	12.93	10 02	10.08
NiO	0.15	0 15	0 14	0.13	0 10	0 01	0.14	0.17	0 14	0.12	0.10	0.15	0.16
MnO	0.18	0.13	0.09	0.16	0 30	0.35	0.29	0 08	0.21	0.44	0 26	0 26	0.13
MgO	49.06	49 03	49.02	48.13	46 29	47.06	46.33	48 66	48.48	44.49	45.31	49 05	48 89
CaO	0 36	0.34	0.29	0.34	0 37	0 33	0 30	0.33	0 30	0 27	0.33	0.36	0 31
Total	99.95	100.10	9959	100.40	100 42	100.45	100 42	100 69	101.31	9887	98.35	100.47	99 88
Fo	89.62	89 75	89.92	88.21	85.94	86 92	86.09	88.92	88.17	84.76	86 20	89 72	89 63

Sample no.													
Analysis no.	46	47	48	49	50	51	52	53	54	55	56	57	58
SiO2	40 30	40 01	3988	39 48	40 43	40 68	4050	39.12	38.99	3929	38.27	40.60	40.67
Cr2O3	0.00	0 06	0 03	0.03	0 02	0 02	0 03	0 04	0.04	0.05	0.06	0.05	0.10
FeO	10 19	10 03	11 20	14.16	10 21	10 04	10 04	13.25	14.69	16.09	18 45	10.03	10.16
NiO	0.16	0 14	0.14	0.07	0 10	0 16	0 12	0.14	0.15	0.08	0.15	0.12	0.08
MnO	0.19	0 12	0.14	0.32	0 23	0 21	0 16	0 33	0 32	0.37	0.38	0.14	0.15
MgO	49 02	48 62	47 46	45 65	49.49	49 22	48 88	4549	44.61	44.31	41.57	48.51	49.26
CaO	0.29	0 35	0.31	0.29	0.32	0.35	0.35	0.30	0.29	0.33	0.25	0.36	0.36
Total	100 14	99.33	99.15	100.00	100 81	100.67	10007	98.66	99 09	100.53	99.12	99.81	100.77
Fo	89 55	89 62	88.31	85.18	89 62	89.73	89 67	85.95	84.40	83.07	80.06	89.61	89.62

Sample no.							
Analysis no.	59	60	61	62	63	64	65
SiO2	39 87	39 71	39.66	38.89	3983	40.52	40 71
Cr2O3	0 10	0.06	0.07	0.09	0.04	0.05	0 00
FeO	16.00	15.12	15.59	18.03	14.27	10.45	10.48
NiO	0.07	0.10	0 15	0 13	0.07	0.17	0.12
MnO	0.33	0.33	0.27	0.43	0.31	0.19	0.22
MgO	44.06	45.04	44.55	42.08	45 62	48.76	48.90
CaO	0.29	0.29	0.29	0.30	0.33	0.30	0.29
Total	100.71	100.66	100.58	99.96	100.48	100.45	100.73
Fo	83.07	84.15	83.58	80.62	85.07	89 26	89.26

Table A4.6. Astrolabe Group spinel

Sample no.	AV186									
Analysis no.	1	2	3	4	5	6	7	8	9	10
SiO2	0.04	0.05	0 07	0.02	0.03	0 03	0.01	0.00	0.02	0.05
TiO2	0.57	0.53	0.49	0.48	0.48	0 49	0.54	0.44	0.50	0.43
Al2O3	6.36	5 64	6.07	6 01	5.88	5 72	5.98	5.96	6.02	5.87
Cr2O3	53.41	54 05	55 11	55.73	55.17	55.13	55.10	54 26	54 74	54.39
FeO	29.26	32.92	27.86	27.73	28.13	29.86	30.13	32 04	27.69	32 10
MnO	0.27	0.48	0.32	0.32	0.29	0.38	0 29	0.43	0.33	0.38
NiO	0.12	0.03	0.09	0.01	0.13	0.00	0.18	0.05	0.04	0.05
MgO	10.22	6.66	9.88	10 70	10.61	8.99	8.65	7.72	10.12	7.25
Total	100.25	100 36	99.89	100.99	100 73	100.59	100.88	100.91	99.46	100.51
Mg#	50 50	34.00	49.40	52.50	52.30	44.80	4320	38.90	50.60	36.70
Cr#	84.89	86.51	85.87	86.13	86.25	86.58	86.04	8590	85.89	86.12
Fe#	39.00	30.10	35.10	37.80	38.80	34.20	32.70	32.50	36.30	30.80
Fo (host olivine)	89.75	86.27	87.94	89.70	8984	87.07	86 50	87 01	89 62	83 30

Table A4.7. Astrolabe Group clinopyroxene

Sample no.	AV185												AV186
Analysis no.	1	2	3	4	5	6	7	8	9	10	11	12	1
SiO2	55.63	55.21	54.97	54.16	54.20	54.91	55.07	54.51	54.40	54.25	54.07	53.54	53.57
TiO2	0 09	0.11	0 14	0.08	0.11	0.09	0.11	0.11	0 11	0.10	0.11	0.11	0.19
Al2O3	0.78	0.86	0 69	0.81	0.67	0.72	0 71	0 68	0 89	0.75	0 85	0.73	1.52
FeO	2.62	2 70	3.20	2.73	2.89	3.01	2.77	2.97	2.56	3.09	3.20	2.72	4.14
MnO	0.04	0.03	0.15	0.00	0.00	0.10	0.00	0.02	0.08	0 03	0.13	0.00	0.25
MgO	18.19	17.86	18.10	17 85	17 93	18.30	18.01	18.19	18 14	18 02	17 74	17.99	17.03
CaO	23.06	23.08	22.56	23.07	22.88	22.79	23.15	23.05	23.15	22.69	23 02	23.06	22.53
Na2O	0.13	0.16	0.17	0.16	0.16	0.14	0.17	0.17	0.16	0 20	0.16	0.18	0.17
Cr2O3	0.31	0.41	0.29	0.64	0.42	0.42	0.45	0 39	0.61	0.46	0.42	0.49	0.50
Total	100.84	100.43	100 26	99.50	99.26	100.47	100.43	100.09	100.09	99 59	99 69	98.81	99 92
Mg#	92.54	92.20	90.98	92.09	91.71	91.55	92.06	91.62	92.67	91 23	90.81	92.19	88.00
Enstatite	50.20	49.68	50.12	49.63	49.81	50.32	49.75	49.94	50.09	49.98	49.17	49.85	47.91
Ferrosilite	4.05	4.20	4.97	4 27	4.51	4.64	4.29	4.57	3 97	4 80	4.98	4.23	6.53
Wollastonite	45.75	46.12	44.91	46.11	45.69	45.03	45.96	45.49	45.95	45.22	45.86	45.93	45.56

Sample no.												AV190	
Analysis no.	2	3	4	5	6	7	8	9	10	11	12	1	2
SiO2	54.19	54.66	54.24	53.99	54.56	53.78	53.95	53.43	53.60	53.43	53.44	48.30	49.66
TiO2	0.15	0.11	0.11	0.11	0.13	0.16	0.15	0 12	0.12	0.16	0.13	0.86	0.67
Al2O3	1.01	0.77	0.98	0.83	0.71	1.01	0.80	1.13	1.09	1.11	1.30	4.94	3 60
FeO	3.11	2.55	2.93	3.13	2.86	3.94	3.35	3.03	2.72	3.14	3.35	8.15	7.58
MnO	0.11	0.00	0.08	0.00	0.10	0.15	0.08	0.05	0.07	0.09	0.09	0.24	0.27
MgO	17.86	18.17	17.77	17.63	18.04	17.39	17.57	17.77	17.91	17.72	17.52	13.65	14.45
CaO	22.97	23.19	22.95	22.65	23.05	22.69	22.63	23.16	23.03	23.12	23.26	23.21	22.92
Na2O	0.14	0.16	0.18	0.17	0.19	0.10	0.18	0.19	0.18	0.17	0.18	0.33	0.30
Cr2O3	0.32	0 61	0.61	0.46	0.48	0.23	0.20	0.59	0.70	0.41	0.47	0.05	0.04
Total	99.86	100.22	99.85	98.99	100.12	99.44	98.90	99.47	99 41	99 34	99.75	99.73	99.48
Mg#	91.11	9270	91.53	90.93	91.84	88.73	90.35	91.28	92.15	90.97	90.31	74.92	77.27
Enstatite	49.46	50 09	49 50	49.43	49.83	48.43	49.21	49.20	49.77	49.09	48.51	39.12	41.08
Ferrosilite	4.83	3 94	4.58	4.93	4 43	6.15	5.26	4.70	4.24	4.88	5.21	13.09	12.08
Wollastonite	45.71	45.96	45.92	45 64	45.75	45.42	45.54	46.10	46.00	46.03	46.28	47.79	46.83

Sample no.													
Analysis no.	3	4	5	6	7	8	9	10	11	12	13	14	15
SiO2	49.76	52 25	48.89	49.71	50.97	53.66	51.04	50 35	50 84	50.12	53.31	53.09	49.54
TiO2	0.57	0.30	0.74	0 61	0.55	0.11	0 49	0.65	0 65	0 64	0.19	0.22	0 77
Al2O3	3.36	1.56	4.06	3 32	2.77	1 11	3.12	3.30	3.63	3 63	1,11	1 36	4.24
FeO	7.37	4.60	8.05	8.42	5 77	3.33	6.92	8.90	7 10	8 20	2.95	3.52	7.33
MnO	0.25	0.14	0 31	0.33	0 18	0.20	0.33	0.36	0 17	0 30	0 10	0.18	0.16
MgO	14.51	16.32	14.09	14.02	15.49	17.62	14.96	13.99	14 60	14.13	17.48	17 08	14 41
CaO	23.09	24.40	22.92	22.51	23.63	22.95	21.57	21.35	22 00	21.48	23.46	23.06	22 06
Na2O	0.26	0.15	0.36	0.33	0.28	0 18	0.34	0.40	0.25	0.33	0.14	0.15	0.34
Cr2O3	0.02	0.13	0.04	0.00	0.17	0.32	0.05	0.01	0 00	0 04	0.36	0.24	0.04
Total	99.18	99.85	99.46	99.25	99 80	99.48	98.82	99.30	99 24	98.88	99.08	98.88	98.89
Mg#	77 82	86.35	75.74	74.80	82.70	90.42	79 40	73.71	78.56	75.44	91.37	89.65	77 80
Enstatite	41.17	44.79	40.17	40.14	43 37	48.98	43.55	40 76	42 44	41.36	48.57	47.94	41.92
Ferrosilite	11.73	7 08	12.87	13.53	9.07	5.19	11.30	14.54	11.58	13 46	4.59	5 54	11.96
Wollastonite	47.09	48.13	46.97	46.33	47.56	4584	45.15	44.70	45.98	45 18	46.84	46 52	46.12

Sample no.				AV176				Traverse from core (C) to rim (R)					
Analysis no.	16	17	18	1	2	3	4	5	6 C				6R
SiO2	52.43	49.40	53 07	50.70	49.23	48.02	48.75	48 14	51 66	51 86	52.39	48.11	49 54
TiO2	0.31	0.76	0.15	0.40	0 57	0.90	0.71	0 70	0.27	0 27	0.17	0 69	0 58
Al2O3	2.17	4.57	1.10	2.80	4.35	4 72	4.38	5 20	1.75	1 58	1.33	4.71	3 51
FeO	5.34	8 23	3.91	5.70	7 48	8 82	8.47	7.85	4 78	4.59	4.07	7.75	7 64
MnO	0.09	0.42	0 16	0.16	0.20	0 29	0.30	0 25	0 08	0.15	0.14	0.22	0 21
MgO	16.14	13.97	17.46	15 75	14 29	13 49	14 04	13.95	16 68	16 69	16 97	13.96	14 92
CaO	22.59	21.79	22.37	22.99	22.44	22.21	22.21	22.59	23 30	23 53	23.82	22.44	22 14
Na2O	0.21	0.33	0.19	0 23	0.34	0.40	0.37	0 29	0 20	0.15	0.14	0.28	0.26
Cr2O3	0.10	0.01	0.44	0.13	0 01	0.06	0 02	0 02	0.14	0 22	0.21	0.03	0 00
Total	99.40	99.49	98.86	98 85	98.93	98.90	99 24	98.99	99 24	99.44	99.62	98.56	99.20
Mg#	84.34	75.16	88.85	83 12	77.30	73.17	74.72	76.01	86.15	86 63	88 14	76 24	77 67
Enstatite	45.63	40.79	48.87	44.40	41 29	39.22	40.40	40 33	46.19	46.13	46 66	40.53	42 47
Ferrosilite	8.47	13.48	6.13	9 02	12.12	14.38	13.67	12.73	7 43	7 12	6.28	12.63	12 21
Wollastonite	45.90	45.73	45.00	46.58	46.58	46 41	45.93	46.94	46.38	46.75	47 06	46 84	45 31

Sample no.													
Analysis no.	7C			7R	8C				8R	9C			
SiO2	51 83	52 11	48.09	47.77	48 38	47 23	48.11	47.16	48.10	49 71	50.31	48.17	50.25
TiO2	0 29	0.22	0 72	0 76	0 59	0 84	0 63	080	0.70	0 57	0.48	0 67	037
Al2O3	1 73	1 42	4 89	4 99	4 14	5 41	4 62	5 27	4 83	3 12	4.47	4.79	2.73
FeO	4 75	4 22	8 14	8 21	7 64	8 46	7 70	8.01	7.76	8.13	6 72	8.03	6.52
MnO	0 11	0.11	0.29	0 29	0.16	0 19	0.18	0 13	021	032	0 14	0 23	0.14
MgO	16 48	16 67	13.61	13 86	14 22	13.30	13.89	13 49	1366	14.49	14 19	13.92	15.23
CaO	2352	2330	21.86	21.99	22 54	22.27	22 51	2236	2208	22.01	21 80	22.52	2340
Na2O	0 20	0 16	0.31	0.28	0 25	0.33	0 29	0 29	0 29	0.29	0 50	0.31	0.19
Cr2O3	0 14	0 26	0.02	0 00	0.07	0 00	0 00	0 03	0.00	0 02	0 11	0.00	0 06
Total	99 42	98 89	98.31	9849	98.36	9837	98 23	9792	98 00	99 03	99 11	99.01	99 31
Mg#	86.08	8757	74.89	75 05	76.83	73 69	76.30	75 02	75 83	76.06	79 02	75.55	8063
Enstatite	45 72	46.59	40.17	4044	40.96	39 06	40.41	39.62	40.31	41 56	42 21	40.22	42 66
Ferrosilite	7.39	6 61	13.47	13 44	12.36	13 94	12.55	13 20	1285	13 08	11 21	13 02	10 25
Wollastonite	46.89	46.80	46.37	46 12	46.68	4700	47.04	47 18	46 84	45 36	4659	46.76	47.09

Sample no.													
Analysis no.	9R	10C				10R	11C			11R	12C		
SiO2	4769	49 11	48.16	48.02	49.34	4771	49.19	48.32	48.07	47 85	49 18	48.88	4674
TiO2	0.76	0.56	0.77	0.90	0.53	0 78	0 71	0.71	0.73	075	0.57	0.61	094
Al2O3	5.22	3.58	4.18	4.42	3 30	4.86	3.79	4.41	4.82	4.97	3 96	3 93	5.24
FeO	8.27	7.68	8.50	8.88	7.30	8.04	8.21	8.85	8.26	7.88	7.61	7.51	8 58
MnO	0.18	0.18	0.31	0.29	0.17	0 19	0.33	0.27	0.22	0 24	0.20	0.16	0 22
MgO	13.63	14.51	13.77	13.49	14.80	13.60	14.26	13.81	13.78	13 63	14.52	14.38	13 25
CaO	22.46	22.52	22.03	22.21	22.66	22.53	22.29	22.12	22.18	22.49	2259	22.56	22 40
Na2O	0.31	0.26	0.33	0.37	0.22	0 29	0 34	0.34	0.31	0 29	0 26	0.29	0 25
Cr2O3	0.00	0.03	0.00	0.06	0 00	0.01	0.04	0.00	0.03	0 00	0.03	0 07	0.06
Total	98.90	98.77	98.43	99 04	9872	98.39	99.55	99.18	98.76	98.49	9932	98 80	9805
Mg#	74.60	77 11	74.28	7303	78 34	75 10	75.59	73.57	7485	7550	77 27	77.34	73.35
Enstatite	39 62	41 46	40.07	39.17	42 08	39 65	40 88	39.83	40.12	39 83	41 46	41 31	38 78
Ferrosilite	13.49	12.31	13.88	14.47	11.63	13 15	13.20	14.31	13.48	12.93	12.19	12.11	14.09
Wollastonite	46 90	46.24	46.05	46.36	46 29	47.20	45 92	45.85	46 40	47 24	46 35	46.58	47 13

Sample no.		AV182		AV187				AV173					
Analysis no.	12R	1	2	1	2	3	4	1	2	3	4	5	6
SiO2	47 10	51.19	51 35	50 85	51.18	51 19	51.83	51 53	52.10	51 82	5147	51.64	51 83
TiO2	0.84	0.37	0.28	037	0.27	032	018	0.51	051	048	049	0.54	048
Al2O3	5.78	2.43	1.78	2.61	2.10	2 22	1.55	2 37	2.15	2 30	2.20	2.50	1 99
FeO	8.20	5.54	6.85	621	7.57	715	7.88	9.55	8.74	978	9.75	9.51	9.23
MnO	0.30	0 12	0.34	0 22	0.34	037	0 38	0.43	041	039	0 56	043	0 56
MgO	13.37	15.42	14.37	15 04	13 51	14 62	13.86	15 02	15 48	15 17	15.14	14.89	14.91
CaO	2258	23.71	23.76	2396	23.64	23 41	23 25	20.18	20.71	1969	19 71	19.86	20.65
Na2O	0 28	0 28	0.59	0.27	0.60	0.41	0.52	0.45	036	047	0.46	0.42	043
Cr2O3	0 02	0.10	0 06	0 00	0.01	004	0 00	001	000	000	004	001	0.00
Total	98 82	99 16	99.40	99.54	99 22	9971	99.45	100 05	10046	100 09	99.82	99.81	100 07
Mg#	74 41	83.24	78.89	81 19	76.10	78 46	7583	7370	75 95	7345	73 47	7362	74 21
Enstatite	39.09	4335	40 71	42.08	38.88	41 23	39 62	43 06	4390	4358	4354	4317	42 67
Ferrosilite	13.45	8 73	10.89	9 75	12.22	11.32	12 63	15.37	13.90	15 76	15 72	15.47	14 83
Wollastonite	47 46	47.92	48 39	48.17	48.90	4745	47 75	41.58	42 21	4066	40 74	41.37	42 50

Sample no.		
Analysis no.	7	8
SiO2	51 92	51 74
TiO2	0.45	0 53
Al2O3	2.04	2 28
FeO	9.38	9.56
MnO	0.46	0 46
MgO	15 10	15 43
CaO	20.10	19 95
Na2O	0.41	040
Cr2O3	0.00	0 01
Total	99 86	100.37
Mg#	74 14	74.21
Enstatite	43 37	4393
Ferrosilite	15.13	15.27
Wollastonite	41.51	40 81

Table A4.8. Astrolabe Group plagioclase

Sample no.	AV182b						AV187						AV190
Element	1	2	3	4	5	6	1	2	3	4	5	6	1
SiO2	53.17	58.78	56.46	57.87	56.06	56 60	51.48	53 34	51 45	48.95	51.14	50.52	49 61
Al2O3	29 16	25.13	26.81	25.93	27.25	26.93	30.22	28.68	30 25	31.29	30.48	30.22	31.13
FeO	0.46	0 35	0.42	0.41	0.43	0.55	0.50	0 49	0.50	0.45	0.63	0.74	0.79
MgO	0.02	0 01	0.02	0 00	0.00	0.07	0.04	0 02	0.03	0.00	0.03	0 17	0.08
CaO	10.95	6 20	7.92	6.92	9.07	8.48	12 46	10.97	12.60	14.09	12.60	12.13	13.91
Na2O	4.68	6.92	6.02	6.45	5.91	5.75	3 79	4 66	3.67	3.07	3.80	3.59	3.01
K2O	0.54	1.26	0.86	0.96	0.30	0.66	0 47	0.63	0.41	0.25	0.38	0.70	0.80
Total	98.98	98.66	98.52	98.54	99.01	99.02	98.94	98.79	98.90	98.10	99.06	98 07	99.34
Albite	42.23	61.93	54.90	59.13	53.16	52.91	34.48	41 85	33 64	27.83	34.48	33.42	26 85
Anorthite	54.57	3066	39.91	35.07	45.09	43.11	62.73	54.44	63.88	70.70	63.24	62.32	68.48
Orthoclase	3.20	7.41	5.18	5.81	1.76	3.99	2.79	3.71	2.48	1.48	2.28	4.26	4 68

Sample no.				
Element	2	3	4	5
SiO2	48.71	46.31	49.52	49.42
Al2O3	31.33	33.32	31.02	31.13
FeO	0.90	0.68	0.79	0.80
MgO	0 17	0.06	0.07	0.10
CaO	14.44	16.46	14.03	13.92
Na2O	2.46	1.90	3.15	3.03
K2O	0.64	0.28	0.65	0.62
Total	98.64	99.00	99.23	99.02
Albite	22.64	16.97	27.83	27.19
Anorthite	73.49	81.41	68.39	69.13
Orthoclase	3.87	1 63	3.79	3.68

Table A4.9. Ngaloa Group olivine-normal conditions (see A2.3. Mineral chemistry analyses)

Sample no.	AV98												
Analysis no.	1	2	3	4	5	6	7	8	9	10	11	12	13
SiO2	40.26	40.28	40.20	40.12	40.18	40.36	40.47	40.27	40.00	40.06	40.04	40.28	39.70
FeO	11.85	11.66	11.95	11.87	11.89	11.21	12.11	13.15	12.16	12.28	12.37	12.29	12.63
NiO	0.16	0.23	0.24	0.20	0.34	0.51	0.38	0.36	0.21	0.35	0.37	0.26	0.35
MnO	0.56	0.48	0.40	0.45	0.36	0.26	0.36	0.28	0.47	0.35	0.25	0.40	0.24
MgO	47.04	47.07	46.73	47.08	46.94	47.67	47.21	46.71	46.92	46.68	46.61	46.74	46.07
CaO	0.14	0.15	0.16	0.15	0.16	0.11	0.15	0.13	0.16	0.14	0.16	0.17	0.12
Total	100.01	99.87	99.67	99.88	99.86	100.13	100.67	100.90	99.91	99.85	99.79	100.14	99.10
Fo	87.62	87.80	87.45	87.60	87.55	88.34	87.42	86.36	87.31	87.13	87.04	87.14	86.66
Sample no.													
Analysis no.	14	15	16	17	18	19	20	22	23	24	25	26	27
SiO2	39.83	39.96	39.94	39.90	40.30	39.97	40.02	40.20	39.84	40.17	39.87	39.90	40.13
FeO	12.45	11.86	11.56	11.10	11.84	12.03	12.14	11.56	11.95	11.86	12.39	11.34	11.03
NiO	0.20	0.32	0.37	0.15	0.36	0.23	0.34	0.45	0.30	0.28	0.31	0.24	0.35
MnO	0.41	0.33	0.35	0.47	0.32	0.51	0.28	0.30	0.36	0.36	0.31	0.42	0.43
MgO	46.36	46.63	47.18	47.16	46.90	46.52	46.33	47.28	46.81	46.84	46.88	47.28	47.67
CaO	0.17	0.14	0.14	0.15	0.14	0.17	0.15	0.12	0.15	0.16	0.14	0.15	0.14
Total	99.42	99.24	99.53	98.93	99.86	99.42	99.25	99.90	99.39	99.66	99.89	99.33	99.75
Fo	86.90	87.51	87.92	88.33	87.59	87.33	87.18	87.93	87.47	87.56	87.08	88.14	88.50
Sample no.													
Analysis no.	28	29	30	31	32	33	34	35	36	37	38	39	40
SiO2	39.90	39.86	40.06	40.27	40.19	40.01	40.27	40.44	39.99	40.18	39.91	40.16	40.11
FeO	11.85	11.79	12.26	11.86	12.57	11.75	11.44	11.30	11.55	12.23	11.44	11.90	12.15
NiO	0.26	0.34	0.36	0.14	0.39	0.31	0.45	0.14	0.23	0.41	0.23	0.36	0.17
MnO	0.43	0.39	0.28	0.53	0.17	0.34	0.22	0.45	0.41	0.28	0.28	0.29	0.51
MgO	46.50	46.73	46.69	47.26	46.84	46.84	47.22	47.34	47.11	46.55	47.16	46.58	46.59
CaO	0.16	0.17	0.15	0.16	0.17	0.18	0.18	0.18	0.15	0.14	0.14	0.15	0.14
Total	99.10	99.28	99.79	100.22	100.32	99.42	99.78	99.84	99.43	99.78	99.16	99.43	99.67
Fo	87.48	87.60	87.16	87.66	86.91	87.66	88.03	88.18	87.91	87.15	88.01	87.47	87.23
Sample no.											AV99		
Analysis no.	41	42	43	44	45	46	47	48	49	50	1	2	3
SiO2	40.12	40.18	40.03	39.79	39.90	40.16	40.25	40.08	40.30	40.15	40.62	40.79	40.65
FeO	11.68	12.10	11.31	11.94	12.28	11.35	11.57	12.01	11.76	12.21	8.86	8.54	9.27
NiO	0.21	0.32	0.14	0.28	0.16	0.38	0.28	0.27	0.36	0.18	0.31	0.21	0.41
MnO	0.48	0.27	0.52	0.31	0.47	0.35	0.41	0.48	0.39	0.46	0.52	0.45	0.31
MgO	46.69	46.90	46.83	46.70	45.97	46.78	46.84	46.58	46.43	46.64	48.81	49.09	48.47
CaO	0.15	0.12	0.14	0.16	0.16	0.17	0.15	0.17	0.17	0.13	0.13	0.14	0.11
Total	99.33	99.89	98.96	99.18	98.94	99.18	99.49	99.60	99.41	99.76	99.24	99.21	99.21
Fo	87.69	87.35	88.06	87.45	86.96	88.02	87.83	87.36	87.56	87.19	90.76	91.10	90.31
Sample no.													
Analysis no.	4	5	6	7	8	9	10	11	12	13	14	15	16
SiO2	40.55	40.80	40.59	40.61	40.87	40.45	40.62	40.99	40.22	40.68	40.53	40.70	40.40
FeO	9.11	8.51	9.27	9.26	8.76	8.90	9.27	8.90	9.21	8.73	8.72	8.85	10.01
NiO	0.26	0.21	0.27	0.25	0.15	0.19	0.16	0.22	0.22	0.34	0.42	0.23	0.43
MnO	0.44	0.55	0.38	0.38	0.47	0.46	0.51	0.44	0.43	0.43	0.33	0.49	0.34
MgO	48.98	49.47	48.86	49.15	49.42	49.25	49.12	49.62	48.99	49.18	48.89	49.22	48.36
CaO	0.13	0.15	0.13	0.13	0.16	0.16	0.13	0.14	0.15	0.11	0.14	0.15	0.14
Total	99.46	99.69	99.49	99.78	99.83	99.40	99.81	100.31	99.23	99.46	99.04	99.64	99.68
Fo	90.55	91.20	90.38	90.44	90.95	90.79	90.42	90.85	90.45	90.95	90.90	90.84	89.60

Sample no.													
Analysis no.	17	19	20	21	22	23	24	25	26	27	28	29	30
SiO2	40.51	40 45	40.77	40.25	40 52	40.53	40.56	40.43	40.46	40.54	40.37	40 71	40 45
FeO	9 22	9.51	8.92	9.00	9 42	8.81	9.03	8.94	9.30	9.18	8.84	9.46	10.36
NiO	0.22	0.33	0 26	0.31	0.30	0.19	0.19	0.33	0.25	0.34	0.26	0.33	0.36
MnO	0.45	0.36	0.42	0 36	0 47	0.46	0.45	0.40	0.46	0.41	0.48	0.46	0.25
MgO	48.87	48 58	48.99	48.73	48.58	48.95	48.84	48 80	48.54	48.55	48.80	49.10	48.40
CaO	0.14	0.16	0.16	0 12	0.13	0.13	0.14	0.11	0.15	0.14	0.17	0.14	0.09
Total	99 41	99.39	99.52	98.76	99.42	99 08	99 20	99.01	99.16	99.15	98.92	100.19	99.90
Fo	90.43	90.10	90.73	90.61	90 19	90.82	90.60	90.68	90.29	90.41	90.77	90 24	89.28
Sample no.													
Analysis no.	31	32	33	34	35	36	37	38	39	40	41	42	43
SiO2	40.39	40.66	40.80	40.63	40 69	40.91	40.88	40.53	40.73	40.53	40.50	40.51	40.48
FeO	9.44	8.70	9.18	8.72	9.17	8 91	8.89	9.52	9.20	9.59	8.63	9.14	9.06
NiO	0.50	0.19	0.44	0.28	0.48	0.21	0.21	0.41	0.23	0.31	0 28	0 30	0.21
MnO	0.32	0.44	0.38	0.40	0.31	0.52	0.49	0.23	0.45	0.35	0.54	0.47	0.42
MgO	48.50	49.43	49.40	49.23	49.08	49.75	49.71	48.49	48.92	48.84	49.19	48 94	48.79
CaO	0.13	0.15	0.13	0.17	0.13	0.11	0.13	0.15	0.16	0.14	0.11	0.15	0.12
Total	99.27	99.57	100.32	99.42	99.86	100.42	100.30	99.34	99.69	99 76	99.24	99.51	99.08
Fo	90.15	91.02	90.56	90.96	90 51	90.86	90.88	90.07	9045	90.07	91.04	90.51	90.57
Sample no.							AV110						
Analysis no.	44	45	46	47	49	50	1	2	4	6	8	9	10
SiO2	40.43	40.70	40.71	40.39	40 77	40.66	40.11	40.17	39.95	39.53	39.70	40.51	39.85
FeO	9 82	9.01	8.83	10.11	8.92	9.12	11.12	11.24	12.60	12.51	13.26	9.29	11 20
NiO	0.39	0.28	0.17	0.42	0.31	0.27	0 47	0.50	0 58	0 54	0.43	0.21	0.42
MnO	0.36	0 38	0.44	0.28	0.43	0.39	0.30	0.22	0.18	0.15	0 18	0.37	0.31
MgO	48.42	49.01	49.54	48.37	48.90	48.96	46 80	46.90	46.16	45.82	45.52	48.70	46.40
CaO	0.13	0.14	0.16	0.12	0.16	0.15	0.12	0.10	0.14	0.11	0.12	0.15	0.12
Total	99.54	99.52	99.86	99.69	99.48	99.55	98.93	99.12	99.60	98.65	99.22	99.23	9830
Fo	89.78	90 65	90.90	89.50	9072	90.54	88.24	88.15	86.72	86.72	85.95	90.33	88.07
Sample no.								AV112					
Analysis no.	11	12	13	14	15	16	17	1	2	3	4	5	6
SiO2	40.19	39.85	39.70	40.27	39.77	39 72	40.38	40.48	40 63	4055	40.79	40.91	40.31
FeO	10.35	11.13	12.46	10.91	11 74	11.06	8.98	9 35	9 02	9.20	9.34	9.19	9.33
NiO	0.35	0.41	0.57	0.52	0.46	0 44	0.22	0.26	0.27	0.22	0 15	0.21	0.26
MnO	0.35	0.26	0.16	0.30	0.25	0 24	0.39	0.37	0.33	0 44	0.28	0.36	0.28
MgO	47.73	46 79	45.87	47 23	46 22	46 66	48.30	48 63	48.83	48.46	48.26	48.54	48.15
CaO	0.13	0.12	0.10	0.09	0.12	0 13	0.14	0.13	0.13	0.14	0.11	0.14	0.16
Total	99 10	98 55	98.86	99.32	98.55	98.24	98.42	99.23	99.20	99.01	98.92	99 34	98.47
Fo	89 15	88 22	86.78	88.53	87 53	88 26	90.55	90.26	90.61	90.38	90 20	90.39	90 20
Sample no.	AV208												
Analysis no.	1	2	3	4	5	7	8	9	10	11	12	13	14
SiO2	39.98	40.29	40.45	40 00	4008	40 14	40.08	40.38	40.20	40.38	40.22	4002	40.03
FeO	9.95	10.09	9.31	9.82	9.85	9 61	10 70	9 14	1025	9 55	8.75	9.31	10.45
NiO	0.49	0 36	0 53	0.51	0 59	0 38	0 43	0.44	0.46	0.50	0 44	0 46	0.22
MnO	0 19	0 31	0 26	0.14	0 27	0 25	0 25	0.25	0.18	0.19	0 34	0 31	0.21
MgO	48.14	47.94	48.62	47.86	4824	4776	47.38	48 76	4759	48.07	48.84	48.20	47 25
CaO	0.14	0.17	0 17	0 14	0 15	0.14	0.16	0.17	0.16	0.14	0.16	0 17	0 12
Total	98.89	99 16	9933	98.47	99.16	98 27	99.00	99.14	98.83	98.83	98 76	98 46	98.28
Fo	89 61	89 44	90.30	89 67	89 72	89 86	88 75	90.48	89.22	89.97	90.86	90.22	88 96

Sample no.													
Analysis no.	15	17	19	20	21	22	23	24	25	26	27	29	30
SiO2	40.36	40 20	40 31	40 08	40 18	40 20	40 33	40 52	40 18	40.50	40 30	40 20	40.40
FeO	9 94	10.19	9 97	9.72	10 28	10 31	10 23	9 82	9 78	9 27	9 99	9 89	9 53
NiO	0 57	0 51	0 56	0 46	0 49	0 49	0 49	0 52	0 57	0 37	0 51	0 56	0 55
MnO	0 20	0 14	0 11	0 21	0 17	0 15	0 16	0.24	0 18	0 28	0.16	0 18	0.15
MgO	47 88	47 34	48 02	47 88	47 54	47 88	47 52	47 97	47 83	48 38	47 44	47 63	48.12
CaO	0 14	0 15	0 13	0 17	0 13	0 18	0 15	0 11	0 14	0 16	0 16	0.14	0 16
Total	99 09	98 51	99 11	98 52	98 79	99 20	98 87	99.18	98 67	98 97	98 55	98.61	98 92
Fo	89 57	89 23	89 56	89 77	89 18	89 21	89 23	89 70	89 71	90 29	89 44	89 56	90 00

Table A4.10
Ngaloa spinel

Sample no	AV208			
oxide names	AV 208 1	2	3	4
SiO2	0 25	0 18	0.31	0 01
TiO2	1.15	1.08	0 94	0.96
Al2O3	8.32	8 90	6 18	7.88
Cr2O3	33.07	33.52	28 45	31.77
FeO	44.77	45 97	52.90	45.24
MnO	0.47	0 34	0 36	0 32
NiO	0 49	0 69	0 56	0.49
MgO	9.35	8.52	8.11	9.54
Total	97.87	99 18	97.81	96 21
Mg #	46.83	42.40	41 45	48.50
Cr#	72.67	71 60	75 60	73.00
Fe #	57.77	55.20	61 45	60 00
Fo (host olivine)	90.22	89.58	89 50	91.07

Table A4.9. Ngaloa olivine continued... (trace element conditions)

Sample no.	AV98												
Analysis no.	1	2	3	4	5	6	7	8	9	10	11	12	13
Trace element conditions													
CaO	0.15	0.14	0.16	0.14	0.15	0.16	0.17	0.14	0.15	0.14	0.15	0.15	0.15
MnO	0.25	0.30	0.47	0.35	0.43	0.50	0 48	0.28	0.32	0.29	0.34	0.35	0.40
NiO	0.42	0.37	0.27	0.36	0 20	0.23	0.24	0.38	0.39	0.36	0.38	0 37	0.29
Normal conditions													
SiO2	40.47	39 87	39.97	39.84	40.15	40.12	40 00	39.96	40.27	40.06	40.04	40.02	39.90
FeO	12.11	12 39	12.03	11.95	12.21	11 68	12.16	11 86	13 15	12 28	12.37	12.14	11.34
MgO	47.21	46 88	46.52	46.81	46.64	46.69	46.92	46.63	46.71	46.68	46.61	46.33	47.28
CaO	0.15	0 14	0 17	0 15	0 13	0.15	0.16	0.14	0.13	0.14	0.16	0.15	0.15
MnO	0 36	0.31	0.51	0.36	0.46	0.48	0.47	0.33	0.28	0.35	0.25	0.28	0.42
NiO	0.38	0.31	0.23	0.30	0.18	0.21	0.21	0.32	0.36	0.35	0.37	0.34	0.24
Total	100.67	99.89	99.42	99.39	99.76	99.33	99.91	99.24	100 90	99.85	99.79	99.25	99.33
Fo	87.42	87 08	87 33	87.47	87.19	8769	87.31	87.51	86.36	87.13	87.04	87.18	88.14
Sample no.	AV99												
Analysis no.	1	2	3	4	5	6	7	8	9	10	11	12	13
Trace element conditions													
CaO	0 14	0.14	0.11	0.11	0.15	0.15	0.14	0.15	0.15	0.15	0.15	0.13	0.14
MnO	0 35	0 51	0.33	0.49	0.44	0.49	0.33	0.52	0.45	0.40	0.45	0.53	0.53
NiO	0.36	0 28	0 46	0.27	0.33	0.27	0.39	0.21	0 28	0.37	0.30	0.24	0.26
Normal conditions													
SiO2	40 62	40.79	40.65	40.55	40.80	40.59	40.54	40.71	40.61	40.68	40.77	40 22	40.91
FeO	8.86	8.54	9.27	9.11	8.51	9.27	9.18	8.83	9.26	8.73	8.92	9.21	8.91
MgO	48.81	49 09	48.47	48.98	49.47	48.86	48.55	49.54	49.15	49.18	48.99	48.99	49.75
CaO	0 13	0.14	0 11	0.13	0 15	0.13	0.14	0.16	0.13	0.11	0.16	0.15	0.11
MnO	0 52	0.45	0 31	0 44	0.55	0.38	0.41	0 44	0.38	0.43	0 42	0.43	0.52
NiO	0.31	0 21	0.41	0 26	0 21	0.27	0.34	0.17	0.25	0 34	0.26	0 22	0 21
Total	99.24	99 21	99 21	99 46	99 69	99.49	99.15	99.86	99.78	99.46	99.52	99.23	100.42
Fo	90.76	91.10	90.31	90.55	91.20	90.38	90.41	90.90	90.44	90.95	90.73	90.45	90.86
Sample no.			AV110										
Analysis no.	14	15	1	2	3	4	5	6	7	8	9	10	11
Trace element conditions													
CaO	0 13	0.15	0 13	0.13	0.12	0.13	0 12	0 11	0.15	0.12	0 13	0 12	0 12
MnO	0 39	0.49	0.29	0 28	0.26	0.20	0.21	0.18	0.46	0.29	0.43	0.28	0.21
NiO	0.38	0.23	0 49	0 47	0 52	0.53	0.53	0.44	0.32	0.46	0.37	0.45	0.53
Normal conditions													
SiO2	40.43	40.88	40 11	40.17	39 74	39 95	39.53	39.70	40 51	39.85	40.19	39.85	39.70
FeO	8 94	8.89	11.12	11.24	11 41	12.60	12.51	13.26	9.29	11.20	10.35	11.13	12.46
MgO	48 80	49 71	46.80	46 90	4606	46.16	45.82	4552	48.70	46.40	4773	46.79	45 87
CaO	0 11	0.13	0 12	0 10	0 11	0.14	0.11	0.12	0.15	0.12	0.13	0.12	0 10
MnO	0 40	0 49	0 39	0 29	0 28	0.23	0.19	0.24	0.48	0.40	0 45	0.34	0 21
NiO	0 33	0 21	0.47	0 50	0 40	0 58	0 54	0.43	0 21	0.42	0 35	0.41	0 57
Total	99 01	100 30	99 02	99 18	98 00	99.65	98 70	99 27	99.34	98.39	99 20	98 63	9890
Fo	90 68	90 88	88 24	88.15	87.80	86.72	86.72	85.95	90.33	88.07	89.15	88 22	86 78

Sample no.				AV112				AV208					
Analysis no.	12	13	14	15	1	2	3	1	2	3	4	5	6
Trace element conditions													
CaO	0 13	0.12	0.12	0.14	0.13	0.13	0.14	0.16	0.17	0.15	0.17	0,16	0.16
MnO	0.34	0.28	0.27	0.51	0.44	0.43	0.44	0.17	0.35	0.27	0.33	0.21	0.24
NiO	0.42	0 50	0.46	0.23	0.34	0.26	0.21	0.50	0.37	0.51	0.46	0.53	0.48
Normal conditions													
SiO2	40.27	39.77	39.72	40.38	40.48	40.63	40.55	39.98	40.29	40.00	40.45	40.08	40.14
FeO	10.91	11.74	11.06	8.98	9.35	9.02	9.20	9.95	10.09	9.82	9.31	9.85	9.61
MgO	47.23	46.22	46.66	48.30	48.63	48.83	48.46	48.14	47.94	47.86	48.62	48.24	47.76
CaO	0 09	0.12	0.13	0.14	0.13	0.13	0.14	0.14	0.17	0.14	0.17	0.15	0.14
MnO	0.39	0.32	0.30	0.51	0.48	0.42	0.56	0.25	0.41	0.19	0.33	0.35	0.33
NiO	0.52	0.46	0.44	0.22	0.26	0.27	0.22	0.49	0.36	0.51	0.53	0.59	0 38
Total	99.41	98 62	98.30	98.53	99.33	99.29	99.13	98.94	99.25	98.51	99.40	99.24	98.34
Fo	88.53	87 53	88.26	90.55	90.26	90.61	90.38	89.61	89.44	89.67	90.30	89.72	89.86

Sample no.						
Analysis no.	7	8	9	10	11	12
Trace element conditions						
CaO	0.15	0.17	0.15	0.16	0.17	0.15
MnO	0.20	0.34	0.16	0.33	0.24	0.15
NiO	0.43	0.39	0.49	0.44	0.52	0.54
Normal conditions						
SiO2	40.08	40.38	40.20	40.22	40.38	40.20
FeO	10.70	9.14	10.25	8.75	9.55	10.19
MgO	4738	48.76	47.59	48.84	48.07	47.34
CaO	0.16	0.17	0.16	0.16	0.14	0.15
MnO	0 32	0.32	0.23	0.44	0.25	0.18
NiO	0.43	0.44	0.46	0.44	0.50	0.51
Total	99.07	99.21	98.88	9886	98.88	98.55
Fo	88.75	90.48	89.22	90.86	89.97	89.23

Table A4.9. continued.... Ngaloa olivine traverses

Sample no.	AV99												
Grain no.	1 RIM												
Analysis no.	1	2	3	4	5	6	7	8	9	10	11	12	13
SiO2	40.67	40 96	40.85	40 95	41.14	40 66	40.77	40 62	41 08	40.73	40 62	40 60	40 67
FeO	8 75	9.09	9.19	9.36	11 03	9 40	9 63	9 97	9 57	9 68	9 66	9 60	9 60
MgO	49.83	49.57	49 63	49.53	47 86	49.24	49.61	48.70	49 47	49 23	49 48	49 09	49 47
NiO	0.17	0.19	0.30	0.31	0.31	0 41	0 24	0 34	0 29	0 36	0 37	0 28	0 30
MnO	0 51	0 41	0.52	0.40	0.35	0 45	0 33	0 39	0 37	0 44	0 29	0 43	0 34
CaO	0.12	0 11	0.11	0 13	0 16	0 12	0 15	0 19	0 12	0.12	0 11	0 11	0 10
Total	100 08	100 35	100 62	100 67	100 87	100 31	100 74	100 23	100 92	100 57	100 53	100 11	100 49
Fo	91.03	90 67	90 59	90.41	88 55	90 32	90 18	89 69	90 21	90 06	90.13	9 0 11	90 18
Sample no.													
Grain no.								RIM	2 RIM				
Analysis no.	14	15	16	17	18	19	20	21	1	2	3	4	5
SiO2	40 51	40 63	40 71	40 66	40 78	40 82	40 86	40 81	40 87	41 11	41.06	41 09	41 28
FeO	9 53	9 60	10 91	9 33	9 22	8 93	9 12	8 67	8 30	8 35	8 22	8 25	8 33
MgO	49.49	49 49	47 84	49 40	49 51	49 64	49.81	49 75	50 37	50.35	50.57	50 48	50 37
NiO	0 33	0 19	0 25	0 24	0 28	0.21	0 22	0.21	0 15	0.19	0 13	0 19	0.20
MnO	0 42	0 37	0.41	0 41	0 37	0 49	0 48	0.57	0 59	0 47	0 56	0 50	0.51
CaO	0 13	0 11	0 21	0 13	0 14	0.10	0 14	0.15	0.14	0 15	0.13	0 15	0 14
Total	100 44	100 40	100 36	100 21	100 34	100.20	100 65	100 15	100 47	100 61	100 68	100 65	100.85
Fo	90 25	90 18	88 66	90.42	90 54	90 83	90.68	91 09	91.54	91 49	91.64	91 60	91.51
Sample no.													
Grain no.												RIM	3 RIM
Analysis no	6	7	8	9	10	11	12	13	14	15	16	17	1
SiO2	40.74	40 80	40 95	40 99	41 08	41 04	41.03	40 95	40.90	41.14	40 73	40 85	40.99
FeO	8 35	8.41	8 30	8 45	8 25	8 18	8.32	8 36	8 29	8 27	8 18	8.19	8 63
MgO	50 38	50 41	50 45	50 49	50 51	50 55	50 32	50.49	50 35	50 37	50 27	50 31	50 12
NiO	0 22	0 24	0 21	0 22	0 28	0 21	0 26	0 23	0 31	0 28	0 23	0 15	0.15
MnO	0.51	0 52	0 50	0 51	0 44	0 44	0 46	0 43	0 46	0.56	0 47	0 55	0.58
CaO	0 12	0 10	0 11	0 12	0 13	0 10	0.12	0 11	0 15	0.14	0 13	0 13	0 14
Total	100 33	100 48	100 56	100 79	100 69	100 52	100.51	100 57	100 45	100 76	100 01	100 17	100 61
Fo	91.50	91 44	91 55	91 41	91 60	91 68	91 51	91 50	91 55	91.56	91.63	91 63	91 19
Sample no.													
Grain no.													
Analysis no	2	3	4	5	6	7	8	9	10	11	12	13	14
SiO2	41 10	40 68	41 03	41 11	41 06	40 83	41 07	40 92	40 87	41.16	40 96	40 99	41 01
FeO	8 85	9 31	8 58	8 60	8 75	8 88	8.76	8 81	8 83	9.17	8 97	9 09	8 89
MgO	50 01	49 46	50 08	50 10	49 91	50 21	49 83	49 79	49.67	49 96	49.36	49 91	49 67
NiO	0 16	0 25	0 35	0 28	0 30	0 31	0 36	0 31	0.39	0 35	0 37	0 35	0 28
MnO	0 54	0 49	0 48	0 38	0 45	0 36	0 48	0 34	0 41	0 42	0 45	0 50	0 48
CaO	0 22	0 11	0 11	0 15	0 12	0 13	0 14	0 13	0 14	0 13	0 12	0 13	0 12
Total	100 89	100 36	100 63	100 64	100 58	100 74	100 66	100 34	100 34	101 19	100 24	100 97	100 44
Fo	90 96	90 45	91 23	91 21	91 04	90 98	91.02	90 96	90.93	90 66	90 74	90 73	90 88
Sample no.													
Grain no.								RIM	4 RIM				
Analysis no.	15	16	17	18	19	20	21	22	1	2	3	4	5
SiO2	40 94	40 98	40 91	40 98	40 91	41 20	40 99	40.75	40 65	40 68	40 73	40 51	40.54
FeO	8 77	8 90	8 85	8 74	8 52	8 55	8 44	8 47	9 78	10 03	10.05	9 87	10.02
MgO	49 90	49.77	49 96	49 75	50 09	49 94	50 10	50 32	48 49	48 30	48 33	48 50	48 37
NiO	0 27	0 34	0 27	0 31	0 29	0 31	0 31	0 20	0 37	0 38	0 38	0 30	0.40
MnO	0 52	0 44	0 45	0 42	0 49	0 47	0 38	0 63	0 33	0 25	0 31	0 30	0 40
CaO	0 11	0 11	0 13	0 13	0 13	0 14	0 15	0 10	0 13	0 14	0 12	0 12	0 14
Total	100 51	100 55	100 57	100 32	100 43	100 65	100 37	100.49	99 75	99.78	99.94	99 63	99 87
Fo	91 02	90 88	90 96	91 02	91 29	91 24	91.36	91 37	89 83	89.56	89 55	89 75	89 59

Sample no.											
Grain no.											RIM
Analysis no.	6	7	8	9	10	11	12	13	14	15	16
SiO2	40 54	40.57	40.44	40.89	40.89	40.62	40.76	40.91	40.77	40.73	40.56
FeO	9 90	9.94	9.78	9.22	9.02	8.99	8.82	8.81	8.54	8.56	8.60
MgO	48.70	48.60	48.78	49.27	49.27	49.59	49.64	49.80	49.90	49.58	49.83
NiO	0 37	0.31	0.38	0.39	0.34	0.36	0.39	0.27	0.30	0.19	0.20
MnO	0 30	0.29	0.38	0.40	0.41	0.37	0.46	0.54	0.48	0.56	0.57
CaO	0.14	0.12	0.13	0.13	0.15	0.18	0.13	0.14	0.16	0.12	0.18
Total	99.95	99.82	99.89	100.30	100 09	100.19	100.21	100.46	100.15	99.75	99.95
Fo	89.76	89.70	89.89	90.49	90.68	90.76	90.94	90.97	91.24	91.17	91.17

Table A4.11. Ngaloa Group clinopyroxene

Sample no.	AV98												
Analysis no.	1	2	3	4	5	6	7	8	9	10	11	12	13
SiO2	51.72	52.19	51.63	51.80	51.38	52.22	49.69	50.52	50.55	50.32	50.19	50.06	49.14
TiO2	0.72	0.22	0.27	0.28	0.31	0.50	1.01	0.80	0.72	0.83	0.81	0.80	1.01
Al2O3	2.84	2.19	2.71	2.67	2.80	2.28	3.99	3.70	2.94	3.53	3.55	3.80	4.74
FeO	4.97	5.27	6.32	6.45	6.14	4.03	4.83	4.31	4.47	4.49	4.21	4.51	4.86
MnO	0.08	0.26	0.24	0.23	0.18	0.09	0.05	0.06	0.01	0.00	0.19	0.08	0.08
MgO	16.78	16.15	15.20	15.37	15.20	17.40	16.45	16.51	16.89	16.68	16.48	16.59	16.21
CaO	22.08	22.48	22.28	22.05	22.37	21.94	21.83	21.85	22.17	22.03	22.06	21.66	21.66
Na2O	0.34	0.36	0.45	0.42	0.42	0.36	0.41	0.45	0.36	0.46	0.43	0.42	0.50
Cr2O3	0.11	0.07	0.18	0.16	0.29	0.49	0.30	0.62	0.18	0.66	0.37	0.57	0.41
Total	99.61	99.19	99.28	99.43	99.09	99.31	98.55	98.80	98.28	98.98	98.27	98.48	98.60
Mg#	85.76	84.53	81.09	80.95	81.53	88.50	85.85	87.22	87.07	86.90	87.47	86.76	85.61
Enstatite	47.35	45.80	43.73	44.12	43.78	49.11	47.20	47.67	47.80	47.63	47.49	47.82	46.98
Ferrosilite	7.86	8.38	10.20	10.39	9.92	6.38	7.78	6.99	7.10	7.18	6.81	7.30	7.90
Wollastonite	44.79	45.82	46.07	45.49	46.30	44.51	45.02	45.34	45.10	45.19	45.70	44.88	45.13
Sample no.						AV99							
Analysis no.	14	15	16	17	18	1	2	3	4	5	6	7	8
SiO2	50.92	51.98	48.53	50.60	48.83	52.69	51.87	51.52	52.28	51.73	50.64	50.92	51.47
TiO2	0.75	0.51	1.24	0.71	1.29	0.45	0.51	0.59	0.50	0.57	0.86	0.89	0.67
Al2O3	3.30	2.12	5.30	3.13	4.88	1.90	2.42	2.44	2.05	2.33	3.37	3.81	2.83
FeO	4.20	4.00	5.75	4.23	5.51	4.03	4.12	4.56	4.14	4.12	5.31	5.01	4.16
MnO	0.09	0.07	0.15	0.09	0.06	0.15	0.09	0.10	0.14	0.15	0.05	0.20	0.18
MgO	16.91	17.84	15.03	16.78	15.70	17.84	17.02	17.23	17.57	17.46	16.52	17.23	17.58
CaO	22.46	21.79	21.62	21.93	21.94	21.98	22.48	22.03	22.18	22.13	22.53	20.84	21.84
Na2O	0.38	0.31	0.48	0.41	0.42	0.29	0.34	0.33	0.34	0.33	0.34	0.38	0.39
Cr2O3	0.33	0.29	0.22	0.54	0.04	0.37	0.37	0.28	0.49	0.34	0.07	0.20	0.47
Total	99.35	98.90	98.31	98.41	98.66	99.70	99.22	99.08	99.69	99.16	99.69	99.49	99.58
Mg#	87.76	88.84	82.32	87.62	83.55	88.75	88.04	87.07	88.33	88.31	84.72	85.98	88.27
Enstatite	47.76	49.91	44.47	48.06	45.42	49.70	47.96	48.37	49.03	48.94	46.29	49.20	49.37
Ferrosilite	6.66	6.27	9.55	6.79	8.94	6.30	6.51	7.18	6.48	6.48	8.35	8.03	6.56
Wollastonite	45.58	43.82	45.98	45.15	45.63	44.01	45.53	44.45	44.49	44.59	45.36	42.78	44.07
Sample no.												AV110	
Analysis no.	9	10	11	12	13	14	15	16	17	18	19	1	2
SiO2	51.03	51.32	50.43	50.53	52.96	51.27	51.60	52.17	50.80	49.88	50.54	51.29	52.32
TiO2	0.74	0.69	0.80	1.01	0.58	0.18	0.74	0.56	0.98	0.77	0.09	0.65	0.50
Al2O3	3.51	3.22	3.56	3.26	2.13	2.75	3.32	2.09	3.47	3.57	3.41	3.03	2.03
FeO	4.27	4.00	4.47	5.66	3.99	5.81	4.48	4.24	5.13	4.53	8.04	4.47	4.60
MnO	0.15	0.13	0.07	0.12	0.10	0.19	0.03	0.00	0.07	0.04	0.28	0.06	0.03
MgO	17.12	17.26	16.96	16.34	18.14	15.77	17.15	17.99	16.48	16.73	14.99	16.95	17.64
CaO	21.97	22.15	22.16	22.12	21.93	22.16	22.00	21.68	21.97	22.07	21.60	21.85	21.03
Na2O	0.43	0.40	0.48	0.33	0.36	0.47	0.43	0.36	0.33	0.45	0.39	0.36	0.38
Cr2O3	0.51	0.66	0.48	0.09	0.41	0.18	0.18	0.40	0.13	0.27	0.02	0.30	0.20
Total	99.73	99.82	99.39	99.46	100.60	98.78	99.93	99.49	99.35	98.31	99.36	98.96	98.73
Mg#	87.72	88.49	87.11	83.73	89.01	82.88	87.21	88.32	85.13	86.80	76.86	87.11	87.24
Enstatite	48.49	48.73	47.92	46.14	50.19	45.12	48.34	50.04	46.89	47.61	42.79	48.21	49.92
Ferrosilite	6.79	6.34	7.09	8.96	6.20	9.32	7.09	6.62	8.19	7.24	12.89	7.13	7.30
Wollastonite	44.72	44.94	44.99	44.90	43.62	45.56	44.57	43.34	44.92	45.15	44.32	44.66	42.77

Sample no.													
Analysis no.	3	4	5	6	7	8	9	10	11	12	13	14	15
SiO2	52.46	50.80	52.42	49 99	50 87	51 91	52.41	51 30	52 19	50 64	52.46	50 08	51.78
TiO2	0.52	0 77	0.58	0 32	0 31	0 59	0 52	0 76	0.61	0 63	0 47	0 88	0.52
Al2O3	2.03	3.55	2 15	3 00	2 99	1 96	1 89	3 25	1 84	3.46	1.93	3.45	2.19
FeO	4.71	5 17	4.56	9 16	9 33	4.47	3 95	4 73	5 10	5 03	4 49	5 36	4.82
MnO	0.11	0.08	0.19	0 36	0 34	0 00	0 15	0 14	0 22	0 13	0 04	0 18	0.05
MgO	17 95	16 67	17 68	14 12	14 27	17 84	17 58	16 61	17 88	16 40	17 75	16 84	18.01
CaO	20 89	21 14	21 84	21 40	21 14	21 71	22.29	22 15	21 25	22 02	22 07	21 47	21.19
Na2O	0.30	0 43	0 32	0.51	0 51	0 36	0 36	0 43	0 28	0 46	0.37	0.44	0.39
Cr2O3	0 16	0 32	0 27	0 00	0 02	0.15	0 36	0 29	0 13	0 42	0 24	0 23	0 22
Total	99.13	98 93	100 00	98 85	99 78	98 98	99 50	99 65	99 50	99.19	99 80	98 92	99.18
Mg#	87 17	85 18	87 35	73 31	73 17	87 66	88 81	86 22	86 22	85 32	87 58	84 86	86.95
Enstatite	50.41	47 95	49 20	40 76	41 13	49 62	49 09	47 20	49 66	46 79	49 12	47 75	50.11
Ferrosilite	7 42	8 34	7 13	14 84	15 08	6 98	6 18	7 55	7 94	8 05	6.96	8 52	7.52
Wollastonite	42.17	43 71	43 67	44 40	43 79	43.40	44 72	45 25	42 41	45 16	43.91	43 74	42.37

Sample no.			AV112										
Analysis no.	16	17	1	2	3	4	5	6	7	8	9	10	11
SiO2	50 65	49 52	51 68	52 72	52 36	51 82	51.55	50.22	50 43	51 24	50.97	51.02	51.20
TiO2	0 69	1.15	0 66	0 49	0 58	0.52	0.68	0 77	0 78	0 70	0 76	0 70	0.78
Al2O3	3 12	3 71	3 06	2 28	2.42	1.95	2.74	3.41	3 06	2.93	3 15	3 12	2.99
FeO	4 66	5 23	4 62	4 40	4.59	4 38	4 32	4.95	4.48	4.61	4 81	4.34	4 87
MnO	0 02	0 17	0.10	0 17	0.10	0 09	0.10	0 00	0 04	0.09	0.10	0.07	0.15
MgO	16 81	16 46	16 86	17 94	17 62	17 66	16.66	16.57	17 07	16.95	16.88	16.96	16.97
CaO	22 04	21 88	21 45	20.96	21.11	21 45	22 68	21.94	22.16	22.12	22.00	22.34	22.15
Na2O	0 45	0 39	0 38	0 36	0 32	0.37	0 40	0.44	0.41	0 46	0.46	0 47	0.35
Cr2O3	0 25	0.14	0 31	0 17	0 28	0 19	0.31	0.30	0 37	0 34	0.34	0.35	0.34
Total	98 68	98 64	99 12	99 49	99 38	98 42	99 44	98 60	98 81	99.44	99 48	99.37	99 81
Mg#	86 54	84 88	86 68	87 91	87 25	87 79	87 29	85 64	87 16	86 76	86.23	87 44	86 13
Enstatite	47 66	46 87	48 35	50.58	49 81	49.69	47 08	47.18	48 07	47 83	47.69	47 85	47 64
Ferrosilite	7 42	8 35	7 43	6.96	7 28	6 91	6.86	7 91	7.08	7 30	7 62	6 87	7.67
Wollastonite	44 93	44 78	44 21	42 47	42.91	43.40	46 06	44.91	44.86	44 87	44.69	45.28	44.69

Sample no.								AV116					
Analysis no.	12	13	14	15	16	17	18	1	2	3	4	5	6
SiO2	52 08	50 80	52 10	51 12	51 30	52 06	51 19	50.33	50 50	51.52	49 97	52 56	51 85
TiO2	0 51	0 71	0 52	0 75	0 71	0 41	0 70	0 33	0 31	0 51	0.58	0 46	0 23
Al2O3	1 95	3 15	1 97	3 11	2 93	1 95	2 82	2.10	2 40	2 17	4 01	1.55	1 27
FeO	4 19	4 83	4 33	4 64	4 36	4 76	4 80	9 31	9 53	5 17	9 00	4 00	7 58
MnO	0 16	0 00	0 12	0 11	0 19	0 00	0 00	0 41	0 28	0 13	0 26	0 09	0 71
MgO	17 65	17 02	17 33	16 75	16 53	18 04	17 09	14 05	14 04	16 26	13 15	17 67	14 59
CaO	21 84	21 65	21 88	21 78	22 65	21 37	21 77	21 58	21 09	22 47	20 30	22 44	22 18
Na2O	0 37	0 50	0 34	0 41	0 44	0 38	0 35	0 46	0 45	0 39	0.64	0.28	0 50
Cr2O3	0 22	0 34	0 17	0 40	0 33	0 13	0 22	0 04	0 02	0 66	0 10	0 40	0 00
Total	98 97	99 00	98 75	99 06	99 45	99 09	98 94	98 61	98 62	99 28	98.01	99 45	98.91
Mg#	88 25	86 27	87 72	86 56	87 11	87 10	86 40	72 90	72 42	84 86	72 26	88 73	77 43
Enstatite	49 45	48 23	48 84	47 85	46 89	50 01	48 24	40 39	40 64	46 05	40 11	49 03	41 95
Ferrosilite	6 58	7 67	6 84	7 43	6 94	7 41	7 59	15 02	15 48	8 21	15 40	6 23	12 23
Wollastonite	43 97	44 09	44 33	44 72	46 17	42 59	44 17	44 59	43 88	45 74	44 50	44 75	45 83

Sample no.		AV152											
Analysis no.	7	1	2	3	4	5	6	7	9	10	11	12	13
SiO2	51.30	50.18	49.98	51.43	51.61	51.45	52.16	52.03	46.75	50.45	49.91	51.80	49.08
TiO2	0.23	0.36	0.33	0.60	0.13	0.12	0.18	0.50	0.73	0.33	0.29	0.15	0.32
Al2O3	1.42	2.63	3.79	2.22	2.25	2.28	1.87	2.08	7.52	3.65	2.37	2.15	4.60
FeO	7.84	10.72	7.51	3.51	6.36	6.34	5.49	3.39	6.48	7.24	11.69	5.21	8.29
MnO	0.52	0.47	0.29	0.13	0.16	0.21	0.16	0.11	0.51	0.14	0.47	0.22	0.28
MgO	14.70	13.61	14.68	17.43	15.66	15.25	16.13	17.60	12.90	15.04	12.72	16.41	13.98
CaO	21.90	20.58	21.65	22.04	21.71	21.98	22.24	22.28	23.41	21.25	20.46	22.84	21.23
Na2O	0.51	0.47	0.42	0.40	0.49	0.51	0.38	0.37	0.17	0.59	0.40	0.33	0.52
Cr2O3	0.00	0.01	0.06	0.86	0.12	0.10	0.12	0.86	0.06	0.08	0.00	0.13	0.05
Total	98.42	99.02	98.71	98.63	98.49	98.24	98.72	99.21	98.51	98.77	98.32	99.23	98.35
Mg#	76.97	69.36	77.70	89.84	81.44	81.08	83.98	90.26	78.01	78.74	65.97	84.89	75.05
Enstatite	42.20	39.55	42.61	49.46	44.96	44.07	45.84	49.55	38.67	43.75	37.42	45.91	41.26
Ferrosilite	12.62	17.48	12.23	5.59	10.25	10.28	8.75	5.35	10.90	11.81	19.30	8.17	13.71
Wollastonite	45.18	42.97	45.15	44.95	44.79	45.65	45.41	45.10	50.44	44.44	43.28	45.91	45.03

Sample no.				AV208									
Analysis no.	14	15	16	1	2	3	4	5	6	7	8	9	10
SiO2	51.27	50.81	49.48	52.66	50.94	49.77	50.47	51.06	51.40	52.04	52.04	51.61	50.36
TiO2	0.17	0.74	1.15	0.44	0.38	0.38	0.42	0.47	0.63	0.27	0.49	0.50	0.42
Al2O3	2.34	3.17	3.77	2.20	3.37	3.40	3.85	3.73	3.39	2.17	2.67	2.07	3.43
FeO	6.37	4.27	5.32	3.72	8.33	8.52	8.43	8.43	5.04	5.19	3.70	3.51	8.26
MnO	0.23	0.05	0.17	0.05	0.24	0.24	0.20	0.24	0.20	0.16	0.11	0.09	0.22
MgO	15.48	16.68	16.10	18.52	14.88	14.39	14.41	14.51	16.98	16.67	18.09	17.77	14.52
CaO	21.96	22.32	22.29	21.24	21.29	21.16	21.50	21.25	21.85	22.52	21.50	22.72	20.99
Na2O	0.49	0.37	0.38	0.44	0.51	0.54	0.53	0.48	0.32	0.34	0.44	0.35	0.51
Cr2O3	0.13	0.23	0.10	1.05	0.11	0.13	0.09	0.14	0.28	0.13	0.86	0.68	0.09
Total	98.43	98.63	98.75	100.31	100.04	98.52	99.89	100.29	100.09	99.50	99.90	99.30	98.79
Mg#	81.24	87.44	84.37	89.87	76.11	75.08	75.29	75.42	85.73	85.12	89.72	90.02	75.79
Enstatite	44.44	47.50	45.86	51.62	42.69	41.86	41.65	42.04	47.82	46.61	50.79	49.27	42.39
Ferrosilite	10.26	6.82	8.50	5.82	13.40	13.90	13.67	13.70	7.96	8.15	5.82	5.46	13.54
Wollastonite	45.30	45.68	45.64	42.57	43.91	44.24	44.68	44.26	44.22	45.25	43.39	45.27	44.07

Table A4.11. continued... Ngaloa Group clinopyroxene traverses

Sample no.	AV116												
cpx type	Reverse zoned												
Analysis no.	1a	2	3	4	5	6	7	8	9	10	11	12	13
SiO2	52.70	52.39	51.96	52.95	51.33	49.85	49.71	49.84	49.52	52.73	52.32	52.22	52.10
TiO2	0.49	0.46	0.47	0.41	0.42	0.51	0.47	0.55	0.58	0.38	0.44	0.44	0.53
Al2O3	1.51	1.61	2.20	1.52	2.27	3.01	2.92	2.89	3.02	1.67	2.11	1.99	2.44
FeO	4.11	3.89	3.59	3.67	7.68	10.57	10.57	10.44	10.48	4.42	3.72	3.76	3.80
MnO	0.11	0.19	0.08	0.07	0.25	0.39	0.32	0.40	0.36	0.27	0.10	0.10	0.09
MgO	18.23	18.04	17.20	18.11	15.81	13.62	13.84	13.70	13.69	18.37	17.51	17.47	17.12
CaO	22.23	22.14	22.46	22.06	21.01	20.46	20.72	20.80	20.61	20.75	22.43	22.56	22.43
Na2O	0.23	0.29	0.42	0.29	0.40	0.46	0.42	0.42	0.50	0.43	0.40	0.44	0.42
Cr2O3	0.23	0.34	0.78	0.58	0.29	0.06	0.05	0.02	0.00	0.64	0.90	0.76	0.96
Total	99.84	99.35	99.15	99.66	99.45	98.91	99.02	99.05	98.77	99.65	99.92	99.72	99.88
Mg#	88.78	89.21	89.53	89.81	78.60	69.67	70.02	70.06	69.95	88.11	89.36	89.23	88.94
Enstatite	49.94	49.93	48.66	50.28	44.90	39.76	39.93	39.71	39.81	51.37	49.03	48.81	48.41
Ferrosilite	6.31	6.04	5.69	5.71	12.23	17.31	17.10	16.97	17.10	6.93	5.84	5.89	6.02
Wollastonite	43.76	44.03	45.66	44.01	42.87	42.93	42.97	43.32	43.09	41.70	45.14	45.30	45.57
Sample no.	AV99												
cpx type													
Analysis no.	1	2	3	4	5	6	7	8	9	10	11	12	13
SiO2	51.22	51.45	52.04	49.74	49.62	49.57	49.99	50.25	50.52	50.26	50.11	49.97	52.10
TiO2	0.59	0.59	0.49	0.32	0.34	0.38	0.34	0.39	0.32	0.38	0.38	0.31	0.38
Al2O3	2.29	2.22	1.97	3.29	3.18	3.16	3.23	3.15	3.31	3.30	3.30	3.25	2.36
FeO	4.49	4.14	3.67	8.94	8.94	9.01	9.28	9.14	8.89	9.17	9.11	8.99	3.98
MnO	0.10	0.18	0.10	0.33	0.30	0.28	0.33	0.33	0.27	0.34	0.36	0.29	0.15
MgO	17.39	17.50	17.90	14.23	14.14	14.13	14.11	14.27	14.22	14.12	14.20	14.09	17.35
CaO	22.30	21.95	22.14	21.41	21.35	21.28	21.05	20.93	21.42	21.38	21.04	21.53	22.49
Na2O	0.31	0.32	0.34	0.47	0.48	0.48	0.48	0.46	0.52	0.45	0.48	0.47	0.35
Cr2O3	0.08	0.25	0.53	0.09	0.06	0.00	0.06	0.10	0.01	0.06	0.11	0.06	0.74
Total	98.75	98.59	99.18	98.82	98.39	98.28	98.86	99.01	99.47	99.45	99.09	98.95	99.90
Mg#	87.36	88.27	89.68	73.94	73.82	73.66	73.05	73.57	74.04	73.31	73.53	73.64	88.61
Enstatite	48.40	49.16	49.90	41.08	40.99	40.99	40.96	41.44	41.09	40.78	41.24	40.72	48.55
Ferrosilite	7.00	6.53	5.74	14.48	14.53	14.66	15.11	14.89	14.41	14.85	14.84	14.57	6.24
Wollastonite	44.60	44.31	44.36	44.43	44.48	44.36	43.93	43.67	44.50	44.37	43.92	44.71	45.22
Sample no.						AV99							
cpx type						Normal zoned							
Analysis no.	14	15	16	17	18	1	2	3	4	5	6	7	8
SiO2	51.66	51.88	52.02	51.64	52.11	48.17	47.33	47.25	47.61	47.57	47.75	47.66	47.67
TiO2	0.47	0.47	0.52	0.61	0.60	1.47	1.73	1.68	1.56	1.61	1.72	1.68	1.54
Al2O3	2.30	2.21	2.57	2.78	2.25	5.04	5.75	5.84	5.35	5.40	5.58	5.60	5.69
FeO	3.63	3.88	3.81	4.46	4.57	5.71	6.33	6.25	5.92	6.30	6.16	6.05	6.19
MnO	0.11	0.06	0.10	0.12	0.13	0.13	0.10	0.15	0.13	0.16	0.09	0.12	0.18
MgO	17.63	18.02	17.84	17.52	17.58	14.89	14.48	14.58	14.78	14.56	14.64	14.49	14.35
CaO	21.94	21.83	21.81	21.80	21.75	23.25	22.91	22.69	23.08	23.13	22.97	22.64	22.68
Na2O	0.36	0.36	0.39	0.35	0.29	0.35	0.38	0.33	0.37	0.34	0.33	0.35	0.36
Cr2O3	0.56	0.54	0.61	0.21	0.08	0.21	0.12	0.16	0.16	0.18	0.16	0.22	0.17
Total	98.66	99.25	99.66	99.48	99.36	99.22	99.12	98.92	98.96	99.23	99.41	98.80	98.83
Mg#	89.65	89.22	89.31	87.51	87.27	82.29	80.32	80.60	81.67	80.47	80.90	81.03	80.53
Enstatite	49.76	50.21	50.04	49.08	49.15	42.78	41.98	42.39	42.62	41.93	42.31	42.43	42.06
Ferrosilite	5.75	6.07	5.99	7.01	7.17	9.21	10.28	10.20	9.57	10.18	9.99	9.93	10.17
Wollastonite	44.49	43.72	43.97	43.91	43.68	48.01	47.73	47.41	47.82	47.89	47.70	47.64	47.76

Sample no.													
cpx type													
Analysis no.	9	10	11	12	13	14	15	16	17	18	19	20	21
SiO2	47.33	48 97	50 24	50 42	50 45	50.48	49 77	50.95	50.72	50.35	50.66	50.37	50.63
TiO2	138	1.09	0 82	0.71	0 74	0 80	0 94	0.75	0.67	0.74	0.67	0.76	0.69
Al2O3	5 95	3 95	3.57	3.32	3 47	3 52	4 03	3 25	3 20	3.56	3.14	3 41	3.04
FeO	5 87	5.61	4 43	4.12	4 45	4.56	4.96	4.22	4.36	4.40	4.28	4.43	4.16
MnO	0 13	0 17	0.11	0.10	0 09	0 12	0.07	0 11	0.13	0.10	0.11	0.11	0.04
MgO	14.56	15.75	16 53	16 75	16 81	16.63	16.23	16.84	16.78	16.63	16.80	16.89	16.92
CaO	22.88	23.03	22.55	22 40	22.58	22.35	22 07	22.42	22.37	22.53	22.43	22.47	22.54
Na2O	0 38	0 35	0 41	0.41	0.39	0 40	0 38	0.37	0 36	0.35	0.39	0.38	0.37
Cr2O3	0 19	0 06	0 52	0.58	0 38	0.26	0.18	0.38	0 45	0 47	0.50	0 62	0.57
Total	98 67	98 97	99 19	98 80	99.36	99 11	98 62	99 29	99 05	99.13	98.98	99 43	98.94
Mg#	81.55	83 35	86.93	87 87	87.07	86 68	85.37	87 68	87 27	87 09	87.50	87.17	87.88
Enstatite	42 45	44 44	46 93	47 64	47 31	47 18	46.53	47 68	47.53	47.13	47.56	47.55	47.73
Ferrosilite	9 61	8 88	7 06	6.58	7.03	7 25	7 97	6.70	6 93	6 99	6.80	7.00	6.58
Wollastonite	47 94	46 69	46 02	45.79	45.66	4557	45 49	45 63	45 54	45 89	45.65	45 46	45.69

Sample no.													
cpx type													
Analysis no.	22	23	24	25	26	27	28	29	30	31	32	33	34
SiO2	50 06	5090	50.51	50.55	50.16	50.17	51.50	51.94	51.52	52.05	51.95	51.82	51.46
TiO2	0 74	0 80	0.80	0.65	0.75	0.79	0.63	0.49	0.47	0.47	0.55	0.58	0.47
Al2O3	3 55	3 25	3.56	3.26	3.32	3.54	2.35	2.09	2 05	1.92	1.94	2.24	1.91
FeO	4 28	4 33	4 33	4.46	4.41	4.22	4.26	4.11	4.25	4 35	4.13	4.10	4.12
MnO	0 14	0 03	0.13	0.14	0.09	0 09	0.10	0.11	0.19	0.15	0.09	0.12	0.15
MgO	16 55	16.59	16.49	16.77	16.82	16.77	17.62	17.96	17.87	17.93	18.01	17 66	18.22
CaO	22 22	22 52	22.40	22.34	22 51	22.27	21.93	21.89	22.16	22.01	21.70	22.09	21.65
Na2O	0 41	0 39	0 40	0.39	0.40	0.43	0.33	0.31	0.30	0 28	0.31	0.34	0.28
Cr2O3	0 65	0 58	0 67	0.49	0.54	0 72	0.39	0.42	0.35	0.40	0.30	0.37	0.45
Total	98 60	99 40	99 29	99 04	99 00	98.99	99.11	99.32	99.17	99.56	98.97	99.32	98.71
Mg#	87 33	87 22	87 15	87.03	87.17	87 62	88.06	88.62	88.23	88 01	88.60	88.47	88.74
Enstatite	47 39	47 13	47 09	47.46	47.41	47.71	49.26	49.90	49.39	49.54	50.13	49.29	50.48
Ferrosilite	6 88	6 90	6 94	7 08	6 98	6 74	6.68	6 41	6.59	6.75	6.45	6 42	6.40
Wollastonite	45 73	45 96	4597	45.46	45.61	45.55	4406	43 69	44.02	43.71	43.42	44 29	43.12

Sample no.													
cpx type													
Analysis no.	35	36	37	38	39	40	41	42	43	44	45	46	47
SiO2	52 11	51 92	51 87	51.56	51.75	51 57	51.46	51.45	50.93	51.24	51.59	51.50	51 51
TiO2	0 45	0 47	0 52	0 46	0 50	0 45	0.56	0 61	0.74	0 55	0 56	0.50	0.55
Al2O3	1 84	1 94	2 15	1 92	1 86	2 01	2.05	2.41	2.89	2 25	2.12	2 24	2 31
FeO	4 12	4 10	4 09	3 82	4.27	4 13	4 06	4.48	4 97	4 46	4.38	3 83	3.86
MnO	0 12	0 07	0 12	0.13	0 22	0.11	0.15	0 14	0 12	0 14	0.14	0 11	0.14
MgO	18 11	17 98	18 10	18 02	17.95	17 86	17 85	17 34	17.19	17 99	17.49	17.53	17.44
CaO	21 69	21 78	21 49	21 92	21.76	22 45	22 23	21.95	21.57	21 58	22 01	22.29	22 80
Na2O	0 29	0 29	0 32	0 32	0 27	0 30	0 30	0.33	0.33	0 34	0 31	0.32	0.35
Cr2O3	0 37	0 38	0 44	0 41	0 31	0 26	0.19	0.06	0.17	0 21	0.20	0 49	0.34
Total	99 09	98 92	99 09	98 54	98 89	99 15	98 85	98.76	98 90	98 75	98 79	98 79	99 28
Mg#	88 69	88 67	88 75	89 38	88 22	88 53	88 68	87 35	86 06	87 80	87 67	89 09	88 95
Enstatite	50 29	50 05	5050	50 17	49 88	49 20	4943	48 68	48 46	49.98	48 90	49 11	48 46
Ferrosilite	6 42	6 40	6 40	5 96	6.66	6 37	6 31	7 05	7 86	6 95	6 88	6 01	6 02
Wollastonite	43 30	4356	43 10	43 86	4347	44 43	44 25	44 27	43 69	43 08	44 23	44 88	45 53

Sample no.										AV99		
cpx type										Sieved cored		
Analysis no.	48	49	50	51	52	53	54	55	56	57	1	2	3
SiO2	48.83	50 16	50.01	50 26	49 73	50 23	49 49	49.53	50.18	50 09	46.08	47 86	4753
TiO2	1.16	0 87	0.97	0.90	0 92	0 89	0 98	1 01	0.82	0.92	1.91	1.45	1.56
Al2O3	4.05	2 80	3 00	2 78	2 99	2 97	3 09	3.28	2 84	2.87	6.30	5 17	5 23
FeO	5.54	5.08	5 11	4 98	5 04	4 98	5 20	5 61	5 12	5.23	6 67	5 81	5.66
MnO	0.10	0 15	0 13	0 10	0 17	0 12	0.08	0.11	0.16	0 09	0.13	0 09	0.11
MgO	15.63	16 39	16 20	16 40	16 17	16.30	16 04	16 14	16.19	16.53	14.06	14.82	14.78
CaO	22.42	23 06	22 88	22.99	22 71	22.87	22 66	22.80	22.75	22.69	22.80	23.16	23.31
Na2O	0 28	0 27	0 26	0 28	0 28	0 29	0.28	0 29	0.27	0 29	0.41	0 43	0.62
Cr2O3	0.15	0 11	0 08	0 07	0.07	0 10	0.12	0 13	0.19	0.10	0.27	0 15	0 21
Total	98 16	9888	98 64	98 76	98 08	98 74	97.94	98.89	98 52	98.79	98.63	98 94	99 02
Mg#	83 41	8520	8495	85 44	85.12	85.37	84 63	83.69	84.93	84.93	79.00	81 96	82.32
Enstatite	44.85	45 76	45 61	45 91	45 78	45.88	45 52	45 25	45 73	46 21	41.14	42.67	42.59
Ferrosilite	8 92	7 95	8 08	7 82	8.01	7 86	8 27	8 82	8.11	8.20	10.94	9 39	9.15
Wollastonite	46 23	46 29	46 31	46 26	46.21	46.26	46.21	45.93	46 16	45.59	47.93	47.94	48.27

Sample no.													
cpx type													
Analysis no.	4	5	6	7	8	9	10	11	12	13	14	15	16
SiO2	50 68	50 92	50 24	50 74	50.64	50 77	50 81	50.84	50.64	50.85	50.21	51 09	51.41
TiO2	0 66	0 59	0 67	0.68	0.77	0 66	0 79	0.70	0.71	0.79	0.76	0.54	0.50
Al2O3	2 82	2 78	3 09	2.86	3.19	2.94	3.18	3.06	3.28	3.34	3.59	2 23	2.32
FeO	4 28	4 14	4 35	4.25	4.85	4.09	4.63	4.87	4.61	4.38	4.47	4.16	4 49
MnO	0 08	0 16	0.13	0.15	0.10	0.14	0.10	0.12	0.11	0.12	0.10	0.10	0.12
MgO	16 95	16.93	16.79	16 63	16.53	16.80	16.80	16.82	16.73	16.90	16.73	17.46	17.49
CaO	23 25	22 90	22 59	23.27	22.57	22.84	22.68	22.50	22.67	22.96	22.35	22.85	22.85
Na2O	0 35	0 38	0 35	0 48	0.40	0.52	0.38	0.39	0.40	0.38	0.40	0.33	0.32
Cr2O3	0 21	0 12	0.11	0.35	0.08	0.23	0 12	0.12	0.31	0.28	0.23	0.15	0 16
Total	99 29	98 92	98.32	99.42	99.13	98.98	99.49	99.42	99 47	99.98	98.83	98.90	99.64
Mg#	87 60	8794	8732	87.46	85 87	87.98	86.60	86.03	86 61	87.30	86.96	88.21	8742
Enstatite	47 00	47 41	47 35	46.53	46.60	47.31	47.06	47.09	46.99	47.12	47.38	48.21	48 01
Ferrosilite	6 66	6.50	6 88	6.67	7 67	6.46	7.28	7 65	7.26	6 86	7 11	6 44	6 91
Wollastonite	46 34	46 09	45.77	46 80	45.74	46 23	45 66	45.27	45.75	46.02	45.51	45 35	45.08

Sample no.					
cpx type					
Analysis no.	17	18	19	20	21
SiO2	48.23	46 77	46 77	47 07	47 85
TiO2	1 10	1 67	1 71	1.60	1 48
Al2O3	4.46	6 35	5 32	5.18	4 85
FeO	5 14	6 89	7.29	7.03	5 98
MnO	0 17	0 14	0 18	0 15	0.14
MgO	15 56	13 77	14 20	14.55	15 03
CaO	22 63	21 82	23 09	23 15	23.40
Na2O	0 38	0 62	0 43	0.39	0 36
Cr2O3	0 39	0 10	0 00	0 00	0 09
Total	98 05	98 12	98 98	99 13	99 18
Mg#	84 37	78 08	77 64	78 68	81 75
Enstatite	44 83	41 33	40 70	41 41	42 70
Ferrosilite	8 31	11 60	11 72	11 22	9 53
Wollastonite	46 86	47 07	47 57	47 37	47 77

Table A4.12. Ngaloa Group plagioclase

Sample no.	AV208				AV112				AV110	AV99			
Analysis no.	1	2	3		1	2	3		1	1	2	3	4
SiO2	52.34	52.88	51.13	52.11	53.41	57 27	57.93	56.20	56.20	58.16	59.94	59.39	59.16
Al2O3	28.91	28.00	29.15	28.69	28.45	26.60	25.90	26.99	27.15	26.26	24.58	25.11	25.31
FeO	1.05	1.05	1.20	1.10	0.39	0.39	0.43	0.40	0.77	0.29	0.28	0.32	0.30
MgO	0.12	0.11	0.07	0.10	0.02	0.03	0.03	0.02	0.06	0.01	0.00	0.02	0.01
CaO	12.58	11.55	13.14	12.42	11.37	9.07	8.01	9.48	9.70	8.33	6.61	7.39	7.44
Na2O	3.81	4.25	3.49	3.85	4.36	5.59	6.25	5.40	5.23	5.77	6.46	6.18	6.14
K2O	0.28	0 39	0.31	0.33	0.20	0.35	0.36	0.30	0.48	0.68	1.02	0.97	0.89
Total	99 08	98.22	98.47	98.59	98.18	99.28	98.90	98.79	99.59	99.50	98.89	99.38	99.26
Albite	34.79	39.00	31.85	35.21	40.46	51.61	57.27	49.82	47.97	53.34	59.91	56.68	56.64
Anorthite	63.51	58.64	66.31	62.83	58.33	46.28	40.55	48.35	49.15	42.53	33.85	37.45	37.95
Orthoclase	1 71	2.36	1.83	1.96	1.21	2.11	2.18	1.83	2.89	4.13	6.24	5.87	5.42

Table A4.13. Ngaloa Group phlogopite

Sample no.	AV99												
Analysis no.	1	2	3	4	5	6	7	8	9	10	11	12	13
SiO2	39.18	39.31	40.44	40.58	40.34	40.50	40.46	40.06	40.67	40.51	40.48	39.89	40.78
TiO2	5.76	5.03	4.73	4.05	4.46	4.46	4.47	4.45	3.85	4.72	4.51	5.37	4.64
Al2O3	11.91	11.73	12.33	11.67	11.55	11.56	11.75	11.89	11.53	12.02	11.96	12.32	11.79
Cr2O3	0.06	0.11	0.06	0.00	0.07	0.00	0.02	0.00	0.00	0.01	0.03	0.04	0.02
FeO	4.38	4.57	4.19	4.19	4.31	4.10	4.11	4.36	3.97	4.36	4.26	4.80	4.25
MnO	0.07	0.05	0.12	0.12	0.09	0.06	0.03	0.08	0.07	0.05	0.06	0.04	0.07
MgO	21.59	21.71	21.77	22.28	22.77	23.25	22.91	22.65	23.19	22.77	23.00	21.98	23.11
Na2O	0.73	0.66	0.97	0.86	0.93	0.91	0.98	0.91	0.75	0.86	0.73	0.80	0.87
K2O	8.55	8.74	8.61	8.09	8.78	9.42	9.45	9.27	9.76	9.30	9.53	9.33	9.50
Total	92.39	92.17	93.31	91.93	93.35	94.43	94.32	93.80	93.94	94.64	94.64	94.62	95.14
Mg#	89.79	89.44	90.26	90.45	90.40	91.01	90.87	90.25	91.23	90.30	90.60	89.08	90.65

Sample no.					
Analysis no.	14	15	16	17	18
SiO2	40.61	3990	40.65	40.73	40.03
TiO2	4.77	5.22	3.89	4.50	4.95
Al2O3	11.90	12.37	11.86	12.29	12.20
Cr2O3	0.01	0.00	0.00	0.04	0.00
FeO	4.12	4.91	3.96	4.32	4.60
MnO	0.09	0.05	0.05	0.06	0.11
MgO	22.91	22.10	22.77	22.93	22.48
Na2O	0.95	0.79	0.81	0.85	0 81
K2O	9 25	9.44	9.11	9.23	9.38
Total	94.68	95.00	93 20	94.98	94.63
Mg#	90.84	88.91	91.10	90.45	89 71

Table A4.14. Western Kadavu clinopyroxene and orthopyroxene

	CPX												
Sample no.	AV54				AV57					AV5	AV78		
Analysis no.	1 C	1 R	2 C	2 R	1 C		1 R	2 C	2 R	1 C	1 C	2 C	3 C
SiO2	52.48	52.23	53.13	49.69	52.02	51.66	52.19	51.88	52.01	52.10	51.73	50.83	51.21
TiO2	0 43	0.49	0.31	0 77	0.34	0.35	0.30	0.23	0.25	0.41	0.40	0.54	0.44
Al2O3	1.84	1 85	1 69	3.70	2.13	1 94	2.13	2.36	2.26	1.84	2.13	3.00	2.38
Cr2O3	0.33	0.21	0.23	0.04	0 16	0.12	0.11	0.07	0.18	0.01	0.39	0.02	0.04
FeO	3 81	4.06	3.66	7.38	4.86	4.92	4.86	6.03	5.90	7.03	6.29	8.97	8.47
MnO	0.06	0.09	0.07	0.15	0.16	0.20	0.19	0.14	0.21	0.33	0.17	0.41	0.31
MgO	17.60	17 51	18.13	14.57	16.98	17.03	16.90	16.24	16.44	16.21	16.70	15.43	15.58
CaO	22.38	22.17	22.48	21.75	22.32	22.08	22.44	22.45	22.05	20.96	20.78	19.60	20.31
Na2O	0 33	0.33	0.31	0.56	0.32	0.29	0.29	0.32	0.28	0.36	0.33	0.37	0.39
Total	99 26	98.94	100.01	98.60	99.28	98.58	99.41	99.70	99.58	99.26	98.93	99.17	99.11
Mg#	89.17	88.48	89.82	77.87	86.17	86.04	86.11	82.75	83.25	80.42	82.54	75.41	76.63
Enstatite	49.14	49.01	49.88	42.42	47.51	47.76	47.27	45.41	46.19	46.02	47.47	44.66	44.60
Ferrosilite	5.97	6.38	5.65	12.06	7.62	7.75	7.63	9.46	9.29	11.20	10.07	14 57	13.60
Wollastonite	44 90	44.61	44.46	45.52	44.87	44.50	45.10	45.12	44.52	42.78	42.46	40.77	41.80

				OPX									
Sample no.					AV5			AV37		AV57		AV78	
Analysis no.	4 C	5 C	6 C	7 C	1C	2C	3C	1C	2C	1C	2C	1C	2C
SiO2	50.57	50.83	52.32	51.57	53.67	53.85	53.89	53.66	53.56	53.13	53.28	52.86	53.18
TiO2	0.51	0.50	0.36	0.43	0.13	0.14	0.14	0.21	0.23	0.14	0.18	0.25	0.20
Al2O3	2.44	3.13	1.77	2.45	1.00	0.76	0.84	1.22	1.34	0.78	0.85	1.17	1.20
Cr2O3	0.02	0.00	0.08	0.04	0.01	0.00	0.02	0.01	0.00	0.01	0.00	0.02	0.01
FeO	8.96	8 03	7.50	7.76	16.14	17.55	16.26	16.11	15.74	18.11	17.42	15.99	16.25
MnO	0.41	0.12	0.23	0.18	1.00	1.11	0.92	0.66	0.60	0.91	0.76	0.59	0.44
MgO	15.40	15.51	15.72	15.61	26.49	26.24	27.06	26.88	26.33	25.60	25.93	26.43	26.28
CaO	19.99	20.48	20.73	20.60	0.83	0.57	0.86	1.38	1.50	0.87	0.90	1.69	1.63
Na2O	0.33	0.44	0.43	0.43	0.01	0.01	0.02	0.00	0.09	0.04	0.03	0.03	0.04
Total	98 64	99.05	99.12	99.08	99.28	100.24	100.01	28.25	27.93	26.50	26.86	28.15	27.95
Mg#	75.38	7749	78.89	78.19	74.53	72.72	74.77	74.83	74.89	71.59	72.63	74.66	74.24
Enstatite	44.26	44.65	45.14	44.90	73.30	71.90	73.52	72.83	72.66	70 37	71.34	72.19	71.87
Ferrosilite	14.45	12 97	12.08	12.52	25.05	26.97	24.80	24.49	24.36	27.92	26 88	24.50	24.93
Wollastonite	41.29	42.38	42.78	42.58	1.65	1.13	1.68	2.68	2.98	1.71	1.78	3 32	3.20

Table A4.15. Western Kadavu plagioclase

Sample no.	AV48						AV54						
Analysis no.	1C	1	1R	2C	2	2R	1C	1R	2C	2	2R	3C	3
SiO2	60.14	60.05	60.32	58.11	60.53	60.64	58.73	57.86	58.27	58.64	58.20	59.22	60.50
Al2O3	25.23	24.92	24.73	26.29	24.80	24.83	25.76	26.45	26.41	26.05	26.44	25.88	24.92
FeO	0.12	0 16	0.10	0.13	0.15	0.20	0.21	0.16	0.12	0.19	0.16	0.21	0.14
MgO	0.01	0 01	0.00	0.00	0.00	0.00	0 00	0.01	0.01	0.01	0.02	0.00	0.01
CaO	6.32	6.27	6.03	7.86	5.93	6.03	7.44	8.01	7.97	7.76	7.91	7.38	6.22
Na2O	7.30	7.20	7 40	6.39	7.31	7.35	6.54	6.20	6.29	6.50	6.35	6.69	7.28
K2O	0.34	0.32	0.36	0.25	0.37	0.34	0.41	0.45	0.29	0.34	0.34	0.42	0.51
Total	99.46	98.93	98.94	99.03	99.09	99.39	99.09	99.14	99.36	99.49	99.42	99.80	99.58
Albite	66.27	66 21	67.46	58.64	67.50	67.40	59.88	56.76	57.79	59.03	58.02	60.57	65.87
Anorthite	31.70	31 86	30.38	3986	30.26	30.55	37.65	40.53	40.46	38.94	39.94	36.93	31.10
Orthoclase	2.03	1.94	2.16	1.51	2.25	2.05	2.47	2.71	1.75	2.03	2.04	2.50	3.04

Sample no.		AV57								AV90			
Analysis no.	3R	1C	1R	2C	2	2R	3C	3	3R	1C	1	1R	2C
SiO2	60.38	57.27	54.26	58.40	57.38	56.38	58.47	58.49	57.38	58.69	57.80	59.07	56.20
Al2O3	24.57	26.78	29.05	26.44	26.82	27.62	26.24	25.93	26.88	25.78	25.73	25.58	27.75
FeO	0.18	0.29	0.36	0.52	0.47	0.38	0.28	0.35	0.39	0.37	0.40	0.31	0.32
MgO	0.01	0.01	0.00	0.03	0.02	0.03	0.03	0.03	0.02	0.01	0.01	0.00	0.02
CaO	6.25	8.69	11.05	8.07	8.50	9.55	7.75	7.62	8.62	7.62	7.51	7.32	9.43
Na2O	7.21	5.98	4.76	6.34	6.16	5.61	6.38	6.54	6.07	6.37	6.18	6.63	5.68
K2O	0.58	0.32	0.18	0.35	0.32	0.28	0.31	0.39	0.28	0.49	0.42	0.49	0.34
Total	99.18	99.34	99.66	100.15	99.67	99.85	99.46	99.35	99.64	99.33	98.05	99.40	99.74
Albite	65.28	54.40	43.33	57.48	55.66	50.67	58.71	59.41	55.09	58.42	58.27	60.29	51.10
Anorthite	31.27	43.69	55.59	40.43	42.44	47.67	39.41	38.25	43.24	38.62	39.13	36.78	46.88
Orthoclase	3.46	1.92	1.08	2.09	1.90	1.66	1.88	2.33	1.67	2.96	2.61	2.93	2.01

Sample no.			AV5				AV78						
Analysis no.	2	2R	1C	1	1	1R	1C	1	1R	2C	2	2	2R
SiO2	56.31	57.01	58.40	60.36	59.35	59.65	54.53	53.86	54.18	54.81	55.01	53.62	54.61
Al2O3	27.59	27.04	25.69	24.89	25.04	25.52	28.05	27.95	28.03	27.37	27.53	28.53	27.61
FeO	0.43	0.38	0.27	0.25	0.26	0.23	0.61	0.63	0.53	0.68	0.68	0.65	0.54
MgO	0.02	0.02	0.00	0.00	0.01	0.00	0.06	0 05	0.06	0.07	0.05	0.04	0.06
CaO	9 29	8.86	7.66	6.16	6.53	6.88	10.95	11.00	10.93	10.39	10.39	11.30	10 65
Na2O	5.62	5.66	6.84	7.25	7.28	6.92	5.03	4.66	5.03	5.16	5.08	4.68	5.18
K2O	0.33	0.36	0.44	0.50	0.51	0.49	0.23	0.27	0.23	0.24	0.24	0.26	0.24
Total	99.59	99 33	9930	99.41	98.98	99.69	99.46	98.42	98.99	98.72	98.98	99.08	98.89
Albite	51.23	52.44	60.23	66.02	64.87	62.64	44.79	42.68	44.83	46 62	46.24	42.19	46.14
Anorthite	46.79	45.36	37.25	31.00	32.14	34.44	53.89	55.70	53.83	51.94	52.33	56.28	52.47
Orthoclase	1.98	2.20	2.52	2.98	2.99	2.92	1.32	1.62	1.34	1.44	1 43	1.53	1.39

Sample no.													AV5
Analysis no.	3C	3	3R	4C	4	4R	5C	5	5R	6C	6	6R	1C
SiO2	55.41	53 25	54.04	54.77	54.62	54.44	53.67	58.66	55.27	55.39	53.57	55 03	52.98
Al2O3	27.44	29 12	28.54	27.52	27.43	27.61	28.60	23.98	27 42	26.90	28.34	27.49	29.32
FeO	0.61	0.59	0.56	0.64	0.64	0.65	0.66	1.56	0.65	0.69	0.64	0.73	0 49
MgO	0.07	0.04	0.05	0.06	0.06	0.05	0.04	0.18	0.06	0.05	0.07	0.05	0 02
CaO	10.08	11.55	11.17	10.51	10.62	10.73	11.44	8.61	10.25	9.74	11.57	10.66	11.99
Na2O	5.25	4.48	4.79	5.06	5.18	5.06	4.65	4.60	5.30	5.49	4.61	5 02	4.42
K2O	0.29	0.20	0.24	0.33	0.26	0.23	0.23	0.76	0.25	0.31	0.20	0.31	0.16
Total	99 15	99.23	99.39	98 89	98.81	98.77	99.29	98.35	99.20	98.57	99.00	99.29	99 38
Albite	47 65	40 73	43.09	45.63	46.18	45.40	41.82	46.64	47 65	49.57	41.38	45.13	39.60
Anorthite	50 59	58.06	55.49	52.43	5230	53.22	56.80	48.27	50.86	4859	57.43	53.01	59.42
Orthoclase	1.76	1.21	1.43	1.94	1.52	1.38	1 38	5.10	1 49	1.85	1.19	1 86	0.97

Sample no.													
Analysis no.	2C	3C	4C	5C	6C	7C	8C	9C	10C	11C	12C	13C	14C
SiO2	54.53	52.98	54.62	52.47	54.92	55.46	54.27	54.99	54.87	54.78	53.56	52.60	52.63
Al2O3	27 94	2943	28.69	29.82	28.19	28.48	28.97	28.28	27.95	28.49	29.59	29.69	29.91
FeO	0.40	0.44	0.33	0.43	0.52	0.39	0.53	0.38	0.48	0.44	0.43	0.49	0.50
MgO	0.03	0.02	0 01	0.03	0.03	0.02	0.04	0.03	0.03	0.04	0.05	0.02	0.03
CaO	10.59	11.79	10 47	12.33	10.36	10.38	10.89	10.27	10.48	10.53	11.58	12.30	12.27
Na2O	5.08	4.52	4.97	4.16	5.11	5.39	5.03	5.05	5.04	5.01	4.52	4.25	4.14
K2O	0.26	0.18	0 23	0.17	0.25	0.20	0.21	0.23	0.26	0.26	0.18	0.19	0.16
Total	98.83	99.36	99.32	99.41	99.38	100.32	99.94	99.23	99.11	99.55	99.91	99.54	99.64
Albite	45.74	40.52	45.60	37.51	46.44	47.84	44.97	46.43	45.77	45.55	40.96	38.03	37.55
Anorthite	52.69	58.41	53.02	61.50	52.07	50.97	53.79	52.18	52.64	52.90	57.98	60.85	61.51
Orthoclase	1.57	1.07	1.39	0.99	1.49	1.20	1.24	1.40	1.59	1.55	1.06	1.12	0.94

Sample no.	AV6										AV78	
Analysis no.	1C	2C	3C	4C	5C	6C	7C	8C	9C	10C	11C	1C	2C
SiO2	54.83	54.68	55.03	54.05	56.49	55.00	54.65	57.03	51.50	53.83	54.47	54.49	54.91
Al2O3	28.20	28.23	28.18	28.95	26.78	28.26	28.20	27 18	30.82	29.21	28.48	27.59	28.03
FeO	0.46	0.40	0.42	0.50	0.29	0.44	0.38	0.26	0.51	0.45	0.47	0.55	0.65
MgO	0.02	0.04	0.02	0.03	0.03	0.02	0.04	0.00	0.04	0.02	0.04	0.06	0.05
CaO	10.36	10.60	10.37	11.07	9.00	10.58	10.53	8.96	13.60	11.47	10.59	10.82	10.46
Na2O	5.07	5.09	5.26	4.72	5.98	5.13	5.14	5.78	3.55	4.61	5.08	4.90	5.04
K2O	0.23	0.24	0.25	0.20	0.29	0.26	0.28	0.31	0.13	0.21	0.22	0.26	0.25
Total	99.17	99.28	99.53	99.52	98.86	99.69	99.22	99.52	100.15	99.80	99.35	98.67	99.39
Albite	46.31	45.82	47.14	43.03	53.64	46.00	46.16	52.88	31.83	41.60	45.84	44.32	45.91
Anorthite	52.28	52.74	51.40	55.75	44.62	52.48	52.21	45.27	67.41	57.16	52.84	54.11	52.62
Orthoclase	1.41	1.44	1.46	1.22	1.74	1.52	1.64	1.85	0.76	1 25	1.32	1.57	1.47

Sample no.								
Analysis no.	3C	4C	5C	6C	7C	8C	9C	10C
SiO2	54.51	54.55	55.41	54.75	54.84	55.02	53.96	54.68
Al2O3	28.14	27.79	27.92	27.77	27.55	27.78	27.94	27.55
FeO	0.57	0.65	0.58	0.60	0.57	0.66	0.65	0.58
MgO	0.06	0.07	0.04	0.05	0 05	0.06	0.07	0.05
CaO	10.76	10.46	10.40	10.88	10.31	10.67	11.11	10.26
Na2O	4.88	4 90	5.13	4.97	5.23	4.91	4.79	5.32
K2O	0.25	0 26	0.25	0.23	0.26	0.23	0.24	0.23
Total	99.17	98.68	99 73	99.25	98.81	99.33	98.76	98.67
Albite	44.39	45.14	46.48	44.66	47.11	44.81	43.21	47.74
Anorthite	54.08	53.27	52.02	53.99	51.34	53.80	55.37	50.90
Orthoclase	1.53	1.58	1.50	1.35	1.55	1.39	1.42	1.36

Table A4.16. Glass inlcusions in plagioclase

Sample no	AV5					AV6				AV78			
Analysis no.	1	2	3	4	5	1	2	3	4	1	2	3	4
SiO2	73 22	74.20	7345	73.35	72.54	70.28	71.41	70.96	70.32	71.20	71.77	71.19	71.79
TiO2	0.53	0.54	0.47	0.45	0.45	0.52	0.45	0.49	0.49	0.75	0.44	0.43	0 65
Al2O3	11 41	10.55	11.95	12.22	12.82	12.96	12.91	12.90	13.15	12.41	13.06	13 21	12.53
FeO	2.47	2.52	2 07	2.09	2.15	2.86	2.41	2.64	2.70	3.07	2.54	2.49	3.05
MgO	0.63	0.65	0 54	0.52	0.51	0.89	0.66	0.79	0 82	0.24	0 18	0.17	0 24
CaO	0.47	0.50	0.44	0.68	0.56	0.88	0.93	0 87	0.92	0.94	0.59	1.14	0.85
Na2O	2.38	2.14	2.59	2.74	3 25	2 51	2.41	2 57	2.47	3.52	3.29	3.50	3.63
K2O	5 65	4.80	5 26	5.04	5.21	5.29	4.95	5.16	5.05	4.62	5.16	4.79	4.63
P2O5	0.11	0 08	0.10	0.09	0.11	0.12	0.09	0.13	0 11	0.16	0.12	0.21	0.18
Total	96.87	95.96	96.88	97.17	97.60	96.31	96 23	96.50	96 02	96.90	97.13	97.13	9754

Table A4.17. Western Kadavu hornblende

Sample no.	AV48							AV90			AV5		
Analysis no.	1	2	3	4	5	6	7	1	2	3	1	2	3
SiO2	48.42	49 10	4762	46.55	49.19	48.61	48.87	43.09	43.12	44.03	46.18	45.16	45.30
TiO2	0 82	0 68	0.98	1.11	0 75	0.81	0.82	2.23	3.03	2.64	1.51	1.71	1.76
Al2O3	6 24	5 36	6.96	7 68	5.67	6.19	5.97	10.58	9.57	8.79	6.56	7.54	7.17
FeO	12.14	11 60	12.34	12.85	11.61	12.00	11.90	11.61	11.78	11.91	11.14	11.43	11.02
MnO	0 61	0.58	0.51	0.48	0.61	0.54	0.58	0.24	0.19	0.25	0.38	0.39	0.29
MgO	15 98	16.33	15.59	14.97	16.51	16.03	16.07	14.46	14 62	14.77	15.53	14.88	15.21
CaO	10.70	11.14	10.69	11.10	10.58	11.12	10.80	11.64	11.68	11.40	11.39	11.25	11.39
Na2O	1.17	1.14	1.35	1.53	1.26	1.27	1.14	2.17	2.21	2.06	1.53	1.72	1.71
K2O	0.20	0.15	0 24	0.30	0.16	0.21	0.18	0.55	0.53	0.56	0.38	0.46	0.43
Total	96.28	96.08	96.27	96.57	96.34	96.78	9632	96.56	96.72	96.41	94.58	94.56	94.28
Mg#	70.12	71.50	69.24	67.50	71.72	70.42	70.64	68.94	68.87	68.85	71.31	69.89	71.10

Sample no.					
Analysis no.	4	5	6	7	8
SiO2	45.59	48.42	46.16	44.57	46.36
TiO2	1.67	1.16	1.60	1.88	1.54
Al2O3	6.98	5.26	6.86	7.79	6.66
FeO	11.41	10.52	11.55	11.62	11.38
MnO	0.28	0.37	0.32	0.35	0.33
MgO	14 99	16.43	15.07	14.37	15.29
CaO	11.37	11.26	11.33	11.41	11.22
Na2O	1.59	1.25	1.60	1.77	1.51
K2O	0.39	0.29	0.40	0.50	0.40
Total	94.27	94.96	94.89	94.26	94.68
Mg#	70.08	73.57	69.94	68.80	70.56

Table A4.18. Central/Eastern/Ono Group pyroxene

	CPX												
Sample no.	AV141			AV117								AV227	
Analysis no.	1C		1R	1C	1R	2C	2R	3C	3R	4C	4R	1C	1R
SiO2	49.61	48.99	50.89	52.59	52.26	51.57	51.35	51.83	52.88	52.95	53.22	51.60	52.06
TiO2	0.80	0.92	0.51	0.19	0.20	0.45	0.48	0.39	0.17	0.13	0.09	0.50	0.42
Al2O3	3.70	4.01	2.66	1.55	1.68	1.63	2.05	1.55	1.27	1.41	1.36	1.77	1.43
Cr2O3	0.12	0.16	0.02	0.95	0.81	0.00	0.03	0.01	0.79	0.43	0.40	0.02	0.00
FeO	6.40	6.74	7.46	3.24	3.31	7.65	7.47	8.34	2.98	5.60	4.88	7.91	7.70
MnO	0.06	0.13	0.21	0.12	0.05	0.31	0.30	0.33	0.09	0.24	0.17	0.32	0.40
MgO	15.30	15.35	15.92	17.55	17.45	15.94	15.77	15.04	17.87	18.23	19.44	15.35	15.58
CaO	22.17	21.86	21.31	23.46	23.44	21.30	21.40	21.64	23.70	20.39	20.32	21.61	21.81
Na2O	0.34	0.31	0.27	0.27	0.20	0.48	0.42	0.42	0.19	0.29	0.22	0.41	0.37
Total	98.50	98.47	99.25	99.92	99.40	99.32	99.26	99.56	99.94	99.67	100.10	99.49	99.76
Mg#	81.00	80.24	79.18	90.63	90.38	78.78	79.01	76.27	91.44	85.30	87.65	77.57	78.30
Enstatite	43.93	44.06	44.95	48.45	48.26	44.85	44.62	42.64	48.85	50.60	52.85	43.47	43.79
Ferrosilite	10.31	10.85	11.82	5.01	5.14	12.08	11.85	13.27	4.57	8.72	7.44	12.57	12.14
Wollastonite	45.77	45.10	43.23	46.54	46.60	43.07	43.53	44.10	46.58	40.68	39.71	43.97	44.07

Sample no.					AV232		AV164						
Analysis no.	2C	2R	3C	3R	1C	1R	1C		1R	2C			2R
SiO2	50.78	51.81	51.79	52.25	50.95	51.36	52.69	52.67	52.53	52.39	52.88	52.61	52.72
TiO2	0.51	0.40	0.26	0.31	0.46	0.36	0.17	0.17	0.18	0.18	0.16	0.30	0.15
Al2O3	2.16	1.54	1.62	0.99	1.75	1.49	0.91	0.86	0.94	0.87	0.77	1.36	1.01
Cr2O3	0.00	0.00	0.38	0.00	0.05	0.04	0.00	0.00	0.00	0.01	0.00	0.02	0.00
FeO	7.76	7.70	7.16	7.59	7.67	7.55	7.13	6.90	7.04	7.01	7.04	6.99	7.07
MnO	0.23	0.34	0.31	0.47	0.34	0.40	0.76	0.69	0.63	0.72	0.79	0.69	0.67
MgO	15.23	15.43	15.77	15.84	15.49	15.28	15.22	15.41	15.13	15.54	15.60	15.13	15.42
CaO	21.68	21.35	21.63	21.75	21.75	21.86	21.87	21.52	21.61	21.87	21.58	21.87	21.84
Na2O	0.40	0.38	0.44	0.45	0.46	0.40	0.35	0.40	0.44	0.42	0.41	0.48	0.44
Total	98.74	98.95	99.36	99.64	98.91	98.73	99.09	98.60	98.49	98.99	99.22	99.45	99.32
Mg#	77.78	78.13	79.71	78.82	78.27	78.30	79.18	79.93	79.31	79.81	79.80	79.42	79.54
Enstatite	43.32	43.96	44.64	44.34	43.74	43.38	43.55	44.35	43.71	44.16	44.50	43.51	43.95
Ferrosilite	12.38	12.31	11.36	11.91	12.14	12.03	11.45	11.14	11.41	11.17	11.27	11.28	11.31
Wollastonite	44.30	43.73	44.00	43.75	44.12	44.60	45.00	44.51	44.89	44.67	44.24	45.21	44.74

						OPX						
Sample no.				AV114		AV114					AV232	
Analysis no.	3C		3R	1C	1R	1C	2C	3C	4C	5C	1C	2C
SiO2	52.77	52.65	52.58	53.33	53.42	53.87	53.20	53.87	52.91	53.28	53.93	52.56
TiO2	0.17	0.23	0.19	0.22	0.19	0.19	0.22	0.20	0.17	0.12	0.23	0.24
Al2O3	0.79	0.88	0.87	1.52	1.49	0.59	0.86	0.71	0.84	0.56	0.89	0.89
Cr2O3	0.00	0.00	0.00	0.15	0.30	0.00	0.00	0.00	0.00	0.00	0.03	0.00
FeO	7.12	6.77	7.00	3.84	3.79	16.28	16.44	15.95	16.17	15.55	16.53	16.45
MnO	0.64	0.58	0.66	0.04	0.22	0.88	0.86	0.90	0.64	0.83	0.55	0.68
MgO	15.07	15.47	15.10	17.77	17.81	26.60	26.61	26.90	26.63	26.74	26.45	26.52
CaO	22.58	22.31	22.63	22.36	21.88	0.92	0.95	0.89	0.92	0.92	0.98	0.99
Na2O	0.41	0.46	0.45	0.23	0.24	0.02	0.02	0.03	0.00	0.02	0.03	0.02
Total	99.55	99.34	99.48	99.45	99.34	99.35	99.15	99.44	98.29	98.00	99.63	98.36
Mg#	79.06	80.28	79.35	89.18	89.33	74.44	74.26	75.04	74.60	75.41	74.04	74.19
Enstatite	42.71	43.82	42.78	49.37	49.95	73.08	72.87	73.73	73.24	74.03	72.60	72.75
Ferrosilite	11.31	10.77	11.13	5.99	5.97	25.10	25.26	24.53	24.94	24.15	25.46	25.31
Wollastonite	45.98	45.42	46.09	44.65	44.09	1.82	1.87	1.75	1.82	1.82	1.94	1.94

Table A4.19. Central/Eastern/Ono plagioclase

Sample no.	AV117 Grain traverses												
Analysis no.	1C		1R	2C		2R	3C		3R	4C	4R	5C	5R
SiO2	54.56	54.20	55.73	51.98	53.09	53.29	54.57	55.99	53.69	53.39	51.71	53.57	54.97
Al2O3	28.27	28.33	27.30	29.68	29.11	28.88	28.01	26.49	28.50	28.50	29.29	29.25	28.08
FeO	0.51	0.56	0.53	0.47	0.47	0.52	0.50	0.77	0.55	0.49	0.54	0.46	0.50
MgO	0.06	0.06	0.06	0.03	0.04	0.04	0.05	0.09	0.05	0.04	0.07	0.06	0.05
CaO	10.10	10.38	9.59	12.53	11.77	10.97	10.44	8.90	10.82	10.79	11.61	11.53	10.18
Na2O	5.04	5.09	5.55	4.10	4.42	4.78	5.07	4.95	4.85	5.02	4.60	4.44	5.15
K2O	0.41	0.40	0.55	0.27	0.39	0.36	0.53	1.33	0.41	0.48	0.33	0.33	0.49
Total	98.95	99.01	99.30	99.06	99.29	98.84	99.17	98.52	98 87	98.71	98.14	99.62	99.43
Albite	46.29	45.87	49.52	36.59	39.57	43.18	45.31	46.07	43.69	44.45	40.95	40.24	46.37
Anorthite	51.24	51.73	47.28	61.81	58.15	54.70	51.55	45.78	53.86	52.76	57.12	57.80	50.72
Orthoclase	2.48	2.40	3.21	1.61	2.28	2.12	3.14	8.16	2.45	2.79	1.93	1.96	2.91

Sample no.	AV227											AV232	
Analysis no.	1C		1R	2C		2R	3C		3R	4C	4R	1C	
SiO2	54.29	56.91	57.57	57.85	55.27	55.70	53.65	53.56	56.87	50.02	53.98	57.59	56.87
Al2O3	28.52	27.02	26.49	26.19	27.82	27.22	28.83	29.10	26.61	31.66	28.87	26.14	26.60
FeO	0.34	0.43	0.36	0.44	0.50	0.62	0.44	0.46	0.47	0.42	0.42	0.41	0.38
MgO	0.02	0.01	0.00	0.03	0.02	0.02	0.04	0.03	0.03	0.02	0.03	0.04	0.02
CaO	10.29	8.55	8.13	8.08	10.16	9.78	10.72	11.17	8.65	14.45	11.05	8.08	8.49
Na2O	4.97	5.75	5.99	5.86	5.27	4.79	4.78	4.60	5.88	3.14	4.89	6.31	6.02
K2O	0.56	0.77	0.78	0 91	0.60	1.21	0.44	0.42	0.70	0.22	0.43	0.74	0.67
Total	98.99	99.45	99.32	99.36	99.62	99.33	98.90	99.35	99.22	99.93	99.67	99.30	99.06
Albite	45.08	52.37	54.47	53.63	46.74	43.61	43.51	41.63	52.84	27.88	43.34	56.05	53.96
Anorthite	51.56	43.04	40.84	40.87	49.77	49.16	53.88	55.86	43.00	70.85	54.15	39.62	42.06
Orthoclase	3.36	4.59	4.69	5.50	3.49	7.23	2.61	2.51	4.17	1.27	2.52	4.33	3.97

Sample no.					AV164								
Analysis no.	1R	2C		2R	1C						1R	2C	2R
SiO2	57.09	55.34	55.68	55.67	60.94	60.38	63 78	59.60	57.98	60.52	60.26	59.54	61.55
Al2O3	2634	27.40	2704	27 13	24.27	24.28	21.89	25.18	26.02	24.11	24.48	25.04	23.44
FeO	0.33	0.41	0.41	0.38	0.35	0.35	0.50	0.28	0 30	0.29	0.30	0 28	0.29
MgO	0.03	0 02	0 02	0 02	0.00	0.03	0.05	0.00	0.01	0.00	0.01	0.02	0.00
CaO	8.00	9.26	9.16	8.99	5.20	5.86	4.12	6.58	7.31	5.93	5.67	6.38	4.81
Na2O	6.10	5.77	5.85	5.81	6.96	6.97	6.77	6.66	6.37	6.76	6.84	6.57	7.13
K2O	0.71	0.54	0.58	0.62	1.17	1.09	1.73	0.86	0.65	1.10	1.20	0.85	1.41
Total	98.59	98.74	98.73	98.61	98.89	98.94	98.84	99.16	98.63	98.71	98.76	98 69	98 62
Albite	55 52	51.36	51.79	51.94	65.62	63.81	66.45	61.29	58.76	62.84	63.57	61.65	66.54
Anorthite	40.24	45.50	44.83	44.39	27.12	29.64	22.37	33.48	37 29	30.44	29.12	33.08	2483
Orthoclase	4.24	3.14	3.38	3.67	7.27	6.55	11.17	5.23	3 95	6.73	7.31	5.27	8.63

Sample no.													
Analysis no.	3C					3R	4C		4R	5C			
SiO2	59 87	61.18	61.26	60.53	61.72	61 37	61.33	59.92	61.49	6075	60.76	59 97	59 96
Al2O3	24.92	24 09	23.76	24.16	23.68	23 66	23.83	24.84	23.54	24.34	24.53	24.71	24.64
FeO	0 25	0.29	0.29	0.33	0.34	0.24	0.35	0.27	0 38	0.25	0.26	0.31	0.27
MgO	0.01	0.00	0.00	0.01	0.02	0.01	0.00	0.00	0.00	0.02	0.02	0.00	0 03
CaO	6.04	5.67	5.03	5.63	4.89	5 18	5.10	6.16	4.89	5.51	5.73	6 18	6 09
Na2O	6 93	7.03	7 04	6.80	7.06	6.93	7.15	6.67	7 08	6.83	6.93	6 60	6 80
K2O	0.99	1.00	1.24	1.07	1.43	1.27	1.17	0 87	1.30	1.23	1.17	0.97	1.11
Total	99 00	99.27	98.63	98.53	99.14	98 66	98.93	98.72	98.67	9893	99.38	98.73	98 89
Albite	63.49	64.95	66.20	64.07	65.96	65.17	66.60	62.64	66.56	63 94	63.79	61.92	62.44
Anorthite	30.55	28.95	26.13	29 28	25.28	26.95	26.23	31.98	25.41	28.48	29.13	32 07	3087
Orthoclase	5.96	6.10	7.67	6.65	8.77	7 89	7.18	5 39	8.03	7.58	7 08	6 01	6 70

Sample no.	AV114												
Analysis no.	5R	6C	6R	1C		1R	2C	2R	3C		3R	4C	
SiO2	60 61	60.83	61.12	55.59	57 33	56.34	56.57	57.06	55 34	56.68	55.71	56.67	57.09
Al2O3	24.31	24.24	23.83	27 66	26 54	26.54	26 49	26.05	27 65	27.09	27.43	26.56	25.78
FeO	0.29	0.31	0.30	0.35	0.32	0 45	0.34	0.36	0 36	0.37	0.35	0.38	0.39
MgO	0.01	0 01	0 01	0 00	0.01	0.01	0.03	0.03	0.02	0.02	0.03	0.04	0.03
CaO	5 64	5 43	5.19	9 81	8 64	8.81	8 92	8.29	10.06	9.11	9.77	8.81	8.34
Na2O	6.83	6 85	6 90	5.44	5 82	5 77	5.66	5.99	5.37	5.68	5.33	5.82	6.15
K2O	1 22	1 08	1 36	0.48	0 62	0.58	0.60	0.71	0.45	0.59	0.48	0.68	0.72
Total	98 90	98 75	98.71	99.33	99.28	98.50	98.62	98.49	99.25	99.54	99.10	98.97	98.50
Albite	63 53	64.84	64 71	48.65	52.89	52.36	51.54	54.29	47 84	51 17	48 26	52.26	54 75
Anorthite	29 02	28 43	26.89	48.51	43.40	44.16	44.87	41.51	49.50	45.33	48.90	43.71	41.02
Orthoclase	7 46	6.73	8.40	2 84	3.71	3.49	3 59	4.21	2 65	3.50	2.85	4.03	4.23

Sample no.													
Analysis no.	4R	5C	6C	7C	8C	9C	10C	11C	12C	13C	14C	15C	16C
SiO2	56 26	57 72	56.86	57.35	55.63	56.14	56.48	54.90	57.27	58.24	56.32	58.52	56.09
Al2O3	26 32	26 28	27.08	26.30	27.09	27.38	26.71	27.62	26.26	25.73	26.69	25.70	27.17
FeO	0.42	0.38	0.43	0.45	0.32	0.42	0.41	0.34	0.33	0.43	0.34	0.33	0.43
MgO	0 02	0 03	0.02	0.04	0.02	0.02	0.03	0.02	0.01	0.02	0.02	0.02	0.03
CaO	8 70	8 46	9.24	8.33	9.69	9.33	9.29	10.36	8.64	7.75	8.86	7.87	9.47
Na2O	5 79	5.84	5.75	5.98	5.42	5.53	5.65	5.12	6.02	6.32	5.68	6.26	5.57
K2O	0 71	0.71	0 63	0.66	0.54	0.63	0.59	0.48	0.68	0.74	0.54	0.83	0.52
Total	98 22	99 42	100.01	99.12	98.70	99.45	99.17	98.84	99.20	99.23	98.46	99.53	99.27
Albite	52.32	53.15	51.01	54.26	48.72	49.84	50.59	45.86	53.55	57 01	51.96	56.14	49.99
Anorthite	43 45	42.57	45.31	41.79	48.10	46.44	45.96	51.33	42.48	38.62	44.77	38.97	46.92
Orthoclase	4.23	4 28	3 68	3.96	3 18	3.73	3.45	2.81	3.97	4.37	3.27	4.89	3.09

Sample no.					
Analysis no.	17C	18C	19C	20C	21C
SiO2	57.91	55 43	54.82	56.80	57.22
Al2O3	25 76	27.29	28 09	26 45	26.59
FeO	0 40	0 42	0.39	0.33	0.30
MgO	0 02	0 02	0.02	0 04	0.01
CaO	7 96	9 66	10.47	8.69	8.79
Na2O	6 28	5 37	5 09	5 92	5.81
K2O	0 73	0.57	0 43	0.59	0.62
Total	99 06	98 76	99.31	98.81	99.34
Albite	56 28	48.44	45.64	53 27	52.47
Anorthite	39 42	48 18	51.84	43.24	43.83
Orthoclase	4 30	3.38	2.52	3.50	3.71

TableA4.20 Glass inclusions in plagioclase

Sample no.	AV114						
Analysis no.	1	2	3	4	5	6	7
SiO2	74 67	74.99	73 34	73 14	75.53	75.12	75.47
TiO2	0.54	0.57	0 48	0.46	0.44	0.48	0.46
Al2O3	11 70	11.13	11 17	13 94	11.50	11.60	11.58
FeO	1 17	1 95	2.19	1.11	1.38	1.52	1.29
MgO	0 08	0.19	0.53	0.09	0.09	0.13	0.10
CaO	0 32	0.42	0.60	0.82	0.40	0.32	0.32
Na2O	2.33	1.95	1 93	3 50	2 24	2 41	2.40
K2O	6 04	5.21	5.43	5.73	6 00	5.67	5.89
P2O5	0 06	0 09	0 07	0 08	0.02	0.09	0.04
Total	96.90	96.51	95 74	98 86	97.61	97.33	97.54

Table A4.21. Central/Eastern/Ono hornblende

Sample no,	AV141											AV232	
Analysis no.	1	2	3	4	5	6	7	8	9	10	11	1	2
SiO2	41.36	41.63	41.97	41.77	42.02	43.07	42.29	43.17	43.28	42.15	42.35	43.72	43.99
TiO2	2.57	2.52	2.35	2.49	2.43	1.86	2.41	1.90	1.94	2.42	2.49	2.79	2.79
Al2O3	11.40	11.52	11.05	11.00	10.86	9.67	10.82	9.91	9.83	10.51	10.93	8.69	8.75
FeO	10.59	10.67	10.69	10.56	10.57	11.94	10.48	11.62	11.72	10.31	10.36	10.99	11.21
MnO	0.09	0.12	0.12	0.21	0.16	0.30	0.19	0.33	0.32	0.13	0.06	0.30	0.26
MgO	15.06	14.90	15.16	14.90	15.01	14.71	15.09	14.87	14.71	15.29	15.08	15.05	15.03
CaO	11.98	11.90	11.44	11.59	11.45	11.17	11.67	11.36	11.31	11.66	11.64	11.40	11.44
Na2O	2.17	2.23	2.21	2.17	2.18	2.13	2.21	2.16	2.12	2.19	2.15	2.09	1.97
K2O	0.64	0.62	0.54	0.62	0.57	0.42	0.54	0.41	0.44	0.59	0.61	0.82	0.84
Total	95.85	96.10	95.52	95.32	95.25	95.27	95.71	95.70	95.67	95.25	95.66	95.84	96.28
Mg#	71.71	71.34	71.69	68.72	71.96	69.53	69.11	72.55	72.18	70.95	70.51	71.73	71.06

Sample no,									
Analysis no.	3	4	5	6	7	8	9	10	11
SiO2	44.25	43.39	43.28	42.28	42.79	41.89	42.71	43.22	43.23
TiO2	2.62	2.95	2.93	1.63	1.67	1.60	1.70	2.87	2.93
Al2O3	8.49	9.16	8.98	11.49	11.32	11.33	11.26	11.85	9.19
FeO	10.80	10.85	11.04	10.46	9.96	10.67	9.87	9.78	10.76
MnO	0.25	0.23	0.19	0.17	0.13	0.10	0.04	0.24	0.09
MgO	15.37	14.95	14.85	15.36	15.76	15.15	15.70	13.19	15.02
CaO	11.48	11.47	11.48	11.33	11.49	11.40	11.55	11.57	11.74
Na2O	2.04	2.10	2.16	2.22	2.15	2.19	2.58	2.48	2.12
K2O	0.83	0.74	0.74	0.49	0.48	0.47	0.48	0.76	0.75
Total	96.12	95.82	9564	95.41	95.76	94.78	95.89	95.96	95.82
Mg#	70.56	72.36	73.83	71.68	73.92	70.63	71.34	71.66	71.55